North Pacific Research Board Bering Sea Integrated Ecosystem Research Program Final Report
Fish forage distribution and ocean conditions (BSIERP - B62)

1. Anne B. Hollowed (NOAA/AFSC/REFM, 7600 Sand Point Way NE, Seattle, WA 98115, Anne.Hollowed@noaa.gov

2. Steven Barbeaux, NOAA/AFSC/REFM,7600 Sand Point Way NE, Seattle, WA 98115, Steve.Barbeaux@noaa.gov

3. Edward D. Cokelet, NOAA/PMEL, 7600 Sand Point Way NE, Seattle, WA 98115, Edward.D.Cokelet@noaa.gov

4. Stan Kotwicki, NOAA/AFSC/RACE, 7600 Sand Point Way NE, Seattle, WA 98115, Stan.Kotwicki@noaa.gov

5. Patrick Ressler, NOAA/AFSC/RACE,7600 Sand Point Way NE, Seattle, WA 98115, Patrick.Ressler@noaa.gov

6. Phyllis J. Stabeno, NOAA/PMEL,7600 Sand Point Way NE, Seattle, WA 98115, Phyllis.Stabeno@noaa.gov

7. Christopher D. Wilson,NOAA/AFSC/RACE, 7600 Sand Point Way NE, Seattle, WA 98115, Chris.Wilson@noaa.gov

8. Robert R. Lauth, NOAA/AFSC/RACE, 7600 Sand Point Way NE, Seattle, WA 98115, Bob.Lauth @noaa.gov

Collaborators, Post-docs or other associated contributors.

1. Matthew Baker, School of Fisheries and Aquatic Sciences, University of Washington, Seattle, WA 98195.

2. John K. Horne, School of Aquatic and Fishery Sciences, University of Washington, Box 355020, Seattle, WA 98195, USA

3. Joy N. Smith, School of Marine and Atmospheric Sciences, Stony Brook University, 239 Montauk Hwy, 5 Southampton, New York 11968

4. Joseph D. Warren, School of Marine and Atmospheric Sciences, Stony Brook University, 239 Montauk Hwy, Southampton, New York 11968

5. Mathieu Woillez, Alaska Fisheries Science Center, National Marine Fisheries Service, NOAA, 7600 Sand Point Way NE, Seattle, WA 98115, USA, and School of Aquatic and Fishery Sciences, University of Washington, Box 355020, Seattle, WA 98195, USA

Submitted October 30, 2013

Overall Project B62 Abstract

This report summarizes the scientific achievements of Project B62 and B91. This report serves to also be the final report for the in-kind project B91 (which is not formally required to have a stand-alone report).

State-of-the-art statistical methods were applied to estimate the functional responses of forage fish and commercial fish to changing climate. Analytical frameworks were developed to project these relationships forward under different climate change scenarios. Innovative new methods were introduced to collect oceanographic and biological data in the eastern Bering Sea. These new methods provided valuable new insights into the impacts of climate variability and change on the spatial distribution, abundance and species interactions in the region. The oceanographic observations provided new data on: water column properties (temperature and salinity), depth, chlorophyll a, oxygen, nitrate, and sea surface temperature. Water column profiles revealed a latitudinal gradient in the upper to lower density difference with stronger stratification north of 59° N. In spring, near surface chlorophyll a, oxygen and nutrient data exhibited relationships consistent with the classical Redfield ratios. Oceanographic conditions were cold throughout the study period which inhibited our ability to compare the strength of density gradients across the shelf in warm and cold years, however, we were able to show that the boundary of the well-mixed, inner shelf was not always located at the 50m isobath. The new data sets were utilized by the BEST-BSIERP modelers to groundtruth coupled biophysical models.

National Marine Fisheries Service standard surveys were augmented to provide new biological observations including: euphausiid vertical and spatial distribution, spatial and vertical distribution of walleye pollock combined from bottom trawl and acoustic surveys, and winter pollock spawing distributions. Retrospective studies showed strong evidence of niche partitioning amongst forage fish, and juvenile and adult groundfish. Depth alone was not sufficient to explain these distributions, light, bottom temperature, prey availability (euphausiids) and predator abundance were all selected as explanatory variables. Comparison of acoustic estimates of euphausiid and juvenile and adult pollock distributions showed evidence of top-down and bottom-up forcing but overall water temperature was a much stronger predictor of euphausiid biomass than pollock biomass (a proxy for predation pressure). The functional responses derived from retrospective studies served as a foundation for the formulation of coupled bio-physical models of the Bering Sea. The projection modeling framework provided a the first quantitative estimate of expected changes in sea surface temperature and wind under future climate change as well as the expected impact of these changes on the cross-shelf advection of northern rock

sole larvae and juveniles. This project contributed to 22 peer reviewed publications and 69 oral presentations at scientific conferences.

Citation

Hollowed, A. B., S. Barbeaux, C. Cokelet, S. Kotwicki, R. Lauth, P. Ressler, P. Stabeno, C. Wilson. 2013. Fish forage distribution and ocean conditions. NPRB BSIERP Project B62 Final Report, 416 p.

Key Words

Bering Sea, tmperature, Chlorophyll a, oxygen, salinity, mixed layer depth, nitrate, redfield ratio, walleye pollock, Pacific cod, northern rock sole, capelin, forage fish, euphausiids, stock projection models, general additive models, random forests, species interactions, niche partitioning, ecoregions, spawning distribution, spatial distribution, climate change, climate variability.

Table of Contents

Overall Project B62 Abstract 3
Citation 4
Key Words 4
Study Chronology 12
Introduction 12
Objectives 12
Chapter 1: Augmentation of Surveys 15
Chapter 1: Overview 15
Chapter 1.a: Underway Oceanographic Measurements on NOAAS Oscar Dyson 15
ABSTRACT 15
INTRODUCTION 15
METHODS 16
CONCLUSIONS 35
Chapter 1.b: Underway Oceanographic Measurements on F/V Aldebaran 36
ABSTRACT 36
INTRODUCTION 36
METHODS 36
RESULTS AND DISCUSSION 40
CONCLUSIONS 44
Chapter 1.c: Bottom Trawl Survey CTD Measurements 45
ABSTRACT 45
INTRODUCTION 45
METHODS 46
RESULTS AND DISCUSSION 50
CONCLUSIONS 66

ACKNOWLEDGEMENTS 67

Chapter 2: Distribution of Euphausiids and Walleye Pollock 68

Chapter 2: Overview 68

Chapter 2.a: Material properties of euphausiids 69

ABSTRACT 69

INTRODUCTION 69

METHODS 71

RESULTS 79

DISCUSSION 94

CONCLUSIONS 101

Chapter 2.b. Target Strength (TS) of euphausiids 103

ABSTRACT 104

INTRODUCTION 104

METHODS 108

RESULTS 114

DISCUSSION 125

ACKNOWLEDGEMENTS 129

Chapter 2.c. Abundance and distribution of euphausiids and walleye pollock, 2004-2010 130

ABSTRACT 130

INTRODUCTION 131

MATERIALS AND METHODS 132

RESULTS 146

DISCUSSION 155

CONCLUSIONS 158

ACKNOWLEDGEMENTS 159

Chapter 2.d. Analysis of the spatial relationship between euphausiids and walleye pollock, and implications for top-down vs. bottom up control of euphausiids 160

ABSTRACT 161

INTRODUCTION 162

MATERIALS AND METHODS 163

RESULTS 168

DISCUSSION 173

CONCLUSIONS 176

ACKNOWLEDGEMENTS 176

Chapter 2.e. Description and spatial distribution of other important acoustic classes 177

ABSTRACT 178

INTRODUCTION 179

MULTIFREQUENCY ACOUSTIC AND TRAWL DATA PROCESSING 179

CLASSIFICATION PROCEEDURE 180

RESULTS AND DISCUSSION 182

CONCLUSION 186

Chapter 2.f. Conclusions 187

Chapter 3: Groundfish Trends in the eastern Bering Sea shelf bottom trawl survey (formerly BSIERP – B91) 188

Chapter 3: Overview 188

Chapter 3.a. Latitudinal trends and temporal shifts in the catch composition of bottom trawls conducted on the eastern Bering Sea shelf. 189

ABSTRACT 189

INTRODUCTION 190

METHODS 192

RESULTS 195

DISCUSSION 201

CONCLUSIONS 207

ACKNOWLEDGEMENTS 208

Chapter 3.b. Detecting temporal trends and environmentally-driven changes in the spatial distribution of groundfishes and crabs on the eastern Bering Sea shelf. 209

INTRODUCTION 209

METHODS 209

RESULTS 211

DISCUSSION 215

CONCLUSIONS 218

Chapter 3.c. Combining bottom trawl and acoustic data to model acoustic dead zone correction and bottom trawl efficiency parameters for semi-pelagic species. 219

ABSTRACT 219

METHODS 219

RESULTS 223

DISCUSSION 224

CONCLUSIONS 227

Chapter 4: Forage fish distribution (age-0 pollock, age-1 pollock, and capelin) 229

Chapter 4.a. Effects of climate variations on pelagic ocean habitats and their role in structuring forage fish distributions in the Bering Sea. 229

ABSTRACT 229

INTRODUCTION 230

MATERIALS AND METHODS 231

RESULTS 238

DISCUSSION 261

ACKNOWLEDGEMENTS 265

Chapter 5: Defining eco-regions 266

Chapter 5.a. Analytical approach to deliniating ecological regions in marine systems 266

ABSTRACT 266

INTRODUCTION 267

METHODS 267

RESULTS 268

DISCUSSION 275

CONCLUSIONS 277

Chapter 5.b. Deliniating ecological regions in marine systems: synthesis of physical structure and community composition to inform spatial management. 278

ABSTRACT 278

METHODS 279

RESULTS 279

DISCUSSION 287

CONCLUSIONS 287

ACKNOWLEDGEMENTS 288

Chapter 6: Predicting eastern Bering Sea adult walleye pollock (*Gadus chalcogrammus*) winter distribution 292

ABSTRACT 292

INTRODUCTION 293

METHODS 295

RESULTS 298

DISCUSSION 320

Chapter 7: Opportunistic Data Collection as an Index of Local Depletion 325

Chapter 7: Overview 325

Chapter 8: A framework for modeling fish and shellfish responses to future climate change 326

Chapter 8: Overview 326

ABSTRACT 326

INTRODUCTION 327

METHODS 329

MANAGEMENT SCENARIOS 336

AN APPLICATION FOR NORTHERN ROCK SOLE 337

DISCUSSION 343

ACKNOWLEDGEMENTS 347

Chapter 9: Summary of key findings and outcomes 348

HYPOTHESIS 1. 348

HYPOTHESIS 2. 349

HYPOTHESIS 3 352

HYPOTHESIS 4 353

NEW SURVEY METHODS 353

Chapter 10: BEST-BSIERP Bering Sea Project Connections 355

Chapter 10.a. Principal Investigators Views on Integrated Research Projects 355

Chapter 10.b. Observations used by other BEST-BSIERP Bering Sea Project investigators 355

Chapter 10.c. Contributions to BEST-BSIERP Bering Sea Project Synthesis 356

Chapter 10.d. Management or Policy Implications and Contributions to inform decisions of the North Pacific Fishery Management Council 357

Chapter 10.e. Integration with BEST-BSIERP Bering Sea modeling projects 359

Chapter 10.f. Contributions to inform research and natural resource management in the Arctic. 359

Chapter 10.g. Oceanographic data shared with other components (Cokelet). 360

Chapter 11: Project Publications 362

Chapter 12: Posters and Oral Presentations at Scientific Conferences or Seminars 365

Chapter 12.a. Oral presentations 365

Chapter 12.b. Posters 372

Chapter 13: Outreach 375

TEACHERS AT SEA: 375

INTERNS: 375

THESES AND DISSERTATIONS: 375

OUTREACH PRESENTATIONS: 376

Chapter 14: Literature Citied 377

Study Chronology

This report documents the activities, analytical methods, results and findings of Project B62 of the Bering Sea Integrated Ecosystem Research Program. The project started in 2007 and ended in April 2013. This project was closely aligned with NPRB BSIERP projects B90 (surface trawl survey, Farley et al.), B59 (Surface trawl survey acoustics, Horne et al.), and B91 (Bottom trawl survey, Lauth et al.) and B61 (Functional foraging response, Aydin et al.). Results from project B91 are also included in this report. Relationships identified in this analysis were used to inform or parameterize the following models: FEAST (B70, Aydin et al.), Spatially Explicit Model of Pollock and Cod (B72, Haynie et al.) and Management Strategy Evaluation (B73, Punt et al.). A no cost extension was requested and granted to allow carry-over of unspent funds to enable two investigators to attend the BEST/BSIERP Open Science meeting that was held in Hawaii in February 2014. Progress reports were submitted biannually and can be found on the North Pacific Research Board website.

Introduction

Project B62 focused on the effect of ocean forcing on fish and euphausiids at different spatial and temporal scales.

Objectives

The objective of Project B62 was to understand the response of fish (including forage fish) and euphausiids to shifts in the characteristics of ocean habitat and use that understanding to model the impacts of climate change on their spatial and temporal distribution. Target species for this project included: walleye pollock, euphausiids, Pacific cod, arrowtooth flounder and capelin.

We simultaneously sampled ocean habitat conditions during acoustic mid-water trawl surveys and groundfish and shellfish bottom trawl surveys during summer and on commercial fishing vessels during summer and winter in order to understand the relation between pollock, euphausiids, Pacific cod, arrowtooth flounder and capelin distributions and ocean habitat. Products included time series, maps and data files for other BSIERP projects. Scientific discoveries helped to define the seasonal movement rules for fish in the Bering Sea ecosystem.

Specific hypotheses addressed by this project include:

H1. Climate-induced changes in physical forcing will modify the availability and partitioning of food for all trophic levels through bottom-up processes. Specifically:

b. Reduced frequency and intensity of summer storms will reduce surface mixing and increase sea surface temperature, thereby increasing stratification. A substantial decrease in summer winds will result in a mixed layer that is shallower than the euphotic zone, extensive subsurface primary production and depletion of nutrients in the entire water column. There will be no fall

phytoplankton bloom. A moderate decrease or no change in the intensity of summer storms will reduce replenishment of nutrients to the euphotic zone, lowering summer primary and secondary production. Both scenarios will reduce juvenile fish production by reducing their condition (energy density) and over-wintering capability.

H2. Climate and ocean conditions influencing water temperature, circulation patterns and domain boundaries impact fish reproduction, survival and distribution, the intensity of predator-prey relationships and the location of zoogeographic provinces through bottom-up processes. Specifically:

a. As heat content increases, the area suitable for spawning and foraging by subarctic species will expand northward and subarctic species will occupy areas formerly occupied by Arctic species.

b. Reduced cold pool extent will increase overlap of inner domain forage fish and outer domain piscivores.

c. Strength of frontal boundaries will weaken due to absence of the summer cold pool, allowing expansion of the inner domain and juvenile and forage fish habitat there. Weaker winds will enhance this effect.

e. Expected decreases in benthic productivity will negatively affect feeding and survival of small flatfish and crab thereby lowering population levels.

H3. Later spring phytoplankton blooms as a result of early ice retreat will increase zooplankton production, thereby resulting in increased abundances of piscivorous fish (pollock, cod and arrowtooth flounder) and a community controlled by top-down processes [Oscillating Control Hypothesis] with the possible trophic consequences:

a. Competition with abundant, piscivorous fish species for forage species will lead to a decline in murres, kittiwakes and fur seals.

c. In a top-down control community, fishing will reduce the degree of top-down control of forage species (including juvenile pollock) by adult pollock, cod and arrowtooth flounder. Owing to light exploitation rates, top-down control by arrowtooth flounder will increase, as will their level of competition with piscivorous fish, seabirds and marine mammals. As a result of these two processes, arrowtooth flounder will determine ultimate community composition, such that the climax community will be arrowtooth flounder-dominated (similar to the Gulf of Alaska).

H4. Climate and ocean conditions influencing circulation patterns and domain boundaries will affect the distribution, frequency and persistence of fronts and other prey-concentrating features and thus the foraging success of marine birds and mammals largely through bottom-up processes. Specifically:

a. Climate-ocean changes will displace predictably located, abundant prey (hot spots).

H5. Climate-ocean conditions will change and thus affect the abundance and distribution of commercial and subsistence fisheries. Specifically:

a. For commercial fishermen, these changes will lead to: 1) a change in home ports and distribution of fishing vessel rents, 2) vessels traveling further, incurring greater fuel costs and peril at sea and 3) greater burden on smaller vessels.

Chapter 1: Augmentation of Surveys

Chapter 1: Overview

This chapter, Augmentation of Surveys, consists of three parts that are presented below as Chapters (1a) Underway Oceanographic Measurements on NOAAS *Oscar Dyson*, (1b) Underway Oceanographic Measurements on F/V *Aldebaran*, and (1c) Bottom Trawl Survey CTD Measurements.

Chapter 1.a: Underway Oceanographic Measurements on NOAAS Oscar Dyson

ABSTRACT

Oceanographic instruments were added to NOAAS *Oscar Dyson* to make underway measurements at 2.5-m depth of water temperature, salinity, nitrate, chlorophyll and oxygen for all 17 Bering Sea cruises in 2008-2010. The system was designed and installed by PMEL EcoFOCI. Discrete samples were collected, analyzed in the laboratory, and used to calibrate the sensors. Maps of variables measured during the same three time periods each year (May, June-August and August-September) show the evolution of these ecosystem parameters on the southeastern Bering Sea shelf. A relationship has been found between nitrate, chlorophyll and oxygen that can be interpreted in terms of the Redfield ratio.

INTRODUCTION

One goal of the BSIERP Project B62, Fish Forage Distribution and Ocean Conditions, was to augment the annual Bering Sea Echo Trawl Integration Survey by adding underway oceanographic instruments to the NOAA fisheries research vessel *Oscar Dyson* to measure ocean habitat coincident with zooplankton and fish observations during the 2008-2010 surveys. We reconfigured the existing system that measured temperature, salinity and chlorophyll fluorescence and added instruments to measure parameters related to the standing stock and primary production of phytoplankton. We also extended the original goal and made these measurements during all 17 Bering Sea cruises in 2008-2010. This had the advantages of

providing much longer sensor-calibration periods with many more discrete measurements and longer time series results.

METHODS

Prior to the 2008 field season, Antonio Jenkins and David Strausz of NOAA/PMEL reconfigured the oceanographic instruments on NOAA ship *Oscar Dyson* and installed nitrate and oxygen sensors and three electronic flow meters. On 10 July 2008, they exchanged the ship's existing Turner Designs 10-AU field fluorometer for a WET Labs ECO fluorometer and rerouted some plumbing lines (Figure 1.1). Starting at the bow inlet at nominally 2.5-m depth, the system consisted of: plastic pipe, a Sea-Bird Electronics (SBE) SBE 38 digital oceanographic thermometer (http://www.seabird.com/products/spec_sheets/38data.htm) to measure water temperature at the water intake, a coarse strainer, a paddlewheel flow meter, a pump and a spare that could be switched, a inverted-U-pipe with air vent to remove air bubbles, two switchable 50-micron filters, a State University of New York MSRC VDB-1 3-inch vortex debubbler to remove air bubbles from the water before it reached the instruments, and three Cole-Parmer pilot-scale electromagnetic flow meters (http://www.coleparmer.com/Product/Pilot_scale_magnetic_flowmeter_115_VAC_60Hz_rated_for_0_8_8_0_gpm_3_0_30_lpm/C-33109-04 or http://www.omega.com/pptst/FMG201_202_203.html) to measure the water flow rates to the thermosalinograph (TSG), nitrate sensor and fluorometer/optode instrument loops. There was also a tap for withdrawing discrete water samples. The TSG loop had an SBE 45 MicroTSG thermosalinograph (http://www.seabird.com/products/spec_sheets/45data.htm) to measure salinity. The nitrate sensor loop had a 1-micron filter followed by a Satlantic MBARI-ISUS V3 nitrate sensor (http://www.satlantic.com/isus) to measure the dissolved nitrate concentration. The chlorophyll-fluorometer/optode loop had a Turner Designs 10-AU field fluorometer (http://www.turnerdesigns.com/products/laboratory/10au-field-fluorometer) until 10 July 2008 and a WET Labs ECO FLNTUS fluorometer (http://www.wetlabs.com/products/eflcombo/fl.htm) with turbidity sensor and bio-wiper after that. The Turner Designs 10-AU fluorometer was transferred to the shore laboratory for analysis of discrete calibration chlorophyll samples. This flow loop also had an Aanderaa Optode 3835 oxygen sensor (http://www.aanderaa.com/productsdetail.php?Oxygen-Optodes-2) to measure the dissolved oxygen concentration. The flow rates were monitored and the filters cleaned whenever the flows dropped too low. The fluorometer, optode and nitrate sensor were cleaned approximately weekly with cotton-tipped swabs, the latter with oxalic acid solution. Data were recorded

on the ship's NOAA SCS (Scientific Computer System) at intervals of 1 second to 6 minutes depending upon the instrument.

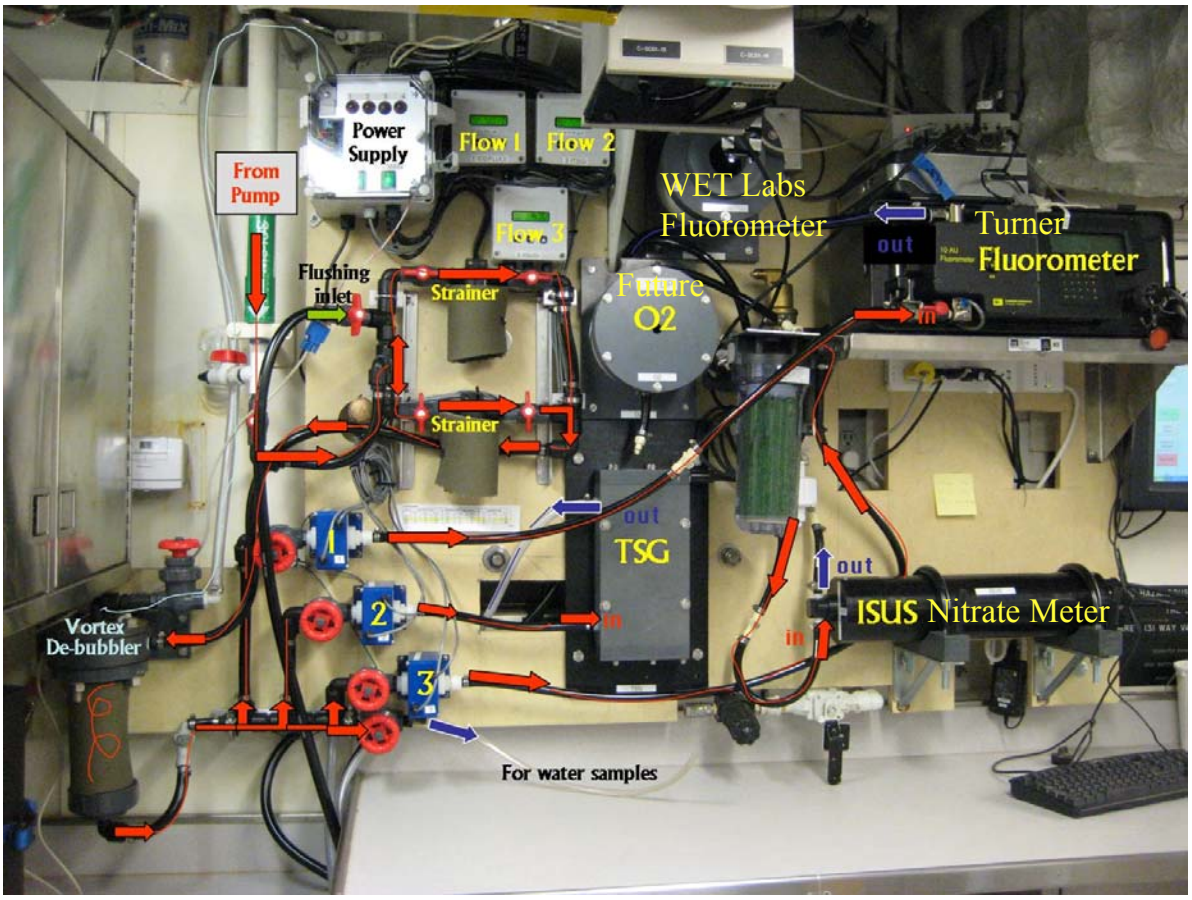

Figure 1.1. The underway seawater sampling system aboard NOAA ship *Oscar Dyson*. Arrows show the seawater flow direction. In this photo the Turner fluorometer was in use, and the WET Labs fluorometer and Aanderaa oxygen sensor were not fully installed.

Dyson's digital position (latitude and longitude), attitude (pitch, roll and heave), speed and course over ground, short- and long-wave solar radiation, wind speed and direction, air temperature and humidity, barometric pressure, underway system flow rates, seawater intake temperature, salinity, nitrate concentration, chlorophyll fluorescence, turbidity, and oxygen concentration were recorded at various rates up to 1 Hz and stored in individual sensor files. Data from each instrument were edited to remove spurious data spikes and extreme values outside ad-hoc thresholds. Also the flow rates through the instrument loops were monitored for low-flow incidents, and those data values flagged as bad. The edited

data were linearly interpolated onto a common equispaced time axis with 1-minute increments. The nitrate sensor operated at a slower rate. For the first cruise, DY0802, the nitrate concentration was recorded at 6-minute intervals, and for subsequent cruises it was recorded at 2-minute intervals. These measurements were linearly interpolated onto a common equispaced time axis with 2-minute increments.

Ship-provided sensors that measured position, attitude, speed and course over ground, short- and long-wave solar radiation, wind speed and direction, air temperature and humidity, and barometric pressure were maintained and calibrated by NOAA's Marine Operations Center-Pacific according to their own schedule. The ship's heading was measured by a gyrocompass and an Applanix POS MV attitude determination system that also measured pitch, roll and heave. The oceanographic thermometer at the water intake was accurate to 0.001°C with a drift within 0.002°C per year according to the manufacturer; therefore a theoretical accuracy of 0.003°C would be predicted. Its output was compared to other sources of seawater temperature (3 hull sensors and the thermosalinograph temperature) to exclude large, spurious deviations. The field accuracy for temperature was probably about 0.01°C. The measured temperature within the thermosalinograph, used to compute salinity, exceeded the seawater intake temperature because the former was mounted in a heated laboratory space. Discrete salinity, nitrate, chlorophyll and oxygen samples were collected on a daily schedule (salinity 1/d, nitrate 1/d, chlorophyll 2/d, oxygen 1/d with occasional replicate samples) and preserved (in stoppered 200-ml Kimax borosilicate bottles for salinity; in acid-cleaned 40 ml HDPE Boston Round sample bottles for nitrate and frozen at -80 C; collected in 60-ml plastic sample bottles, filtered through 0.7 micron glass fiber filters and frozen at -80 C for chlorophyll; or collected in 300-ml BOD bottles and 'pickled' with manganous sulphate and alkaline iodide solutions for oxygen) for later analysis in the laboratory aboard ship or in Seattle. Salinity samples were analyzed with a Guildline Autosal laboratory salinometer with laboratory accuracy better than 0.0001 psu. Nitrate samples were analyzed using a modified method of Armstrong, Stearns and Strickland (1967) with a typical laboratory accuracy of 0.5 μg/L. Chlorophyll samples were analyzed via the acidification method (Lorenzen, 1966) using a Turner Designs AU-10 fluorometer with a typical laboratory accuracy of 10-20%. Oxygen samples were analyzed via the Winkler method (Strickland and Parsons, 1968) with a typical laboratory accuracy of 1 μmole/L.

For each instrument with corresponding discrete samples, the instrument and discrete time series were differenced, and the difference trend was assumed to be from instrument drift. The instrument time series was detrended and calibrated against the discrete samples with a linear least-squares fit. Figure 1.2 shows the fits for salinity for which the correlation coefficients, r^2, exceeded 0.99. The blue-dashed line of slope 1 through the origin represents an exact fit, the green solid line represents the actual fit, and any outliers

not included in the fit are designated by red squares. Clearly the TSG made accurate salinity measurements. For nitrate, chlorophyll and oxygen, the 2008 time series were independently calibrated

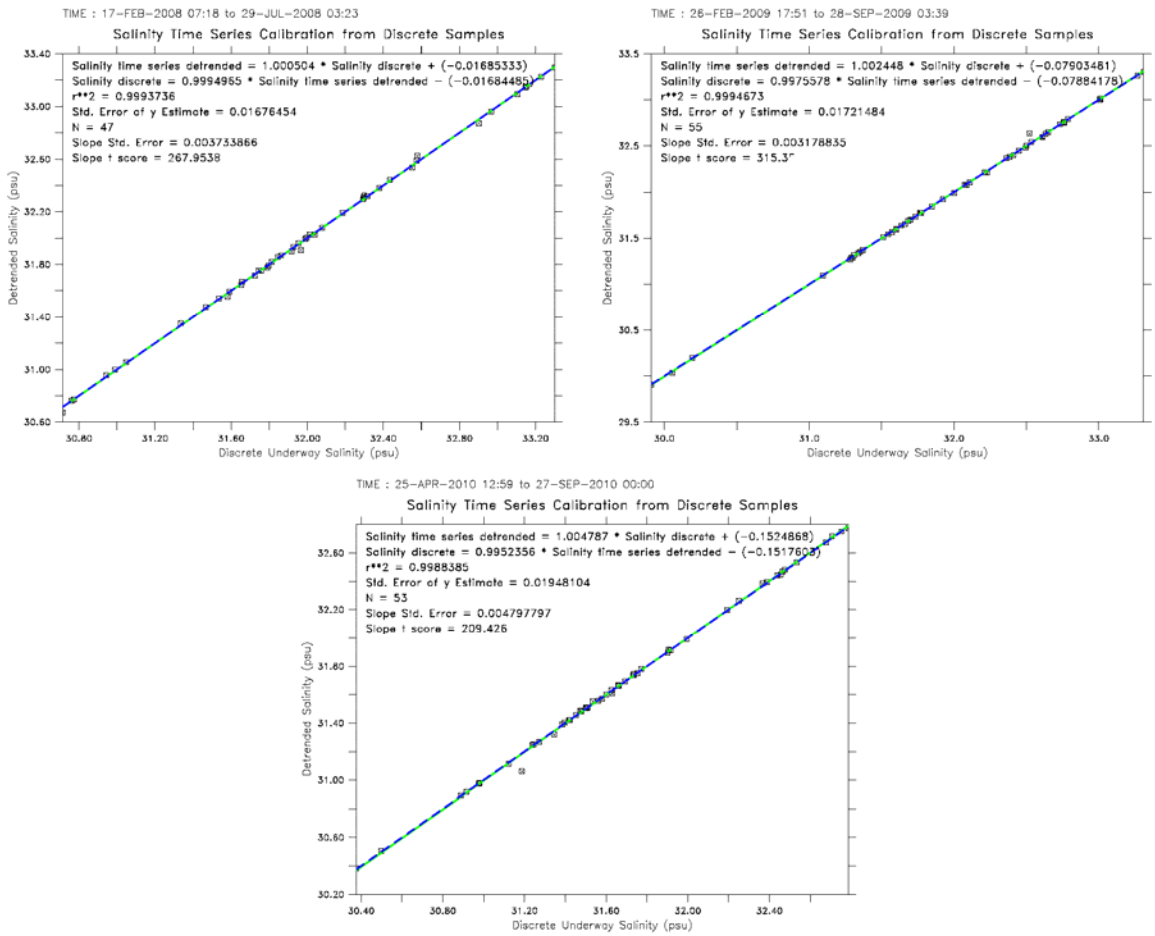

Figure 1.2. Salinity calibration fit with discrete sample values on the abscissa and detrended underway instrument values on the ordinate. The blue-dashed line represents an exact fit, and the green solid line is the linear least-squares fit.

before and after 10 July 2008 when the system plumbing was modified and some instruments swapped out. Figure 1.3 shows the calibration fits for nitrate with r^2 varying between 0.88 and 0.99 with standard error estimates of 0.6-1.6 micromolar. Such good fits and relatively small error estimates show the value of the ISUS for measuring dissolved nitrate continuously. However regular comparisons against discrete samples are very important because the instrumental reading can drift over time. For some years, large ISUS nitrate trends were removed prior to the fits shown here. The largest trend was in 2008 when the ISUS nitrate drifted downward by about 2 micromolar per month. In contrast, in 2009 it drifted upward at about 0.2 micromolar per month. Figure 1.4 shows the fits for chlorophyll for which the data

indicated that the 2010 field season calibrations should also be split into two parts. The chlorophyll fits are less precise than for the other variables with r^2 of 0.30-0.72 perhaps due to species variations and light

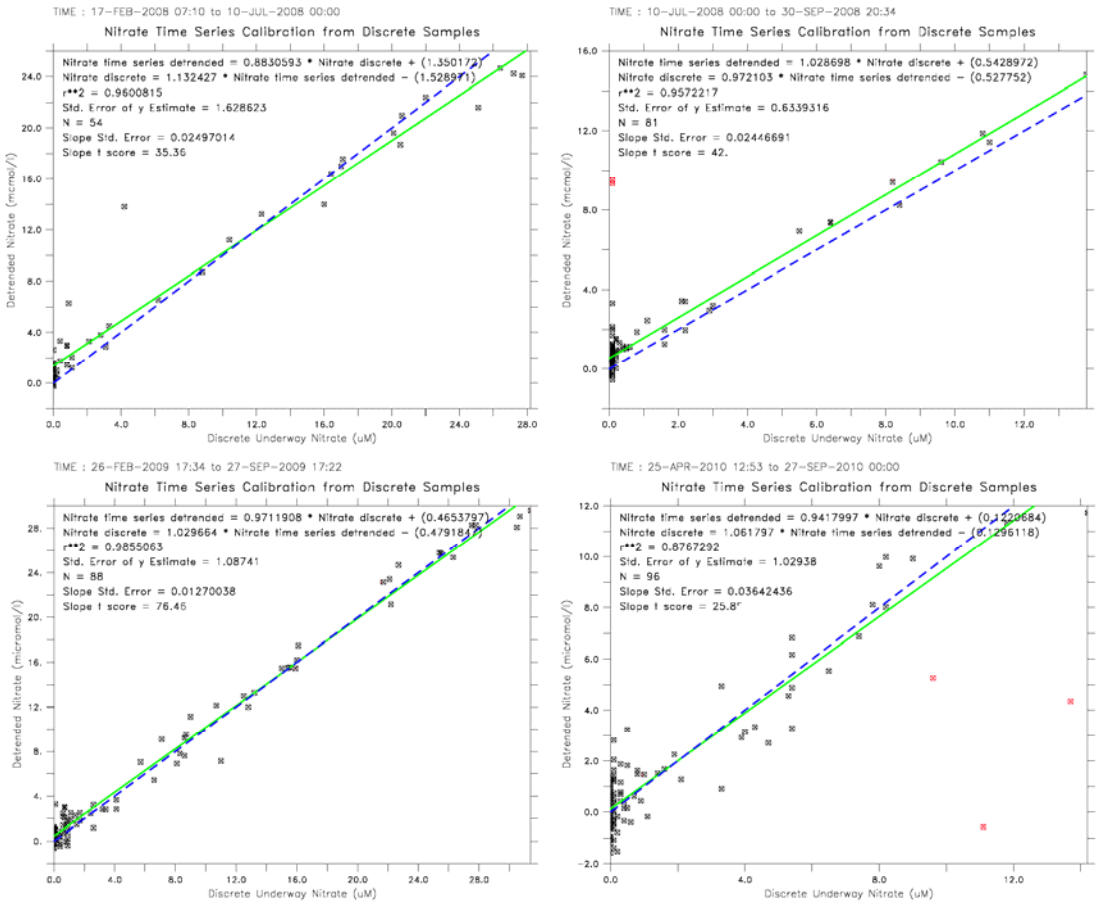

Figure 1.3. Nitrate calibration fits with discrete sample values on the abscissa and detrended underway instrument values on the ordinate. The blue-dashed line represents an exact fit, and the green solid line is the linear least-squares fit. Outliers excluded from the fit are shown as red squares.

adaptation. The oxygen calibrations are shown in Figure 1.5 with r^2 varying between 0.72 and 0.98. These are good fits, and the continuously measuring oxygen sensor represents a great instrumental advance over the routine measurement of oxygen concentrations via discrete water samples that must be preserved with chemicals and titrated in the laboratory.

No attempt was made to force the best-fit calibration curves through their origins; therefore some of the calibrated nitrate and chlorophyll time series take on slightly negative, non-physical values. That can be taken as another measure of their accuracy.

These time series data and supporting metadata with plots are available on the BSIERP Data Archive (http://www.eol.ucar.edu/projects/bsierp/) in NetCDF (Network Common Data Form, http://www.unidata.ucar.edu/software/netcdf/) format.

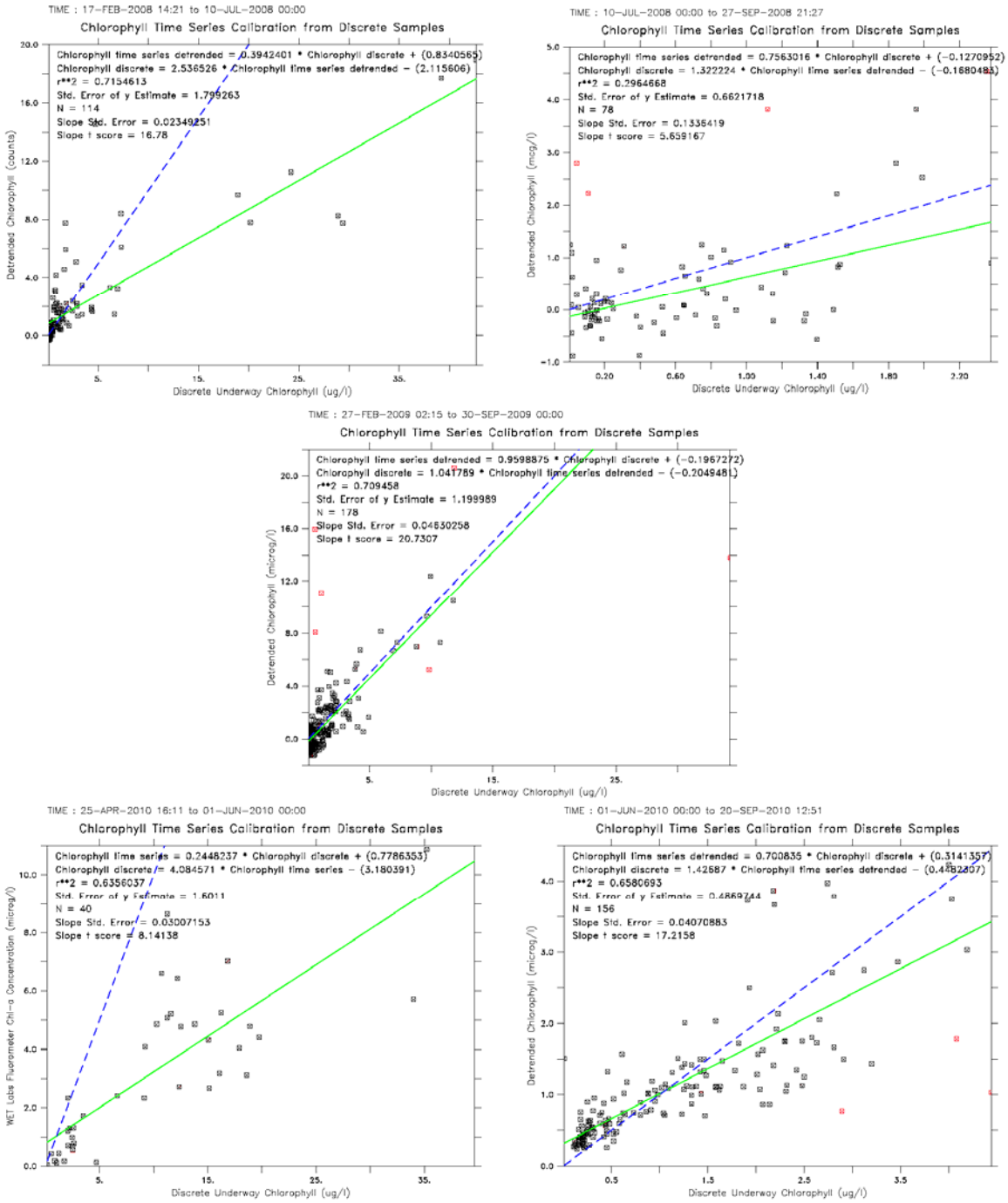

Figure 1.4. Chlorophyll-a calibration fits with discrete sample values on the abscissa and detrended underway instrument values on the ordinate. The blue-dashed line represents an exact fit, and the green solid line is the linear least-squares fit. Outliers excluded from the fit are shown as red squares.

208

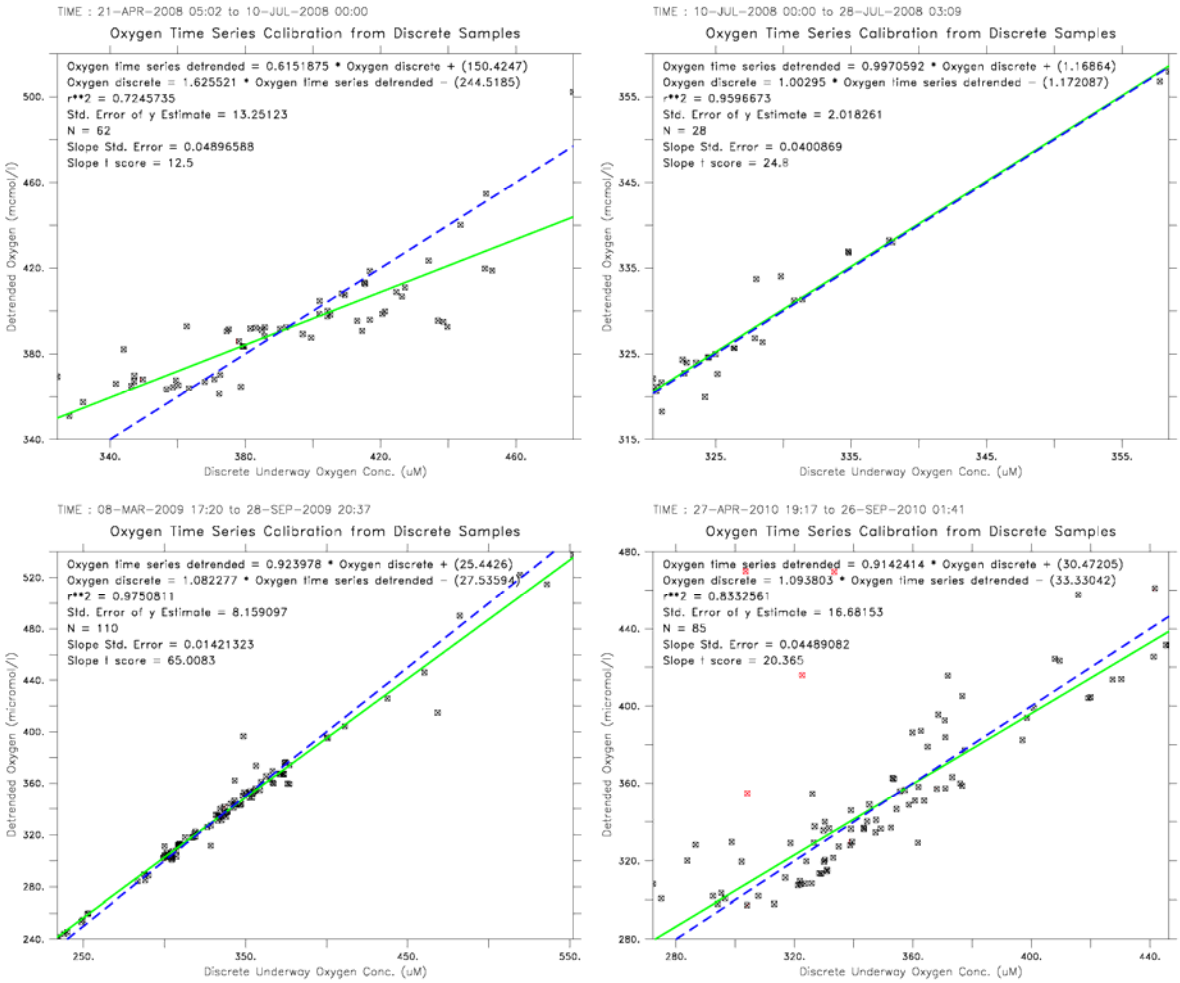

Figure 1.5. Oxygen calibration fits with discrete sample values on the abscissa and detrended underway instrument values on the ordinate. The blue-dashed line represents an exact fit, and the green solid line is the linear least-squares fit. Outliers excluded from the fit are shown as red squares.

RESULTS AND DISCUSSION

Table 1.1 shows the 17 Bering Sea cruises on NOAAS *Oscar Dyson* in 2008-2010 for which we made underway oceanographic measurements. These included midwater echo integration trawl surveys operated by the AFSC/RACE Midwater Assessment and Conservation Engineering Program (MACE), ice seal surveys by the National Marine Mammal Laboratory, EcoFOCI mooring deployment cruises by PMEL/OERD, ichthyoplankton surveys by AFSC/RACE EcoFOCI, and salmon surveys by the

AFSC/RACE Bering-Aleutian Salmon International Survey (BASIS). The surveys spanned February through September 2008 and 2009, and April through September 2010. This large data set contains 30 variables occupying 112 megabytes of binary data in NetCDF format. To manage the difficult task of displaying the data, we have chosen to map, along the ship's track, five oceanographic variables (water temperature, salinity, nitrate concentration, chlorophyll concentration and dissolved oxygen saturation) that relate directly to primary production. Each along-track cell is the average over 4 time steps of the final processed data, i.e. 8 minutes for nitrate and 4 minutes for all other variables. Table 1.1 shows that each year, three cruises – the spring ichthyoplankton, echo integration trawl and BASIS surveys – were repeated on approximately the same dates, thus providing a sequence for comparison.

Table 1.1 Underway oceanographic measurements made aboard NOAAS *Oscar Dyson*

Cruise	Cruise Type	Start Date	End Date
DY0802	Echo Integration Trawl Survey	17-Feb-2008	1-Mar-2008
DY0804	Ice Seals	20-Apr-2008	1-May-2008
DY0806	EcoFOCI Moorings	4-May-2008	11-May-2008
DY0807	Spring Ichthyoplankton Survey	12-May-2008	22-May-2008
DY0809	Echo Integration Trawl Survey	2-Jun-2008	1-Aug-2008
DY0811	BASIS	10-Sep-2008	1-Oct-2008
DY0902	Winter Ichthyoplankton Survey	26-Feb-2009	4-Mar-2009
DY0903	Echo Integration Trawl Survey	7-Mar-2009	16-Mar-2009
DY0906	EcoFOCI Moorings	24-Apr-2009	5-May-2009
DY0907	Spring Ichthyoplankton Survey	8-May-2009	21-May-2009
DY0909	Echo Integration Trawl Survey	9-Jun-2009	8-Aug-2009
DY0910	Right Whale	12-Aug-2009	29-Aug-2009
DY0911	BASIS	2-Sep-2009	29-Sep-2009
DY1003	EcoFOCI Moorings	24-Apr-2010	3-May-2010
DY1004	Spring Ichthyoplankton Survey	6-May-2010	19-May-2010
DY1006	Echo Integration Trawl Survey	5-Jun-2010	8-Aug-2010
DY1007	BASIS	17-Aug-2010	27-Sep-2010

The data set consisting of 31 variables occupies 112 megabytes of binary data in NetCDF format. The time series data and supporting metadata with plots are available on the BSIERP Data Archive (Cokelet, 2013d, e, f).

Water temperature and salinity describe the basic physical state of the ecosystem. Figure 1.6 shows the temperature along the cruise tracks. Each row represents a year, 2008-2010. Each column represents one of the three repeated cruises. The temperature varied between -1.72°C, near the freezing point of seawater owing to recent contact with sea ice, to 12.40°C due to summer warming. These diagrams are scans of the Bering Sea shelf, lasting up to two months, and not instantaneous snapshots. As the ship moved north from its point of debarkation in Dutch Harbor, the ocean surface warmed as summer advanced. Therefore, the northward increase in temperature shown on the map, say during an echo integration cruise, is influenced by the progression of solar heating during the warm summer months and does not represent the state of the ocean at the same instant. In fact, the shelf is generally cooler in the north at a given time. It is meaningful to compare temperatures between different years at fixed geographical locations because the cruises were run in much the same pattern each year. For instance, Figure 1.6 shows that the ocean was warmer at the far northwestern edge of the echo integration survey in 2010 than in other years.

Figure 1.7 shows maps of the near-surface salinity that varied between 27.58 and 33.46 psu. Generally the salinity is greatest at the shelf break at 200-m depth and decreases landward owing to dilution by river inflow and to less-salty Alaska Coastal Current water that enters the Bering through Unimak Pass and hugs the Alaska Peninsula and coast. The lowest salinity measured was in 2008 near St. Matthew Island at about 60°N, probably owing to thick ice that rafted against the island and melted slowly leaving a fresher upper layer.

Nitrate is an essential nutrient for phytoplankton growth and primary production at the base of the food chain. Our ISUS nitrate meter with repeated discrete calibration samples gave accurate, continuous time series measurements (Figure 1.3). Figure 1.8 shows the nitrate concentrations that varied between 0 and 30+ µmole/L. (Non-physical negative values are considered zero for this discussion.) Nitrate was available at 10-20 µmole/L at the SW corner of the study area in the basin and over Bering Canyon at all times of the year. It was also available on the southern shelf near the Alaska Peninsula, especially in May 2009, and at some locations on the mid-shelf during the echo integration survey in July 2009. The latter

coincided with somewhat higher salinities in that region (Figure 1.7) indicating that saltier, nutrient-rich water probably extended onto the middle shelf in summer 2009.

The chlorophyll-a concentration is a measure of the standing stock of phytoplankton, the ocean's primary producers. It varied from trace amounts to over 80 µg/L (Figure 1.9). High values were measured near the shelf break where nutrients from the basin were available and in inflow water through Unimak Pass. Concentrations were vanishingly small in the later months where nitrate was depleted (Figure 1.8).

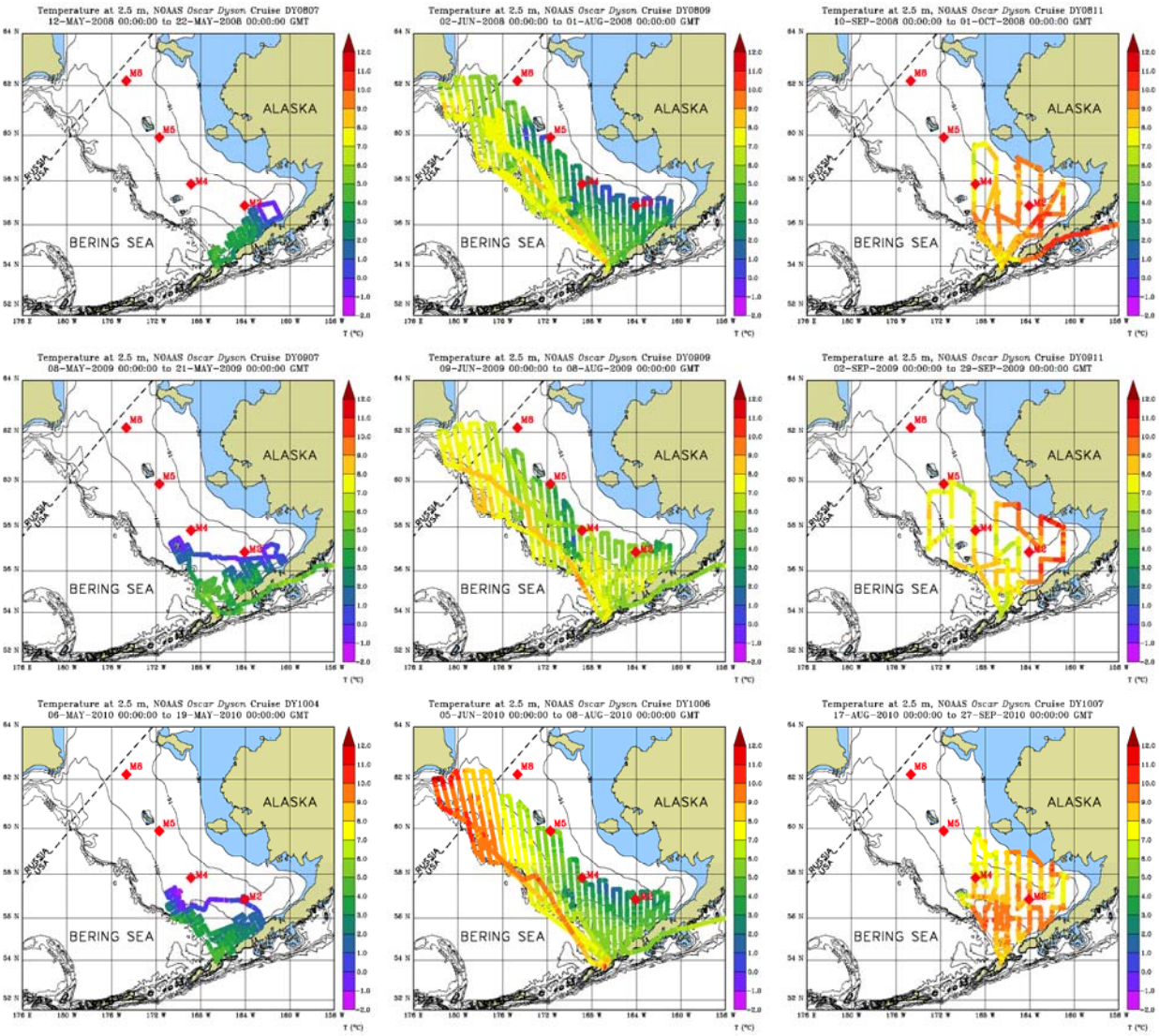

Figure 1.6. Temperature (°C) at 2.5 m in the Bering Sea measured by NOAAS *Oscar Dyson* during the spring ichthyoplankton (May), echo integration trawl (June-August) and BASIS surveys (August-September) in 2008-2010. Water depths are contoured at 30, 50, 100, 200, 500, 1000 and 2000 m. Red diamonds show the locations of PMEL EcoFOCI moorings M2, M4, M5 and M8.

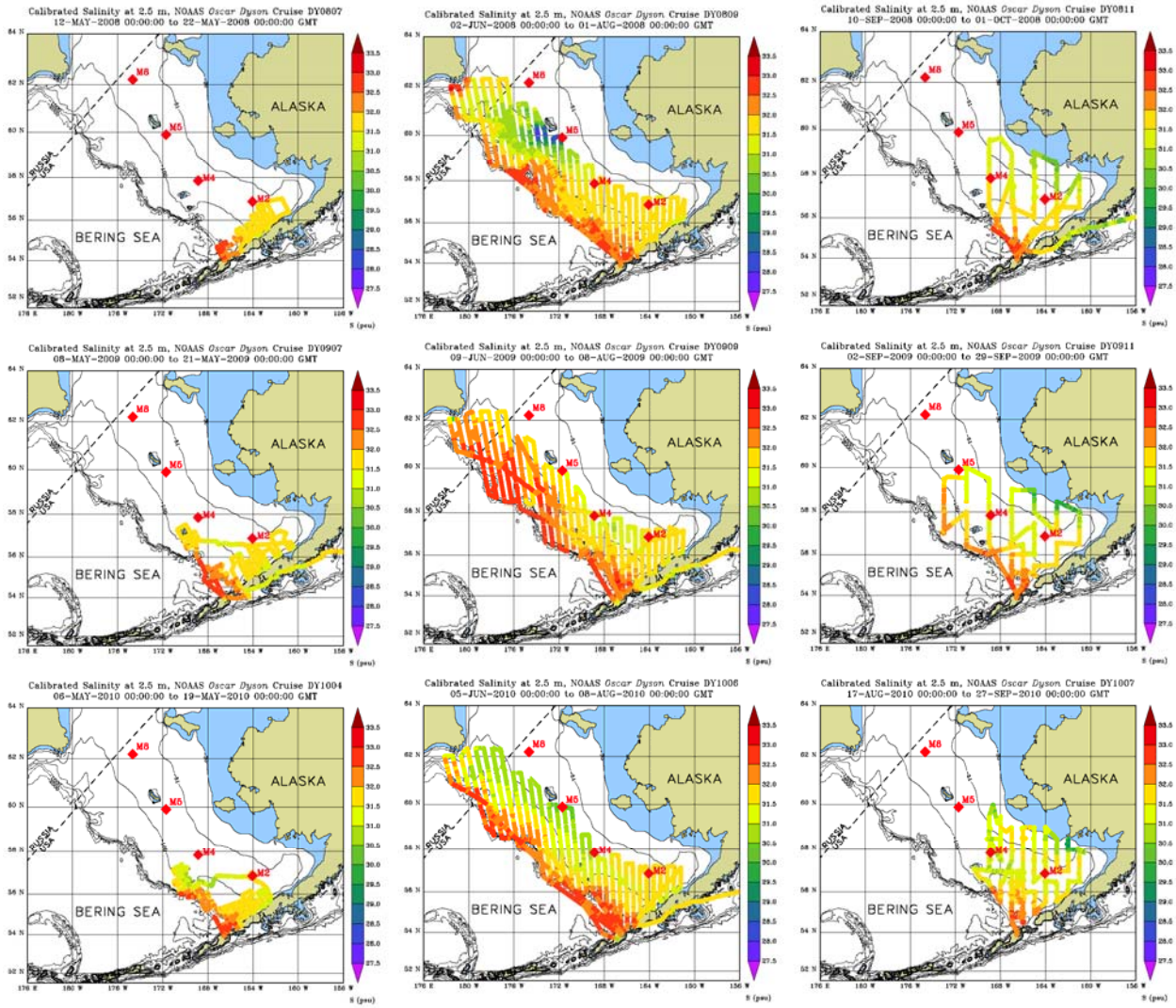

Figure 1.7. Salinity (psu) at 2.5 m in the Bering Sea measured by NOAAS *Oscar Dyson* during the spring ichthyoplankton (May), echo integration trawl (June-August) and BASIS surveys (August-September) in 2008-2010. Water depths are contoured at 30, 50, 100, 200, 500, 1000 and 2000 m. Red diamonds show the locations of PMEL EcoFOCI moorings M2, M4, M5 and M8.

Figure 1.10 shows maps of the oxygen saturation. Oxygen is produced by phytoplankton photosynthesis; therefore oxygen saturation values are high (over 180%) where chlorophyll is high (Figure 1.9). Saturation rarely dropped below 80% because the underway measurements were made in the near-surface water at 2.5 m where exchange with the atmosphere is active.

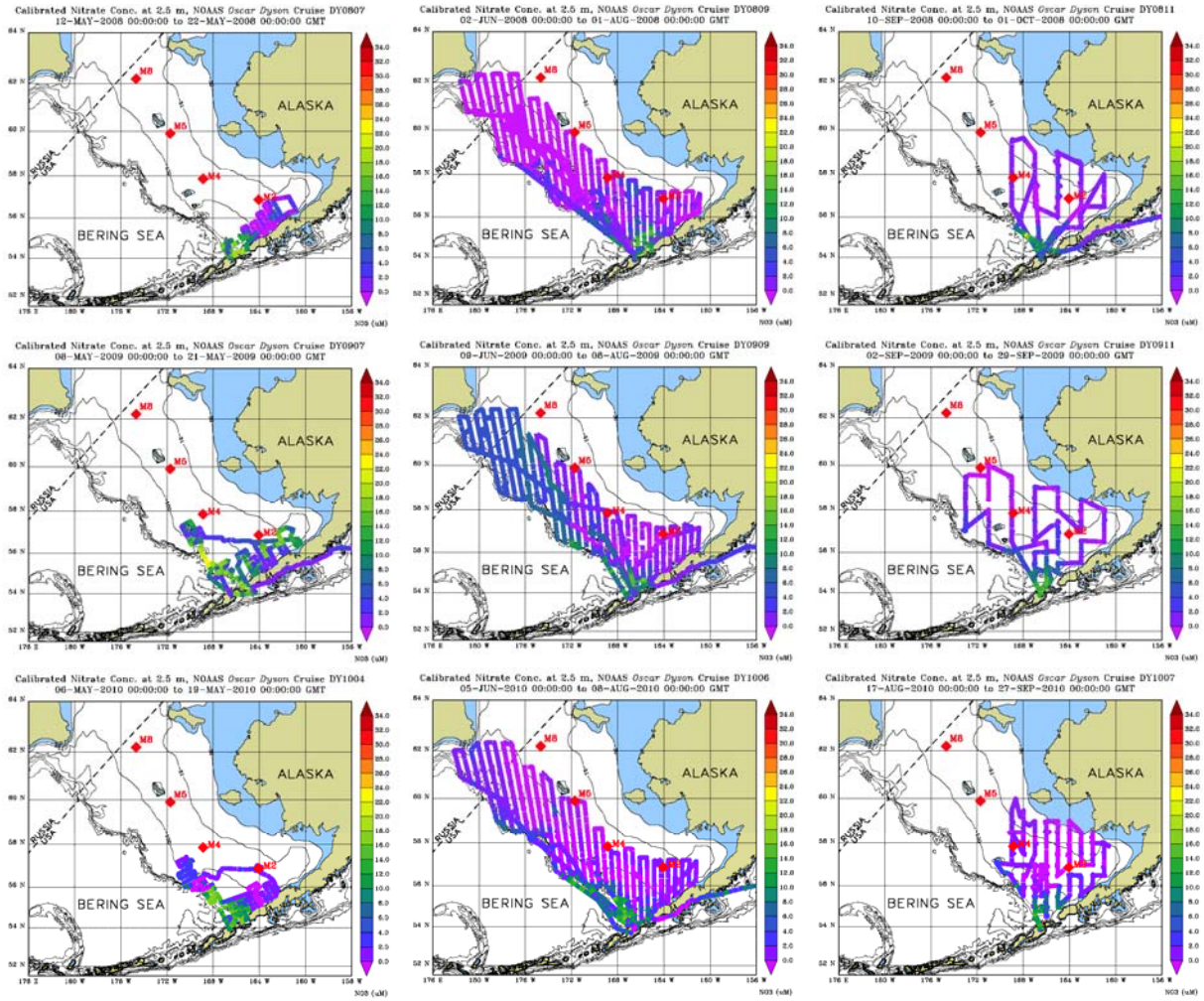

Figure 1.8. Nitrate concentration (µmole/L) at 2.5 m in the Bering Sea measured by NOAAS *Oscar Dyson* during the spring ichthyoplankton (May), echo integration trawl (June-August) and BASIS surveys (August-September) in 2008-2010. Water depths are contoured at 30, 50, 100, 200, 500, 1000 and 2000 m. Red diamonds show the locations of PMEL EcoFOCI moorings M2, M4, M5 and M8.

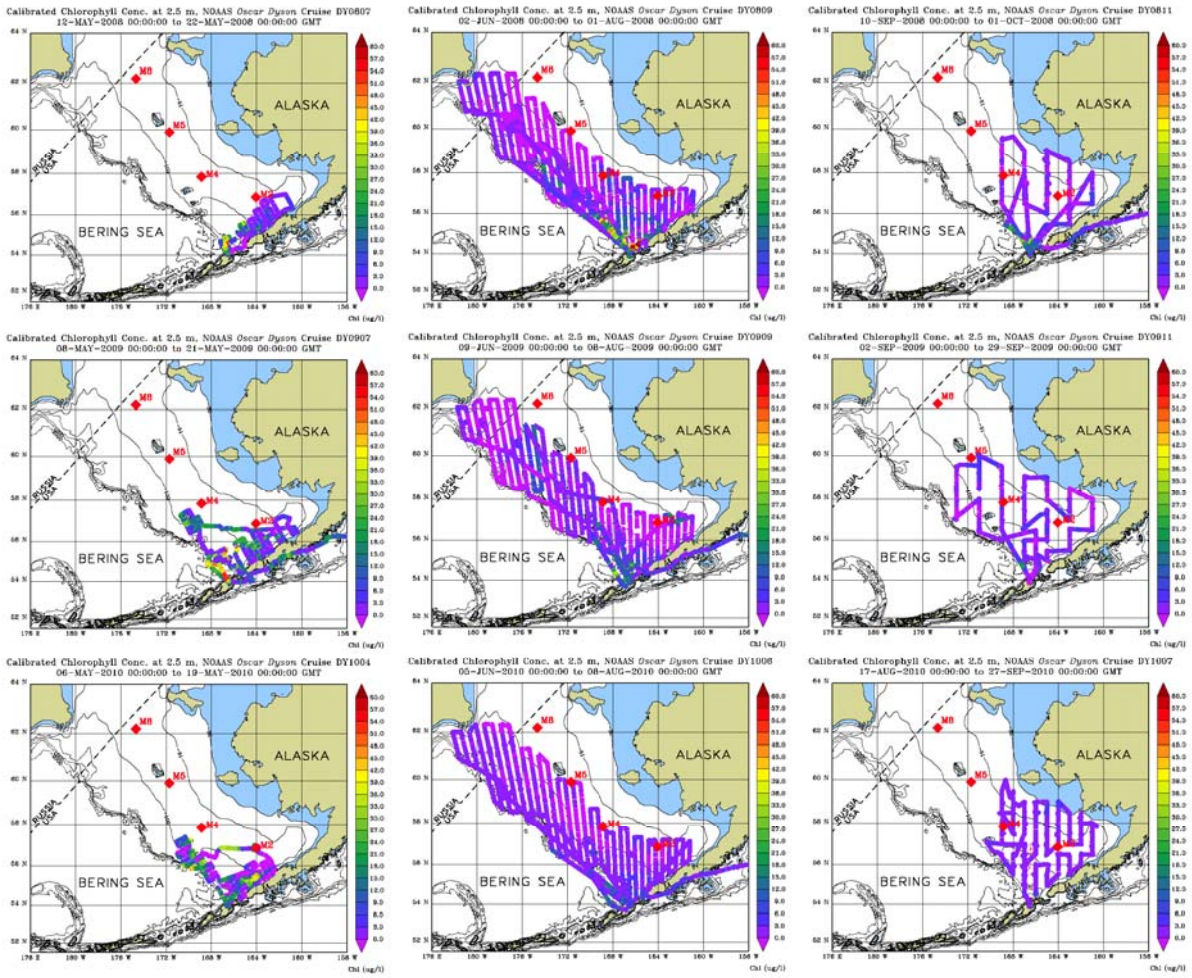

Figure 1.9. Chlorophyll-a concentration (µg/L) at 2.5 m in the Bering Sea measured by NOAAS *Oscar Dyson* during the spring ichthyoplankton (May), echo integration trawl (June-August) and BASIS surveys (August-September) in 2008-2010. Water depths are contoured at 30, 50, 100, 200, 500, 1000 and 2000 m. Red diamonds show the locations of PMEL EcoFOCI moorings M2, M4, M5 and M8.

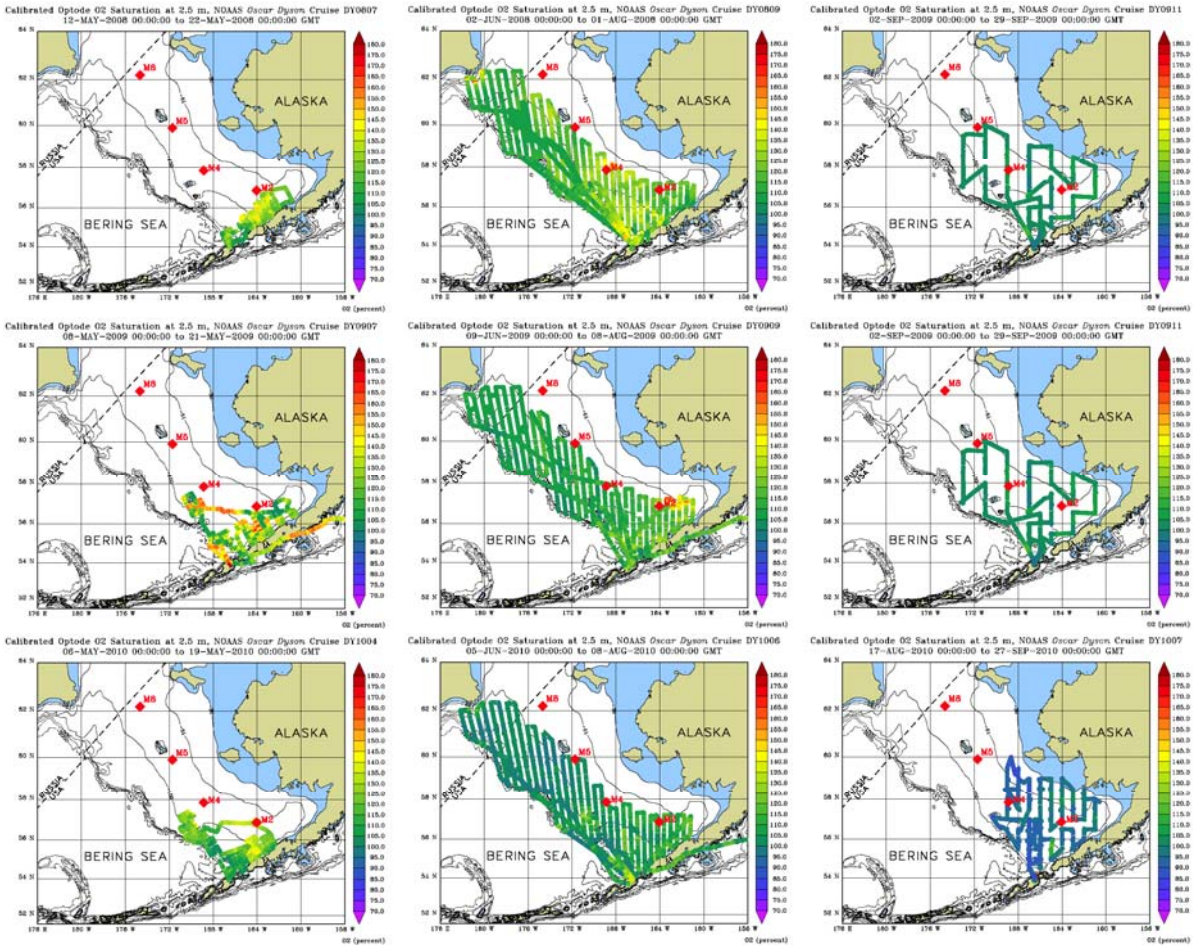

Figure 1.10. Dissolved oxygen saturation (%) at 2.5 m in the Bering Sea measured by NOAAS *Oscar Dyson* during the spring ichthyoplankton (May), echo integration trawl (June-August) and BASIS surveys (August-September) in 2008-2010. Water depths are contoured at 30, 50, 100, 200, 500, 1000 and 2000 m. Red diamonds show the locations of PMEL EcoFOCI moorings M2, M4, M5 and M8.

The underway measurements reveal relationships between nitrate, chlorophyll and oxygen that are related to primary production. From the classical work of Redfield (1934), plankton, on average, contain carbon, nitrogen and phosphorous in the molar ratios C:N:P = 106:16:1. Therefore during photosynthesis, for each mole of phosphate taken up, 16 moles of nitrate and 106 moles of carbon dioxide are utilized. Oxygen is both consumed and liberated during photosynthesis, but its stoichiometry is not known as precisely. Research indicates that about 150 moles of oxygen are released for every 16 moles of nitrate utilized so that $-O_2$:N = −150:16 where the minus sign indicates net oxygen production during

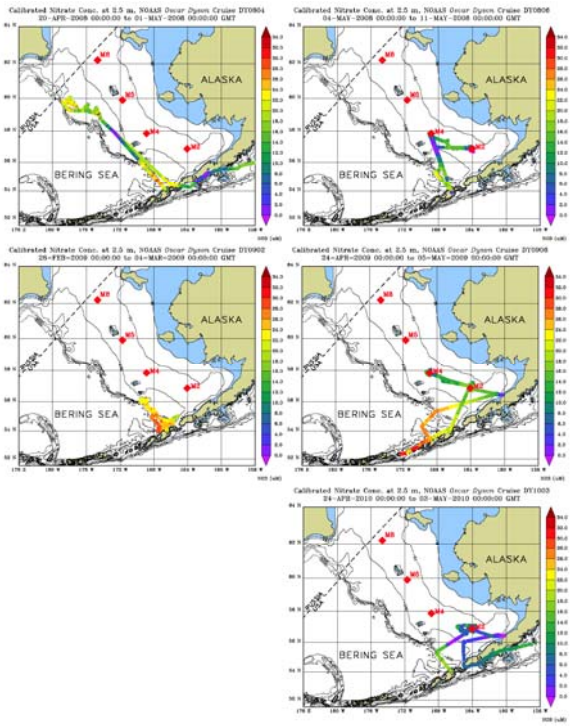

Figure 1.11. Nitrate concentration (µmole/L) at 2.5 m in the Bering Sea measured by NOAAS *Oscar Dyson*, during early spring cruises, 2008-2010. Water depths are contoured at 30, 50, 100, 200, 500, 1000 and 2000 m. Red diamonds show the locations of PMEL EcoFOCI moorings M2, M4, M5 and M8.

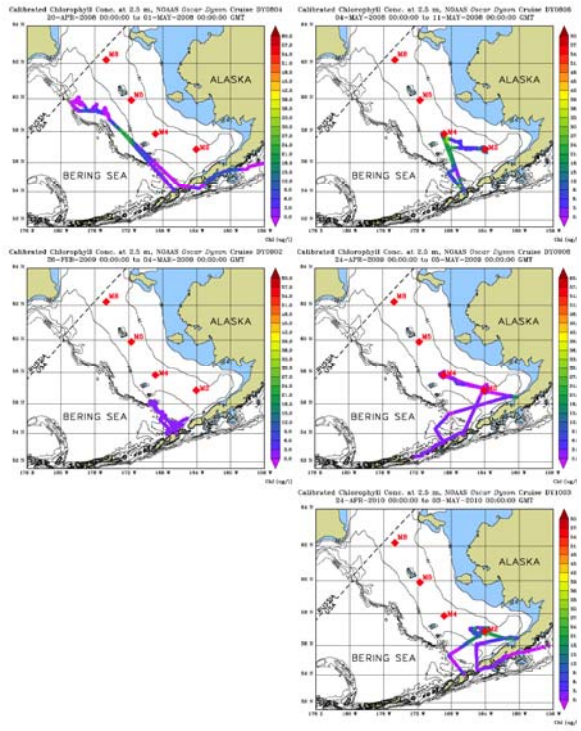

Figure 1.12. Chlorophyll-a concentration (µg/L) at 2.5 m in the Bering Sea measured by NOAAS *Oscar Dyson*, during early spring cruises, 2008-2010. Water depths are contoured at 30, 50, 100, 200, 500, 1000 and 2000 m. Red diamonds show the locations of PMEL EcoFOCI moorings M2, M4, M5 and M8.

positive nutrient consumption (Anderson, 1995; Hedges et al., 2002; Redfield et al., 1963; Richards, 1965). If the same basic process of photosynthesis is occurring throughout the study region, will measurements of nitrate, chlorophyll and oxygen reflect the Redfield ratios even though made at varying locations in water pumped from just 2.5 m below the sea surface on a ship underway in the stormy Bering Sea? Consider measurements confined to the Bering Sea shelf and Bering Canyon during March-May of 2008-2010 – the spring growing seasons. Figures 1.11-1.13 show the nitrate, chlorophyll and oxygen concentrations for additional cruises in this time span, but not discussed previously. As before, there is a general sense that regions of high nitrate correspond to low chlorophyll and oxygen, and vice versa. We computed the hourly median concentrations to obtain independent, low-noise samples. Figure 1.14a shows there is indeed a negative relationship between oxygen and nitrate. The fitted linear least squares solid line with $r^2 = 0.52$ has a slope of −4.64 with a greater than 99% chance that it differs from zero

(standard error 0.122, 1360 degrees of freedom, student's-t score of 38.1). For comparison, a Redfield-ratio curve of slope, −O2:N = −150/16 = −9.38, is shown by a dashed line. Its intercept was chosen at the highest projected oxygen concentration, and the fact that the Redfield curve serves as an upper bound to the measurements shows there is a relationship. The fitted oxygen-to-nitrate ratio is less than the Redfield ratio because the seawater cannot retain the liberated oxygen in solution. Most of it has or will outgas to the atmosphere because the water is supersaturated (denoted by the red dots in Figure 1.14a) and not undersaturated (denoted by blue dots), especially at the lowest nitrate concentrations where the Redfield ratio predicts more oxygen will have been produced. The relationship of carbon to nitrate can be determined based upon a typical carbon-to-chlorophyll mass ratio of 60 as approximated for phytoplankton in the Gulf of Alaska (Booth et al., 1988; Frost, 1993) and converted to its molar equivalent at 12 g carbon per mole. Figure 1.14b shows a weak negative correlation between inferred carbon and nitrogen with a linear-least-squares fit line whose slope of -2.58 is non-zero with over 99% confidence. Some of the scatter is due to the quality of the chlorophyll calibrations (Figure 1.4), and some is due to assuming a constant carbon-to-chlorophyll ratio. The dashed Redfield-ratio line, drawn to pass through the highest nitrogen measurements, has a

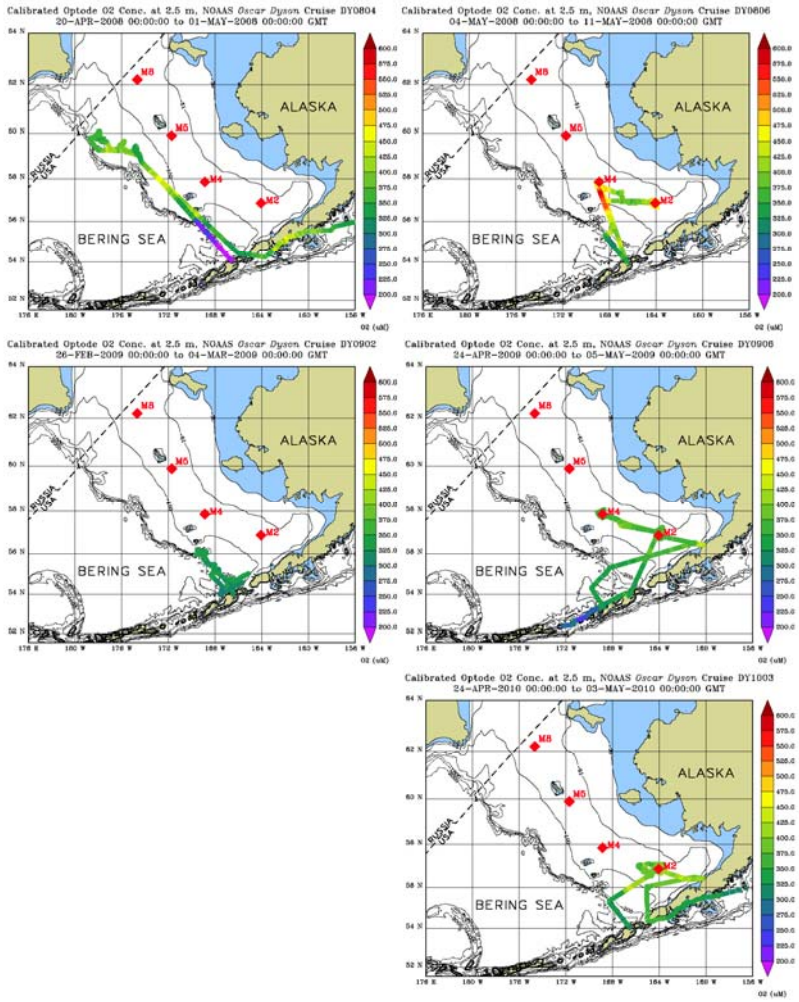

Figure 1.13. Dissolved oxygen concentration (µmole/L) at 2.5 m in the Bering Sea measured by NOAAS *Oscar Dyson*, during early spring cruises, 2008-2010. Water depths are contoured at 30, 50, 100, 200, 500, 1000 and 2000 m. Red diamonds show the locations of PMEL EcoFOCI moorings M2, M4, M5 and M8.

steeper slope of -6.63 and bounds almost all the observations. Why doesn't the best-fit curve have the Redfield-ratio slope? One reason is that the *Dyson* measurements were made at a constant depth of 2.5 m, but the upper mixed layer is considerably deeper. Being a dissolved constituent, nitrate would have a nearly uniform distribution in the mixed layer, but phytoplankton cells sink toward the pycnocline. Therefore at 2.5 m there will be a deficit of phytoplankton carbon compared to nitrate, lessening the steepness of the best-fit line. Another reason is that the ship moves across regions of different initial nitrate concentrations at the outset of the spring bloom. Therefore the bloom begins at different nitrate levels and follows different nitrogen-carbon trajectories leading to scatter in Figure 1.14b and diminishing the steepness of the best-fit curve of the amalgamated points. To demonstrate this, consider a simplified, hypothetical scenario illustrated by the red line in Figure 1.14b. Suppose the spring bloom at a fixed location 2.5 m below the sea surface begins at 15-µmole/L nitrate concentration with no chlorophyll in the water column. As it progresses along the N-C trajectory at the Redfield-ratio slope of 106:16, it consumes nitrate until it reaches 12 µmole/L when it receives an injection of 4 µmole /L owing to a wind-mixing event. The bloom continues at the Redfield-ratio slope but with increased nitrate. When it reaches 5 µmole /L nitrate and 92 µmole /L carbon, 80 µmole /L of phytoplankton carbon sink below the 2.5 m depth horizon. Then the bloom continues to 36 µmole /L carbon when the nitrate is exhausted. The total trajectory will have an average slope shallower than the Redfield ratio. Trajectories like this, combined over hundreds of km of ocean, will lead to a C:N distribution similar to Figure 1.14b.

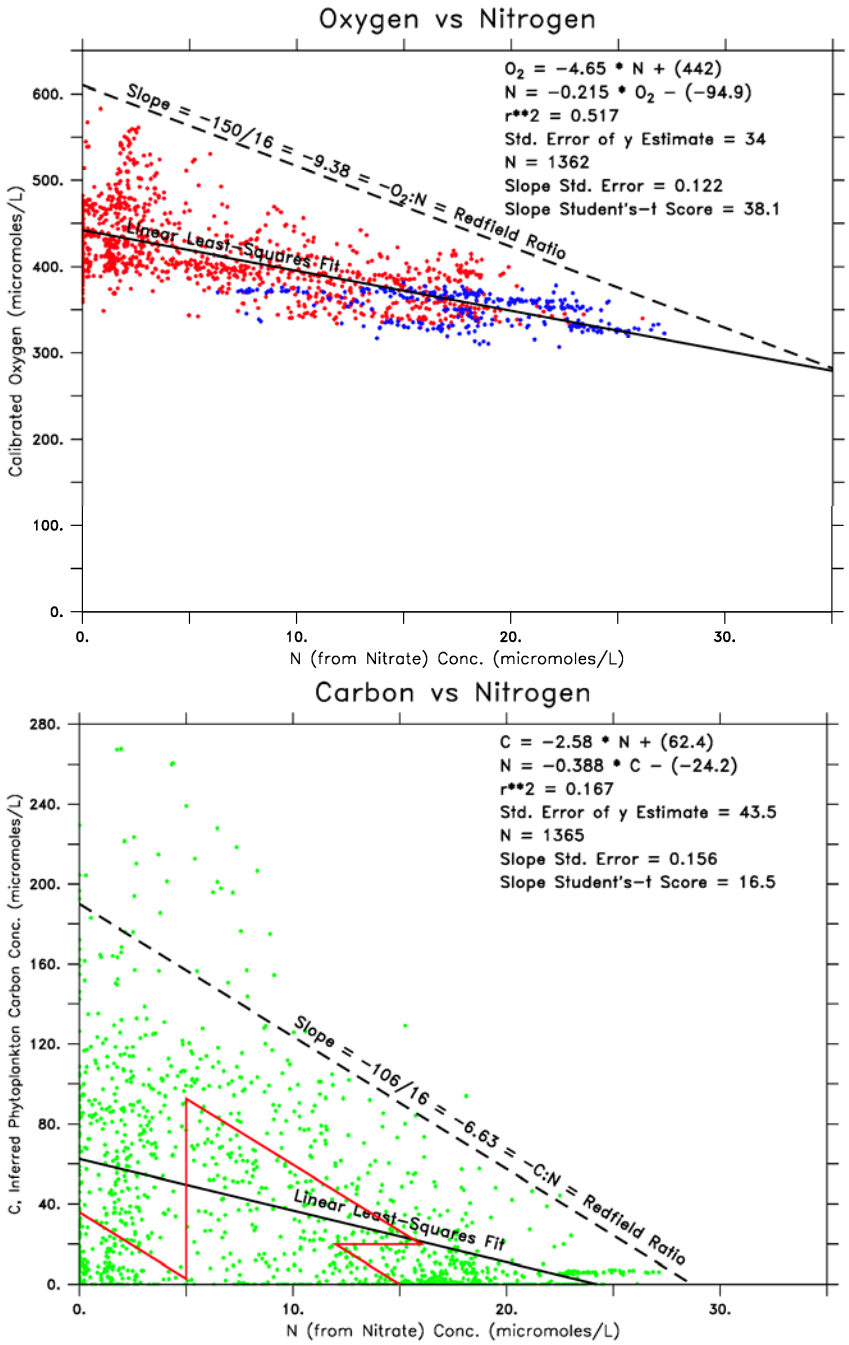

Figure 1.14. (a) Underway oxygen and (b) carbon versus nitrogen concentrations (µmole /L) for the spring 2008-2010 *Oscar Dyson* cruises over the Bering Sea shelf and Bering Canyon. Black solid lines represent least-squares-linear fits, and dashed lines are at Redfield-ratio slopes. Red dots in (a) denote supersaturated and blue dots under saturated concentrations. The red line in (b) represents a hypothetical phytoplankton growth-sinking scenario.

CONCLUSIONS

We augmented the underway oceanographic measurement system on NOAAS *Oscar Dyson* by reconfiguring the system and adding meters to measure the flow through the instruments, a vortex debubbler to remove air bubbles, an ISUS nitrate sensor, and an oxygen sensor. Although our original charge was to make these measurements during the three echo integration surveys in 2008-2010, we expanded that to measure during all 17 *Dyson* cruises in the Bering Sea in 2008-2010. Electronic measurements of salinity, nitrate, chlorophyll and oxygen were calibrated against discrete samples analyzed in the laboratory. The optode oxygen sensor was a new instrument, and it provided valuable measurements, once calibrated. The underway observations at 2.5 m depth of ocean temperature, salinity, nitrate, chlorophyll and oxygen over three years provide a unique and comprehensive data set that shows how these ecosystem variables change with season and year. We have shown that near-surface measurements from a moving ship in rough seas can reveal relationships between nitrate, oxygen and phytoplankton carbon that can be understood in terms of the classical Redfield ratio during the spring bloom when nitrate is depleted, and oxygen and chlorophyll increase owing to primary production. At the time of writing this report, the results from the augmented underway oceanographic system on NOAAS *Oscar Dyson* are being analyzed. They have not yet been incorporated into a scientific publication. However we did leverage the expertise gained from working with *Dyson* to calibrate and analyze underway measurements from USCG *Healy*, R/V *Knorr* and R/V *Thomas G. Thompson* during five BEST cruises in 2008-2010. Underway solar radiation and chlorophyll-a measurements from *Healy* and *Knorr* were used in a vertically generalized productivity model (VGPM) to estimate net primary production on the Bering Sea shelf (Lomas et al., 2012). Likewise, underway measurements of temperature, salinity, nitrate and chlorophyll-a were employed to estimate the air-sea CO_2 flux, net community production rate and phytoplankton population abundance as *Thompson* crossed the Gulf of Alaska in 2010 on its way to a BEST Bering Sea cruise (Palevsky et al., 2013).

Chapter 1.b: Underway Oceanographic Measurements on F/V Aldebaran

ABSTRACT

Oceanographic instruments were added to F/V *Aldebaran* to make underway measurements at 3-m depth of water temperature, salinity and chlorophyll during the Pollock A Season and the summer bottom trawl survey in 2008-2010. The system was designed and installed by PMEL EcoFOCI. Discrete samples were collected, analyzed in the laboratory, and used to calibrate the sensors. Maps of variables measured during January-March and June-August show the evolution of these ecosystem parameters on the southeastern Bering Sea shelf. The summer bottom trawl survey measurements of temperature and salinity were used to check the calibration of CTDs that were added to the bottom trawl survey nets.

INTRODUCTION

A second goal of BSIERP Project B62 was to add underway oceanographic instruments to the F/V *Aldebaran*, a 125-foot Bering Sea pollock trawler. Each summer *Aldebaran* was employed as a survey vessel under contract to NOAA for the eastern Bering Sea continental shelf bottom trawl survey of groundfish and invertebrate resources. Ocean habitat measurements of water temperature, salinity and chlorophyll complemented the fisheries survey. As a bonus, the measurements continued while *Aldebaran* fished commercially during the harsh winter (January-March) Pollock A Season, a time when observations are scarce.

METHODS

In December 2007, David Strausz and Antonio Jenkins of NOAA/PMEL designed, built and installed an oceanographic instrument system on *Aldebaran*. The instruments were plumbed using copper-nickel pipe by shipyard workers at Trident Seafoods, the ship's owner, in Seattle. The underway seawater sampling system consisted of: 3/4-inch copper-nickel piping from the ship's sea chest in the engine room drawing water from about 3-m depth to the instruments; a Sea-Bird Electronics (SBE) SBE 38 digital

oceanographic thermometer (http://www.seabird.com/products/spec_sheets/38data.htm) to measure water temperature at the water intake; a Perko 493 seawater intake 1-inch strainer to remove large particles; a Hydracell MO3 positive displacement pump with 1/4 hp Baldor motor and variable speed controller pumping water at 0.5 gal/min; a State University of New York MSRC VDB-1 2-inch vortex debubbler to remove air bubbles from the water before it reached the instruments; a Cole-Parmer pilot-scale electromagnetic flow meter (http://www.coleparmer.com/Product/Pilot_scale_magnetic_flowmeter_115_VAC_60Hz_rated_for_0_8_8_0_gpm_3_0_30_lpm/C-33109-04 or http://www.omega.com/pptst/FMG201_202_203.html) to measure the flow; an SBE 45 MicroTSG thermosalinograph (http://www.seabird.com/products/spec_sheets/45data.htm) to measure salinity; a WETLabs ECO fluorometer with bio-wiper (http://www.wetlabs.com/products/eflcombo/fl.htm) to measure chlorophyll fluorescence; a GPS receiver to measure the ship's position; and a Windows computer running NOAA's SCS (Scientific Computer System) to record the observations at intervals of 1 second to 1 minute dependent upon the instrument. Discrete salinity and chlorophyll samples were taken daily by a NOAA Fisheries Observer during the Pollock A Season or by a NOAA fisheries scientist during the summer bottom trawl survey. Salinity samples were preserved in stoppered 200-ml Kimax borosilicate bottles. Chlorophyll samples were collected in 60-ml plastic sample bottles, filtered through 0.7 micron glass fiber filters and frozen in the ship's food freezer. Samples were transported to Seattle for later laboratory analysis. Salinity samples were analyzed with a Guildline Autosal laboratory salinometer with laboratory accuracy better than 0.0001 psu. Chlorophyll samples were analyzed via the acidification method (Lorenzen, 1966) using a Turner Designs AU-10 fluorometer with a typical laboratory accuracy of 10-20%.

Digital position, flow rate, temperature, salinity and chlorophyll fluorescence observations recorded were linearly interpolated onto a common time axis with 1-minute increments. Data were determined to be invalid if values fell outside threshold ranges, most commonly because the flow rate was too low or the intake and thermosalinograph temperature difference was too large, both conditions indicating restricted flow. The threshold values were based on common sense and experience gained from working with the data. The oceanographic thermometer at the water intake was accurate to 0.001°C with a drift within 0.002°C per year according to the manufacturer; therefore a theoretical accuracy of 0.003°C would be predicted. The field accuracy for temperature was probably about 0.01°C. Chlorophyll fluorescence was scaled to chlorophyll concentration based upon the fluorometer manufacturer's specifications. Values from this time series were extracted at the times of the discrete chlorophyll samples that had been analyzed in the laboratory.

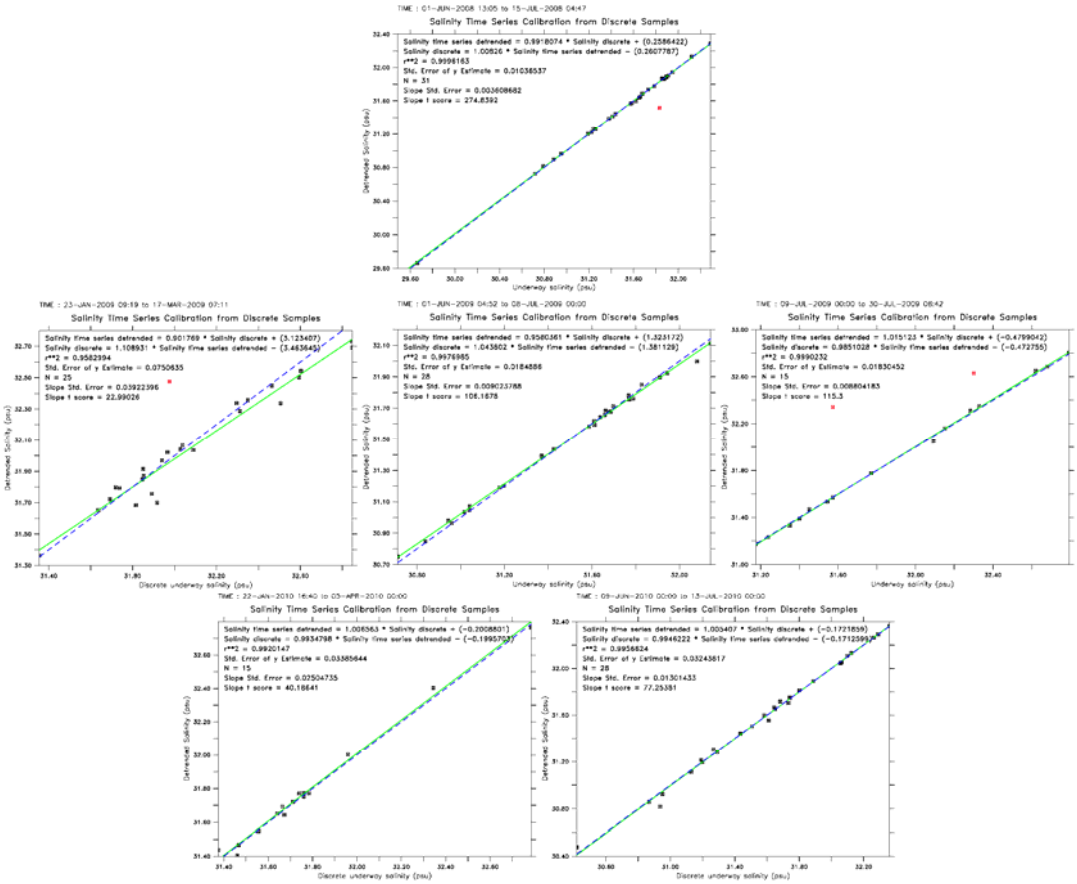

Figure 1.15. Salinity calibration fit with discrete sample values on the abscissa and detrended underway instrument values on the ordinate. The blue-dashed line represents an exact fit, and the green solid line is the linear least-squares fit. Outliers excluded from the fit are shown as red squares.

The thermosalinograph salinity and discrete-sample time series were differenced, and the difference trend was assumed to be from instrument drift. The instrument time series were detrended and calibrated against the discrete samples with linear least-squares fits. Figure 1.15 shows the fits for salinity which the data indicated should be split into various time segments for best fits. The salinity calibrations were very accurate with correlation coefficients, r^2, exceeding 0.95 and standard errors less than 0.08 psu.

Figure 1.16 shows the fits for chlorophyll-a for which no detrending was done. The chlorophyll fits are less precise than for the other variables with r^2 of 0.36-0.78 perhaps due to species variations and light adaptation.

During the Pollock A Season, sea ice covered much of the Bering Sea shelf. Daily ice edge locations were obtained from the National Ice Center Daily Ice Analysis Products webpage as ASCII files (http://www.natice.noaa.gov/products/daily_products.html).

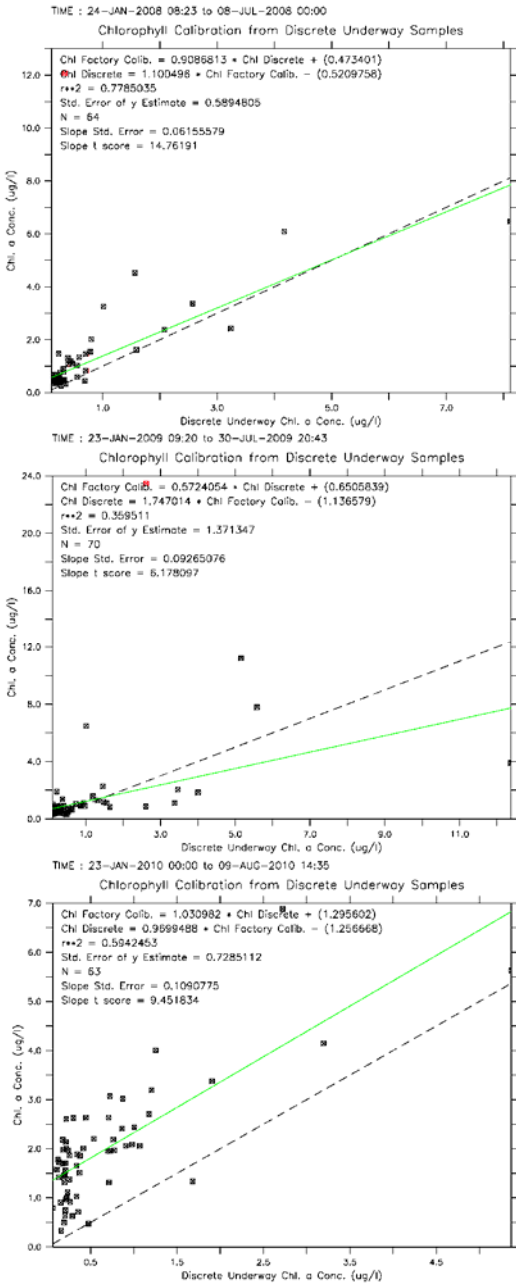

Figure 1.16 Chlorophyll-a calibration fits with discrete sample values on the abscissa and underway instrument values on the ordinate. The blue-dashed line represents an exact fit, and the green solid line is the linear least-squares fit. Outliers excluded from the fit are shown as red squares.

RESULTS AND DISCUSSION

Table 1.2 shows the six Bering Sea cruises on F/V *Aldebaran* in 2008-2010 for which we made underway oceanographic measurements. The underway system worked well during all but one of the cruises, the 2008 bottom trawl survey cruise for which it stopped logging data at about the half-way point. The data

Table 1.2 Underway oceanographic measurements made aboard F/V *Aldebaran*

Cruise Type	Start Date	End Date
Pollock A Season	19-Jan-2008	12-Mar-2008
Bottom Trawl Survey	3-Jun-2008	8-Jul-2008
Pollock A Season	19-Jan-2009	19-Mar-2009
Bottom Trawl Survey	29-May-2009	1-Aug-2009
Pollock A Season	17-Jan-2010	6-Apr-2010
Bottom Trawl Survey	5-Jun-2010	12-Aug-2010

set consisting of five variables (latitude, longitude, water temperature, calibrated salinity and calibrated chlorophyll-a concentration) occupies 23 megabytes of binary data in NetCDF format. The time series data and supporting metadata with plots are available on the BSIERP Data Archive (Cokelet, 2012a, b, c)). We map water temperature, salinity and chlorophyll-a concentration along the ship's track with each along-track cell representing a 6-minute average.

Figure 1.17 shows the temperature along the *Aldebaran*'s cruise tracks. Temperatures varied from −1.33°C near the freezing point to 10.81°C in summer. The Pollock A Season and bottom trawl surveys occupied approximately the same time spans each year thus providing some basis for year-to-year comparisons. But as pointed out earlier, these diagrams are scans of the Bering Sea shelf that last over periods of two months or longer during which time the region as a whole may have cooled or warmed. A warming example can be seen in the 2010 bottom trawl survey plot. After the ship finished its usual survey, it transited from near Nunivak Island into Bristol Bay, south and east of Cape Newenham, to sample that area in more detail. The water was warmer on the second visit. The Pollock A Season cruise tracks were governed by optimizing fish catch while at the same time remaining outside the sea ice field. The progressive ice edge is shown in Figure 1.17 as a sequence of date-stamped, color-coded lines plotted

every 8 days. The color-code sequence is black, red, green, blue, cyan and magenta. The ice edge usually advanced southward during the Pollock A Season, reached a maximum extent and then retreated somewhat. The fishing vessel usually fished along the Alaska Peninsula in the early season, and then switched to northwestward trips to near the ice edge.

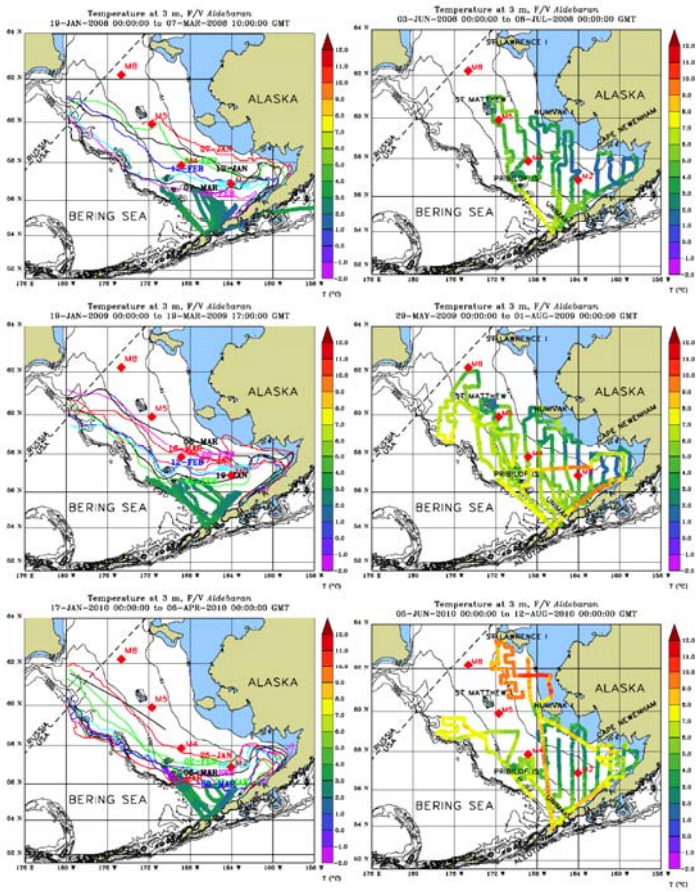

Figure 1.17. Temperature (°C) at 3 m in the Bering Sea measured by F/V *Aldebaran* during the Pollock A Season (January-March) and bottom trawl surveys (June-August) in 2008-2010. Water depths are contoured at 30, 50, 100, 200, 500, 1000 and 2000 m. Red diamonds show the locations of PMEL EcoFOCI moorings M2, M4, M5 and M8. Date-stamped, color-coded lines represent the ice edge every 8 days during the Pollock A Season cruises.

Figure 1.18 shows maps of the near-surface salinity that varied between 26.35 and 33.06 psu. The highest salinities were encountered in basin water near the shelf break and over Bering Canyon. The lowest salinities were measured shoreward of the 30-m contour in Bristol Bay. Low-salinity water, probably due to ice melt, was observed near St. Matthew Island, as shown earlier for the 2008 echo integration survey (Figure 1.7).

The Pollock A Season occurs in low winter light during short days before the spring bloom, so it is no surprise that no chlorophyll-a was detected during that time (Figure 1.19). The bottom trawl survey takes place well after the spring bloom when nutrients have been stripped from the water column by phytoplankton production; therefore most of the region has negligible chlorophyll. Mid-range concentrations were found near Unimak Pass and along the Alaska Peninsula owing to

nutrient-rich water that had entered the Bering through mixing and transport in Unimak Pass. A few random patches of low chlorophyll were observed on the shelf perhaps due to local wind-mixing events that injected nutrient-rich water into the mixed layer.

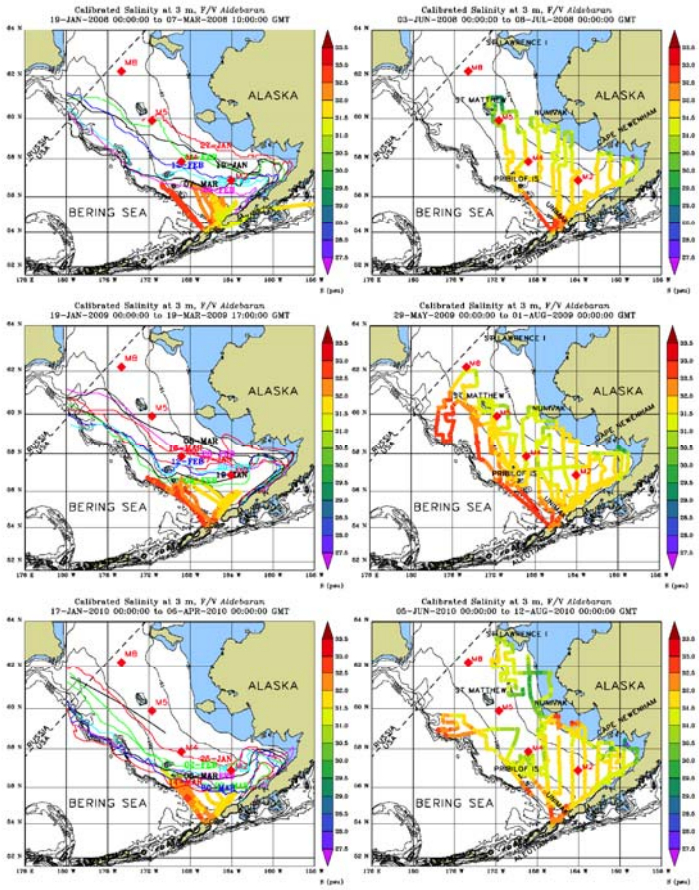

Figure 1.18. Salinity (psu) at 3 m in the Bering Sea measured by F/V *Aldebaran* during the Pollock A Season (January-March) and bottom trawl surveys (June-August) in 2008-2010. Water depths are contoured at 30, 50, 100, 200, 500, 1000 and 2000 m. Red diamonds show the locations of PMEL EcoFOCI moorings M2, M4, M5 and M8. Date-stamped, color-coded lines represent the ice edge every 8 days during the Pollock A Season cruises.

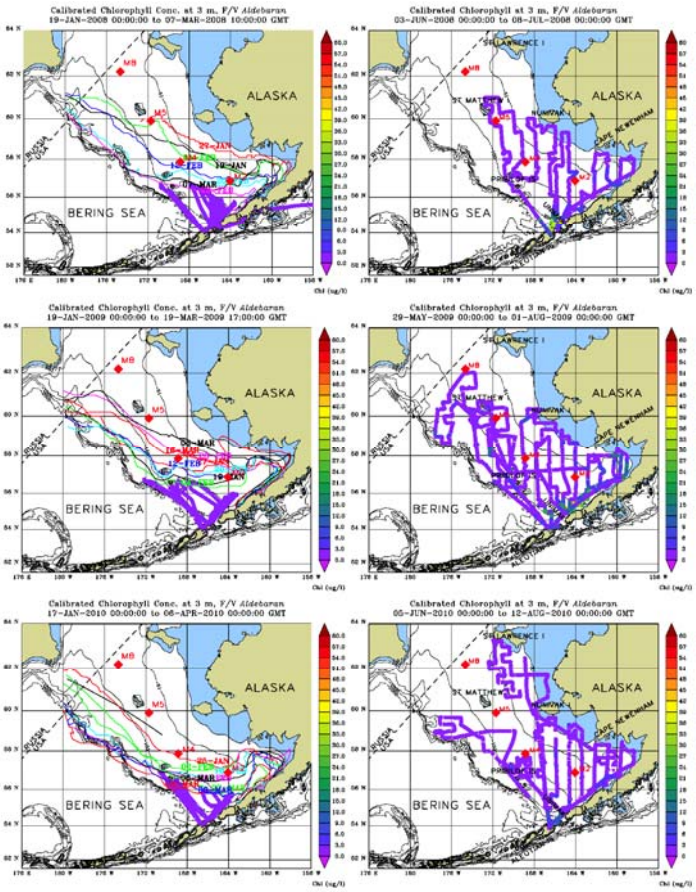

Figure 1.19. Chlorophyll-a concentration (µg/L) at 3 m in the Bering Sea measured by F/V *Aldebaran* during the Pollock A Season (January-March) and bottom trawl surveys (June-August) in 2008-2010. Water depths are contoured at 30, 50, 100, 200, 500, 1000 and 2000 m. Red diamonds show the locations of PMEL EcoFOCI moorings M2, M4, M5 and M8. Date-stamped, color-coded lines represent the ice edge every 8 days during the Pollock A Season cruises.

CONCLUSIONS

We installed an underway oceanographic measurement system on F/V *Aldebaran* to measure ocean temperature, salinity and chlorophyll at 3-m depth during three Pollock A Season and three bottom trawl survey cruises in the southeastern Bering Sea in 2008-2010. Salinity and chlorophyll measurements were calibrated against discrete samples analyzed in the laboratory. Maps of variables measured during January-March and June-August show the evolution of these ecosystem parameters on the southeastern Bering Sea shelf. The winter data set is valuable because oceanographic measurements made in this area are rare. The summer bottom trawl survey measurements of temperature and salinity provided a valuable independent check on the calibration of CTDs that were added to the bottom trawl survey nets.

Chapter 1.c: Bottom Trawl Survey CTD Measurements

ABSTRACT

The NOAA/AFSC bottom trawl survey samples demersal fish at over 350 sites on the southeastern Bering Sea continental shelf each summer on a 37 x 37 km grid. We have added rugged CTDs to the net hauls to obtain gridded data sets of temperature and salinity measurements for 2008 to 2010. Results reveal the three-dimensional thermohaline structure of the shelf including the Cold Pool and areas of fresher water around St. Matthew Island and in Bristol Bay. Horizontal gradients are often strongest roughly along the 50-m and 100-m isobaths that traditionally separate the inner- and outer-shelf from the middle-shelf centered along the 70-m isobath. The mixed layer depth is less than 30 m over much of the region. It reaches deeper to the bottom along the coast southeast of Nunivak Island in water depths both less and greater than 50 m, implying that the boundary of the well-mixed, inner shelf is not always at the 50-m isobath. The greatest upper-to-lower layer density difference is found across the shelf north of 59°N. The temperature difference is the main contributor to this density difference over most of the region, but salinity can play a stronger role at times near Unimak Pass, at the shelf-break, around St. Matthew Island and near the coast. The geostrophic velocity relative to the bottom shows northwestward flow seaward of the 100-m isobath and northwestward transports integrated across the shelf of 0.10 to 0.25 Sv. In 2008 and 2010 there was clockwise circulation in a region of less-dense water around St. Matthew Island. In 2009 that less-dense lens did not exist, and flow was concentrated along the 100-m isobath bringing saltier water across the shelf.

INTRODUCTION

A third goal of BSIERP Project B62 was to add CTD measurements to the annual bottom trawl survey. NOAA's Alaska Fisheries Science Center (AFSC) has conducted standardized bottom trawl surveys each summer on the eastern Bering Sea continental shelf since 1982, trawling at over 350 sites to determine the composition, distribution and abundance of demersal fish, shellfish and epibenthic invertebrates (Lauth, 2011; Stauffer, 2004). Besides providing an important long-term view of this resource needed for fisheries management, the survey has made concomitant temperature measurements to help understand the progression between cold and warm years and the size of the Bering Sea Cold Pool defined by water in which the summer temperature is less than 2°C. The repeated, regular nature of the bottom trawl

survey presented an opportunity to add other oceanographic measurements. Funded by BSIERP, we added conductivity-temperature-depth (CTD) instruments to the net hauls in 2008-2010. The temperature and salinity measurements allowed us to compute the mass density field, its gradients, the mixed layer depth and the bottom-referenced geostrophic circulation on a three-dimensional grid covering a large region of the shelf from the Alaska Peninsula to 62°N and from the 30-m to the 200-m depth contours.

METHODS

The CTDs needed to be small and light so as not to affect how the nets fished, be rugged enough to survive hundreds of trips up and down the trawl ramps on the typical 38- to 45-m-long commercial fishing trawlers employed as contract vessels, have long battery life to minimize the chances of waterproof-seal failures when the instruments were opened for battery changes, and sample rapidly to resolve sharp thermoclines. We chose Falmouth Scientific Instruments (FSI) NXIC CTDs that later became Teledyne RD Instruments (RDI) Citadel CTD-NVs (http://www.rdinstruments.com/citadel.aspx)

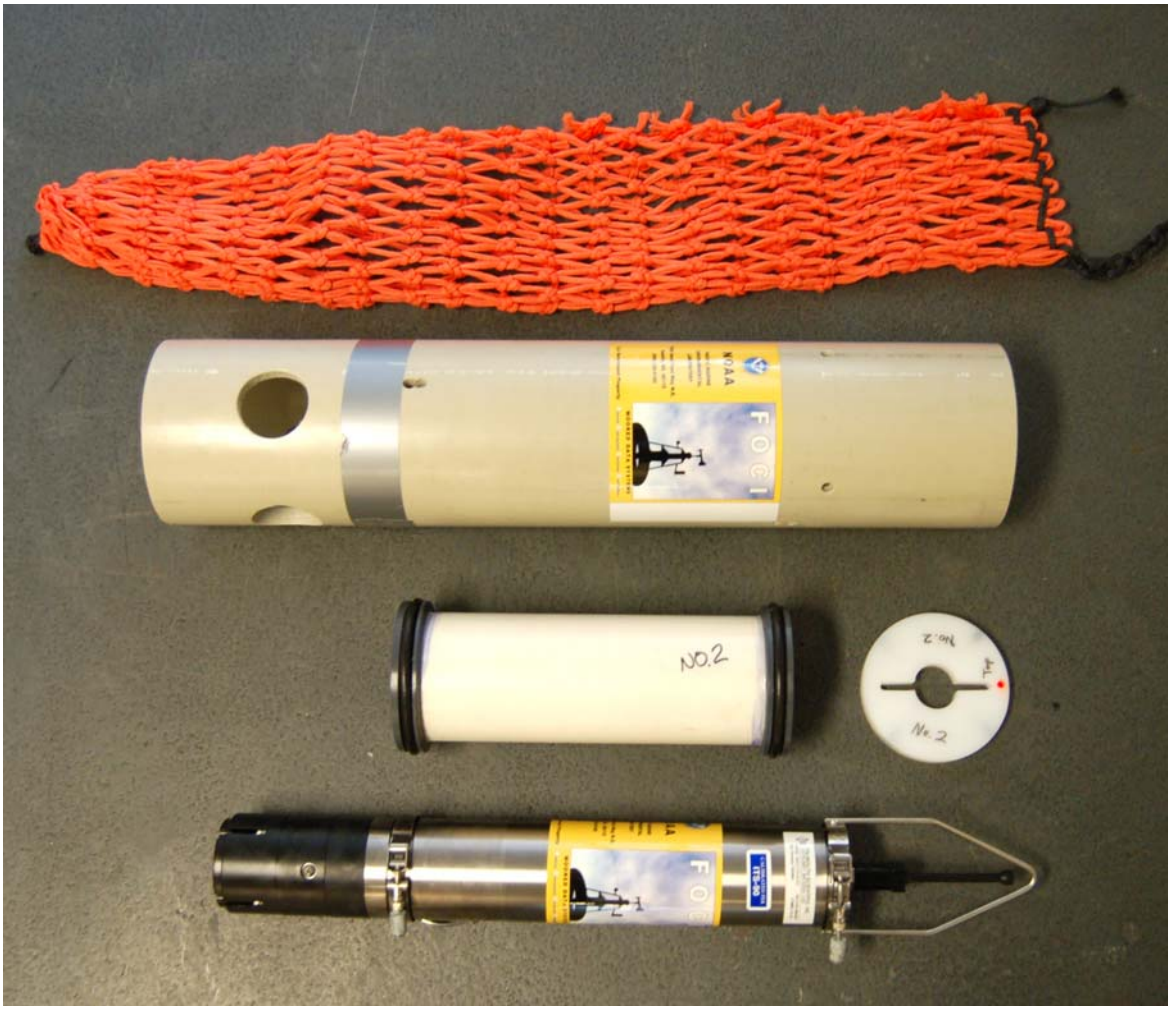

Figure 1.20. NXIC CTD with protective polypropylene case components and net bag.

when the product line changed hands. Each CTD was 67 cm long, 8 cm in diameter and weighed 3.8 kg in air with a titanium case. It had a rugged thermistor and non-external inductive conductivity sensor (NXIC). The batteries lasted most of the summer field season, requiring only one battery change per instrument. The instruments were deployed at their maximum sampling rate of 15 Hz.

Although the CTDs were designed to be rugged, for extra protection we mounted them in sturdy cases constructed from 160-mm-diameter Asahi/America Proline Pro-150 polypropylene pipe with a 14.6 mm wall thickness (Figure 1.20). Each case was placed in a mesh bag made from fishing net material and attached to the trawl net's headrope (Figure 1.21). This configuration was a compromise between adding to the thermal mass and reducing the flow through the conductivity cell of each instrument, and protecting it from damage. The conductance cell faced forward into the flow as the net fished. In a standard net haul, the ship steamed at 1.5 m/s (3 knots) while the net was lowered to the bottom at a vertical speed of ~0.3 m/s, towed with the headrope 2.5 m above the bottom for 30 minutes, and brought up to the surface at ~0.3 m/s (Stauffer, 2004).

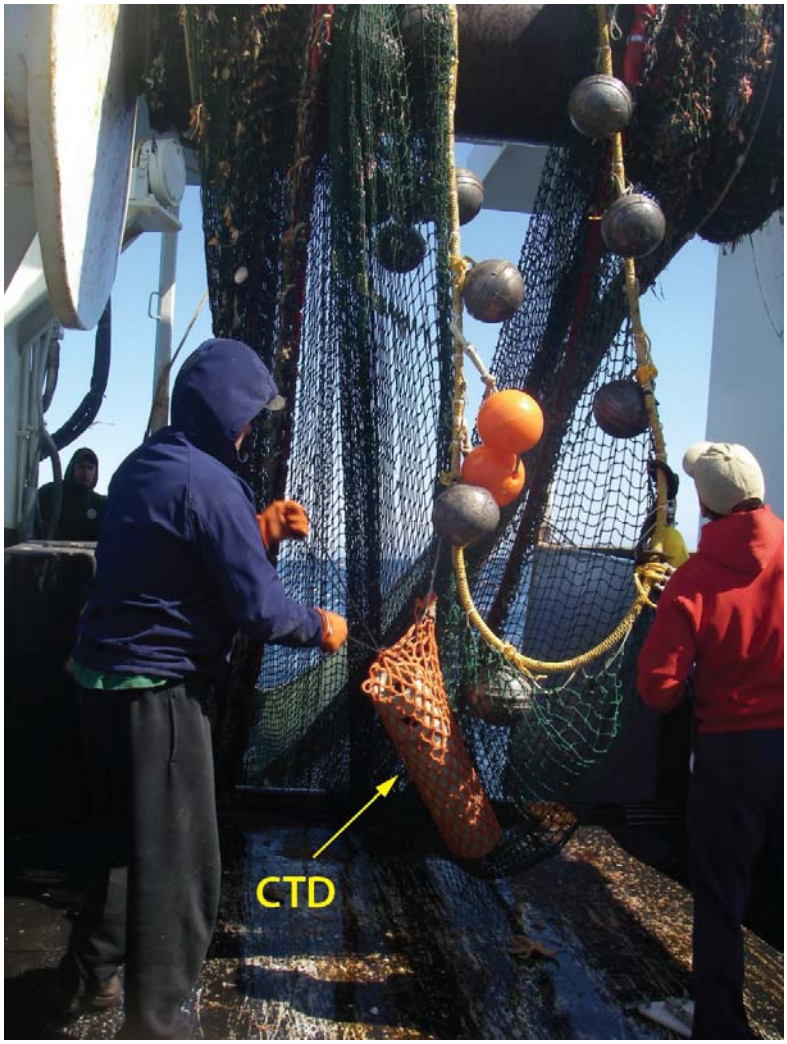

Figure 1.21. Photograph of an NXIC CTD mounted inside a 160-mm diameter polypropylene pipe and attached to the trawl net's

The CTD manufacturers specified temperature, conductivity and pressure accuracies of 0.005ºC, 0.009 mS/cm and 0.05% of full scale, respectively. These convert to salinity and pressure accuracies of 0.006 psu (PSS78) at 5ºC and 0.25 dbar (decibar $=10^4$ Pa ≈ 1 m of water depth) for the 500-m pressure transducers that the CTDs carried. These values are for CTDs factory-calibrated annually in constant temperature and salinity conditions, but the accuracy in a dynamic field environment is undoubtedly less. As the CTD is lowered or towed, water flows through the inductive cell and past the thermistor; therefore no pump is required, thus enhancing battery life. However the residence time of a water parcel within the inductive cell and the time lag between the conductance and temperature measurements vary with flow speed. Temperature effects dominate conductance measurements, and salinity plays a secondary role. It is well known that to determine the changing salinity accurately, one must account for the changing temperature at the instant and location of the conductance measurement. If time constants and lags are not accounted for properly, salinity spikes and inaccuracies result. Some other CTD systems mitigate these problems by pumping water through a small diameter cell at a known, constant rate and fine-tuning time constants and offsets with factory-supplied data processing software. The NXIC CTDs came with no such software; therefore we wrote our own using the Ferret data visualization and analysis computer program (Hankin et al., 1992; Hankin et al., 1991).

Our data processing scheme had several steps. First, with software provided by the manufacturer, we converted each of the CTD's binary data files into an ASCII comma-separated-value (csv) file whose unique name was composed of the instrument's serial number and the date and time of the first sample. Each csv file was a time series of pressure, temperature, conductivity, salinity and battery voltage. Second, we read each csv file and eliminated bad and unwanted values. The CTDs were set up to begin recording when they entered salt water. Data values with conductivities below 5 mS/cm, owing to initial startup transients, were removed at this processing stage. During initial net deployment and final retrieval, the CTDs remained on the surface for a few minutes just behind the moving ship. These measurements in the ship's wake did not represent the undisturbed water column; therefore we removed values for pressures less than 1 dbar. Owing to data handling errors within the CTDs' factory software, especially in the early years of this study, the csv files sometimes had bad sections with blocks of repeated data making it appear that the sampling time had jumped backwards or did not progress. These sequences were detected and removed. The remaining values were linearly interpolated onto an equispaced time axis with an increment of $1/15^{th}$ second – the instrument's sampling interval – and stored in a NetCDF file (network common data form, Rew et al., 2009). The third step in our processing scheme involved correcting the measured pressures, temperatures and conductivities for sensor lag times. RD Instruments gave the following values for the response times of their sensors: pressure 0.025 s,

temperature 0.100 s and conductivity 0.05 s at a flow rate of 1 m/s (Teledyne RD Instruments, 2009). We used the method of Fofonoff et al. (1974) to correct for these lags. In general, the true value of a variable, $f_T(t)$, is approximated by its measured value, f_M, by

$$f_T \approx f_M + \tau_f \left\langle \frac{df_M}{dt} \right\rangle \qquad (1)$$

where τ_f, is the response time for variable f and the bracket represents a smoothing operation applied to reduce noise in the time derivative. The CTD's pressure measurements were noisier than the other variables; therefore we smoothed them first with a 15-point (1-s duration) Hanning window (Press et al., 1986) before computing the three-point centered time derivative and the "true" pressure in **Error! Reference source not found.**. For temperature we computed the three-point centered time derivative of the measured temperature and then smoothed it with a 5-point Hanning window before applying **Error! Reference source not found.**. For conductivity, we assumed that the more massive conductivity cell's temperature lagged that of the "true" temperature measured with a downstream thermistor. We experimented with lagging the "true" temperature and its 5-point-Hanning-smoothed derivative by various times, used that and the measured conductivity to compute the salinity and checked for salinity spikes. By trial and error, we found that a lag time between the "true" temperature and the conductivity temperature of 0.3 s gave the best results in general, but it did not always entirely eliminate salinity spikes. The fourth step in CTD data processing involved matching the CTD time series with net haul times and positions. The pressure time series was smoothed with a Hanning window whose width in time (51 points) was chosen to be equivalent to 1 dbar at the sampling frequency of 15 Hz and a typical vertical net speed of 0.3 dbar/s. We designated that portion of each net haul a down- or upcast when the down- or upward velocity exceeded 0.08 dbar/s, respectively. Net haul logs provided by the bottom trawl survey scientists gave the time and geographic position when each haul reached and left the sea bottom, and the down- and upcasts were assigned those times and positions. The down- and upcast time series were linearly interpolated onto pressure axes with one-dbar increments, missing values above 3 dbar were assigned their nearest-neighbor values from below, and the results stored as separate NetCDF files. Usually the downcast was chosen to represent each CTD station, but each was compared graphically with its upcast and the latter was chosen if it had smaller spurious density inversions (heavy water above light water) owing to salinity spiking.

Two ships (F/V *Aldebaran* and either F/V *Arcturus*, *Alaska Knight* or *Vesteraalen*) conducted the bottom trawl survey, sailing parallel north-south tracks in tandem, 37 km apart, repeating the same pattern each year. For each survey year, CTD casts (321 in 2008, 292 in 2009 and 377 in 2010) were gridded onto an

equispaced (2/3˚ longitude x 1/3˚ latitude) grid between 178.6667˚W and 157.6667˚W and 54.6667˚N and 66.0000˚N using a Laplacian algorithm with a spline-smoothing parameter of 2 and interpolating no more than 1 grid point away from any data point (Denbo, 1993; Hankin et al., 1992; Hankin et al., 1991). This regular grid approximated the bottom trawl survey grid that was spaced at 37 x 37 km over most of the region, but with finer spacing in areas of enhanced fisheries interest (Lauth, 2011). Some CTD casts were lost owing to equipment failure, dead batteries or corrupt data files such that an interpolated value was not available at every grid point. Unless otherwise mentioned, the results that follow are based upon the gridded data set.

In addition to the CTDs, one ship, F/V *Aldebaran*, was equipped with an underway seawater sampling system consisting of a Sea-Bird Electronics SBE 38 digital oceanographic thermometer, an SBE 45 MicroTSG thermosalinograph to measure salinity, and a WETLabs ECO fluorometer with bio-wiper to measure chlorophyll fluorescence. Water was sampled every 60 s from the ship's sea chest, drawing water from approximately 3 m depth. Discrete salinity and chlorophyll samples were taken daily, analyzed in the laboratory after the field season and used to calibrate the salinity and chlorophyll fluorescence sensors (see Chapter 1.b of this report). These temperature and salinity measurements were used as an independent check on the CTD measurements.

RESULTS AND DISCUSSION

The NOAA bottom trawl survey required about two months to cover the eastern Bering Sea continental shelf. It can best be characterized as a scan of the region, not a snapshot. Figure 1.22 shows maps of the age of the survey since it commenced for each of the years 2008-2010. The survey began in early June in the southeast corner of the region and moved toward the northwest. The sampling scheme was designed so that the same sites were sampled at about the same time each year. While the sampling was not synoptic over the entire region, sampling at adjacent sites was no more than a few days apart.

The FSI/RDI CTDs were new instruments to us. They were factory calibrated at the beginning of each field season, but because they were deployed on towed fishing nets instead of on vertical hydrographic wire casts, it was not possible to take discrete samples for in-situ calibration. However as a check on the CTD's performance, we compared measurements with the underway system on F/V *Aldebaran*. Figure 1.23 shows time series of temperature and salinity from the underway system and the CTD measurements at 3 m depth for the 2009 bottom trawl survey. The CTD measurements track the near-surface variations

very well with correlation coefficients, r^2, for temperature and salinity over the three years exceeding 0.99 and 0.98, respectively. The CTDs were not recalibrated against the underway measurements because the turbulent wake of a ship moving in a stratified fluid is a poor calibration environment. The CTD cast data and supporting metadata with plots are available on the BSIERP Data Archive (Cokelet, 2013a, b, c).

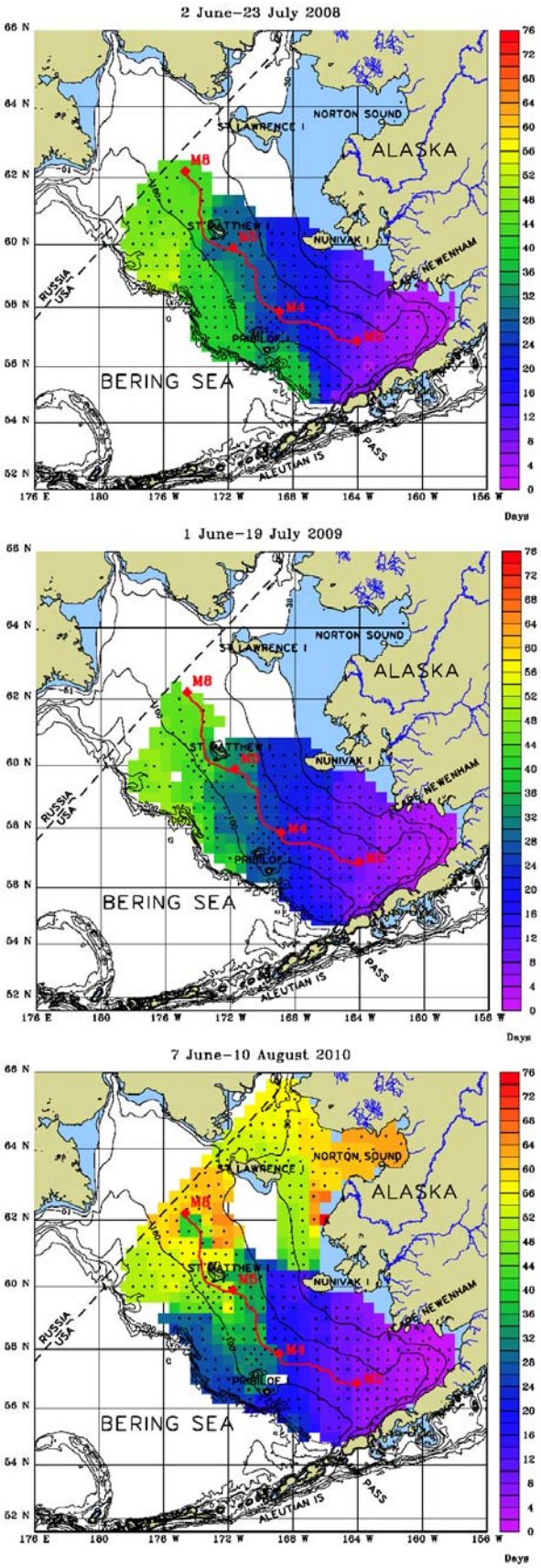

Figure 1.22. Maps of each year's bottom trawl survey history in days since inception for 2 June-23 July 2008, 1 June-19 July 2009, and 7 June-10 August 2010. The black dots represent the CTD cast sites. The long-term EcoFOCI mooring sites (M2, M4, M5 and M8) and 70-m isobath section are shown in red. Depths are contoured at 30, 50, 100, 200, 500, 1000 and 2000 m.

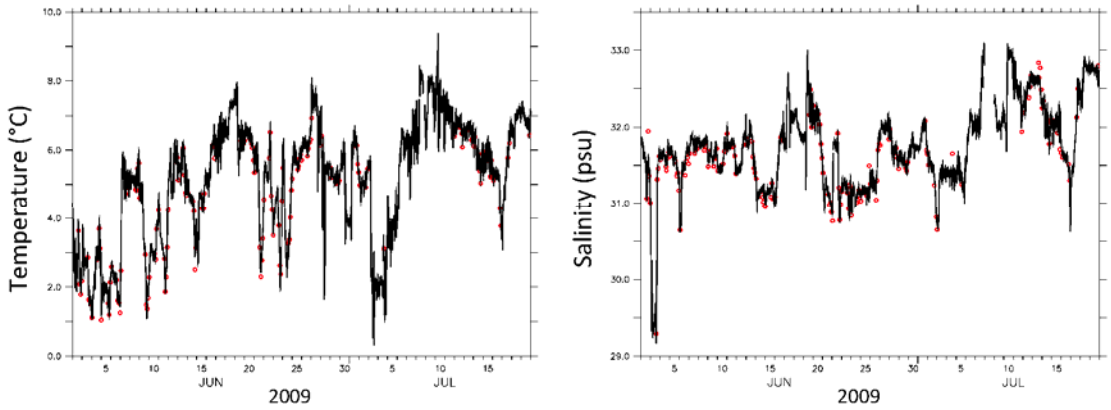

Figure 1.23. Time series of the underway (black lines) and CTD (red circles) measurements of (a) temperature and (b) salinity at 3 m on F/V *Aldebaran*, summer 2009.

Temperature

The area covered by the bottom trawl survey provides a large-scale picture of ocean properties. The left column of Figure 1.24 shows the gridded temperature at 5 m over the three study years. This temperature is representative of the surface mixed layer. The measured water temperature at 5 m for all years varied between 0.54 and 15.20ºC. For bottom depths exceeding 30 m, the surface water was coldest on the inner shelf owing to winter cooling and generally increased seaward influenced by warmer basin water. The warming from southeast to northwest tracks with the survey age (Figure 1.22) and is strongly influenced by summer solar heating during the cruises's progress. We have few actual measurements at shallower bottom depths in 2008 and 2009, but those that exist show warmer water near the coast due to summer heating of fresher water derived from coastal rivers that is confined along the coast by shallow fronts (Danielson et al., 2011). In 2010 the measurements extended into Norton Sound where the warmest water was found in shallow water late in the season.

The bottom temperature at each grid point is defined to be the deepest temperature that is within 10 m of the bottom or within 10% of the bottom depth for water depths greater than 100 m. For locations where the mixed layer depth is less than the bottom depth, the bottom temperature represents the lower layer temperature. The right column of Figure 1.24 shows the bottom temperature for each year. The most striking feature is the tongue of cold water with temperatures below 0ºC along the much-studied 70-m

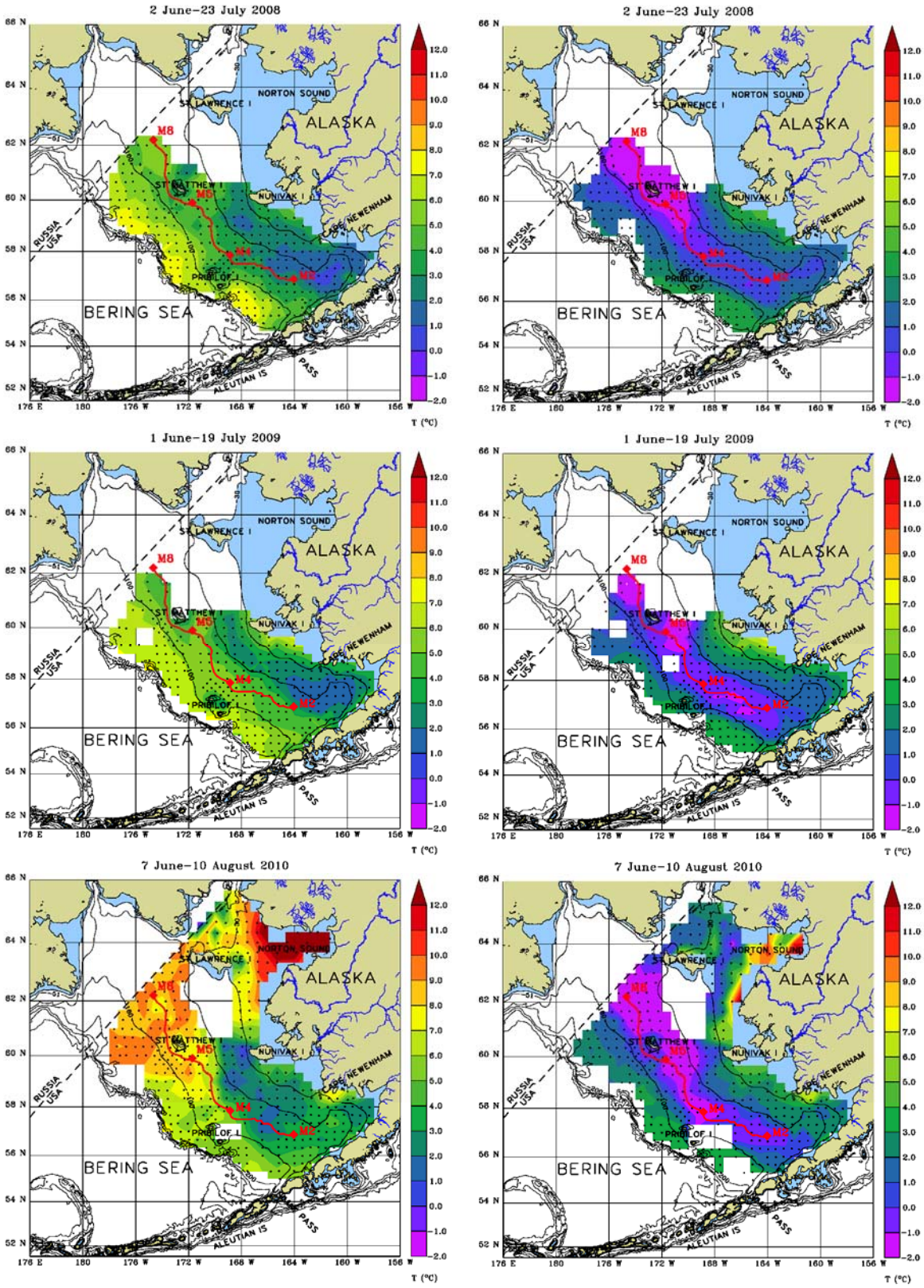
2 June–23 July 2008
2 June–23 July 2008
1 June–19 July 2009
1 June–19 July 2009
7 June–10 August 2010
7 June–10 August 2010
NORTON SOUND
ST LAWRENCE I
ALASKA
ST MATTHEW I
NUNIVAK I
CAPE NEWENHAM
PRIBILOF I
RUSSIA
USA
BERING SEA
ALEUTIAN IS
PASS
M8
M6
M4
M2
T (°C)

797

Figure 1.24. Maps of the ocean temperature at 5 m depth (left column) and the sea bottom (right column) for the 2008, 2009 and 2010 bottom trawl surveys. The black dots represent the CTD cast sites. The long-term EcoFOCI mooring sites (M2, M4, M5 and M8) and 70-m isobath section are shown in red. Depths are contoured at 30, 50, 100, 200, 500, 1000 and 2000 m. The red line represents the 75m isobath section (Stabeno et al., 2010; Stabeno et al., 2012a).

The three study years are considered to be cold years on the Bering Sea shelf (Stabeno et al., 2012b). Even at the height of summer, the bottom temperature did not exceed 2ºC that defines the Cold Pool boundary (Wyllie-Echeverria and Wooster, 1998). The Cold Pool forms by cooling due to sea-ice formation and melting during the previous winter or succession of winters. The large temperature difference between the 5-m and bottom temperatures (Figure 1.24) contributes to the vertical density stratification.

Salinity

The unique aspect of adding CTDs to the bottom trawl survey is the measurement of salinity over the region. Figure 1.25 shows the salinity at 5-m and on the bottom. Salinity is a more conservative quantity than temperature, being affected slowly by circulation and river inflow near the coast. In a general sense, the upper-layer salinity (Figure 1.25, left column) increases offshore from less-saline water influenced by coastal river inflow to saltier basin water at the shelf break. However secondary variations exist along isobaths. A southeast-northwest gradient occurs in all three years with a lower-salinity area centered near St. Matthew Island. Seaward of the 100-m isobath, higher-salinity shelf-break water encroaches onto the shelf in varying degrees, with the greatest extent in 2009. Low salinity water is found in Bristol Bay all three years. The lowest salinity was measured in shallow Norton Sound in 2010, but in that same year anomalous high-salinity water of unknown origin was observed south of Nunivak Island. This measurement was confirmed independently by the underway seawater system aboard F/V *Aldebaran* (Figure 1.18).

The bottom salinity exceeds the surface-layer salinity and reflects its distribution in the southeast (Figure 1.25, right column). The low-salinity region around St. Matthew Island is smaller. Higher-salinity shelf-break water extends to the 100-m isobath in all years. In 2010 when measurements are available to the north, shelf-break water extended across the shelf past St. Lawrence Island and toward Bering Strait. This is the Anadyr Water as identified by Coachman (Coachman et al., 1975).

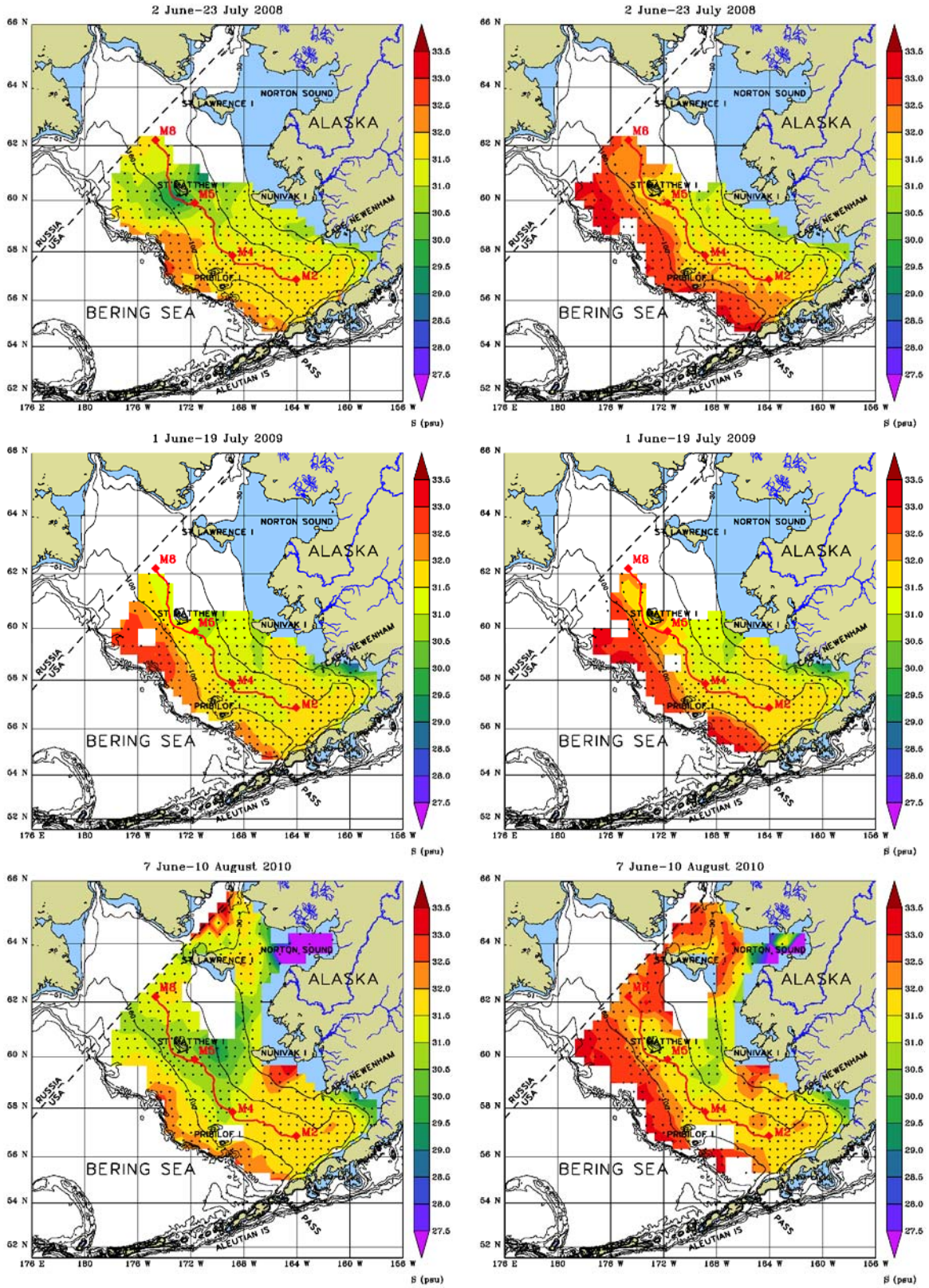
2 June–23 July 2008
2 June–23 July 2008
1 June–19 July 2009
1 June–19 July 2009
7 June–10 August 2010
7 June–10 August 2010
NORTON SOUND
ST LAWRENCE I
ALASKA
ST MATTHEW I
NUNIVAK I
NEWENHAM
PRIBILOF I
RUSSIA
USA
BERING SEA
ALEUTIAN IS
PASS
M8
M6
M4
M2
66 N
64 N
62 N
60 N
58 N
56 N
54 N
52 N
176 E
180
176 W
172 W
168 W
164 W
160 W
156 W
33.5
33.0
32.5
32.0
31.5
31.0
30.5
30.0
29.5
29.0
28.5
28.0
27.5
S (psu)

832

Figure 1.25. Maps of the salinity at 5 m depth (left column) and the sea bottom (right column) for the 2008, 2009 and 2010 bottom trawl surveys. The black dots represent the CTD cast sites. The long-term EcoFOCI mooring sites (M2, M4, M5 and M8) and 70-m isobath section are shown in red. Depths are contoured at 30, 50, 100, 200, 500, 1000 and 2000 m.

Gradients

The availability of gridded measurements in three dimensions allows one to compute gradients. Figure 1.26 shows the magnitudes of the horizontal gradients, $\left|\nabla_H T_B\right|$ and $\left|\nabla_H S_B\right|$, of the bottom temperature, T_B, and bottom salinity, S_B. Bands of strong temperature gradient lie approximately along the 100-m isobath in all three years and along the 50-m isobath in 2009 and 2010. Strong salinity gradient bands lie along the 100-m isobath, but are not so clearly demarcated. These bands are shelf-wide affirmation of the fronts separating the outer, middle and inner domains of the continental shelf as first observed along isolated cross-shelf sections by Schumacher et al. (1979) and Kinder and Schumacher (1982). In simple terms, the outer domain has mixed upper and lower layers separated by a thick, diffuse density gradient layer, the middle domain has two mixed layers separated by a sharper, thinner gradient region, and the inner domain is mixed top to bottom. The thermal fronts in Figure 1.26 can be traced throughout lower layer of the water column. Such fronts provide sharp thermal boundaries to organisms capable of living only within narrow temperature ranges. At mid shelf is the oft-studied 70-m-isobath CTD section occupied several times a year by PMEL (Stabeno et al., 2010; Stabeno et al., 2012a). As by design, it coincides with a region weakly varying temperature and salinity with small gradients.

Mixed Layer Depth and Stratification

The upper and lower layers of the water column define separate habitats – the upper with ample light for photosynthesis but stripped of essential nutrients, and the lower deficient in light but with ample nutrients. The mixed layer depth denotes the bottom of the upper layer, i.e. the top of the pycnocline. After some trial and error, we settled on a similar definition of the mixed layer depth as Danielson et al. (2011) – that depth at which the density anomaly, $\sigma_t = \rho$ (S, T, p=0) – 1000 (where ρ is the fluid mass density in kg/m^3 and p is the pressure above atmospheric), first exceeds its average value over the upper 5 m by 0.1 kg/m^3. If that criterion is not met upon reaching the bottom, then the mixed layer depth is set to the bottom depth,

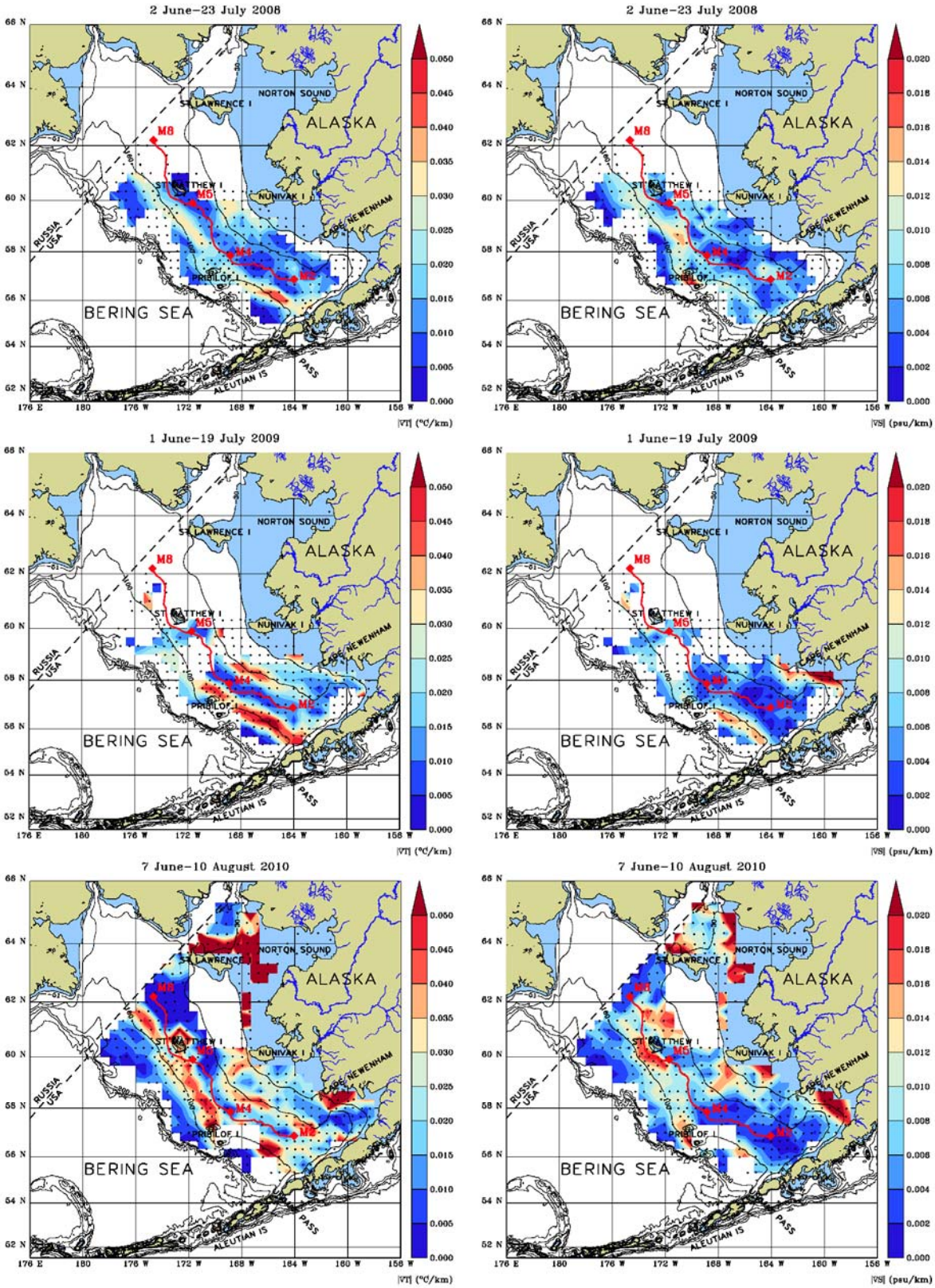
2 June–23 July 2008
2 June–23 July 2008
1 June–19 July 2009
1 June–19 July 2009
7 June–10 August 2010
7 June–10 August 2010
NORTON SOUND
ST LAWRENCE I
ALASKA
ST MATTHEW I
NUNIVAK I
CAPE NEWENHAM
PRIBILOF I
BERING SEA
ALEUTIAN IS
PASS
RUSSIA
USA
M1
M2
M4
M5
M8
|∇T| (°C/km)
|∇S| (psu/km)

866

Figure 1.26. Maps of the horizontal temperature gradient magnitude, $\left|\nabla_H T_B\right|$ (left column), and salinity gradient magnitude, $\left|\nabla_H S_B\right|$ (right column), at the sea bottom for the 2008, 2009 and 2010 bottom trawl surveys. The black dots represent the CTD cast sites. The long-term EcoFOCI mooring sites (M2, M4, M5 and M8) and 70-m isobath section are shown in red. Depths are contoured at 30, 50, 100, 200, 500, 1000 and 2000 m.

and the water column is deemed well mixed. Figure 1.27 (left column) shows the mixed layer depth that varies between 3 and 79 m during the three bottom trawl surveys. It is less than 30 m over most of the region but deepens south of Nunivak Island, paralleling the coast, and at some locations near the shelf break. The white, hatched pattern delineates areas where the mixed layer reached the bottom. This often occurs in water shoreward of the 50-m isobath, the traditional outer boundary of the well-mixed inner shelf (Ladd and Stabeno, 2012, and other references cited there), but our results show that the well-mixed region can both extend beyond, and at other sites not reach, the 50-m isobath.

It is instructive to compute the density difference between the upper and lower layers and to determine the individual contributions of temperature and salinity. Where the water column is two-layered, the pycnocline can be thin as on the middle shelf, or thick as on the outer shelf. Through experimentation, we find that density 30 m below the mixed layer depth, or at the ocean bottom if shallower, is a good indicator of lower-layer values. Figure 1.27 (right column) shows the lower-to-upper layer density difference. It is much greater north of 58°N and around St. Matthew Island in 2008 and 2010 than in 2009. Where the difference is less than 0.1 kg/m^3, the upper layer depth equals the bottom depth, and values are denoted by hatched areas. To determine the individual contributions of potential temperature, θ, and salinity to the potential density, ρ, difference, consider its vertical derivative

$$\frac{d\rho(S,\theta)}{dz} = \frac{\partial\rho}{\partial S}\frac{dS}{dz} + \frac{\partial\rho}{\partial\theta}\frac{d\theta}{dz} = \rho\left(\beta\frac{dS}{dz} - \alpha\frac{d\theta}{dz}\right)$$

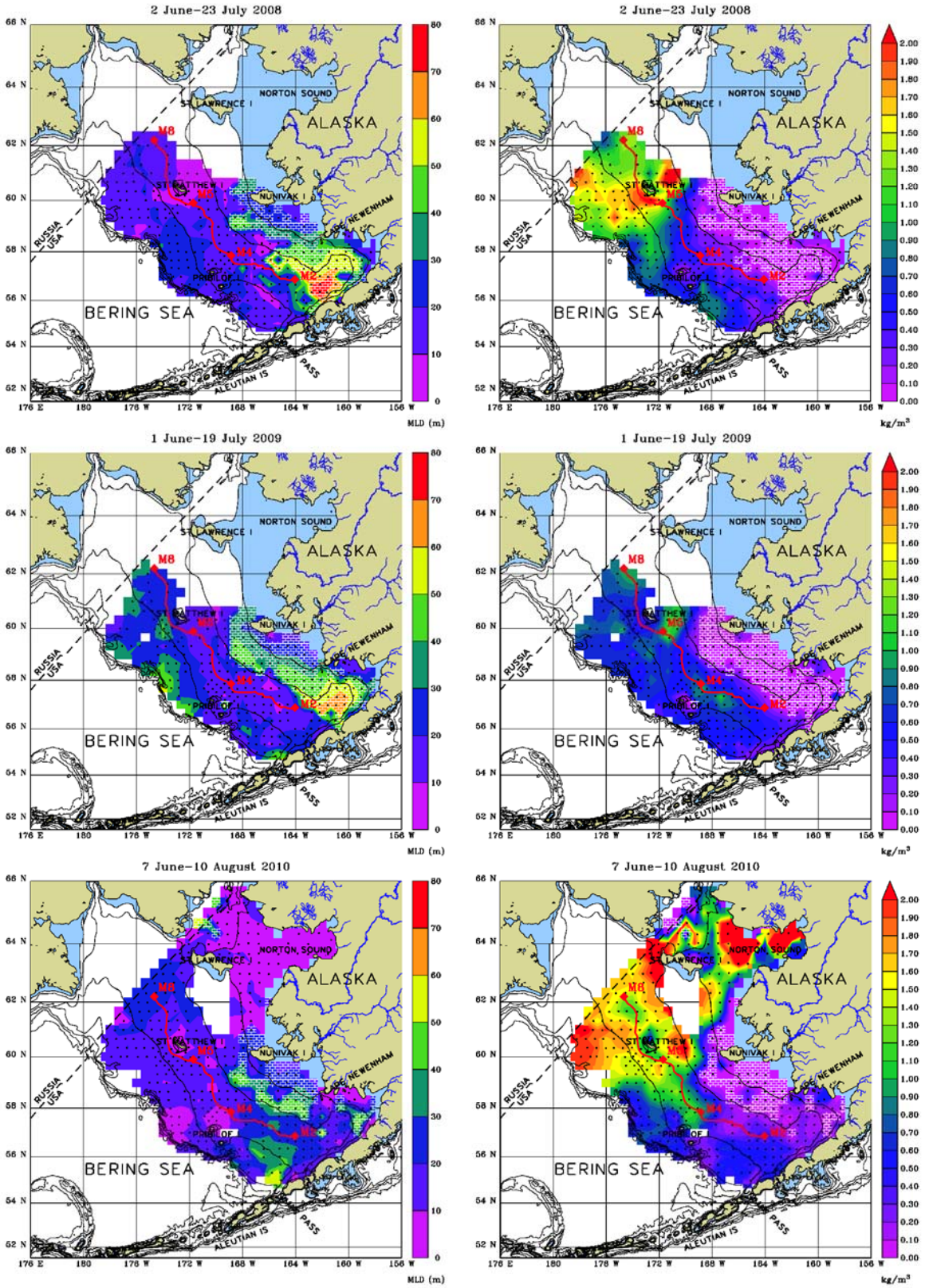
2 June–23 July 2008
1 June–19 July 2009
7 June–10 August 2010
NORTON SOUND
ST LAWRENCE I
ALASKA
ST MATTHEW I
NUNIVAK I
NEWENHAM
PRIBILOF I
BERING SEA
ALEUTIAN IS
PASS
RUSSIA
USA
M8
M6
M4
M2
MLD (m)
kg/m³

892

Figure 1.27. Maps of the mixed layer depth (left column), and upper-to-lower-layer density difference, $\Delta\sigma_t$ (right column), for the 2008, 2009 and 2010 bottom trawl surveys. White hatching represents areas where the upper mixed layer reaches the ocean bottom. The black dots represent the CTD cast sites. The long-term EcoFOCI mooring sites (M2, M4, M5 and M8) and 70-m isobath section are shown in red. Depths are contoured at 30, 50, 100, 200, 500, 1000 and 2000 m.

where $\beta = \frac{1}{\rho}\frac{\partial\rho}{\partial S}$ is the haline contraction coefficient and $\alpha = \frac{1}{\rho}\frac{\partial\rho}{\partial\theta}$ is the thermal expansion coefficient. The ratio of temperature to salinity effects is $-\alpha\frac{d\theta}{dz}\Big/\beta\frac{dS}{dz}$, but this quantity can vary between -∞ and ∞ depending on the signs of the numerator and denominator as the salinity gradient approaches zero, much like the trigonometric function tan(x) as x approaches ±90°. This inconvenient metric can be rendered useful by defining its inverse tangent, called the gradient Turner angle (Ruddick, 1983), T_u, by

$$T_u \equiv \tan^{-1}\left(-\alpha\frac{d\theta}{dz}\Big/\beta\frac{dS}{dz}\right) - 45°$$

that varies between -90° and 90° for stable density gradients and equals 0° when the temperature and salinity gradients contribute equally to the density gradient. By analogy, the bulk density difference between the lower and upper layers, $\Delta\rho/\Delta z$, defines the bulk Turner angle

$$T_u \approx \tan^{-1}\left(-\langle\alpha\rangle\frac{\Delta\theta}{\Delta z}\Big/\langle\beta\rangle\frac{\Delta S}{\Delta z}\right) - 45°$$

where Δ signifies the lower-to-upper layer difference operator, and ⟨⟩ refers to the average of the upper and lower layer coefficients. The Turner angle has an advantage over the stability-index (Ladd and Stabeno, 2012) and the Brunt-Vaisala-frequency (Danielson et al., 2011) methods to measure the effects of temperature and salinity on density stratification. In both applications, the authors compared their indices in two hypothetical cases, one with assumed uniform temperature in the water column and one with assumed uniform salinity – conditions that almost never actually occur. Conversely, T_u is a measure of the *actual* stratification without hypothetical assumptions. Figure 1.28 shows an example of the Turner angle for each CTD cast from the 2010 bottom trawl survey, plotted on axes representing the salinity and temperature contributions. Dashed red lines are isolines of density gradient. For negative Turner angles, salinity differences outweigh temperature differences, and for positive Turner angles, temperature outweighs salinity. For Turner angles between -45° and 45°, as is usually the case, salinity increases and

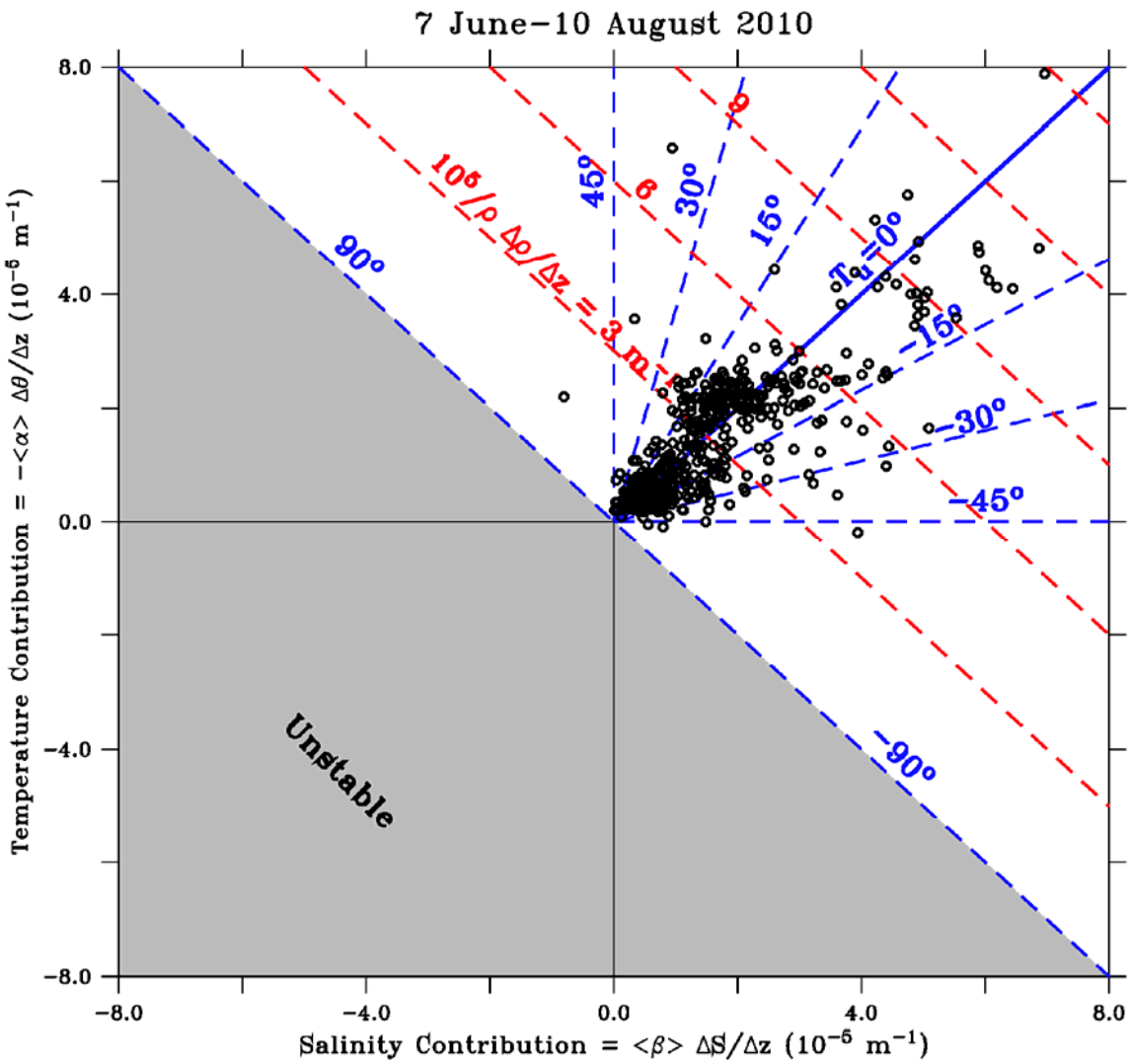

Figure 1.28. The bulk Turner angle, T_u, for the 2010 bottom-trawl-survey CTD casts, plotted against the contributions of the upper-to-lower-layer salinity and temperature differences. The red dashed curves are isolines of the density difference, $1/\rho\ \Delta\rho/\Delta z$ in increments of 3×10^{-5} m^{-1}. Salinity differences dominate temperature differences for negative T_u and vice versa for positive T_u.

temperature decreases with depth, both increasing the density difference and water column stability. For Turner angles less than -45° temperature increases with depth, and for Turner angles greater than 45° salinity decreases with depth – both conditions reducing stability. Past -90° and 90°, the water column becomes statically unstable.

Figure 1.29 shows maps of the Turner angle for the three bottom trawl surveys. Over most of the region T_u is positive, meaning that the temperature difference contributes most to the density difference between the upper and lower layers. There are exceptions. In all three years, salinity dominates the density difference near Unimak Pass and at varying sites along the coast between Nunivak Island and Bristol Bay. Where the surface mixed layer reaches the bottom, what little density difference that exists can be dominated by either temperature or salinity differences (Figure 1.29, hatched areas). In 2008 salinity dominates around St. Matthew Island and in 2010 on the outer shelf. The large upper-to-lower-layer density differences near St. Matthew in 2008 and 2010 (Figure 1.27) are due to salinity in the first instance and temperature in the second. Along the 70-m isobath, salinity controls density in the north more in 2008 than in 2009, but not so in 2010 when it controls slightly ($-15° < T_u < 0°$) only near mooring M4. These results for 2008 and 2009 agree qualitatively with the stratification index results of Ladd and Stabeno (2012), but our observations, on a

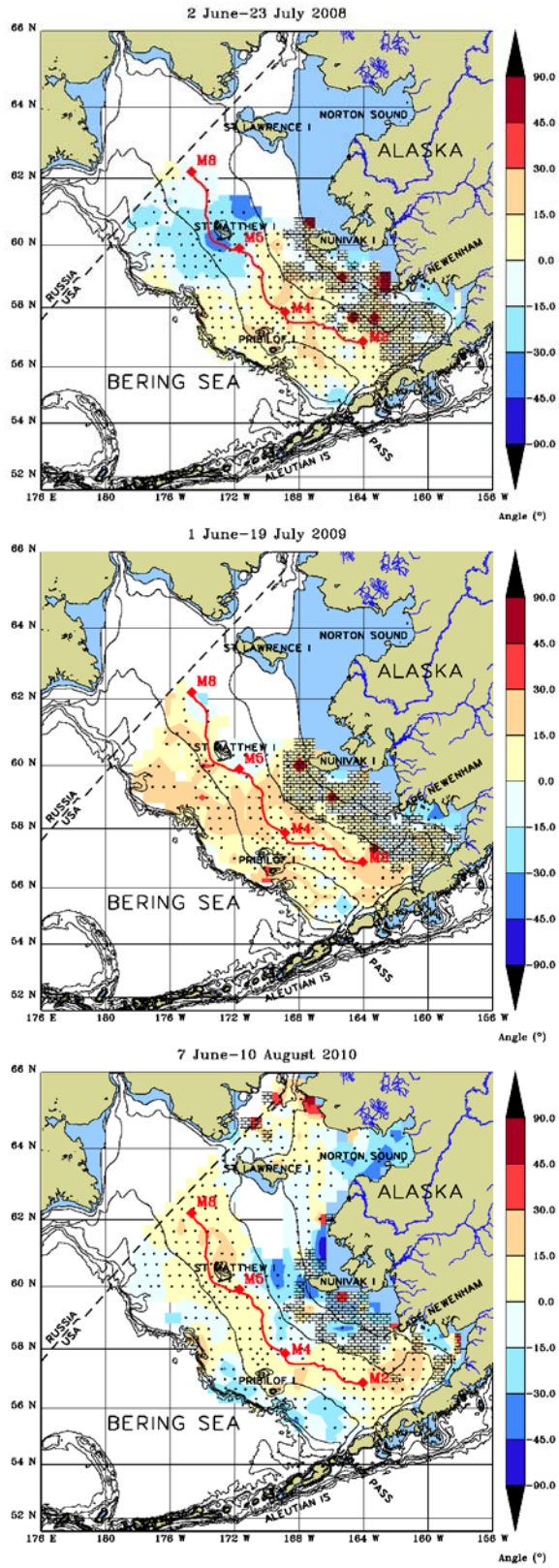

Figure 1.29. Maps of the bulk Turner angle, T_u, for the 2008, 2009 and 2010 bottom trawl surveys. Black hatching represents areas where the upper mixed layer reaches the ocean bottom. The black dots represent the CTD cast sites. The long-term EcoFOCI mooring sites (M2, M4, M5 and M8) and 70-m isobath section are shown in red. Depths are contoured at 30, 50, 100, 200, 500, 1000 and 2000 m.

regular grid reoccupied annually, reveal a more complex regional interplay between temperature and salinity than has been observed along the 70-m isobath alone.

Geostrophic Velocity and Circulation

Ocean currents are driven by the tide, the wind and density differences – the latter being a function of the temperature and salinity fields as we have measured. With certain assumptions, this thermohaline component of the velocity field can be computed from the geostrophic equations

$$-fv = -\frac{1}{\rho}\frac{\partial p}{\partial x}$$

$$fu = -\frac{1}{\rho}\frac{\partial p}{\partial y}$$

(Gill, 1982) where f is the Coriolis parameter related to the earth's rotation, x and y are the eastward and northward coordinates with velocity components u and v, ρ is the water mass density, g is the acceleration of gravity in the downward z-direction measured from a level surface, $z = \eta(x,y)$ is the sea surface, and p is the pressure given by

$$p = g\int_{\eta}^{z} \rho(S,T)\,dz.$$

Here we assume that the equations are time-averaged over tidal periods to remove the back-and-forth effect of the tides, and that tidally averaged components are steady. The geostrophic velocities are local in that they depend upon the local horizontal derivatives of the pressure field that ultimately depends on the measured temperature and salinity fields. Neighboring grid points are usually sampled no more than a few days apart owing to how the survey grid is occupied (Figure 1.22), so that the geostrophic components need only be assumed time-invariant over a few days for these equations to be valid locally. However if the geostrophic velocity vectors are interpreted together over an entire survey region, then there is an implicit assumption of steadiness over the survey's duration. Nonlinear effects are neglected in the geostrophic dynamics because geostrophic currents are slow, and their radius of curvature large. Frictional effects are also neglected. This can be problematic near boundaries, but we shall define the geostrophic currents to vanish at the ocean bottom. This is called the reference level or the level of no motion. Put another way, the computed geostrophic velocities will be relative to the bottom. This is the most restrictive assumption that makes the computed geostrophic currents only one element of the complete flow field. The velocity field is related to the density field such that velocity vectors have

denser water on their left in the northern hemisphere. Viewed looking downstream, denser water on the left means that the isopycnals tilt upward to the left causing a cross-flow baroclinic pressure gradient whose magnitude usually increases downward. The sea surface tilts upward to the right at the proper angle to cause its barotropic gradient to cancel the baroclinic gradient at the bottom, by assumption, thus causing the velocity to vanish there.

Figure 1.30 shows the geostrophic velocity vectors at 5 m, referred to the bottom, overlaying the density anomaly, σ_t, field. As mentioned above, denser water is on the left of each vector. Seaward of the 100-m isobath, there is strong northwestward flow in all three years. The flow is broader north of the Pribilof Islands in 2008 and 2010. In 2009 the flow is confined more to the 100-m isobath and saltier, denser water (Figure 1.25) has intruded across the shelf where the 100-m isobath bends landward away from the shelf break. South of the Pribilofs is strong flow that may veer offshore at the north wall of

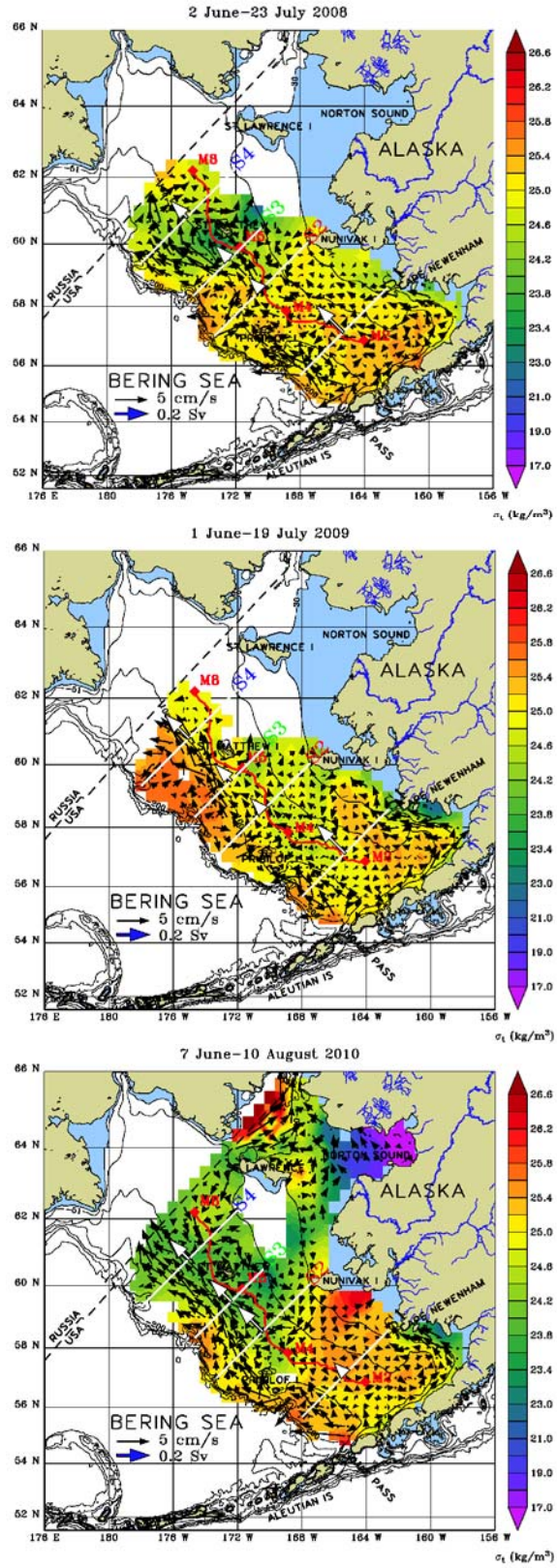

Figure 1.30. Maps of the density anomaly, σ_t, at 5 m with geostrophic velocity vectors referred to the bottom for the 2008, 2009 and 2010 bottom trawl surveys. White arrows represent the net transport across sections S1-S4, and black dots mark the CTD cast sites. The long-term EcoFOCI mooring sites (M2, M4, M5 and M8) and 70-m isobath section are shown in red. Depths are contoured at 30, 50, 100, 200, 500, 1000 and 2000 m.

Pribilof Canyon, but measurements are sparse where the 100-m and 200-m isobaths pinch together. In 2008 and 2010 there is clockwise circulation around St. Matthew Island owing to the low-density water there caused by low salinity in 2008, perhaps due to ice melt, and by high temperature and low salinity in 2010 (Figures 1.24, 1.25 and 1.29). Farther south along the middle shelf, geostrophic flow is weak near moorings M4 and M2. Flow is weak landward of the 50-m isobath and southeast of Nunivak Island, except for a strong coastal jet south of Cape Newenham due to low-salinity, low-density water in Bristol Bay. The bottom trawl survey only sampled north of St. Lawrence Island in 2010, where a strong jet caused by salty Anadyr Water to the northwest flows along the Russia-USA border toward Bering Strait.

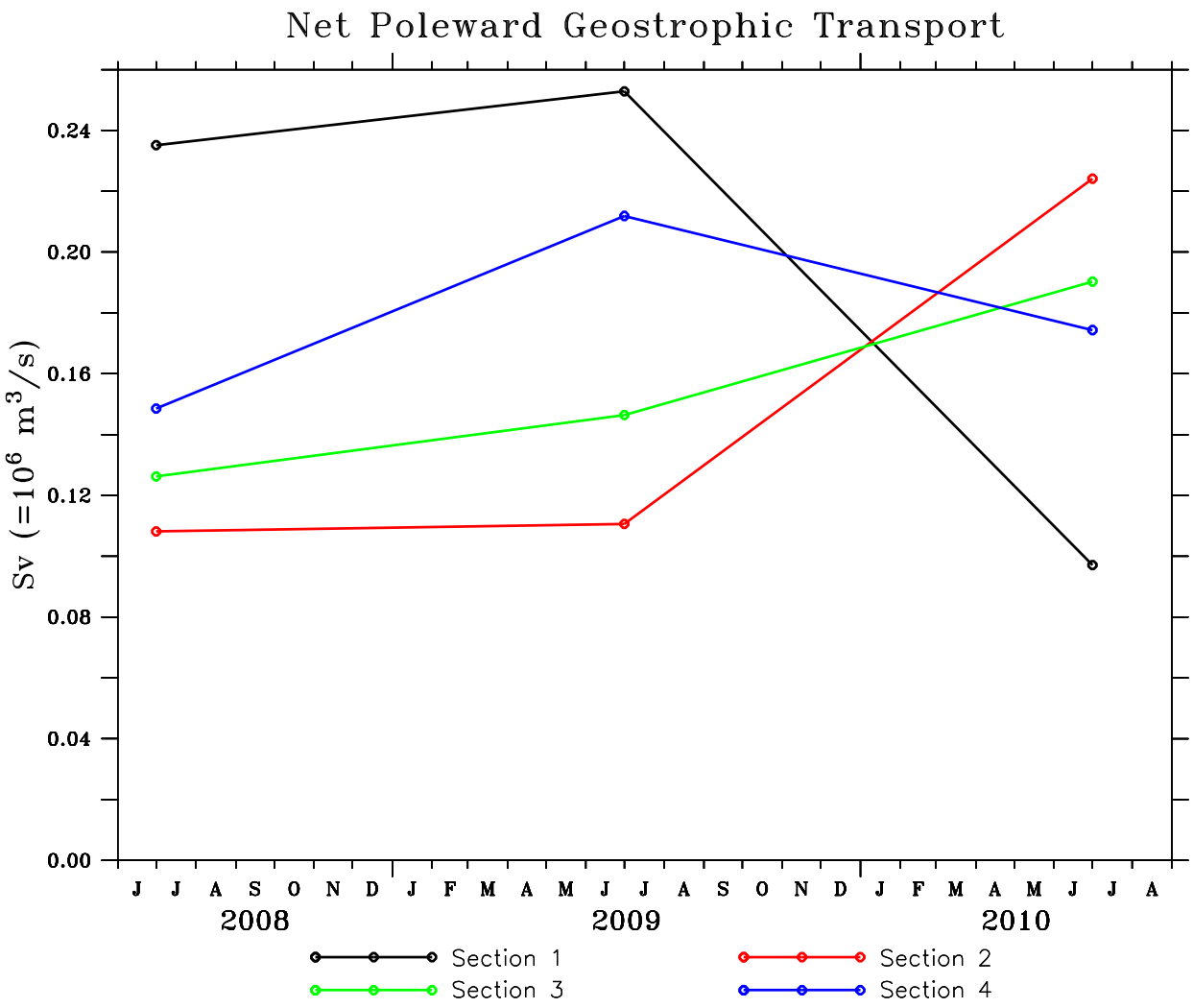

Figure 1.31. Time series of the volume transport through sections S1-S4 as shown in Figure 1.30.

Overall, the bottom-referenced geostrophic flow is northwestward. We define four sections, S1-S4, common to all years and denoted by white lines across the shelf in Figure 1.30. White arrows represent the net poleward volume transport through each section that varied between 0.10 and 0.25 Sverdrups (Sv=10^6 m^3/s). Figure 1.31 displays the volume transport time series. The transport between sections is not conserved because they are open at one (S1 and S2) or both (S3 and S4) ends. The net transport is primarily governed by the flow at their deep, seaward ends. Measurements are few in the deep water between S1 and S2, but we can speculate as to why their ranking order changed dramatically in 2010. In 2008 and 2009, S1 exceeded S2, implying transport off-shelf between the two. 2010 had weak flow south of the Pribilofs through S1 and strong flow through S2, implying transport onto the shelf between them. This could be due to eddies in the Bering Slope Current and merits further investigation (Ladd et al., 2012; Mizobata et al., 2002; Mizobata et al., 2008; Okkonen, 2001).

CONCLUSIONS

This BSIERP project to augment the Bering Sea bottom trawl survey with CTD measurements was very successful. We obtained 990 CTD casts between 2008 and 2010 with no increase in ship-time usage. The nature of the bottom trawl survey, on its regular three-dimensional grid that is occupied in the same way each year, provides a unique data set that is rarely equaled in oceanography. Its grid lends itself to straightforward analysis and interpretation, and has been used for comparison with numerical models, which are often expressed on a grid (Hermann et al., 2014). Results reveal the three-dimensional thermohaline structure of the continental shelf between the 30-m and 200-m isobaths from the Alaska Peninsula to 62°N in 2008-2009 and to 65°N in 2010 (Cokelet, 2014). The sharp temperature gradient between the Cold Pool and the surrounding waters can provide a boundary to fish habitat (De Robertis and Cokelet, 2012). The new measurements give a fuller view of the salinity and density structure on the shelf than those along the 70-m transect alone, or at other widely spaced hydrographic sections. They enable the computation of horizontal gradients that are often strongest roughly along the 50-m and 100-m isobaths that traditionally separate the inner- and outer-shelf from the middle-shelf. A regional view of the summer mixed-layer depth shows it to be less than 30 m over much of the region. It reaches deeper to the bottom along the coast southeast of Nunivak Island in water depths both less and greater than 50 m, implying that the frontal boundary of the well-mixed, inner shelf is not always at the 50-m isobath as had been deduced from scattered, cross-shelf transects. The greatest upper-to-lower layer density difference is found across the shelf north of 59°N, but its horizontal extent was much less in 2009. The temperature difference is the main contributor to the vertical density difference over most of the shelf, but salinity

plays a larger role at times near Unimak Pass, at the shelf-break, around St. Matthew Island and near the coast. Horizontal density gradients give the geostrophic velocity relative to the bottom. Velocity vectors show northwestward flow seaward of the 100-m isobath and northwestward transports integrated across the shelf range from 0.10 to 0.25 Sv. In 2008 and 2010 there was clockwise circulation in a region of less-dense water around St. Matthew Island. In 2009 that less-dense lens did not exist, and flow was concentrated along the 100-m isobath bringing saltier water across the shelf. The CTD measurements have been used to help establish the effects of ocean habitat on the distribution forage fish across the Bering Sea shelf (Hollowed et al., 2012).

ACKNOWLEDGEMENTS

This research was funded in part by the North Pacific Research Board under the Bering Sea Integrated Ecosystem Research Program (BSIERP). We thank the captains and crews of NOAAS *Oscar Dyson,* F/Vs *Aldebaran*, *Arcturus*, *Alaska Knight* and *Vesteraalen* and the fishing vessel owner, Trident Seafoods, Seattle. Tony Jenkins and David Strausz designed and installed the underway seawater sampling systems on *Oscar Dyson* and *Aldebaran*. *Oscar Dyson* Survey Technician Kathy Hough conscientiously looked after the underway sampling system and drew many of the discrete samples for calibration. Various fisheries observers extracted and logged discrete samples on *Aldebaran* during the Pollock A Seasons. The members of NOAA's Alaska Fisheries Science Center (AFSC) Bering Sea bottom trawl survey, led by Robert Lauth, graciously attached the CTDs to their nets, downloaded data daily and looked after the equipment at sea. Dennis Holzer and PMEL's Machine/Fabrication Shop built the CTD polypropylene cases, and AFSC's net shed constructed the net bags. Calvin Mordy, Eric Wisegarver and Fred Menzia analyzed the discrete nitrate and chlorophyll samples, as did Colleen Harpold for chlorophyll. Scott McKeever and Bill Floering analyzed the salinity samples. Various scientists on *Oscar Dyson* cruises took discrete samples and analyzed oxygens at sea. Tiffany Vance provided the positions of the Alaskan rivers. The Ferret program for analysis and graphics was used in this paper **(**http://ferret.pmel.noaa.gov/Ferret/**)**.

Chapter 2: Distribution of Euphausiids and Walleye Pollock

Chapter 2: Overview

To understand the distribution of fish in relation to ocean habitat conditions, we needed to develop better information on both predator and prey distribution. Chapter 2 describes our efforts to describe the spatial and temporal distribution of 1) walleye pollock (*Theragra chalcogramma*), the dominant zooplanktivorous pelagic fish that is important as both predator and prey in the eastern Bering Sea ecosystem, and 2) euphausiids (*Thysanoessa* spp.), a key zooplankton prey for pollock as well as many other species. Survey information on walleye pollock in the eastern Bering Sea has been available for some time from bottom trawl and acoustic surveys, but our project spatially combined data from both of these surveys and analyzed them along with new survey information on euphausiid prey. The new survey information on euphausiids (or "krill") required measurement of the physical properties of euphausiids (their "material properties", the animal's density (g) and sound speed (h) with the surrounding seawater), modeling of the acoustic backscatter from a single euphausiid individual (the "target strength", TS), and a methodology for using these parameters, euphausiid net samples, and backscatter data from the acoustic-trawl pollock survey to estimate euphausiid biomass. In our project, the survey data on pollock and euphausiids were then used to analyze the spatial relationship between predator (pollock) and prey (euphausiids) under the different physical environmental conditions encountered during the study years. Euphausiid and pollock biomass data were also used by other BSIERP projects. Finally, we described the distribution and abundance of several other important classes of acoustic backscatter on the eastern Bering Sea shelf.

The following sections detail the work completed and are organized as follows:

a. Material properties of euphausiids
b. Target strength of euphausiids
c. Abundance and distribution of euphausiids and walleye pollock, 2004-2010
d. Analysis of the spatial relationship between euphausiids and walleye pollock, and implications for top-down vs. bottom up control of euphausiids
e. Description and spatial distribution of other important acoustic classes

Each section includes a brief introduction and citation to the full publication. An overall Conclusions section follows.

Chapter 2.a: Material properties of euphausiids

This section describes measurement and analysis of the physical properties of Bering Sea euphausiids, which was necessary to develop a model of the acoustic backscatter from a single animal (target strength). The material in this section is the work of Smith (MS student in part supported by B62), Ressler (B62 PI), and Warren (scientist supported under contract by B62), and was published as:

Smith, J.N., P.H. Ressler, and J.D. Warren. 2010. Material properties of Bering Sea euphausiids and other zooplankton. Journal of the Acoustical Society of America 128(5): 2664-2680. http://asadl.org/jasa/resource/1/jasman/v128/i5/p2664_s1?isAuthorized=no

ABSTRACT

Acoustic assessment of Bering Sea euphausiids and their predators can provide useful data for ecosystem studies if the acoustic scattering characteristics of these animals are known. The amount of acoustic energy that is scattered by different marine zooplankton taxa is strongly affected by the contrast of the animal's density (g) and sound speed (h) with the surrounding seawater. Density and sound speed contrast were measured in the Bering Sea during the summer of 2008 for several different zooplankton and nekton taxa including: euphausiids (*Thysanoessa inermis, Thysanoessa raschii,* and *Thysanoessa spinifera*), copepods, amphipods, chaetognaths, gastropods, fish larvae, jellyfish, and squid. Density contrast values varied between different taxa as well as between individual animals within the same species. Sound speed contrast was measured for monospecific groups of animals and differences were found among taxa. The range, mean, and standard deviation of g and h for all euphausiid species were: g = 1.001-1.041; 1.018 ± 0.009 and h = 0.990-1.017; 1.006 ± 0.008. Changes in the relationship between euphausiid material properties and animal length, seawater temperature, seawater density, and geographic location were also evaluated. Results suggest that environmental conditions at different sample locations led to significant differences in animal density and material properties.

INTRODUCTION

Zooplankton form a key trophic link between primary producers and higher trophic level consumers in pelagic marine ecosystems (Springer and Roseneau, 1985; Brodeur et al., 2002). Euphausiids, along with more variable contributions from calanoid copepods and juvenile walleye pollock, are the most important prey items for the walleye pollock (*Gadus chalcogrammus*) stock on the Bering Sea shelf (Dagg et al., 1984; Livingston, 1991; Ciannelli et al., 2004). Ecologically, walleye pollock are a keystone species (Springer, 1992) in the Bering Sea and are important prey for northern fur seals and other marine mammals, as well as for foraging fish and seabirds (Coyle et al., 1992;

Sinclair, 1994; Decker and Hunt, 1996). Economically, the pollock fishery is the largest U.S. fishery by mass and makes up over 40% of the global whitefish production (Ianelli et al., 2008). Walleye pollock are broadly distributed throughout the North Pacific, with the largest concentrations found throughout the Eastern Bering Sea (Ianelli et al., 2008). Acoustic surveys along with net trawls are regularly conducted to estimate the abundance and distribution of the walleye pollock population there (e.g., Honkalehto et al., 2009). These survey data sets may also be used to identify and quantify the abundance of some zooplankton taxa.

Acoustic techniques allow scientists to observe the spatial and temporal variability in zooplankton distributions with a greater resolution and broader areal coverage than traditional net sampling. Acoustic surveys using multiple frequencies (e.g. 38, 120, and 200 kHz) have previously been applied to the study of zooplankton in the Bering Sea (Coyle and Pinchuk, 2002, Honkalehto et al., 2002). However, in order for acoustic backscatter measurements to be used as a quantitative tool for studying these populations, it is necessary to have a well-constrained estimate of target strength (TS) to convert acoustic energy into a particular biological metric (e.g. numerical density, animal taxon, biomass; Simmonds and MacLennan, 2005). TS estimates are available for many species including walleye pollock (Traynor, 1996), other commercially-important fish species (Simmonds and MacLennan, 2005), and Antarctic euphausiids (Demer and Conti, 2005), but such estimates do not exist for Bering Sea zooplankton. In the absence of direct measurements, TS can be estimated through the use of acoustic scattering models for zooplankton (see review by Foote and Stanton, 2000). TS is a function of the acoustic frequency and the size, shape, orientation, and material properties of the animal (Stanton and Chu, 2000; Chu et al., 2000; Warren et al., 2002). If more information is known about the physical characteristics of the target, then more accurate scattering model predictions will result in improved acoustic predictions of biological information (Stanton and Chu, 2000).

The two material properties most important to zooplankton scattering model predictions are g, the density contrast between a target and the surrounding seawater, and h, the sound speed contrast between a target and the surrounding seawater (Anderson, 1950). Along with animal length, the density and sound speed contrasts are particularly critical parameters for predicting scattering from crustacean zooplankton because these animals are modeled as weakly scattering fluid-like objects with material properties similar to that of the surrounding seawater. Small changes in these parameters can cause large changes in the predicted scattering from the animal (Stanton et al., 1994; Wiebe et al., 1997; Stanton and Chu, 2000). Modeling by Chu et al. (2000) has predicted up to a 20

dB difference in TS for weakly scattering euphausiid-like zooplankton (g = 1.0357, h = 1.0279) with only a 2 -4 % change in g and h. Relatively few studies have measured the material properties of specific zooplankton taxa. The available data show that g and h vary significantly among different types of zooplankton (Greenlaw and Johnson, 1982; Foote et al., 1990; Chu and Wiebe, 2005; Warren and Smith, 2007), as well as within the same zooplankton taxon from individual to individual (Forman and Warren, 2009), between geographic regions, and through time both seasonally and as the organisms age (Hagen et al., 1996; Køgeler et al., 1987). For each geographical area under study, it would be ideal to measure parameters such as animal length and material properties of living specimens from different zooplankton groups for use in these scattering models. This study measured the physical characteristics and material properties of several types of zooplankton from the Bering Sea during the summer of 2008. Animals were grouped into different taxonomic categories for analysis of their size and material properties and the ranges in g and h values for each zooplankton taxon were measured. These taxa included *Thysanoessa raschii* and *Thysanoessa inermis*, the two euphausiid species that dominate zooplankton biomass in the Bering Sea (Smith, 1991), along with a less dominant euphausiid species, *Thysanoessa spinifera*. Several other zooplankton taxa were collected and studied including: copepods (*Neocalanus sp.*), amphipods (*Themisto libellula*), chaetognaths (*Sagitta sp.*), gastropods (*Clione limacina*), larval fish (*Gadus chalcogrammus*), and jellyfish (*Chrysaora melanaster* and an unidentified species, possibly *PoIyorchis penicillatus*). One nektonic taxon, a squid of the family Gonatidae (species undetermined), was also collected and the material properties of some of their body parts were measured. Although squid are not zooplankton, they are often present in the water column and can be significant scatterers of acoustic energy (Greenblatt, 1981; Brierley and Watkins, 1996). Material properties of euphausiids and copepods were compared to previous measurements of these zooplankton in the Barents Sea and elsewhere (Greenlaw and Johnson, 1982; Køgeler et al., 1987; Foote, 1990; Chu and Wiebe, 2005). We also examined the influence on g from animal length, environmental factors (such as seawater temperature and salinity), geographic location, and food availability as measured by fluorescence.

METHODS

Zooplankton collection and husbandry

Live zooplankton were collected using a Methot trawl (MT) at nine stations sampled during an acoustic-trawl pollock survey in the Bering Sea aboard the NOAA ship *Oscar Dyson* from 20 June to 09 July 2008 (Honkalehto et al., 2009; Fig. Ch2.a.1). The Methot trawl is a rigid frame trawl with a mouth area

of 5 m^2, 2 mm by 3 mm oval mesh in the body of the net, and 1 mm mesh in the hard codend (Methot, 1986). In order to obtain live specimens in a minimally-stressed, healthy condition and to maximize the number of animals captured, short duration (average 4.5 min) and shallow (average maximum depth 12.1 m) hauls were conducted at night when zooplankton aggregations in surface waters were expected to be abundant. Upon retrieval of the net, the contents of the codend from each tow were immediately transferred to a large container (~ 100 L) containing surface seawater. The taxa collected in the Methot trawls included euphausiids, copepods, amphipods, chaetognaths, gastropods, fish larvae, and jellyfish. All zooplankton (or a subset consisting of the mostly healthy animals depending on the number of animals caught) were then sorted by hand into smaller containers (2 or 34 L) by taxon. They were kept alive until measurements of the physical characteristics and material properties could be made. Animal density measurements were typically made within 6 hours (and all measurements were made within 48 hours) of being collected.

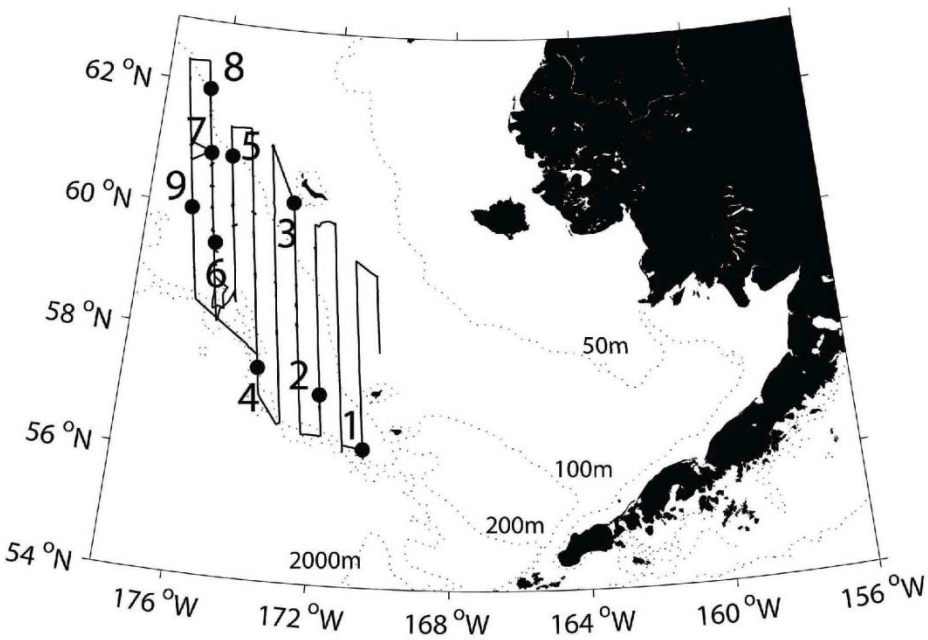

Figure Ch2.a.1. Cruise trackline (solid line) of the NOAA Ship *Oscar Dyson* from 20 June to 09 July 2008. Methot trawl locations are identified (filled circles) and numbered. Bathymetry contours (dotted lines) are shown for 50, 100, 200, and 2000 m.

In addition to the Methot trawl sampling, animals collected in large mid-water trawls conducted as part of the pollock survey (an Aleutian Wing trawl with a mouth area of about 650 m^2; Honkalehto et al., 2002) were also used in this study. While some jellyfish were caught in the Methot trawl, large jellyfish (e.g., *Chrysaora melanaster* with bell diameters ranging from 15 to 24 cm) and squid specimens were caught in

the mid-water trawl nets, along with pollock and other large nekton. Both the large jellyfish and squid specimens were alive and moving when brought onboard the vessel and were placed in containers (~ 10 L) of seawater. Unlike the zooplankton captured by the Methot trawl, these animals were likely traumatized or damaged by the net tow collection process. Due to the size of these animals, material property measurements were made on excised parts.

Measurements were taken for a variable number of animals from each taxon depending on the number of animals caught and sorted from each tow. For example, a typical tow contained several hundred to thousands of euphausiids and copepods, while ten to fifty animals from the other taxa were collected. Measurements on individual animals included: species identification (when possible), animal length and width, and animal density (*P*). Measurements on groups of animals from each taxon included sound speed contrast (*h*). Animals used for the density measurements were separated by taxon and placed into large (34 L) and small (2 L) aerated plastic tanks containing pumped, ambient surface seawater (average temperature 4 °C) in a controlled environment room (air temperature ranging from 2.7 -7.2 °C). The large containers held euphausiids and copepods, while the small containers held amphipods, chaetognaths, gastropods, fish larvae, and jellyfish. Animals used in the sound speed experiments were placed in small (2 L) tanks with ambient surface seawater and were then transferred into the chamber used for the *h* measurements shortly after the sorting process was completed. The temperature and salinity of the surrounding seawater in the tanks were recorded for each experiment.

Length measurements

Animal lengths were measured for a subsample of animals collected by each Methot trawl. Every animal that had its density measured also had its length recorded. Organisms from a separate subset of animals from each MT had both their lengths and widths measured. Euphausiid lengths were measured from the front of the eye to the end of the telson with the animal positioned as straight as possible. Lengths measured for other zooplankton taxa were total lengths in which the animal was positioned as a straight as possible. Length and width are input variables used in many target strength models (Stanton and Chu, 2000). The relationship between animal length and *g* was evaluated through linear regressions for those taxa in which *g* was measured for the entire animal (as opposed to pieces of the animal) and there were a sufficient number of animals collected.

Material properties measurements

Density

The density (*P*) of individual animals from each taxon was measured and the density of the surrounding seawater was calculated from the temperature and salinity measurements. These values were then used to

calculate the density contrast (*g*). Animal density was measured for the following: euphausiids, copepods, amphipods, chaetognaths, gastropods, fish larvae, jellyfish and squid body parts. Density measurements for most taxa were made on live organisms, so their movement had to be suppressed in order to accurately monitor any changes in buoyancy. Individual zooplankton were placed in a small container holding approximately 50 ml of seawater and 1 drop of clove oil until they stopped moving. Density measurements for fish larvae and most jellyfish were not conducted on live animals; however, the measurements were taken shortly after their death. Fish larvae typically did not survive the Methot trawl, while large jellyfish (*Chrysoara melanaster*) had to be cut into small pieces in order to fit into the equipment used to measure animal density. For squid, separate density measurements were recorded for different parts of the body (mantle, pen, beak) after each part was removed from the rest of itself. Beaks were stored in seawater while the pens and mantle pieces were frozen. The density of all three body parts of the squid were measured separately in the laboratory after the cruise. In the cases where live animals of a taxon were not measured, we assume that any changes in density as a result of decomposition or time elapsed between capture and measurement were negligible (except where noted for the squid specimens).

Two different methods were used to measure the density of an animal: the titration method onboard the ship and the pipette method on land. The titration method (Warren and Smith, 2007) for all density measurements, except those of squid material, involved placing the animal in a beaker containing a known volume of ambient sea water (V). A solution of higher-salinity seawater was created by dissolving Instant Ocean (Aquarium Systems, Inc., Mentor, OH) into ambient seawater. This saltier water was then titrated into the beaker until the buoyancy of the animal was altered and the animal began to rise. The volume of the hypersaline solution required to make the animal float was recorded (V_{hs}). For some individual animals that were positively buoyant, fresh water was titrated into the container until the buoyancy of the animal changed and the animal began to sink. Prior to each measurement, the temperature, salinity, and conductivity of the water were recorded (YSI 65, YSI Incorporated). The temperature and salinity of the ambient, fresh, and hypersaline seawater solutions were used to calculate the solution density using the CSIRO MATLAB Seawater Library. With the information collected, the density of the individual animal was calculated based on the following equation:

$$\rho_{animal} = \frac{\rho_{sw} V_{sw} + \rho_{hs} V_{hs}}{V_{sw} + V_{hs}} \quad , \qquad (1)$$

where p is the density of seawater (g ml^{-1}), V is the volume of seawater water used initially to hold the organism (ml), p is the density of the solution (g ml^{-1}), and V is the volume of solution used in the titration (ml). Once the density of the animal was measured, *g*, the ratio of the animal density to the

density of the seawater, was calculated using the following equation:

$$g_{animal} = \frac{\rho_{animal}}{\rho_{sw}} \quad . \qquad (2)$$

The maximum potential error that can result from calculating animal density has previously been estimated for material property measurements of different zooplankton species collected from Antarctic waters (Chu and Wiebe, 2005). The maximum potential error associated with the equation used to calculate the density of Bering Sea euphausiids (Eq. 1) was also estimated with the equation:

$$\delta\rho_{animal} = \left(V_{sw}\frac{\rho_{sw}}{V_{sw}+V_{hs}}\right)\left(\frac{\delta V_{sw}}{V_{sw}} + \frac{\delta\rho_{sw}}{\rho_{sw}} + \frac{\delta V_{sw}+\delta V_{hs}}{V_{sw}+V_{hs}}\right)$$

$$+\left(V_{hs}\frac{\rho_{hs}}{V_{sw}+V_{hs}}\right)\left(\frac{\delta V_{hs}}{V_{hs}} + \frac{\delta\rho_{hs}}{\rho_{hs}} + \frac{\delta V_{sw}+\delta V_{hs}}{V_{sw}+V_{hs}}\right) \quad . \qquad (3)$$

The estimated uncertainty of the instrumentation for each parameter was $op_{sw} = 4x10^{-5}$ g ml^{-1}, $\delta\rho_{hs} = 4x10^{-5}$ g ml^{-1}, $\delta V_{sw} = 0.05$ ml and $\delta V_{hs} = 0.05$ ml. The maximum potential error for the animal density was, $\delta\rho_{animal} = 0.0129$. As the name implies, the maximum potential error gives the greatest possible value of error, however this value is likely to be an overestimation if the uncertainty from the instrumentation is independent and random, as it is in this study. Therefore, a more realistic estimate of the combined uncertainty can be made through quadrature addition. This error analysis technique is based on the principle that measurements from two independent instruments (for example, x and y) will have a normal distribution (thus, an associated σ_x and σ_y) around their true value (X and Y). The associated error from summing x and y would then be governed by statistical rules and be described by sqrt[$(\sigma_x)^2 + (\sigma_y)^2$ 1] (Taylor, 1982). Applying the quadrature technique to Eq. 1, the error estimated through quadrature was calculated using Eq. 4:

$$\delta\rho_{animal} = \rho_{animal}\sqrt{\left(\frac{\rho_{sw}}{V_{sw}\rho_{sw}+V_{hs}\rho_{hs}} - \frac{1}{V_{sw}+V_{hs}}\right)^2 \delta V_{sw}^2 + \left(\frac{V_{sw}}{V_{sw}\rho_{sw}+V_{hs}\rho_{hs}}\right)^2 \delta\rho_{sw}^2}$$

$$\cdot\sqrt{+\left(\frac{\rho_{hs}}{V_{sw}\rho_{sw}+V_{hs}\rho_{hs}} - \frac{1}{V_{sw}+V_{hs}}\right)^2 \delta V_{hs}^2 + \left(\frac{V_{hs}}{V_{sw}\rho_{sw}+V_{hs}\rho_{hs}}\right)^2 \delta\rho_{hs}^2} \qquad (4)$$

The estimated uncertainty for each parameter remained the same for both error analysis equations, ($\delta\rho_{sw} = 4x10^{-5}$ g ml^{-1}, $\delta\rho_{hs} = 4x10^{-5}$ g ml^{-1}, $\delta V_{sw} = 0.05$ ml and $\delta V_{hs} = 0.05$ ml), however the calculated error

through quadrature was approximately two orders of magnitude lower than the error calculated using the maximum potential error equation and had a value of $\delta\rho_{animal_quad} = 1.1721 \times 10^{-4}$. Since the error estimated through quadrature was small, fluctuations in the *g* measurements were likely the result of variability from animal to animal instead of error from the instrumentation. The titration method was used to measure the density of squid beak pieces, but instead of a hypersaline solution being used as the titrant, glycerine ($\rho = 1.173$ g ml^{-1}) was used since the beaks were substantially more dense than the hypersaline solution. Squid beaks were excised from the surrounding tissue, stored in seawater, and brought back to the laboratory. There was no visible deterioration or dissolution of the squid beaks from when they were collected and when they were measured. The jaw was divided into top and bottom portions and the density of each piece was measured. Two measurements were taken for each squid beak piece and the mean percent difference between the trials was 0.46 %. We had hoped to also measure the density of the squid pen in addition to the beak and mantle; however, the pens deteriorated even more than the squid mantle by the time the density measurements were taken, so no results for the pens are reported.

The pipette method (Warren and Smith, 2007; Forman and Warren, 2009) was used to measure squid mantle density, since this material was too dense to be properly measured using the titration method. Squid mantles were cut into multiple pieces which were frozen, transferred back to the laboratory, then thawed. The mass of a piece of mantle was measured after excess water had been removed and then the tissue was placed in a graduated cylinder containing a known volume of seawater. The amount of water displaced by the mantle was extracted and weighed. The density of the mantle was calculated using the following equation:

$$\rho_{animal} = \frac{m_a}{\left(\frac{m_d}{\rho_{sw}}\right)} \quad , \qquad (5)$$

where m_a is the mass of the animal (*g*); m_d is the mass of water displaced by the organism (*g*), and ρ_{sw} is the density of the seawater (g ml^{-1}). The density of each mantle piece was measured twice and the mean percent difference between trials was 1.55%. Similar to the titration method, *g* was calculated using Eq. 2. As the squid mantle measurements were made on frozen and thawed samples, the mantle was slightly deteriorated by the time the measurement was taken. Considering the interest in material properties of squid (Kang et al., 2004), we present these data with the caveat that our measurements may be biased due to degradation of the tissue.

Sound speed

The sound speed contrast (*h*) was measured for euphausiids, copepods, jellyfish, amphipods, and gastropods. Animals were placed in a small chamber (PVC t-tube), with a volume of either 26 or 84 ml depending on the size and number of the animals being measured. Two 500 kHz transducers (one transmitter, one receiver) were clamped on either end of the containers. The time it took for a sound wave to travel from one end of the container to the other was recorded when the compartment contained only seawater and when it was full of a mixture of zooplankton and seawater. Knowing the difference in travel time, along with the container volume and zooplankton volume, *h* (the ratio of sound speed through zooplankton tissue (c) compared to sound speed through seawater (c)) was calculated with the following equation:

$$h=\frac{c_a}{c_{sw}}=1+\frac{\Delta t}{\Phi t_d} \quad , \qquad (6)$$

where Δt is the travel time difference between two received waveforms (one waveform where the chamber was filled with animals and one waveform where the chamber was only filled with seawater), < is the volume fraction (< = V_{animal}/V_{tube} where V_{animal} is the volume (ml) of the zooplankton and V_{tube} is the volume (ml) of the PVC-tube chamber), and t_d is the travel time (s) of sound from transducer to receiver with an empty chamber (Greenlaw and Johnson, 1982; Køgeler et al., 1987; Chu et al., 2000; 265 Chu and Wiebe, 2005; Warren and Smith, 2007). The animal volume (V_{animal}) was measured using the animal displacement method in which a known volume of water filled the chamber, animals were then placed inside the chamber, and the volume of water displaced by the animals was measured. The maximum potential error attributed to the instrumentation was estimated from Eq. 6 using the following:

$$\delta h_{max}=h\left(\frac{\delta\Delta t}{\Delta t}+\frac{\delta\Phi}{\Phi}+\frac{\delta t_d}{t_d}\right) \quad , \qquad (7)$$

while the error estimated through quadrature was calculated with:

$$\delta h_{quad}=\sqrt{\left(\frac{1}{\Phi t_d}\right)^2\delta\Delta t^2+\left(\frac{-\Delta t}{t_d\Phi^2}\right)^2\delta\Phi^2+\left(\frac{-\Delta t}{\Phi t_d^2}\right)^2\delta t_d^2} \quad . \qquad (8)$$

The uncertainties corresponding to each variable were estimated as $\delta\Phi = 0.04$, $\delta\Delta t = 5.44\text{x}10^{-8}$ s, and $\delta t_d = 1.62\text{x}10^{-7}$ s. The volume fraction uncertainty was estimated using the uncertainty of the graduated cylinder used to measure the volumes of the animals and chamber (0.5 ml). The typical volume of animals in the chamber was 20 ml which results in an uncertainty in the volume fraction of 0.04. The uncertainty of t was determined from the resolution of the cross correlation technique used to determine the time shift in the two waveforms. The uncertainty of td was the difference between the maximum and minimum time delay for the transmitted waveform as it traveled from transmitter to receiver for each trial. The maximum potential error calculated for all zooplankton groups was $\delta h_{max} = 0.1922$ while the error calculated through quadrature was $\delta h_{quad} = 1.5\text{x}10^{-3}$. Similar to the error analysis used for *g*, the maximum potential error calculated for *h* was likely to be an overestimate of the true error since the uncertainties of each parameter were independent and random. Thus, a more reasonable estimate of our measurement uncertainty was obtained from the quadrature method using Eq. 8.

The criteria for determining which zooplankton groups would be measured for *h* depended on the volume of each zooplankton group caught in the net tow. The volume of zooplankton had to be enough to fill (or nearly fill) the measurement chamber in order to get an accurate measurement of sound speed contrast.

Other parameters measured

Biomass Density

The wet weight of all zooplankton collected by each Methot trawl (MT) was measured and the total volume of water filtered by the MT was calculated by multiplying the area of the opening of the MT and the distance sampled. Both the wet weight and total volume filtered were used to calculate zooplankton biomass density (g m^{-3}).

Environmental variables

Animal density contrast is a function of both the density of the animal and the density of the surrounding seawater. Since both temperature and density vary vertically and horizontally (e.g., across frontal regions) in the ocean, changes in *g* as a function of these parameters were examined. The average water temperature of the containers holding zooplankton was 4 °C. Several experiments were conducted in which this temperature was manipulated to see if it affected the animal density contrast (*g*). Water temperature was cooled by placing the container with the live animals in an ice bath. Subsequently, temperatures warmed naturally through time as the water adjusted to the surrounding air temperature. Water temperatures ranged from 0.6 °C to 6.3 °C, which lies within the range of water temperatures that

zooplankton may experience throughout the year within the Bering Sea (Coyle et al., 2008). Experiments in which water temperature was manipulated were conducted only for euphausiids since they were the main zooplankton group of interest and most common animal in the Methot trawl catches. We also recorded the changes that occurred in the salinity and density of the water the euphausiids were kept in over the course of the experiments. The influence of ambient water conditions (temperature, salinity, and density) on *g* was evaluated. Chl-a fluorescence data were collected from a WETStar (WETLabs) sensor on a ConductivityTemperature-Depth (CTD) rosette deployed at multiple stations during the cruise. Seven of the MT locations (MT01, MT02, MT04, MT05, MT07, MT08, MT09, Fig. 1) had CTD profiles conducted either immediately before or after the MT, while two MT locations (MT03, MT06) did not. Chlorophyll-a (chl-a) concentration (mg m^{-3}, based on a factory calibration of chl-a fluorescence from the WETStar sensor) was used as a proxy of zooplankton prey (phytoplankton) at each location. Pearson correlations were computed between euphausiid *g* and the chl-a concentration at the water depth from which the zooplankton were collected. Pearson correlations were also computed between *g* and the integrated chl-a over the entire water column.

Statistical analysis

Since the variables that potentially have an effect on *g* may also be inter-related, a principal component analysis was performed in order to reduce the variables with redundant behavior into several factors which account for the variance in the observed data. The relationships among variables and between groups of variables and *g* were also explored. Secondly, a linear regression was performed to evaluate the effect of length on *g*. Finally, factorial ANOVAs were used to determine whether or not particular variables affected *g* by themselves or whether or not those variables interacted with one another to simultaneously affect *g*.

RESULTS

Total zooplankton biomass density in Methot catches varied from 2.5 g m^{-3} (MT04, the largest value observed) to 0.03 g m^{-3} and 0.05 g m^{-3} (MT06 and MT07, respectively) and were dominated by euphausiids, copepods, and parts of gelatinous zooplankton. Not all taxa were collected at each station; of all the zooplankton taxa that were collected and measured (Fig. Ch2.a.2) euphausiids were most common and present in all MTs. However, the relative abundance of the three euphausiid species differed with location (Fig. Ch2.a.3). The two dominant euphausiid species were *T. inermis* and *T. raschii*, while *T. spinifera* were only present in MT04.

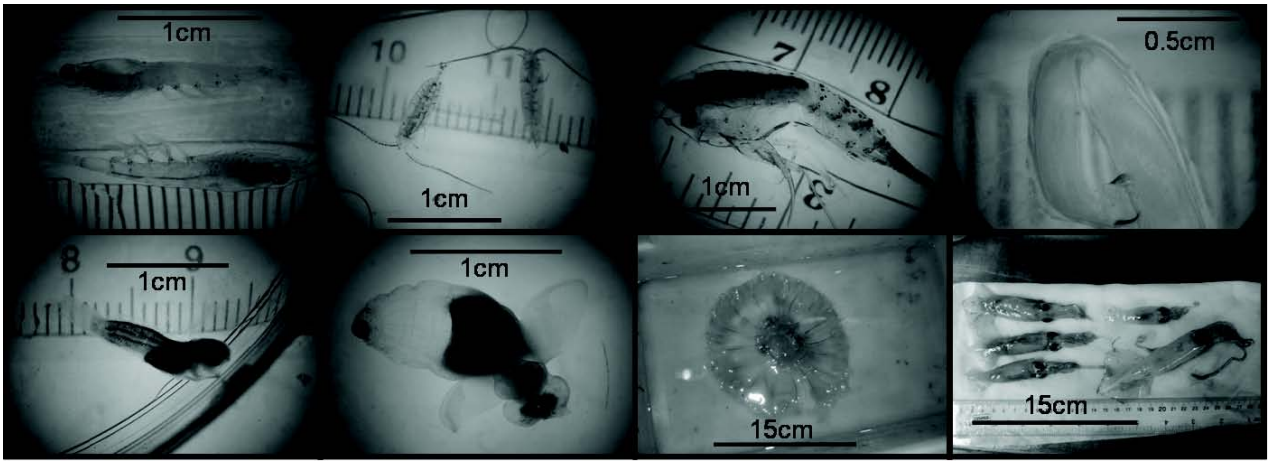

Fig. Ch2.a.2. (Color online) Representative photographs of taxa collected and measured for their material properties. Top row (from left to right): euphausiid, copepod, amphipod, chaetognath. Bottom row (from left to right): fish larvae, gastropod, jellyfish, squid.

The average and standard deviation of *g* and animal length for euphausiids were calculated for each species; whereas the average and standard deviation of *h* were calculated for each MT (Table 1). Environmental parameters measured for the ambient water the euphausiids were kept in during the experiments (a function of both natural environment and experimental manipulation; Table 1), and for the water column at each location were also reported (Table 2). These data are representative of environmental conditions and material properties for euphausiids during summer in the Bering Sea.

Length distributions

Animal lengths varied both within and between different taxa (Table 3). There were a sufficient number of specimens to determine the length distribution for euphausiids, copepods, and amphipods. The length distributions of euphausiids (for all species combined and each separate species) were roughly similar, with smaller animals being more abundant than larger animals (Fig. Ch2.a.4, Table 3). The mean length (mm) and standard deviation (sd) for all euphausiid species combined as well as for each species was as follows: all (18.2 ± 5.0), *T. inermis* (19.2 ± 2.4), *T. raschii* (17.2 ± 2.5), and *T. spinifera* (20.6 ± 2.4). The length distribution of copepods was also unimodal with a mean and standard deviation of 8 ± 0.45 mm, although the range in lengths was much narrower compared to euphausiids.

TABLE 1. Mean and standard deviation (sd) of material properties, physical features, and environmental variables for euphausiids at each MT. Density contrast (g) values are presented for all euphausiid species combined as well as for each individual species. The sd for all water density measurements was negligible (0.001). The average volume fraction (<) of the chamber used for the *h* measurements is also reported for each MT.

MT	Taxonomic group	Animal length (mm)		Density contrast		Sound speed contrast (*h*)	Temperature (°C)	Salinity (ppt)	Water density (g ml^{-1})	Φ
		length	n	*g*	n					
MT01	all euphausiids	19.6 ± 9.1	94	1.005 ± 0.002	61	1.008	4.4 ± 2.4	32.1 ± 0.1	1.025	0.94
	T. inermis	20.1 ± 2.5	53	1.006 ± 0.002	29					
	T. raschii	18.7 ± 1.8	41	1.004 ± 0.002	15					
MT02	all euphausiids	20.4 ± 2.5	104	1.007 ± 0.005	54	1.002	5.5 ± 0.5	32.9 ± 0.5	1.026	1.00
	T. inermis	20.3 ± 2.6	65	1.007 ± 0.005	38					
	T. raschii	20.6 ± 2.1	39	1.009 ± 0.005	16					
MT03	all euphausiids	15.3 ± 1.7	117	1.019 ± 0.007	67	0.996	4.7 ± 0.8	30.4 ± 0.4	1.024	0.63
	T. raschii	15.3 ±1.7	117	1.019 ± 0.007	67					
MT04	all euphausiids	20.0 ± 3.3	118	1.017 ± 0.007	58	1.006	4.0 ± 1.3	33.4 ± 0.9	1.026	0.94
	T. inermis	19.4 ± 1.3	31	1.018 ± 0.004	20					
	T. raschii	19.0 ± 1.0	8	1.016 ± 0.003	3					
	T. spinifera	20.5 ± 2.4	76	1.017 ± 0.005	32					
MT05	all euphausiids	16.3 ± 1.3	122	1.024 ± 0.006	72	1.012	4.1 ± 2.0	33.0 ± 1.2	1.026	0.85
	T. raschii	16.3 ± 1.3	122	1.024 ± 0.006	72					
MT06	all euphausiids	17.5 ± 1.4	98	1.023 ± 0.006	48	n/a	3.9 ± 2.6	33.2 ± 1.4	1.026	n/a
	T. raschii	17.5 ± 1.4	98	1.023 ± 0.006	48					
MT07	all euphausiids	16.9 ± 1.1	62	1.027 ± 0.003	12	0.990	4.9 ± 0.0	32.7 ± 0.0	1.027	0.77
	T. raschii	16.9 ± 1.1	62	1.027 ± 0.003	12					
MT08	all euphausiids	19.1 ± 3.0	98	1.022 ± 0.008	48	1.006	3.3 ± 2.4	34.5 ± 0.3	1.027	0.71
	T. inermis	17.9 ± 2.2	14	1.018 ± 0.006	10					
	T. raschii	19.4 ± 3.1	83	1.024 ± 0.008	38					
MT09	all euphausiids	19.0 ± 2.3	77	1.019 ± 0.006	27	1.014	2.6 ± 2.2	32.1 ± 0.4	1.026	1.00
	T. inermis	18.8 ± 1.9	36	1.016 ± 0.004	17					
	T. raschii	19.3 ± 2.8	41	1.024 ± 0.005	10					

TABLE 2. Average water column properties for MT stations, based on nearby CTD casts. No data were available for MT03 and MT06.

Location	Top 5 m water temperature (C)	Average water column temperature (C)	Average water column salinity (ppt)	Average water column density (kg m^3)	Average water column chlorophyllla (mg m^{-3})
MT01	5.8	3.8	32.3	25.9	4.0
MT02	5.4	3.4	32.4	26.1	3.1
MT04	6.3	3.5	32.8	25.7	6.0
MT05	5.5	-0.4	32.0	26.1	3.6
MT07	5.3	0.3	32.1	26.0	1.8
MT08	5.7	0.1	32.1	26.0	3.0
MT09	3.9	0.8	32.4	26.3	1.7

TABLE 3. Range, mean, and standard deviation (sd) of animal length, density contrast (*g*), and sound speed contrast (*h*) for different zooplankton taxa; regardless of location. The number of animals measured (n) for *g* from each taxon is also presented along with the number of animal groups (nn) for which *h* was measured. The volume fraction (<) of animals relative to the chamber used for the *h* measurements is averaged for each zooplankton taxon. Data presented for *Chrysaora melanaster* is from pieces of their bell, not the whole animal.

Zooplankton taxon	n	**Animal length (mm)**		**Density contrast (*g*)**		**nn**	**Sound speed contrast (*h*)**		
		Range	**Mean ± sd**	**Range**	**Mean ± sd**		**Range**	**Mean ± sd**	**Φ**
Euphausiids (all species)	448	12 to 27	18.2 ± 5.0	1.001 to 1.041	1.018 ± 0.009	12	0.990 to 1.017	1.006 ± 0.008	0.88
T. inermis	114	15 to 26	19.2 ± 2.4	1.001 to 1.027	1.011 ± 0.007	n/a	n/a	n/a	n/a
T. raschii	282	12 to 27	17.2 ± 2.5	1.001 to 1.041	1.021 ± 0.008	n/a	n/a	n/a	n/a
T. spinifera	32	17 to 27	20.6 ± 2.4	1.004 to 1.029	1.017 ± 0.005	n/a	n/a	n/a	n/a
Copepods	90	7 to 9	8.0 ± 0.45	0.995 to 1.015	1.005 ± 0.006	3	1.003 to 1.010	1.007± 0.004	0.88
Amphipods (all)	66	8 to 32	21.3 ± 8.3	1.001 to 1.029	1.010 ± 0.006	n/a	n/a	n/a	n/a
Small (<20 mm)	22	8 to 14	10.0 ± 1.7	1.001 to 1.009	1.005 ± 0.002	n/a	n/a	n/a	n/a
Large (>20 mm)	44	23 to 32	26.9 ± 2.4	1.002 to 1.029	1.013 ± 0.006	3	0.990 to 1.007	1.001 ± 0.009	0.59
Chaetognaths	14	13 to 35	25.6 ± 6.4	1.007 to 1.026	1.014 ± 0.007	n/a	n/a	n/a	n/a
Gastropods	17	9 to 23	14.9 ± 4.1	1.008 to 1.031	1.016 ± 0.006	1	n/a	1.008 ± 0.0	0.88
Fish larvae	15	20 to 33	23.8 ± 3.3	1.008 to 1.039	1.023 ± 0.008	n/a	n/a	n/a	n/a
Jellyfish (all)	40	20 to 95	49.0 ± 25.3	1.001 to 1.006	1.003 ± 0.001	n/a	n/a	n/a	n/a
Chrysaora melanaster	36	35 to 95	53.0 ± 28.0	1.001 to 1.006	1.003 ± 0.001	8	0.996to 1.007	1.002 ± 0.004	0.97
unidentified	4	21 to 31	24.0 ± 4.5	1.004 to 1.005	1.005 ± 0.001	n/a	n/a	n/a	n/a
Squid beak	30	25 to 17	5.0± 3.1	1.125 to 1.180	1.149 ± 0.013	2	1.010	1.010 ± 0.0	0.51

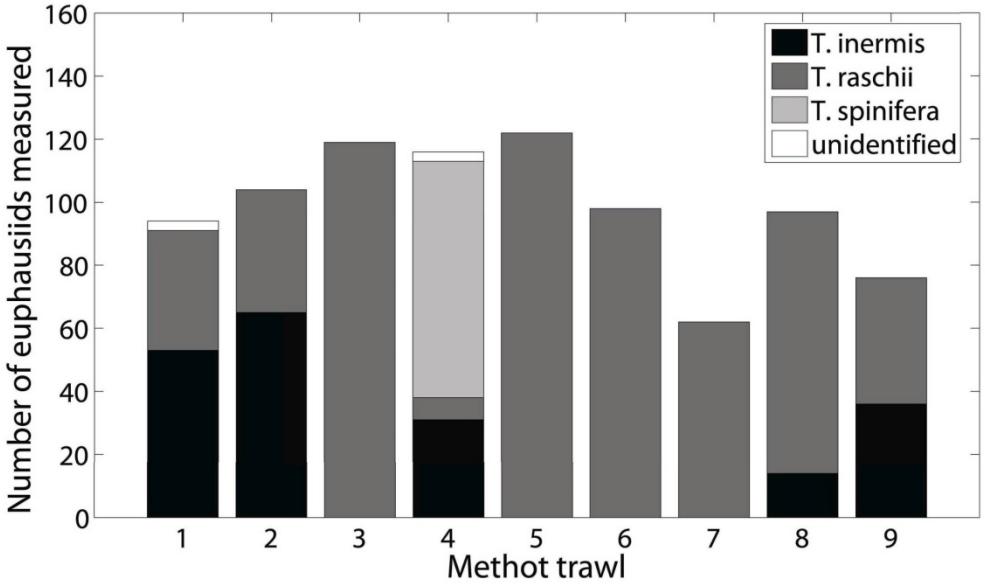

Fig.Ch2.a.3. Species composition of euphausiids caught in Methot trawls that were measured for their 955 physical (length) or material (*g*, *h*) properties.

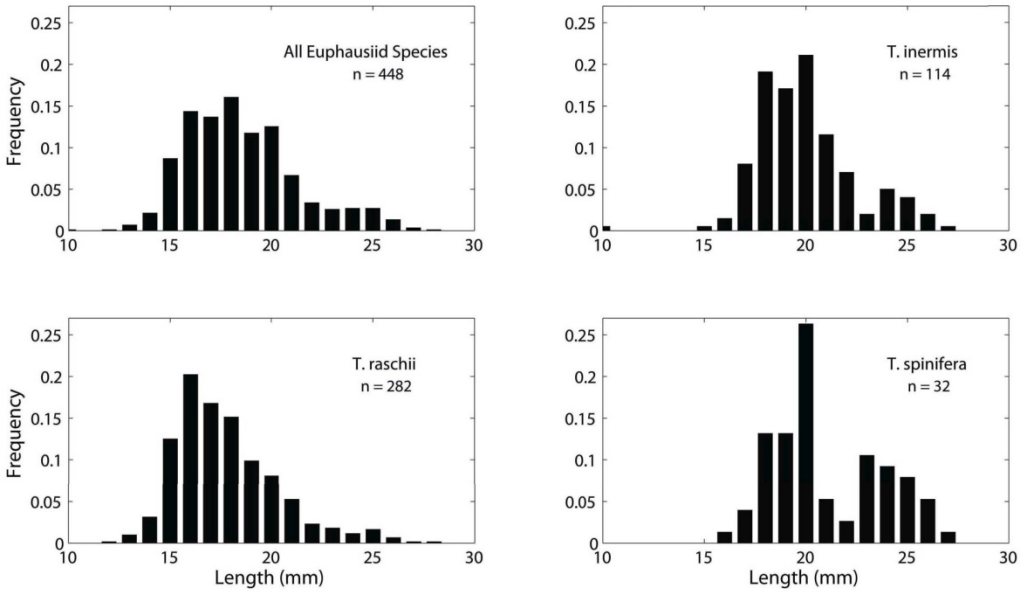

Fig.Ch2.a.4. Length-frequency distributions for all euphausiids (upper left), *T. inermis* (upper right), *T. raschii* (lower left), and *T. spinifera* (lower right).

The length distribution of amphipods was bimodal. There were two size classes of amphipods: small (20 mm) and large (>20 mm). Amphipods were found only in MT05 and MT08. With the exception of one animal, all of the small amphipods were collected from MT05 while large amphipods were collected at both MT05 and MT08. The bell diameter of the larger jellyfish species (*Chrysaora melanaster*) ranged from 150 to 240 mm with a thickness of 15 to 30 mm. They were drastically larger than the smaller, unidentified jellyfish (a bell-shaped hydromedusae) which had a bell diameter ranging in length from 20 to 31 mm with a bell thickness ranging from 5 to 9 mm.

Density

The density contrast varied among and within the different taxa (Fig. Ch2.a.5). A more detailed examination of the density contrast results for each taxon is presented below.

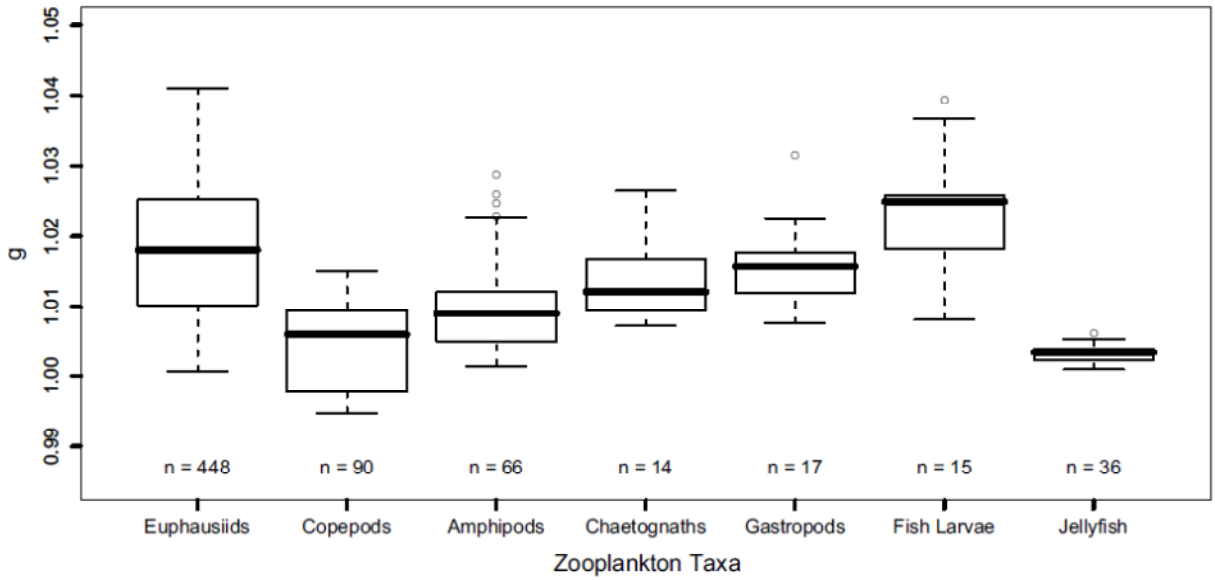

Fig.Ch2.a.5. Density contrast of each zooplankton taxon. The lower line of the box represents the 1st quartile, the thick black line is the median, and the upper line of the box is the 3rd quartile while the whiskers are the maximum and minimum values. Circles represent outliers. The zooplankton taxa are all fluid-like and subsequently have lower values of *g*. Euphausiids have the largest range in *g* values while jellyfish (data from two species combined) have the smallest range in *g* values.

Euphausiids

Euphausiids were collected at all MT stations and the densities of 448 euphausiids were measured. As a group (all species), *g* ranged from 1.001 to 1.041 with a mean and sd of 1.018 ± 0.009 (Table 3). Pairwise scatter plots suggest a positive relationship between location (MT) and both *g* and the animal density for all euphausiids: both *g* and animal density increased in samples taken further to the west (Fig. 1, Fig. Ch2.a.6). Similarly, we also examined the effects of temperature, salinity, and density of the water in which the animals were kept during the experiments on *g* (Table 1, Fig. Ch2.a.7); however, the relationships were weak for these variables. A principal component analysis (PCA) examined variation among these explanatory variables: MT, species, animal length, temperature, salinity, and water density. The PCA was conducted using only euphausiids with data for all variables, thus only 429 animals were used. The components were orthogonally rotated so correlations between the variables and the components could be more easily interpreted. The results indicated that PC1, PC2, and PC3 explained

39%, 23%, and 17% respectively (total 79 %) of the total variance. The major loadings on each primary component varied: PC1 (location (MT), salinity (ppt), and water density (g ml^{-1})), PC2 (location, temperature (°C), and animal length (mm)), and PC3 (species). These results suggest that spatial location and correlated changes in physical water properties (density, salinity, and temperature) were responsible for most of the variance among explanatory variables, while animal length and species had measurable but weaker contributions. Average *g* was slightly different among species (Table 3), but the uneven distribution of species by station (Fig. Ch2.a.3) makes it difficult to separate species effect from that of location. There was a similar trend in changes in *g* with location for both *T. inermis* and *T. raschii,* the euphausiid species found at more than one station (Fig. Ch2.a.8). There was no strong relationship between euphausiid length and *g* for any species or for all species combined, as there was a large variability in *g* between different animals of the same length (Fig. Ch2.a.9). Linear regressions between animal length and *g* indicated a very weak negative relationship for all euphausiids (R^2 = 0.062) and for each species individually (*T. inermis* - R^2 = 0.014; *T. raschii* - R^2 = 0.004; *T. spinifera* - R^2 = 0.063). The seawater surrounding the animals during their measurements was maintained at the ambient temperature of the seawater at the collection site. Occasionally, the temperature of the water in the container holding the animals was lowered (by placing the container in an ice bath) or raised (by exposing the container to warmer, ambient air) to provide a greater experimental temperature range. To evaluate the complexity of multiple factors impacting *g*, two-way factorial ANOVAs were used to determine the relationship between location, temperature, and the interaction between the two variableson animal density, water density, and *g*. These statistical analyses were performed on each species separately. *T. inermis* were exposed to water temperatures ranging from 0.5°C to 6.3°C and *T. raschii* were exposed to similar temperature ranges of 0.5°C to 6.4°C. Results for *T. inermis* indicated that location, temperature, and the interaction between the two variables had a significant effect on the animal density, the water density, and *g* (p 0.001 for all tests): animal density, water density, and *g* increased at stations located further to the west and with colder ambient water temperatures, and ambient water temperature was related to station location. The relationship between location and water density on *g* was analyzed through two-factorial ANOVAs. This analysis was applied to *T. inermis* and *T. raschii* separately and the results differed for each species. *T. inermis* were exposed to water densities ranging from 1.0252-1.0282 g ml^{-1}. Results from the two-factorial ANOVA for *T. inermis* indicated that location, water density, and the interaction between the two variables had a significant effect on *g* (p 0.001 for all three results). *T. raschii* were kept in water with densities with a larger range (1.0234-1.0282 g ml^{-1}) and yet only location had a significant effect on *g* (p 0.001). The results from the PCA and previously described two-factorial ANOVAs have indicated that location influences *g*. Furthermore, a piecewise multiple comparison procedure (Dunn's

Method) indicated that the western locations (MT05, MT06, MT07, MT08, MT09) were significantly different from the eastern locations (MT01, MT02, MT03, MT04) for both *T. inermis* and *T. raschii* (p 0.05 for all pairwise comparisons between eastern and western sites). The *g* values of *T. inermis* and *T. raschii* were grouped into eastern and western sites and a Kruskal-Wallis one-way ANOVA on ranks was evaluated between the two groups for both species. Results from both ANOVAs indicated that there was a significant difference in *g* between the eastern and western sites (p 0.001, for both species) with the animals from western sites having a significantly lower *g* than those from the eastern sites (Fig. Ch2.a.10). Water column properties at each MT station (rather than the properties of the ambient water in which the animals were kept) indicate that the western stations were characterized by generally colder and denser water with lower chlorophyll concentrations (Table 2). Since location was shown to have an effect on *g*, we examined the hypothesis that differences in chl-a between the sites explained the differences in *g* with location that were observed. The maximum chl-a concentration varied at each location and occurred at different depths (ranging from 16.9 m to 50.0 m). The results from the Pearson correlation between *g* and the chl-a measured at the same depth at which the zooplankton were collected indicated that there was a weak relationship between the two variables ($r^2 = 0.025$, p 0.05). Euphausiids migrate vertically and move throughout the water column over the course of a diel cycle (Schabetsberger *et al*., 2000); thus, a Pearson correlation was also computed between *g* and chl-a integrated over the entire water column which found a significant relationship ($r^2 = 0.172$, p 0.001). The correlation between chl-a and *g* was negative, that is *g* decreased as chl-a increased. Finally, the chl-a data were divided into the same two areas (eastern and western) and t-tests were used to determine whether there was a significant difference in chl-a between the two areas. There was no significant difference between the eastern (MT01,02,04) and western (MT05,07,08,09) locations for the chl-a measured at the depth from which the zooplankton were collected (p = 0.06). However, there was a significant difference between the integrated water column chl-a concentration for the eastern and western sites (p 0.05). Chl-a was higher in the eastern MTs compared to the western MTs (Fig. Ch2.a.11). Furthermore, the mean integrated chl-a of the western sites was 2.45 mg m^{-3} while the mean of the eastern sites was nearly double that at 4.56 mg m^{-3}.

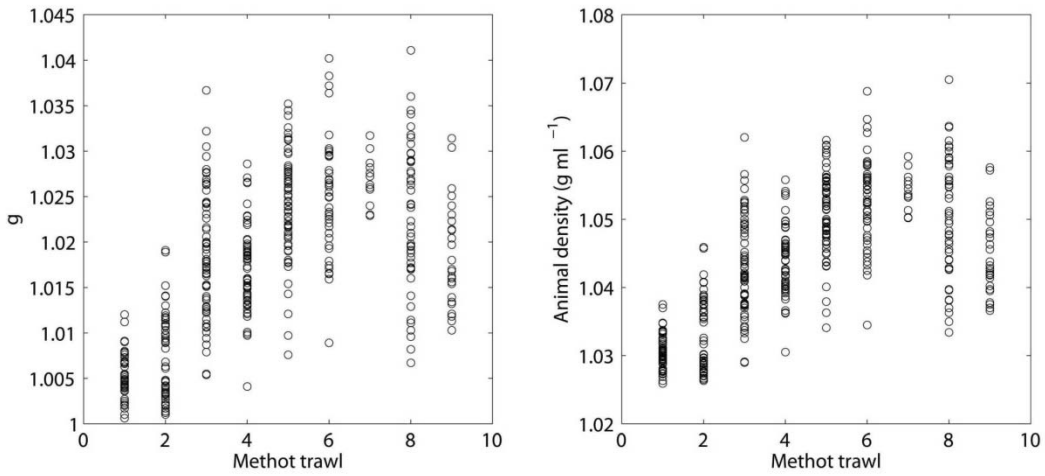

Fig.Ch2.a.6. Pairwise scatterplots of *g* and animal density as a function of location for all euphausiids.

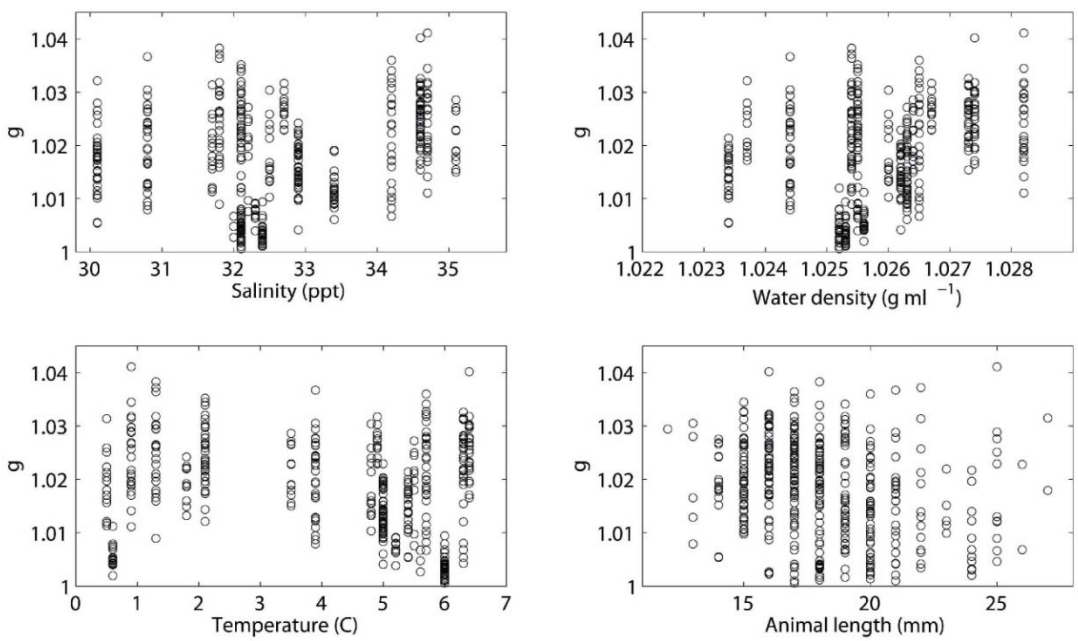

Fig.Ch2.a.7. Pairwise scatter plots for ambient salinity, water density, temperature, and animal length against g. Location, salinity, and water density are components of PC1 and location, temperature and animal length are components of PC2. Although the relationship is weak, as PC1 increases so does *g*. On the contrary, as PC2 increases, *g* decreases.

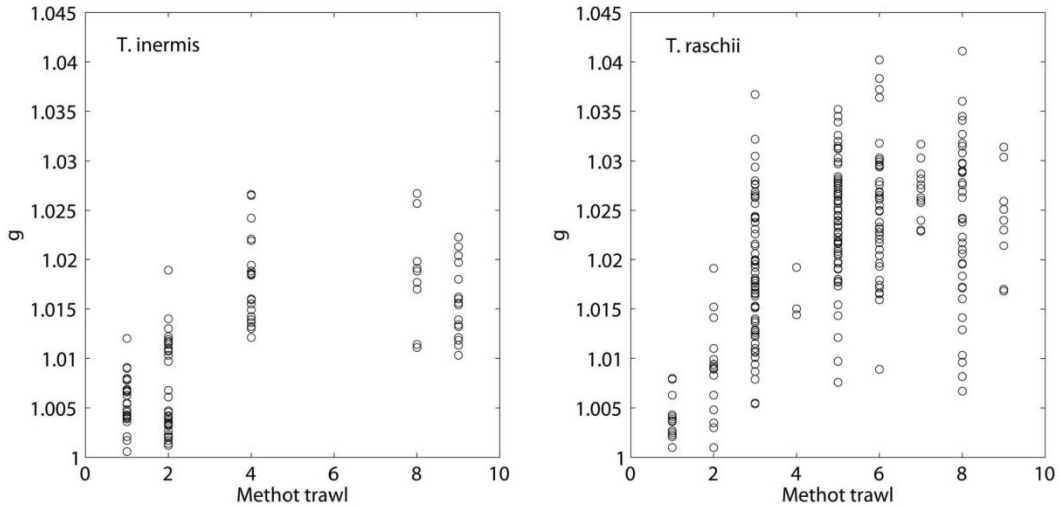

Fig.Ch2.a.8. Density contrast for *T. inermis* and *T. raschii* for each MT. Overall *g* values are lower for the East region (MT01,02,03,04) compared to the West (MT05,06,07,08,09).

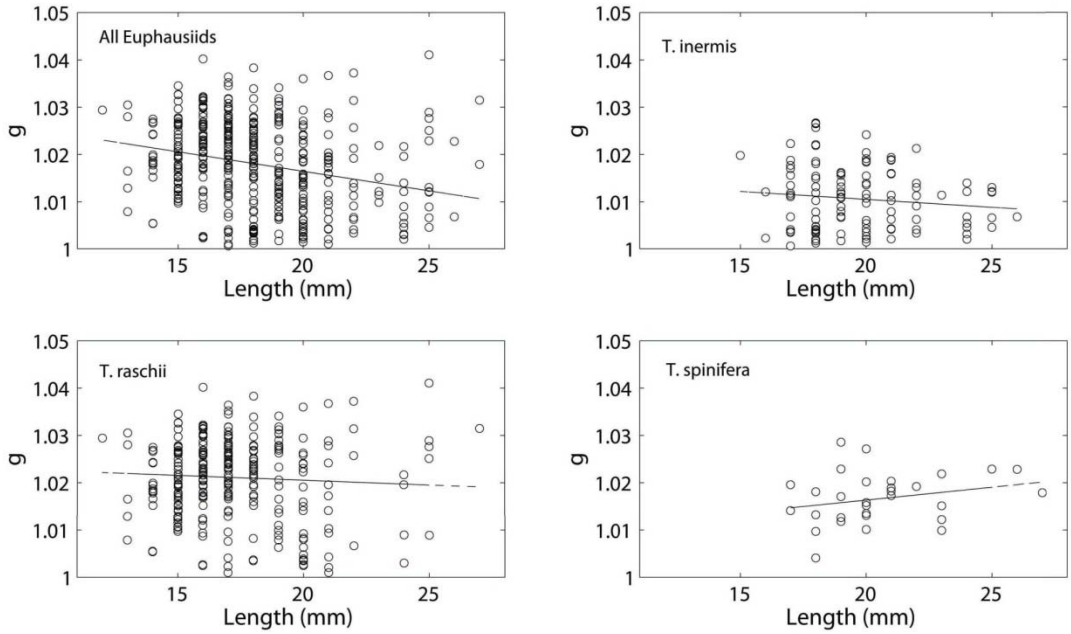

Fig.Ch2.a.9. Density contrast (*g*) as a function of animal length for all euphausiids (n=448), *T. inermis* (n=114), *T. raschii* (n = 282), and *T. spinifera* (n = 32). There is a large range in *g* values for all animal lengths. A linear regression showed that there is little correlation between the two variables for all euphausiids and each species. All species: R^2=0.062; g = -0.000825* Length(mm)+1.03; *T. inermis*: R^2=0.014; g = -0.000336* Length(mm)+1.02; *T. raschii*: R^2=0.0035; g = -0.000203* Length(mm) +1.02, and *T. spinifera*: R^2=0.063; g = -0.000545* Length(mm)+1.01.

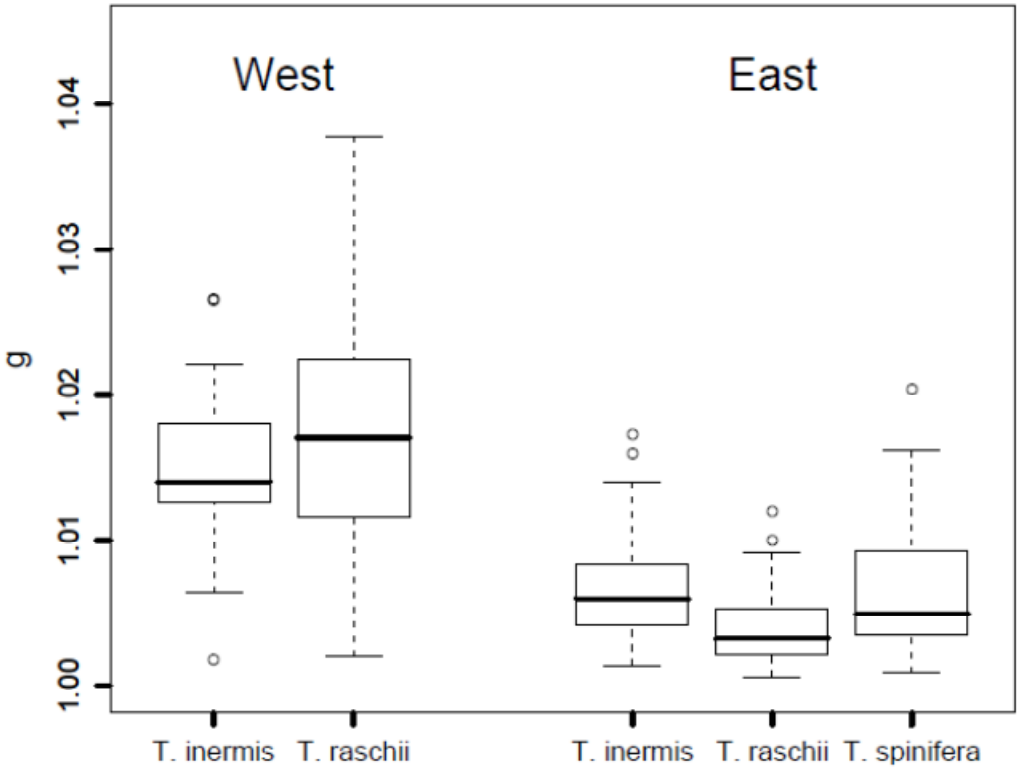

Fig.Ch2.a.10. Density contrast (*g*) distributions for different euphausiid species between the East (MT01, MT02, MT03, MT04) and West (MT05, MT06, MT07, MT08, MT09) locations. Density contrast was 985 significantly different between the western and eastern sample sites for euphausiids (p 0.001).

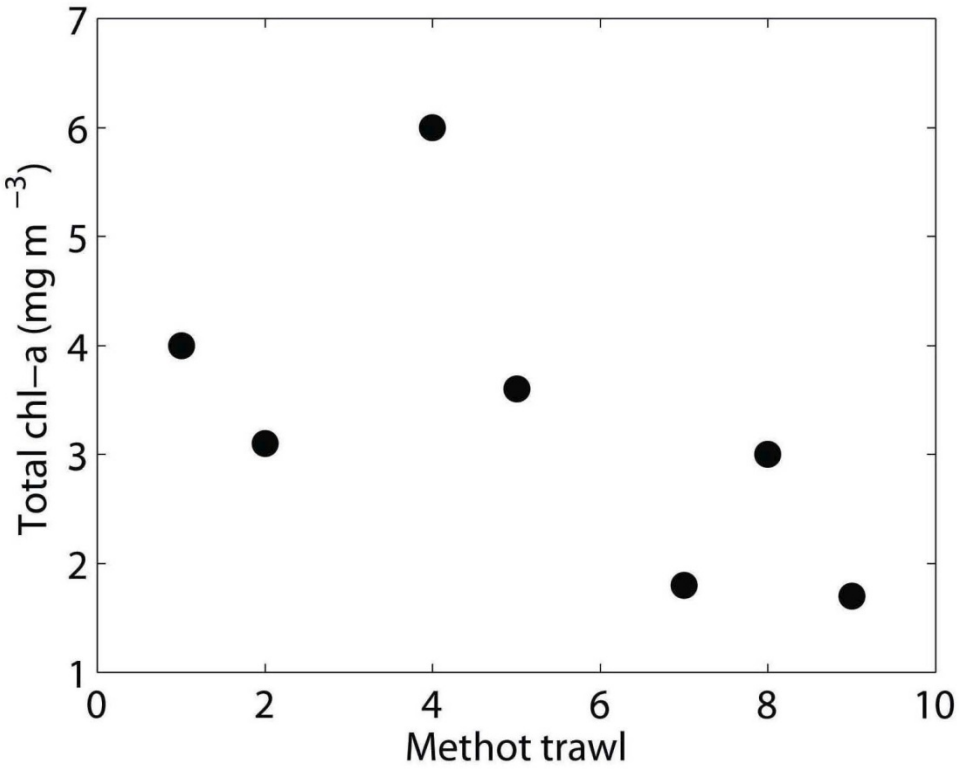

Fig.Ch2.a.11. Chlorophyll-a integrated over the water column varied with Methot trawl location. Sites in the western region (MTs 5 and higher) had lower levels of chl-a than eastern sites (MTs 4 and lower).

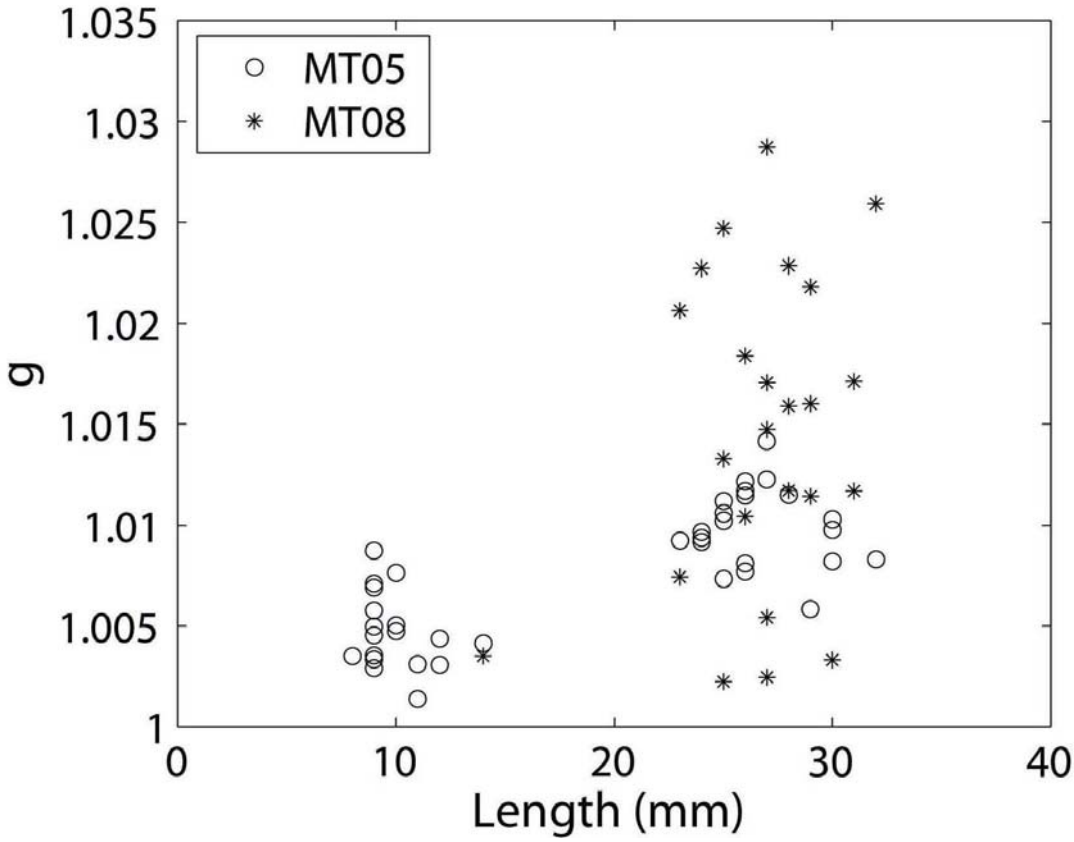

Fig. Ch2.a.12. Amphipod density contrast (*g*) was weakly correlated with animal length. Amphipods from Methot trawl 05 were split between small (20 mm) and large (> 20 mm) animals, whereas animals from Methot trawl 08 were almost all large animals. The large animals showed a greater range in *g* values. Density contrast was significantly different between the small and large amphipods (t-test, p 0.001). Results from a linear regression showed that R^2=0.33 and $g = 4.35 \times 10^{-4}$ Length (mm) + 1.

Other zooplankton groups

Along with euphausiids, other abundant zooplankton taxa in the Methot trawl catches included copepods and amphipods, however there were relatively few chaetognaths, gastropods, fish larvae, jellyfish, and squid specimens collected. Material properties and length measurements for each zooplankton group were measured, however relatively small data sets did not allow for environmental and spatial analysis to be conducted as was done for the euphausiid data.

a. Copepods. Ninety copepods (*NeocaIanus* sp.) were analyzed from MT02 (n = 18), MT04 (n = 31), and MT09 (n = 41). Density contrast ranged from 0.995 to 1.015 with a mean and sd of 1.005 ± 0.006 (Table

3). A linear regression showed little relationship (R^2 = 0.007) between copepod length and *g* . The regression fit was likely affected by the small range in copepod length and by the presence of both positively (g 1) and negatively (g > 1) buoyant copepods.

b. Amphipods. A total of 66 amphipods (*Themisto IibeIIuIa*) were collected from MT05 and MT08. Twenty-two amphipods were classified as small (20 mm length) and 44 amphipods were classified as large (> 20 mm length). The density contrast of small amphipods ranged from 1.001 to 1.009 with a mean and sd of 1.005 ± 0.002 (Table 3). The density contrast of large amphipods ranged from 1.002 to 1.029 with a mean and sd of 1.013 ± 0.006 (Table 3; Fig. Ch2.a.12). A linear regression showed that a weak correlation (R^2 = 0.33) existed between amphipod length and *g*. Density contrast varied both between and within the small and large amphipods. The large amphipods had a greater range in *g* than the smaller animals and *g* was significantly different between the two groups (t-test, p 0.001).

c. Chaetognaths. Although they were found in small numbers in multiple MTs, a total of 14 chaetognaths (*Sagitta* sp.) all from MT09 were measured. Their density contrast (*g*) values ranged from 1.007 to 1.026 with a mean and sd of 1.014 ± 0.007 (Table 3). Chaetognaths had the highest correlation of all taxa between length and *g* (g = -7.16×10^{-3} * Length(mm) + 1.03; R^2 = 0.503).

d. Gastropo s. Seventeen gastropods (*CIione Iimacina*) collected from two MTs (13 from MT06, 4 460 from MT07) had a *g* ranging from 1.008 to 1.031 with a mean and sd of 1.016 ± 0.006. A linear regression between length and *g* produced a low coefficient of determination (R^2 = 0.03).

e. Fish Larvae. Fifteen larval fish (*Theragra chaIcogramma*) were collected and measured (6 from MT06, 9 from MT07). Their *g* values ranged from 1.008 to 1.039 with a mean and sd of 1.023 ± 0.008 (Table 3). A linear regression between length and *g* produced a low coefficient of determination (R^2 = 465 0.00062).

f. JeIIyfish. Two species of jellyfish were measured, *Chrysaora meIanaster* and an unidentified hydromedusa. *Chrysaora meIanaster* were too large in size (bell diameters ranged from 15 to 24 cm) for density measurements with the available equipment, so the bells were cut into smaller pieces (n = 36) and measurements performed immediately after this. The mean length, width, and thickness of the pieces were 49 mm, 25 mm, and 8 mm respectively. The density contrast ranged from 1.001 to 1.006 with a mean and sd of 1.003 ± 0.001 (Table 3). The density contrast was calculated for the entire body of the unidentified jellyfish species (n=4), and ranged from 1.004 to 1.005 with a mean and sd of 1.005 ± 0.001

(Table 3).

g.Squid . The density of the squid mantle was measured in a laboratory using the pipette method, while the densities of the squid beaks were measured in the laboratory using the titration method, but with glycerine as the titrate instead of a hypersaline solution. As noted previously, measurements on the squid pens were not possible due to deterioration of the samples. Seven pieces of squid mantle were measured and *g* ranged from 1.023 to 1.116 with a mean ± sd of 1.073 ± 0.030 (Table 3). The mantle pieces were slightly deteriorated, so *g* may differ from that of live tissue. Fifteen squid beaks were collected and separated into upper and lower aw pieces for a total of 30 density measurements. Their *g* ranged in value from 1.125 to 1.180 with a mean of 1.149 ± 0.013 (Table 3). The squid beaks showed no evidence of deterioration.

Sound Speed

Sound speed contrast data were collected for those zooplankton taxa abundant enough to fill a 485 26 ml or 84 ml PVC T-tube measurement chamber. The sound speed contrast was measured for groups of animals from the same taxon in each haul. When a particular taxon was abundant within the MT, several different groups of those animals were measured for their *h* value. In total, *h* was measured for 11 separate groups of euphausiids representing all MTs except MT06. The number of group measurements of *h* for each taxon were: copepods (3), amphipods (3), gastropods (1), jellyfish (*Chrysaora meIanaster*, 8), and squid mantle (2). Three trials were conducted for each group and the results were averaged. The mean percent difference in *h* between trials was 0.076%. As a taxon, euphausiids had both the greatest number and the widest range of *h* measurements (range 0.990 to 1.017; mean 1.006, sd 0.008; Table 3). The two squid mantle measurements were the most consistent with *h* = 1.010. Copepods, amphipods, and jellyfish also displayed a range in *h* values (Table 3).

Location was found to be an important factor influencing *g*, hence euphausiids (the taxon with the most measurements of *h*) were separated into eastern (MT01, MT02, MT03, MT04) and western (MT05, MT07, MT08, MT09) groups and a t-test was used to evaluate the difference in *h* between the two groups. Unlike the density data, there was no significant difference in *h* of groups of euphausiids from the eastern (n = 4) and western (n = 7) sites, although this result may have been affected by the small sample size for the sound-speed measurements.

DISCUSSION

Although there are a small number of previous studies on the material properties of several of the taxa we measured, there have been no such measurements on specimens from the Bering Sea. There

are also several relatively common zooplankton groups (such as chaetognaths) which have had no information reported about their material properties at all prior to this study. A major contribution of this study are measurements of zooplankton material properties from this ecosystem; these data (Table 1) can be used in scattering models to provide more accurate estimates of zooplankton biomass or abundance. Little is known about how material properties might be affected by or related to factors such as animal length, geographic location, surrounding environmental conditions, age, gender, fecundity, feeding state, or numerous other factors which are likely to affect the body composition of these organisms and thus their density and sound speed (Chu et al., 2000; Chu and Wiebe, 2005; Forman and Warren, 2009). Therefore, we also examined the effects of various parameters on the material property measurements, focusing principally upon euphausiid *g*, the zooplankton group and material property for which we had the most observations. The variables considered were species, length, water temperature, water density, location, and water column chl-a concentration as a proxy of zooplankton prey abundance. Principal component analysis determined how these different explanatory variables were related to one another. Separate analyses were used to further examine specific relations between a given variable (or variables) and *g*.

Density contrast

All of the explanatory variables examined appeared to contribute to the variance in *g* to some degree. The confounding effects and interactions between these variables makes it difficult to reach any definitive conclusions about direct relationships between a single variable and animal density, however these data do provide insight into some of these relationships and offer avenues for future investigations. Both euphausiid density and *g* were greater at western MT locations than at eastern stations, and increased with increasing water density and salinity, and decreasing temperatures. These relationships occurred for both ambient (at the MT station) or experimental (in the tank the animals were maintained) conditions. However, if all other factors are constant and the animals are not altering their own density, increasing ambient water density should cause a decrease, not an increase, in *g*. We suspect that the increase in *g* was due to an increase in animal density at the western stations (Fig. Ch2.a.6) which was greater than any increase in ambient water density; as *g* was significantly different between the western and eastern sample sites for euphausiids (p 0.001). These western sample sites were characterized by colder water and lower chlorophyll concentrations. Water temperature changes both spatially and seasonally and can alter the material properties of zooplankton throughout the year (Forman and Warren, 2009). Changes in lipid composition were suggested by Køgeler et al. (1987) to explain the differences in *g* between seasons. Many zooplankton increase their lipid composition in colder months as a means to store energy through winter (Campbell and Dower, 2003). Female euphausiids alter their lipid composition throughout egg

reproduction (Smith, 1991). Such changes in lipid composition are likely triggered by temperature changes, though the exposure time to different temperatures in our experiments (several hours to a day) may have been too short to allow the animals to adjust their body composition. Long term exposure to the ocean temperatures at the locations from which the euphausiids were collected (average water column temperature for the stations in the eastern group was 2.6 °C compared to 0.4 °C for the west) could partially explain the difference in animal density between MTs (Fig. Ch2.a.6). It is also possible that zooplankton that are well-fed have different material properties than those animals without a sufficient food supply. The concentration of phytoplankton varies both spatially and seasonally, and we used chl-a concentration as a crude indicator of the abundance of phytoplankton, the primary prey for euphausiids in these waters. Chl-a had a significant correlation with animal density and *g* ($r^2 = 0.17$), with western MT sites having less chlorophyll than eastern sites. The r^2 value is fairly low, but the mean chl-a values differ by a factor of two (western region = 2.45 mg m^{-3}; eastern region = 4.56 mg m^{-3}). This difference may be substantial when considering the difference in surface chl-a values between a spring bloom (3.5 -6.0 mg m^{-3}) and summer months (0.8 -1.0 mg m^{-3}) where nutrient consumption limits phytoplankton production for the middle and outer shelf of the Bering Sea (Iida and Saitoh, 2007). The difference in mean chl-a concentrations between the eastern and western sites is not as large as the difference between a spring bloom and and the subsequent decline for a similar region. However, the difference might be great enough to potentially influence the material properties of euphausiids. We did not examine the specific mechanism responsible for this relationship; it may be the result of the phytoplankton prey being less dense than the euphausiids and as the euphausiids eat the less dense material they themselves become less dense, or it may be that well fed animals are storing energy as lipids which will affect their density relative to the surrounding seawater. Information on euphausiid gut contents, gut volume, and phytoplankton densities would need to be measured to determine the differences in *g* for euphausiids that are well-and poorly-fed. Future studies examining material properties of zooplankton should include an examination of lipid content in order to better resolve this issue.

We found differences in *g* for the same species due to changing environmental conditions over relatively small distances (10s -100s km). Differences due to environmental conditions that vary with location may explain the differences between our data for *T. inermis* and *T. raschii* from the Bering Sea and those of Køgeler et al. (1987) for the same species of euphausiids collected off Norway. Greenlaw and Johnson (1982) also measured the density contrast of *T. raschii* in two widely separated locations; the density contrast of *T. raschii* from Norway ranged from 1.013 to 1.018 while *g* ranged from 1.045 to 1.050 in Saanich Inlet, British Columbia. Results reported by Greenlaw and Johnson (1982) for *T. raschii* in

Norway are similar to our *g* estimates for the same species in the Bering Sea, while their results for *g* of *T. raschii* from British Columbia are similar to Køgeler et al. (1987)'s results from the Barents Sea. Variation of material properties among different locations, environmental conditions, and times of year is not yet well understood. Even though the euphausiid species we examined are of the same genus and have a roughly similar morphology, there were enough differences between each species to suggest an effect on *g,* though we were not able to conclusively separate a species effect from that of sample location. Køgeler et al. (1987), working in the Barents Sea, examined the material properties of three euphausiid species (*Thysanoessa inermis*, *T. raschii*, and *Meganyctiphanes norvegica*) over the course of a year. The *Thysanoessa* species they measured are also the dominant euphausiids on the Bering Sea shelf (Smith, 1991). Although Køgeler et al. (1987) did not test for any significant difference in density contrast values among the three euphausiid species, they showed that *g* values were slightly different among the species and that *g* fluctuated with season. The density contrast of *T. inermis* and *T. raschii* fluctuated in a similar pattern in which the maximum *g* occurred in February and the minimum *g* occurred in mid-November for *T. inermis* and mid-December for *T. raschii.* The *g* values that we report are generally smaller and have a wider range, and yet they overlap with the range of measurements described in Køgeler et al. (1987) and Greenlaw and Johnson (1982) for the same euphausiid species (this study: 1.001 to 1.041; Køgeler et al. (1987): 1.022 to 1.054; Greenlaw and Johnson (1982): 1.013 to 1.050). Comparing *g* values between euphausiid species is also appropriate considering that the material properties of a particular species has often been applied to modeling the scattering of other species. The *g* values we obtained for *Thysanoessa* spp. appear to be somewhat lower than *g* values reported for *Euphausia superba* by other studies (1.021 to 1.040, Greenlaw and Johnson (1982); 1.021 to 1.040, Chu and Wiebe (2005)). Data on *E. superba* from these studies (as well as Foote, 1990) are often used for scattering models for any euphausiid-like animal, even though there are large differences between different euphausiid species particularly in their size (adult *E. superba* are roughly two to three times as large as *T. inermis* or *T. raschii*).

The density contrast of our copepods ranged from 0.995 to 1.015 with a mean of 1.005 ± 0.006. The mean copepod *g* value from our results lies within the range of copepod density measured by Køgeler et al. (1987). However, the copepods examined in our study (*NeocaIanus* sp.) are larger (7 to 9 mm in length) compared to the copepods examined in Køgeler et al. (1987) (*CaIanus finmarchicus*, 2.2 to 3.0 mm and *CaIanus hyperboreus*, 3.5 to 5.5 mm in length). The density contrast of copepods measured by Køgeler et al. (1987) ranged from 0.999 (February through September) to 1.003 (in late-February) for *CaIanus hyperboreus*; for *CaIanus finmarchicus*, *g* ranged from 0.996 at the end of July to 1.010 in late-February. Unlike the measurements of euphausiids, both our study and that of Køgeler et al. (1987) measured copepods with positive and negative buoyancy (g 1): approximately a quarter of our

copepods were less dense than the seawater, while Køgeler et al. (1987) showed that copepods were less dense than seawater the majority of the year and only became denser immediately prior to spawning in March. Copepods with both positive and negative buoyancy have also been reported elsewhere for the same genera and species. *CaIanus* sp. found in Antarctic waters were all measured to have densities less than seawater (Chu and Wiebe, 2005), but none of the copepods measured by Greenlaw and Johnson (1982), including representatives of the species *CaIanus finmarchicus,* were less dense than seawater. It is possible that the majority of the copepods measured in this study had recently spawned or otherwise did not contain sufficient lipid stores to be less dense than water.

Our examination of the effect of animal length on *g* revealed that for most zooplankton taxa in this study there was little or no correlation between the two variables. Amphipods ($R^2 = 0.33$) and chaetognaths ($R^2 = 0.50$) were the only taxon with a coefficient of determination greater than 0.10 between length and *g*. Though our results indicated no significant relationship between euphausiid length and *g*, we calculated a linear regression between animal length and *g* for euphausiids in order to compare to the linear regressions for the same species found in Køgeler et al. (1987). Their euphausiids (*T. inermis* and *T. raschii*) ranged in length from 10 to 25 mm while our euphausiids ranged in length from 12 to 27 mm. They provided multiple regression equations (g = a*Length(mm) + b) for each month that data were collected. The slopes for their linear regressions were all small negative numbers (ranging from -0.01×10^{-3} to -2.5×10^{-3} with a mean slope of -1.27×10^{-3}) and their coefficients of determination ranged from $R^2 = 0.01$ to $R^2 = 0.90$. We calculated a similar slope of -0.93×10^{-3} for the linear regression between euphausiid length and *g* and a small coefficient of determination ($R^2 = 0.06$). Greenlaw and Johnson (1982) examined euphausiids of the genus *Thysanoessa* (but from unspecified locations) and demonstrated a positive relationship between animal length and the density contrast, but their data represented a very small range (15 to 18 mm) of lengths. Chu and Wiebe (2005) also reported a positive correlation between euphausiid length and *g*, however all of their animals were larger (25 -52 mm) and of a different species (*Euphausia superba*) than the euphausiids in our study.

Sound speed contrast

While density contrast was measured for individual zooplankton, *h* was measured on groups of animals (Table 3). Unfortunately the sound speed contrast could not be measured for all zooplankton groups since not enough individuals of some taxa were collected. Overall, *h* was fairly close to unity for all zooplankton groups for which measurements were made and in some cases it was less than one, which signifies that sound travels slower through the group of zooplankton compared to the surrounding

seawater. It is likely that these bulk measurements, containing multiple sizes and species for each taxon, are intrinsically more variable than measurements made on individuals of a single type and size. The sound speed contrast for euphausiids ranged from 0.990 to 1.017 with a mean and standard deviation of 1.006 ± 0.008, lower than *h* measured for two of the same species (a mixture of *T. inermis* and *T. raschii*) by Køgeler et al. (1987), who reported a mean of 1.026 ± 0.005. Greenlaw and Johnson (1982) measured *h* for *T. raschii* ranging from 1.032 to 1.045, which is also higher than the *h* measurements collected for euphausiids from the Bering Sea. Similarly, Bering Sea euphausiid *h* measurements were lower than the average *h* value measured for *E. superba* by Chu and Wiebe (2005) which was 1.030 ± 0.004 and by Foote (1990) which was 1.0279 ± 0.0024. Euphausiid *h* did not exhibit the east-west spatial pattern observed for euphausiid *g*. Bering Sea copepod *h* measurements were lower then the results Køgeler et al. (1987) reported for a different genus, species, and animal size of copepod: our average *h* for *NeocaIanus* sp. copepods was 1.007 ± 0.004, while Køgeler et al. (1987) for several species of the genus Calanus showed a mean *h* of 1.027 ± 0.007. Greenlaw and Johnson (1982) report similar *h* values to this study ranging from 1.006 to 1.012, even though they measured a smaller copepod species (*CaIanus pIumchrus*).

Sources of Uncertainty

Measurements of both the density and sound speed contrast of animals have several sources of uncertainty. Because the titration method involved adding a saltier solution to the seawater surrounding the animal, it is possible that the resulting osmotic pressure could have altered the density of the animal. We observed that a change in the buoyancy occurred over several minutes if the animal was allowed to remain in the solution after the saltier solution had been added. In this study, the measurement needed for estimation of animal density using the titration method was completed within approximately 30 seconds of the saltier solution being added, which we believe minimized the chance of osmotic adjustment by the animal. In addition, the titration method was performed multiple times on each animal; the density measurements were similar between iterations and had a mean percent difference of 0.41 %. This small mean percent difference, with no systematic change in animal density after repeated iterations, suggests that there was no bias due to osmotic effects in density measurements using the titration method.

Another possible source of uncertainty with this method is that seawater bound to the animal by surface tension will bias the measurement towards unity, since the titration method measures the density of the animal along with any seawater that is attached to the animal by surface tension. This factor will increase in importance as animal volume decreases and thus is most likely to impact the smallest animals we measured, the copepods. However, other studies have used similar density measurement methods on even

smaller copepods than those in this study (Køgeler et al., 1987; Greenlaw and Johnson, 1982; Greenlaw, 1977). The density contrast measurements also may be underestimated due to seawater viscosity. Viscous friction at the interface between the animal and seawater could potentially affect the accuracy of the density measurements, however any such effect is difficult to quantify. The *h* measurements were likely biased minimally (towards unity) considering the difficulty in entirely removing excess water from around the animals and the difficulty in completely filling the chamber with animals (i.e., < is always less than 1). In other words, interstitial water between the animals being measured when using displacement volume to estimate volume fraction (Eq. 6) may explain some of the variation in *h* for each zooplankton taxon. It is preferable that animals be uniformly distributed within, and appear to fill, the horizontal section of the measurement tube (Foote, 1990). Køgeler et al. (1987) reported that the maximum volume fraction within their measurement chamber was 65%, but the mean volume fraction in this study ranged from 63% to 100% with a mean of 89%. Indirect methods of measuring volume fraction involve measuring the resistivity of a group of animals and then calculating its theoretical volume fraction; Chu et al. (2000) showed that this method can significantly reduce the error in calculating *h*, but this technique has not yet been widely used.

Effect on predictions of target strength (TS)

Material properties appear to be a function of the environment as well as a function of the physical parameters of the various zooplankton groups. It is very difficult to understand the relationship of each parameter on *g* considering many of the factors are inter-related (e.g. location, water temperature). The importance of these relationships is that very small differences in *g* and *h* (0.01 or less for each) that may result from differences in, for example, location, species, or animal size can produce different TS values that will result in vastly different estimates of numerical abundances of animals when used in con unction with acoustic backscatter survey data. Forman and Warren (2009) showed that using the lowest, average, and highest values of *g* and *h* that they measured for coastal zooplankton can result in differences in population estimates of up to three orders of magnitude. Given the wide range of *g* and *h* values in the literature and the fact that bioacousticians often use material property values from species other than the ones they are studying (primarily because the data they need do not exist), it is imperative that more material property measurements are made. For example, many studies use the values reported for *Euphausia superba* by Foote et al. (1990) or more recently Chu and Wiebe (2005) for any fluid-like crustacean, even when the animal being studied is either much smaller in size or a completely different family or order of animal. Chu and Ye (1999) show that the differential backscattering cross section (σ_{bs}) is proportional to the square of the sum of the deviations of *g* and *h* fromunity (σ_{bs} a(h+ g)^2 where h=h-

1and g = g-1). Since σ_{bs} is related to target strength by the equation TS = 10log σ_{bs} (Stanton et al., 1996), we can calculate how much TS will change when different *g* and *h* values are used. Both *g* and *h* are proportional to the backscattering cross-section; however, we cannot be certain that *g* and *h* are correlated given that *h* can only be measured on groups of animals while *g* is measured for individual animals. For instance, euphausiids measured in this study had a range in *g* from 1.001 to 1.041 and a range in *h* from 0.990 to 1.017, which would result in TS estimates that vary by as much as 16 dB. As a difference in TS of 10 dB corresponds to an order of magnitude difference in the numerical density of a scatterer, the variation in *g* and *h* from our study needs to be taken into account to produce zooplankton population estimates that are accurate enough for studies of ecosystem processes.

Since location appeared to be a significant factor influencing *g* for euphausiids in the Bering Sea, the variation in TS was calculated using the ranges in *g* and *h* found in the eastern and western groups. TS estimates could vary by 19.5 dB for eastern euphausiids and 16.7 dB for western euphausiids. These large dB ranges are the maximum differences that could occur within a population based on data collected in the Bering Sea; the likely range of TS estimates based on the combinations of mean *g* and *h* observed in our data from each MT may be substantially smaller. In addition to estimating the maximum possible difference in TS due to *g* and *h* measurements of euphausiids in the Bering Sea, a more likely estimate of the variability in TS can be found by computing the proportional effect on the backscattering cross-section (σ_{bs}) from the average *g* and *h* for each MT (using the equation presented in Chu and Ye, 1999). Using this method, the estimated difference in the range of 725 TS values (between 95% confidence bounds approximated as twice the standard error of the mean) was 5.7 dB for all euphausiids, 9.0 dB for the East, and 4.8 dB for the West. The larger range for the East region is the result of *g* values being very close to unity, where small changes in *g* will produce larger variations in TS. The actual TS distribution for a population of animals may need to be calculated on an individual-by-individual basis to determine the impact of the variability in material properties on numerical estimates of animal abundance.

CONCLUSIONS

This study presents material property values for Bering Sea zooplankton. We measured the material properties for euphausiids, copepods, amphipods, chaetognaths, gastropods, fish larvae, jellyfish, and body parts of squid. In those cases where there were prior measurements of the same taxa using specimens collected from different regions, our measurements showed significant variation; these differences suggest that uncertainty in scattering model predictions should be reduced if material property values are specific to each target taxon in the location being studied. Potentially, if an environment is relatively stable from year to year, the material properties of a particular zooplankton group may also be stable. The only way to verify this is to measure the

material properties for a specific location and group of animals during the time period of interest. If material properties are shown to be stable or predictable, then less frequent measurements of material properties would be needed. With improved knowledge of material properties, including what factors cause these properties to change, as well as other scattering model inputs such as animal orientation (Demer and Conti, 2005; Warren et al. 2002); more accurate estimates of zooplankton abundance and distribution could be made from acoustic surveys which would improve our ability to understand the status and trends of these populations.

ACKNOWLEDGEMENTS

This project was supported by the Alaska Fisheries Science Center, National Marine Fisheries Service, NOAA, and the North Pacific Research Board's Bering Sea Integrated Ecosystem Research Program. The captain, crew, and scientists aboard the NOAA ship *Oscar Dyson* provided excellent logistical support and sampling assistance. Abigail McCarthy helped us greatly with the set up and maintenance of the on board aquaria as well as with the trawl sampling operations. We acknowledge the taxonomic advice of Elaina Jorgensen (squid) and Claudia Mills (hydromedusae). We would like to thank Alex De Robertis and Neal Williamson for their comments and suggestions on this manuscript. The statements, findings, conclusions, and recommendations in this manuscript are those of the authors and do not necessarily reflect the views of NOAA or the U.S. Department of Commerce. Also, reference to trade names (such as Instant Ocean) does not imply endorsement by the National Marine Fisheries Service, NOAA. This paper was BEST-BSIERP Publication 7.

Chapter 2.b. Target Strength (TS) of euphausiids

This section describes a mathematical model of the acoustic backscatter from a single euphausiid (target strength, or TS), a parameter necessary to the conversion of acoustic backscatter into biologically meaningful quantities, such as numerical density and biomass. Estimates of TS were not previously available for Bering Sea euphausiids, and no shelf-wide survey of euphausiids on the Bering Sea shelf (acoustic or otherwise) had ever been done. The material in this section is the work of Smith (MS student in part supported by B62), Ressler (B62 PI), and Warren (scientist supported under contract by B62), and was published as

Smith, J.N., Ressler, P.H., and Warren, J.D., 2013. A distorted wave Born approximation target strength model for Bering Sea euphausiids. ICES Journal of Marine Science 70:204-214. http://icesjms.oxfordjournals.org/content/70/1/204.short

Joy N. Smith, School of Marine and Atmospheric Sciences, Stony Brook University, 239 Montauk Hwy, Southampton, New York 11968

Patrick H. Ressler, National Marine Fisheries Service, Alaska Fisheries Science Center, Resource Assessment and Conservation Engineering Division, 7600 Sand Point Way NE, Seattle, Washington 98115

Joseph D. Warren, School of Marine and Atmospheric Sciences, Stony Brook University, 239 Montauk Hwy, Southampton, New York 11968

ABSTRACT

Acoustic surveys monitor euphausiid populations in the Bering Sea because of their importance as prey for walleye pollock and other organisms. Various scattering models exist to convert acoustic backscatter data to estimates of euphausiid numerical density or biomass, but a target strength (TS) model specific to Bering Sea euphausiids has not been available. This study parameterized a distorted wave Borne approximation (DWBA) scattering model using physical (length, body shape) and material (density contrast, *g*, and sound speed contrast, *h*) properties measured from live euphausiids. All model parameters (length, shape, material properties, orientation) were evaluated for their effect on predicted TS. A polynomial function was used to describe animal shape and produced smaller TS estimates compared to a taper function, which is traditionally used in DWBA scattering models of euphausiids. Animal length was positively correlated with TS, but variations in other parameters (including material properties and orientation) also produced large changes in TS. Large differences in TS between estimates calculated using measured and literature material property values caused large variations in acoustic estimates of euphausiid numerical densities (animals m^{-3}) which emphasizes the importance of collecting site-specific *g* and *h* measurements when possible.

Keywords: euphausiids, target strength (TS), distorted wave Born approximation (DWBA)

INTRODUCTION

Euphausiids ("krill", principally *Thysanoessa* spp.) are an important part of the Bering Sea ecosystem. These crustacean zooplankton are prey for many species, including murres (Decker and Hunt, 1996), northern fur seals (Sinclair, 1994), puffins (Hatch and Sanger, 1992), and most notably walleye pollock (*Gadus chalcogrammus;* Bailey, 1989; Lang et al., 2000, 2005) as pollock are the target of one of the largest single-species fisheries in the world (FAO, 2009). There are interests in a quantitative estimate of the abundance of euphausiids in the eastern Bering Sea because of the trophic linkage between euphausiids and pollock (Ianelli et al., 2009). Acoustic-trawl resource assessment surveys conducted in the Bering Sea by the National Marine Fisheries Service (Honkalehto et al., 2009) provide a potential source of this information. Acoustic surveys sample large areas at high spatial and temporal resolution (Simmonds and MacLennan, 2005), but net sampling must also be conducted to ground-truth the acoustic data and determine the types of animals being detected (Kasatkina et al., 2004). Once the identity of the dominant acoustic targets are known, a model of the acoustic scattering from these targets is required to convert acoustic backscatter measurements into units of animal abundance and biomass (Foote and Stanton, 2000).

The prevailing approach to modeling the scattering of euphausiids is via physics-based scattering models. These models require input parameters describing the acoustic wave (frequency or wavelength) and the target (shape, length, orientation relative to the acoustic wave, and material properties) (Stanton and Chu, 2000; Lavery et al. 2002; Demer and Conti, 2003a,b; Lawson et al. 2006). The material properties used in acoustic modeling are: density contrast (*g*), which is the ratio of the density of the animal to the density of the ambient seawater, and the sound speed contrast (*h*), which is the ratio of the speed of sound in the animal to the surrounding seawater. Material property data are often measured through laboratory studies of individual specimens (Greenlaw and Johnson, 1982; Køgeler et al., 1987; Forman and Warren, 2010), although these measurements have also been made at sea (Chu and Wiebe, 2005; Smith et al., 2010). One purpose of this study was to examine the influence of material properties, specifically *g* and *h*, on model predictions of Bering Sea euphausiid target strength.

A variety of scattering model formulations have been proposed for euphausiids. Initially, euphausiids were modeled as straight cylinders (Stanton 1988a, b), but more advanced models considered their shape to be deformed (bent) cylinders (Stanton et al. 1993a; Stanton et al., 1993b; Stanton and Chu, 2000). Ray-based solutions were used to compute the scattering at different euphausiid orientations; however, ray-based models work best for angles of incidence near normal to the lengthwise axis of the body (Stanton et al. 1993b) and most are only valid at high frequencies where the acoustic wavelength is smaller than the cross-sectional radius of the euphausiid (Urick, 1983). However, Stanton et al. (1993b) presented a ray-based solution with a phase correction that worked at a wider range of frequencies (ka > 0.3 where ka is the product of the acoustic wave number (k) and the equivalent cylindrical radius of the animal (a)).

More recently, the distorted wave Born approximation (DWBA) model has been used to model the backscatter from euphausiids. The DWBA model is valid for all acoustic frequencies, can be evaluated for all angles of orientation (Chu et al., 1993), and can be applied to arbitrary shapes (Stanton et al., 1998a,b). In the DWBA model, a scattering function is integrated over the length of the axis of the body, taking into account the phase shift that results from the bent body. The model assumes that the targets are comprised of weakly scattering material, which is true for euphausiids. The general formula for modeling acoustic scattering with the DWBA model was first given by Morse and Ingard (1968) as:

$$f_{bs} = \frac{k_1^2}{4\pi} \iiint_V \left(\gamma_k - \gamma_\rho\right) e^{i2\left(\vec{k}_i\right)_2 \cdot \vec{r}_{pos}} dv \qquad (1)$$

The integration is within the volume (v) of the body and has a position vector $([r_{pos}])$, $[(\vec{k}_i)_2]$ is the incident wave number vector inside the body, and γ_κ and γ_ρ are terms used to describe the material properties within the body. The parameters γ_κ and γ_ρ are expressed in regards to the compressibility (κ), density contrast (*g*), and sound speed contrast (*h*) and are described as follows:

$$\gamma_\kappa \equiv \frac{\kappa_2 - \kappa_1}{\kappa_1} = \frac{1 - g\,h^2}{g\,h^2} \qquad (2)$$

$$\gamma_\rho \equiv \frac{\rho_2 - \rho_1}{\rho_2} = \frac{g - 1}{g} \qquad (3)$$

where

$$\kappa = \left(\rho c^2\right)^{-1}; h = \frac{c^2}{c_1}; g = \frac{\rho_2}{\rho_1} \qquad (4)$$

In this paper, we define the term $|\gamma_\kappa - \gamma_\rho|$ as the material property parameter (M). It will later be parameterized based on *g* and *h* measurements for Bering Sea euphausiids.

Since the general formula for the DWBA model is complex and requires knowledge of the animal's shape and material properties in three dimensions, a simplified form of the DWBA model with only one integral has been developed (Stanton et al., 1993a). The single integration assumes that the cross-section of the elongated zooplankton is circular throughout the length of the body and the material properties are constant throughout the animal; therefore the integration follows the length of the body (Stanton et al., 1993a; Stanton et al., 1998a; Stanton and Chu, 2000). It is written as follows:

$$f_{bs} = \frac{k_1}{4} \int_{\vec{r}_{pos}} a\left(\gamma_\kappa - \gamma_\rho\right) e^{2i\left(\vec{k}_i\right)_2 \cdot \vec{r}_{pos}} \frac{J_1\left(2k_2 a \cos\beta_{tilt}\right)}{\cos\beta_{tilt}} \left|d\vec{r}_{pos}\right| \qquad (5)$$

where a is the radius of the euphausiid as it changes along the length of the animal's body (L), k_1 refers to the acoustic wave number in the surrounding medium, k_2 is the acoustic wave number inside the body,

$[(\vec{k}_i)_2]$ is the wave number vector of incident field evaluated inside the body, $ß_{tilt}$ is the angle between the incident wave (k_i) and the cross section of the cylinder at each point along its axis, and J_1 is the Bessel function of the first kind of order one. For modeling purposes, each euphausiid is divided into multiple cross-sectional areas and the energy reflected by each section is calculated separately and added together for the entire animal. The scattering amplitude, f_{bs}, is related to the backscattering cross section of the target (σ_{bs}) and target strength (TS) by the following relation (Urick, 1983; Medwin and Clay, 1998):

$$TS = 10\log_{10}|f_{bs}|^2 = 10\log_{10}\sigma_{bs} \qquad (6)$$

TS is a logarithmic measure of the proportion of the incident intensity backscattered from the target measured in units of dB relative to 1 m^2.

The DWBA model may not properly capture the phases of the backscattered signal for angles away from normal incidence. TS predictions from the DWBA model have been experimentally validated for euphausiids near broadside incidence with angles less than 15-30º; however, the model predictions of TS at larger angles in the same experiment were approximately 5-10 dB lower than direct measurements (McGehee et al., 1998). Demer and Conti (2003a) proposed that the variability in the phases had three possible explanations: scattering variability in a field with stochastic noise, euphausiid shape is more complex than the assumed cylinder with varying radii, and euphausiids flex their body as they swim. They attempted to account for this phase variability using a stochastic distorted wave Born approximation (SDWBA) model validated for Antarctic krill (Demer and Conti 2003a,b). Unfortunately their potential explanations for phase variability in echoes from euphausiids have not been conclusively demonstrated or individually analyzed and there is yet no consensus on the best model for euphausiid scattering, though the SDWBA model has been adopted by the Commission for the Conservation of Antarctic Marine Living Resources (CCAMLR) community for krill biomass assessments (Reiss et al., 2008).

In general, the DWBA model has been more widely used than the SDWBA to model backscatter of euphausiids (Lawson et al., 2006; Amakasu and Furusawa, 2006; Lee et al., 2008; Lawson et al., 2008) as well as other animals such as mackerel (Gorska et al., 2005), Japanese anchovy (Miyashita, 2003), salps (Wiebe et al., 2010), and squid (Jones et al., 2009). Recent studies suggest that euphausiids spend most of their time at orientations where they are nearly horizontal in the water column (Demer and Conti, 2005,

Conti and Demer, 2006; Lawson et al., 2006), and for this range of animal orientations there may be little difference between DWBA and SDWBA model predictions. For these reasons we elected to use the DWBA model parameterized using recent measurements of the material properties and shape of Bering Sea euphausiids (Smith et al., 2010) to estimate TS, and evaluate the effects of animal shape, length, material properties, orientation, and curvature on these estimates.

METHODS

Animal length, shape, species, and material properties were measured at sea for live euphausiids (Smith et al., 2010) collected in short tows made near the surface at night using a Methot trawl (MT; Methot, 1986). A Methot trawl is a rigid-frame trawl and depressor vane with a 5 m^2 mouth opening, 2 mm x 3 mm oval mesh in the body of the net, and 1 mm mesh in the codend, towed at 2-3 kts. Zooplankton samples were collected at nine stations from 20 June to 09 July, 2008 during the Bering Sea acoustic-trawl pollock survey aboard the NOAA Ship *Oscar Dyson* (Figure Ch2.b.1). These data, as well as several different distributions of animal orientation from the literature, were used to parameterize the DWBA model. Since strong species-specific differences in length and material properties were not observed in these data (Smith et al., 2010), euphausiids of all species are modeled using the same parameters. The effect of each model parameter on TS estimates for acoustic frequencies from 10 to 1000 kHz was calculated. Methot trawls conducted on euphausiid layers during daytime were used for comparisons of acoustic and net capture estimates of euphausiid density.

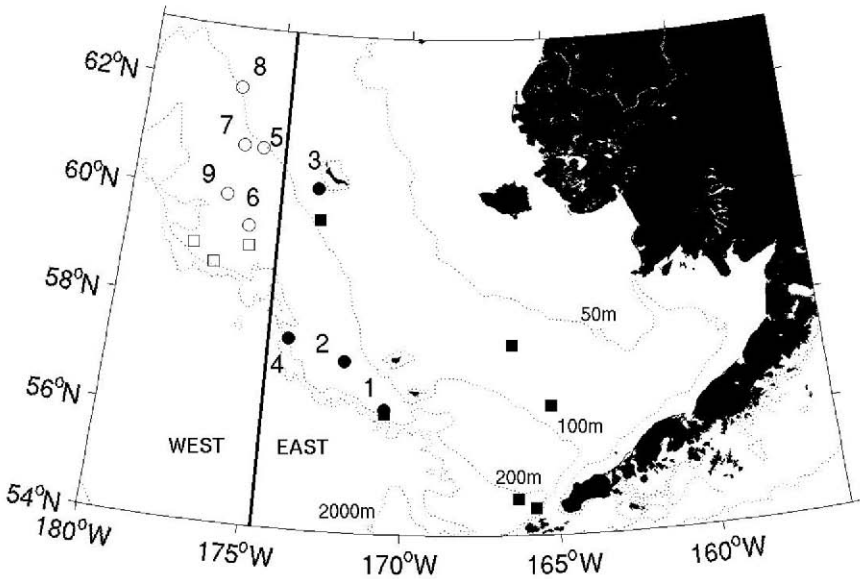

Figure Ch2.b.1. Station locations are shown for Methot trawl (MT) (numbered circles) where material property measurements were made and daytime trawl (DT) (squares) stations where concurrent acoustic and net data were collected. Stations were divided into East (filled) and West (open) regions. DT and MT stations were conducted on different cruise legs during the summer of 2008. Bathymetry contours (dotted lines) are shown for 50, 100, 200, and 2000 m.

Model Parameterization and Sensitivity

Target strength predictions from the single integration DWBA model (equations 5 and 6) rely on the shape of the euphausiids (L and *a*), their material properties (γ_κ and γ_ρ), and their orientation and curvature ($ß_{tilt}$).

Animal Shape

Chu et al. (1993) described the shape of the euphausiids using a taper function:

$$a(z) = a_0 * \sqrt{\left[1 - \left(\frac{z}{(L/2)}\right)^T\right]} \qquad (7)$$

where T is the taper variable, a_0 is the radius at the midsection of the euphausiid (z = 0) which is half of the measured width (widest part of the first thoracic segment), and L is the length of the animal from the anterior tip of its eye stalk to the posterior tip of its telson (Foote, 1990; McGehee et al., 1998, Demer and Conti, 2005). Previous studies of Antarctic krill (Chu et al. 1993, Lawson et al. 2006) used a taper value of 10 (taper occurs rapidly near the edge of both ends of the animal), but a taper variable equal to 2 (taper is gradual and begins near the mid-section of the animal) was a better visual match to the shape of the Bering Sea euphausiids. However, a more realistic shape model was created by measuring the animal's height (dorsal to ventral distance), which was later used to calculate the radius, in 0.5 mm increments along the length of the body from digitized images of four Bering Sea euphausiids. The radii was normalized by dividing each radii measurement by the largest radius measurement so that the radius values ranged from 0 to 1. The length of the euphausiid's body was also normalized (to a value of two) and shifted so that the animal's telson was considered to be point -1, the midpoint was 0, and the end of the eye was 1 (Figure Ch2.b.2). This was done to create a length-independent shape function applicable to krill of any size. The normalized radius measurements were then averaged for all animals, and two shape functions (a smoothly-varying sixth-degree polynomial and a segmented five-part piecewise) were fit to these measurements. The new shape function was based on measurements of four animals, but there was little variation between each animal (mean standard deviation in normalized radii was 0.04). The sixth-degree polynomial function, the piecewise function, and the two taper functions (with T = 10 and 2), were separately used to describe the shape of the animal in the DWBA model to estimate the TS of euphausiids.

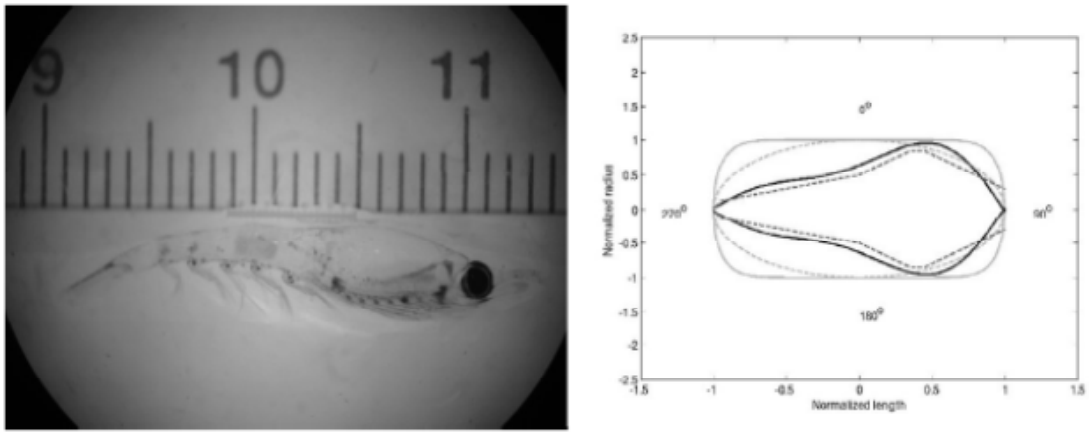

Figure Ch2.b.2. An image of a euphausiid (left, scale is cm) and the different functions (right) used to define the euphausiid shape in the target strength model: taper (T=10) (solid grey, taper (T=2) (dashed grey), polynomial (solid black), and piecewise (dashed dark grey). The incidence angle is also included where 0° is broadside incidence. Notice that the polynomial and piecewise functions more accurately represent the shape of the euphausiid.

To compare the differences in model predictions of TS for the four shapes, the scattering spectra were calculated for each shape function for two different cases, all shapes with the same mean radii (1.5 mm) and different volumes (taper (T = 10) V = 5.98 mm^3, taper (T = 2) V = 5.03 mm^3, polynomial V = 2.34 mm^3, and piecewise V = 1.68 mm^3), and all shapes with the same volume (5.98 mm^3) but different radii (different radii (r) of each shape: taper (T=10) r = 1.0 mm; taper (T=2) r = 1.1 mm; polynomial r = 1.6 mm; piecewise r = 0.9 mm). In general, TS models are parameterized using length and width (or height) measurements (not using animal volume); however, varying volumes can have an effect on TS as well as the frequency response of the scattering. Thus, both scenarios (constant radii and varying volumes, varying radii and constant volumes) were examined and calculations were made over the frequency range of 10 – 10 00 kHz.

Animal length

TS was estimated with the DWBA model for each euphausiid measured in this study using the measured values in animal length, *g*, and *h*. Assuming the orientation of a euphausiid does not change, the TS will increase with the length of the animal, although this relationship is not linear (Chu et al., 2000). By applying the measured *g* and *h* values to the DWBA model, the range of TS values for different length measurements was examined at a frequency of 120 kHz.

Material properties

Measurements of material properties of live Bering Sea euphausiids (Smith et al., 2010) were used to parameterize the TS model. In that study, the density contrast (*g*) was measured for individual euphausiids, whereas the sound speed contrast (*h*) measurements were made on multiple groups of euphausiids from the same MT. These measurements were averaged together and the mean *h* value was assigned to each individual euphausiid in that MT. We also examined whether *g* and *h* measured at the same location were correlated.

The effects of *g* and *h* on TS model predictions were examined by calculating TS values using the minimum, maximum, and mean *g* and *h* values observed in the Bering Sea, as well as selected *g* and *h* values from other studies (Greenlaw and Johnson, 1982; Køgeler et al., 1987; Chu and Wiebe, 2005) for an animal with mean length and broadside incidence at a frequency of 120 kHz while the other parameters (orientation, shape, length) were kept constant. The material property value (M) was calculated for each individual animal using measured values of *g* and *h* and then averaged for each MT to produce a site-specific M value. This value was used to calculate the mean TS for euphausiids at each location.

Animal orientation and curvature

Animal orientation (θ) is the angle between the line joining the bent cylinder's ends and the horizontal plane (Lawson et al., 2006). In order to determine the influence of orientation on TS estimates, several different Gaussian distributions describing animal orientation were applied to the DWBA model. The distribution of orientations observed for euphausiids measured in an aquarium was found to be $N(\theta,\sigma_\theta)=N(45.3,30.4)$ by Kils (1981) and $N(\theta,\sigma_\theta)=N(45.6,19.6)$ by Endo (1993), where θ is the mean angle of orientation and σ_θ is the associated standard deviation. *In situ* observations of euphausiid orientation include N(9.7,59.3), N(0,27.3) (Lawson *et al*., 2006), and N(0,30) (Kristensen and Dalen, 1986). Distributions of *in situ* euphausiid orientation estimated by inversion of euphausiid scattering models include N(15,5) (Demer and Conti, 2005) and N(11,4) (Conti and Demer, 2006).

Both the animal's orientation and the radius of curvature (ρ_c) are used to define the parameter $ß_{tilt}$. Assuming the echosounder is pointing down through the water column, an animal is at normal (broadside) incidence (θ = 0°) if it is horizontal in the water column. At the midpoint of the euphausiid, $ß_{tilt} = \theta$, however this relationship does not hold true along the length of the euphausiid because of the

curvature of its body. The mean radius of curvature was determined for the euphausiids examined in this study (using the geometry described in Stanton, 1989). Assuming that ρ_c remains constant for all euphausiids, a single value of ρ_c was applied.

Estimates of euphausiid numerical density

A Simrad EK 60 echosounder and vessel-mounted acoustic transducers located on a lowered centerboard 9.15 m below the sea surface were calibrated via the standard target method (Foote *et al*., 1987) and used to measure volume backscattering strength (S_v, dB re 1 m^{-1}) at five frequencies (18, 38, 70, 120, 200 kHz). S_v is the logarithmic measure of combined echo intensity from multiple scatterers in a given volume, which can be used to estimate the numerical abundance of scatterers. The linear form of S_v is the volume backscattering coefficient (s_v, m^{-1}) (Simmonds and MacLennan, 2005).

Concurrent comparisons of s_v and the density of euphausiids estimated from nighttime Methot tows used to capture live specimens for *g* and *h* measurements were not possible. These nighttime tows collected euphausiids in the upper 10-20 m of the water column where s_v data were not available because of the depth of the vessel-mounted transducers and the necessary blanking distance beneath the transducers to account for pulse transmission and transducer ringing. Instead, nine daytime Methot tows that were deployed to sample length and species composition of euphausiid scattering layers located well below the sea surface (identified based on their frequency response; De Robertis et al., 2010; Ressler et al. 2012) were used to compare acoustic and net tow estimates of euphausiid numerical density. Smith et al. (2010) found spatial variation in euphausiid material properties between east and west sides of the study site, so the nine daytime tows (DTs) were grouped accordingly, with DT 1-6 constituting the East region and DT 7-9 comprising the West region (Figure 1). Values of M were determined for each DT (based on the region) and the length distribution data gathered from each DT were used to estimate a length-weighted σ_{bs} for each DT using the DWBA model. The mean s_v over the portion of the water column sampled by each daytime Methot trawl was calculated, accounting for the mouth area of the net, the amount of wire out during the net deployment, and the setback between acoustic transducers and the net

frame. Observed s_v and σ_{bs} were used to solve for the number of animals (N) present in one m^3 of water using the equation

$$s_v = \sum_{i=1}^{m} N_i \sigma_{bs_i} \qquad (8)$$

where m is the number of different types of scatterers in the volume. It was assumed that euphausiids were the dominant acoustic target (m=1). This acoustically-estimated quantity was compared with numerical density estimated from the flowmeter-equipped Methot trawl. This procedure was followed for all nine DTs.

RESULTS

Target strength values for individual euphausiids were calculated for all MTs and scattering model input parameters were varied to determine their effect on euphausiid TS. In order to evaluate the influence of one parameter on TS estimates, other parameters were kept constant and the mean material properties and animal length were used (Table 1; Smith et al., 2010).

Animal shape

From measurements of radius along the length of the body, an average euphausiid shape was defined by fitting a sixth-degree polynomial to the data:

$$a = 0.83z^6 + 0.36z^5 - 2.1z^4 - 1.2z^3 + 0.63z^2 + 0.82z + 0.64 \qquad (9)$$

where z is the normalized length of the animal ranging from -1 to 1 and a is the animal radius in mm. The same data are also described by the following piecewise function:

$$\begin{aligned} z &= -1 \text{ to } -0.95 & a &= 2.5z + 2.5 \\ z &= -0.95 \text{ to } 0 & a &= 0.39z + 0.5 \\ z &= 0 \text{ to } 0.35 & a &= z + 0.5 \\ z &= 0.35 \text{ to } 0.45 & a &= 0.85 \\ z &= 0.45 \text{ to } 1 & a &= -1z + 1.3 \end{aligned} \tag{10}$$

The polynomial shape function is smoothly-varying along the animal length and resembles the actual animal shape more closely. In contrast, the piecewise function has sharp changes in the shape of the animal along the body length. The taper function (using both taper variables T=10 and 2) assumed that the euphausiid was symmetrical (dorsal-ventral) while the polynomial and piecewise functions do not (Figure 2).

When the radius was kept constant but the volume changed for each shape equation, the polynomial and piecewise functions had smaller TS values compared to the taper functions for most frequencies although this varied with some frequencies depending on the behavior of the function (Figure Ch2.b.3). There was a considerable difference in TS values between the functions; for example, at 120 kHz it resulted in TS estimates 7 dB higher than those using the polynomial shape function, and nearly 10 dB higher than those using the piecewise shape function. The resulting higher TS values are not unexpected considering the animal volume is larger for both taper functions than for the more realistic polynomial or piecewise shapes (Figure 2). To compare different shaped animals with an equivalent volume, TS was also calculated as a function of frequency for animals with the same volume of 5.98 mm^3 (not shown). To maintain the same volume, the radius for each shape function was different (taper (T = 10) r = 1 mm; taper (T = 2) r = 1.1 mm; polynomial r = 1.6 mm; piecewise r = 1.89 mm). As was true for the same radius but different volumes scenario, in nearly all cases where the volume was constant but the radius changed, the polynomial and piecewise functions had smaller TS values compared to the taper function for most frequencies. In both cases, the use of different shape models also changed the shape of the TS curve as a function of frequency, altering the location of peaks and nulls (Figure 3). Since the polynomial shape model most closely matched the shape of the euphausiids we examined, it was used in subsequent scattering model calculations.

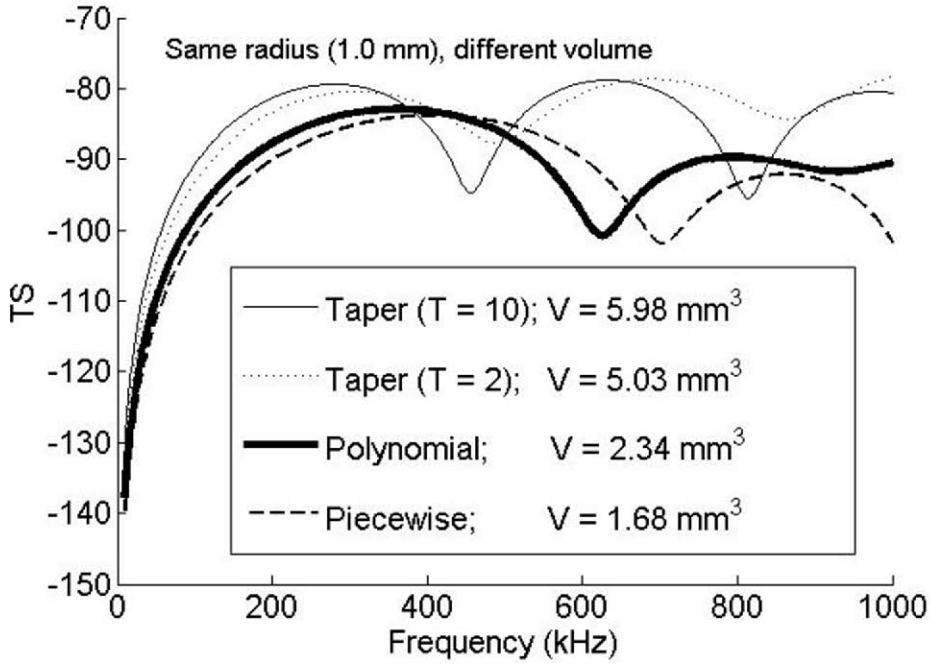

Figure Ch2.b.3. TS (dB re 1 m^2) calculated as a function of frequency for individual euphausiids with mean length, *g*, and *h* values measured from the Bering Sea. Calculations were made for an animal with broadside incidence and polynomial shape. Constant radius (r = 1 mm) used for each euphausiid shape, while the volume (V) varied among shape models.

Animal length

As expected when TS was calculated for different lengths using the *g* and *h* measurements for each individual euphausiid, TS increased with animal length (Figure Ch2.b.4). There was, however, a wide range in TS for each length measurement, with some lengths having nearly a 30 dB difference. This range in TS values for one length measurement indicates that a significant portion of variability in TS comes from the other parameters.

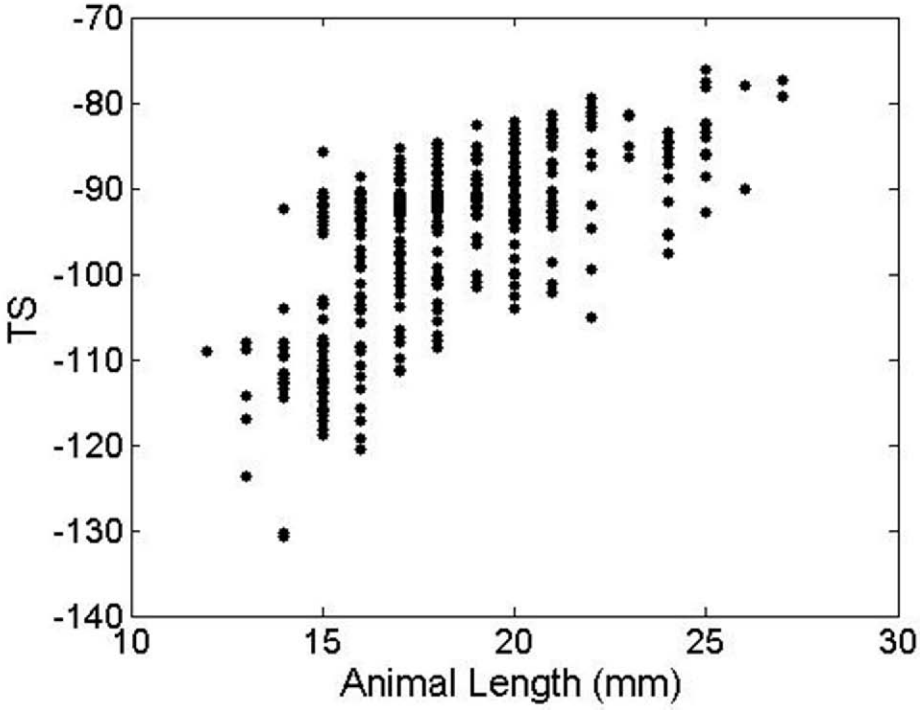

Figure Ch2.b.4. TS (dB re 1 m^2) calculated for each individual euphausiid collected from the Bering Sea (N = 380) using the measured length, width, *g*, and *h*, the polynomial shape function, a frequency of 120 kHz, and a broadside orientation.

Material properties

TS was evaluated as a function of frequency for the most common echosounder frequencies used in fishery surveys (18, 38, 70, 120, and 200 kHz) over a range of *g* and *h* values including the minimum, mean, and maximum values from measurements of individual Bering Sea euphausiids, as well as measurements of euphausiids in other studies. Each calculation of TS was made with either *g* or *h* varying while other model parameters were held constant at the mean values observed for Bering Sea specimens (Table 1) and at broadside incidence using the polynomial shape function. As both material properties increased, so did the TS estimates, although not linearly (Figure Ch2.b.5; these calculations were made at 120 kHz, but the relationship holds true for all frequencies in the geometric scattering regime). Linear regression was used to test for a relationship between the two material properties, but there was no significant correlation between mean *g* and *h* for Bering Sea euphausiids at each MT station where both properties were measured ($r = -0.22$, $p = 0.59$, $n = 8$; Figure Ch2.b.6). However, the relationship between *g* and *h* is difficult to evaluate, because *g* is measured on individual animals and *h* is measured on groups of animals.

TABLE 1. Minimum, maximum, and mean of physical and material properties measured for Bering Sea euphausiids (N = 380).

	Min	**max**	**mean**
Length (mm)	12	27	18.2
Height (mm)	1	5	2.5
g	1.001	1.041	1.017
h	0.9898	1.014	1.005

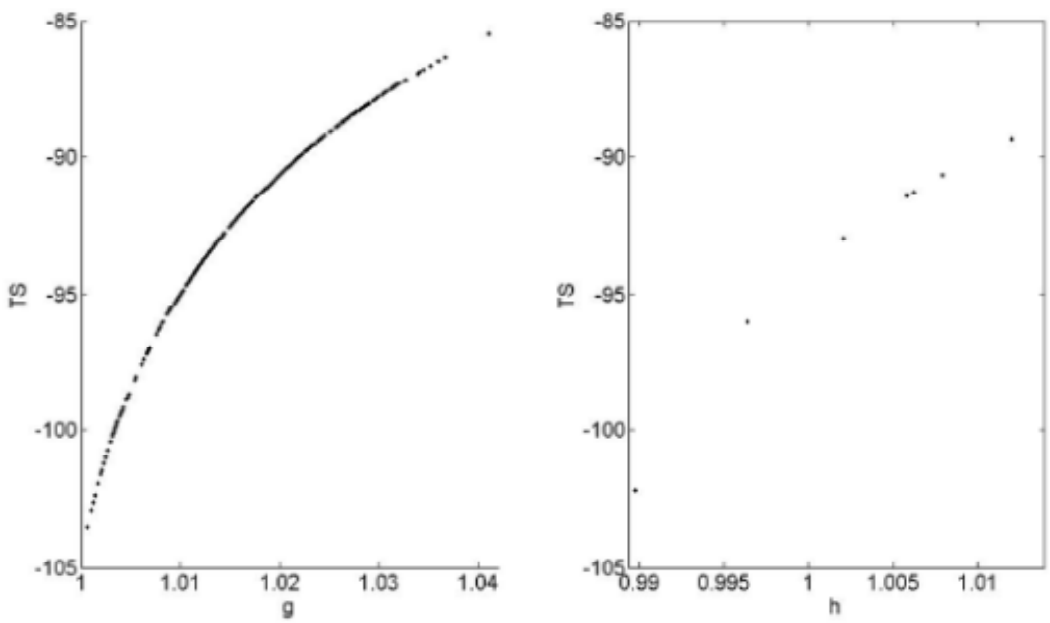

Figure Ch2.b.5. TS (dB re 1 m^2) estimates as a function of *g* (left panel, other parameters: mean length, mean *h*, 120 kHz, broadside incidence, polynomial shape) and as a function of *h* (right panel, other parameters: mean length, mean *g*, 120 kHz. broadside incidence, polynomial shape). Measurements of *h* were made on groups of animals, so there are fewer observations than for the *g* measurements.

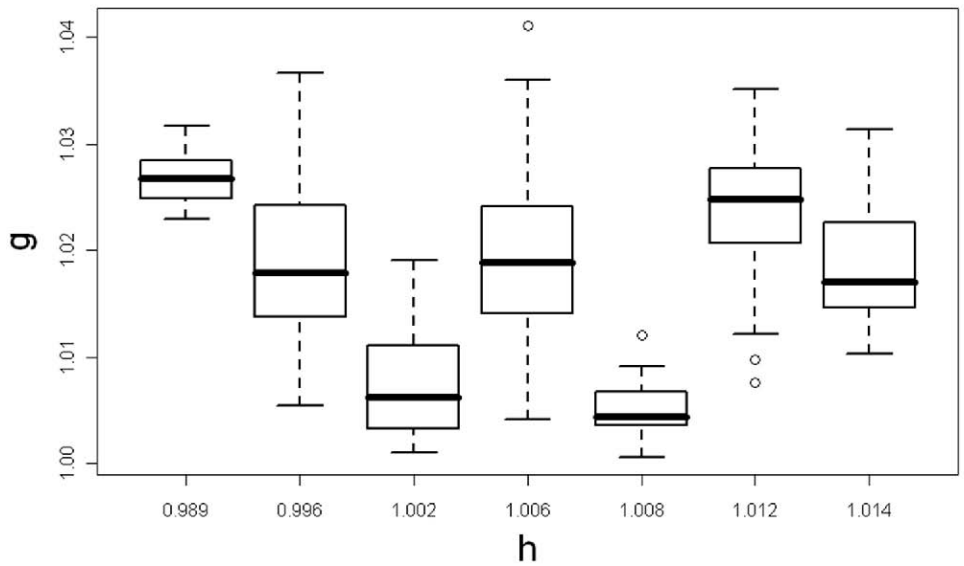

Figure Ch2.b.6. Boxplot of density contrast (*g*) as a function of sound-speed contrast (*h*). Boxplots indicate 25th, 50th, and 75th percentiles, whiskers indicate the 95% confidence interval, and outliers are shown as circles. Note that *g* is measured on individuals while *h* is measured on groups of animals. No correlation between the two properties is indicated.

Since there is not a simple relationship between *g* and *h*, the minimum *g* and *h* values do not necessarily produce the minimum TS value; likewise, the maximum *g* and *h* values do not necessarily produce the maximum TS value, and the mean material properties of Bering Sea euphausiids may not be correctly represented by mean (*g*) and mean (*h*). To determine average TS values, mean TS was calculated for each MT using the mean M (material property parameter, a function of both *g* and *h*) instead of mean *g* and *h* (Table 2).

Table 2. The mean material property parameter (M) and associated standard deviations calculated for each MT and the resultant mean Target Strength (TS). M was not calculated for MT06 because there was no *h* value collected for that location. Calculations were made using the M value and mean length from each MT at 120 kHz and broadside incidence.

MT	M		TS
	mean	sd	
1	0.026	0.005	-98.6
2	0.018	0.009	-101.5
3	0.032	0.022	-96.8
4	0.045	0.009	-93.7
5	0.070	0.010	-89.9
7	0.032	0.005	-96.7
8	0.067	0.016	-90.3
9	0.057	0.011	-91.7

The large variability in *g* and *h* measurements emphasizes the importance of measuring material properties at each new study site, since differences in *g* and *h* measurements can have large effects on TS estimates (Chu et al., 2000). Often literature values of *g* and *h* (from other geographic locations or even different species) are used in TS models, however this approach (while practical) can produce substantially different TS estimates compared with a site-specific approach (Table 3).

Table 3. Target Strength (TS) values were calculated by maintaining mean parameters and altering either *g* or *h* separately. This table gives the difference in TS values away from the TS estimate using mean parameters (i.e .difference in TS away from g_{mean} or h_{mean}). Material properties used from other studies are as follows: $g_{Greenlaw\ and\ Johnson}$=1.050, $g_{Køgeler}$=1.062, h_{Foote}=1.0279, $h_{Køgeler}$=1.031, and $h_{Chu\ and\ Wiebe}$=1.048. Mean length was used in calculations for an animal at broadside incidence with a polynomial shape.

g	*H*	ΔTS
g_{min}	h_{min}	-7.3
	h_{mean}	-11.2
g_{mean}	h_{min}	-1.8
	h_{max}	+2.9
	h_{Foote}	+6.0
	$h_{Køgeler}$	+6.6
	$h_{Chu\ and\ Wiebe}$	+9.1
g_{max}	h_{mean}	+6.2
	h_{max}	+7.7
$g_{Greenlaw\ and\ Johnson}$	h_{mean}	+7.7
$g_{Køgeler}$	h_{mean}	+9.3

Animal orientation and curvature

The mean radius of curvature for the euphausiids examined was $\rho_c = 3.3L$. Stanton et al. (1993a) estimated euphausiid curvature to be 3L, although they also showed that when backscattering cross-sections are averaged over a range of angles then they are nearly independent of ρ_c when $\rho_c \geq 2L$ (which is true in this study). A linear regression found no significant difference in the TS estimate when using either $\rho_c = 3.3L$ or $\rho_c = 3L$; thus, 3.3L was used for all subsequent computations.

Across a range of frequencies, orientation had a large impact on TS estimates made using various distributions of euphausiid orientation reported by other studies (Figure Ch2.b.7). Polynomial shape, mean length, and mean material properties were used to compute TS at each combination of orientation and frequency. Broadside incidence (i.e. dorsal insonification) produced the largest TS values and the least amount of peaks and nulls across the range of frequencies. As expected, orientation distributions near broadside incidence (N(15,5) from Demer and Conti, 2005 and N(11,4) from Conti and Demer, 2006) produced TS estimates similar to those produced when the animal was oriented at broadside incidence. The euphausiids described by Kils' (1981) orientation distribution are not horizontal in the water column and are at an angle (45.3º) with a large standard deviation (30.4); consequently, this orientation distribution produced the lowest TS estimates.

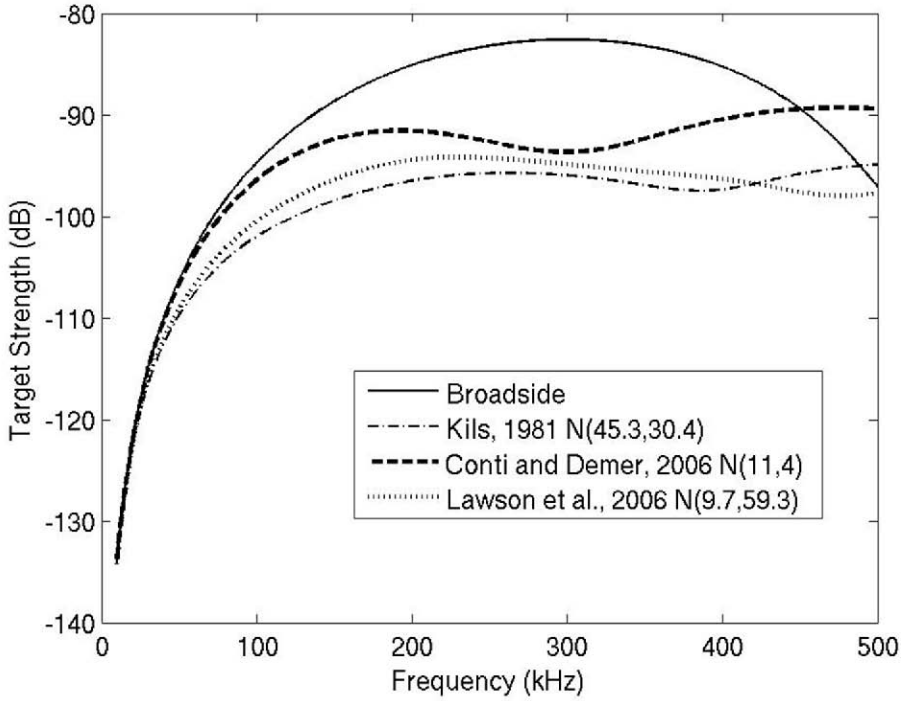

Figure Ch2.b.7. Modeled euphausiid target strength as a function of frequency for several different orientation distributions N(mean, standard deviation): N(0,0) broadside incidence, N(45.3,30.4) from Kils (1981), N(11,4) from Conti and Demer (2006), and N(9.7,59.3) from Lawson et al. (2006). The mean length and material properties were used to calculate the TS for a polynomial shaped euphausiid.

Estimates of numerical density at these tow locations

Numerical densities were calculated for nine DT locations using observed S_v, measured euphausiid lengths, and either the mean M for the study or the east or west region containing the tow. DWBA model calculations were made at 120 kHz for euphausiids at broadside incidence with a polynomial shape. When the numerical densities derived from acoustic data were compared to those estimated from the net tow catches, the acoustic estimates were always larger, often by several orders of magnitude (Figure Ch2.b.8). Site-specific information on material properties in TS model computations changed acoustic estimates of euphausiid density in scattering layers by a factor of 0.6 – 2.1 across these locations, and increased the overall mean numerical density by a factor of 2 when compared to acoustic estimates which used a single mean M value for the entire region. Averaging over all sites in the study, euphausiid numerical densities (# m^{-3}) were 6 (net), 1200 (acoustic using site-specific M values), and 600 (mean M value).

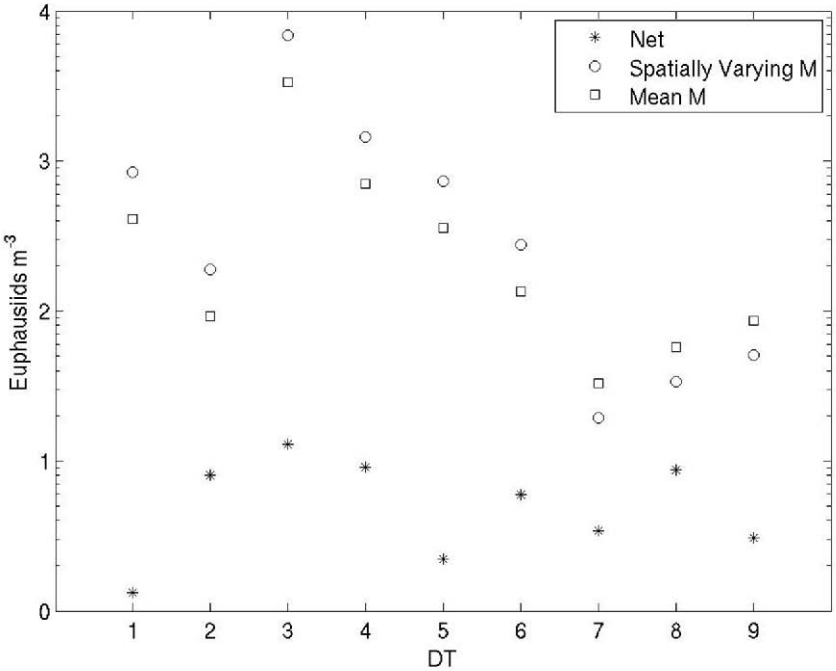

Figure Ch2.b.8. Comparison of numerical densities at nine daytime trawl (DT) stations from net measurements and two acoustic methods which used measured S_v data, euphausiid length data from the DT net tows,, and material property measurements from nearby MT stations. S_v data were inverted for euphausiid numerical densities by calculating a length-weighted, mean Target Strength (TS) value for each DT location. Material property (*g* ,*h)* values in the model were either the mean M value for all data collected or were averages for the East and West regions of the study area (see Smith et al., 2010 for reasons for the differences). Target strength calculations were made for backscatter at 120 kHz for polynomial-shaped euphausiids at broadside incidence. Note that numerical densities are presented on a logarithmic scale.

The potential importance of using site-specific animal information for TS can be further demonstrated by a closer examination of the DT numerical density data. Station pairs were selected that had equivalent acoustically-estimated numerical densities using either the site-specific or mean M values. Only one pair (DT 2 and 9) met this criteria where the acoustic estimates of numerical density (using a mean M value) were equivalent (92 and 86 animals m^{-3} respectively). Using single values of animal material properties is the standard procedure in acoustic surveys, so these data reflect what most acoustic surveys of euphausiid abundance would produce and suggest that the animal abundance at these two sites were similar. However, net tow numerical density data showed the numerical densities at DT 2 to be approximately three times greater than at DT 9 (8 and 3 animals m^{-3} respectively). This pattern was also seen when site-

specific M values were used to acoustically estimate numerical densities, with DT 2 being 3.5 times as dense as DT 9 (188 and 50 animals m^{-3} respectively). Given that only one pair of sites could be compared in this manner, these results are not conclusive.

DISCUSSION

A DWBA model was parameterized using observed physical and material properties from live Bering Sea euphausiid specimens. Examination of model results indicated that the more realistic empirical model of euphausiid shape and locally-measured, spatially-varying material properties could have a significant effect on model predictions of TS and resulting estimates of numerical density. Parameterization of the expected distribution of euphausiid orientations *in situ* also had a strong influence on model results.

Effect of shape

The sixth degree polynomial model presented in this study most realistically portrays the animal as being asymmetrical from head to tail. Unlike the piecewise function, it does not contain inflection points or abrupt changes in the animal width. The taper function produced higher TS estimates than polynomial and piecewise functions for animals of the same length but different volumes, as well as for animals of the same volume but different lengths, furthermore suggesting that the chosen shape function is important to model predictions. TS estimates for Bering Sea euphausiids in this study produced using the more realistic polynomial model of animal shape will be lower (and lead to higher acoustic estimates of euphausiid density) than those produced with models that use a taper function.

Effect of length

There was a clear, positive relationship between animal length and their model-estimated TS (Figure 4), varying by approximately 30 dB over the lengths observed in this study. Length and width measurements are critical to more accurately parameterizing scattering models in acoustic surveys, and these measurements are relatively easy to collect with standard net or optical zooplankton sampling techniques.

Effect of material properties

Material properties were highly influential to model predictions. Both *g* and *h* were shown to increase TS as *g* or *h* diverged from unity, with TS varying by 15-20 dB, although this relationship was not linear (Figure 5) as was found by Chu et al., 2000. Density contrast (*g*) had a greater influence on the TS estimate compared to sound speed contrast (*h*), although this may be the result of the measured *g* being more variable than measured *h*. The range of TS calculated using the highest and lowest M values measured in the Bering Sea was smaller than the range of TS calculated from material properties measured in this study and values reported in the literature (Table 3), demonstrating that taxon- and area-specific measurements of material properties help reduce and characterize uncertainty in model predictions.

Even with site-specific measurements of g and h, there are uncertainties associated with the measurement methods (in particular the time-of-flight method) which may produce error (or uncertainty) in the modeled TS (Smith et al., 2010). Our estimates of the TS of Bering Sea euphausiids are generally lower than what would have been calculated had we assumed material property values for other euphausiid species from other locations as is typically done in acoustic surveys. Since *g* and *h* measurements showed large variability, and the way in which these physical quantities vary together in individual animals is unclear, we contend that mean M (a function of both *g* and *h*) should be used in scattering model predictions instead of the mean *g* and mean *h*.

Material properties which are difficult to measure have been shown to be related (Smith et al., 2010) to a variety of different factors including animal size; water temperature, density, or soundspeed; or chlorophyll-a concentration which are often simpler to measure. In the future, it may be possible to predict values of material properties from these more easily-measured parameters but this requires a better understanding of how and why g and h vary in animals. Until we have more knowledge on this subject, measuring g and h directly is the best way to have the most accurate TS estimates for a particular acoustic scatterer.

Effect of orientation

We were not able to measure the *in situ* orientation of Bering Sea euphausiids, so distributions of euphausiid orientations from other studies (Kils, 1981; Endo, 1993; Demer and Conti, 2005; Conti and Demer, 2006) were used to evaluate the effect on DWBA model predictions. Orientation has a large effect on model predictions of euphausiid TS, particularly at higher frequencies (Figure Ch2.b.7). As expected, broadside incidence produced the largest TS values (Figure Ch2.b.7) and distributions with animals swimming nearly horizontally (Demer and Conti, 2005 and Conti and Demer, 2006 orientation distributions) had TS estimates close to measurements made at broadside incidence. Properly

characterizing the distribution of orientation for the specific animals and location being studied is clearly important, although these observations are difficult to collect *in situ*.

Numerical density estimates

While there were large differences in euphausiid numerical densities measured acoustically and by net tow, there were also significant differences in euphausiid numerical density depending on what material property values were used in the target strength model. Different spatial regions of our study area had euphausiids with significantly different material property values (Smith et al., 2010), and we showed a case (DTs 2 and 9) in which using site-specific information (rather than mean values) in the TS modeling revealed the same relative patterns as the net data. Although this is not conclusive, it does suggest that using site-specific information may provide a more accurate representation of spatial patterns or differences in acoustic estimates of zooplankton biomass. It may be difficult to implement for every acoustic survey, but the most accurate numerical density estimates would result from a TS model parameterized with site-specific material and physical animal properties.

We do not fully understand what factors cause the spatial variation in g and h that have been found previously (Smith et al., 2010) although internal changes in the animal's physiology or composition are logical explanations. Forman and Warren (2010) found that gravid and non-gravid crustaceans (and the eggs) all had different g values which may be the result of different levels of energy storage or expenditure by individual animals. Smith et al. (2010) showed that g values varied with animal size and environmental factors (specifically chlorophyll-a and temperature) which is consistent with the theory that material properties are related to levels of food availability or metabolic requirements of the krill as it uses or stores lipids or builds muscle or other structures.

The acoustic estimates of euphausiid density in euphausiid layers sampled with trawls were much higher than densities estimated from the catch in the trawls. This is universally true when such comparisons have been made in the literature (e.g., Coyle and Pinchuk, 2002, Warren et al., 2003; Warren and Wiebe, 2008). It is not clear whether the net capture or acoustic estimates more correctly represent the true density of euphausiids at these stations. It is difficult to quantify the uncertainty or possible bias in single net sample estimates (Clutter and Anraku, 1968), but it has been shown experimentally that euphausiids can often avoid capture by nets, leading to 2-20 fold underestimates by net samples (Sameoto et al., 1993; Wiebe et al., 2004). Other explanations for an overestimate of euphausiid density by acoustic techniques could include contributions to S_v from organisms other than euphausiids, or a low bias in model-derived TS predictions.

Methot tows where scattering from age-1 and older walleye pollock occurred in the trawl path were not used for the comparison we presented here, since the Methot trawl is not effective at capturing large nekton. Ressler et al. (2012) showed that euphausiids often dominated the measured scattering from crustacean mesozooplankton in the Bering Sea, and in some cases our site-specific acoustic estimates of numerical density (e.g. compare estimated densities at DT 2 and 9, Fig. Ch2.b.8) were greater than the net data by a factor of approximately 20 or less, which could be due entirely to net avoidance. However, since we cannot rule out contributions to scattering from unretained organisms (Warren and Wiebe, 2008), the acoustic estimates of the numerical density of euphausiids presented here may be overestimated (Warren *et al*., 2002).

In addition, since the animals used for material properties measurements were collected from different tows than those used for comparison of numerical densities estimated acoustically and via net capture (Table 2), there may be additional uncertainties in comparing net and acoustic estimates due to the horizontal (Smith *et al*., 2010) or vertical spatial variation in the material properties of euphausiids. Measurement of material properties at depth is difficult and has only successfully been done for h (and not g) for Southern Ocean euphausiids and copepods (Chu and Wiebe, 2005). Results from their study were mixed with one krill species (E. superba) having no variation in h with depth, but copepods and a different krill (E. crystallorophias) did. Further work on material properties, *in situ* orientation, TS model validation, and comparisons of acoustic estimates of euphausiid density with other techniques are needed to resolve this question. At present, acoustic estimates may best be considered an upper bound (and net capture estimates a lower bound) on the numerical density of euphausiids (Warren and Wiebe, 2008).

Recommendations

Several of the parameters we evaluated have the potential to alter model predictions of euphausiid TS by several orders of magnitude, leading to similar uncertainties in euphausiid population estimates. Since many of these parameters (e.g., length, orientation, material properties) will vary within a typical survey area (and sometimes even within a single aggregation of krill), values used to calculate a mean TS value to produce biomass estimates should be chosen (and tested) carefully. Measurements of the material properties and shape of Bering Sea euphausiids constrained the uncertainty in model TS estimates in this study, but despite the demonstrably improved information on shape and material properties, the disparity between acoustic and net sample estimates of euphausiid densities remained large. Correctly characterizing the *in situ* orientation of euphausiids remains a challenge, and more observations are needed. Our results demonstrate that uncertainty in TS model predictions is reduced if models are parameterized for specific zooplankton taxa in the region of study, rather than applying parameters for other taxa in other regions (commonly done due to a lack of data for many species).

Though it presents logistical challenges, acoustic surveys over large areas may need to measure scattering model inputs at multiple sites, particularly in regions where environmental or zooplankton characteristics may vary greatly.

ACKNOWLEDGEMENTS

This project was supported by the Alaska Fisheries Science Center, National Marine Fisheries Service, NOAA, and the North Pacific Research Board's Bering Sea Integrated Ecosystem Research Program. The captain, crew, and scientists aboard the NOAA ship Oscar Dyson provided excellent logistical support and sampling assistance. Abigail McCarthy helped us greatly with the set up and maintenance of the on board aquaria as well as with the trawl sampling operations. The comments of Dezhang Chu, Kresimir Williams, and several anonymous reviewers helped improve this manuscript. This was NPRB publication number 352 and BEST-BSIERP publication number 64. The findings and conclusions in the paper are those of the authors and do not necessarily represent the views of the National Marine Fisheries Service.

Chapter 2.c. Abundance and distribution of euphausiids and walleye pollock, 2004-2010

The research on euphausiid material properties and target strength described in the previous two sections allowed us to develop an acoustic survey of Bering Sea euphausiids. Chapter 2.c describes the method we used to convert acoustic backscatter collected during the acoustic-trawl survey pollock survey to estimate euphausiid biomass. Secondly, we spatially combined bottom trawl and acoustic-trawl surveys of pollock to develop a shelf-wide estimate of the spatial distribution of pollock. Thirdly, we provide a first comparison of the distribution of predator (pollock) and prey (euphausiids) over multiple years of changing ocean conditions (2004-2010), as well as a survey-based estimate of the fraction of euphausiid standing stock likely consumed by pollock during summer. The material in this section is the work of Ressler (B62 PI), De Robertis, Warren, Smith, and Kotwicki (B62 PI), and was published as:

Ressler, P.H., De Robertis, A., Warren, J.D., Smith, J.N., and Kotwicki, S., 2012. Developing an acoustic index of euphausiid abundance to understand trophic interactions in the Bering Sea ecosystem. Deep-Sea Research II 65-70: 184-195. http://www.sciencedirect.com/science/article/pii/S096706451200029X

Patrick Ressler, Alex De Robertis, and Stan Kotwicki: Resource Assessment and Conservation Engineering Division, Alaska Fisheries Science Center, National Marine Fisheries Service, National Oceanic and Atmospheric Administration, 7600 Sand Point Way NE, Seattle, WA 98115, USA

J. Warren and J. Smith: Stony Brook University, School of Marine and Atmospheric Sciences, 239 Montauk Highway, Southampton, NY, 11968, USA

ABSTRACT

Euphausiids (principally *Thysanoessa* spp.) are a key group of organisms in the Bering Sea ecosystem, linking production at lower trophic levels to top predators and important commercial fish stocks such as walleye pollock (*Gadus chalcogrammus*). Here, we combine multifrequency acoustic survey methods, physics-based models of euphausiid backscatter, and net sampling to provide a means of monitoring the status and trends of euphausiid standing stock biomass on the Bering Sea shelf. Observations made using this approach during six summers (2004 and 2006 – 2010) indicate that standing stocks of euphausiids and pollock were inversely correlated over time as well as in space across the continental shelf. First-order calculations show that when pollock abundance was at its peak during these years, the pollock stock could have consumed 10 - 87% of the euphausiid standing stock between May and September. We hypothesize that predation by pollock is a significant top-down control on euphausiid standing stock in this system.

Keywords: USA, Alaska, Bering Sea, walleye pollock, euphausiids, acoustic survey; 54° N, 64° N, 155° W, 185° W

INTRODUCTION

Euphausiids (Family Euphausiidae) or 'krill' play a key role in the Bering Sea ecosystem. Euphausiids are important prey for many species, forming an important node in the food web and a major pathway for transfer of energy from primary production to higher trophic levels (Aydin and Mueter, 2007). They are also one of the most important prey items for walleye pollock (*Gadus chalcogrammus*, hereafter 'pollock'; Brodeur et al., 2002; Lang et al., 2000; Lang et al., 2005), which supports one of the largest single-species fisheries in the world and the largest fishery by volume in the United States (FAO, 2009; NMFS, 2010). The principal euphausiid species on the Bering Sea shelf are *Thysanoessa inermis* and *T. raschii*; the typical length of adult animals in midsummer is ca. 18 - 19 mm (Coyle, 2000; Coyle and Pinchuk, 2002; Smith, 1991; Stockwell et al., 2001). *Thysanoessa inermis* begins to spawn in April and is more common on the outer shelf (100 – 200 m bottom depth), while *T. raschii* begins to spawn in May and is the dominant euphausiid further inshore; each species is thought to spawn once per year (Dalpadado and Skjoldal, 1996; Pinchuk and Hopcroft, 2006; Smith, 1991). There is some recent evidence that the abundance of euphausiids on the Bering Sea shelf is greater in years with cold, icy springs and cold summers versus years with warmer conditions (Coyle et al., 2008; Coyle et al., 2011; Hunt et al., 2011). Despite their great importance in the Bering Sea ecosystem, however, knowledge of the stock size and factors controlling the population dynamics of euphausiids in the Bering Sea remains limited. For example, the net sampling methods used in existing long-running time series of Bering Sea zooplankton abundance are better suited to capturing smaller zooplankton taxa (such as copepods; Napp et al., 2002) than the larger euphausiids. Time series observations of the abundance and distribution of euphausiids would fill a gap in what is known about this important group of animals in the Bering Sea, benefitting both resource management and our understanding of trophic interactions and ecosystem function.

Seminal observations by Balls (1948) and Sund (1935) in the first half of the 20th century showed that ship-based acoustic echosounders could detect fish schools, and since that time there has been substantial development of acoustic equipment and methods to estimate the abundance of both fishes (Simmonds and MacLennan, 2005) and zooplankton including euphausiids (Foote and Stanton, 2000; Holliday and Pieper, 1995; Sameoto, 1980). Acoustic methods have been applied to studies of euphausiid distribution in the Bering Sea (Coyle, 2000; Coyle and Pinchuk, 2002; Swartzman et al., 2002) as well as in other

locations (Brierley et al., 1997; Lawson et al., 2008; Ressler et al., 2005; Simard,and Lavoie, 1999; Stevick et al., 2008; Warren and Demer, 2010), but the application of these methods to routinely monitor euphausiid stocks has been uncommon due to the limited availability and complexity of the necessary data. The major exceptions are surveys of Antarctic krill, *Euphausia superba*, for which acoustic-trawl surveys are the method of choice (Brierley et al., 1997; Hewitt and Demer, 2000; Hewitt et al., 2004; Reiss et al., 2008). In the Bering Sea, the large-bodied crustacean zooplankton assemblage is dominated by euphausiids (Vidal and Smith, 1986), and multifrequency acoustic data are available from existing resource monitoring surveys (Honkalehto et al., 2010). Recent work on multifrequency classification and ground-truth identification of target species (De Robertis et al., 2010), and new area- and species-specific work on modeling acoustic backscatter from euphausiids (Smith et. al., 2010; Smith, 2010), have made the application of acoustic techniques to monitoring this euphausiid standing stock feasible. This study demonstrates that acoustic methods are a suitable means of monitoring euphausiid standing stock and distribution on the Bering Sea shelf. These standing stock estimates, along with recent pollock survey results, allow us to draw some first-order inferences about the predation impact of pollock on euphausiids and the potential for top-down control of the euphausiid standing stock by predation.

MATERIALS AND METHODS

Survey data sets

Acoustic backscatter and net capture data for midwater pollock and euphausiid distribution and abundance were collected during summertime acoustic-trawl surveys conducted by scientists from NOAA's Alaska Fisheries Science Center (NOAA-AFSC) aboard NOAA Ships *Oscar Dyson* or *Miller Freeman* using standard acoustic survey methods (Simmonds and MacLennan, 2005). Honkalehto et al. (2002) and (2010) provide more details on the routine methods used for estimation of midwater pollock biomass; only an overview, with additional details pertinent to the estimation of euphausiid biomass (which has not been a routine survey product), is given here. The surveys consisted of acoustic backscatter measurements averaged into 0.5 nmi (0.926 km) elementary distance sampling units (EDSUs) along north-south oriented transects spaced 20 nmi (37 km) apart (Figure Ch2.c.1). Acoustically detected aggregations were opportunistically sampled with large midwater and bottom trawls to verify size and species composition of acoustic targets. The survey speed of the vessel averaged approximately 12 nmi hr^{-1} (6 m s^{-1}). Operations were conducted during daylight hours only. The echosounder used was a Simrad[1] EK500 or a Simrad EK60 operating at frequencies including 18, 38, 70, 120, and 200 kHz, at a ping interval of 1 s^{-1}, and calibrated using a standard target (Foote, 1987). Midwater pollock biomass was estimated from 16 m below the sea surface to 3 m above the seafloor. In some years, areas of both the

[1] Reference to trade names does not imply endorsement by the National Marine Fisheries Service, NOAA.

U.S. and Russian exclusive economic zones (EEZs) were surveyed, but we present results only for the U.S. EEZ.

Observations of demersal pollock distribution and abundance were obtained from bottom trawl surveys on the Bering Sea shelf conducted by NOAA-AFSC using chartered fishing vessels. The bottom trawl survey was also conducted only during daylight hours. Area-swept pollock density estimates of pollock within approximately 3 m of the seafloor were made at standard stations located nearby to the acoustic survey transects and spaced at a distance of 20 nmi (37 km, Figure Ch2.c.1; see Lauth, 2010 for details). The bottom trawl survey covered most of the U.S. EEZ sampled by the midwater acoustic survey, as well as areas further inshore where most or all of the pollock stock is found very close to the bottom (Honkalehto et al., 2002; Kotwicki et al., 2005). Both midwater and bottom trawl surveys were conducted from early June to early August in 2004 and 2006 – 2010.

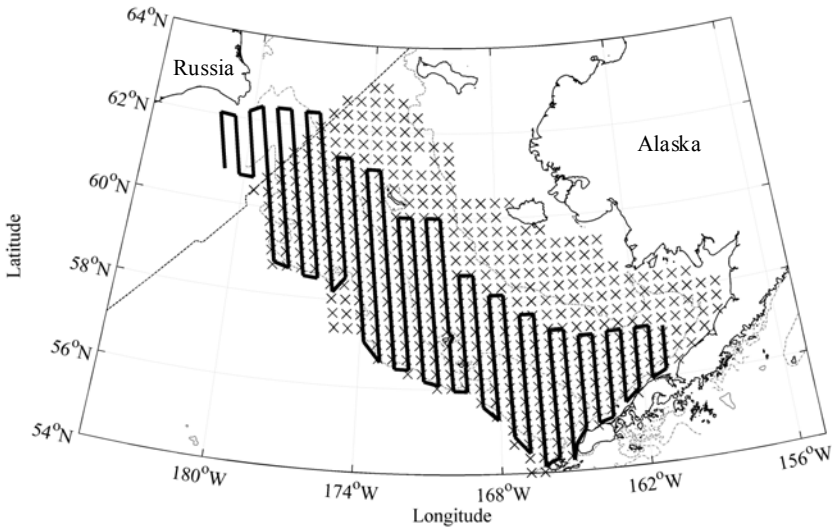

Figure Ch2.c.1. Areas covered by NOAA-AFSC surveys of walleye pollock on the Bering Sea shelf. X symbols indicate locations of bottom trawls deployed by the bottom trawl survey of demersal pollock, while bold black north-south lines indicate transect sampling by the acoustic survey of midwater pollock. The 50, 100, and 200 m isobaths are indicated by gray dotted lines. The convention line dividing the U.S. and Russian EEZ is indicated by a black dotted line.

Classification of euphausiid backscatter

Euphausiid backscatter was identified by comparing the observed backscatter frequency response at 18, 38, 120, and 200 kHz from acoustic survey transects to a reference data set obtained from trawl-verified measurements of frequency response collected between 2004 and 2007 using the method of De Robertis et al. (2010), who present the details of this classification method as well as a rigorous evaluation of its application to classification of backscatter from pollock. Echoview software (Myriax Pty, Hobart, Australia) and custom Matlab (The Mathworks, Natick, MA) routines were used for this work. Briefly, volume backscattering strength (S_v, dB re 1 m^{-1}; see MacLennan et al., 2002 for a review of acoustic terminology) was averaged over 5 ping (horizontal) by 5 m (vertical) cells, and then all pairwise differences between S_v at different frequencies were computed for each of these cells. The absolute value of the mean normal deviate (Z-score) over all frequency pairs for each 5 ping by 5 m cell was computed relative to the expected pairwise frequency differences for each of several taxonomic groups (including euphausiids; see Table 2 in De Robertis et al., 2010). This mean Z-score indicates how well the observed frequency response matches the expectation for the various taxa and can be used to classify each cell; for example, a mean Z-score of 2 relative to the expectation for euphausiid frequency response ($\overline{Z}_{euph} = 2$) indicates that the observed frequency response of S_v in that cell is within approximately two standard deviations of the mean frequency response for euphausiids in the reference set.

Table 1. Parameterization of DWBA model for σ_{bs} of Bering Sea euphausiids

	Low σ_{bs}	Med σ_{bs}	High σ_{bs}
Material properties[a]	$\bar{M}$ - 2 SE = 0.030	$\bar{M}$ = 0.043	$\bar{M}$ + 2 SE = 0.057
Orientation[b]	N(9.7, 59.3)	N(0, 30)	N(11, 4)
Length	Average length composition from 2004 – 2009 Methot tows in inshore (bottom depth < 100 m, n = 21 tows) and offshore (bottom depth > 100 m, n = 38 tows) strata, 1 mm length bins, converted from euphausiid length to krill standard length for model computations		
Width	Computed from krill standard length using a regression based on n = 412 euphausiid specimens measured in 2008		
Shape[c]	Empirical sixth-degree polynomial function with a cylindrical shape and radius of curvature 3.3		

[a] The term 'material properties' refers to sound speed contrast (h) and density contrast (g) of animal tissue with seawater. In the DWBA model, the combined effect of g and h is parameterized using the function $M = | (1-gh^2/gh^2) * (g-1/g) |$; M is positively related to σ_{bs} (Smith, 2010). The mean M and standard errors of the mean (SE) are from n = 448 euphausiid specimens collected at nine stations in the Bering Sea during summer 2008 (Smith et al., 2010).

[b] σ_{bs} model predictions for each 1 mm length bin were averaged over 100 animals with orientations drawn randomly from a normal distribution with parameters N(mean, standard deviation). The references for these distributions of *in situ* euphausiid orientation are Lawson et al. (2006), Kristensen and Dalen (1986), and Conti and Demer (2006).

[c] More details on modeling of euphausiid shape are given in Smith (2010).

Table 2. Estimation of predation impact on euphausiids by pollock. Table parameters are as follows: B_p is the biomass of pollock in the area covered by both surveys, R_d is the fraction of body weight in prey that pollock consumes per day, F_e is the fraction of euphausiids in pollock diet, C_d is the biomass of euphausiids consumed per day by pollock, B_e is the survey estimate of euphausiid biomass, and C is the fraction of euphausiid standing stock consumed by pollock from May – September (150 d).

	2004	2006	2007	2008	2009	2010
B_p[a]	6.5×10^9	4.3×10^9	5.8×10^9	3.9×10^9	3.1×10^9	5.7×10^9
R_d	0.02	0.02	0.02	0.02	0.02	0.02
F_e	0.53	0.53	0.53	0.53	0.53	0.53
C_d	6.9×10^7	4.6×10^7	6.2×10^7	4.1×10^7	3.3×10^7	6.0×10^7
$B_{e, low}$[b]	1.2×10^{10}	2.2×10^{10}	3.0×10^{10}	3.3×10^{10}	3.6×10^{10}	2.9×10^{10}
$B_{e, med}$	2.7×10^{10}	5.1×10^{10}	6.8×10^{10}	7.6×10^{10}	8.2×10^{10}	6.6×10^{10}
$B_{e, high}$	1.1×10^{11}	2.0×10^{11}	2.7×10^{11}	3.0×10^{11}	3.3×10^{11}	2.6×10^{11}
$C_{, low}$	0.87	0.31	0.31	0.19	0.14	0.31
$C_{, med}$	0.38	0.14	0.14	0.08	0.06	0.14
$C_{, high}$	0.10	0.03	0.03	0.02	0.02	0.03

[a] All biomass values are in kg wet weight.

[b] Low, med, and high euphausiid biomass estimates (B_e) and corresponding fractions consumed by pollock relative to euphausiid standing stock (C) correspond to high, medium, and low σ_{bs} scenarios, respectively. See Equation 1.

The signal-to-noise ratio (SNR) of the S_v in each cell was evaluated before multifrequency classification occurred, following De Robertis and Higginbottom (2007). SNR is range- and frequency-dependent. In practice, S_v at 38 kHz has a SNR of > 10 dB up to a range of 500 m or more. S_v at 120 and 200 kHz exhibit a significant reduction in SNR at ranges > 200 m. At 18 kHz, transducer ringing generated noise that decayed rapidly with depth, but which sometimes dominated the received signal at shorter ranges (20

- 80 m). SNR was estimated for 18, 120, and 200 kHz, and cells with SNR < 10 dB were not used in the analysis. In 2006, the 18 kHz cells often failed this criterion in the upper 50 m due to ringing noise; in these cases, frequency differences between 38, 120, and 200 kHz were used for classification of euphausiid backscatter in these cells.

The S_v of all cells where SNR $\geq$ 10 dB, $\overline{Z}_{euph} \leq 2$, and $\overline{Z}_{euph}$ was the minimum Z-score for any other class in the analysis was classified as euphausiid backscatter (Figure 2). The four known classes of acoustic targets included were pollock, euphausiids, jellyfish, and myctophids; discrimination power for euphausiids is likely to be high given the difference in frequency responses among these classes (cf. De Robertis et al., 2010, Table 3). In cells meeting these criteria, S_v at 120 kHz above a -80 dB integration threshold was then integrated into 0.5 nmi (0.926 km) x 20 m bins between depths of 20 m from the sea surface and 0.5 m above the seafloor to a maximum range of 500 m. These larger bins were required to have a mean $\overline{Z}_{euph}$ of $\leq$ 1.5 before being subjected to further processing and analysis. The nested approach of thresholding Z_{euph} at the scale of both the 5 ping by 5 m and 0.5 nmi by 20 m scales has the effect of classifying marginal analysis cells (i.e., $1.5 < \overline{Z}_{euph} < 2$) as consistent with euphausiids only when the surrounding cells are more consistent with the expectation for euphausiids (cf. De Robertis et al., 2010).

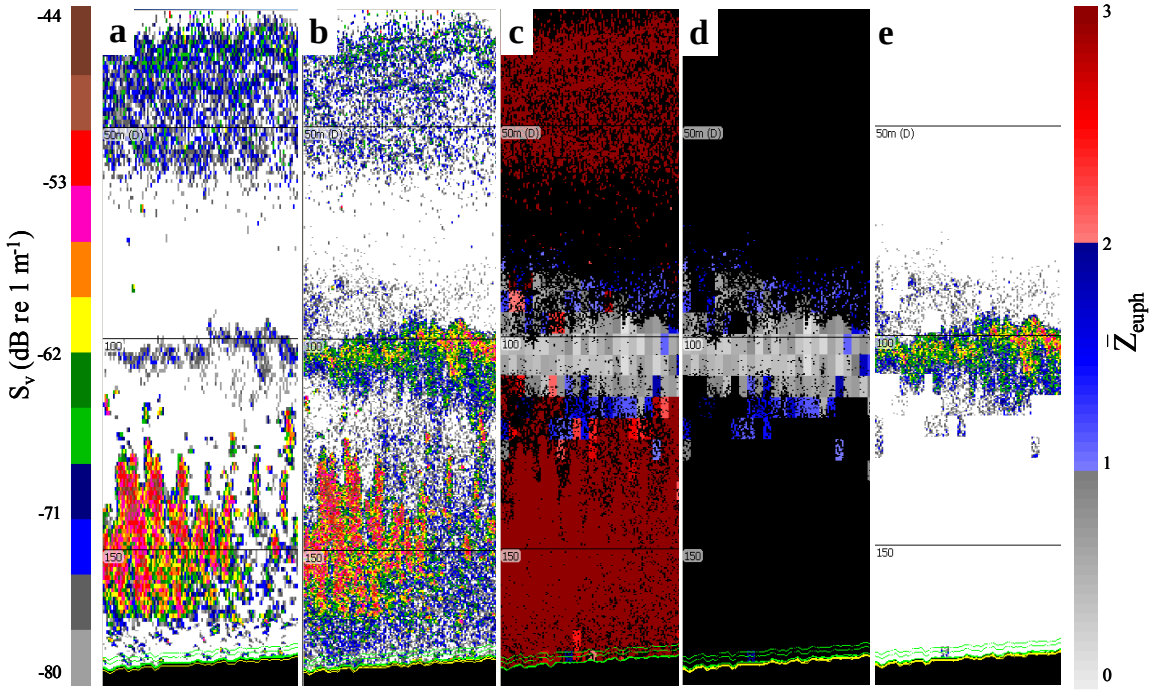

Figure Ch2.c.2. Multifrequency classification sequence for euphausiid backscatter from left to right, including a) S_v at 38 kHz and b) S_v at 120 kHz with SNR > 10 dB, c) $\overline{Z}_{euph}$ for all cells with SNR > 10 dB and 120 kHz S_v exceeding a -80 dB integration threshold, d) $\overline{Z}_{euph} \leq 2$ and minimum for all classes in the analysis, and finally e) euphausiid S_v at 120 kHz for cells with SNR > 10 dB, $\overline{Z}_{euph} \leq 2$ and minimum for all classes, and 120 kHz S_v exceeding a -80 dB integration threshold. S_v at 18 and 200 kHz are not shown. Color scales for S_v are at left, and $\overline{Z}_{euph}$ at the right. Horizontal black lines indicate depth increments of 50 m. S_v below the euphausiid layer is from a large school of pollock, and S_v above the euphausiid layer is from a near surface mixture of unknown composition; both of these layers are rejected by the classification algorithm because they do not have a frequency response consistent with euphausiids.

Corrections for overlap with pollock and diel period

Two potential biases in the euphausiid backscatter data set were examined in greater detail. Walleye pollock are relatively strong acoustic targets (ca. 10^5 times stronger scattering per individual than euphausiids, e.g., Demer and Conti, 2005; Traynor, 1996) with a relatively flat S_v response at the frequencies in use here (De Robertis et al., 2010). Backscatter from pollock and euphausiids located in the same cubic meter of water will typically be dominated in terms of frequency response by scattering from the pollock, which could lead to underestimates of euphausiid densities (Coyle and Pinchuk, 2002). In practice, the size of this bias depends on the vertical and horizontal overlap of pollock and euphausiids

during the daytime acoustic surveys. To examine the significance of this potential bias in our data, we computed a correction factor by using the 'background' euphausiid S_v surrounding detected pollock schools to estimate the S_v of euphausiids that might be within the area encompassed by those schools but obscured by scattering from the pollock. Vertical bins (5 nmi (9.26 km) by 20 m) were used for this local average of euphausiid backscatter. The cumulative impact of this correction was small on a survey-wide basis, ranging from an 0.5 to 4.2 % increase in mean euphausiid backscatter (averaging 1.4 %) for all surveys. The data presented in this paper include this correction.

The second potential bias is related to the vertical distribution of euphausiids. As noted, the acoustic pollock survey transects were sampled almost entirely during daytime hours (Honkalehto et al., 2010), but for logistical reasons, small portions of the transects were sampled near dusk, and occasionally even at night. Euphausiids in the Bering Sea and elsewhere exhibit a regular diel vertical migration to near-surface waters each night (Mauchline, 1980), eventually moving above where they can be detected by vessel-mounted transducers. After examining the ratio of euphausiid backscatter integrated over the water column (s_A, m^2 nmi^{-2}) to daytime mean backscatter as a function of time of day, we suspected that some measurements of euphausiid density were biased low (Figure Ch2.c.3); pollock backscatter data did not exhibit this pattern (not shown). Therefore, we corrected the euphausiid data set for this diel bias by removing data collected after sunset and before sunrise from further analysis. As with the correction for pollock overlap with euphausiids, on a survey-wide basis the magnitude of this bias was extremely small, ranging from an 0.8 to 3.6 % increase in mean euphausiid backscatter (averaging 2.0 %) over successive surveys.

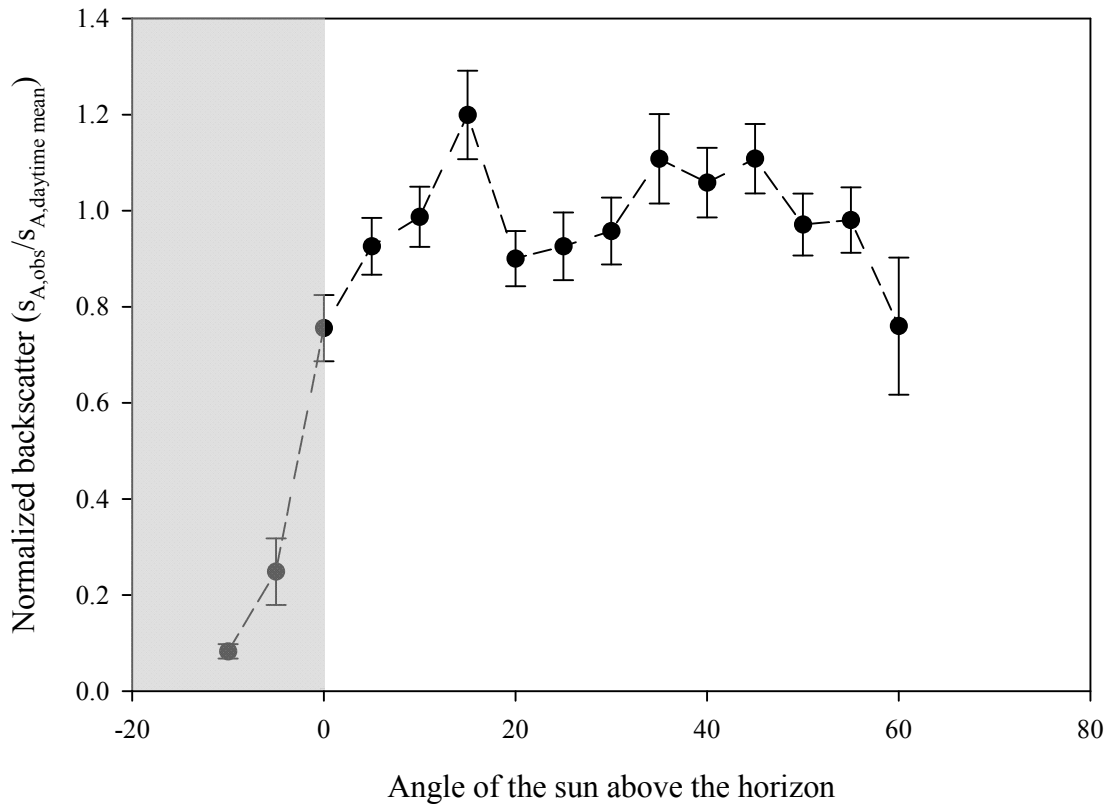

Figure Ch2.c.3. Average ratios of euphausiid backscatter integrated over the water column (s_A, m^2 nmi^{-2}) to daytime mean values as a function of sun angle, 2004 - 2010. A sun angle of 0 degrees represents sunrise or sunset. A ratio was computed for each survey day between mean vertically integrated euphausiid backscatter at each sun angle and the average vertically integrated euphausiid backscatter at all daytime sun angles on that day. Averages were then taken for each sun angle over all survey days. The shaded area represents sun angles for which data were excluded from further analysis to avoid a negative bias to estimated euphausiid biomass due to diel migration of euphausiids to surface waters between sunset and sunrise. Error bars indicate $\pm$ 1 standard error of the mean.

Quality control and verification of acoustic backscatter classification

The average, backscatter-weighted $\overline{Z}_{euph}$ computed over all EDSUs for each survey transect (De Robertis et al., 2010) was used to measure how well observed data classified as euphausiids compared to the reference data set. Since the reference set is a fixed and separate data set, it can be used to evaluate relative quality and internal consistency of euphausiid backscatter classifications in the data analyzed here.

Backscatter layers identified as being composed of euphausiids were also sampled to verify species composition and obtain length-frequency information with targeted tows using a rigid frame Methot trawl with a 5 m^2 mouth area, 2 mm x 3 mm mesh in the body of the net, and 1 mm mesh in the codend (Methot, 1986). Tows were made at a nominal vessel speed of 3 nmi^{-1} h^{-1} (1.5 m s^{-1}). Larger organisms such as juvenile fish and jellyfish medusae were removed from the catch and enumerated, and then a subsample of the remainder was preserved in 5% buffered formalin and sent to the Polish Plankton Sorting and Identification Center (Szczecin, Poland) for enumeration. Organisms with length $\geq$ 5 mm were identified to species when possible, and the lengths of up to 25 individuals of each taxon were measured. Euphausiid lengths were measured from the curve of the carapace behind the eye to the posterior of the telson (body length + telson length as given by Shaw et al., 2006). Euphausiid density was estimated using the volume of water filtered by the net as computed from flowmeter measurements and mouth area dimensions, and counts of euphausiids in the preserved samples. These net capture estimates of euphausiid numerical density were compared with S_v from euphausiids measured in the path of each Methot trawl deployment between 2004 and 2009, accounting for the mouth area of the net and the setback between acoustic transducers and the net frame (Zhou et al., 1994). Samples from summer 2010 are not included as they have yet to be enumerated.

Target strength model and biomass computation

The acoustic scattering from an individual organism can be expressed as a backscattering cross-section (σ_{bs}, m^2) or its logarithmic counterpart, target strength (TS = 10 * $\log_{10}(\sigma_{bs})$, dB re 1 m^2). This quantity is fundamental to estimation of number of targets from S_v measurements. When a single organism type dominates the acoustic scattering in a volume, number of targets in the volume can be calculated using the equation

$$N = s_v / \bar{s}_{bs} \qquad (1)$$

where N is the number of organisms per unit volume (m^{-3}), s_v is the volume backscattering coefficient ($s_v = 10^{(Sv/10)}$, m^{-1}), and $\bar{s}_{bs}$ (m^2) is the average backscattering cross-section weighted by the distribution of organism lengths.

Currently, the most common way to estimate euphausiid σ_{bs} is via a physics-based scattering model (Conti and Demer, 2006; McGehee et al., 1998; Reiss et al., 2008; Stanton and Chu, 2000). For the analysis presented here, a distorted wave Born approximation (DWBA) model (Lawson et al., 2006; McGehee et al., 1998; Stanton and Chu, 2000) is employed. The parameterization and use of the DWBA model for Bering Sea euphausiids is described in detail by Smith et al. (2010) and Smith (2010). Briefly, the euphausiid is modeled as a fluid-filled cylindrical shape described by key parameters including length, width, sound speed and density, and orientation with respect to the impinging acoustic wave.

There were not enough data in every survey year to fully parameterize the DWBA model: there were relatively few Methot tows in 2004 and 2006, width, sound speed, and density measurements were only available for 2008 specimens, and no measurements of *in situ* euphausiid orientation were made. The Methot catch data that are available from 2004 – 2009 indicate that euphausiid length and species composition were very consistent among years: offshore of 100 m bottom depth, species composition was dominated by *T. inermis* (56% by number) with mean length 19.3 mm (SD 1.5, n = 38 tows, unimodal length distribution), while inshore *T. raschii* were more common (75% by number) with mean length 18.3 mm (SD 2.3, n = 21 tows, unimodal length distribution). Given the limited information available, we used the DWBA model to estimate σ_{bs} at 120 kHz in 1 mm length bins between 8 and 28 mm for the average length distribution in two strata, inshore and offshore of the 100 m isobath. For DWBA model runs, our euphausiid lengths were converted to CCAMLR (Convention on the Conservation of Antarctic Marine Living Resources) 'standard krill lengths' (anterior of eye to posterior of telson; Demer and Conti, 2005; McGehee et al., 1998) using a regression obtained using 2008 measurements (standard krill length = 1.07 * euphausiid length + 0.1041, $r^2 = 0.96$, n = 231); estimates of numbers and density are subsequently reported in terms of euphausiid length. Widths were computed from a regression of standard krill length on width (width = 0.0024 * standard krill length$^{2.3679}$, $r^2 = 0.61$, n = 412) and average values for sound speed and density contrast with seawater (both obtained from euphausiid specimens measured in 2008; Smith et al., 2010) were used to parameterize DWBA model runs for both strata in all survey years. Smith et al. (2010) did not observe differences in sound speed and density contrast across species, so the same values for these model parameters were used for all euphausiids. However, species composition of Methot catches was used to apportion numbers of euphausiids among species and to convert numbers of animals to biomass when species specific information was available. Likely distributions of *in situ* euphausiid orientation were obtained from the literature (Conti and Demer, 2006; Kristensen and Dalen, 1986;

Lawson et al., 2006). To express possible uncertainty in DWBA model estimates of σ_{bs} and resulting computations of numbers and biomass, we implemented three σ_{bs} scenarios that encompass likely values of the least well-constrained model parameters, material properties (combined effects of sound speed and density contrast with seawater) and *in situ* orientation. Model parameterization is summarized in Table 1.

The number of euphausiids at length in each 0.5 nmi (0.926 km) x 20 m cell in all survey data sets was computed for each species using the equation

$$N_{ij} = (s_A * 0.5 * 20) / (\bar{s}_{bs} * 4\pi) * P_{ij} \quad (2)$$

where N_{ij} is number of euphausiids at length i and species j, s_A is euphausiid backscatter density per unit area at 120 kHz (m^2 nmi^{-2}) in each cell, 0.5 nmi and 20 nmi are constants needed to expand the cell s_A to the area comprising the length of the EDSU and halfway to the adjoining survey transect on either side, 4π converts backscattering cross-section $\bar{s}_{bs}$ to spherical scattering cross-section $\bar{s}_{sp}$ (see MacLennan et al., 2002), and P_{ij} is the proportion of euphausiids at length i and species j in Methot net tow catches. P_{ij} differed by onshore and offshore strata, but was constant within each stratum over all years. $\bar{s}_{bs}$ varied for each of the three DWBA model scenarios; within each of these scenarios, it also differed by onshore and offshore strata, but was constant within each stratum in a DWBA model scenario over all years.

Biomass at length was computed from numbers using a length-wet weight regression determined in a study of euphausiid proximate composition (Harvey et al., 2012); we report biomass here in terms of the wet weight of euphausiids, but in principle other currencies such as carbon, lipid, or energy content given by Harvey et al. could be used, as well. When species-specific information on biomass conversion was available (for *T. inermis*, *T. raschii*, and *T. longipes*), it was used to compute biomass of the proportion of animals from each of those species in the Methot net catches. For other species, a length-wet weight regression using average parameters of the equations for other species was employed. The biomass calculation from estimated numbers of animals can be summarized in the following equation

$$B_{ij} = N_{ij} * P_j * W_{ij} \quad (3)$$

where B_{ij} is biomass of species j at length i, P_j is proportion of euphausiids in species j from Methot net catches, and W_{ij} is the wet weight of a euphausiid of length i and species j computed from length-wet weight regressions given in Harvey et al. (2012). P_j differed between onshore and offshore strata, but was constant within each stratum over all years. The length-wet weight regression used for W_{ij} is based upon specimens collected from 2008 - 2010. Both euphausiid numbers and biomass were summed across length, species, and strata in each year to compute a survey total for each quantity. Sampling variability in these survey totals was estimated using a 1-D geostatistical method (Petitgas, 1993), the same technique used for acoustic-trawl pollock survey data.

Spatial and temporal patterns in euphausiid and pollock biomass

Acoustic and bottom trawl surveys detect different portions of the pollock stock. Bottom trawls capture only near-bottom pollock, while acoustic surveys cannot detect pollock in very close proximity to the seafloor (within about 1.5 m in this case; cf. Ona and Mitson, 1996). Thus, neither survey alone provides a complete picture of pollock abundance and distribution, and both are treated as separate relative indices for stock assessment purposes, rather than as absolute estimates (Ianelli et al., 2010). Similarly, acoustic surveys cannot detect euphausiids located very close to the seafloor, but limited net sampling in the study area using a Tucker trawl modified with runners for epibenthic sampling suggests that a relatively small fraction of euphausiid biomass is located there; estimates of integrated euphausiid density within 2 m of the seafloor from these samples averaged only 5.4% of integrated water column density (SD = 8.3, n = 6; Ressler, P.H., NOAA-Alaska Fisheries Science Center, unpublished data). In order to evaluate both spatial and temporal patterns of pollock (predator) relative to that of euphausiids (prey) in this study, we made the necessary assumptions that acoustic and bottom trawl survey biomass results sum to the total amount of midwater and demersal pollock throughout the water column, and that the acoustic survey detects the total amount of euphausiid biomass in the water column.

We used both bottom trawl and acoustic survey time series to evaluate temporal patterns in the standing stocks of pollock and euphausiids and the potential for their interaction in the U.S. EEZ from 2004 – 2010. The demersal pollock survey does not produce euphausiid biomass estimates, but we assumed that the temporal pattern of euphausiid biomass in the acoustic survey area reflects the shelf-wide temporal

pattern in euphausiid standing stock. For spatial comparison of pollock and euphausiids, vertically integrated midwater pollock biomass density estimated by the acoustic survey (kg ha^{-1}) was averaged in 20 nmi x 20 nmi (37 x 37 km or 1.4 x 10^{-5} ha) blocks surrounding each demersal survey station, while bottom trawl catch per unit effort at each station was used to compute average pollock density in these same blocks (kg ha^{-1}). The two survey estimates were summed in each block. In the shallow areas (bottom depth < 50 m) surveyed only by the bottom trawl survey where pollock is mostly or entirely demersal, we assume that the bottom trawl survey detects all pollock. Euphausiid biomass was similarly vertically integrated and block-averaged. Spatial distributions of pollock and euphausiid density were compared using contoured surfaces of these block-averaged data. The covariance of pollock and euphausiid density at each block was computed over the 6 year time series for the area sampled by both surveys.

Estimation of predation impact by pollock on euphausiids

The approximate predation impact by pollock on euphausiids was estimated by taking the sum total of pollock and euphausiid biomass in each survey year *only* in the area sampled by both the acoustic and bottom trawl pollock surveys in each year (since euphausiid estimates are not made by the bottom trawl survey), and making some simplifying assumptions about the rate of pollock consumption, using the equation

$$C_d = B_p * R_d * F_e \tag{4}$$

where C_d is the biomass of euphausiids consumed per day by pollock (kg d^{-1}), B_p is the sum of pollock standing stock biomass from acoustic and demersal surveys (kg) in the area covered by both surveys, R_d is the fraction of body weight in prey that pollock consumes per day (0.02; K. Aydin and T. Buckley, personal communication; Springer, 1992) for a population currently dominated by younger fish (Ianelli et al., 2010), and F_e is the fraction of pollock diet consisting of euphausiids between May and September (mean 0.53, range 0.37 – 0.70, for the years 1997 - 2001; Lang et al., 2005). The daily rate of pollock consumption of euphausiids relative to the standing stock of euphausiids can then be calculated (C_d/B_e, d^{-1}), where euphausiid biomass (B_e, in kg) is the acoustic survey estimate of euphausiid biomass B_{ij} summed over all lengths and species. This rate can be multiplied by the number of days over which feeding takes place to estimate the fraction of euphausiid standing stock consumed by the pollock

standing stock over that time period. Standing stock estimates for both pollock and euphausiids come from surveys conducted from early June to early August during the summer northward and shoreward 'feeding migration' by pollock (Kotwicki et al., 2005). The pollock food habits data reported by Lang et al. (2005) were based on samples collected between May and September. Therefore, the computation of euphausiid consumption by pollock relative to the size of the euphausiid standing stock (C) was based on the May - September time period (5 months or ca. 150 days) in each survey year:

$$C = (C_d / B_e) * 150 \text{ d} \quad (5)$$

RESULTS

Quality control and verification of acoustic backscatter classification

Over all survey years, $\overline{Z}_{euph}$ for acoustic survey transects averaged 0.91 (SD 0.16) (Figure Ch2.c.4), indicating that backsatter classified as euphausiids closely matched the reference frequency response reported by De Robertis et al. (2010). The performance of the method appears relatively consistent, although $\overline{Z}_{euph}$ in 2004 was noticeably higher than the mean of other survey years (by ca. 0.2 SD). We do not know the reason for this difference, but backscatter classified as euphausiids in that year nevertheless had a frequency response that was on average within 1.15 (SD 0.10) standard deviations of the reference set. There was no spatial pattern in $\overline{Z}_{euph}$ among transects (not shown), indicating spatial as well as temporal consistency of classification. This level of classification performance is comparable to that shown by De Robertis et al. (2010) for Bering Sea pollock using the same acoustic data set.

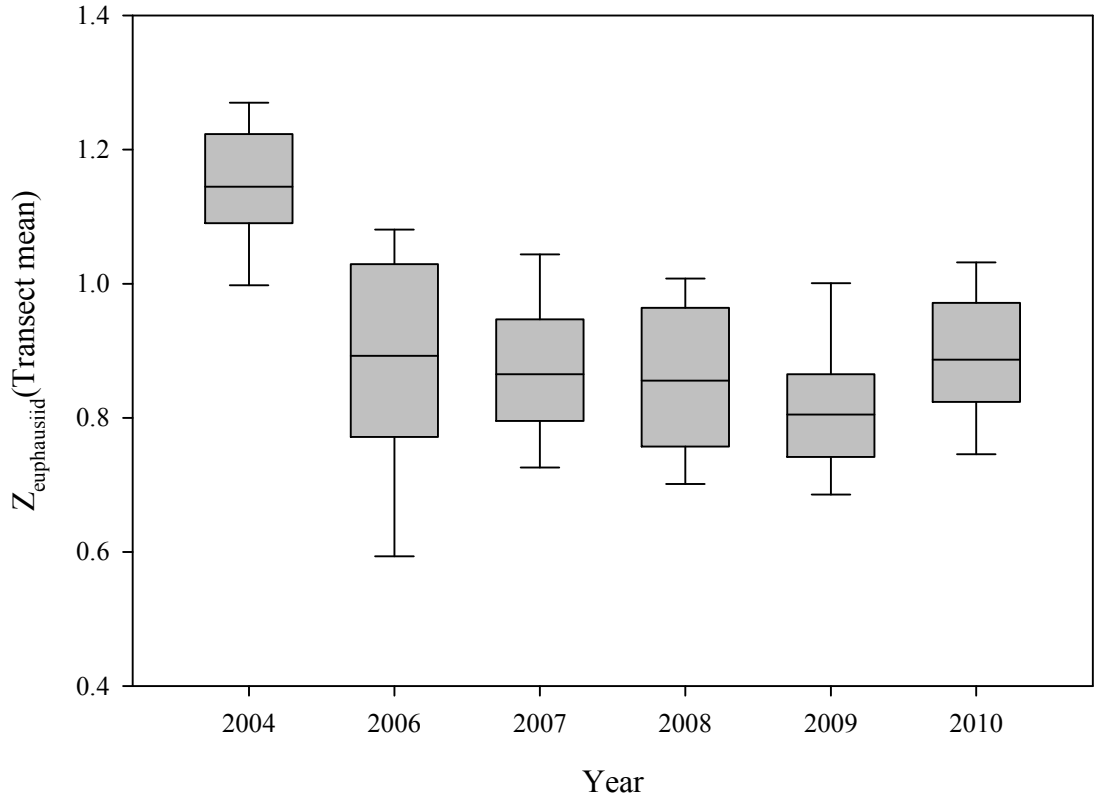

Figure Ch2.c.4. Boxplots of transect mean $\overline{Z}_{euph}$ for each survey year, indicating the 10th, 25th, 50th (median), 75th, and 90th percentiles of the observations.

Since Methot samples collected between 2004 and 2007 were used to develop the frequency classification reference set (De Robertis et al., 2010), only Methot tow catches collected in 2008 and 2009 (n = 38) were used here to verify classification of euphausiid backscatter, providing an out-of-sample comparison. The proportion of catch comprising euphausiids and large copepods in these Methot samples averaged 0.94 (SD 0.06) by number. Other organisms such as chaetognaths, small gelatinous zooplankton, and amphipods (listed in order of their relative abundance in the samples) were not encountered consistently in these Methot tow catches, and represented a negligible fraction on average (0.06 by number) of the total catch. Of the euphausiid and copepod portion, euphausiids averaged 0.85 (SD 0.16) by number and 0.98 (SD 0.04) on a biomass basis (Figure Ch2.c.5a). The biomass of euphausiid and copepods were estimated using published length-wet weight regressions (Harvey et al., 2012; Kobari et al., 2003) and observed lengths; in 2008 and 2009, the average length of euphausiids was 18.6 mm (SD 2.1), and the average copepod length was 7.7 mm (SD 0.9). Small organisms with lengths less than about 10 mm are probably underestimated by the Methot trawl. However, the relatively high densities of euphausiids, their

larger size and biomass per individual relative to the next most common organism in the catches (copepods), and their exponentially stronger $\overline{s}_{bs}$ compared to the largest copepods (one 18 mm euphausiid as modeled here is likely a 10^2-fold stronger acoustic target than a *Neocalanus* sp. copepod 8 mm in body length; Matsukura et al., 2009) support the contention that most backscatter in these layers is dominated by scattering from euphausiids.

Based on Equation 1 and its underlying assumptions, we expected a positive and directly proportional relationship between euphausiid s_v at 120 kHz and the density of euphausiids captured by the Methot trawl, though we anticipated that the relationship would have a significant amount of scatter. As is often done in such cases (e.g., Warren and Wiebe, 2008), logarithmic forms of these quantities were used to improve the homogeneity of variance and linearity of the data set before statistical evaluation; we used S_v and 10 * $\log_{10}$(euphausiids m^{-3}) and expected a slope of approximately 1 (Figure Ch2.c.5b). The observed correlation was positive and statistically significant ($r^2 = 0.49$, $p < 0.001$, $n = 38$). A functional regression (Ricker, 1973) of log-transformed euphausiid density on S_v was also performed, and approximate 95% confidence bounds on the slope of this regression ($t_{0.05/2} = 2.03$, slope = 0.78 ± 0.21, df = 36) narrowly failed to include 1. When a single, highly influential datum obtained from a Methot tow on a relatively weak and patchy euphausiid layer (Figure Ch2.c.5b) was excluded and the correlation and regression were recomputed, the correlation coefficient was reduced but remained significant ($r^2 = 0.32$, $p < 0.001$, $n = 37$) and the slope value changed to 0.97, with the hypothesized slope of 1 well within the recomputed 95% confidence bounds ($t_{0.05/2} = 2.03$, slope = 0.97 ± 0.32, df = 35). These results are consistent with the contention that despite substantial variance in the relationship, volume backscattering attributed to euphausiids is directly proportional to euphausiid density in Methot trawl catches, particularly since factors such as variation in euphausiid $\overline{s}_{bs}$ due to size, material properties and orientation, and variable catchability of euphausiids by the Methot trawl are not accounted for.

a)

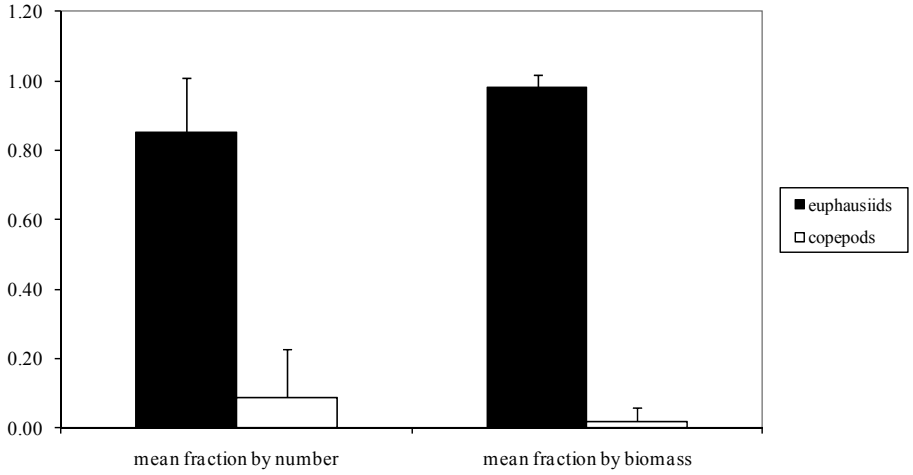

b)

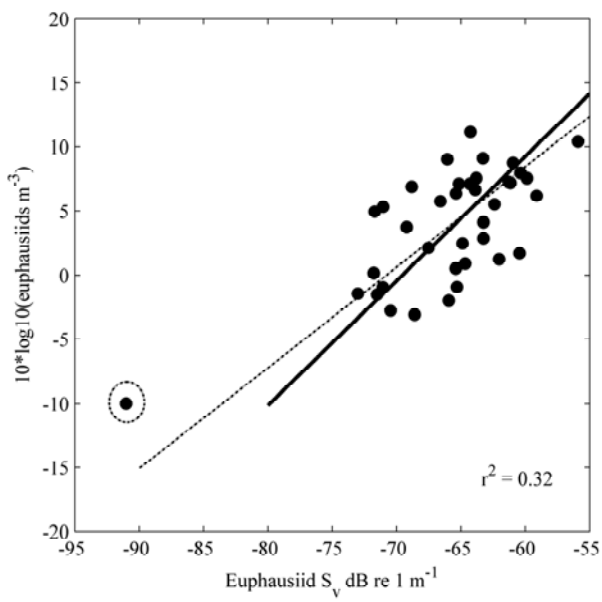

Figure Ch2.c.5. a) Average fraction of Methot trawl catches composed of euphausiids and copepods in tows targeting euphausiid scattering layers during summers 2008 and 2009. Error bars indicate 1 standard deviation of the mean. b) Regression of log-transformed euphausiid density on euphausiid S_v. On both axes, 10 units indicate a change of one order of magnitude. The dotted line indicates a functional regression slope including all data, and the solid line and r^2 value indicate a regression fit excluding the circled outlier. The equation for the functional regression fit that excluded the circled outlier was y = 0.971 x + 67.5.

3.2 Target strength model and biomass computation

DWBA model runs indicated that euphausiid TS varies by a factor of ca. 40 dB across the range of euphausiid lengths observed in Methot catches (but only by ca. 8 dB within 1 SD of the mean length), and by a little less than 10 dB between low and high σ_{bs} scenarios (Figure Ch2.c.6). However, modeled $\overline{TS}$ varied relatively little between inshore and offshore strata (-91.63 dB inshore vs. -90.54 dB offshore, using the med σ_{bs} scenario) as euphausiid lengths were not very different between these areas. We will interpret results from the medium σ_{bs} scenario, which we consider the most reasonable estimate, but will occasionally refer to high and low σ_{bs} scenarios in discussion of possible bias in biomass results (note that the *highest* σ_{bs} scenario will produce the *lowest* estimate of euphausiid biomass; see Equation 1). Uncertainty due to sampling variability (error bars in Figure Ch2.c.7) is much smaller than potential bias due to σ_{bs}.

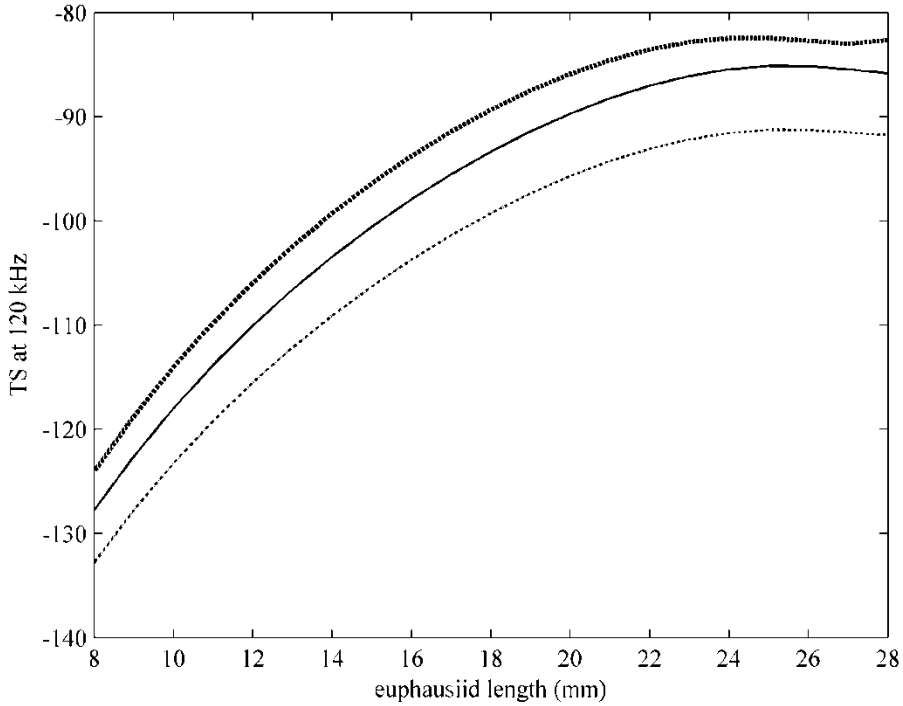

Figure Ch2.c.6. Euphausiid TS = 10 * $\log_{10}(\sigma_{bs})$ at 120 kHz predicted by DWBA model runs for the range of euphausiid lengths observed in Methot tows 2004 – 2010. The DWBA model was parameterized as described in Table 1. The three curves indicate high (dark dotted line), medium (dark solid line), and low (light dotted line) σ_{bs} scenarios.

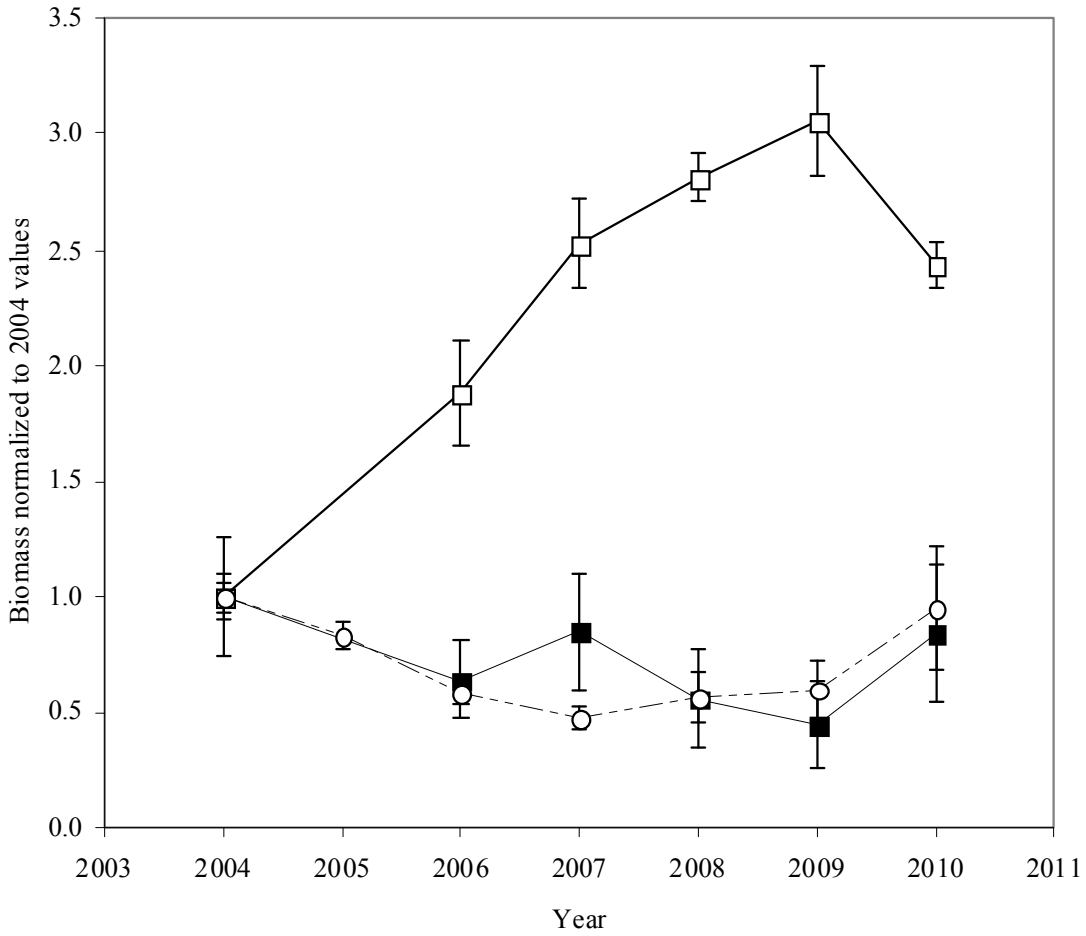

Figure Ch2.c.7. Time series of pollock biomass (solid line with black squares), euphausiid biomass from the acoustic survey (solid line with white squares), and pollock biomass for ages 1-7 estimated by a stock assessment model (dotted line with white circles). The stock assessment model data are courtesy of J. Ianelli and are described in detail by Ianelli et al. (2010). All three time series are normalized to their value in 2004 to indicate the relative change over time. Error bars indicate sampling variability in the form of 95% confidence intervals. For pollock survey data, the intervals were constructed as the sum of the 95% bounds for acoustic and bottom trawl pollock survey estimates.

Spatial and temporal patterns in euphausiid and pollock biomass

Euphausiid biomass (kg) summed across length, species, and stratum in each survey year increased more than 3-fold between 2004 and 2009, before decreasing by approximately 20% in summer 2010 (Figure

Ch2.c.7). The sum of pollock biomass in both acoustic and bottom trawl surveys declined by ca. 50% between 2004 and 2009, before nearly doubling from 2009 to 2010. Pollock and euphausiid survey time series were inversely correlated ($r^2 = 0.54$). The pollock stock assessment time series (Figure Ch2.c.7) is an estimate of biomass for ages 1-7 in January using a mean annual weight at age, and incorporates data from both surveys as well as fishery landings and fishery observer data, while both acoustic and bottom trawl pollock surveys take place in summer and each has a different age- and size-selectivity. Thus, the survey and model time series are not expected to show identical patterns (Ianelli et al., 2001, 2010). Nevertheless, the general temporal patterns in both survey data and model results are the same: pollock biomass declined while euphausiid standing stock increased, and when pollock biomass rebounded to near 2004 levels by 2010, euphausiid standing stock dropped.

Euphausiids were present throughout the acoustic survey area (Figure Ch2.c.8), but their biomass density was usually highest in the southeastern portion of the shelf. Both acoustic and bottom trawl surveys showed that pollock biomass density was usually highest in the northwestern part of the shelf. Pollock biomass appeared to have a negative spatial relationship with euphausiid biomass. By comparing the covariance at each station between euphausiid biomass and pollock biomass for six annual summer surveys between 2004 -2010 (Figure Ch2.c.9), it is apparent that there are large areas of negative covariance between euphausiids and pollock, though this is not true in every location. Overall, biomasses of predator and prey appear to have a negative relationship in both space and time.

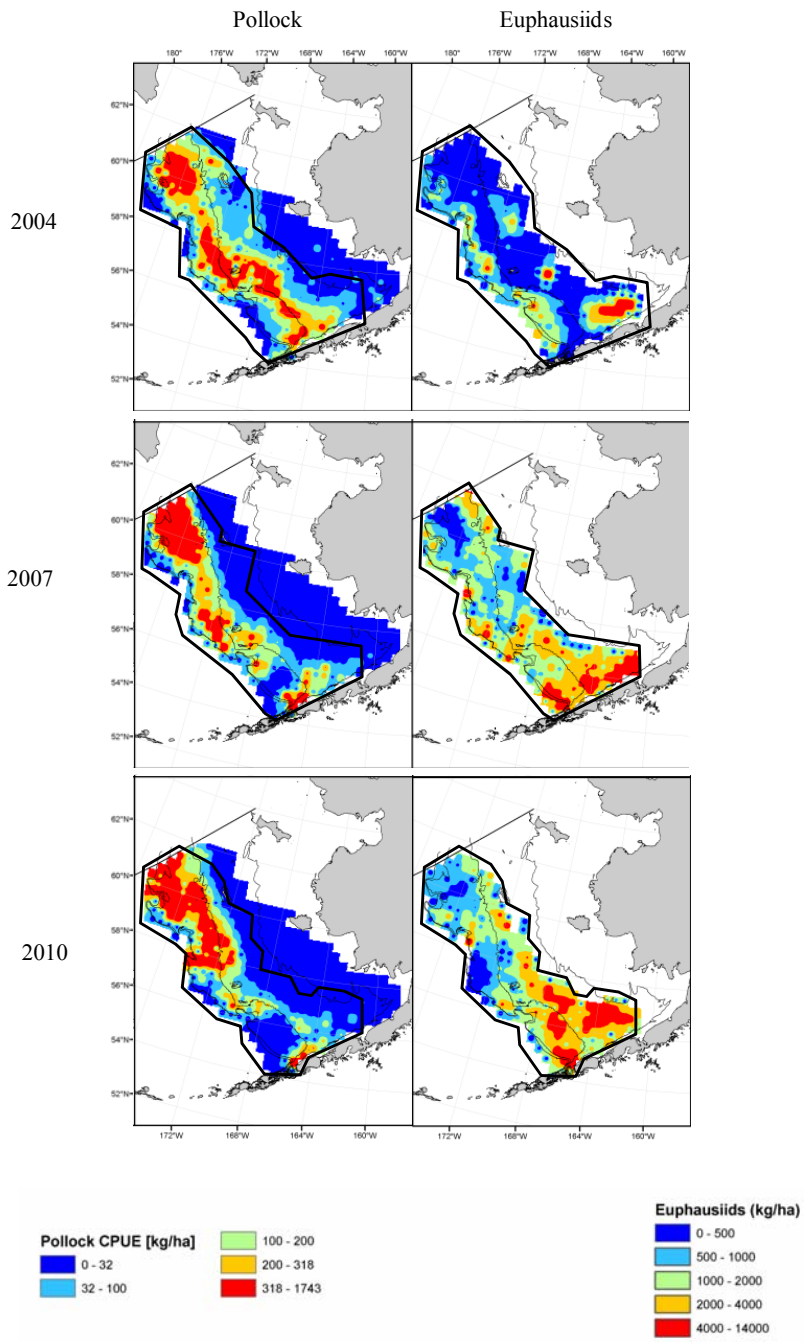

Figure Ch2.c.8. Spatial distribution of pollock biomass density (kg ha^{-1}) observed by acoustic and bottom trawl surveys (left column) and euphausiid biomass (kg ha^{-1}) observed by the acoustic survey (right column) in 2004 (top row), 2007 (middle) and 2010 (bottom). Data from 2006, 2008, and 2009 surveys are not shown. The medium σ_{bs}scenario was used for euphausiid biomass. Contours were drawn by interpolation from 37 x 37 km (20 x 20 nmi) block-averaged data. Black polygons approximately bound the acoustic-trawl survey area, which changes slightly from year to year.

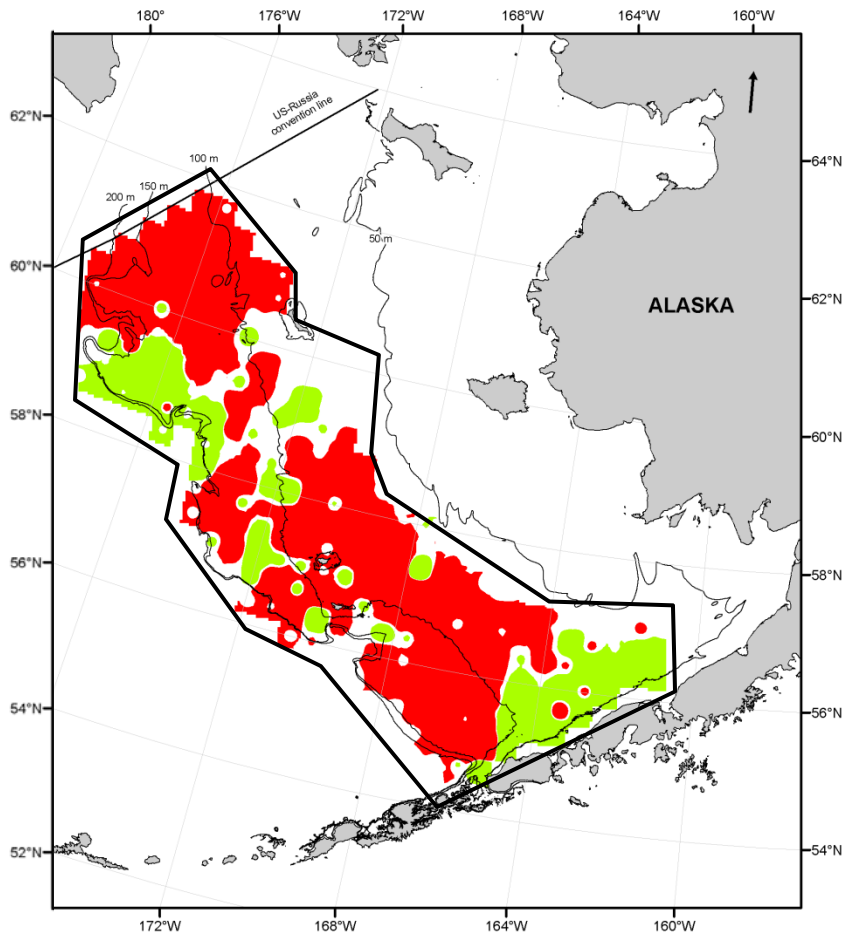

Figure Ch2.c.9. Covariance between pollock and euphausiid biomass over six summers, 2004 – 2010. The covariance was calculated between pollock and euphausiid biomass density in each 37 x 37 km (20 x 20 nmi) block in the area covered by both acoustic and bottom trawl surveys, and the contoured surface was drawn by interpolating those values. Red indicates strong negative covariance (< -10,000) while green indicates strong positive covariance (> 10,000). The black polygon approximately bounds the area for which covariance was computed.

Estimation of predation impact by pollock on euphausiids

Although we were not able to compare production rates of pollock and euphausiids to evaluate predation impact, biomass comparisons are probably reasonable since both species have only a single generation per year (Smith, 1991; Ianelli et al, 2010), and the survey biomass estimates are done in summer after both species have reproduced. Calculations using Equations 4 and 5 indicated that the fraction of euphausiid standing stock consumed by pollock between May and September varied from a high of 0.38

(in 2004) to a low of 0.06 (in 2009), using the medium σ_{bs} scenario for euphausiid biomass; corresponding ranges for high and low σ_{bs} scenarios respectively were 0.87 – 0.14 and 0.10 – 0.02 (Table 2). Despite the large range in uncertainty, these estimates indicate that feeding by a single important predator population between May and September (5 months) could have consumed a measurable and substantial fraction of the euphausiid standing stock.

DISCUSSION

Acoustic estimates of euphausiid biomass on the Bering Sea shelf

The acoustic estimates of euphausiid distribution and biomass presented here are an important new source of information about the distribution, abundance, and role of these animals in the Bering Sea ecosystem, augmenting the relatively small body of work that already exists on this topic (Coyle and Pinchuk, 2002; Coyle et al., 2008; Smith, 1991; Swartzman et al., 2002). In terms of scope and potential for long term monitoring of this key ecosystem component, no comparable time series exists for the Bering Sea, and the observations are derived from existing monitoring surveys for pollock at a relatively modest additional cost of ship and sample processing time. These data are beginning to inform pollock stock assessment and management (Ianelli et al., 2010; Zador and Gaichas, 2010) and contribute to an improved understanding of patterns in pollock recruitment (Hunt et al., 2011).

Top-down control of euphausiids (prey) by pollock (predator)

Although top-down control of crustacean zooplankton by fish in lakes is well-documented (e.g., Brooks and Dodson, 1965; Carpenter and Kitchell, 1993; Gliwicz, 1986), the relative importance of fish predation for controlling crustacean zooplankton populations in marine systems remains an open question (Dalpadado and Skjoldal, 1996; Mullin and Conversi, 1988; Reid et al., 2000; Robinson, 2000; Stevick et al., 2008; Wilson et al., 2009; Worm and Myers, 2003). In the Bering Sea, it has been proposed that bottom-up forcing through climate, spring water temperatures, and sea ice are an important control on large copepods (Baier and Napp, 2003; Coyle et al., 2011) and perhaps euphausiids (Coyle et al., 2008; Coyle et al., 2011; Hunt et al., 2008) - cold, icy springs are thought to be favorable, though the mechanism has not been demonstrated. The time period of 2004 – 2010 is particularly interesting in terms of bottom-up forcing of euphausiids by ocean conditions. 2004 was a relatively warm year (Stabeno et al., 2012) in which the summertime Bering Sea shelf was relatively depauperate of euphausiids and large copepods (Coyle et al., 2008; Hunt et al., 2008). In contrast, very cold conditions have prevailed since

2006 (Stabeno et al., 2012), and increases in the abundance of both large copepods and euphausiids during that time have been documented (this study; Coyle et al., 2011; Hunt et al., 2011). These observations are consistent with bottom-up forcing of large crustacean zooplankton stocks and favorable conditions for large copepods and euphausiids in cold years. However, the decrease of euphausiid biomass in 2010, another cold, icy spring in the Bering Sea, does not fit this pattern.

We show that in addition to variation in spring ice cover and water temperatures, another important factor changed over the 2004 - 2010 time period: the standing stock of pollock. Pollock is an enormous predatory force in the Bering Sea (Aydin and Mueter 2007; Springer, 1992). Its recruitment may also be tied to cold, icy conditions like those experienced in recent springs and summers (Hunt et al., 2011). The increase of euphausiid biomass coincided with decreasing predation as pollock standing stock declined after 2004. Though it is not conclusive, following Dalpadado and Skjoldal (1996) and Worm and Myers (2003) we contend that such a pattern is consistent with the hypothesis of top-down control through predation (Aydin and Mueter, 2007; Springer, 1992; Smith, 1991). In particular, the 2010 observations support the notion that top-down forcing is important in spite of potentially favorable ocean conditions for euphausiids: as the pollock stock climbed again in 2010 toward stock levels observed in the early 2000s, its predatory influence increased proportionately, which could explain the drop in euphausiid standing stock in in 2010 despite continued cold conditions. The negative spatial association between euphausiid and pollock standing stocks would also be consistent with top-down forcing due to fish predation (Genin et al., 1988; Koslow, 1981); certainly, current hypotheses of direct bottom-up forcing of euphausiids in the Bering Sea do not offer an easy explanation for these spatial patterns.

The summer surveys described here are two-month snapshots that may confound spatial and temporal variability, but they do take place at a consistent point in the year, subsequent to reproduction of euphausiids and inshore movement by pollock for feeding (Smith, 1991; Kotwicki et al., 1995). Our euphausiid length data do not suggest that some of our surveys were ‘early’ or ‘late’ in terms of euphausiid reproduction. It is possible that bottom-up effects (forcing of pollock distribution by physical environmental conditions) could influence top-down processes (predation impact on euphausiids by pollock). Changes in pollock distribution during non-summer months are not completely understood, but migration and movement of pollock throughout the year appears to be limited by physical conditions such as water temperature and sea ice (Kotwicki et al., 2005; De Robertis and Cokelet, 2012) which could

mediate the impact of pollock predation upon euphausiids by changing the temporal and spatial overlap of predator and prey.

The calculations presented here suggest that particularly at high stock levels, predation by pollock is large enough to make a substantial impact, though it is not clear whether this alone could control the standing stock of euphausiids. Many other animals prey upon euphausiids as well (Aydin and Mueter, 2007), and pollock feed on euphausiids throughout most of the year, not just from May through September (Dwyer et al., 1987; Smith, 1981), so Equation 5 is probably a conservative estimate of the total amount of euphausiid standing stock removed annually. At the same time, some unknown amount of euphausiid biomass is inshore of our area of comparison (Coyle and Pinchuk, 2002), while the pollock biomass on the inner shelf appears to be relatively small (Figure 8). If the amount of euphausiid biomass on the inner shelf is very large compared to the standing stock estimated here, it would reduce the apparent impact of pollock predation in our calculations. It is worth noting that ecosystem modeling has independently suggested the possibility of top-down control of zooplankton by pollock predation in the Bering Sea (Aydin and Mueter, 2007; Springer, 1992). Springer (1992) claimed very close coupling between pollock and zooplankton; his estimate of annual zooplankton consumption by pollock was 1.7×10^{13} g C y^{-1}, which is of the same order of magnitude as our acoustic euphausiid standing stock estimates for the entire acoustic survey area expressed in terms of carbon (1.1×10^{13} g C, using the med σ_{bs} scenario).

Order of magnitude (or greater) discrepancies between acoustic and net capture estimates of euphausiid density are the rule in the literature (Coyle, 2000, Coyle and Pinchuk, 2002, Warren and Wiebe, 2008), and our data are no exception. The mean density of euphausiids in our acoustic data set was about 30 m^{-3} using the med σ_{bs} scenario, while our Methot net capture density estimates averaged about 4 m^{-3}; a euphausiid biomass estimate derived from any net capture data set would almost certainly be much lower than what we estimated acoustically. This discrepancy could be explained by a systematic low bias to modeled TS estimates (which inflates acoustic estimates of euphausiid density); though such models have been experimentally validated (McGehee et al., 1998, Demer and Conti, 2003), considerable uncertainty in model predictions still exists because of the difficulty in correctly parameterizing the models in terms of material properties and orientation to reproduce *in situ* TS (Chu et al., 2000; Smith et al., 2010; Stanton and Chu, 2000). Net avoidance by euphausiids could also explain the discrepancy between net capture and acoustic estimates of density (Coyle, 2000; Everson and Bone, 1986; Smith, 1991; Wiebe et al., 1982). The size of this effect is difficult to measure directly (Clutter and Anraku, 1968); however,

artificial lights have been shown to increase net estimates of euphausiid density by a factor of 2 – 20 fold, implying that the effect of avoidance could be of that magnitude (Sameoto et al., 1993; Wiebe et al., 2004). We currently lack the data to make a conclusive determination of the source of this discrepancy, but additional measurements of the material properties of euphausiids, their *in situ* orientation during surveys, and further experimental validation of the application of TS model estimates would help answer this question. Until more is known, acoustic and net capture estimates might be considered upper and lower bounds on euphausiid density, respectively (Warren and Wiebe, 2008).

The conclusions drawn here are necessarily tentative, given the simplified nature of the calculations (for example, variation in pollock diet within years, among years, and among predator size groups was not specifically accounted for) and the potentially wide uncertainty in euphausiid standing stock estimates. Yet, the calculations illustrate that the impact of pollock predation on euphausiid biomass could be substantial and explain in part the negative association between pollock and euphausiid biomass that was observed spatially as well as among survey years. More detailed pollock diet data collected concurrently with the acoustic observations of euphausiid prey, as well as extensive observations of physical environmental conditions in the Bering Sea, is becoming available through research conducted as part of the BEST-BSIERP Ecosystem Partnership (http://bsierp.nprb.org/). These new observations will allow a better examination of both interannual and spatial variation in pollock predation rates in comparison to the available euphausiid prey field, and further evaluation of the interplay of predation and oceanographic conditions in controlling euphausiid standing stock.

CONCLUSIONS

Acoustic estimates of summertime euphausiid standing stock on the Bering Sea shelf derived from regular resource assessment surveys represent a valuable new source of information for fisheries and ecosystem management. Results show that euphausiid biomass increased between 2004 and 2009 while the pollock stock declined after a series of years with poor recruitment. Pollock and euphausiid time series appear closely coupled, however; as pollock biomass climbed again toward 2004 stock levels in 2010, euphausiid biomass dropped by about 20%. Calculations of the approximate predation impact by pollock on euphausiids suggest this top-down effect could be significant, particularly when pollock biomass is high. While cold, icy springs and cool summers also coincided with the period of increasing euphausiid standing stock, the negative association between pollock and euphausiid biomass in both space and time is more consistent with ‘top-down’ than ‘bottom-up’ control. Physical environmental conditions probably

still play a role in this trophic interaction, perhaps by mediating overlap between predator and prey throughout the year.

ACKNOWLEDGEMENTS

This work was supported by the Alaska Fisheries Science Center, National Marine Fisheries Service, National Oceanic and Atmospheric Administration (NOAA), the North Pacific Research Board (NRPB) as part of the BEST-BSIERP Ecosystem Partnership. This work would not have been possible without fellow survey scientists of the Resource Assessment and Conservation Engineering (RACE) Division, skippers and crew of NOAA Ships *Miller Freeman*, *Oscar Dyson* and F/Vs *Arcturus*, *Aldebaran*, *Northwest Explorer*, and *Alaska Knight*. We thank Jim Ianelli for providing stock assessment model output data for use in Figure 7 and for helpful discussions. Jeff Napp (NOAA) and the Polish Plankton Sorting and Identification Center are thanked for plankton sample enumeration. Technical editing by Christine Baier and the comments of Troy Buckley, Kresimir Williams, Chris Wilson, and several anonymous reviewers helped improve this manuscript. This was NPRB publication number 336 and BEST-BSIERP publication number 50. The findings and conclusions in the paper are those of the authors and do not necessarily represent the views of the National Marine Fisheries Service.

Chapter 2.d. Analysis of the spatial relationship between euphausiids and walleye pollock, and implications for top-down vs. bottom up control of euphausiids

The following section takes the euphausiid and pollock survey data one step further. The possibility of top-down control of euphausiid standing stock by pollock predation was proposed in section iii, along bottom-up forcing by temperature and other physical processes. In this section, we hypothesize that in the presence of strong top-down control by predation, there should be a negative relationship between the local abundances of pollock and euphausiids, all other factors being equal. We approached the problem with a multivariate statistical regression model (GAM), where the effect of each covariate on the response could be considered simultaneously. We found that water temperature was a much stronger predictor of euphausiid biomass than pollock biomass (a proxy for predation pressure), which is not consistent with the idea of top-down control. This manuscript is one of several synthesis products supported by our project.

The following material is the work of Ressler (B62 PI), De Robertis, and Kotwicki (B62 PI), and will be submitted to Marine Ecology Progress Series as:

Ressler, P.H., De Robertis, A., and Kotwicki, S., in review. The spatial distribution of euphausiids and pollock in the eastern Bering Sea does not imply top-down control by predation. Marine Ecology Progress Series.

Patrick H. Ressler, Alex De Robertis, and Stan Kotwicki, Resource Assessment and Conservation Engineering Division, Alaska Fisheries Science Center, National Marine Fisheries Service, National Oceanic and Atmospheric Administration, 7600 Sand Point Way NE, Seattle, WA 98115, USA; patrick.ressler@noaa.gov, alex.derobertis@noaa.gov, stan.kotwicki@noaa.gov

ABSTRACT

Although euphausiids ('krill') are a key zooplankton taxon in the Bering Sea ecosystem, the processes controlling variation in the standing stock of these animals are not well understood. Both forcing by temperature ('bottom up') and predation ('top down') have been proposed. We developed multivariate regression models to examine the spatial distribution of euphausiids and walleye pollock (their single most important predator) using survey data collected over multiple years, to test the hypothesis that if strong top-down control dominated, there would be a strong negative relationship between the standing stocks of these animals. We used the models to evaluate the relative importance of pollock biomass and water temperature in predicting euphausiid biomass, and found that temperature was a far better predictor, a result that is not consistent with dominant top-down control of euphausiids by predation.

Keywords: USA, Alaska, Bering Sea, walleye pollock, euphausiids, acoustic survey, top-down, bottom-up, GAM; 54° N, 64° N, 155° W, 185° W

INTRODUCTION

Euphausiids are a key group of zooplankton in the eastern Bering Sea shelf ecosystem. The dominant euphausiid species are *Thysanoessa raschii*, found principally on the middle continental shelf (< 100 m bottom depth), and *T. inermis*, found more commonly on the outer shelf (100-200 m bottom depth).). Both species reproduce on the shelf in April and May (Smith 1991), and euphausiids can be found there throughout the year (De Robertis and Cokelet 2012). Euphausiids form an important trophic link between phytoplankton and microzooplankton and animals at upper trophic levels (Aydin and Mueter 2007), including walleye pollock (*Gadus chalcogrammus*), which supports one of the world's largest commercial fisheries (FAO 2012). Walleye pollock (hereafter 'pollock') dominates the fish assemblage of the eastern Bering Sea shelf, spawning in late winter and early spring on the outer shelf and moving inshore and north to feed on the middle and outer shelf during summer (Kotwicki et al. 2005).

Sea temperature and ice cover play a key role in the annual cycle of phytoplankton, zooplankton, and fish production in this system (Hunt et al. 2002, Stabeno et al. 2007, Stabeno et al. 2012b). In particular, cold, icy conditions may favor recruitment and survival of *Calanus* spp. copepods (Baier and Napp 2003), and this argument has been extended to euphausiids based on observations in recent years (Coyle et al. 2011; Hunt et al. 2011). Temperature and ice cover have also been linked to the distribution and abundance of walleye pollock (Kotwicki and Lauth 2013, De Robertis and Cokelet 2012, Kotwicki et al. 2005, Wylie-Echeverria and Wooster 1998; Swartzman et al. 1994). From 2001-2005, conditions on the Bering Sea shelf were warm, euphausiid abundance was low, and pollock recruitment (cf. Ianelli et al. 2012) was poor; a series of cool years followed, characterized by increases in copepods and euphausiids and a rebound of the pollock stock after a nadir sometime between 2007 and 2009 (Ressler et al. 2012, Stabeno et al. 2012b). Such observations led to the hypotheses that warm conditions and poor zooplankton prey availability between 2001 and 2005 may have reduced the recruitment and survival of young pollock (Coyle et al. 2011, Hunt et al. 2011, Stabeno et al. 2012b), and that the subsequent reduction in the biomass of the adult pollock stock and coincident increase of euphausiid biomass could have been due in part to a significant release of pollock predation pressure (Ressler et al. 2012).

However, a complete understanding of the mechanisms driving these patterns has been elusive. Conceptual models of the interplay of predation pressure ('top-down') and environmental drivers ('bottom-up') on euphausiids in the eastern Bering Sea have been largely limited to categorical (e.g., warm vs. cold, high vs. low) comparisons, mostly relying on the synthesis of disparate types of field

observations (Coyle et al. 2011, Hunt et al. 2011, Stabeno et al. 2012a,b) or the results of mass-balance modeling (Aydin and Mueter 2007, Springer 1992). The recent availability of high-resolution surveys of euphausiids and pollock conducted over multiple years (2004-2012) and covering most of the continental shelf (Ressler et al. 2012) offers a new opportunity for a multivariate examination of the hypothesis that pollock predation is a dominant control of the standing stock of euphausiids on the Bering Sea shelf.

We developed multivariate regression models to evaluate the relative importance of pollock predation and temperature in predicting euphausiid density. In these models, water temperature serves as a proxy for 'bottom-up' forcing of euphausiid biomass by environmental conditions, and pollock biomass as a proxy for 'top-down' predation by the single largest consumer of euphausiids in this ecosystem. A multivariate model framework allows the power of all explanatory variables to be competed simultaneously. The expectation in the case of strong top-down control by predation in our models is clear: all other factors being equal, pollock biomass should be the best predictor of euphausiid density, and the relationship between pollock and euphausiid biomass should be negative.

MATERIALS AND METHODS

Hypothesis: We hypothesized that if there was strong top-down control of euphausiids by pollock predation, then a strong negative spatial relationship would exist between theiMar local abundances.

Pollock biomass. Pollock biomass data analyzed here came from two types of surveys of the Bering Sea shelf conducted by scientists of the Alaska Fisheries Science Center in the summers of 2004, 2006, 2007, 2008, 2009, and 2010. An annual bottom trawl survey (Lauth et al. 2011) collected observations of the number of demersal pollock caught per area swept by a bottom trawl with a headrope height of approximately 3 m at fixed stations spaced at a distance of 37 km (20 nmi). The density of pollock was converted to biomass per area at length using a length-weight regression. Water temperature (C) at each trawl location was measured with a Seabird[2] SBE-39 temperature-depth sensor mounted on the trawl. Midwater pollock in the remainder of the water column was observed by an annual or biennial acoustic-

2 Reference to trade names does not imply endorsement.

trawl survey (Honkalehto et al. 2012), which estimates biomass density at length using acoustic backscatter at 38 kHz, length and species composition from midwater trawl catches, a target strength model (Traynor, 1996), and a length-weight regression. The acoustic and bottom trawl estimates of pollock biomass density (kg ha^{-1}) in 37 x 37 km (20 x20 nmi) blocks around each bottom trawl survey station were added to yield a combined estimate of pollock biomass density throughout the water column, as described by Ressler et al. (2012) (Fig. Ch2.d.2; data from 2007 are shown as an example).

Euphausiid biomass. Euphausiid biomass was estimated using acoustic and zooplankton trawl data from the acoustic-trawl surveys of pollock described above (see Ressler et al. 2012 for complete details). Briefly, acoustic backscatter at 120 kHz throughout the water column was classified by analyzing the frequency response measured at 18, 38, 120, and 200 kHz (De Robertis et al. 2010), converted from backscatter to biomass at length using length and species composition from Methot trawl samples (Methot, 1986), a target strength model (Smith et al. 2012), and a length-weight regression (Harvey et al. 2012). Euphausiid biomass was vertically integrated and spatially averaged in the same manner as the acoustic-trawl pollock survey biomass estimates, to produce density estimates (kg ha^{-1}) in the same 37 x 37 km blocks as the pollock biomass data (Fig. Ch2.d.2).

Model fitting. Data from 6 surveys with between 195 and 216 stations per survey were analyzed. Only stations at which data for all variables were measured were included in this analysis. This excluded inshore stations sampled only by the bottom trawl survey, where no estimates of midwater pollock and euphausiid biomass were available. Survey data show that relatively little pollock biomass is found in this inshore region (Ressler et al. 2012; Kotwicki and Lauth, 2013), but some unknown amount of euphausiid biomass exists there (Smith, 1991; Coyle and Pinchuk, 2002); our study is necessarily limited to the area covered by both surveys.

Generalized additive models (GAMs) were fit to the data using the R mgcv package (version 1.7-13; Wood 2006) in R (version 2.15.0; The R Foundation for Statistical Computing 2012). These models assume that effects of the predictors are additive, and use smooth functions (penalized regression splines; Wood and Augustin 2002) to model the effect of each term on the response variable. The full model had the following form

Eqn. 1: s(log10(euph + 10)) ~ s(log10(pk + 10)) + s(bot_temp) + s(ann_surf_temp) + s(lon, lat)

where euph= euphausiid biomass (kg ha^{-1}), pk= pollock biomass (kg ha^{-1}), bot_temp is bottom temperature (C), ann_surf_temp is the annual average surface temperature (C), lon= longitude, and lat= latitude. Both bottom temperature and annual average surface temperature were included in the model because they appeared to have separate, significant effects on euphausiid density, and are only weakly correlated spatially ($r^2 = 0.11$). Summer bottom temperatures are closely related to the spatial extent of ice cover in the previous winter, and they change little over the course of the summer while the survey is conducted, while surface temperatures change substantially during the survey due to seasonal warming and wind mixing after ice retreat (Stabeno et al. 2007; Lauth, 2011). The geographic term s(lon,lat) was included to model any large-scale spatial trend that was present and not attributable to the other covariates we included (Wood and Augustin 2002); essentially, this controls for the average spatial distribution over all years in the data set. We considered all possible combinations of latitude, longitude, and depth when deciding how to specify the geographic term in our models, choosing to use only one pair of these variables since knowing latitude and longitude will specify the value of depth. We chose s(lon, lat) as it was the most intuitive and provided the best model performance.

Backward variable selection was performed by fitting the full model, and then dropping terms one at a time if several criteria were met: a non-significant F-test for the model term, estimated degrees of freedom equal to one with 95% confidence intervals of the partial fit including zero throughout the range of the predictor, and an increase in Akiake Information Criterion (AIC) and the generalized cross-validation (GCV) score for the model (Wood and Augustin 2002). The model in which all terms were significant by these measures was retained as the best model. Plots of the partial residuals and functions for each covariate were scrutinized to evaluate model performance. Transformation of euphausiid and pollock data was required to achieve approximately normally distributed model residuals. After trying several different data transformations, we selected a logarithmic transformation and the addition of a constant as it provided satisfactory residual plots and intuitive scaling of the partial plot axes.

Since pollock are thought to avoid the coldest bottom temperatures on the Bering Sea shelf in summer (De Robertis and Cokelet 2012, Kotwicki et al. 2005, Wylie-Echeverria and Wooster 1998; Swartzman et al. 1994), an interaction between bottom temperature and pollock in these models might be expected. We examined this interaction by including smooths of pollock biomass variables and bottom temperature (e.g., s(pk, bot_temp)) in the models, but found that these terms were not significant and produced inferior GAMs based on the model selection criteria described above.

Prediction of out-of-sample surveys: Because a) GAMs are very flexible and capable of fitting many types of relationships, b) it is likely that the stations in these data sets are not completely independent, and c) the full model of Eqn. 1 was selected, we suspected that overfitting could have occurred. We further supposed that additional out-of-sample prediction (beyond the cross-validation that is normally part of fitting GAM models; Wood 2006) would allow us to evaluate the relative importance of the predictors we retained and judge how robust the model predictions were to out-of-sample data. Jensen et al. (2005) approached this problem by fitting GAM models to single years of a data set and then evaluating out-of sample model prediction of the remaining years. Loots et al. (2010) fit a GAM to half of a spatial fisheries time series and used the other half of the data set for cross-validation. We used a method analogous to the latter, in which we iteratively fit Eqn. 1 to five of the six surveys in our data set, leaving one survey out in turn for prediction, and then computed the mean-squared prediction error as a measure of a model's ability to predict the remaining out-of-sample survey data set. Mean-squared prediction error (mspe) was computed for each of several selected models as follows

$$\textbf{Eqn. 2:}\quad \mathrm{mspe}_j = \mathrm{Sum}_{n,i}\left((\text{predicted euph}_{ij} - \text{observed euph}_{ij})^2\right) / n_j$$

where mspe_j is the mean-squared prediction error for survey j, predicted predicted euph_{ij} is the euphausiid density predicted by the model for station i of survey j, observed euph_{ij} is the euphausiid density from the survey at the same station, n is the number of stations in survey j, and $\mathrm{Sum}_{n,i}$ is the sum over all n stations in survey j.

Relative importance of bottom temperature and pollock: To further examine the importance of temperature and pollock to model predictions of euphausiid density, we used the GAM in Eqn. 1 to make

sets of predictions for two contrasting survey years and for a 'base case' of average temperature and average pollock biomass, as follows:

P1: average temperature, average pollock biomass (base case)

P2: temperature in the coldest year (2009), average pollock biomass

P3: temperature in the warmest year (2004), average pollock biomass

P4: average temperature, pollock biomass in year with most pollock (2004)

P5: average temperature, pollock biomass in year with least pollock (2009)

Bottom temperatures and pollock biomass for these predictions were either the average at each station for all years or the value at each station in one of the contrasting years, 2004 or 2009. Average surface temperatures were either the average value for all stations in all years, or the average value for all stations in one of the contrasting years. The spatial term s(lon,lat) was the same for all prediction data sets. We used these sets of predictions to draw contrasts between the predicted change in euphausiid density due to the effect of temperature and of pollock biomass relative to the base case predictions, as follows:

C1: relative effect of temperature, (P2 - P3)/P1 x 100

C2: relative effect of pollock biomass, (P5 - P4)/P1 x 100

In each case, predicted euphausiid biomass in 2004 is subtracted from predicted biomass in 2009 and divided by predicted euphausiid biomass in the base case. Note that we removed the log10 + 10 transformation of the response before drawing these contrasts, and that only the 183 stations sampled in both 2009 and 2004 (the years used for the warm/cold high pollock/low pollock contrasts) were included in this exercise.

RESULTS

Euphausiids, pollock, and temperature. Annual averages of euphausiid biomass have varied inversely with average pollock biomass (r^2 = 0.43), average bottom temperature (r^2 = 0.94), and average surface temperature (r^2 = 0.81) over the surveys analyzed here (Fig. Ch2.d.1). Euphausiids were found throughout the surveyed area in all years, with patchy regions of high density especially in the southeastern part of the shelf (Fig. Ch2.d.2; Ressler et al. 2012). Pollock biomass was typically concentrated between about 75 and 200 m bottom depth and in the northwestern portion of the continental shelf. Shelf-wide patterns in bottom temperature data are dominated the by the cold pool (< 2° C; Wyllie-Echeverria 1998; Stabeno et al. 2007), with coldest temperatures inshore and to the north; the warmest part of the shelf was usually near the shelf break in the southeast (Fig. Ch2.d.2). As noted in the Methods, summer surface temperatures (not shown) are dominated by seasonal warming and wind mixing; since the survey progresses from east to west in June and July, surface temperatures are always warmest in the westernmost part of the surveyed area (cf. Lauth 2011).

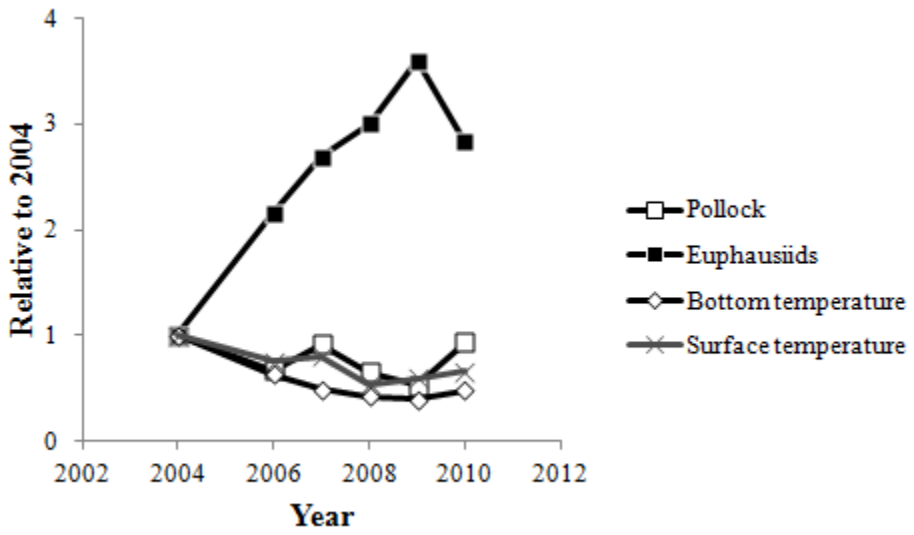

Fig. Ch2.d.1. Interannual pattern in average euphausiid biomass (kg ha^{-1}), pollock biomass (kg ha^{-1}), bottom temperature (C), and sea surface temperature (C). Values for each series are shown relative to the value in 2004.

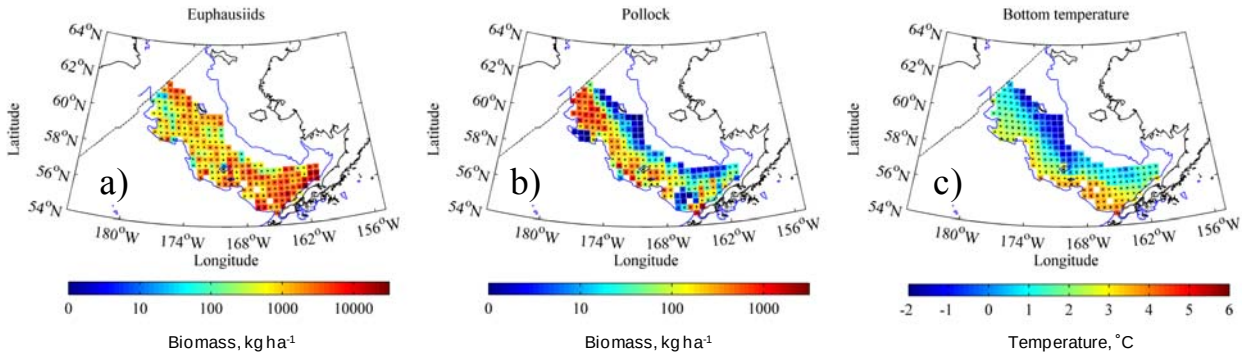

Fig. Ch2.d.2. Example of survey data sets from summer 2007. Blocks with black dots in the center represent 37 x 37 km (20 nmi x 20 nmi) averages around each bottom trawl survey station. Panels show a) sum of age-1+ pollock biomass (kg ha^{-1}) from both surveys, b) euphausiid biomass (kg ha^{-1}) from the acoustic-trawl survey, c) water temperature (C) at the bottom measured during bottom trawl survey. The 50 and 200 m isobaths are shown as blue line contours. The boundary between the U.S. and Russian exclusive economic zone is shown as a diagonal line across the top left corner in each panel.

Model results. The full model was selected as the best model: all terms were statistically significant, AIC was minimized, and deviance explained (47.0%) was highest when all terms were retained (Table 1). Examination of partial residual plots (Fig. Ch2.d.3) indicate a strong negative effect of bottom temperature on euphausiid density, and a moderate negative effect of annual average surface temperature, while the effect of pollock was relatively flat in comparison. There was a significant geographic trend in the data over all years: the s(lat,lon) term was positive in the southeast part of the continental shelf, and negative inshore and to the west. Both environmental and geographic covariates contributed substantially to model fit: a model using only the environmental covariates (pollock biomass and bottom temperature) explained 34.2% of the deviance in euphausiid biomass, while a model using only the geographic term had even less explanatory power (10.7%). Both environment-only and geographic-only models had inferior AIC and residual structure compared to the selected model (Table 1). Finally, it is important to note that more than half of the variability in the euphausiid data remained unexplained by the best model.

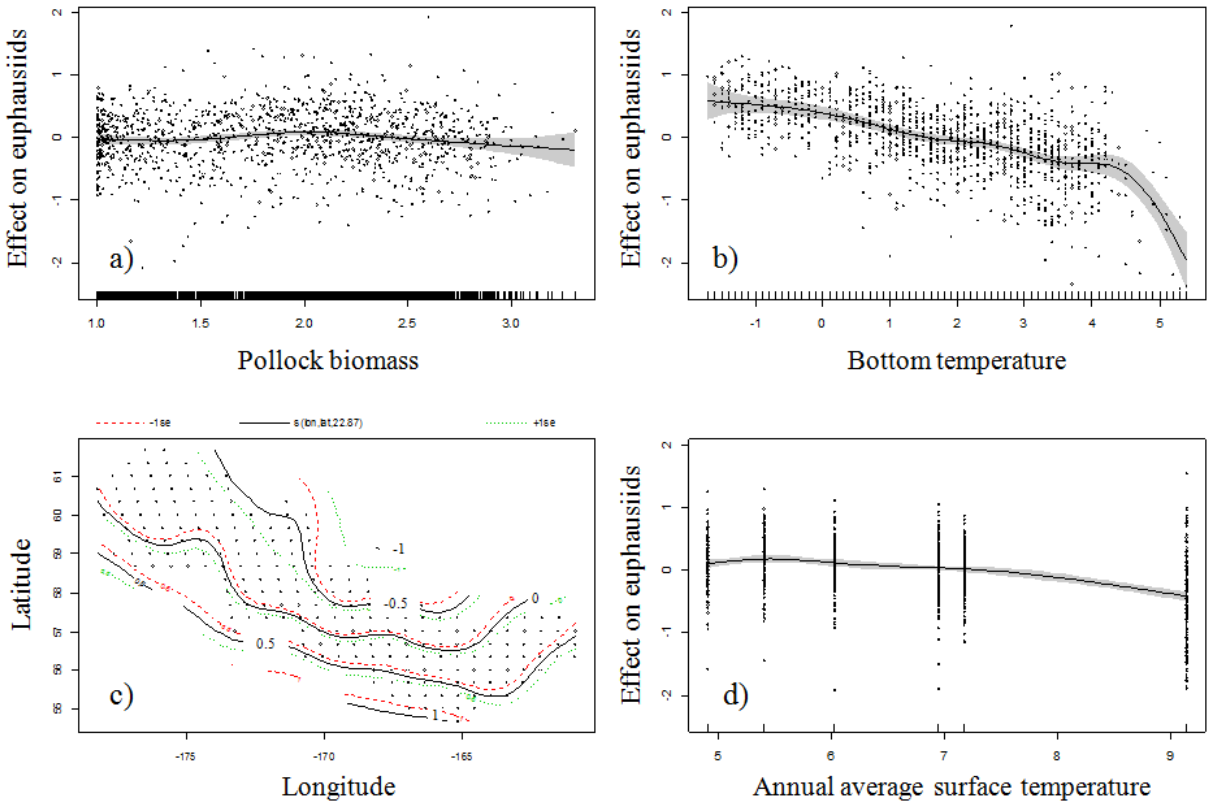

Fig. Ch2.d.3. Effect of each term in the best GAM model of euphausiid biomass density (kg ha^{-1}). Covariates shown by each panel are as follows: a) age-1+ pollock biomass (kg ha^{-1}), b) bottom temperature (C), c) latitude and longitude, and d) annual average surface temperature (C). Note that the units of pollock and euphasiid biomass have undergone a log10(x +10) transformation. In each panel, the points on the plots are residuals from the full model without the effect of the covariate on the x-axis, and the solid lines are smooth functions indicating the modeled effect of that covariate on predicted euphausiid density. In panels a), b), and d), the shading denotes a 95% confidence around the fit, while in panel c) red dotted lines indicate +1 SE, and green dotted lines -1 SE.

Table 1. Model statistics for several GAMs based on Eqn. 1.

	Pollock biomass			Bottom temperature			Longitude x Latitude			Annual average surface temperature			Deviance explained	AIC
	edf	f	p	edf	f	p	edf	f	p	edf	f	p		
best model	4.05	3.59	0.003	8.43	17.16	< 2E-16	22.86	10.25	< 2E-16	3.63	27.32	< 2E-16	47.0%	1618.94
environmental terms only	3.96	8.77	4.35E-08	8.62	4.43	1.05E-05		N/A		3.86	99.20	< 2E-16	34.2%	1839.37
geographic terms only		N/A			N/A		21.00	4.98	1.55E-14		N/A		10.7%	2220.69

Prediction of out-of-sample surveys. When five model variants of Eqn. 1 were iteratively fit using five of six survey years, leaving one survey year out in turn for cross-validation, the full model had the lowest AIC and highest deviance explained on average (Table 2), as would be expected from the results of backward variable selection using Eqn. 1. In terms of out-of sample prediction, the full model also had the lowest mspe on average. Mean-squared prediction error decreased when annual average surface temperature was dropped from the model, and was slightly smaller when pollock was dropped from the model, but the largest changes by far occurred when either s(bot_temp) or s(lon,lat) were dropped. The mspe of a model with only bottom temperature and spatial location differed by only about 5% on average from that of the full model. Eliminating the pollock term from the model, although it was statistically significant, appeared to have only a marginal effect on predictive power.

Table 2. Leave-one-out cross validation for several selected models. Darker shades of gray indicate poorer performance on each model statistic.

	model	average AIC	average deviance explained	average mspe	average % difference in mspe from full model
full model	log10(euph+10) ~ s(log10(pk_all+10)) + s(bot_temp) + s(ann_avg_sst) + s(lon,lat)	1336.43	45.38	0.30	0.00
no annual average surface temperature	log10(euph+10) ~ s(log10(pk_all+10)) + s(bot_temp) + s(lon,lat)	1402.54	41.58	0.31	4.95
no annual average surface temperature or pollock	log10(euph+10) ~ s(bot_temp) + s(lon,lat)	1407.74	40.85	0.31	5.34
geographic terms only	log10(euph+10) ~ s(lon,lat)	1801.45	12.01	0.42	34.80
environmental terms only	log10(euph+10) ~ s(log10(pk_all+10)) + s(bot_temp) + s(ann_avg_sst)	1521.95	31.75	0.52	13.88

Relative effect of temperature and pollock: Compared to 'base case' model predictions made using average temperature and average pollock biomass, the change in predicted euphausiid density from 2004 to 2009 was greatest when temperature was varied (Figure Ch2.d.4). Under our hypothesis, a positive value would be expected for each contrast (euphausiid biomass peaked in 2009, coinciding with both the coldest temperatures and lowest pollock biomass); if top-down control by pollock predation dominated variability in euphausiid biomass, the effect of pollock biomass on predicted euphausiid density should be largest. On average, the relative change in predicted euphausiid density at each station given temperatures in the coldest year (2009) and the warmest year (2004) with average pollock biomass was 160.53% (min 51.45, max 363.78). The relative change in predicted euphausiid density from given pollock biomass in 2009 and 2004 with average temperatures was close to zero and slightly negative on average (mean -3.02%, min -49.85, max 44.70).

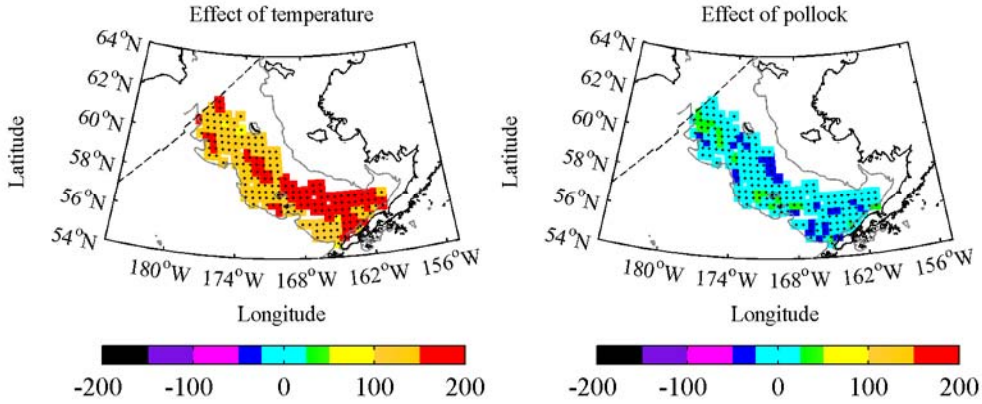

Fig. Ch2.d.4. Comparison of the relative effect of pollock and temperature. At left, the relative change (%) in predicted euphausiid density due to the temperature change from the warmest year (2004) to the coldest year (2009) given the average effect of pollock. The red and orange colors indicate the relatively large increases in euphausiid biomass at each station attributed to temperature in the model as temperatures cooled between 2004 and 2009. At right, the relative change (%) in predicted euphausiid density due to the change in pollock biomass from the year with the least pollock (2009) to the year with the most pollock (2004) given the average effect of temperature. The blue and green colors indicate the relatively small change in euphausiid biomass at each station attributed to pollock biomass in the model.

DISCUSSION

The results presented here are not consistent with dominant top-down control of euphausiids by pollock predation on the Bering Sea shelf. We hypothesized that if predation by pollock were the dominant factor affecting the standing stock of euphausiids on the eastern Bering Sea shelf ('top-down control'), we would have observed a strong, negative spatial relationship between the biomass of the two species. Instead, while pollock biomass was a statistically significant model covariate, there was only a modest reduction in explanatory power when pollock terms were dropped from our GAMs. Further, the effect of pollock on euphausiid biomass was rather flat and not strongly negative (Fig. Ch2.d.2). The effects of temperature were much stronger, a robust observation that held true during both stepwise model selection (Table 1) and leave-one-out cross validation (Table 2). When model predictions based on the temperature and pollock biomass extremes in the data set (2004: warm, high pollock; 2009: cold, low pollock) were compared with euphausiid biomass predicted under average conditions, the change in euphausiid biomass indicated by the range of temperatures in this data set was much larger than for observed changes in pollock biomass (Fig. 4).

Effect of temperature. The effect of temperature on euphausiid biomass appeared relatively strong and negative in all of the GAMs (Fig. Ch2.d.2), consistent with the negative bivariate correlations of interannual averages (Fig. Ch2.d.1) of euphausiid biomass and temperature. Bottom temperature was also the most important single covariate in predictions of out-of-sample data (Table Ch2.d.2). Annual average surface temperature also had an independent, negative effect on euphausiid biomass in these models. Water temperature on the Bering Sea shelf is uniform and well-mixed from surface to bottom in winter, but after ice retreat in spring, seasonal warming of surface waters occurs over the course of the summer while bottom temperatures remain cold, reflecting the extent of winter ice cover (Stabeno et al. 2007). The negative effect of both surface and bottom temperatures in the models are consistent with the idea that warmer conditions with reduced ice cover and early ice retreat, greater spring and summer insolation, and reduced wind mixing leading to smaller 'cold pools' and warmer, stratified summer surface temperatures are somehow unfavorable for euphausiids.

De Robertis and Cokelet (2012) reported that the effect of bottom temperature on the spatial distribution of acoustic backscatter from zooplankton (principally euphausiids) on the Bering Sea shelf during spring and summer of 2007 and 2008 was weaker than the effect on the spatial distribution of fish backscatter (principally pollock), but they did note that on average euphausiids were found in somewhat colder water temperatures than pollock. This is consistent with the negative effect of temperature on euphausiid biomass observed here. However, the temperatures on the Bering Sea shelf are not near physiological (Pinchuk and Hopcroft 2006) or distributional (Brinton et al. 2000) limits for these euphausiid species, and a negative association of biomass and temperature for these species is not universally found (Zhukova et al. 2009, Dalpadado et al. 2012). Potential mechanisms underlying positive 'bottom-up' forcing of euphausiid standing stocks during the recent cold, icy conditions on the Bering Sea have been proposed, including release from metabolically demanding warmer temperature conditions (Pinchuk and Coyle 2008), favorable timing of phytoplankton blooms on and in association with sea ice, or increased new production in summertime (Hunt et al. 2011, Coyle et al. 2011), but the question of which if any of these predominate remains unresolved.

Effect of pollock biomass. Pollock biomass had a relatively flat effect on euphausiid density in our models, slightly positive at low pollock densities and slightly negative at high pollock densities (Fig. Ch2.d.2). A consistently strong, negative effect of pollock biomass on euphausiid density was not observed; rather, it was weak and variable compared with the effect of temperature (Fig. Ch2.d.4). Overall, inclusion of pollock terms lent a statistically significant amount of predictive power to the model, but particularly when compared to the impact of bottom temperature and spatial location, the predictive power of pollock biomass in the GAM was weak.

We did not observe the negative association between pollock and euphausiid biomass that we expected based on previous comparisons of pollock and euphausiid standing stocks showing that annual predation could be significant (Ressler et al. 2012), and previous studies suggesting tight coupling between zooplankton and higher trophic levels (Aydin and Mueter 2007, Springer 1992) in the Bering Sea. Though top-down control of zooplankton by fish predation has been shown in closed freshwater systems (Brooks and Dodson 1965, Carpenter and Kitchell 1993, Gliwicz 1986) clear demonstrations of this in marine systems are rare. In the present study, negative univariate associations of pollock and euphausiid standing stock (Ressler et al. 2012) appeared much weaker when included with other potential covariates in a multivariate regression model.

Effect of spatial location. Spatial location lent a significant amount of predictive power to the models. Though the environmental covariates are clearly more important in the models, the spatial term s(lon,lat) was able to explain 10-12% of the deviance in euphausiid biomass on its own, and models that included the spatial term had better predictive power than those including only environmental covariates (Tables 1, 2). Accounting for large-scale trends when fitting regression models to spatial data has been recommended to avoid incorrectly attributing that trend to other model covariates (Legendre 1993), and a geographic term is often included in spatial regression models of fisheries data (Swartzman et al. 1992, Wood and Augustin 2002, Mueter and Litzow 2008, Planque et al. 2011). However, the ecological interpretation of this term can be problematic (Wood, 2006): for example, the spatial trend is present in all years of this data set, and it is not clear what environmental or life history processes could have produced this pattern in euphausiid biomass, or how long it has persisted (nor is it possible to examine these questions with the data set in hand). The effect of s(lon,lat) is probably best interpreted as a proxy for spatial processes unresolved by the other covariates in these models.

Weaknesses of the method and data set. GAMs are vulnerable to overfitting and non-independence of observations. We addressed this by comparing traditional model selection with leave-one-out cross validation of out-of-sample survey data sets. This approach showed that the conclusions drawn about the relative predictive importance of pollock and bottom temperature from traditional model selection were robust. It is also important to note that the shape of the smooths for each covariate (Fig. 3) remained consistent when a year of observations was left out of the model; no single year in the data set drove these results.

Our analysis is limited to the 2004-2010 time period, and we do not know for certain whether the relationships modeled in our study are representative of all conditions in the eastern Bering Sea. We

cannot, for example, address what might have set up the large-scale spatial trend represented by the geographic term in the model, or how long such a pattern could have been present. The string of very warm years in the early 2000s followed by cold years from 2007-2010 is an unusual pattern in environmental conditions in this region (Hunt et al. 2011, Stabeno et al. 2012b), but it is not statistically unexpected given historical variability (Overland et al. 2012). Likewise, the standing stock of Bering Sea pollock was lower during our study period than peak biomass values in the mid-1980s and late 1990s, and was very low from 2007-2010, but it was nevertheless within the envelope of past stock estimates (Ianelli et al. 2012). Finally, our hypothesis regarding control of euphausiid standing stock by pollock predation relies on a spatial comparison of biomass, rather than of production rates. However, given the difficulty of obtaining robust production estimates for the two species at the spatial resolution of our data sets, we think our approach is a reasonable one.

CONCLUSIONS

The amount of euphausiid biomass consumed annually by walleye pollock is substantial and we cannot categorically exclude predation as one of several possibly important factors affecting the standing stock of euphausiids on the Bering Sea shelf. However, the effect of pollock predation does not appear predominant. Despite negative univariate interannual and spatial relationships between pollock and euphausiid biomass, the effect of pollock on euphausiid density was weak when competed with other covariates in a multivariate model.

ACKNOWLEDGEMENTS

This work was supported by the Alaska Fisheries Science Center, National Marine Fisheries Service, National Oceanic and Atmospheric Administration (NOAA), the North Pacific Research Board (NRPB) as part of the BEST-BSIERP Bering Sea Project, and NSF as part of the Bering Sea Synthesis xxxx. Technical editing by xx and comments by xx and several anonymous reviewers helped improve this manuscript. This is NPRB publication xxx and BEST-BSIERP Bering Sea Project publication xx. The findings and conclusions in the paper are those of the authors and do not necessarily represent the views of the National Marine Fisheries Service.

Chapter 2.e. Description and spatial distribution of other important acoustic classes

Other important parts of the Bering Sea ecosystem are not well described or monitored by any survey. We investigated what other acoustic classes might be amenable to acoustic surveys. This work is described in the following section. In addition to pollock and euphausiids, there are at least two other dominant acoustic classes in the eastern Bering Sea shelf. The composition of these classes is uncertain and provides a direction for future research.

The following material is the work of Woillez (postdoc supported by B62), Ressler (B62 PI), Wilson (B62 PI), and Horne, and was published as:

Woillez, M., P.H. Ressler, C.D. Wilson, and J.K. Horne, 2012. Multifrequency species classification of acoustic-trawl survey data using semi-supervised learning with class discovery. JASA Express Letters 131(2), DOI: 10.1121/1.3678685.
http://asadl.org/jasa/resource/1/jasman/v131/i2/pEL184_s1?bypassSSO=1

M. Woillez
Alaska Fisheries Science Center, National Marine Fisheries Service, NOAA, 7600 Sand Point Way NE, Seattle, WA 98115, USA, and School of Aquatic and Fishery Sciences, University of Washington, Box 355020, Seattle, WA 98195, USA

P. H. Ressler and C. D. Wilson
Alaska Fisheries Science Center, National Marine Fisheries Service, NOAA, 7600 Sand Point Way NE, Seattle, WA 98115, USA

J. K. Horne
School of Aquatic and Fishery Sciences, University of Washington, Box 355020, Seattle, WA 98195, USA

ABSTRACT

Acoustic surveys often use multifrequency backscatter to estimate fish and plankton abundance. Direct samples are used to validate species classification of acoustic backscatter, but samples may be sparse or unavailable. A generalized Gaussian mixture model was developed to classify multifrequency acoustic backscatter when not all species classes are known. The classification, based on semi-supervised learning with class discovery, was applied to data collected in the eastern Bering Sea during summers 2004, 2007, and 2008. Walleye pollock, euphausiids, and two other major classes occurring in the upper water column were identified.

INTRODUCTION

Estimating abundance in acoustic-based surveys depends on allocating fish species to measured acoustic backscatter. To help either interpretation by experts or classification by algorithms, trawl samples are collected to provide information (e.g. species, length) about the targeted aggregations[1]. However, as most surveys focus on few commercial species, little direct sampling effort is available to determine species composition of other taxa. Backscatter classification of non-target species may provide added ecological insights.

Classifications used in fishery acoustics differ regarding statistical techniques, discriminatory variables, and spatial resolutions of data[2,3]. For statistical techniques, when classification models are built from validation samples and used to predict known classes, the learning is said to be supervised[4,5]. If no validation samples are used and classes are not specified, then the classification is unsupervised[6]. Classification models can be improved by using both types of information (semi-supervised learning)[7], but detected classes must be present in validation samples. Here a semi-supervised classification procedure is implemented that also allows discovery of unknown classes[8]. A generalized Gaussian mixture model (GGMM), adapted to repeated surveys of the same ecosystem, is applied to multifrequency acoustic data collected from summer acoustic-trawl surveys in the Eastern Bering Sea (EBS). Walleye pollock (*Gadus chalcogrammus*) and euphausiids (*Thysanoessa* spp.) comprise dominant acoustic classes, but other classes with unique frequency responses also occur. Classification results for pollock and euphausiids (two of the three known classes) are compared to results provided by two other classification methods: interpretation by experts[9] and an empirical multifrequency method[4]. Two other major classes (one known and one unknown) are also identified and described.

MULTIFREQUENCY ACOUSTIC AND TRAWL DATA PROCESSING

Acoustic data were collected at 18, 38, 120, and 200 kHz with Simrad EK60 echosounders in the EBS during summers 2004, 2007, and 2008 during NOAA acoustic-trawl surveys[9]. Data acquisition is described in De Robertis et al.[4]. Background noise at 120 and 200 kHz, and transducer ringing at 18 kHz were estimated[10]. Only data with a signal-to-noise ratio ≥ 10 dB at any frequency, and with Sv > -80 dB re 1 m^{-1} at one or more frequencies were used (e.g., Fig. 1). Three pair-wise frequency differences relative to 38 kHz (ΔSv18-38, ΔSv120-38 and ΔSv200-38) were considered as discriminatory variables for the classification. An existing library of concurrent multifrequency and trawl data characterizing midwater aggregations of single species[4] was used to determine the species-specific pair-wise frequency differences. Known acoustic classes included pollock, euphausiids, and a third class of uncertain

taxonomic composition showing S_v values highest at 18 kHz (hereafter named high18). Preliminary results[4] suggested that high18 may be jellyfish, but more validation trawls are needed.

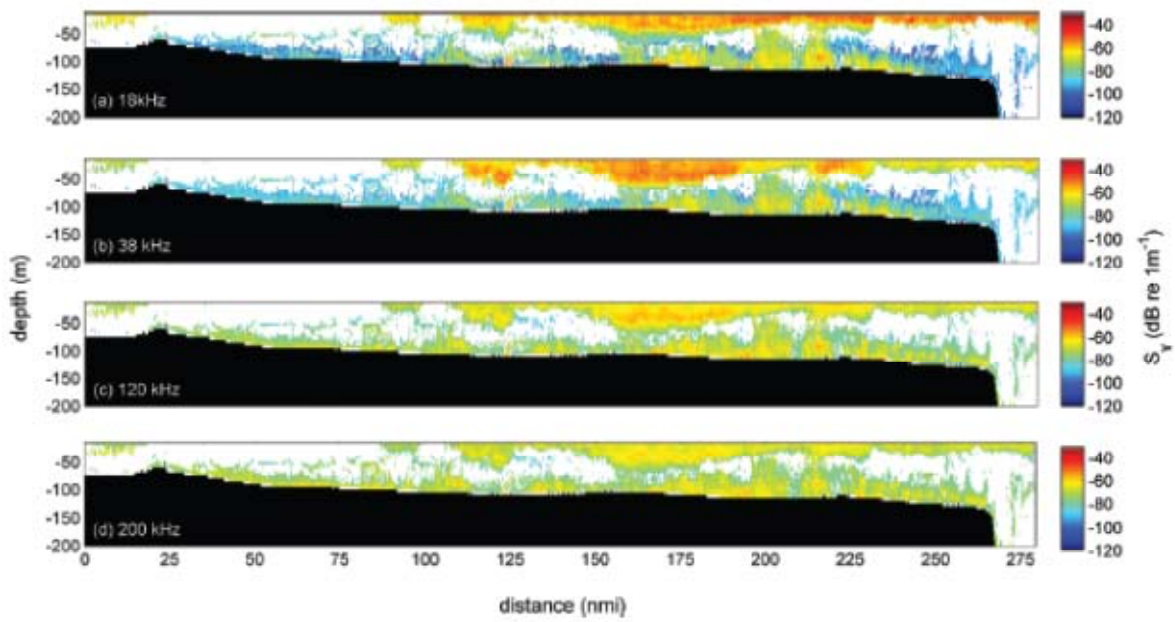

Figure 1. Volume backscattering strength (Sv in dB re 1 m^{-1}) at 18, 38, 120 and 200 kHz (a, b, c, and d) that met signal-to-noise (SNR ≥ 10 dB at any frequency) and threshold (Sv > -80 dB re 1 m^{-1} at one or more frequencies) criteria from representative transect across the EBS shelf, summer 2007.

CLASSIFICATION PROCEEDURE

Labeled acoustic data, where the acoustic class is known (library data) and unlabeled data, where class is unknown (survey data), are learned separately. Then, both models and data are merged together and learned using the GGMM.

Supervised learning of labeled data

Species-specific pair-wise frequency differences were used to determine a classification model, where each known class is assumed to follow a Gaussian distribution[11]. Each class is modeled independently and parameters (mixing coefficients, means, and variance-covariance matrix) are inferred. A single classification model is then built by merging all known class components.

Unsupervised learning of unlabeled data

The unlabeled pair-wise frequency differences are modeled using a mixture of multivariate Gaussian distributions, where the class label is an unobserved latent variable that needs to be inferred[6]. For the purpose of estimating parameters of this statistical model, an Expectation-Maximization (EM) algorithm[12] can be used. It is an iterative method that allows computing the maximum likelihood estimates of the model parameters. First, a k-means algorithm is used to provide initial estimates of the parameters. Then, the EM iteration alternates between 'expectation' (E) and 'maximization' (M) steps until the convergence is reached (a property of the EM algorithm is that it is guaranteed to increase the likelihood at each iteration). The E-step computes the expectation of the log-likelihood evaluated using the current estimate for the parameters, in this case the probability that a data point belongs to a Gaussian model component. The M-step computes parameters maximizing the expected log-likelihood found on the E-step. These parameter estimates are then used to determine the distribution of the latent variables (here the class label) in the next E step. Finally, all unlabeled data are associated with unknown classes.

Semi-supervised learning based on generalized Gaussian mixture model

All known and unknown class components obtained previously are merged and initialize the semi-supervised GGMM learning[8]. All labeled and unlabeled data are now considered together in the analysis. Thus, some unlabelled data will be classified as belonging to known classes. Known class component parameters are then updated. The remaining unlabelled data stay associated with unknown class components, whose parameters are also updated.

The GGMM treats the label presence ($L = l$) or absence ($L = m$) as a random variable. Thus, 2 types of mixture model components can be defined: (i) predefined components C_{pre}, representing known classes, which generate both labeled and unlabeled data; and (ii) non-predefined components $\overline{C}_{pre}$, which generate only unlabeled data. These latter components represent outlier regions of known classes or possibly unknown (undiscovered) classes. In addition to mixing coefficients π_k, means μ_k and the variance-covariance matrix Σ_k of Gaussian mixture components, the GGMM introduces three new parameters: (i) the probability of data being labeled when belonging to a generic predefined mixture component M_g, $P(L = l \mid M_g \in C_{pre})$ (identical for all predefined components), (ii) the probability mass function associating each predefined mixture component M_k with all known classes $P(C = c \mid M_k \in C_{pre}, L = l)$, and (iii) the categorical variable v_k indicating the component type (predefined or non-predefined). The joint log-likelihood of the observed data for the model with N components is then:

$$\log L_M = \sum_{x \in X_l} \log(\sum_{k=1}^{M} v_k \pi_k P(x \mid \mu_k, \Sigma_k) P(L = l \mid M_g \in C_{pre}) P(C = c(x) \mid M_k \in C_{pre}, L = l)) + \sum_{x \in X_u} \log(\sum_{k=1}^{M} v_k \pi_k P(x \mid \mu_k, \Sigma_k) P(L = m \mid M_g \in C_{pre}) + (1 - v_k) \pi_k P(x \mid \mu_k, \Sigma_k)) \quad (1)$$

Semi-supervised learning uses a generalized EM algorithm to estimate model parameters. It alternates between choosing component types to maximize the log likelihood of the GGMM when all other parameters are fixed, and using a classic EM algorithm to estimate the remaining model parameters when component types are fixed. The choice of the component type is an iterative 'one at a time' selection among all possible combinations. That is, a component type is assigned, the model log likelihood evaluated, and the component type yielding the higher likelihood selected. The next component is considered until no further changes are observed. Remaining parameters are estimated using a classic EM, where the expected complete data likelihood is evaluated (E-step), and then model parameters are maximized (M-step). The log likelihood to maximize differs as component types are now determined. Probabilities of component ownership are determined based on whether the data are labeled or unlabeled, and whether a component is predefined or non-predefined. Mixture parameters are then maximized using latter probabilities of ownership[8].

Treatment of the year effect and model selection

As dominant acoustic classes are expected to occur repeatedly, a year effect was added to the GGMM framework[8]. Means and variance-covariances of class-components are held constant across years, while mixing coefficients are allowed to vary. The ability of a mixture model to identify classes is quantified using the Integrated Complete-data Likelihood (ICL) criterion, as it includes a penalty term to account for classification uncertainty[13].

RESULTS AND DISCUSSION

Classification of multifrequency data

Gaussian components were fitted to the labeled data for each of three known classes, and unsupervised learning of unlabeled data was completed using 8 Gaussian components as suggested by the ICL criterion. Then, GGMM classification was used to detect and map 8 classes with different acoustic frequency responses based on 4 recorded frequencies (Fig. 2).

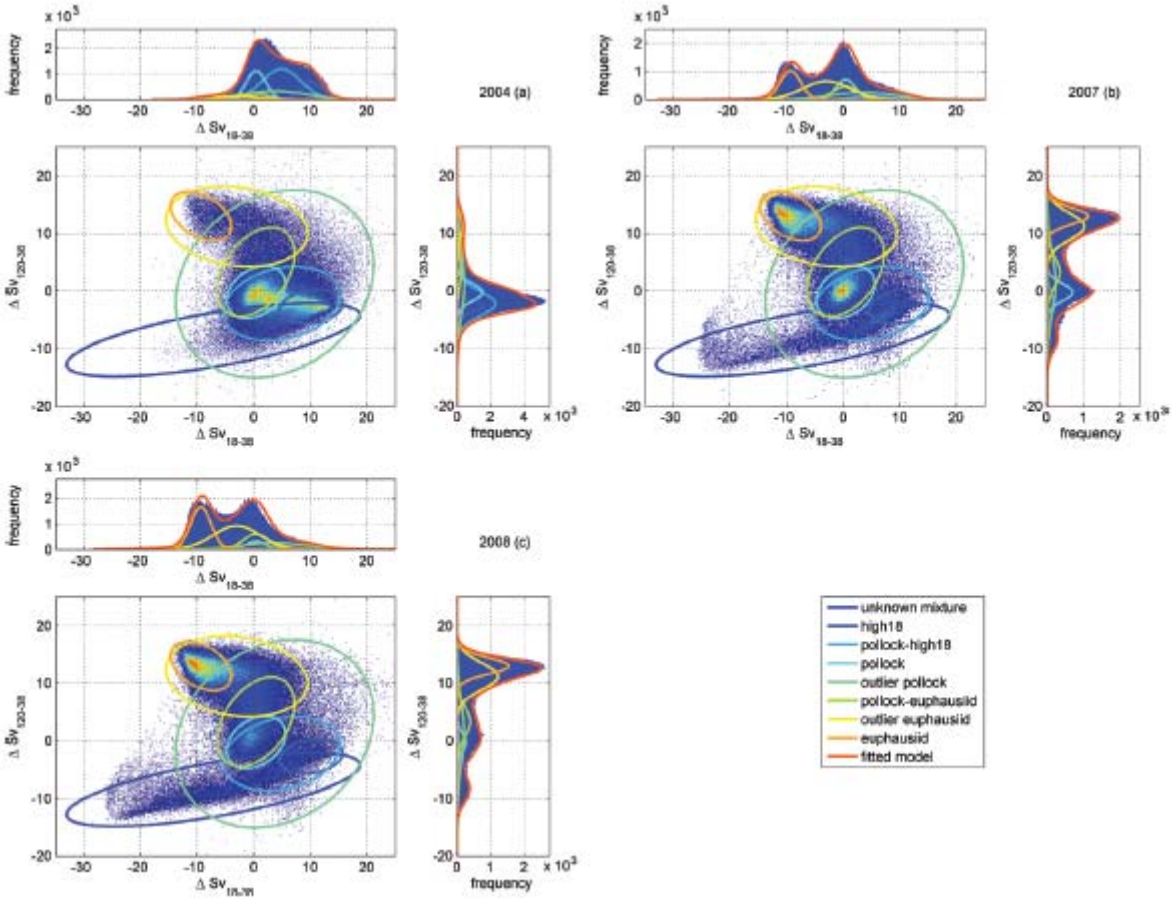

Figure 2. Example pairwise frequency differences in survey backscatter data for years 2004 (a), 2007 (b) and 2008 (c). 1D and 2D histograms from ΔSv 18-38 and ΔSv 120-38 are represented, as well as the 8 fitted multivariate Gaussian class components (colors orange to blue). The fitted mixture model, representing the sum of all class components, is represented by a red line in each 1D histogram. The known class components, pollock, euphausiids, and high18, are indicated concurrently with the unknown class components.

Two classes identified by the GGMM were known classes corresponding to pollock and euphausiids. A third known class, high18, was consistent with the frequency response of jellyfish trawl catches[4]. Two of the five remaining classes were interpreted as outliers distributed around known classes, two as mixtures between two known classes, and one as an undiscovered class, which was different from known classes, outlier distributions, or mixtures. The relative frequency response of the unknown class was similar to that of myctophid trawl catches[4], but myctophids are not typically found over the EBS shelf. The general shape of the frequency response (peak at 38 kHz) may indicate fish larvae or macroplankton (e.g., siphonophores) containing a small, resonant gas enclosure[14].

Vertical distribution patterns differed among GGMM scattering classes (Fig. 3). Pollock and euphausiids appeared in the lower two-thirds of the water column during the day (>95% and >97%) in 2007 and 2008, as has been reported elsewhere[9,15]. High18 and the unknown class occurred in the upper third of the water column (>98% and >63%) during these years. However, high18 occurred over most of the water column, overlapping with pollock and euphausiids in 2004.

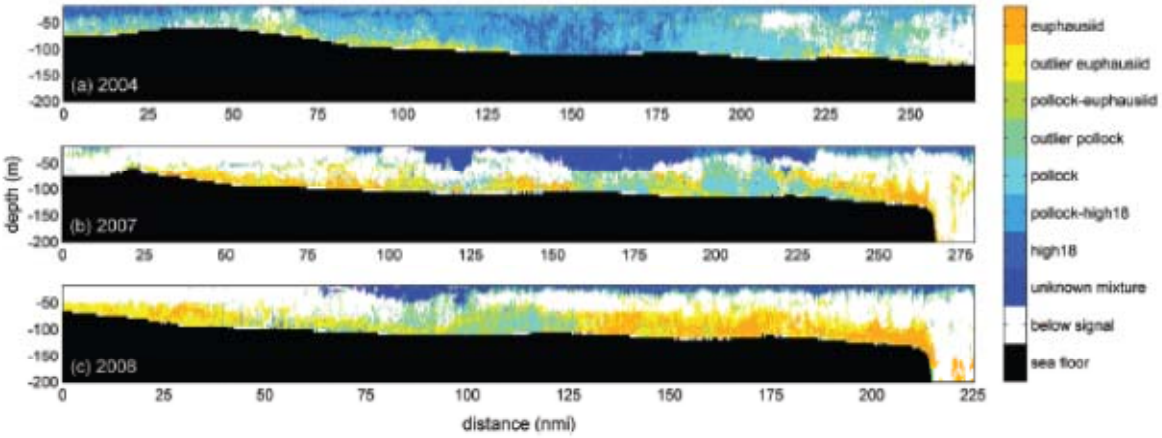

Figure 3. Corresponding classes obtained by the classification procedure for a representative transect during summer 2004 (a), 2007 (b), and 2008 (c). Known classes are pollock, euphausiid and high18. Unknown classes correspond to outliers from a known class, mixtures of known classes, or an undiscovered class.

Comparison with other classification methods

The GGMM results for two known classes (pollock and euphausiids) and mixtures containing these classes were compared with classification results based on expert classification and/or empirical multifrequency classification for pollock[4] and euphausiids[15]. Mean backscatter attributed to each class for each transect was regressed linearly between methods for each year (Table 1). GGMM results generally agreed with the expert classification of pollock in every year (Table 1) and the empirical multifrequency classification of pollock and euphausiids in two of three years, though in all cases GGMM estimates were lower (slope <1).

Table 1. Class estimates of alternative classification methods for pollock and euphausiid were compared to corresponding GGMM class estimates by linear regression. Transect mean backscatter was used as the comparative variable. From all possible comparisons (= 51), only significant ($\alpha < 0.001$) models with a high r^2 and a slope greater than 0.5 are shown.

alternative methods' class estimates	GGMM class estimates	year	intercept	slope	r^2
expert classification for pollock	pollock (k)	2004	35.80	0.733	0.850
		2007	-1.54	0.685	0.888
		2008	-12.02	0.513	0.861
	pollock (k) + outlier pollock	2004	53.934	0.794	0.862
		2007	3.381	0.746	0.906
	pollock (k) + pollock-euphausiid	2008	-17.054	0.770	0.909
empirical multifrequency classification for pollock[4]	pollock-high18	2004	-169.33	1.013	0.741
	pollock (k)	2007	-21.70	0.737	0.951
		2008	-16.66	0.552	0.903
	pollock-high18 + pollock (k)	2004	121.029	1.039	0.891
	pollock (k) + outlier pollock	2007	-17.725	0.799	0.960
	pollock (k) + pollock-euphausiid	2008	-22.639	0.818	0.930
empirical multifrequency classification for euphausiids[13]	outlier euphausiid	2004	-12.53	1.099	0.887
	euphausiid (k)	2007	-30.88	0.821	0.956
		2008	-14.03	0.699	0.937
	outlier euphausiid + euphausiid (k)	2004	-10.54	1.180	0.949
		2007	-11.536	0.903	0.970
		2008	12.883	0.770	0.939

k: for known class component.

For classification challenges associated with mixed aggregations, the 3 methods produced different results as illustrated in 2004 when the high18 class vertically overlapped with that of pollock and euphausiids on some transects (Fig. 3). The GGMM and expert classification for pollock agreed, but the empirical

multifrequency classification pollock results were better correlated with the GGMM pollock-high18 mixture than with GGMM pollock (Table 1). A significant amount of unlabeled data was allocated to a pure class by the empirical multifrequency method, but split into several pure and mixed classes by the GGMM. When combining these two classes, the correlation improves (Table 1). Combining resolves other cases of disagreement (e.g. euphausiids in 2004; Table 1). Indeed, expert and empirical multifrequency classifications aggregated around target classes, while the GGMM classification tended to subdivide into classes.

CONCLUSION

Semi-supervised learning using a GGMM effectively classified backscatter from known and unknown classes. The GGMM results for known scattering classes, pollock and euphausiids, compared well with classification results from established methods, although differences occurred when scattering types were mixed. The GGMM was able to create mixtures of classes, whereas expert scrutiny and empirical multifrequency classification assume pure classes. The main advantages of the GGMM method are that i) it can discover unknown classes while accounting for the presence of known classes, and ii) it can include mixtures between identified classes. To improve the GGMM method, future work should include labeled data based on mixed aggregations, other discriminatory variables (e.g., morphological descriptors, depth), and direct sampling of unknown scattering classes.

ACKNOWLEDGEMENTS

Support was provided by Alaska Fishery Science Center, NMFS, NOAA and the Bering Sea Integrated Ecosystem Research Program, North Pacific Research Board. We thank Alex De Robertis for review and labeled data, Jim Ianelli for review, and Ainhoa Lezama-Ochoa for helpful discussions. Findings and conclusions are those of the authors and do not necessarily represent views of NMFS, NOAA and reference to trade names does not imply endorsement. This was BEST-BSIERP publication 34.

Chapter 2.f. Conclusions

We determined that a high-resolution, wide-area acoustic survey of euphausiids in the EBS (concurrent with the acoustic-trawl pollock survey) was possible. We gathered this information on the biomass of euphausiids during the BSIERP field years, and it is feasible for NOAA-AFSC to continue to do so in support of stock and ecosystem assessment in the eastern Bering Sea. Pollock predation on euphausiids is probably substantial, but multivariate analysis suggest that the "bottom-up" effect of temperature has a larger effect on the spatial distribution of euphausiid biomass than the "top-down" predation pressure exerted by pollock. In addition to euphausiids and pollock, there are at least two other dominant acoustic backscatter classes on the eastern Bering Sea shelf; further research is required detmermine their composition.

Chapter 3: Groundfish Trends in the eastern Bering Sea shelf bottom trawl survey (formerly BSIERP – B91)

Chapter 3: Overview

The Resource Assessment and Conservation Engineering Division of the Alaska Fisheries Science Center conducts annual bottom trawl (BT) surveys to monitor the condition of the demersal fish and crab stocks of the eastern Bering Sea (EBS) continental shelf. The EBS shelf BT survey (BSIERP - B91) was a matching project that did not receive BSIERP funding but was a very important component augmenting other BSIERP projects and providing broad scale biological and environmental data during 2008-2010 and dating back to 1982. The EBS shelf BT time-series is a rich data source for investigating complex ecological interactions amongst the biota and for understanding trends and temporal shifts in response to climate change. This chapter has three sections, each which investigates a different type of trend using data from the EBS shelf BT survey. The first section investigates general latitudinal trends in the structure of the seafloor community over a broad geographical area spanning from the Alaska Peninsula to the Chukchi Sea, and how those general latitudinal trends on the EBS shelf respond to major temperature shifts during warm and cold periods during the last decade. The second section investigates how temporal changes in a major environmental driver on the EBS shelf, the "cold pool," affects the temporal and spatial distribution and abundance of bottom fishes and crabs. The final section focuses on initial research into the continuing development of a new index for analyzing abundance trends in semi-pelagic fishes such as walleye pollock and Pacific cod. The investigation uses an empirical approach to incorporating environmental variables with a combination of BT survey and acoustic data to predict the relative catchability of BT and acoustic surveys for different environmental factors. Independent of this report are data reports detailing the methodology and results for the EBS shelf BT surveys for each of the three field years of BSIERP (Lauth 2011, 2010; Lauth and Acuna, 2009). These data reports, as well as those for all other survey years since 1982, are available online from the AFSC Publications Database (http://access.afsc.noaa.gov/pubs/search.cfm).

Chapter 3.a. Latitudinal trends and temporal shifts in the catch composition of bottom trawls conducted on the eastern Bering Sea shelf.

The material in this section was published as:

Stevenson, D.E., and R.R. Lauth. 2012. Latitudinal trends and temporal shifts in the catch composition of bottom trawls conducted on the eastern Bering Sea shelf. Deep-Sea Research II 65-70(2012):251-259.

ABSTRACT

Latitudinal species diversity gradients are well known in both terrestrial and aquatic ecosystems throughout the world. However, trends in relative abundance and other shifts in community structure with latitude, which can be more sensitive to environmental shifts such as climate change, have received less attention. Here we investigate latitudinal trends in the seafloor community of the eastern Bering Sea using catches of fishes and epibenthic invertebrates in bottom trawl surveys conducted from 1982 through 2010. Our results indicate that the overall biomass of the epibenthic community declines with increasing latitude in the eastern Bering Sea. This latitudinal trend is primarily driven by declining fish catches in the northern Bering Sea, which in turn reflects changes in the structure of the fish community. The fish fauna in northern latitudes is increasingly dominated by gadids, though the species composition of the gadid fauna also changes with latitude, with smaller species becoming more common in the north. The biomass of the invertebrate megafauna remains relatively consistent throughout the eastern Bering Sea, but invertebrates make up a larger proportion of the catch in bottom trawls conducted at higher latitudes. The epibenthic invertebrate megafauna in the eastern Bering Sea is composed primarily of sea stars (Asteriidae) and oregoniid crabs (*Chionoecetes* and *Hyas*), though no clear latitudinal trends in the invertebrate community are evident. Limited trawl data from the eastern Chukchi Sea indicate that the fish community farther north is even more heavily dominated by gadids, and the epibenthic invertebrate community is dominated by asteriid sea stars. Temperature data from bottom trawl surveys in the southeastern Bering Sea over the past decade indicate that there was a distinct temperature shift around 2005, and the relatively warm years of 2001–2005 were followed by five relatively cold years. This shift in the summer temperature regime of the Bering Sea has resulted in lower fish catches, particularly in the "cold pool" region (58–61°N), and a higher proportion of epibenthic invertebrates in the bottom trawl catches of the past 5 years leading up to 2010

INTRODUCTION

Latitudinal species diversity gradients are well known in both terrestrial and aquatic ecosystems, and have been extensively examined for decades (e.g. Pianka, 1966; Clarke, 1992; Rohde, 1992; Rosenzweig and Sandlin, 1997). One of the pervasive themes of these studies is the tendency for species diversity to decline with increasing latitude. In the eastern North Pacific Ocean, declining diversity with increasing latitude has been demonstrated on a broad scale in marine gastropods (Roy et al., 1998), bivalves (Roy et al., 2000), and decapod crustaceans (Boschi, 2000). This pattern is not universal, and latitudinal trends can be interrupted by regions of particularly high diversity, such as the rocky intertidal zone of the Gulf of Alaska, which supports an unusually high diversity of benthic invertebrates given its high latitude location (Iken et al., 2010; Pohle et al., 2011). However, it is clear that in a broad variety of biomes throughout the world, species diversity is highest at low latitudes and lowest near the poles (Hillebrand, 2004). A multitude of hypotheses have been suggested to explain the underlying causes of these trends, including many that focus on climatological variables such as incident solar energy and temperature, as well as overall stability in climate (Currie et al., 2004).

Latitudinal trends in species diversity have been well documented, but trends in relative abundance and other shifts in community structure with latitude have received less attention, though some recent studies have begun to address this need (Bluhm et al., 2009; Iken et al., 2010; Konar et al., 2010). Because relative abundance is a more sensitive measure than simple presence/absence, latitudinal trends in the relative abundances of taxa may be more revealing over relatively small geographic scales, and changes in climatic forcing variables should affect relative abundance measures over shorter temporal scales. In the northern Bering and Chukchi Seas, much of the primary production settles directly to the benthos, and as a result the pelagic-benthic coupling in these regions is strong (Grebmeier et al., 1988). Given the large spatial area contained within the Bering and Chukchi Seas and the annual variability in ice cover (Wyllie-Echeverria and Wooster, 1998), we expect latitudinal trends in the seafloor community structure to reflect the spatial variability of the pelagic-benthic coupling process, and that long-term temporal shifts in these latitudinal trends may be indicative of fundamental changes in the process due to climate change.

A number of previous studies have examined benthic communities in the Alaskan arctic and subarctic regions. Many of these studies have used bottom grabs to examine the macrobenthic epifauna and infauna (Haflinger, 1981; Stoker, 1981; Grebmeier et al., 1988, 1989; Feder et al., 1994, 2007; Jewett et al., 2009). Others have utilized bottom-trawling gear to examine the larger components of the epifauna in the Chukchi Sea (Feder et al., 2005; Bluhm et al., 2009) or in Norton Sound (Hamazaki et al., 2005). Jewett and Feder (1981) characterized the epifaunal invertebrate community of the eastern Bering Sea and Chukchi Sea using bottom-trawl surveys conducted in 1975 and 1976, and Cui et al. (2009) examined

groundfish distribution around St. Lawrence Island in the northern Bering Sea. However, few of these studies have addressed the relative contributions of the ichthyofauna to the epibenthic biomass or the temporal changes in the characteristics of the epibenthic community, and those that have (e.g., Cui et al., 2009) were based on relatively limited spatial and temporal sampling.

Here we analyze bottom-trawl catches of fishes and epibenthic macroinvertebrates from National Marine Fisheries Service (NMFS) standardized bottom-trawl surveys in the eastern Bering Sea. We examine latitudinal trends in the biomass of fishes and invertebrates and in the species composition of the epibenthic megafauna across the entire latitudinal range of the eastern Bering Sea shelf. We also compare latitudinal trends in the composition of the benthic community of the southeastern Bering Sea from the warm years and cold years of the past decade, and comment on limited historical bottom trawl survey data from the Chukchi Sea. This data set is particularly valuable in that it represents a vast quantity of sampling effort (over 18,000 ha of area sampled) distributed over a broad geographic and temporal scale.

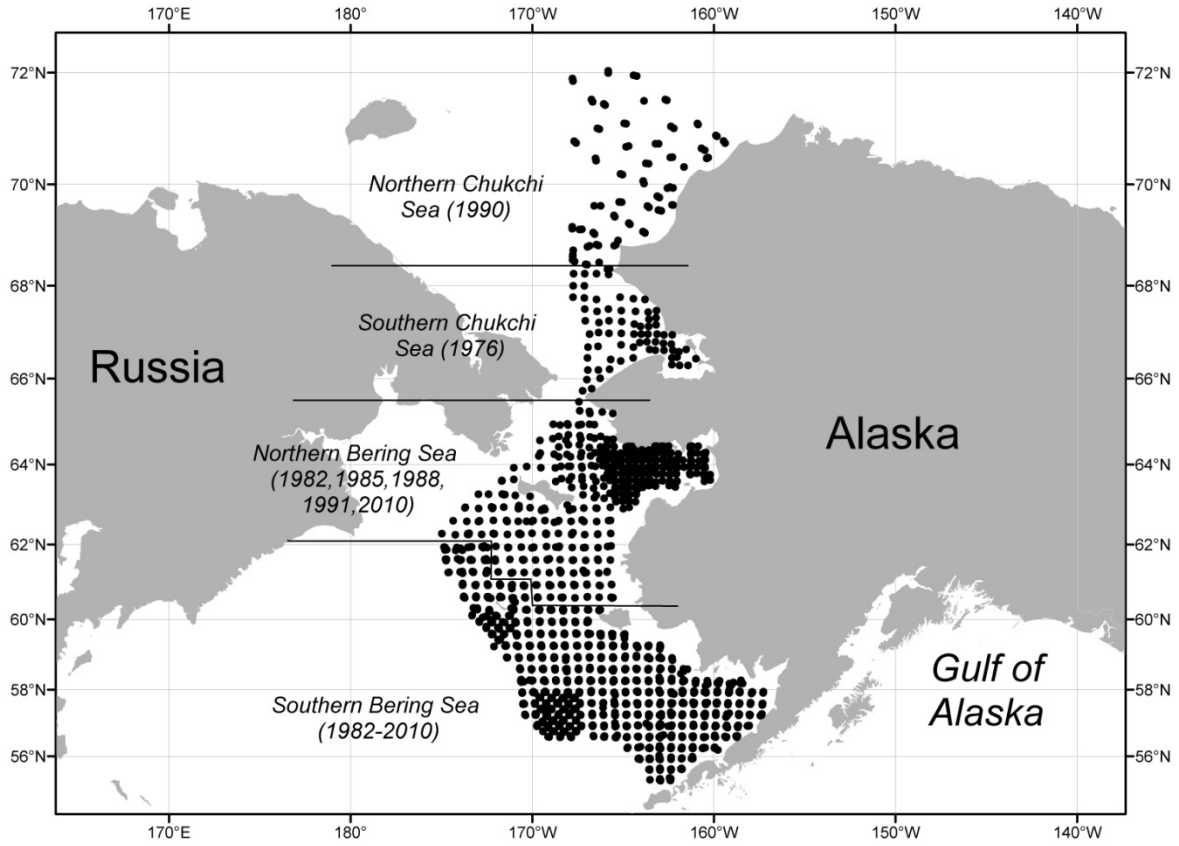

Figure 1. Map of areas sampled by Alaska Fisheries Science Center bottom trawl surveys included in this study.

METHODS

Surveys

This study includes standardized catch data from the annual NMFS eastern Bering Sea shelf bottom trawl surveys conducted during the summer months of 1982–2010 (Fig. 1), as well as smaller-scale NMFS trawl surveys conducted in the southeastern Chukchi Sea in 1976 and the northeastern Chukchi Sea in 1990. Portions of the trawl data presented here for the northern Bering Sea have previously been analyzed by Hamazaki et al. (2005), and data from the southeastern Chukchi Sea were used by Jewett and Feder (1981), Barber et al. (1997), and Feder et al. (2005). NMFS trawl survey data are maintained in a database by the Alaska Fisheries Science Center's RACE (Resource Assessment and Conservation Engineering) Division. Data for standard survey stations back to 1982 can be accessed online at http://www.afsc.noaa.gov/RACE/groundfish/survey_data/default.htm, and data for surveys prior to 1982 can be obtained by contacting the authors.

Survey trawl gear and research trawling operations adhered to the specifications and protocols found in Stauffer (2004). All bottom trawl surveys used an 83-112 Eastern otter trawl constructed with a 102-mm (4-in) stretched mesh body, 89-mm (3.5-in) stretched mesh intermediate, 32-mm (1.25-in) mesh codend liner, 25.3-m (83 ft) headrope, and a 34.1-m (112 ft) footrope. The research trawl was spread by a pair of 1.8 x 2.7-m (6 x 9 ft) 816-kg steel V-doors connected to the trawl by a pair of 54.9 m (30-fathom) dandylines. Net opening width for trawls included in this study averaged approximately 16 m, and the distance towed averaged 2.75 km. Catch data were standardized by converting catch weight to catch per unit effort (CPUE), expressed as kg/ha. CPUE was calculated by dividing catch weight by area swept, which was determined by multiplying the mean net width by the distance towed (Alverson and Pereyra, 1969). The survey data examined here were geographically limited to trawls conducted at or north of 55°N, and because the entire sampled area in the northern portion of the Bering Sea (north of 62°N) consists of depths less than 100 m, we limited analyses to trawls at bottom depths of 100 m or less throughout the study area. Only trawls with satisfactory gear performance (i.e., no gear damage and no indication that the net was not fishing properly) were used in our analyses.

Latitudinal trends in the eastern Bering Sea (1982-2010)

Bottom trawl surveys of the eastern Bering Sea shelf are conducted annually, extending from the north side of Unimak Island as far north as 62°N, so haul data for those latitudes span the entire study period, from 1982 through 2010. However, the northern Bering Sea (from 62°N to the Bering Strait) has not been surveyed as frequently. Survey data for the northern Bering Sea consist of a synoptic bottom trawl survey done in 2010, as well as triennial surveys conducted in 1982, 1985, 1988, and 1991. In order to minimize

the effect of temporal variation, analyses of latitudinal trends in the Bering Sea data are limited to the five survey years in which the entire latitudinal range of the eastern Bering Sea was surveyed.

Survey data from the Chukchi Sea are even more limited. The southeastern part of the Chukchi Sea, from the Bering Strait approximately to Point Hope, was surveyed in 1976, and a limited survey was conducted from Point Hope north to about 72°N in 1990. Although the gear used for these surveys is comparable to those conducted in the eastern Bering Sea, their limited sample size and temporal incongruence with the other surveys included in this study precludes a detailed comparison with the Bering Sea data, so our analysis of the Chukchi data is limited to general comments.

General latitudinal trends in CPUE were investigated by plotting log-transformed CPUE vs. start latitude for all trawls conducted during the five synoptic survey years, and by plotting the proportion of fishes (fish catch weight/total catch weight) vs. latitude for each trawl. Latitudinal trends in catch composition were further investigated by computing CPUE for each of the most abundant fish and invertebrate taxa for each trawl. Both fish and invertebrate taxa were grouped at the family level, except for taxa in which field identifications are routinely more general, such as tunicates (Ascidiacea), sponges (Porifera), and sea anemones (Actiniaria). In order to summarize latitudinal trends in the catch composition, each haul was assigned a latitude category by rounding the start latitude to the nearest degree, so that for example the 58° category includes all hauls with recorded start latitude from 57.5°N to 58.499°N (Fig. 2A). Because the most southern and most northern latitude categories (55° and 65°) were each represented by less than 20 total hauls over the five included survey years, these were combined with the adjacent latitude category (56° and 64°, respectively). A mean CPUE and standard error were then calculated for each taxon for each latitude category (including “zero” hauls, in which the taxon was not present).

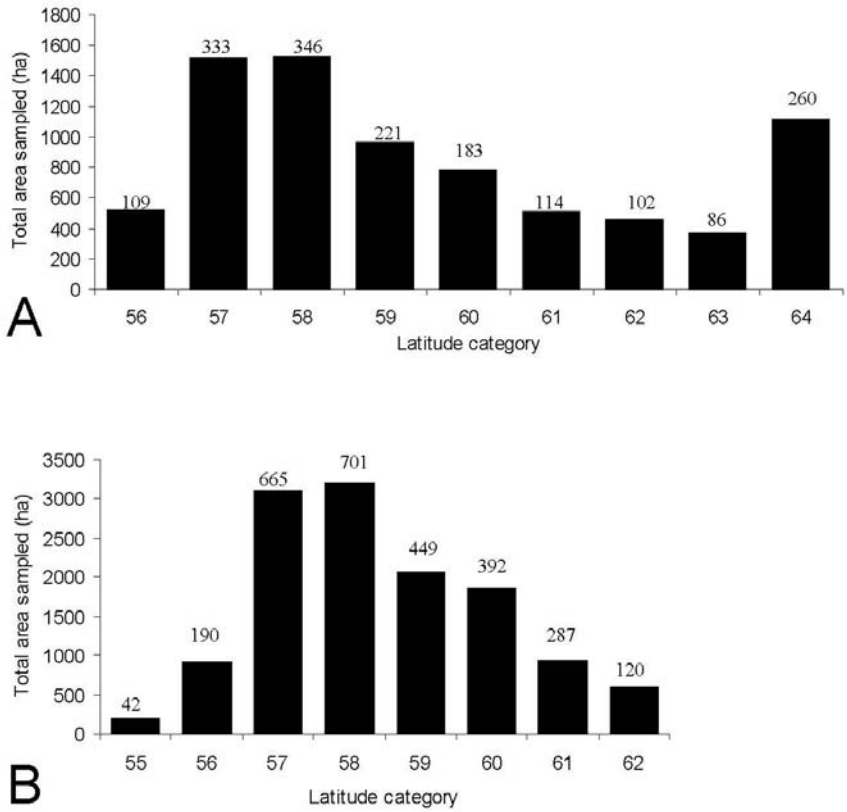

Figure 2. Total area sampled by latitude category for (A) years in which the entire latitudinal range of the eastern Bering Sea was surveyed (1982, 1985, 1988, 1991, and 2010), and (B) the southeastern Bering Sea for the ten most recent survey years (2001–2010). Numbers above the bars indicate total haul count for each category.

Temporal trends in the southern Bering Sea (2001-2010)

Bottom trawl surveys covering a standard 20 X 20 nmi grid of stations on the southern part of the eastern Bering Sea shelf were conducted annually from 1982–2010. Over that time period, temperature data were collected at each station by one of three methods: 1) expendable bathythermograph (XBT) casts from 1976–1992, 2) a Branker XL-200 temperature logger attached to the headrope of the trawl from 1993–2001, or 3) a SeaBird SBE-39 attached to the headrope from 2002–2010. A single bottom temperature for each station was taken from each XBT cast or it was calculated using the mean of temperature logger readings taken between brake-set and haulback. Mean annual temperature, $\bar{t}$, was calculated as:

$$\bar{t} = \sum_{i=1}^{h} \sum_{j=1}^{n_i} \frac{w_i}{n_i} x_{ij} ,$$

where w_i is the proportion of the survey area in stratum i (see Lauth (2010) for stratum classification), n_i is the number of hauls in stratum i, x_{ij} is the measured bottom temperature in haul j of stratum i, and h is

the number of strata in the survey area. Warm and cold years were then defined by comparing $\bar{t}$ for each year with the grand mean temperature for the study period, which was calculated by taking the simple average of all mean annual temperatures.

In order to summarize latitudinal trends in bottom temperatures in the eastern Bering Sea over the past decade, each haul conducted on the standard eastern Bering Sea survey grid from 2001–2010 was assigned a latitude category by rounding the start latitude to the nearest degree, so that hauls ranging from 54.66°N to 62.35°N were assigned to latitude categories 55–62 (Fig. 2B). Bottom temperature data from each haul were averaged within survey year by latitude category and plotted for the years 2001–2010. Means and standard errors for the proportion of fish, total fish CPUE, and total invertebrate CPUE were calculated by year for each latitude category and plotted to investigate temporal patterns between warm versus cold years from 2001–2010 relative to the long-term average of the 1982–2010 eastern Bering Sea shelf bottom trawl survey time series (2.29°C; Lauth, In Press).

RESULTS

Latitudinal trends in the eastern Bering Sea (1982-2010)

Bottom trawl data from the eastern Bering Sea show clear trends in CPUE with increasing latitude. The slope of the regression relating log-transformed total CPUE to latitude (Fig. 3A) is significantly negative ($P < 0.0001$), as is the slope of the regression relating fish CPUE (Fig. 3B) to latitude ($P < 0.0001$). In contrast, invertebrate CPUE (Fig. 3C) does not change significantly with latitude ($P = 0.05$). The general decline in total CPUE with increasing latitude is accompanied by a significant (regression $P < 0.0001$) decline in the proportion of fishes in the catch (Fig. 4). In the southern Bering Sea, fishes make up roughly 70% of the total catch weight, but this proportion decreases to about 30% in the northern Bering Sea. Therefore, the decline in total CPUE in the Bering Sea is primarily a reflection of the decline in fish catch, as hauls in the northern portion of the region are increasingly dominated by invertebrates. Our limited data from the Chukchi Sea indicate that overall biomass begins to increase again north of the Bering Strait, primarily due to increases in the invertebrate biomass.

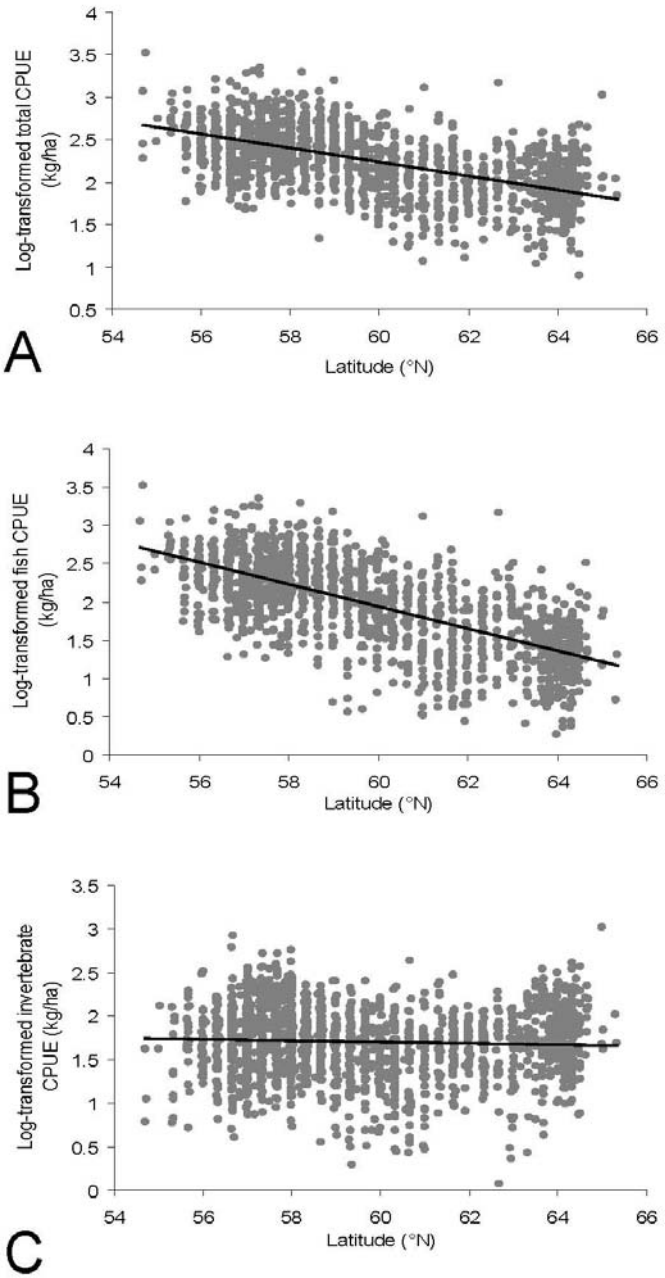

Figure 3. Log-transformed (A) total catch per unit effort (CPUE), (B) fish CPUE, and (C) invertebrate CPUE vs. latitude for bottom trawls conducted in the eastern Bering Sea during the survey years of 1982, 1985, 1988, 1991, and 2010.

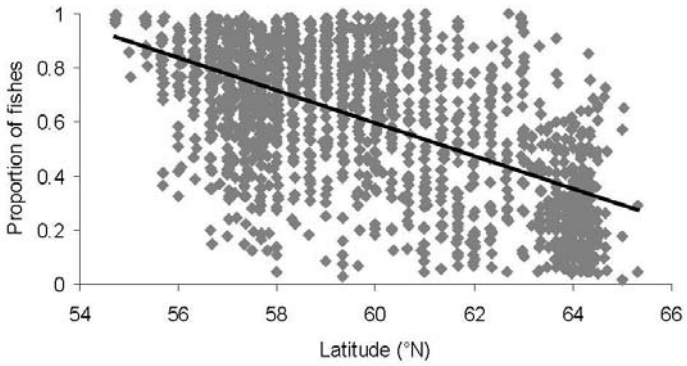

Figure 4. Proportion of total catch weight represented by fishes vs. latitude for bottom trawls conducted in the eastern Bering Sea during the survey years of 1982, 1985, 1988, 1991, and 2010.

As the relative proportions of fishes and invertebrates change with latitude in the eastern Bering Sea, so does the composition of the catches. Pleuronectid CPUE is consistently high throughout the southern Bering Sea (56–59°N), then declines rapidly in more northern latitudes (Table 1). Gadid CPUE is highest in the southernmost hauls, and declines rapidly with increasing latitude. In the southernmost latitudes flatfishes (Pleuronectidae) and cods (Gadidae) together make up about 90% of the overall fish catch (Fig. 5A). However, as pleuronectid and gadid catches decline in the northern Bering Sea, other fishes, such as sculpins (Cottidae) and eelpouts (Zoarcidae) make up an increasing proportion of the fish catch. In the northernmost portion of the eastern Bering Sea (64°N), the catches are dominated by gadids, which make up about 60% of the fish catch, followed by flatfishes and sculpins. Skates do not make up more than 10% of the mean fish catch in any latitude category. Skate (Rajidae) biomass generally decreases with increasing latitude in the Bering Sea, while eelpout (Zoarcidae) biomass generally increases with increasing latitude, but both groups makes up a relatively small proportion of the fish catch at all latitudes. In the Chukchi Sea, the fish catch is even more dominated by gadids, which may account for 60% or more of fish biomass, and cottids are the only other fish family consistently encountered.

Table 1. Summary of CPUE (kg/ha) for dominant fish and invertebrate taxa, presented as mean ± SE, by latitude category for the combined bottom trawl surveys of the eastern Bering Sea conducted in 1982, 1985, 1988, 1991, and 2010.

	Latitude category									Overall Mean
	56	57	58	59	60	61	62	63	64	
Fishes										
Pleuronectidae	174.8 ± 16.2	160.2 ± 11	194.3 ± 9.2	150.6 ± 11	60.9 ± 5.2	41.7 ± 5.6	27.9 ± 3.7	34 ± 7.8	8.0 ± 0.6	111.1 ± 3.7
Gadidae	175 ± 33.3	92.3 ± 8.3	64.5 ± 6.2	54.9 ± 8.5	45.9 ± 6.4	28.7 ± 11.2	22.1 ± 6.1	29 ± 10.8	14.4 ± 1.3	59.1 ± 3.4
Cottidae	2.1 ± 0.3	5.3 ± 0.7	5.9 ± 0.6	6.1 ± 0.5	14.1 ± 3.2	6.7 ± 1.9	3.6 ± 0.5	6.8 ± 1.2	5.6 ± 0.5	6.3 ± 0.4
Rajidae	7.8 ± 1.2	5.2 ± 0.6	4.3 ± 0.4	3.3 ± 0.4	2.3 ± 0.4	2.6 ± 0.4	2.5 ± 0.6	2.5 ± 1.1	0.1 ± 0.1	3.4 ± 0.2
Clupeidae	1.3 ± 0.9	0.6 ± 0.3	3.2 ± 2.8	0.2 ± 0.1	1.3 ± 1.1	0.3 ± 0.1	0.1 ± 0.0	0.3 ± 0.1	0.6 ± 0.2	1.1 ± 0.6
Zoarcidae	0.2 ± 0.1	0.2 ± 0.0	0.3 ± 0.0	0.8 ± 0.3	2 ± 0.5	2.7 ± 0.8	2.1 ± 0.4	2 ± 0.9	0.8 ± 0.6	0.9 ± 0.1
Agonidae	0.6 ± 0.1	0.9 ± 0.1	0.7 ± 0.1	0.5 ± 0.1	0.4 ± 0.1	0.1 ± 0.0	0	0	0.1 ± 0.0	0.5 ± 0.0
Osmeridae	0.1 ±0.1	< 0.1	0.1 ± 0.0	0.1 ± 0.0	0.1 ± 0.0	0.2 ± 0.1	0.5 ± 0.2	0.6 ± 0.1	0.4 ± 0.1	0.2 ± 0.0
Liparidae	0	0	0.1 ± 0.0	0.2 ± 0.1	0.5 ± 0.1	0.2 ± 0.1	0.5 ± 0.1	0.3 ± 0.0	0.1 ± 0.0	0.2 ± 0.0
Hemitripteridae	< 0.1	0.7 ± 0.1	< 0.1	0.1 ± 0.0	0.1 ± 0.1	0	0	< 0.1	< 0.1	0.2 ± 0.0
Invertebrates										
Asteriidae	13.9 ± 3.8	27.3 ± 2.5	25.3 ± 1.6	23.7 ± 2.1	13.9 ± 2.1	9.0 ± 1.6	7.7 ± 1.6	14.6 ± 2.7	41.5 ± 2.1	23.5 ± 0.8
Oregoniidae	5.8 ± 1.5	11.4 ± 1.2	13.8 ± 1.4	11.7 ± 1.5	10.8 ± 1.3	26.1 ± 4.5	24.4 ± 2.2	17.8 ± 3.1	3.8 ± 0.8	12.3 ± 0.6
Ascidiacea	0.3 ± 0.1	6.7 ± 1.1	17.5 ± 2.6	3.9 ± 1.0	3.7 ± 0.7	3.8 ± 1.3	4.0 ± 1.0	6.1 ± 1.4	11.1 ± 3.4	8.1 ± 0.8
Paguridae	8.9 ± 1.2	6.9 ± 0.6	11.7 ± 1.0	3.3 ± 0.4	5.5 ± 0.6	3.0 ± 0.7	3.7 ± 0.5	7.5 ± 1.1	5.1 ± 0.6	6.7 ± 0.3
Buccinidae	6.8 ± 1.1	5.6 ± 0.5	8.4 ± 0.7	5.6 ± 0.5	6.3 ± 0.7	2.9 ± 0.7	5.5 ± 0.8	7.6 ± 1.4	4.3 ± 0.7	6.0 ± 0.3
Lithodidae	6.9 ± 1.8	5.4 ± 1.0	1.6 ± 0.2	0.2 ± 0.0	1.2 ± 0.2	0.5 ± 0.4	< 0.1	0.1 ± 0.0	1.2 ± 0.2	2.1 ± 0.2
Porifera	7.9 ± 2.7	6.3 ± 3.0	0.3 ± 0.1	< 0.1	0.9 ± 0.4	< 0.1	< 0.1	0.3 ± 0.2	0.3 ± 0.2	1.9 ± 0.6
Gorgonocephalidae	0.6 ± 0.2	2.0 ± 0.3	1.9 ± 0.2	1.1 ± 0.2	1.6 ± 0.5	1.0 ± 0.2	1.4 ± 0.2	1.1 ± 0.3	2.7 ± 0.5	1.7 ± 0.1
Actiniaria	1.8 ± 0.5	4.3 ± 1.0	1.7 ± 0.5	< 0.1	0.2 ± 0.0	0.1 ± 0.0	0.2 ± 0.0	0.2 ± 0.0	1.4 ± 0.4	1.5 ± 0.2
Strongylocentrotidae	0.9 ± 0.9	0.8 ± 0.6	0.1 ± 0.1	< 0.1	0.1 ± 0.1	< 0.1	< 0.1	0.1 ± 0.0	2.8 ± 0.7	0.7 ± 0.2
Holothuroidea	0.2 ± 0.1	1.1 ± 0.3	< 0.1	0	0.1 ± 0.0	< 0.1	< 0.1	< 0.1	0.3 ± 0.1	0.3 ± 0.1
Cheiragonidae	0.1 ± 0.0	0.4 ± 0.1	1.0 ± 0.0	0.4 ± 0.1	0.1 ± 0.0	0.1 ± 0.0	< 0.1	< 0.1	1.1 ± 0.1	0.3 ± 0.0
Ophiuridae	< 0.1	0.8 ± 0.2	0.1 ± 0.0	< 0.1	< 0.1	< 0.1	0.3 ± 0.1	0.2 ± 0.1	< 0.1	0.2 ± 0.0
Alcyonacea	< 0.1	0.1 ± 0.0	0.2 ± 0.0	0.1 ± 0.0	0.1 ± 0.0	0.1 ± 0.0	0.2 ± 0.0	0.5 ± 0.1	0.19 ± 0.1	0.2 ± 0.0

Latitudinal trends in invertebrate catches are difficult to characterize. Invertebrate catches throughout the eastern Bering Sea are dominated by sea stars, crabs (oregoniids and pagurids), ascidians, and buccinid gastropods (Table 1). In the southern latitudes of the Bering Sea, asteriid sea stars dominate the invertebrate catch (Fig. 5B), but in much of the northern Bering Sea (61–63°N) oregoniid crabs make up a larger proportion of the invertebrate catch. Catch rates for buccinid gastropods and hermit crabs (Paguridae), which utilize empty gastropod shells for shelter, track closely with each other throughout the survey area, each accounting for about 10% of the overall invertebrate catch. Ascidians also account for about 10% of the invertebrate catch in the study area, though there is no clear latitudinal trend in their catch proportions. Lithodid crabs comprise a noteworthy portion of the invertebrate catch only at southern latitudes. Trawl data from the Chukchi Sea indicate that sea stars continue to dominate the invertebrate community farther north, followed by oregoniid crabs and sponges (Porifera).

Our analysis of bottom trawl data also shows a decline in average fish size with increasing latitude in the study area, which is evident in at least two of the dominant fish families of the region (Fig. 6). This decrease in fish size is most dramatic for the cottids, which average almost 1 kg each in the southernmost latitudes of the eastern Bering Sea, but less than 0.2 kg each in the northern Bering Sea. Similarly, gadids average over 0.8 kg in the southern Bering Sea, but less than 0.1 kg in the northern Bering Sea. A smaller

but notable decline in size is evident for pleuronectids. Zoarcids, which are relatively small in the southern Bering Sea, tend to be larger in the northern Bering Sea.

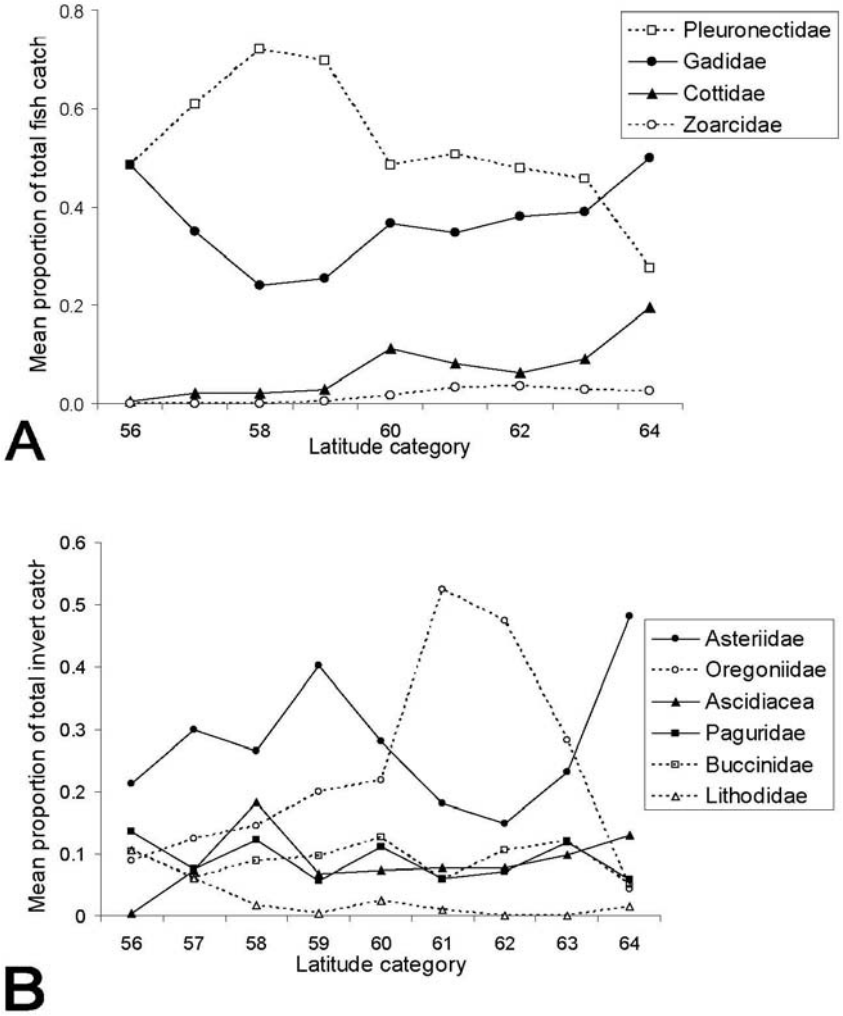

Figure 5. Mean proportion by latitude category of (A) total fish catch for dominant families, and (B) total invertebrate catch for dominant taxa.

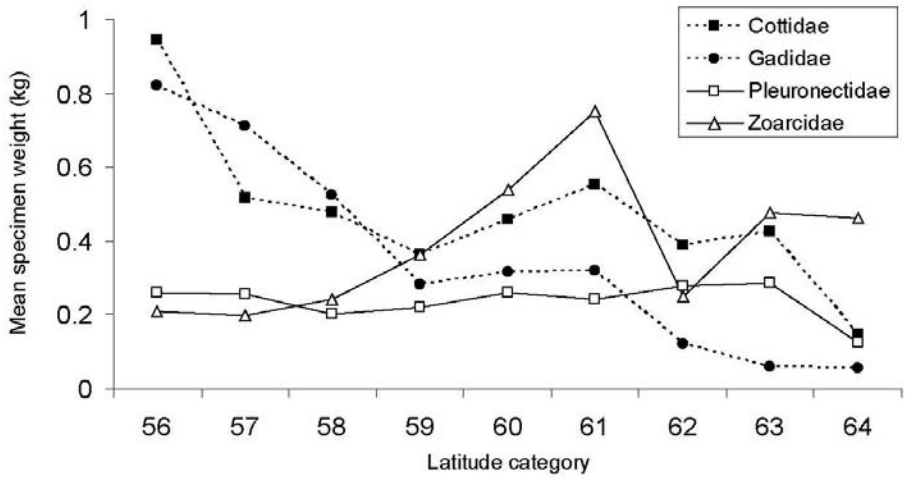

Figure 6. Mean specimen weight for dominant fish families by latitude category.

Temporal trends in the southern Bering Sea (2001-2010)

Survey mean bottom water temperature declines with increasing latitude in the eastern Bering Sea (Fig. 7). Trawl-derived bottom temperatures are generally uniform in the southeastern Bering Sea, from 56–59°N, and then drop significantly from 59–62°N. These bottom temperatures are subject to considerable interannual fluctuation. For the first half of the last decade (2001–2005) survey bottom temperatures were relatively high, ranging from 4–5°C in the southern Bering Sea to about 0°C in the north, near St. Matthew Island. The latitudinal trend in bottom temperatures is the same for the last half of the decade (2006–2010), but the absolute values are lower, ranging from 3–4°C in the south to almost -2°C in the north. Thus, 2001–2005 represent warm years relative to the 30 year mean, while 2006–2010 were relatively cold years (Fig. 8).

Latitudinal trends in bottom-trawl catches in the eastern Bering Sea are correlated with the overall temperature regime. The overall mean proportion of fishes in the catch (Fig. 9A) was similar in the southernmost (55–56°N) latitudes of the study area during warm years (2001–2005) and cold years (2006–2010) of the past decade. Furthermore, the general shape of the curve was similar for the warm and cold years, with the proportion of fishes generally declining farther north. However, the proportion of fishes in the catch in the central latitudes of the eastern Bering Sea shelf (58–62°N) was significantly lower during the cold years. This difference between warm and cold years was not driven by an increase in invertebrate catch, but rather by a relative decline in overall fish CPUE at these latitudes during cold years (Fig. 9B). The difference in fish catch was most dramatic from 58–61°N, where overall mean fish

CPUE during the warm years was as much as three times greater than that during the cold years. Invertebrate CPUE values were not notably different in warm and cold years.

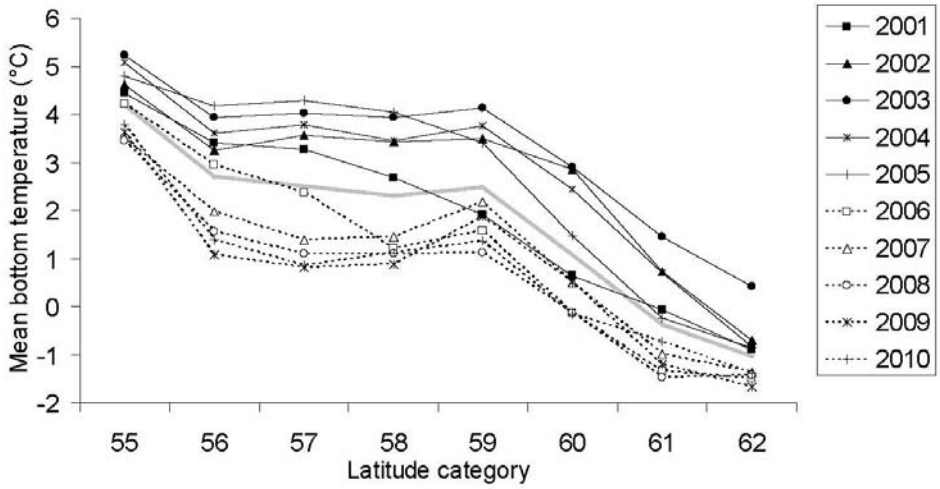

Figure 7. Mean bottom temperature (°C) for bottom trawls conducted in the Bering Sea for each year from 2001–2010, rounded to the nearest degree latitude. Gray line represents 10-year mean.

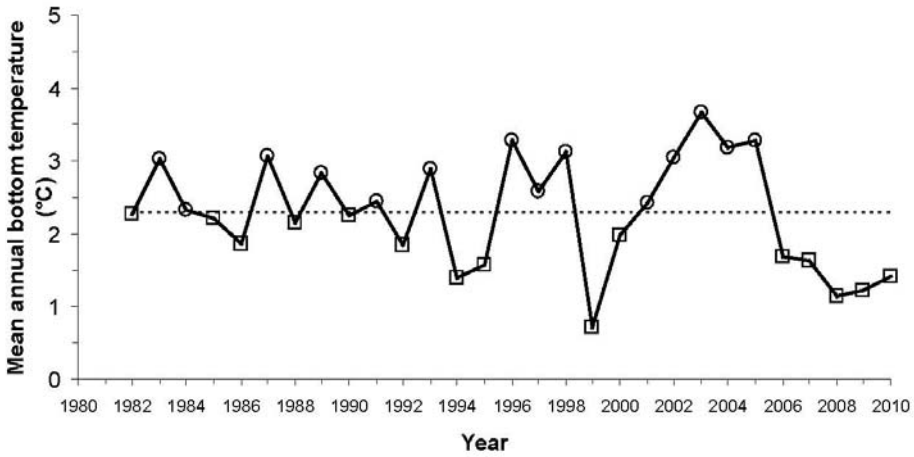

Figure 8. Mean annual bottom temperatures, weighted by stratum, measured during the eastern Bering Sea bottom trawl surveys from 1982–2010. The dashed line represents the grand mean temperature for 1982–2010, open squares represent annual means below the grand mean (cold years), and open circles represent means above the grand mean (warm years).

DISCUSSION

Numerous studies have documented declines in species diversity with increasing latitude. This study compliments those results by documenting a decline in the overall trawl-caught biomass of the epibenthic community with increasing latitude in the eastern Bering Sea. The trend of declining biomass with latitude in the Bering Sea is primarily a reflection of reduced fish catches in northern latitudes. Invertebrate catches do not decline significantly with increasing latitude in the Bering Sea, and therefore the relative proportion of invertebrates in the overall catch increases dramatically at higher latitudes. These changes are consistent with a shift from a pelagic-dominated ecosystem on the southern Bering Sea shelf, in which demersal fishes and epibenthic invertebrates consume the primary production of the overlying water column, to a more benthic ecosystem in the north, in which seasonal pulses of primary production in the water column more directly support large standing stocks of infaunal and epifaunal biomass (Grebmeier et al., 1988, 2006).

The species composition of the benthic fish fauna changes markedly with latitude in the eastern Bering Sea. Pleuronectids, including yellowfin sole (*Limanda aspera*), northern rock sole (*Lepidopsetta polyxystra*), Pacific halibut (*Hippoglossus stenolepis*), and others, account for more than half of the survey fish catch from the southern Bering Sea and support large commercial fisheries in the region (Wilderbuer and Nichol, 2010; Wilderbuer et al., 2010; Hare, 2010). However, most pleuronectid species (with the notable exception of Bering flounder, *Hippoglossoides robustus*) are more abundant on the southern portion of the Bering Sea shelf (Lauth, 2010) than they are farther north. Thus, pleuronectid biomass declines in northern latitudes, and the relative proportion of gadids, a group that includes commercially important species such as walleye pollock (*Gadus chalcogrammus*) and Pacific cod (*Gadus macrocephalus*), becomes greater. Although gadid CPUE actually declines with increasing latitude, as it does for all fish groups, gadids make up an increasing proportion of the fish catch in the northern Bering Sea. Cottids and zoarcids also make up increased proportions of the fish catch in more northern latitudes, though the trends in those families are not as striking as in the flatfishes and cods. Cui et al. (2009) found similar trends in the northern Bering Sea, reporting groundfish assemblages south of St. Lawrence Island dominated by gadids and flatfishes and those north of St. Lawrence Island dominated by sculpins. The increasing dominance of gadids and sculpins with increasing latitude in the Bering Sea apparently continues into the Chukchi Sea, as Norcross et al. (2010) reported catches dominated by sculpins in a recent survey of the Chukchi Sea, and Barber et al. (1997) reported catches dominated by gadids in the northeastern Chukchi Sea.

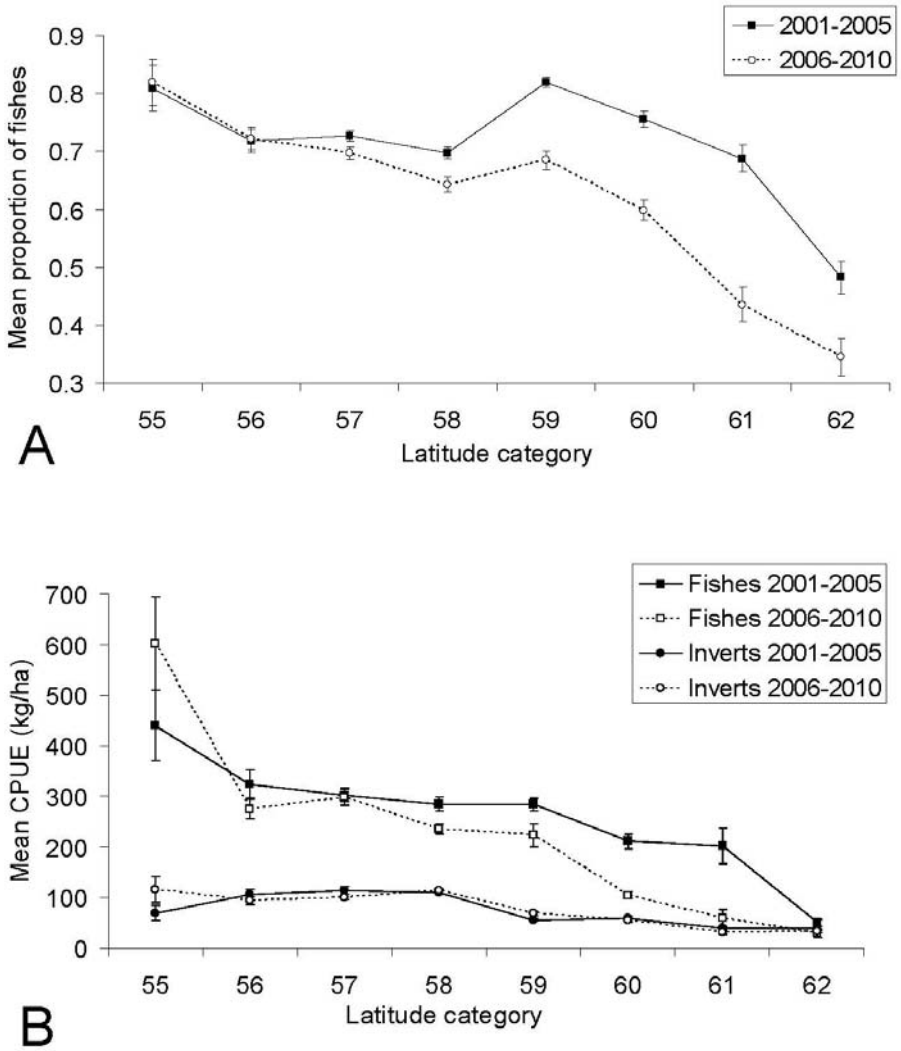

Figure 9. Comparison of trawl catches by latitude category during the warm years (2001–2005: solid lines) and cold years (2006–2010: dashed lines) of the past decade: (A) mean (± SE) proportion of total catch weight accounted for by fishes, and (B) mean (± SE) catch per unit effort (CPUE) for fishes (squares) and invertebrates (circles).

Unlike the fish fauna, the dominant taxa of the epibenthic invertebrate fauna do not appear to change in any consistent way with increasing latitude, at least at the taxonomic and geographic scales reported here. Echinoderms, arthropods, and tunicates dominate the invertebrate catches at nearly all latitudes, though their relative contributions to the catch vary substantially. The most dominant epibenthic invertebrate species in the eastern Bering Sea is the northern Pacific sea star (*Asterias amurensis*), which makes up over 25% of the invertebrate biomass reported on surveys included in this study. However, in some areas of the eastern Bering Sea, particularly in the northern latitudes, crabs actually make up a higher

proportion of the invertebrate biomass than sea stars. This is primarily due to the abundance of the snow crab (*Chionoecetes opilio*), although lyre crabs (genus *Hyas*) are also common. These results are consistent with previous studies of the epibenthic macrofauna (Jewett and Feder, 1981; Ambrose et al., 2001; Feder et al., 2005; Bluhm et al., 2009), which indicate that sea stars and crabs are the dominant benthic macroinvertebrate taxa throughout the region. Ascidians, hermit crabs, and buccinid snails each account for a relatively consistent 10% of the invertebrate biomass throughout the latitudinal range of the eastern Bering Sea. Both compound and solitary ascidians can be locally abundant throughout the region, though solitary species (*Halocynthia*) tend to be more common in the southern Bering Sea while compound species (*Aplidium*) are more common at northern latitudes. The biomass of hermit crabs tracks closely with the biomass of buccinid gastropods, which is not a surprising result given their dependence on empty snail shells for shelter. Hermit crabs and buccinid gastropods are both diverse groups in the eastern Bering Sea, and field identification has historically been problematic at the species level, so species-level latitudinal trends for these groups can not be reliably concluded from our data. In fact, historical changes in priorities and resources have led to fluctuations in the specificity and consistency of field identifications for invertebrates over the study period (Stevenson and Hoff, 2009), therefore for many invertebrate groups we cannot confidently report catches at lower taxonomic levels.

Previous studies have indicated that in portions of the northern Bering and Chukchi seas benthic infaunal biomass may be related to high water column productivity and sediment heterogeneity (Grebmeier et al., 1988, 1989; Feder et al., 2007). Those studies used finer scale tools, such as benthic grabs, which sample a different component of the benthic fauna than that sampled in this study and measure heterogeneity over a smaller spatial scale than we were able to measure with bottom trawls. We were unable to correlate invertebrate biomass with water masses or sediment characteristics because the necessary data have not been collected during the NMFS bottom trawl surveys described here, and differences between the dominant invertebrate groups reported in those studies (bivalves, amphipods, and polychaetes) and those reported here are likely due to differences in sampling gear.

Our data show that the decline in fish catch at higher latitudes is at least partially due to a decline in the average individual weight of the fishes. That decline in average fish weight is in large part driven by changes in the species composition of the fish catch. The gadid fauna of the southern Bering Sea is dominated by walleye pollock and Pacific cod, which are both large-bodied species that may weigh several kg each, while gadid catches in the north are dominated by saffron cod (*Eleginus gracilis*) and Arctic cod (*Boreogadus saida*), both of which reach much smaller maximum sizes. Likewise, larger species of cottids, such as the great sculpin (*Myoxocephalus polyacanthocephalus*) and yellow Irish lord

(*Hemilepidotus jordani*) are more common in the southern portion of the study area, while smaller sculpin species (e.g., *Myoxocephalus jaok*, *Gymnocanthus* spp.) are relatively abundant throughout the region. *Hemitripterus bolini*, another very large cottoid species, is common only in the southern latitudes of the eastern Bering Sea. For zoarcids, the average specimen size is relatively small in the southern Bering Sea, but somewhat larger in the northern Bering Sea. Again, this is due to changes in the species composition of the catch, as the only large zoarcid commonly encountered in this region, *Lycodes raridens*, is only found consistently in the northern Bering Sea. The other zoarcids common in the shallow waters of the Bering Sea, *Lycodes palearis* and *L. brevipes*, are both much smaller species. This decline in average fish size, coupled with the overall decline in fish biomass, has important implications for potential commercial fisheries. At this time there do not appear to be any fish species in the northern Bering Sea, or in the Chukchi Sea, that could support large-scale commercial exploitation, nor are there any common species that reach a large enough maximum size to be commercially desirable.

Temperature data from summer bottom trawl surveys in the eastern Bering Sea over the past 29 years exhibit notable interannual fluctuations. These fluctuations have increased in magnitude and periodicity in recent years. The most recent decade of survey data include five relatively warm years and five cold years, and indicate a distinct temperature shift in the eastern Bering Sea between 2005 and 2006. The warming trend in the Bering Sea that was broadly reported in the middle of the decade (Overland and Stabeno, 2004; Grebmeier et al., 2006; Mueter and Litzow, 2008) based on data collected through 2005 or 2006 has reversed over the past 5 years, and the spatial extent of the eastern Bering Sea shelf cold pool (defined as the region in which the early summer bottom temperature is < 2°C; Wyllie-Echeverria and Wooster, 1998) has again expanded southward nearly to the Alaska Peninsula (see Fig. 6 in Lauth , 2010). This mid-decade shift in the summer temperature regime of the Bering Sea shelf provides a convenient opportunity for comparison of latitudinal trends among warm and cold survey years.

In general, overall fish catches for the trawls included in this study are lower during the cold years (2001–2005) than during the warm years (2006–2010), and as a result, the proportion of invertebrates present in survey catches is higher during cold years. This indicates that either the biomass of the surveyed populations has declined during the recent cold period or that fish populations are less likely to be caught in bottom trawl surveys during cold years, either due to migration out of the survey area or changes in capture probability. A decline in biomass over the most recent cold period is consistent with, and complimentary to, the findings of Mueter and Litzow (2008), who reported an increase in groundfish biomass during the warming period of 1985–2005. Temperature shifts, particularly consistent trends extending over multiple years, may affect larval recruitment, food availability, predation patterns, and

other ecological variables that could cause population declines in fish and invertebrate species (Hunt et al., 2002, 2011; Coyle et al., 2011). Furthermore, recruitment success for walleye pollock in the eastern Bering Sea during the warm years of 2004–2005 was low (Moss et al., 2009), and recruitment failures during the first part of the decade may have contributed to lower population biomass in later years, so the declining biomass during the most recent cold period may simply be a delayed effect from the earlier warm years.

Shifts in temperature regime may also affect the availability of fish populations to the trawl survey, as well as the capture probability of some species, which may be confounded with population declines. For example, yellowfin sole (*Limanda aspera*) migrate to nearshore areas to spawn soon after the annual ice-edge retreat, and the timing of this migration may be affected by fluctuations in bottom temperature (Nichol, 1998). Thus, the proportion of the population in the nearshore spawning areas, which are not sampled by annual bottom trawl surveys, may affect the biomass estimated by the trawl survey. Some fish species, such as Arctic cod, saffron cod, shorthorn sculpin, and Alaska plaice possess an antifreeze protein in their blood sera (Hargens, 1972; Osuga and Feeney, 1978; Knight et al., 1991) and are able to tolerate water temperatures near the freezing point. Other subarctic species, such as Pacific cod, walleye pollock, and yellowfin sole, lack this physiological adaptation to extremely cold water, and the presence of cold water masses may force them to migrate off the shelf and outside the survey area. In addition to changes in the spatial distribution of populations, the overall catchability of the benthic fauna may not be spatially or temporally constant. We have documented species composition changes in the ichthyofauna with increasing latitude, and catchability rates for many fishes are not well known. Thus, it is possible that some southern species are simply more susceptible to capture by bottom trawl than their more northern counterparts (i.e., they have higher catchability rates). For both fishes and invertebrates, smaller species may have lower catchability than larger species (Somerton and Otto, 1999; Weinberg et al., 2004; Kotwicki and Weinberg, 2005) due to the fact that smaller specimens can more easily escape through the net mesh or under the footrope, and it is clear that specimen size, at least in fishes, declines with increasing latitude in the eastern Bering Sea. The relationship of a species with the substrate may also affect catchability, as species that burrow in the sediment or tend to remain motionless on the substrate at the approach of the trawl are more likely to be missed by the trawl and therefore have lower catchability. Finally, for fishes and other mobile species, other factors such as herding and schooling behavior and swimming performance may affect catchability (Somerton et al., 2007), and temperature changes may affect these behaviors. Therefore, the magnitude of the latitudinal decline in biomass and the effects of temperature regime on this biomass trend may be somewhat affected by lower catchability in northern species.

The region of greatest impact for the 2005–2006 temperature shift is 58–61°N, where mean fish catches were depressed by anywhere from 20% to 75% during the cold years of the past decade, while there is no detectable difference in mean fish CPUE south of 58°N or north of 61°N for warm vs. cold years. This lack of effect in the southern Bering Sea may be due to the relatively short lifespan of the southernmost portion of the cold pool, which rapidly shrinks northward as summer progresses, but is much more persistent north of the Pribilof Islands and therefore may affect fish distributions more profoundly in the north. Furthermore, at its southern terminus the cold pool tends to be much narrower than it is farther north, thus it covers only a small proportion of the southern Bering Sea sampling area, but may extend over almost the entire shelf area north of St. Matthew Island. Thus, the area of coverage and the temporal persistence of the cold pool are more extensive north of 58°, and fish abundance in those areas may be more sensitive to interannual variations in the temperature regime. In the northern latitudes of the Bering Sea, interannual temperature variation is less pronounced, and recent evidence suggests that north of about 60°N there is little difference between the temperature regime of warm years and cold years (Stabeno et al., 2012). Our data suggest that this reduced interannual temperature variation in the northern Bering Sea is associated with reduced interannual variation in groundfish biomass in this region. Thus, the benthic ecosystem of the southern Bering Sea is very different in warm years than in cold years, while in the northern Bering Sea the ecosystem does not fluctuate as dramatically.

CONCLUSIONS

This study highlights some latitudinal trends in the epibenthic community of the eastern Bering Sea, as well as some changes correlated with interannual temperature fluctuation. In the eastern Bering Sea, epifaunal biomass declines with increasing latitude. Overall fish biomass declines as the community dominated by large gadids and flatfishes in the south transitions to a fauna increasingly dominated by small-bodied gadids, flatfishes, and sculpins. As overall epibenthic biomass declines, macroinvertebrates account for an increasing proportion of the fauna, with sea stars and oregoniid crabs dominating the invertebrate biomass throughout the region. Over the past decade, the eastern Bering Sea shelf has experienced a significant temperature shift, with five relatively warm years (2001–2005) followed by five cold years (2006–2010). During the cold years, the benthic fish biomass present on the central portion of the eastern Bering Sea shelf (58–61°N) was considerably lower than that recorded during the preceding warm years, indicating that long-term climate changes may have considerable impact on the benthic communities of this region.

ACKNOWLEDGEMENTS

We thank the multitude of field scientists involved in NMFS bottom-trawl surveys in the eastern Bering Sea and southeastern Chukchi Sea over the past 30 years, as well as the captains and crews of the charter vessels used for these surveys and the programmers and database managers responsible for maintenance of the RACE database. We also thank Dan Nichol (AFSC) for comments on an earlier version of the manuscript. The findings and conclusions in this paper are those of the authors and do not necessarily represent the views of the National Marine Fisheries Service, NOAA. This was BEST-BSIERP publication number 55.

Chapter 3.b. Detecting temporal trends and environmentally-driven changes in the spatial distribution of groundfishes and crabs on the eastern Bering Sea shelf.

This paper was published, for details refer to:

Kotwicki, S. and Lauth R.R. 2013. Detecting temporal trends and environmentally-driven changes in the spatial distribution of bottom fishes and crabs on the eastern Bering Sea shelf. Deep-Sea Research Part II: Topical Studies in Oceanography, 94: 231-243

INTRODUCTION

This study used a 30-year time series of standardized bottom trawl survey data (1982-2011) from the eastern Bering Sea shelf to model between-year responses of spatial distribution indices of selected bottom fishes and crabs against between-year differences in the areal extent of the cold pool at three different temperature levels. There are other factors besides changes in temperature that can affect distribution, including natural fluctuations in population abundance (Spencer, 2008) and the temporal autocorrelation of spatial patterns (Pyper and Peterman, 1998) also known as the time lag effect; i.e., snapshots of a spatial distribution for a particular species that are closer in time may be more similar than those separated by longer periods of time. Hence, in addition to temperature, we investigate variability in spatial distribution patterns due to between-year changes in population abundance as well as the time lag between survey years.

METHODS

The temporal scale we used was limited to the available survey data, but to determine how distribution patterns varied over different spatial scales, we chose two indices as dependent variables in the model: 1) a shelf-wide index comparing between-year responses of population centers across the eastern Bering Sea shelf, and 2) a spatially-explicit local index comparing between-year responses of abundance location-by-location. A generalized additive model (GAM) framework was used to model responses using the two spatial indices for all possible survey year combinations. The basic thesis is that these models will explain the observed variability in spatial distribution of populations and make it possible to determine the relative contribution of a changing cold pool, fluctuating population abundance, and time lag between surveys to the distributional changes observed in various bottom fishes and crabs on the eastern Bering Sea shelf.

The primary criterion for selecting the taxa used in the analysis was that bottom trawl abundance for a taxon had to be a credible index of abundance over time. Excluded taxa failed to meet this criterion for a

variety of reasons: 1) bottom trawl not designed for quantitative sampling of pelagic species, 2) historical changes in the specificity and consistency of field identifications (Stevenson and Hoff, 2009), 3) historical changes in the consistency of subsampling rare or singular species from large catches, and 4) rare or patchily distributed with insufficient data for analyses. Accordingly, Alaska skate (*Bathyraja parmifera*) and northern rock sole (*Lepidopsetta polyxystra*) were combined into the broader taxonomic groups *Bathyraja* spp. and *Lepidopsetta* spp., respectively. In both cases, the other species combined into these taxonomic groups had overlapping spatial distributions but composed only a small percentage of the total abundance within that group in any given year (<5%). Flathead sole (*Hippoglossoides elassodon*) and Bering flounder (*H. robustus*) are difficult to differentiate; however, their zoogeography differs (Mecklenburg et al., 2002) and there was a concerted effort to separate the two species since 1982, so the two species were analyzed separately. Two other similar species, arrowtooth flounder (*Atheresthes stomias*) and Kamchatka flounder (*A. evermanni*) were not identified separately in the survey until 1992, so the analysis for arrowtooth flounder was confined to the 1992-2011 time period. A separate analysis for Kamchatka flounder was not conducted due to insufficient data.

Two spatial indices were used for analyzing pairwise comparisons among all bottom trawl survey years: the global index of collocation (*GIC*) and the local index of collocation (*LIC*; Bez, 2007). Survey catch data from all 376 stations were included for calculating the *LIC* if they were available. The *GIC*s and *LIC*s were pooled for all years by taxa to calculate a range, mean, and standard deviation for each. A GAM was used to investigate how the *GIC* and the *LIC* responded to the between-year absolute differences in the areal extent (km^2) of the cold pool (ΔCPA_T) at a threshold temperature T (°C), the absolute difference in population abundance ($\Delta ABUND$), and the time lag ($\Delta YEARS$) by taxon. For simplicity, absolute differences in predictor variables will be referred to as "differences" in the remainder of the paper. The GAMs were run using the "mgcv" package in R (Wood, 2006) with the smoothing spline protocol (Wood, 2003). The basic form of the GAM used in the analysis was:

$$LIC \text{ or } GIC \sim s(\Delta CPA_T) + s(\Delta ABUND) + s(\Delta YEARS) + factor(VESSEL) + factor(YEAR1),$$

where *s()* indicated variable fitted with cubic spline and *factor()* indicated categorical variable.

To investigate more specific responses to a range of cold pool bottom temperatures, backward variable selection was performed for three different temperature thresholds: *CPA_ 0°C*, *CPA_ 1°C*, and *CPA_ 2°C*, where a temperature threshold defines the two-dimensional boundary within the cold pool. Factors representing survey *VESSEL* and the first year of the comparison pair (*YEAR1*) were included in the model to account for the random or systematic errors that were considered to be artifacts of sampling

methodology such as vessel or skipper effects (Munro, 1998; von Szalay and Brown, 2001), survey timing, and technology creep (Zimmerman et al., 2003).

Our null hypothesis was that there is no relationship between the interannual differences observed in an organism's spatial distribution and the interannual differences observed in the predictor variables. Rejection of the null hypothesis implies that a predictor variable has an effect on the spatial index, and thus affects the spatial distribution of a taxon. For example, if the magnitude of the difference in $\Delta ABUND$ is negatively correlated with a spatial index (i.e., greater $\Delta ABUND$ corresponds to decreasing similarity of the spatial index) then the population abundance influences the spatial distribution.

RESULTS

Results are summarized in the attached tables 1, 2, and 3.

Survey bottom temperatures and extent of cold pool

Mean survey bottom temperatures and areal extent of the cold pool showed considerable interannual variability from 1982 to 2011. The coldest year in 1999 resulted in the largest deviation from the mean and the largest areal extent of cold pool in the time series (393,595 km^2). This extremely cold year was followed by a 5-year warm period (2001-2005) during which the average survey bottom temperature on the eastern Bering Sea shelf included the warmest year (2003) and the areal extent of cold pool reached its minimum size (48,000 km^2). The *CPA_0°C* was absent (1996) or generally small during years when the mean survey bottom temperature was above the long-term mean. From 2005 to 2006, the warm trend reversed and there was a sharp decline in the mean bottom temperature, coinciding with a cold period that lasted for 5 years (2006-2010). In 2011, the cold pool decreased in size, especially the *CPA_0°C*, resulting in a mean survey bottom temperature that was slightly above the 30-year mean.

Model results

The *LIC*s generally had lower similarities and greater variability than *GIC*s for all taxa. The mean *LIC* ranged from 0.32 to 0.78 compared to the mean *GIC* which ranged from 0.83 to 0.98, and standard deviations were on average 2.5 times greater for *LIC* than *GIC*. Also, the highest *GIC* for every taxon was 1.0, compared to the highest *LIC* values which varied from 0.67 to 1.0.

As expected, we observed a significant *YEAR1* effect for all taxa and a *VESSEL* effect for most taxa, which together accounted for the differences in the survey catchability between vessels and years. A closer examination of results or a discussion for the *YEAR1* and *VESSEL* effects was omitted because they were sampling artifacts without biological relevance to the primary purpose of this study.

Table 1. List of taxa considered for the analysis. An "*" next to the common name indicates that the taxa was included in the analysis and a number in the last column indicates the rationale (see below) for those taxa excluded from the analysis.

Common name	Scientific name	Exclusion
Skates*	*Bathyraja* spp.	
Arrowtooth flounder*	*Atheresthes stomias*	
Kamchatka flounder	*Atheresthes evermanni*	2,4
Greenland turbot*	*Reinhardtius hippoglossoides*	
Pacific halibut*	*Hippoglossus stenolepis*	
Flathead sole*	*Hippoglossoides elassodon*	
Bering flounder*	*Hippoglossoides robustus*	
Rex sole*	*Glyptocephalus zachirus*	
Yellowfin sole*	*Limanda aspera*	
Longhead dab*	*Limanda proboscidea*	
Sakhalin sole	*Limanda sakhalinensis*	4
Starry flounder*	*Platichthys stellatus*	
Rock sole*	*Lepidopsetta* spp.	
Alaska plaice*	*Pleuronectes quadrituberculatus*	
Sawback poacher	*Leptagonus frenatus*	2,3
Sturgeon poacher*	*Podothecus accipenserinus*	
Bering poacher	*Occella dodecahedron*	4
Pacific sand lance	*Ammodytes* spp.	1
Searcher	*Bathymaster signatus*	3,4
Pacific herring	*Clupea pallasi*	1
Yellow Irish lord	*Hemilepidotus jordani*	4
Buterfly sculpin*	*Hemilepidotus papillio*	
Warty sculpin	*Myoxocephalus verrucosus*	2
Great sculpin	*Myoxocephalus polyacanthocephalus*	2
Plain sculpin	*Myoxocephalus jaok*	2
Spinyhead sculpin	*Dasycottus setiger*	3,4
Bigmouth sculpin	*Hemitripterus bolini*	3
Pacific sandfish	*Trichodon trichodon*	4
Pacific cod*	*Gadus macrocephalus*	
Arctic cod	*Boreogadus saida*	1,2
Saffron cod	*Eleginus gracilis*	4
Walleye pollock*	*Theragra chalcogramma*	
Whitespotted greenling	*Hexagrammos stelleri*	3,4
Eulachon	*Thaleichthys pacificus*	1
Capelin	*Mallotus villosus*	1
Rainbow smelt	*Osmerus mordax*	1
Marbled eelpout	*Lycodes raridens*	2,4
Wattled eelpout*	*Lycodes palearis*	
Shortfin eelpout*	*Lycodes brevipes*	
Decorator crab	*Oregonia gracilis*	2
Tanner crab*	*Chionoecetes bairdi*	
Snow crab*	*Chionoecetes opilio*	
Helmet crab	*Telmessus cheiragonus*	4
Red king crab*	*Paralithodes camtschaticus*	
Blue king crab*	*Paralithodes platypus*	
Horsehair crab	*Erimacrus isenbeckii*	4

1. Bottom trawl not designed for quantative sampling of pelagic species.
2. Historical changes in the specificity and consistency of field identifications.
3. Historical changes in the consistency of subsampling rare or singular species.
4. Rare or patchily distributed species with insufficient data for spatial analyses.

Table 2.-- Range, average, and standard deviation of local (*LIC*) and global (*GIC*) collocation indices and general additive model results of *LIC* and *GIC* indices of collocation for selected taxa from the eastern Bering Sea shelf. Predictor variables include pairwise interannual comparisons of survey cold pool area (ΔCPA_T) within isothermal boundaries of T = 0°, 1°, and 2°C, abundance ($\Delta ABUND$), and survey time lag ($\Delta YEARS$). The level of signifcance for listed predictor variables is $P < 0.01$. Dashes indicate that the variable dropped out from the model during the selection process, and "d", "n", and "i" indicate whether trend in the response variable was decreasing, neutral or increasing, respectively.

	LIC								*GIC*							
Common name	Min.	Max.	Avg.	SD	Trend ΔCPA_T	Trend $\Delta ABUND$	Trend $\Delta YEARS$	Deviance explained (%)	Min.	Max.	Avg.	SD	Trend ΔCPA_T	Trend $\Delta ABUND$	Trend $\Delta YEARS$	Deviance explained (%)
Skates	0.19	0.72	0.49	0.11	d 1°	d	d	69.6	0.79	1.00	0.97	0.03	n 1°	-	d	76.6
Arrowtooth flounder	0.27	0.84	0.64	0.13	d 1°	d	-	56.6	0.88	1.00	0.98	0.02	d 1°	-	-	39.7
Greenland turbot	0.26	0.83	0.54	0.11	d 1°	-	d	48.1	0.60	1.00	0.93	0.08	-	n	d	67.2
Pacific halibut	0.23	0.71	0.46	0.09	d 2°	d	d	41.9	0.80	1.00	0.97	0.03	n 1°	-	i	66.9
Flathead sole	0.08	0.85	0.44	0.16	-	d	d	67.3	0.85	1.00	0.97	0.04	-	d	d	30.6
Bering flounder	0.04	0.84	0.46	0.15	d 0°	-	d	48.0	0.71	1.00	0.92	0.06	d 2°	d	n	48.5
Rex sole	0.38	0.99	0.78	0.13	d 0°	-	d	60.4	0.84	1.00	0.97	0.03	i 0°	i	i	52.6
Yellowfin sole	0.35	0.87	0.59	0.09	d 2°	i	d	58.3	0.88	1.00	0.98	0.02	-	-	d	51.6
Longhead dab	0.09	0.92	0.57	0.16	-	d	d	41.7	0.58	1.00	0.93	0.08	-	-	-	64.4
Starry flounder	0.03	0.84	0.37	0.18	d 0°	-	n	55.9	0.44	1.00	0.90	0.12	d 1°	-	n	76.9
Rock sole	0.28	0.91	0.57	0.12	d 1°	d	d	62.7	0.69	1.00	0.96	0.05	n 1°	-	n	87.4
Alaska plaice	0.21	0.82	0.53	0.13	d 2°	-	d	43.7	0.83	1.00	0.97	0.03	-	-	d	23.1
Sturgeon poacher	0.07	0.89	0.46	0.17	-	-	d	61.9	0.51	1.00	0.91	0.09	d 1°	-	d	65.2
Butterfly sculpin	0.01	1.00	0.46	0.25	n 1°	-	-	43.8	0.47	1.00	0.84	0.13	-	i	-	49.4
Pacific cod	0.12	0.80	0.37	0.12	d 1°	d	n	54.8	0.81	1.00	0.97	0.03	-	i	d	58.3
Walleye pollock	0.08	0.67	0.32	0.10	-	d	-	37.0	0.74	1.00	0.95	0.05	d 0°	-	d	36.8
Wattled eelpout	0.08	0.71	0.38	0.13	d 0°	-	d	53.4	0.56	1.00	0.90	0.10	n 1°	i	n	39.0
Shortfin eelpout	0.00	0.85	0.48	0.19	d 1°	d	d	62.1	0.09	1.00	0.85	0.21	n 1°	-	-	66.3
Tanner crab	0.09	0.89	0.36	0.17	d 1°	i	d	55.3	0.55	1.00	0.92	0.08	-	i	n	81.1
Snow crab	0.08	0.73	0.43	0.11	i 1°	d	d	47.5	0.66	1.00	0.95	0.06	-	-	n	48.5
Red king crab	0.03	0.95	0.38	0.19	d 2°	d	d	53.4	0.45	1.00	0.91	0.10	d 0°	-	n	61.6
Blue king crab	0.03	0.97	0.44	0.22	-	-	d	54.9	0.31	1.00	0.83	0.18	-	n	d	51.2

Table 3. The distance and bearing associated with a change in the center of gravity (ΔCG) by species for warm relative to cold years, high relative to low abundance years, and early relative to recent years are shown to illustrate the magnitude and direction of the predictor variables ΔCPA_T (cold pool area at isotherm temperature T), $\Delta ABUND$ (change in abundnace), and $\Delta YEARS$ which had a significant effect on the global index of collocation (GIC).

Species	Approximated predictor variable	ΔCG Distance (km)	ΔCG Bearing (degrees)
Skates	$\Delta CPA_1°$	30	196
	$\Delta YEARS$	61	28
Arrowtooth flounder	$\Delta CPA_1°$	36	136
Greenland turbot	$\Delta ABUND$	16	147
	$\Delta YEARS$	24	336
Pacific halibut	$\Delta CPA_1°$	35	119
	$\Delta YEARS$	54	306
Flathead sole	$\Delta ABUND$	33	131
	$\Delta YEARS$	90	301
Bering flounder	$\Delta CPA_2°$	37	205
	$\Delta ABUND$	20	135
	$\Delta YEARS$	21	45
Rex sole	$\Delta CPA_0°$	6	264
	$\Delta ABUND$	17	294
	$\Delta YEARS$	22	132
Yellowfin sole	$\Delta YEARS$	19	85
Starry flounder	$\Delta CPA_1°$	21	116
	$\Delta YEARS$	35	20
Rock sole	$\Delta CPA_1°$	31	161
	$\Delta YEARS$	42	316
Alaska plaice	$\Delta YEARS$	21	52
Sturgeon poacher	$\Delta CPA_1°$	5	244
	$\Delta YEARS$	36	230
Butterfly sculpin	$\Delta ABUND$	13	334
Pacific cod	$\Delta ABUND$	32	292
	$\Delta YEARS$	40	303
Walleye pollock	$\Delta CPA_0°$	42	262
	$\Delta YEARS$	50	309
Wattled eelpout	$\Delta CPA_1°$	79	296
	$\Delta ABUND$	16	296
	$\Delta YEARS$	113	112
Shortfin eelpout	$\Delta CPA_1°$	54	128
Tanner crab	$\Delta YEARS$	42	211
Snow crab	$\Delta ABUND$	35	152
	$\Delta YEARS$	57	303
Red king crab	$\Delta CPA_0°$	31	240
	$\Delta YEARS$	11	90
Blue king crab	$\Delta YEARS$	68	337

The Δ*YEARS* was a significant effect for most *LIC*s (86%) and *GIC*s (82%) with the dominant trend being decreasing similarity in spatial indices with increasing Δ*YEARS*. The *LIC* was significantly affected by the areal extent of the cold pool for a majority of taxa (77%), compared to about half (55%) for the *GIC*. The Δ*CPA_ 1°C* most frequently affected both *LIC* and *GIC* (61%), followed by Δ*CPA_ 0°C* (23%) and Δ*CPA_ 2°C* (16%). The Δ*ABUND* was a significant effect for a greater percentage of the *LIC* models (59%) than for the *GIC* models (41%), with most taxa showing decreasing similarity with the *LIC* and variable trends in similarity with the *GIC*.

The *GIC* for all taxa except longhead dab showed a significant response to at least one of the predictor variables, indicating a community shift in the shelf-wide distribution of demersal fauna on the eastern Bering Sea shelf. The Δ*YEARS* was significant for a majority of taxa (82%), and compared to the temperature and abundance effects, the Δ*CG* for early relative to recent years showed the largest magnitude of displacement (mean = 45 km) and the broadest range of directional shifts with 14 of the 22 taxa undergoing a northward shift. The effect of increasing Δ*CPA_T* on Δ*CG* had a mean displacement of 34 km and the directional shift for all taxa was southward except for the wattled eelpout. Changes in abundance had the smallest effect on Δ*CG*, with a mean displacement of 23 km along a relatively narrow southeast-northwest axis.

DISCUSSION

Studies have shown that both density-independent and density-dependent factors can affect bottom fish distribution (Cianelli et al., 2008; Spencer, 2008). The prevalence of the time lag variable suggests that the density-independent factors (other than temperature) and partially density-dependent factors (other than population abundance) may have more influence on the spatial distribution of a species than do changes in the cold pool or population abundance. Density-independent environmental factors have often been limited to the effects of climate change as approximated by water temperature (e.g., Mountain and Murawski, 1992; Swain, 1999; Spencer, 2008); however, distribution shifts can also result from changes in other density-independent biological factors such as migrations involving ontogeny, spawning, and feeding (Nichol, 1998; Ernst et al., 2005; Kotwicki et al., 2005; Sohn et al., 2010), *in situ* light conditions (Kotwicki et al., 2009), primary production patterns, or fishing pressure (Garrison and Link, 2000). Additionally partially density-dependent factors such as food availability (e.g. Dorn, 1995, Nøttestad et al., 1999) and competition between species, predation (Ciannelli et al., 2008), could also influence spatial distribution in other ways than changes in the cold pool area or population abundance.

The change in area occupied by the cold pool was the second most common significant effect, suggesting that, it is a major environmental feature affecting spatial patterns of distribution on the eastern Bering Sea

shelf. The cold pool affected a much higher percentage of taxa on the local scale (77%) than shelf-wide scale (55%) indicating that distributional changes due to the cold pool are more prevalent on spatial scales smaller than the eastern Bering Sea shelf. The cold pool area enclosed by the 1°C isotherm was the temperature threshold most commonly affecting spatial indices on both scales, suggesting it is an important boundary for describing temperature preferences of more migratory species on the eastern Bering Sea shelf.

Fluctuations in population abundance also affected distribution patterns on both scales, but it was more apparent with taxa locally (59%) than shelf-wide (41%). Population growth creates greater competition for resources, forcing animals within a population to spread more into outlying areas (Swain and Wade, 1993; Atkinson et al., 1997). In the 1980s, there was rapid growth in the populations of several eastern Bering Sea flatfish species, which corresponded to significant increases in the dispersion of those species (McConnaughey, 1995). Increases in the population abundance of "arrowtooth flounder" (combined *Atherethes stomias* and *A. evermanni*) and rock sole (*Lepidopsetta* spp.) on the eastern Bering Sea shelf have been strongly related to increased spatial coverage of their populations, while increases in the area occupied by the cold pool have been associated with decreased spatial coverage of these species (Spencer, 2008).

Immigration and emigration to and from the survey area can cause fluctuations in population size that can affect spatial distribution patterns. The Bering Sea shelf extends hundreds of kilometers to the north where fishes and crabs such as Alaska plaice (*Pleuronectes quadrituberculatus*), yellowfin sole (*Limanda aspera*), and snow crab (*Chionoecetes opilio*) have contiguous distributions (Lauth, 2011) and can easily move into and out of the survey area. The same is true for deeper shelf species such as arrowtooth flounder and Greenland turbot (*Reinhardtius hippoglossoides*) that undergo ontogenetic migrations from the shelf down the upper continental slope, but older aged individuals are known to inhabit both the shelf and slope regions (Alton et al., 1988; Sohn et al., 2010; Spies et al., 2011).

Changes in spatial distribution of many fish populations have been attributed to warmer temperatures associated with climate change (Perry et al., 2005; Mueter and Litzow, 2008; Nye et al., 2009). Our analyses show that increasing cold pool size is partly responsible for driving the short-term interannual variability in the spatial distributions on both shelf-wide and local scales. However the fact, that despite the lack of warming trend over last 30 years on the EBS shelf and despite inclusion of recent data from the extended cold period (2006 to 2010), we still observe a temporal northward shift, provides an argument that a general warming trend is not the main driving mechanism for the temporal northward distributional shift as was proposed in the previous study by Mueter and Litzow (2008). Our results

indicate though that if the warming trend was to appear in the future we should expect further northward shift in fish distributions. Current predictions are that winter ice cover and a summer cold pool will persist on the Bering Sea shelf and continue to act as a barrier to northward migration of subarctic species (Sigler et al., 2011; Stabeno et al., 2012a, 2012b).

We took the analysis a step further by carefully selecting taxa that provide a meaningful index of abundance, and we looked at the spatio-temporal displacement in all directions rather than just along a north-south axis. Twelve of the 14 taxa that were found to have a northward displacement in the Mueter and Litzow (2008) study were also found to have a northward displacement in our study, and four taxa that were found to have a southward displacement in that study also were also found to have a southward displacement in our study. Despite the similarities, directional vectors representing temporal shifts in populations varied considerably among taxa and vectors for some taxa were greater in magnitude to the east or west than to the north. The cross-shelf shifts in populations of pollock and arrowtooth flounder in response to the cold pool size were more noticeable than northerly latitudinal shifts. Population shifts along different axes for the different taxa suggest a variety of species-specific biological or environmental mechanisms or perhaps different responses to the same mechanism.

Another possible mechanism for the northward temporal displacement is disproportional commercial fishing effort on the southeastern Bering Sea shelf. Commercial fishing can impact fish distribution and can change community structure (Garrison and Link, 2000). There is a major fishing port in close proximity to the Bering Sea shelf located in Dutch Harbor, Alaska. Among all U.S. fishing ports, Dutch Harbor was ranked number one in total commercial fishery landings for most of the past 20 years with annual totals ranging from 230 to 413 thousand metric tons (NMFS, 2012). Practical considerations such as winter ice cover and regional management closures, or financial incentives such as travel time and fuel costs, may favor fishable waters closer to Dutch Harbor and result in disproportionate fishing pressure on the southeast portion of the shelf. Ten of the 22 taxa investigated here have been, or continue to be, targeted by a commercial fishery on the Bering Sea shelf, and 8 of the 10 commercially exploited taxa show a northward temporal displacement. The largest trawl fishery on the Bering Sea shelf by weight is walleye pollock, and the relative commercial fishing effort between the southeast and northwest shelf varies by season and by year (Ianelli et al., 2011). Another major trawl fishery for yellowfin sole and rock sole catches a majority of their annual quota on the southeastern shelf (Wilderbuer and Nichol, 2011; Wilderbuer et al., 2011). Commercial harvest of king crabs (*Paralithodes* spp.) occurred around the Pribilof Islands and St. Matthew Island until the late 1990's; however, population declines in both areas resulted in closures that are still in effect. The only remaining major commercial harvest of king crab on the eastern Bering Sea shelf is in Bristol Bay. Historical area- and species-specific commercial fishery

data are available and should be analyzed to investigate whether disproportional fishing effort on the southeastern Bering Sea shelf during the last 30 years is a contributing factor to the apparent northward temporal shift in crab and fish populations.

CONCLUSIONS

This investigation is the first to include data for the 2006-2010 cold period and to use between-year comparisons of shelf-wide and local spatial indices to test specific responses to a range of cold pool temperatures. Model results for shelf-wide and local indices show that cold pool extent and survey time lag more greatly affect spatial distribution than population abundance, suggesting that density-independent mechanisms may play a major role in shaping distribution patterns on the eastern Bering Sea shelf. The area enclosed by the 1°C isotherm most commonly affects spatial indices on both scales, suggesting it is an important boundary for describing temperature preferences of eastern Bering Sea crabs and groundfishes. Distributional shifts in population varied considerably among species and directional vectors for some species were greater in magnitude to the east or west than to the north or south; however, in general, eastern Bering Sea shelf populations shift southward in response to the increasing cold pool size, and after accounting for differences in temperature and population abundance, there is a temporal northward shift in populations over the last three decades.

Chapter 3.c. Combining bottom trawl and acoustic data to model acoustic dead zone correction and bottom trawl efficiency parameters for semi-pelagic species.

This paper was published, for details refer to:

Kotwicki, S., De Robertis, A., Ianelli, J. N., Punt, A. E., and Horne, J. K. 2013. Combining bottom trawl and acoustic data to model acoustic dead zone correction and bottom trawl efficiency parameters for semi-pelagic species. Canadian Journal of Fisheries and Aquatic Sciences. 70: 208-219.

ABSTRACT

Abundances of semi-pelagic fishes are often estimated using acoustic trawl or bottom trawl surveys, both of which sample only a fraction of the water column. Acoustic instruments are effective at sampling the water column, but they have a near-bottom acoustic dead zone (ADZ), where fish near the seafloor cannot be detected. Bottom trawl surveys cannot account for fish that are located above the effective fishing height (EFH) of the trawl. We present a modeling method that combines acoustic and bottom trawl abundance measurements and habitat data to estimate ADZ correction and bottom trawl efficiency parameters. Bottom trawl and acoustic measurements of walleye pollock (*Gadus chalcogrammus*) abundance and available habitat data from the eastern Bering Sea (EBS) are used to illustrate this method. Our results show that predictions of fish abundance in the ADZ can be improved by incorporating bottom habitat features such as depth and sediment particle size, as well as pelagic habitat features such as water temperature, light level, and current velocity. We also obtain predictions for trawl efficiency parameters such as EFH, density-dependent trawl efficiency, and catchability ratio for trawl and acoustic data by modeling bottom trawl catches as a function of acoustic measurements and the environmentally dependent ADZ correction. We conclude that the detectability of pollock by acoustic-trawl surveys and the catchability of pollock by bottom trawl surveys are spatially and temporarily variable. Our modeling method can be applied to other semi-pelagic species to obtain estimates of ADZ correction in relation to habitat and environmental factors, and bottom trawl efficiency parameters.

METHODS

In this study, we propose a modeling approach that combines simultaneously collected bottom trawl and acoustic data and environmental data to estimate the ADZ correction, bottom trawl efficiency parameters

(effective fishing height, density-dependence), and the catchability ratio between acoustic and BT abundance estimates. Our approach builds on present understanding of the processes associated with the collection of fish abundance data from acoustics and bottom trawl. Acoustics detects fish in the water column between near-surface and near-bottom dead zones, while the bottom trawl detects fish that are near the bottom up to the effective fishing height (Hjellvik et al., 2003). The near-surface acoustic dead zone is not a concern for a majority of semi-pelagic species because they are rarely in this zone, and we consequently use the term "ADZ" to refer to the near-bottom acoustic dead zone. Direct measurement of fish density in the ADZ is difficult. However, bottom trawl sampling can be used to estimate the density of fish near the seafloor. We obtain information about unknown processes (e.g. ADZ, trawl efficiency) associated with data collection by both methods by combining acoustic and bottom trawl data in one model. We have chosen semi-pelagic pollock from the EBS as a test case because it has been assessed using both BT and AT surveys since the 1980s (Ianelli et al., 2009). Both of these surveys detect substantial parts of the pollock population, indicating that pollock resides in both pelagic and near-bottom habitat (Kotwicki et al., 2005). Although the data used in this study are for EBS pollock, the method is broadly applicable to AT and BT surveys of other semi-pelagic or semi-demersal species.

Model construction

We assume that a functional relationship exists between density estimates that are obtained from the acoustics and bottom trawl given that data collection took place simultaneously. We can specify this relationship as: $s_{A,BT} \sim f(s_A)$. The form of this functional relationship can be constructed using knowledge of the processes involved in acoustic data collection and bottom trawl catch. Bottom trawl equivalent s_A ($s_{A,BT}$) can be predicted using acoustic backscatter that was detected above the ADZ up to the effective fishing height plus unknown equivalent s_A in ADZ, which results in equation:

$$s_{A,BT_i} = r_q\left(\sum_{b}^{h_1} s_{Ai} + D_i\right)e^{\varepsilon_i} \qquad [5],$$

where r_q is the catchability ratio between the bottom trawl, and acoustics, that accounts for differences in catchability between both methods, h_1 is the effective fishing height of the trawl, D_i is the unobserved fish backscatter in the ADZ in s_A units (thereafter referred to as the ADZ correction), b is the backstep in meters used in processing acoustic data, i is a tow subscript, and e^{ε} is log-normally distributed error. A log-normal error was assumed following Walters and Martell (2004), who argue that a log-normal distribution is appropriate because most quantitative observations in fish dynamics arise as a product of a model component and a proportional observation (r_q in this case), and the sum of logs of such proportions is likely to be normally distributed because of the Central Limit Theorem.

To determine the most appropriate model for relating acoustic and bottom trawl data, a set of alternative models was developed and compared using AICc (Akaike's Information Criterion corrected for finite sample size; Burnham and Anderson, 2010). The first term in all models is of the same form as in equation [5] and represents acoustic backscatter up to the effective fishing height. The second term, which represents the ADZ correction, differs among models.

Model A:

$$s_{A,BT_i} = r_q(\sum_{0.5}^{h_1} s_{Ai} + D_{const})e^{\varepsilon_i} \quad [6]$$

is the simplest with the ADZ term (D_{const}) independent of all covariates and constants. This type of model has been used in past attempts to estimate the effective fishing height of the BT (e.g. Aglen, 1996, Rose and Nunnallee, 1998, von Szalay et al., 2007).

Model B:

$$s_{A,BT_i} = r_q(\sum_{0.5}^{h_1} s_{Ai} + D_{ui}(h_2))e^{\varepsilon_i} \quad [7]$$

has the ADZ term ($D_{ui}(h_2)$) is independent of all environmental covariates, however, the ADZ term is not constant but rather determined by the backscatter observed immediately above the ADZ. This term represents the ADZ correction based on geometric approach of Ona and Mitson (1996). This correction is appropriate for flat bottom areas (Patel et al., 2009) such as in the EBS, and assumes that fish density in the ADZ is uniform from an acoustically visible layer just above the ADZ to the bottom. One improvement to the method incorporated here is use of the observations to estimate the parameter h_2, which determines height of the acoustic layer that is used for ADZ correction, and which is usually chosen arbitrarily.

To apply the Ona and Mitson (1996) ADZ correction a theoretical height of the ADZ (h_{ADZ}) was estimated using formula:

$$h_{ADZ} = h_{eq} + h_{\tau} + h_b \text{, [8]}$$

where h_{eq} is equivalent lost height, h_τ is partial integration zone height, and h_b is the height of the backstep. h_{eq} is the height of the near-bottom layer that is lost due to the curved nature of the leading edge of the acoustic beam and equals $2.83\times10^{-3}\times BD$ for a 7 degree beam, where BD is the bottom depth. h_τ is the height that is lost due to the inability to resolve backscatter associated with the bottom from backscatter associated with fish that are in close proximity to the bottom. This value depends on the length of transmitted pulse and equals $c\tau/4$ where c is the speed of sound, and τ is the pulse duration. h_b is the height of the zone above the echosounder-detected bottom that is used to avoid echo integration of the seafloor. This height has been set at 0.5 m to equal the value used in pollock AT surveys in the EBS.

Model C:

$$s_{A,BT_i} = r_q\left(\sum_{0.5}^{h_1} s_{Ai} + e^{\mathbf{b[X_i]}}\sum_{0.5}^{h_2} s_{Ai} + e^{\mathbf{c[X_i]}}\right)e^{\varepsilon_i} \qquad [9]$$

has the ADZ correction term specified as $e^{\mathbf{b[X_i]}}\sum_{0.5}^{h_2} s_{Ai} + e^{\mathbf{c[X_i]}}$ which represents an ADZ correction based on acoustic backscatter data up to height h_2 (similar to model B) as well as a constant parameter c (intercept in **c[X$_i$]**; similar to model A). Inclusion of c was necessary because at times all fish caught by the BT were located in the ADZ, making it impossible to predict their density using s_A data exclusively. This model does not assume that fish density in the ADZ is the same as in the layer above. Instead, it assumes that fish density in the ADZ can be a function of s_A observed above the ADZ and environmental variables. This assumption seems reasonable in light of recent findings that density of pollock in the layers close to the bottom can be predicted using environmental variables (Kotwicki et al., 2009). Environmental variables and mean fish length are included in model C as the linear covariates **b[X$_i$]** and **c[X$_i$]**, where **b** and **c** are vectors of parameters and **[X$_i$]** is a matrix of the predictor variables including: bottom depth, bottom temperature, surface temperature, sediment size, current speed, bottom light level, and mean fish length.

Model D:

$$s_{A,BT_i} = \left(\frac{1}{r_q\left(\sum_{0.5}^{h_1} s_{Ai} + e^{\mathbf{b[X_i]}}\sum_{0.5}^{h_2} s_{Ai} + e^{\mathbf{c[X_i]}}\right)} + \frac{1}{a}\right)^{-1} e^{\varepsilon_i} \qquad [10]$$

is the same as Model C, but allows for density dependence in bottom trawl efficiency. The parameter *a* represents density dependence of the efficiency of the bottom trawl within the bottom trawl effective fishing zone, defined as the layer from the sea floor to the effective fishing height. When fish densities are much lower than *a,* the term *1/a* is negligible, and model D converges to model C. However, with increased fish density, *a* becomes more influential, resulting in reduced BT efficiency. For example, at fish density equal to the value of *a,* BT efficiency will be approximately half of the efficiency at lowest densities.

Estimation of predictor effects

The relative impact of the linear predictors was determined using parameter estimates from the final model and mean values of all linear and non-linear predictors estimated from the data. For example, the ADZ correction was calculated from the best model for all observed values of bottom depth, while all other predictors were fixed at their means to estimate relative effect of the bottom depth on the ADZ correction. All calculated ADZ values were then divided by their mean to show a change in ADZ correction relative to its mean value. These analyses were conducted for the ADZ correction factor and the BT predicted catch.

RESULTS

Model selection

Model D, which used both acoustic data as well as the intercept for the ADZ correction, had lowest AICc score even without using environmental predictors, indicating that model D fit the data best among models examined. Since all four models have the same structure for the prediction of bottom trawl catches from the acoustic data, and they differ only in the form of the ADZ correction and density-dependence, it can be concluded that the ADZ correction used in model D performed best at predicting fish density in ADZ. Selection of model D also indicated that inclusion of the parameter *a,* that accounts for density-dependence in the efficiency of the bottom trawl, was appropriate.

Including environmental predictors in model D improved the fit of the model to the data significantly by reducing the AICc by 51.72 (negative log likelihood 329.16). Bottom depth, mean fork length, surface temperature, sediment size, bottom light, and current speed proved to be important predictors of fish density in the ADZ. Bottom temperature did not improve model fit and it was eliminated from final model in variable selection process.

Bottom trawl efficiency parameters

The parameters r_q, h_1, and a can be used to describe BT efficiency relative to observed acoustic backscatter in the effective fishing zone and predicted fish density in the ADZ because they provide information necessary to relate the two types of data. The estimate of h_1 indicates that the effective fishing height of the BT is on average ~ 16 m. The estimate of r_q was 0.96 and not significantly different from 1, indicating that the catchabilities of the two surveys are effectively the same. However, the catchabilities are comparable only at low densities because the estimate of a = 4133 implies that bottom trawl efficiency is reduced at higher densities. For example, the BT will be only half maximum efficiency, at fish densities equivalent to the value of a (or ~ 778,911 40 cm fish /nmi^2). Such a density will result in an estimated pollock catch of approximately 3 metric tons (t) during 30 min tow; catches of this size (and greater) occurred on average in 2.5% of tows in EBS BT surveys.

Acoustic dead zone correction parameters

Estimates of pollock densities in the ADZ confirmed our expectations that a large proportion of EBS pollock may be located in the ADZ. ADZ corrections for the stations used in this analysis ranged between 8-97% (mean 60%, median 63%) of all the fish in the entire water column. The estimate of h_2 indicates that fish density in the ADZ is predicted best using acoustic backscatter data from the first layer above it. Our results also indicate that predictors such as environmental variables and fish length can be used to predict fish density in the ADZ. Low estimates of VIFs indicated that possible correlations between predictor variables are not of a concern. Bottom depth was by far the most influential environmental predictor for fish density in the ADZ, and its effect ranged from ~ 0.6 of the mean prediction in the shallowest depths of 40-60 m to 2 at the depths of 160 m. The surface temperature effect increased from 0.8 to 1.5 over 2 to 10°C. Pollock densities in the ADZ increased from 0.9 to 1.2 relative to the mean as sediment size was decreased from 1 to 7 phi. Increasing light levels decreased pollock densities in the ADZ. Inclusion of current speed in the model was supported by AICc, but this variable had a minor effect on pollock densities in the ADZ. On the other hand, an increase in mean pollock length led to large increases in the density of pollock in the ADZ (0.6 for the smallest pollock (~20 cm fork length) to 1.60 for the largest pollock (>60 cm fork length).

DISCUSSION

Best fit to the data by model D indicated that the catchability of either BT or AT survey for pollock is variable in space and time because it depends on environmental variables, and is density-dependent in the case of the BT survey. However, it is likely that environmental variables are affecting catchability

indirectly by impacting fish distribution patterns and behavior. Similar conclusions have been reported by Godø and Wespestad (1993), where they state that the "survey conditions", or environmental impacts on distribution patterns impact catchability differently from year to year. Additinally, Aglen et al. (1999) found environmentally driven variable availability and efficiency of the bottom trawl and variable availability to an echosounder for Atlantic cod, haddock and redfish. These studies indicate that achieving constant survey catchability across time and space for semi-pelagic species may be impossible regardless of survey standardization efforts (Stauffer, 2004). Catchability is unknown for most fishery-independent surveys, but it is assumed to be stationary in time and space (Kimura and Somerton, 2006) because survey data are often perceived to be of better quality than fishery data (Harley et al., 2001). Our findings indicate that problems associated with non-stationary catchability in the fishery-dependent data (i.e. commercial fishery data; e.g. Godø and Engås, 1989; Hilborn and Walters, 1992; Wilberg et al., 2010) may also arise with survey data. This can be problematic for example, in geostatistical estimates of fish abundance because they require that underlying local CPUE data are proportional to abundance (Rivoirard et al. 2000). The fact that local CPUE data from either the AT or the BT survey may not be proportional to fish density can introduce errors in these estimates. The same assumption is often made in spatial dynamics studies, which use CPUE data to investigate relationships between fish distributions and environmental factors (e.g. Bartolino et al. 2011). In the case of these studies, the presence of non-stationary, environmentally-dependent catchability makes it impossible to distinguish environmental effects on fish spatial distribution from environmental effects on catchability. This conundrum can be resolved by combining results from two surveys, conducted simultaneously, in a model that accounts for factors influencing both surveys as was presented here. In the EBS pollock example, the models predicted an ADZ correction and BT efficiency parameters. The next logical step will be to use these results to estimate environmental effects on catchability and correct local density estimates for environmental effects, thereby providing spatial distribution data that is reflective of actual species distributions.

Environmental effects

This investigation provides evidence that the density of pollock in the ADZ depends on many environmental factors and shows that s_A alone is a rather poor predictor of fish density in the ADZ. Semi-pelagic fish behavior in the water column can be affected by the fish size as well as environmental factors (e.g. Michalsen et al., 1996; Aglen et al., 1999; Kotwicki et al., 2009). Changes in behavior may influence fish vertical distribution close to the bottom and hence abundance in the ADZ. Therefore it is preferable to use the experimentally-derived ADZ correction, that accounts for environmental effects, over one that uses geometric approach exclusively.

Higher fish abundance in the ADZ with depth is expected because the volume of the ADZ increases with depth (Ona and Mitson, 1996). The surface temperature effect detected in the model may be explained by pollock avoidance of warmer temperatures that would result in increased need for oxygen and food consumption (Clarke and Johnston, 1999). In the EBS, areas with high surface temperatures have a greater vertical temperature gradient than areas with colder surface temperatures. Pollock, therefore, may have more incentive to be near bottom (in colder water) in areas with a higher surface temperature to conserve energy. Additionally, zooplankton availability in the water column generally decreases in the EBS by the end of summer (Springer et al., 1989; Chuchukalo et al., 1996; Coyle et al., 1996), indicating that this energy saving behavior may be reasonable when surface temperatures are highest. The model predicted higher fish densities in the ADZ with decreasing sediment size ranging from sand to mud. A possible explanation may be that pollock prefer to be closer to the sandy-mud bottom, prevalent on the middle EBS shelf (Smith and McConnaughey, 1999), due to higher food availability on the inner shelf with 10-fold larger infaunal biomass than on the outer shelf (Walsh and McRoy, 1986). Our study also predicted that pollock density in the ADZ is lower with increased near-bottom light levels. This finding seemingly contradicts a previous study on the effect of light on pollock vertical distribution, which indicated that pollock tend to be higher off bottom in low near-bottom light conditions (Kotwicki et al. 2009). However this study did not look explicitly at the ADZ, but only at pollock observed by the AT. Lastly, although current speed was selected (based on AICc), the magnitude of the current speed effect proved to be very small and at this point we consider it negligible. Future research, using presented here methodology, could explore additional environmental factors which are likely to influence pollock densities in the ADZ.

This study also found a size-dependent effect with pollock abundance in the ADZ, with larger pollock more likely to be present in the ADZ. This result was expected because larger pollock are more demersal (Karp and Walters, 1994). Also, survey selectivity curves derived in pollock stock assessments show that the selectivity of the AT survey is lower for larger pollock (Ianelli et al., 2009), suggesting that larger pollock are more likely to be present in the ADZ.

Implications for stock assessment

Looking forward, we advocate that a combined acoustic-bottom trawl survey be considered in place of the separate AT and BT surveys to minimize possible biases associated with environmental variability (Godø and Wespestad, 1993). If the surveys are performed on separate vessels, it is important to schedule them at approximately the same time and location. Both AT and BT surveys have shortcomings that can complicate interpretation of survey abundance data. In the AT survey, the ADZ causes bias (e.g. McQuinn et al., 2005), and can lead to spatial and temporal changes in the AT survey catchability

(Kotwicki et al., 2009) because of the dependence of the fish density in the ADZ on environmental variables. In the case of the BT survey, the existence of a bottom trawl blind zone and density-dependence of BT catches indicate similar bias and catchability problems. However, performing both surveys on one platform, and using models such as the one presented here, could mitigate these problems. Further research on the models that quantify the ADZ correction incorporating environmental factors and BT efficiency parameters could concentrate on two aspects that have been shown here but remain still unresolved. First, variability in catchability of both AT and BT surveys needs to be better understood. Parameters estimated in models that combine bottom trawl and acoustic data could provide the means to estimate changes in catchability of either survey in relation to environmental factors, allowing estimation of the magnitude of these effects on survey abundance indices. Second, this knowledge would also be useful for deriving one abundance index by combining results from both BT and AT surveys and testing these new indices in stock assessment models.

Ecosystem monitoring to better understanding ecosystem patterns and processes is a dominant theme of the ecosystem-based approach to management (Grumbine, 1994; Christensen et al., 1996, Mangel et al., 1996). However, our understanding of the abundance of key organisms in the ecosystem can be negatively impacted by the environmental variability that affects monitoring tools (BT and AT surveys in this case; Godø and Wespestad, 1993; Godø, 1994). To account for this impact we need to understand how the monitoring is affected by the environment and integrate environmental data into stock assessment process. We perceive our study as a step toward this goal. This topic requires further research that could concentrate on either including environmental variables in the process of estimating abundance indices, or by integrating environmental variability into catchability estimates within stock assessment models. Regardless of the avenues that are pursued in the future, collection of environmental data during stock assessment surveys is essential.

CONCLUSIONS

Abundances of semi-pelagic fishes are often estimated using acoustic trawl or bottom trawl surveys, both of which sample only a fraction of the water column. Acoustic instruments are effective at sampling the water column, but they have a near-bottom acoustic dead zone (ADZ), where fish near the seafloor cannot be detected. Bottom trawl surveys cannot account for fish that are located above the effective fishing height (EFH) of the trawl. We presented a modeling method that combines acoustic and bottom trawl abundance measurements and habitat data to estimate ADZ correction and bottom trawl efficiency

parameters. Our results show that predictions of fish abundance in the ADZ can be improved by incorporating bottom habitat features such as depth and sediment particle size, as well as pelagic habitat features such as water temperature, light level, and current velocity. We also obtain predictions for trawl efficiency parameters such as EFH, density-dependent trawl efficiency, and catchability ratio for trawl and acoustic data by modeling bottom trawl catches as a function of acoustic measurements and the environmentally dependent ADZ correction. We conclude that the detectability of pollock by acoustic-trawl surveys and the catchability of pollock by bottom trawl surveys are spatially and temporarily variable. Our modeling method can be applied to other semi-pelagic species to obtain estimates of ADZ correction in relation to habitat and environmental factors, and bottom trawl efficiency parameters.

Chapter 4: Forage fish distribution (age-0 pollock, age-1 pollock, and capelin)

Chapter 4.a. Effects of climate variations on pelagic ocean habitats and their role in structuring forage fish distributions in the Bering Sea.

This paper was published, for details refer to:

Hollowed, A. B., S. J. Barbeaux, E. Farley, E. D. Cokelet, S. Kotwicki, P. H. Ressler, C. Spital, C. D. Wilson. 2012. Effects of climate variations on pelagic ocean habitats and their role in structuring forage fish distributions in the Bering Sea. *Deepsea Research II,* 65-70: 230-250.

ABSTRACT

This paper examines how climate variations influence the boundaries of suitable ocean habitat, and how these changes affect the spatial distribution and interactions between forage fishes in the southeastern Bering Sea shelf. The study focuses on the summer distributions of forage fish age-0 and age-1 walleye pollock, *Gadus chalcogrammus*, and capelin, *Mallotus villosus,* observed during National Marine Fisheries Service summer acoustic trawl, surface trawl and bottom trawl surveys conducted in the Bering Sea between 2004 and 2009. We compare the responses of these forage fish to climate-induced shifts in ocean habitats. Habitat boundaries were defined using key explanatory variables including depth, bottom temperature and surface temperature, using general additive models. Bathymetry, bottom temperature and frontal zones formed boundaries between different groups of forage fishes. Age-0 pollock were dispersed throughout the middle domain (50-100m depth) in well-stratified regions. In cold years the highest densities of age-0s were found in the southern regions of the middle domain waters in waters warmer than approximately 1°C. In contrast, age-1 pollock were observed on the sea floor over the middle domain and in midwater in the northern outer domain in cold years and more broadly dispersed across the middle and outer domain in warm years. The demersal concentrations of age-1 pollock in the middle domain shows age-1 pollock tolerate a wide range of bottom temperatures. Midwater and demersal distributions of age-1 pollock exhibited a patchier distribution than age-0 pollock. Midwater concentrations of age-1 pollock tended to be associated with the outer domain and regions where higher levels of lower trophic level production are expected. Capelin were concentrated in the inner domain, a well-mixed region. The overlap of age-1 pollock and capelin was higher in cold years than in warm years.

Keyword: Forage fish, zoogeography, Bering Sea, climate change, cold pool

INTRODUCTION

Shifts in the volume and spatial extent of ocean habitats can influence fish distributions and species interactions (MacCall 1990, Agostini et al., 2006; Ciannelli and Bailey, 2005; Hollowed et al., 2007, Logerwell et al., 2007; Logerwell et al., 2010, Planque et al., 2011). Climate change is expected to influence the distribution and volume of ocean habitats resulting in shifts in marine fish distributions (Ressler et al., 2007; Nye et al., 2009; Cheung et al., 2009; Overland et al., 2010). Predicting the responses of forage fish to climate-driven change requires knowledge of their habitat associations and environmental tolerances, and has motivated a renewed interest in understanding factors influencing the biogeography of marine fish (Rijnsdorp et al., 2009; Lenior et al., 2011).

Previous studies provide evidence that shifts in climate can influence the spatial distribution of eastern Bering Sea groundfish. A recent warming event in 2001-2005 in the eastern Bering Sea (EBS) coincided with an apparent shift in the spatial distribution of groundfish species (Overland and Stabeno, 2004; Mueter and Litzow, 2008; Spencer, 2008). These studies focused primarily on adult fishes. Some studies of juvenile pollock (a common prey fish) and other small forage fishes (e.g. capelin) have been conducted; however, these studies examined fish distribution relative to place-based foragers (e.g. Decker et al., 1995) in a restricted region (e.g. Swartzman et al., 2002 and 2005). There is a need to understand and predict the effect of climate change on forage fishes since they represent a major node through which energy flows in the EBS (Aydin and Mueter, 2007). This paper extends previous studies by Mueter and Lizow (2008) and Spencer (2008) by providing a detailed focus on the spatial distribution of three potentially interacting forage fish groups (capelin, age-0 pollock and age-1 pollock). We build on previous studies by Ciannelli and Bailey (2005) by providing new information on distributions of forage fishes in cold years and we introduce new statistical models that detail the distribution of these three major forage fish groups in the Bering Sea. Understanding the behavioral responses of forage fishes to climate variations and the expected impact of these responses on the top trophic level species is particularly important because this region supports one of the world's largest sustainably managed commercial fisheries (Worm et al. 2009, Livingston et al., 2011).

Three forage fish groups (defined by size or species) make up a large proportion of the forage fish complex in the EBS: age-0 and age-1 walleye pollock (*Gadus chalcogrammus,* hereafter referred to as pollock), and capelin (*Mallotus villosus*). In this study age-0 and age-1 pollock were defined by size. The spatial distribution of forage fishes relative to oceanographic features in the Bering Sea has been

discussed previously (Wyllie-Echeverria, 1998; Ciannelli and Bailey, 2005; Moss et al., 2009). The work of these authors focused on the following hypothesis:

> *Hydrography and bathymetry define the boundaries of ocean habitats and contribute to spatial segregation of predators and prey (Francis and Bailey, 1983; Wyllie-Echeverria and Wooster, 1998; Ciannelli and Bailey, 2005).*

Recent studies have considered the role of environmental forcing on plankton distribution and abundance and its effect on the diet and energetics of age-0 pollock in the Bering Sea (Baier and Napp, 2003, Moss et al. 2009, Hunt et al., 2011, Mueter et al., 2011). The work of these authors focused on the following hypothesis:

> *Spatio-temporal patterns of ocean conditions influence sea ice extent and impact the survival of energy rich prey which in turn regulates lipid acquisition in juvenile pollock.*

This paper evaluates these hypotheses by examining the spatial distribution of forage fishes relative to each other and relative to large-scale physical oceanographic patterns during summer and early fall. In doing so, this paper addresses elements of the more comprehensive hypothesis posed by the Bering Sea Ecosystem Study (BEST, funded by the National Science Foundation) and the Bering Sea Integrated Ecosystem Research Program (BSIERP, funded by the North Pacific Research Board):

> "*Climate and ocean conditions influencing water temperature, circulation patterns and domain boundaries impact fish reproduction, survival and distribution, the intensity of predator-prey relationships and the location of zoogeographic provinces through bottom-up processes; Reduced cold pool extent will increase overlap of inner domain forage fish and outer domain piscivores; Strength of frontal boundaries will weaken due to absence of the summer cold pool, allowing expansion of the inner domain and juvenile and forage fish habitat there. Weaker winds will enhance this effect*". (http://bsierp.nprb.org/)

MATERIALS AND METHODS

The Study Region

The study region for this analysis is the eastern shelf of the Bering Sea south of St. Lawrence Island. The shelf region is characterized by three major oceanographic domains (inner middle, and outer) bounded by inner and outer fronts (Macklin and Hunt, 2004, Fig. 1). The inner domain is characterized as being well

mixed due to wind and tidal effects (Kachel et al., 2003). The middle domain lies between the 50- and 100-m depth contours and is stratified during summer, and the annual extent of the 'cold pool' is a prominent feature of ocean habitat there (Spencer, 2008). The cold pool is a large body of cold water that forms from the annual freezing and melting of sea ice, and is defined to be contained within the 2°C isotherm in summer (Fig. 1). In warm years, the cold pool retreats to the northern portion of the middle shelf domain (Stabeno et al. 2010). Recent oceanographic studies revealed that salinity is a key variable that determines density stratification in the northern regions of the middle domain although geographic differences are often found within this domain. Salinity and temperature together determine density stratification in the southern region (Stabeno et al., 2010). For example, water in the northern portion of the middle shelf was less stratified in summer than the well-defined, two-layered system in the southern portion. The outer front is roughly located along the 100 m isobath. The outer domain is those waters between the outer front and the shelf break (Coachman, 1986), and the offshore side of the outer domain is bounded by the Bering Slope current offshore, a productive region known as the 'green belt' (Springer et al., 1996).

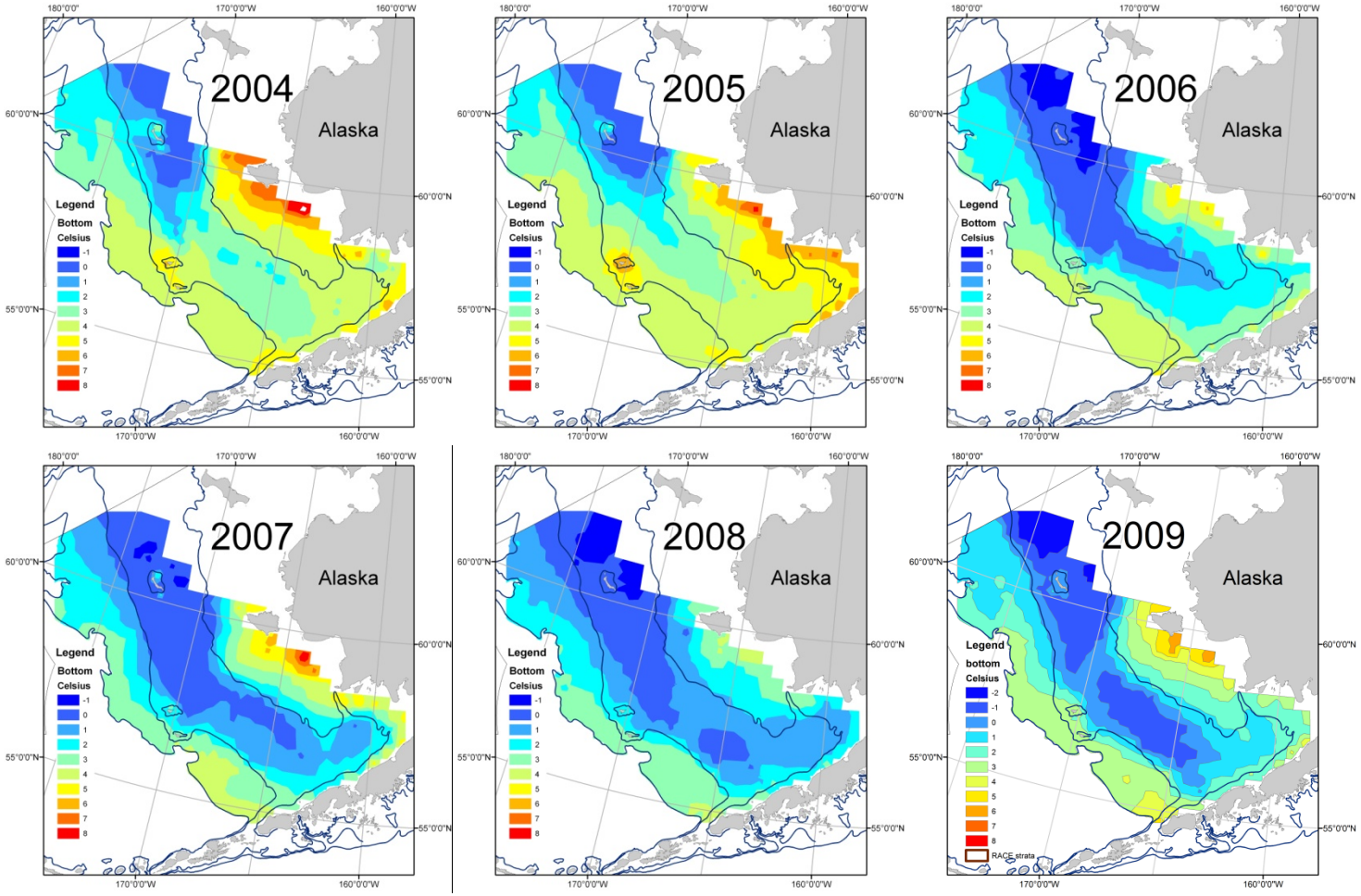

Figure 1. Bottom temperature (° C) from National Marine Fisheries Service bottom trawl survey during the summers (June-July) of 2004-2009. Contour lines identify the inner front (~50m depth), the middle front (~100 m depth) and the shelf break.

Data Sources and Surveys

National Marine Fisheries Service (NMFS), Alaska Fisheries Science Center (AFSC) researchers conduct three types of fishery-independent surveys of the Bering Sea shelf: surface trawl (Moss et al., 2009), acoustic-trawl (primarily midwater; Honkalehto et al., 2010), and bottom trawl (Lauth, 2010). Data from each of these types of surveys were used in this study and they are briefly described below. None of the surveys provide a complete view of the distribution of forage fishes in the EBS because they sampled only part of the available habitat. Given that the focus of this study was the assessment of forage fish biogeography, integration of results from the different survey types provide a general view of the broad-scale distribution of forage fish in the southeast Bering Sea shelf region.

Age-0 pollock distributions in surface waters were assessed in August - September using data collected during the Bering-Aleutian Salmon International Survey (BASIS) survey (now known as the Bering Arctic Subarctic Integrated Surveys). A complete description of the sampling methods is found in Moss et al. (2009). Briefly, the BASIS survey used a 198-m-long midwater rope trawl that was modified to sample near surface waters. The codend was fitted with a 1.2 cm mesh cod-end liner. Thirty-minute tows were conducted at tow speeds of 6.5-9.3 km/hr. Catch was sampled for species, and CPUE was estimated based on the volume of water filtered by each tow. This analysis was limited to surface trawls that sampled the upper ca. 20 m of the water column.

Age-1 pollock and capelin near-bottom distributions were annually assessed in June-July using data collected during the NMFS EBS continental shelf bottom trawl survey. A complete description of the sampling methods for this survey can be found in Lauth (2010). Briefly, data were generally collected from a tow conducted within each of approximately 376, 37x37 km grid cells. Stations were located at the center of each grid cell, and additional stations were added in some strata to address crab distributions at smaller spatial scales. An 83-112 Eastern otter trawl with 25.3 m headropes and a 34.1 m footrope was used. The net mesh sizes ranged from 10.2 cm to 8.9 cm and the codend was fitted with a 3.2 cm mesh liner. The catch was sorted to lowest taxonomic level and species densities were estimated based on the number (age 1 pollock) or weight (capelin) per hectare of area swept by the trawl. The area swept by the trawl was estimated by multiplying distance the net was on the bottom and net width. Bottom trawl estimates of capelin numbers per area swept were based on actual count from tows with less than 50 capelin or the average weight of capelin from more abundant tows. Bottom trawl estimates of age-1 pollock density were based on numbers rather than weight because the age-1 pollock were not weighed. Total sample weight, subsample numbers, and length frequency data were used to estimate numbers/per hectare at length. The catch-at-age 1 data was then estimated using the age-length key method described

by Kimura (1989). The data were then converted from number or weight/hectare to number or weight/per km^2.

Semi-pelagic age-1 pollock distribution patterns were also described for June-July using data collected during the NMFS-AFSC acoustic-trawl survey (hereafter acoustic survey). A complete description of the methods used for the acoustic surveys can be found in Honkalehto et al. (2010). Surveys were conducted during June and July in 2004, and 2006 – 2009 on either the NOAA ships *Miller Freeman* or *Oscar Dyson*. The surveys were conducted during daylight hours along parallel transects uniformly spaced 37 km apart. Acoustic backscatter data were collected with calibrated echosounders operating at 18, 38, (70 *Dyson* only), 120 and 200 kHz.. The nautical area scattering coefficient (s_A, m^2 nmi^{-2}, MacLennan et al., 2002) was estimated for each 926 m segment of the trackline. Acoustic-trawl surveys have traditionally provided abundance and distribution estimates of semi-pelagic pollock from near the ocean surface to within 3 m of the sea floor. A midwater trawl with headrope/footrope lengths of 81.7 m and mesh sizes ranging from 325.1 cm to 8.9 cm and fitted with a 1.27 cm codend liner was primarily used to confirm the species classification of acoustic backscatter and collect other biological information to convert the echo integration data to estimates of abundance. Estimates of age-0 pollock and capelin are typically not made by the NMFS-AFSC acoustic-trawl survey as capelin are rarely encountered and age-0 pollock are poorly detected in early summer.

For this study we selected the years 2004-2009. This time period provided contrasting oceanographic conditions with 2004-2005 being relatively warm and 2006 - 2009 being relatively cool (Fig. 1, Stabeno et al. 2012b). Data were not available for all years for the acoustic trawl and BASIS surveys. Acoustic trawl surveys were not conducted in 2005 and the BASIS surface trawl data collected in 2008 were too limited (sample spacing was wider and too coarse for use in this study).

Oceanographic measurements

A core suite of oceanographic measurements were collected during the three different types of surveys. During the BASIS cruises, CTD profiles and surface water temperatures were taken at each station. During the bottom trawl surveys, a micro-bathythermograph was attached to the headrope of the trawl to provide a temperature profile of the water column at each station and a record of bottom temperature. During the acoustic surveys, continuous underway measurements of surface temperature and salinity were obtained as well as profiles of water column properties at selected stations using CTDs, trawl-mounted microbathythermographs and expendable bathythermographs.

Beginning in 2008, the BEST-BSIERP program funded the collection of underway measurements on the NOAA ship *Oscar Dyson* and the chartered fishing vessel, F/V *Aldebaran*. Both vessels measured near-

surface water temperature, salinity and chlorophyll fluorescence. These continuous underway measurements identified horizontal changes in the oceanography across the region. The BEST-BSIERP program also funded the collection of temperature and salinity profiles using rugged CTDs attached to the trawl headropes of contract survey vessels. These profiles provided a three-dimensional view of the water column structure and were used to estimate the geostrophic velocity in 2008.

Analysis Methods

Spatial patterns of forage fish distribution relative to surface and subsurface oceanography were examined using Geographical Information Systems (GIS). Statistical analyses were performed to verify relationships. Non-linear relationships were explored using general additive models (GAMs). Measures of aggregation (D95; Swain and Benoit, 2006) were evaluated to detect age-0 pollock behavioral differences among different years.

Vertical Stratification 2004-2007

An index of the vertical stratification of the water column, or its static stability, is the potential energy anomaly, ϕ, given by $\phi = \frac{1}{h}\int_{-h}^{0}(\overline{\rho}-\rho)gzdz$ where $\overline{\rho} = \frac{1}{h}\int_{-h}^{0}\rho dz$ is the mean fluid density over the water column of depth h, z is the vertical Cartesian coordinate, and g is the acceleration of gravity (Simpson 1981). This anomaly is the amount of work per unit volume of fluid required to completely mix the water column. ϕ is large for a highly stratified system and vanishes with complete vertical mixing. It was computed from the surface to the shallower of 70 m or the bottom from CTD casts during the BASIS cruises of August-September 2004-2009.

Aggregation-strength 2004-2007

Swain and Benoit (2006) developed the "D95" approach as a measure of the occupied area in relation to environmental variables. D95 is defined as the minimum number of stations over which 95% of the population is distributed. D95 may reflect a limited geographic range or the patchiness of the species over its observed range. Given that age-0 pollock exhibit a broad, geographic range in the Bering Sea, it is used as a measure of relative patchiness for this analysis. If animals are patchily distributed or have a limited geographic range, D95 is small, whereas if the animals were uniformly distributed, D95 is large. The number and spatial distribution of BASIS stations sampled varied between years. D95 estimates were not made for the 2009 BASIS data because the sample spacing differed from the other years. For the 4 study years (2004-2007), D95 estimates were limited to a standard group of 100 stations located primarily on the southern Bering Sea shelf that were occupied in all years. For these selected stations,

cumulative density distributions were developed for CPUE and D95 was computed for the BASIS survey data.

Spatial overlap of bottom trawl survey age-1 pollock and capelin

Exploratory analysis was performed to examine the spatial overlap of bottom trawl survey age-1 pollock and capelin. GIS maps were drawn to show the relative fraction of the total capelin+age-1 pollock in a tow comprised of age-1 pollock or capelin. The expectation was that if age-1 pollock and capelin exhibited spatial partitioning, that the two species would generally not co-occur.

GAM analyses of EBS Surveys 2004-2009

Non-linear relationships were explored with generalized additive models (GAM; Hastie and Tibshirani 1990) using the R (R Core Development Team 2009) package mgcv (Wood 2004, 2006). The dependent variable for all analyses was catch per unit effort (CPUE) measured as the numbers of fish per square kilometer. For surface and bottom trawl surveys the CPUE was the number of fish per square kilometer trawled per trawl haul. For the acoustic surveys, the CPUE was the estimated number of fish per square kilometer insonified along 0.5nmi (926 m) of trackline averaged into 20 nmi (37 km) blocks to match the resolution of the BASIS and bottom trawl survey data sets. The distribution of CPUE was examined in relation to location and environmental variables. For the acoustic and bottom trawl surveys, bottom depth (BD), surface temperature (ST) and bottom temperature (BT) were included as environmental variables for all surveys. For the surface trawl analyses bottom depth and surface temperature were used in this study. We further examined the annual trends with year as a factor and the influence of being in a period with on-average warm (2004-2005) or cold (2006-2009) spring water temperatures (Stabeno et al. 2012b).

We examined presence-absence data using quasi-binomial Generalized Additive Models (GAMs, Zuur 2009). For the analysis of fish density we used quasi-lognormal GAMs. The underlying assumption in using this modeling method was that there were two independent ecological processes playing a role, one governing presence or absence of fish and another determining density when fish were present. The presence or absence of fish was modeled using a quasi-binomial logit regression having over dispersion accounted for using a dispersion parameter (θ) with a full model of the form:

$$
\begin{aligned}
&Ki = B(1, \pi_i) \\
&E(K_i) = \pi_i, \mathrm{var}(K_i) = \pi_i \times (1 - \pi_i) \times \theta \\
&\log it(\pi i) = \alpha_j + s(Z_i)AS_{1i} + s(Z_i)AS_{2i} + te(BD_i, ST_i, BT_i)AS_{1i} + te(BD_i, ST_i, BT_i)AS_{2i}
\end{aligned}
$$

where K is the binary response variable B coded as 1 (presence) or 0 (absence), and π is the probability parameter in the binomial. The logit includes an independent intercept (α) for each year (j), with bottom

depth (BD) in meters, and surface temperature (ST) and bottom temperature (BT), in tenths of a degree C. To address spatial autocorrelation (Swartzman et al. 1992) we used thin plate regression splines (s) over location (Z) in universal transverse mercator (UTM) coordinates in kilometers. We employed tensor product smooths (te) for analyses of models with interaction terms among temperatures and depth. Tensor product smooths are more appropriate than other smoothers here because the interactions were fit over different units (i.e. temperatures in ^{o}C and bottom depth in m). In the full models, both the thin plate regression splines and tensor product smooths were fit with a factor for either warm periods (AS_1; 2004-2005) or cold periods (AS_2; 2006-2009) where warm and cold periods were based on mean spring water temperatures. This formulation was used to explore the hypothesis of different functional responses for the two periods. The dimensions of the marginal basis for the thin plate regression splines were restricted to 20 and for the tensor product smooths to 4 to reduce overfitting of the data (Wood 2006).

Where fish were present, the CPUE was modeled as an over-dispersed log-normal process using a quasi-approach (Zuur et al., 2009) where over-dispersion was accounted for using a dispersion parameter (θ). The full model where CPUE was greater than zero was of the form:

$$
\begin{aligned}
&LN(CPUE_i) = N\left(\mu_i, \sigma^2 + \theta\right) \\
&\mu_i = \alpha_j + s(Z_i)AS_{1i} + s(Z_i)AS_{2i} + te(BD_i, ST_i, BT_i)AS_{1i} + te(BD_i, ST_i, BT_i)AS_{2i}
\end{aligned}
$$

BT was not included in the tensor product smooths of the surface trawl age-0 pollock analyses as these data were not available. Model selections were conducted separately for the quasi-binomial and quasi-log normal models for all datasets using generalized cross validation (GCV; Wood 2006). Four model configurations were tested for each dataset and family: the full model, a model without the spring water temperature factors, models without accounting for autocorrelation, and models without the temperatures and bottom depth smooth.

The predicted CPUE for a given location, temperature, bottom depth, year, and average spring temperature period was calculated as the product of the binomial prediction of probability of occurrence and the quasi-log normal predicted CPUE. The interpretation of the results and these models are not meant to be predictive beyond the bounds of the data and all figures were clipped to the bounds of the datasets.

RESULTS

Ocean conditions

Summer (June – July) bottom trawl survey data revealed that on the eastern Bering Sea shelf, the cold pool (temperature <2º C) was restricted to the middle domain and regions north of the Pribilof Islands in

2004-2005. In 2006-2009, the cold pool extended into the southern regions of the EBS shelf (Fig. 1). While the bottom temperatures were cool, surface waters away from the 50 m isobath were relatively warm in the middle domain (Fig. 2) leading to strong stratification there (Fig. 3). The spatial pattern of this vertical stratification index shows vanishing-to-weak stratification in the inner domain (50 m<depth), strong stratification in the southern middle domain (50 m<depth<100 m) and variable stratification in the middle domain north of 58 – 59 ° N (Fig. 3).

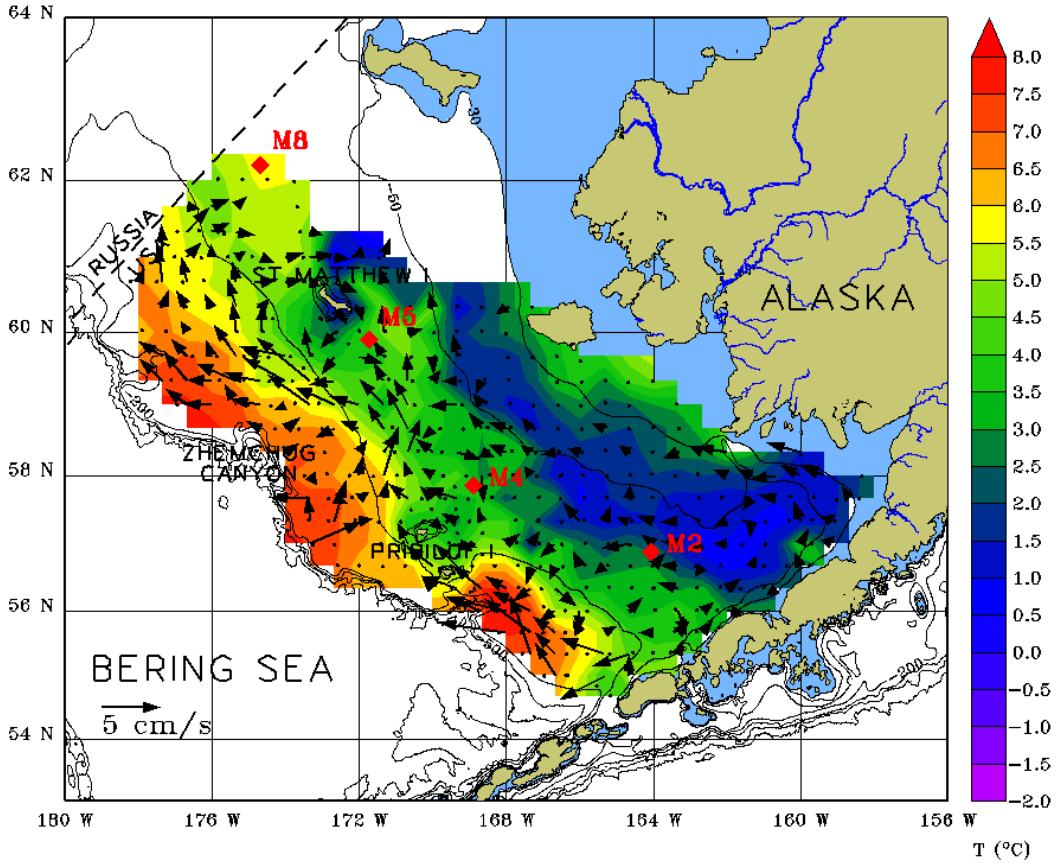

Figure 2. The near-surface (10 m) temperature from CTD measurements during the bottom trawl survey, 3 June-26 July 2008. The arrows represent geostrophic velocity vectors exceeding 1cm/s, relative to 100 m or the bottom, whichever is shallower and also shown are EcoFOCI mooring sites M2, M4, M5 and M8. Depths are contoured at 30, 50, 100, 200, 500, 1000 and 2000 m.

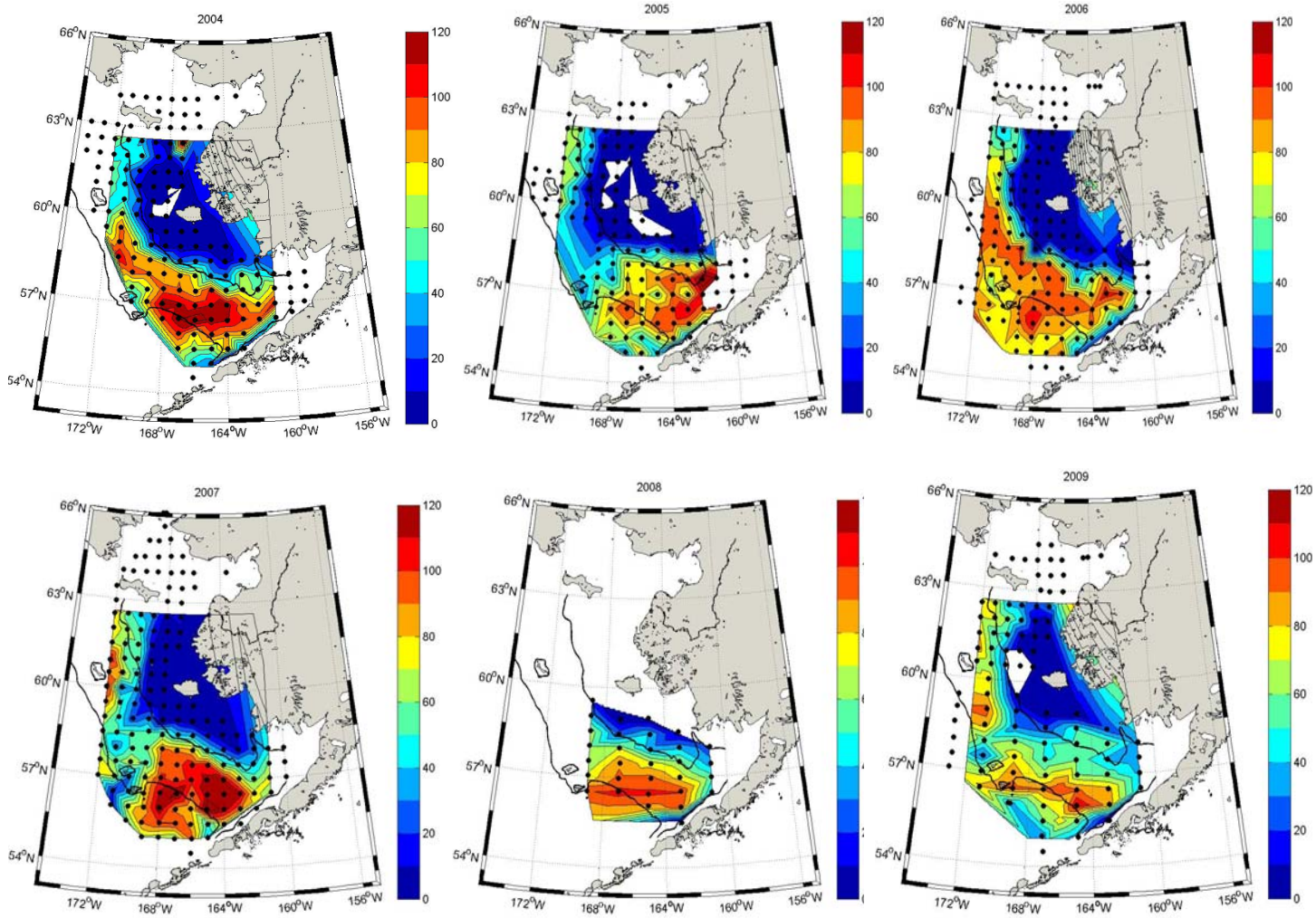

Figure 3. The potential energy anomaly, ϕ (J/m^3), based upon CTD casts during the August-September 2004-2009 BASIS cruises in the eastern Bering Sea. The 50- and 100-m isobaths are also shown to distinguish the inner (<50 m), middle (50-100 m) and outer (100-200 m) domains.

The geostrophic velocity vectors relative to 100 m show the thermohaline circulation on the continental shelf (Fig. 2). The flow crosses from the outer to the middle domain north of the Pribilof Islands with clockwise circulation around St. Matthew Island. South and east of the Pribilof Islands the flow is generally northwestward but weak with areas of recirculation. On the inner shelf, landward of the 50 m isobaths, the thermohaline flow is very weak. These findings show that while flow is generally along the traditional frontal boundaries at 100 and 50 m, advective corridors can cross the 100 m outer front and enter the middle domain.

Spatial Distributions

Data revealed that frontal boundaries generally partition the summer and early fall distribution of forage fish in the EBS (Fig. 1, 4, 5 and 6). Bottom trawl survey data revealed that capelin were found in the inner domain in all years (Fig. 4). Capelin were also found in the northern and southern middle domain in some years. Late summer / early fall distributions of age-0 pollock at the surface were broadly distributed in the middle and outer domains and to a lesser extent, the inner domain during a few years (Fig. 5). Examination of the higher density observations shows that the spatial distribution of age-0 pollock contracted in the cold years of 2006 and 2007 compared to prior, warmer years (Fig. 5). In most years, age-1 pollock observed in the bottom trawl survey during June and July were patchily distributed in the middle domain bounded by the 50 and 100 m isobaths (Fig. 6). Summer distributions of age-1 pollock from in the acoustic trawl survey in 2007 and 2009 were found in the region of cross-shelf flow northwest of the Pribilof Islands and in the region of geostrophic flow along the 100 m isobath north of Zhemchug Canyon (Figs. 2 and 7). In years associated with the 2006 and 2008 strong year classes (Ianelli et al. 2010, evidenced by the higher CPUE of age-1 fish in 2007 and 2009), age 1 pollock were observed throughout the northern portion of the shelf (Figure 6 and 7), with concentrations just NE of the Pribilof Islands and farther north, up to the U.S. Russia convention line.

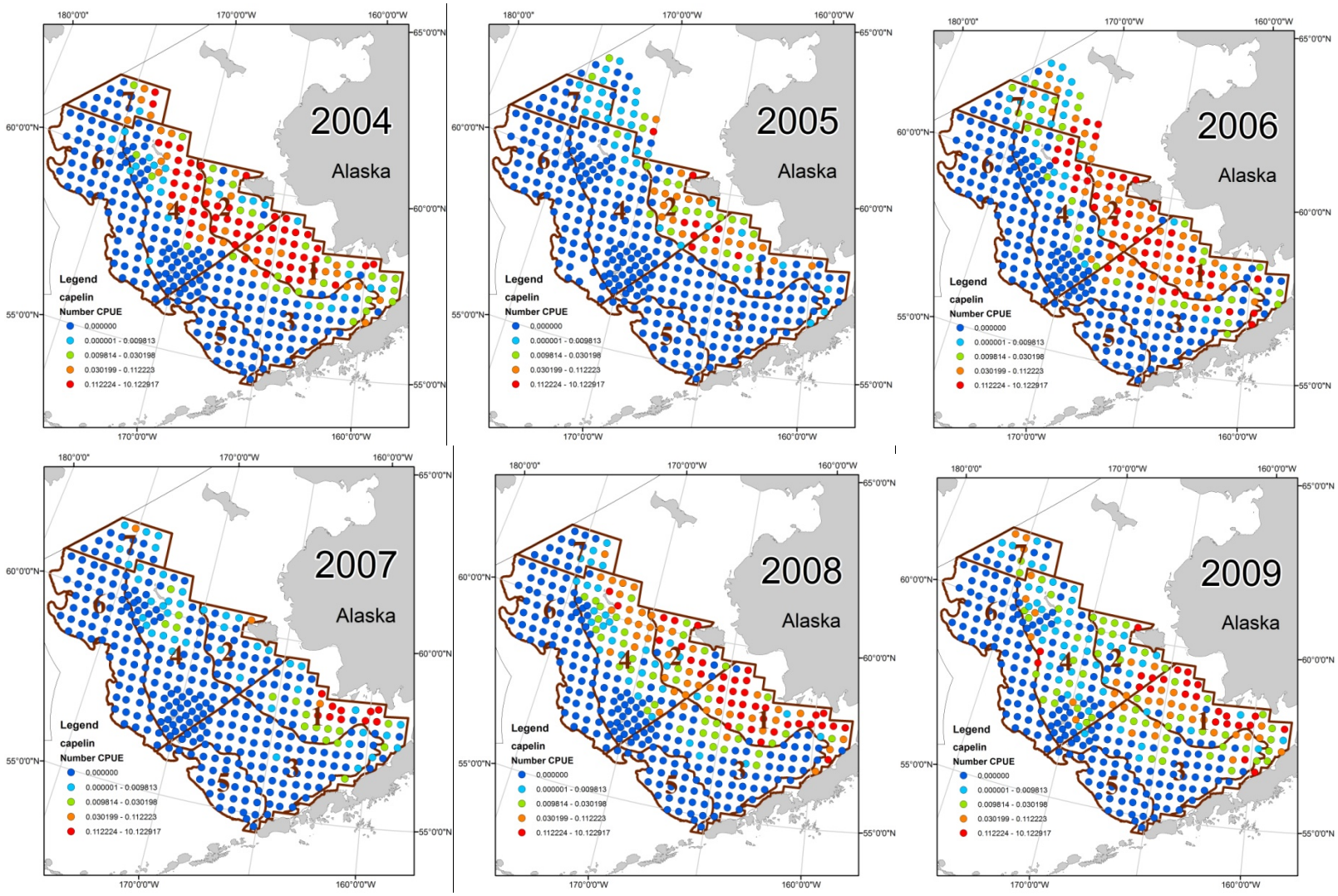

Figure 4. Distribution of capelin numbers/km^2 from bottom trawl data in 2004-2009 overlain with the NMFS bottom trawl survey grid and strata boundaries (5-southern outer domain, 3-southern middle domain, 1 southern inner domain, 6 northern outer domain, 4 northern middle domain, 2 northern inner domain).

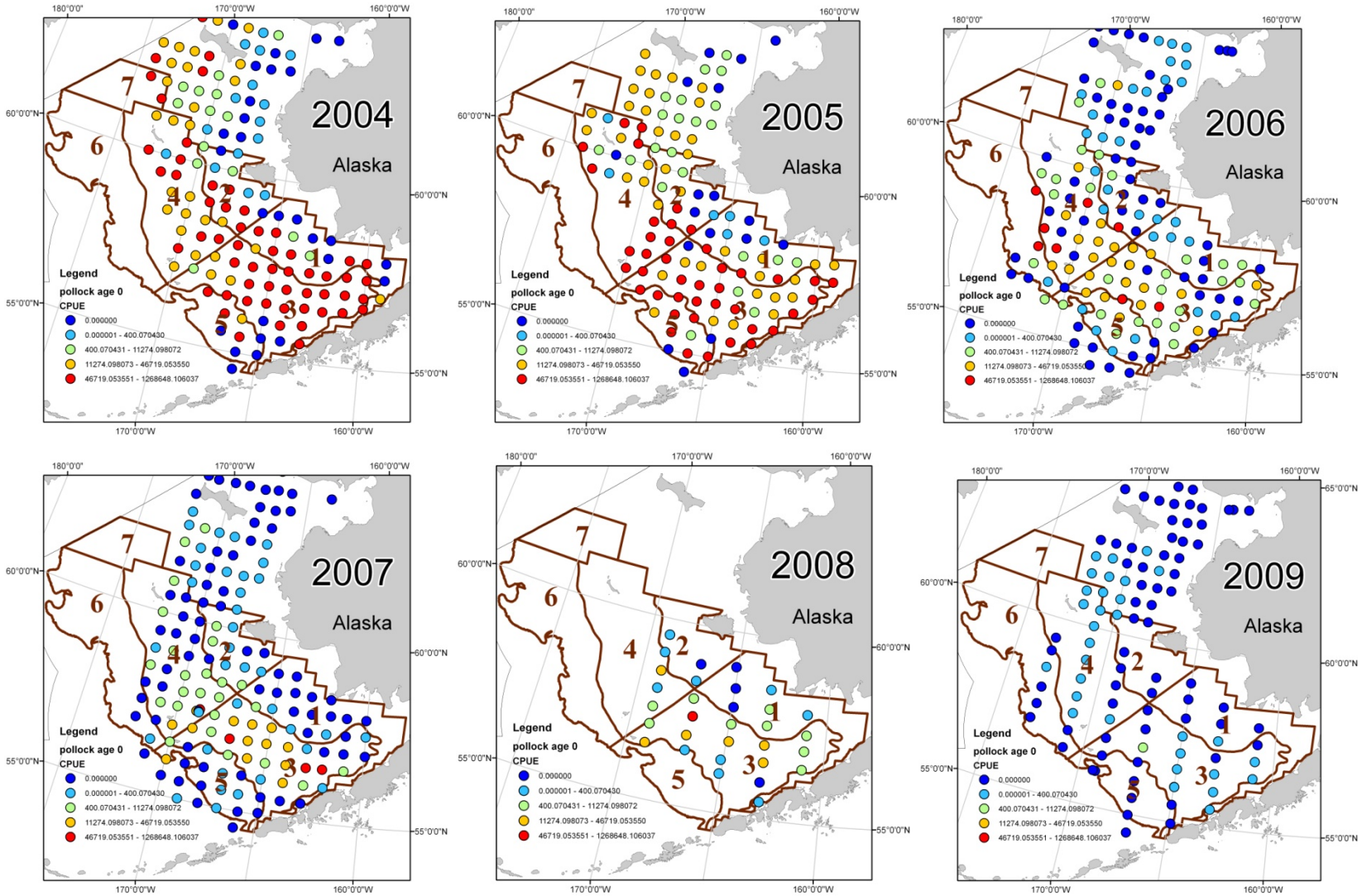

Figure 5. Age-0 pollock log transformed CPUE from BASIS survey data in 2004-2009 overlain with the NMFS bottom trawl survey grid and strata boundaries (as in Figure 4).

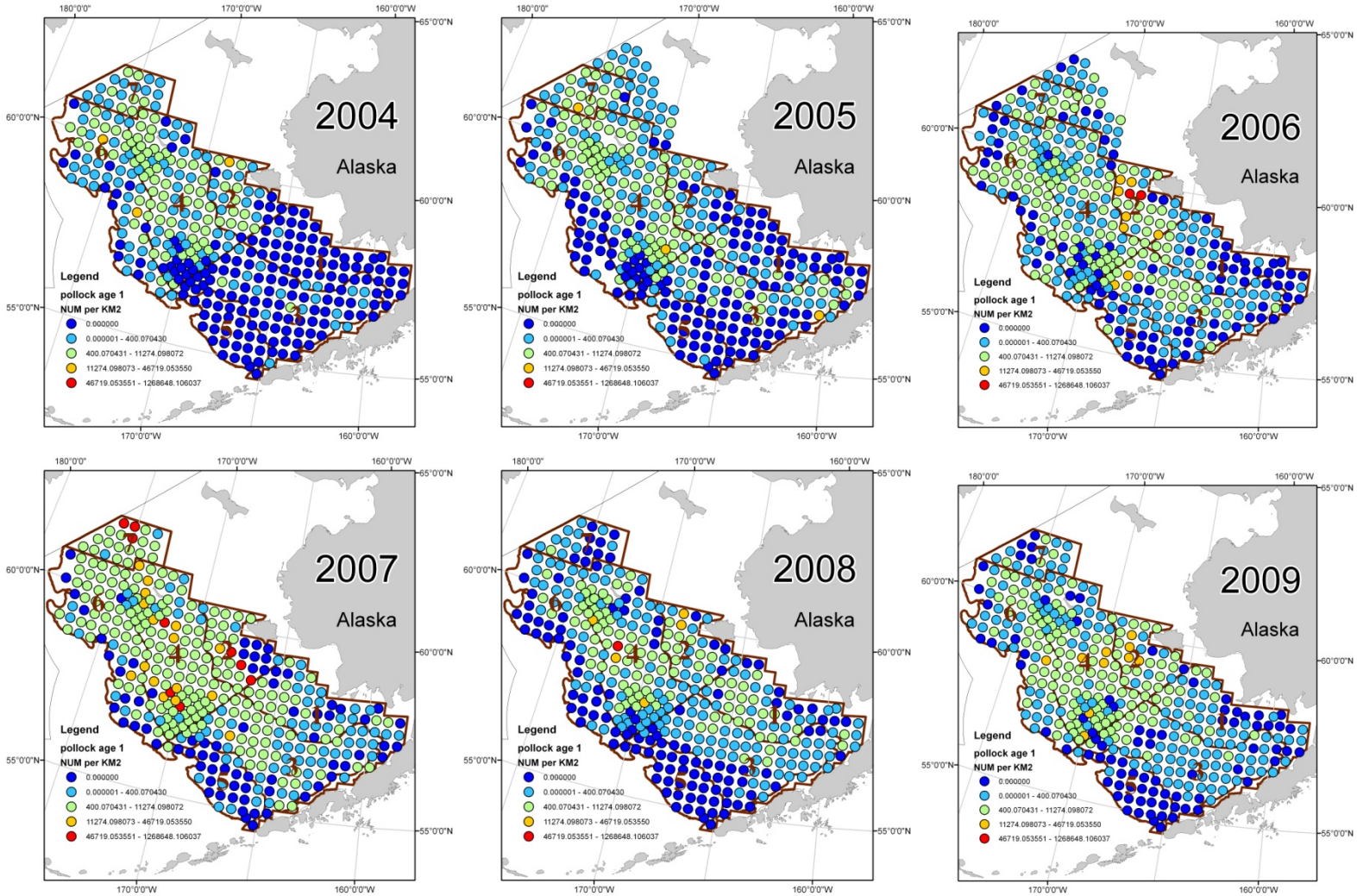

Figure 6. Distribution of age-1 pollock number per km^2 from bottom trawl data collected in 2004-2009 overlain with the NMFS bottom trawl survey grid and strata boundaries (as in Figure 4).

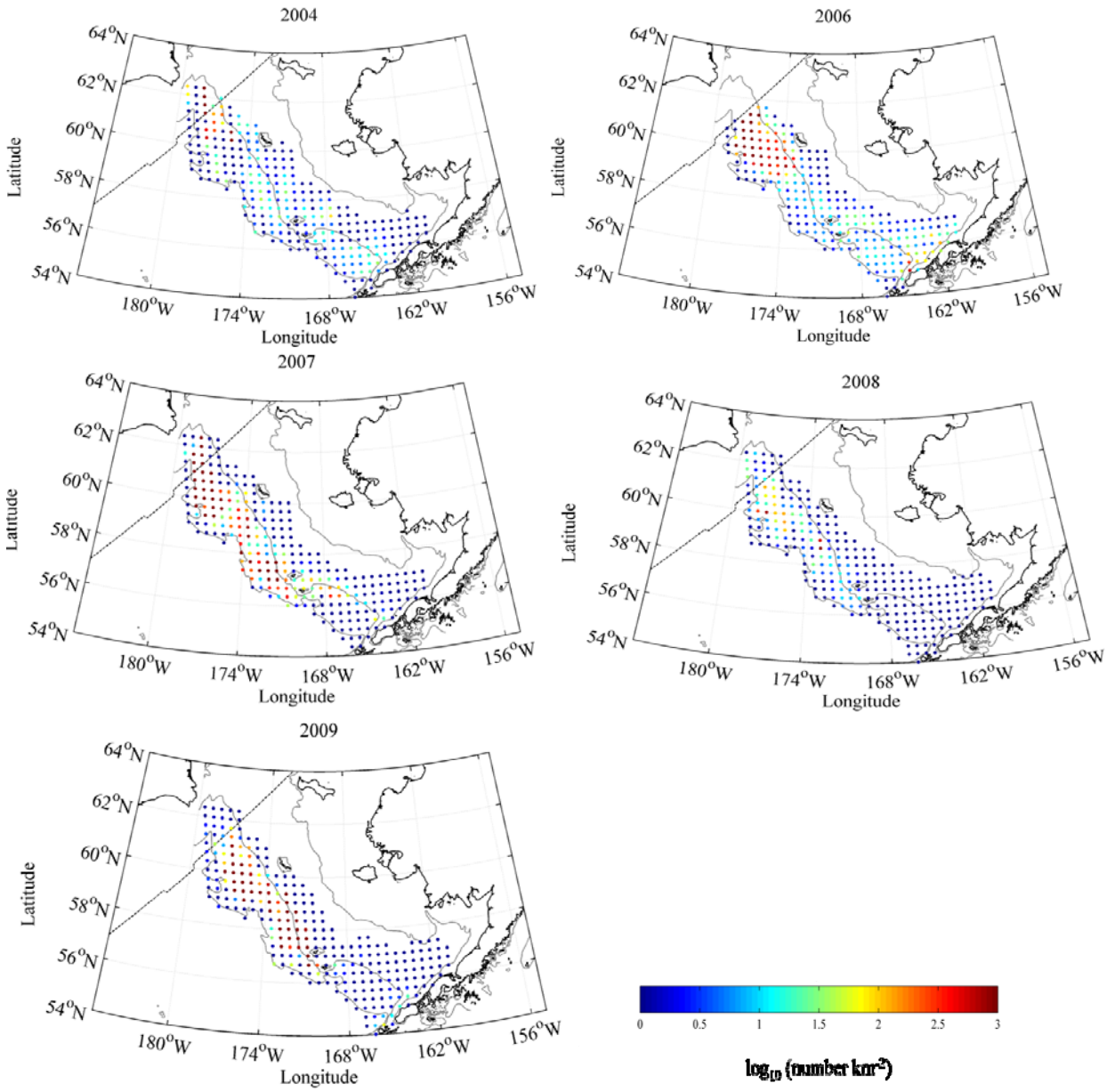

Figure 7. Distribution of age-1 pollock from the midwater acoustic survey. Color scale indicates $\log_{10}$ of density (number per km^2), while circle area is proportional to the square root of density. Gray lines indicate the 50m, 100m, and 200 m isobaths.

Spatial concentration of age-0 in EBS 2004-2007

Age-0 pollock captured in the BASIS surface trawls in August and September were more localized (more patchily distributed) in the EBS in cold years (2006 and 2007) than in warm years (2004 and 2005). The D95 threshold was reached in 23 and 21 stations in 2006 and 2007, respectively, as compared to 44 and 47 stations in 2004 and 2005.

Spatial overlap of bottom trawl survey age-1 pollock and capelin

GIS mapping of the relative proportion of bottom trawl age-1 pollock and capelin present at a given station shows that age-1 pollock and capelin seldom co-exist in the middle domain where age-1 pollock are most abundant (Fig. 8). Age-1 pollock and capelin co-occurred in the northern regions of the survey area, particularly along the 50 m isobaths in 2004. In the southern regions of the survey area, the frequency of stations with both species increased in cold years (2006-2009) relative to warm years (2004 – 2005) (Fig. 8). The average number of stations where age-1 pollock and capelin co-occurred was 67.5 for warm years and 117 for cold years.

GAM analysis of capelin, age-0 pollock and age-1 pollock in EBS 2004-2009

Statistical analysis of the presence-absence data for age-0 pollock in a warm year (2004) revealed that age-0 pollock were broadly dispersed throughout the EBS shelf (deviance explained in Table 1) particularly in stratified waters (above 10° C surface temperature) of the middle domain between 50 and 150m (Fig. 9 top, left). Analysis of age-0 pollock density in a warm year (2004) also showed a region of high CPUE stations between 50 and 150 m and 8° – 12° C (see color scale surfaces, Fig. 9 bottom, left). Statistical analysis of the age-0 pollock probability of occurrence data in a cold year (2009) revealed that age-0 pollock were less abundant over all relative to 2004. Age-0 probability of occurrence data in a representative cold year showed that they were broadly distributed over the shelf with the highest probability of occurrence deep water 100 – 150 m (Fig. 9 top, right). Age-0 density in 2009 was broadly dispersed throughout the EBS shelf (deviance explained in Table 1) particularly in stratified waters (above 10° C surface temperature) of the middle domain between 50 and 150m (Fig. 9 bottom, right). GAM derived maps of probability of occurrence for warm and cold years shows age-0 pollock expanded east of the 50 m isobath and to the north in warm years. In cold years age-0 pollock the density surfaces are more restricted to the southern regions of the middle domain and outer domain (Figure 10). Plots of GAM derived maps of predicted density show similar results and more clearly shows the contraction of the spatial distribution towards the boundary of the outer domain and in the southern portion of the shelf (Fig. 10).

Table 1. Generalized additive model selection results with effective degrees of freedom (EDF), deviance explained, and generalized cross validation score (GCV). Model selected is shaded gray. The models include Year(Y) as a factor, a tensor product smooth of surface temperature (ST), bottom temperature (BT), bottom depth (BD) and their interactions and a thin plate regression spline (s) on UTM position (Z). In the full model splines, smooths are fit separately (AS) for the periods of warm (1; 2004-2005) and cold (2; 2006-2009) spring water temperatures.

Dataset	Quasi Family	Model	EDF	Deviance Explained	GCV
Pollock Age 1	Binomial	=Y+s(Z)$AS_{1,2}$+te(ST,BT,BD)$AS_{1,2}$	87.43	60.7%	0.67
Acoustic		=Y+s(Z)+te(ST,BT,BD)	47.22	39.2%	0.93
		=Y+te(ST,BT,BD)	32.21	29.6%	1.03
		=Y+s(Z)	17.78	20.5%	1.12
	Log Normal	=Y+s(Z)$AS_{1,2}$+te(ST,BT,BD)$AS_{1,2}$	47.16	66.4%	6.91
		=Y+s(Z)+s(Z)AS_2+te(ST,BT,BD)AS_2	43.08	66.6%	6.73
		=Y+s(Z)+te(ST,BT,BD)	39.42	43.1%	11.27
		=Y+te(ST,BT,BD)	24.62	34.1%	12.18
		=Y+s(Z)	18.98	32.2%	12.20
Pollock Age 1	Binomial.	=Y+s(Z)$AS_{1,2}$+te(ST,BT,BD)$AS_{1,2}$	69.67	38.7%	0.83
Bottom Trawl		=Y+s(Z)+te(ST,BT,BD)	52.73	35.2%	0.86
		=Y+te(ST,BT,BD)	23.70	25.7%	0.94
		=Y+s(Z)	22.80	27.9%	0.92
	Log Normal	=Y+s(Z)$AS_{1,2}$+te(ST,BT,BD)$AS_{1,2}$	55.84	36.6%	2.11
		=Y+s(Z)+te(ST,BT,BD)	36.19	33.5%	2.13
		=Y+te(ST,BT,BD)	26.25	18.5%	2.56
		=Y+s(Z)	21.12	28.0%	2.24

Pollock Age 0	Binomial.	=Y+s(Z)$AS_{1,2}$+te(ST,BD)$AS_{1,2}$	28.68	30.5%	1.01
Surface Trawl		=Y+s(Z)+te(ST,BD)	23.59	29.6%	1.00
		=Y+te(ST,BD)	14.15	25.5%	1.01
		=Y+s(Z)	18.69	26.2%	1.02
	Log Normal	=Y+s(Z)$AS_{1,2}$+te(ST,BD)$AS_{1,2}$	32.22	75.3%	4.18
		=Y+s(Z)+te(ST,BD)	13.78	69.1%	4.57
		=Y+te(ST,BD)	12.58	68.7%	4.58
		=Y+s(Z)	18.79	68.9%	4.76
Capelin	Binomial.	=Y+s(Z)$AS_{1,2}$+te(ST,BT,BD)$AS_{1,2}$	74.11	59.6%	0.58
Bottom Trawl		=Y+s(Z)+te(ST,BT,BD)	48.56	55.6%	0.62
		=Y+te(ST,BT,BD)	32.40	51.6%	0.66
		=Y+s(Z)	24.62	51.4%	0.66
	Log Normal	=Y+s(Z)$AS_{1,2}$+te(ST,BT,BD)$AS_{1,2}$	39.05	42.8%	1.73
		=Y+s(Z)+te(ST,BT,BD)	33.66	39.7%	1.78
		=Y+te(ST,BT,BD)	24.49	34.6%	1.86
		=Y+s(Z)	18.43	33.2%	1.86

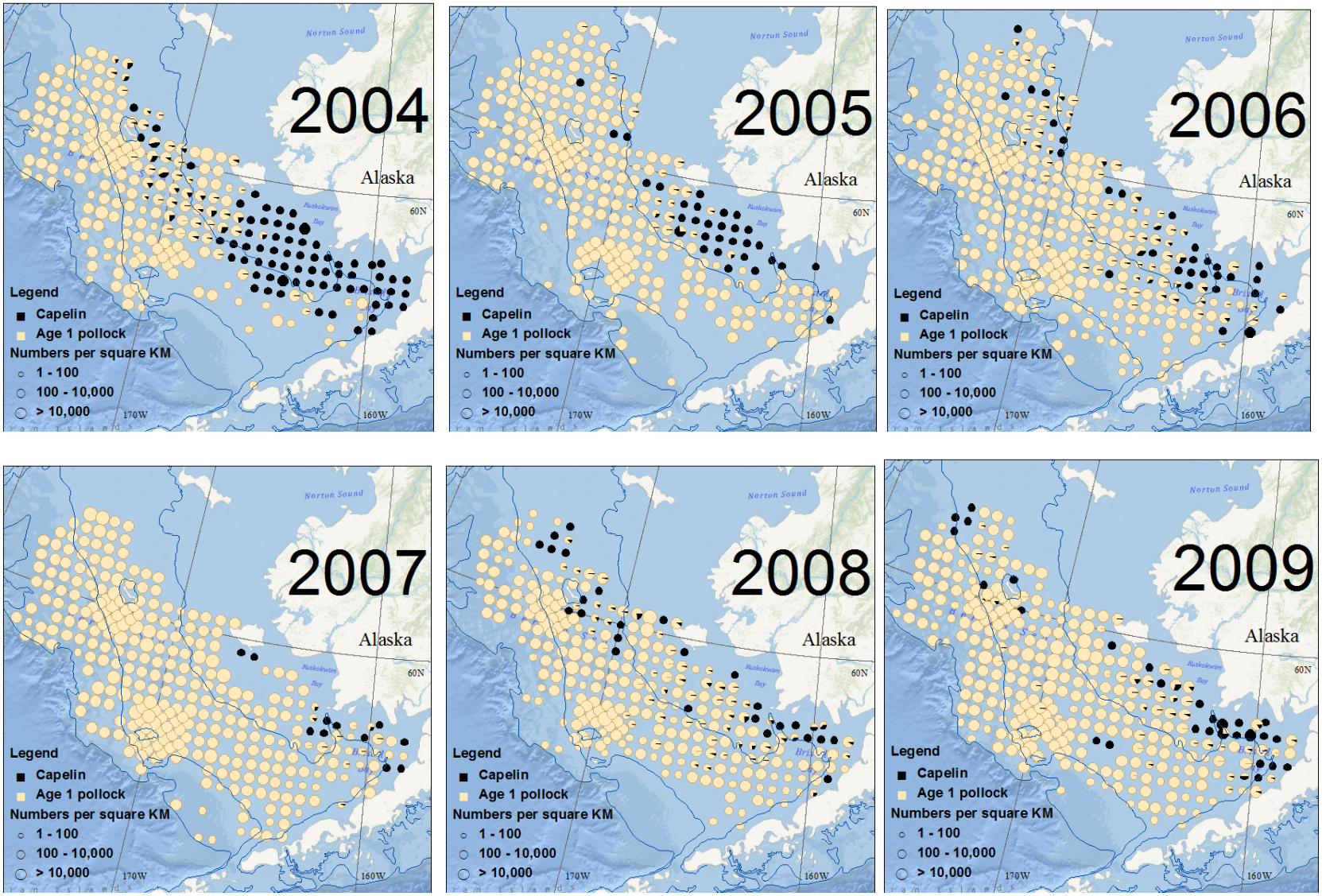

Figure 8. Spatial distribution and co-occurrence of age-1 pollock and capelin from NMFS bottom trawl survey in July 2004-2009. Contour lines as in Figure 1.

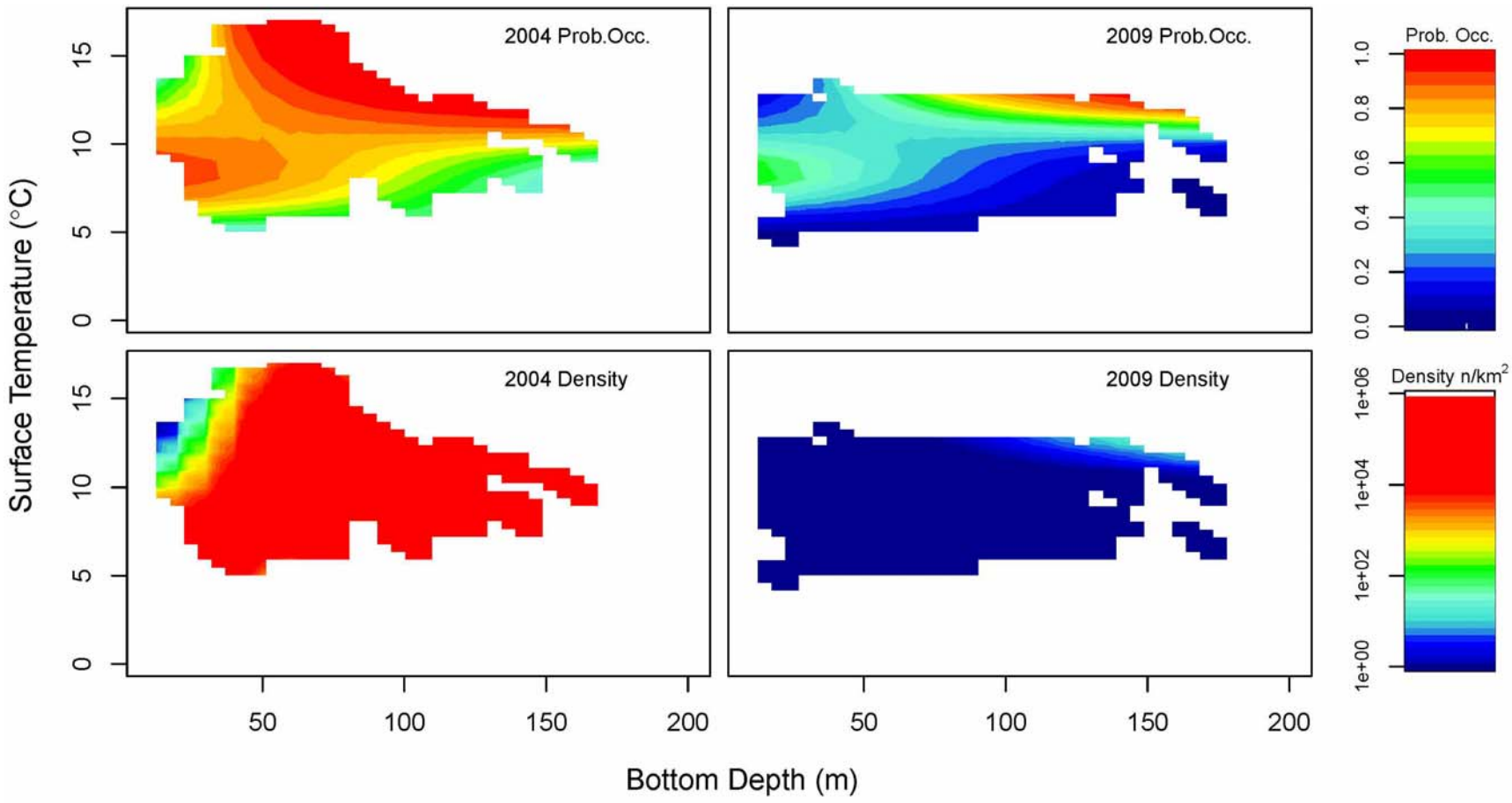

Figure 9. GAM derived BASIS surface trawl age-0 probability of occurrence (top) and density (bottom; number per km^2) profiles over surface temperature and bottom depth for 2004 (left) and 2009 (right). Only the area of the modeled surface for which data were available is presented.

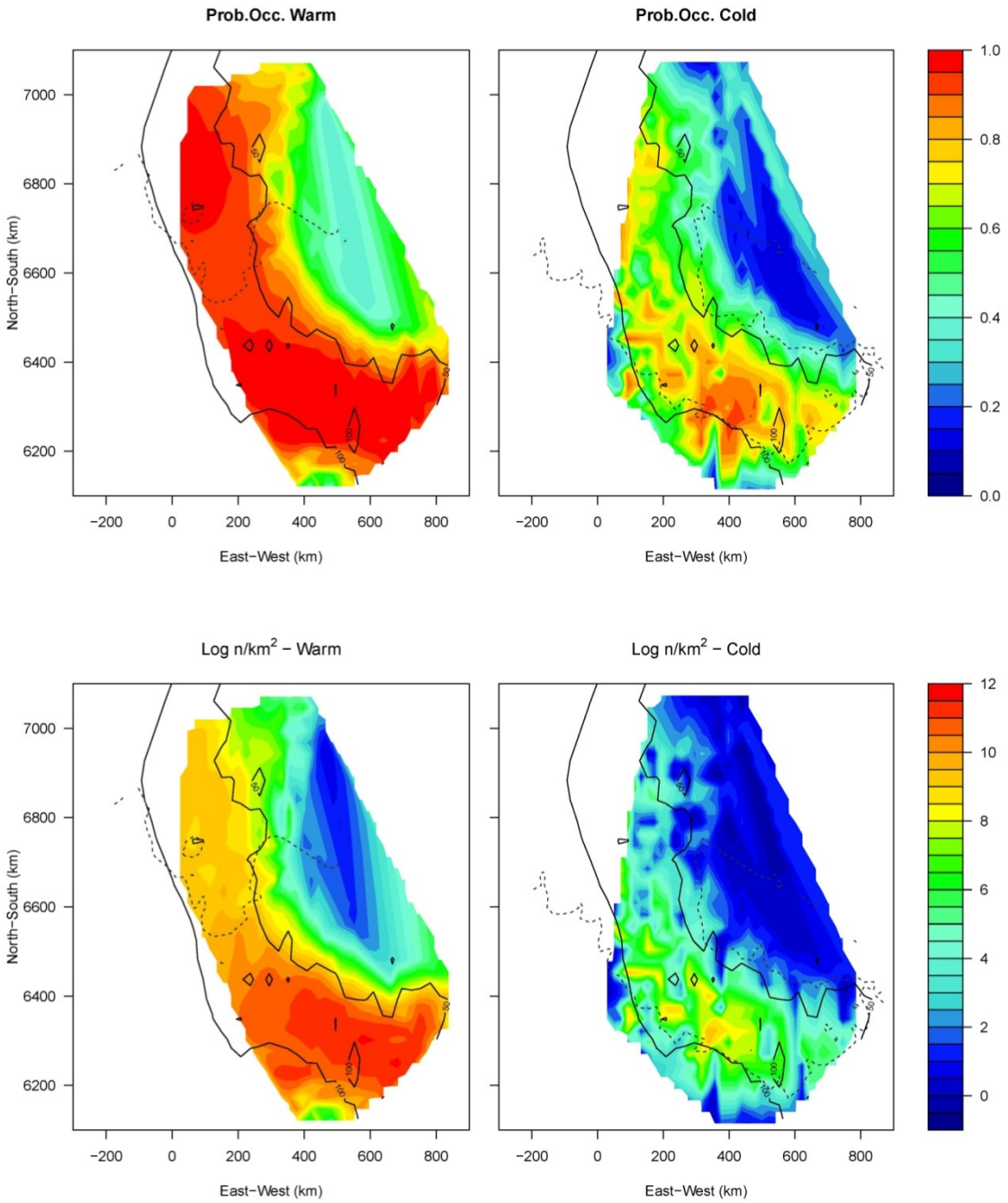

Figure 10. GAM predicted probability of occurrence (top panels) and GAM predicted spatial surfaces of BASIS age-0 density (log(number per km^2)) (bottom panels) for years with warmer (2004-2005; left) and colder (2006, 2007 and 2009; right) spring water temperatures. Black solid lines are the 50 and 100 m isobaths. Dotted line indicates the average location of the 2°C bottom temperature isotherm in warm or cold years

Analysis of the age-1 pollock data revealed significant interactions between bottom depth, surface temperature and bottom temperature (Table 1). Therefore, response surfaces were plotted over surface temperature and bottom temperature by six depth bins (20m, 50m, 70m, 100m, 120m and 150m). Statistical analysis of demersal distributions of age-1 pollock from bottom trawl surveys revealed that presence-absence and density for representative years (2004 and 2009) show a strong depth relationship with a high probability of occurrence or density in the middle domain within the 50-100m depth range (Table 1, Fig. 11). In the warm year (2004), age-1 pollock density within the middle domain (50-100 m) was highest in waters above 2°C (Fig. 11). In contrast, in the cold year (2009), high density pockets of age-1 pollock were observed in stratified waters within the cold pool (<2°C, Fig. 11). GAM derived maps of probability of occurrence or predicted density of age-1 pollock in warm and cold years shows the spatial distribution expands in the middle domain in response to the change in the cold pool. In cold years the area of probability of occurrence and density surfaces expand to the south (Fig. 12).

Acoustic survey age-1 pollock presence absence data in representative warm (2004) and cold (2009) years show a high probability of occurrence in waters greater than 100 m (Fig. 13). Comparison of GAM derived maps of probability of occurrence and density surfaces for 2004 and 2009 shows age-1 pollock occurred in a smaller surface of bottom and surface water temperatures in warm years 2004 than in cold years 2009 (see overall size of surfaces plotted on Fig. 13). This finding may reflect the high abundance of age-1 fish in 2009 resulting from an incoming 2008 year class. GAM derived maps of probability of occurrence in warm or cold years show age-1 pollock expand into the middle domain in warm years, especially in the south (Fig. 14). GAM derived maps of predicted density of acoustic survey age-1 pollock suggests that the northern outer shelf is the region of high density in cold years (Fig. 14). The CPUE plots show that the highest predicted age-1 pollock midwater density was found in the vicinity of the outer front near 100 m in the south during cold years. In the north, the highest predicted densities were in the outer domain (Fig. 14).

Capelin tended to be present in bottom depths of less than 100 m (Figs. 15). In shallow depths, i.e. less than 50 m, capelin were widely distributed across all sampled surface and bottom temperatures (Fig. 1, 5, 15). GAM derived maps of probability of occurrence of bottom trawl capelin in warm and cold years shows capelin tend to remain in the inner domain in warm and cold years, and in warm years there was a higher probability of finding them over the middle shelf, than in cold years (Fig. 16).

Analysis of the year effect for age-0, age-1 and capelin revealed large often order-of-magnitude inter-annual variation. The density of age-0 pollock declined from 2004-2009 (Fig. 17). The density of age-1 pollock in the bottom trawl shows the influence of the strong 2006 (age-1 in 2007) and 2008 year classes

(Fig. 17). The density of age-1 pollock was higher 2006 – 2009 than 2004-2005. The midwater assessment of age-1 pollock does not show these same features or trends although the CPUE in 2004 was lower than 2005 – 2009. The density of capelin showed no clear trend other than a possible annual oscillation (Fig. 17).

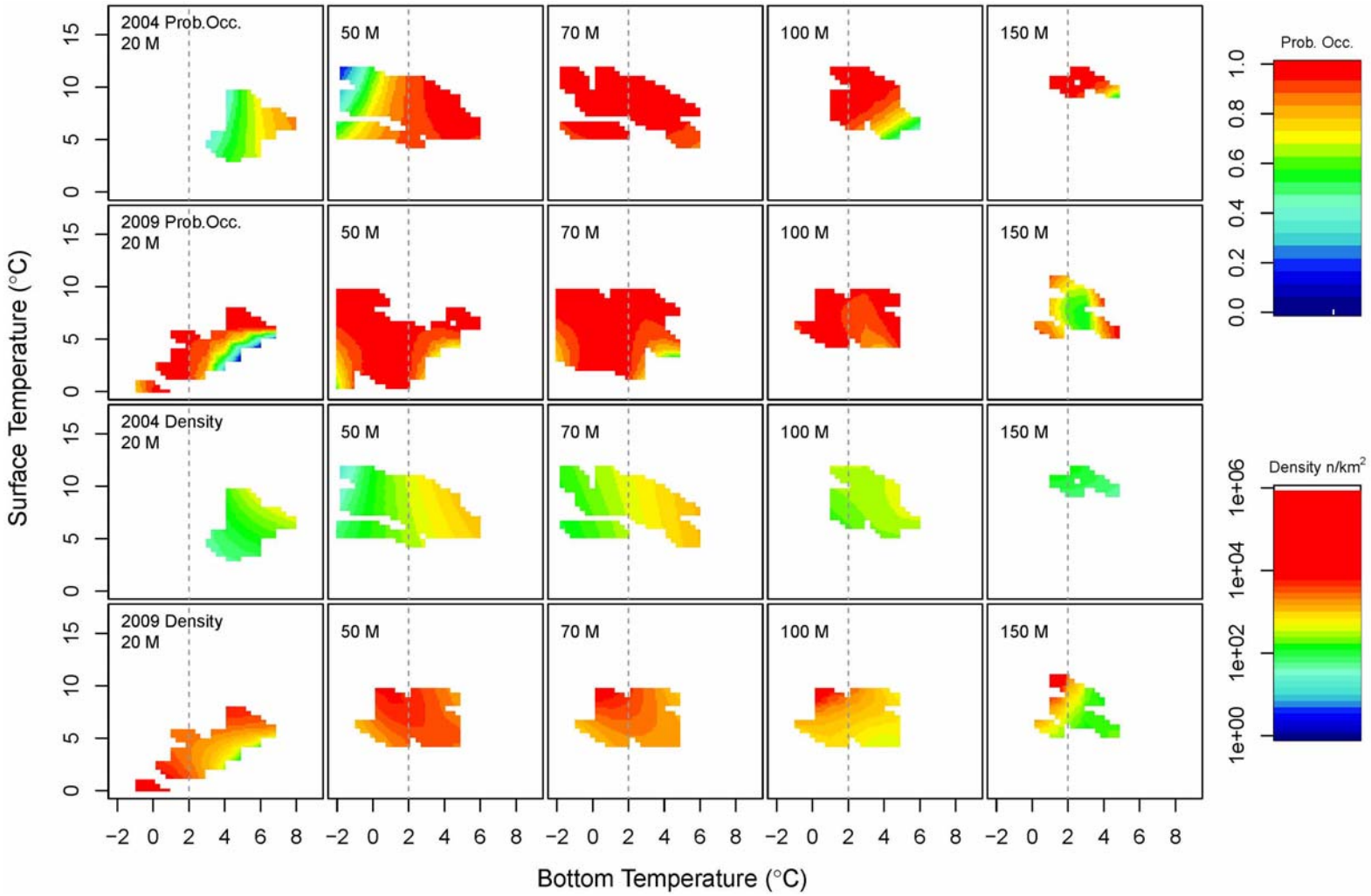

Figure 11. GAM derived bottom trawl survey age-1 pollock probability of occurrence (top two rows) and density (bottom two rows; number per km^2) profiles for 2004 and 2009, over surface and bottom temperature for bottom depth increments of 20, 50, 70, 100, and 150 meters. Only the area of the modeled surface for which data were available are presented. Dotted line indicates the 2°C bottom temperature isotherm which marks the boundary of the cold pool.

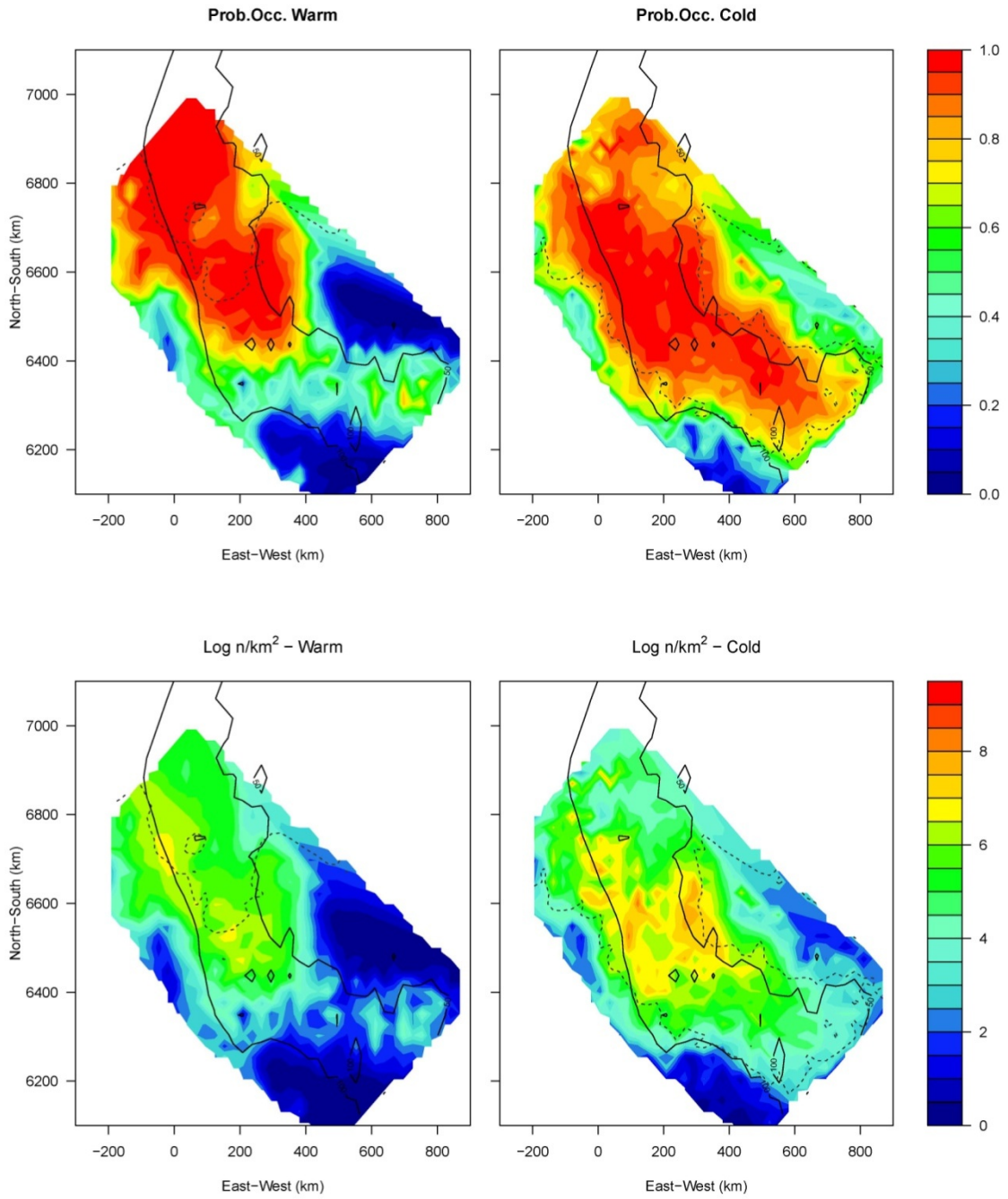

Figure 12. GAM predicted probability of occurrence (top panels) and GAM predicted spatial surfaces of bottom trawl survey age-1 density (log(number per km^2)) (bottom panels) for years with warmer (2004-2005; left) and colder (2006-2009; right) spring water temperatures. Black solid lines are bathymetry in meters. Dotted line indicates the average location of the 2°C bottom temperature isotherm in warm or cold years.

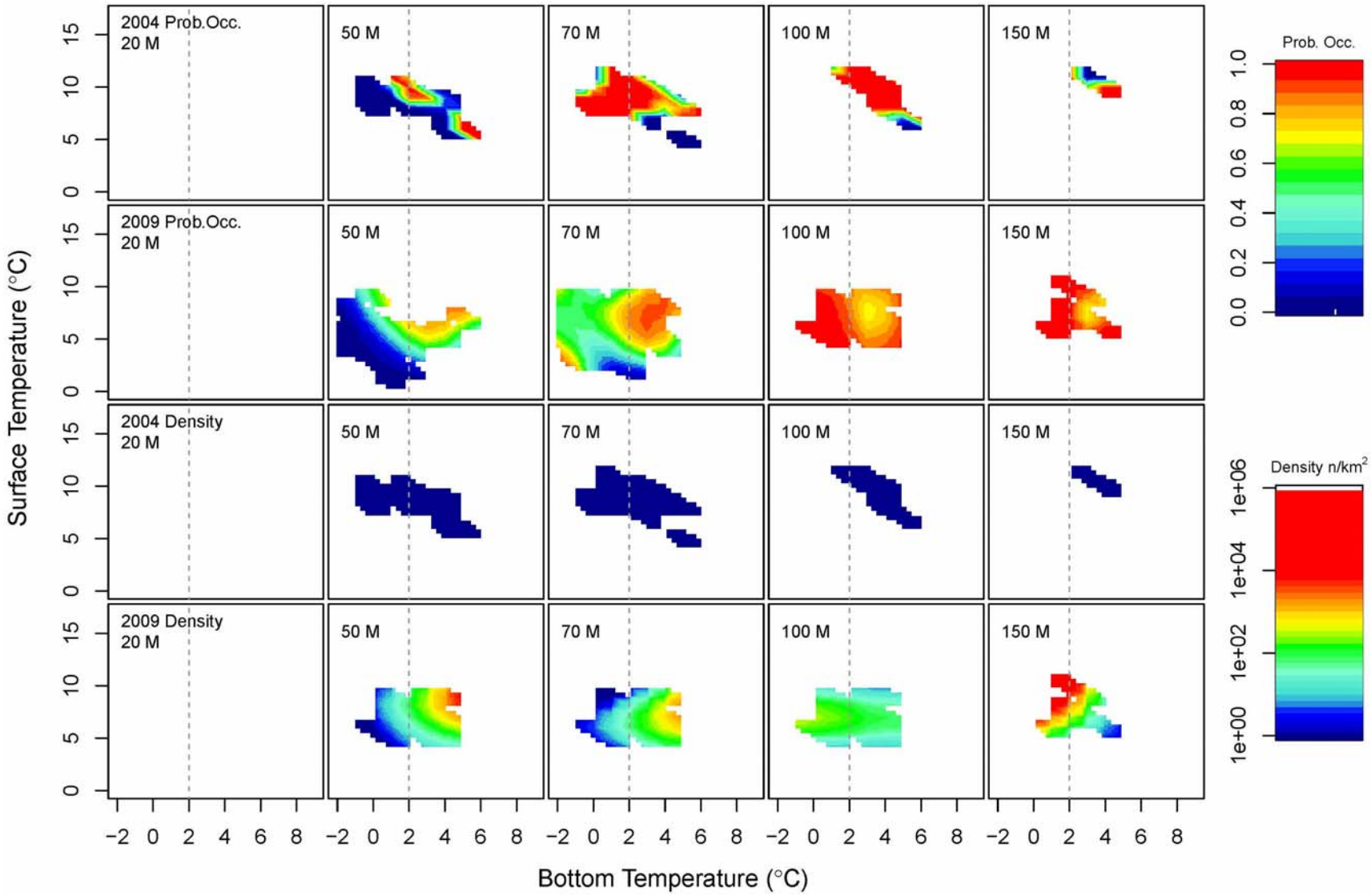

Figure 13. GAM derived acoustic survey age-1 pollock probability of occurrence (top two rows) and density (bottom two rows; number per km^2) profiles for 2004 and 2009. Isotherms as in Figure 11

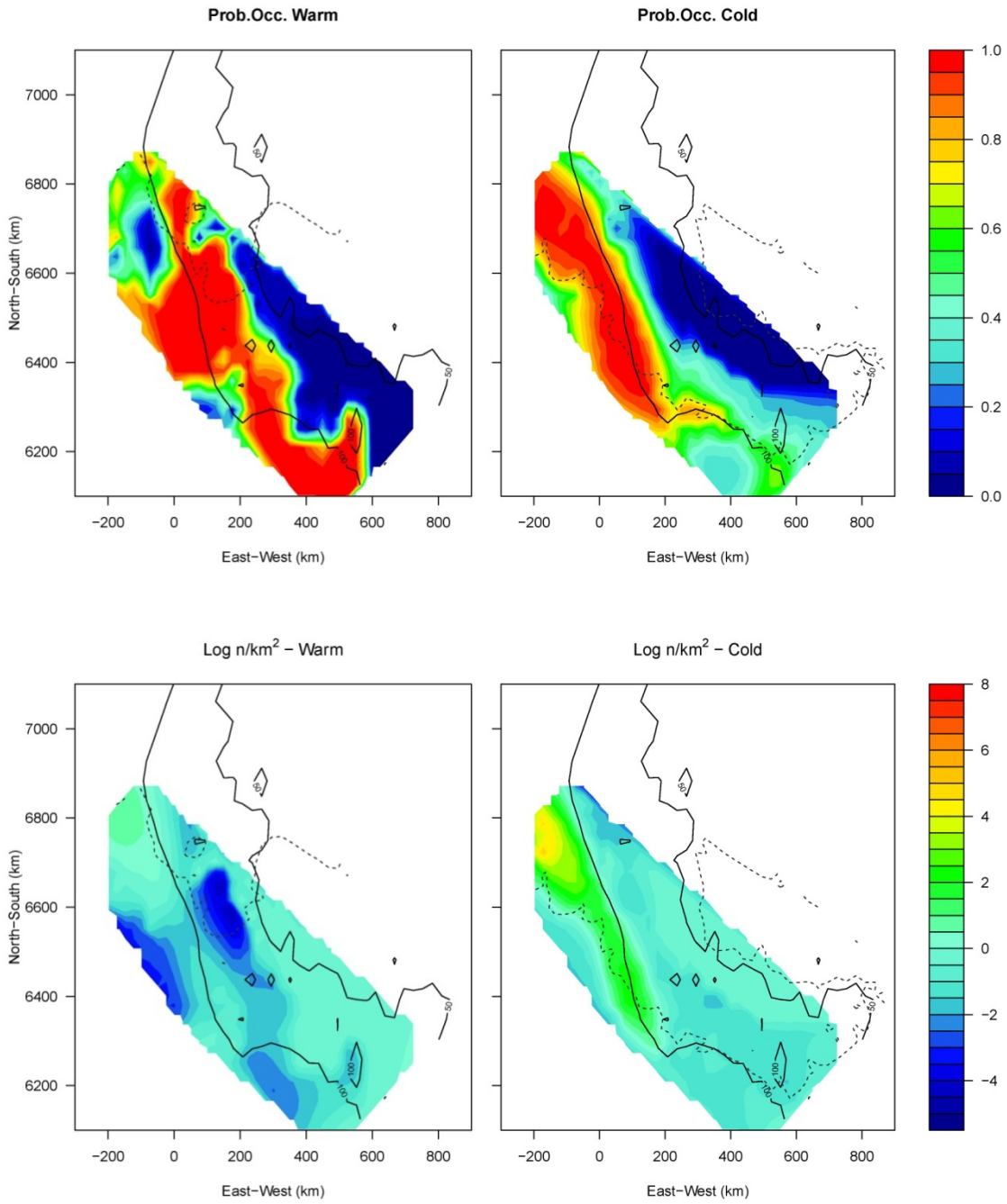

Figure 14. GAM predicted probability of occurrence (top panels) and GAM predicted spatial surfaces of acoustic survey age-1 density (log (number per km^2)) (bottom panels) for years with warmer (2004; left) and colder (2006-2009; right) spring water temperatures. Contours as in Figure 12.

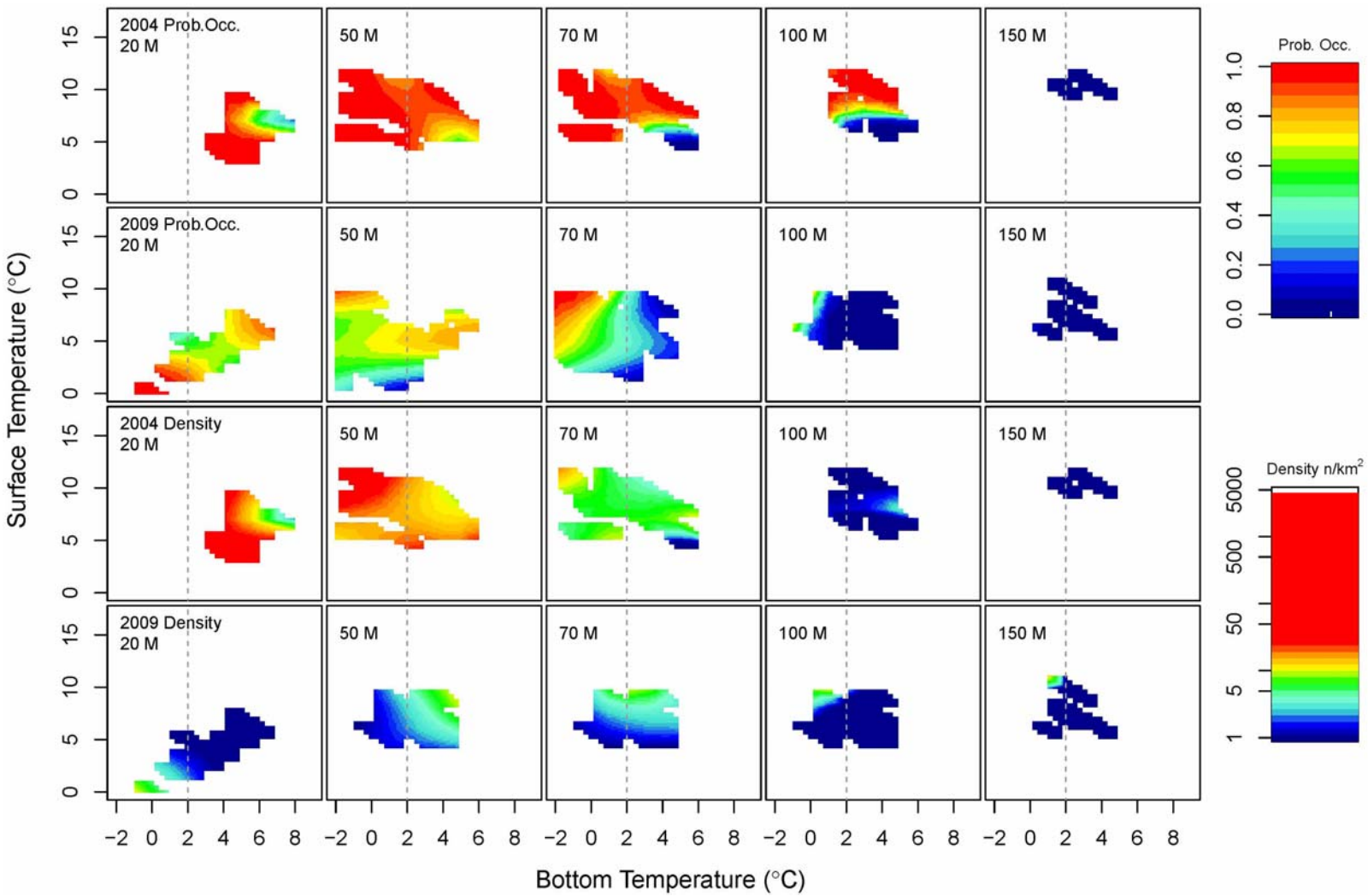

Figure 15. GAM derived NMFS bottom trawl survey capelin probability of occurrence (top two rows) and density (bottom two rows; number per km^2) profiles for 2004 and 2009, over surface and bottom temperature for bottom depth increments of 20, 50, 70, 100, and 150 meters. As in Figure 11.

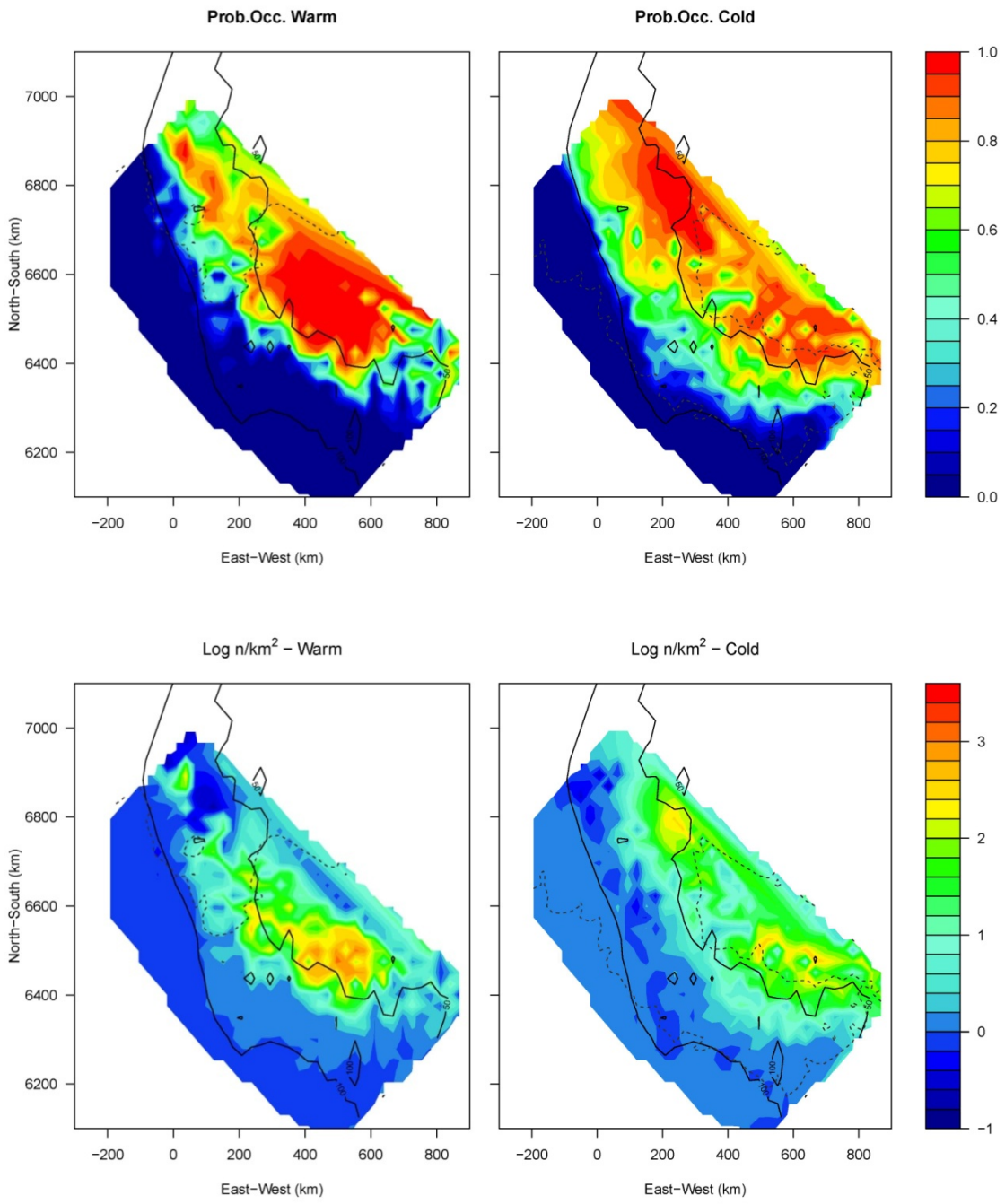

Figure 16. GAM predicted probability of occurrence (top panels) and GAM predicted spatial surfaces of capelin density (log (kg per km^2) (bottom panels) for years with warmer (2004-2005; left) and colder (2006-2009; right) spring water temperatures Isotherms as in Figure 12.

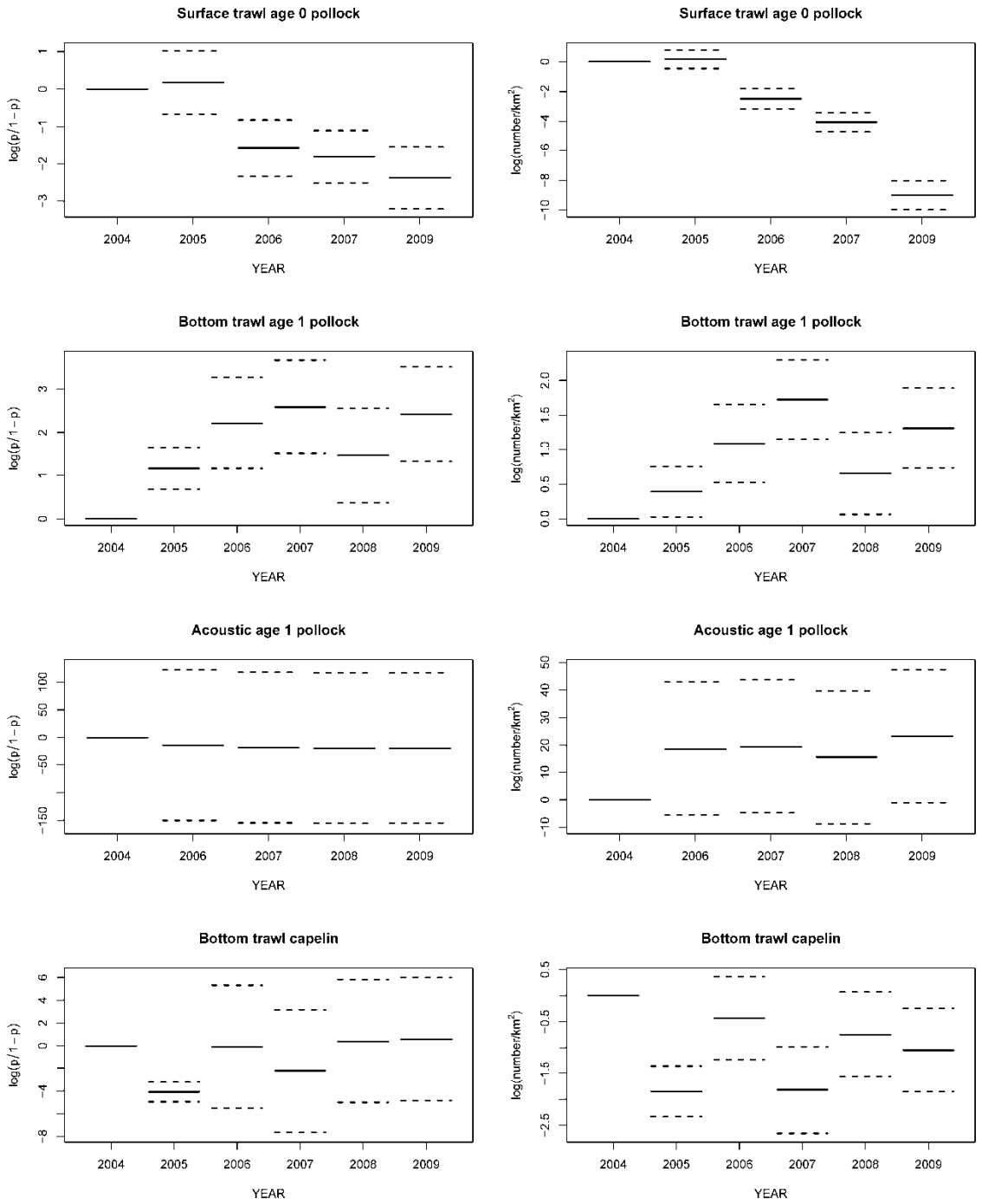

Figure 17. Partial year effect from selected GAMs in either logit(p) in the presence/absence models or log(number per km^2) in the presence only model.

DISCUSSION

Age-1 pollock and capelin

In the Bering Sea, the frontal boundary at 50m bottom depth appeared to partition age-1 pollock and capelin in most years. Age-1 pollock were found in midwater and on the bottom in the middle domain in association with the cold pool. In cold years, midwater, pollock were associated with regions of the northern outer shelf near and along the 100 m isobath. In contrast, capelin were primarily located in the inner domain and the northern middle shelf. These findings are consistent with previous studies by Wyllie-Echeverria and Wooster (1998) and Ciannelli and Bailey (2005).

There are several possible explanations for the observed spatial differences in area occupied by capelin and age-1 pollock. Summer distributions may reflect seasonal behavior. Capelin spawn in spring and summer in nearshore regions (Mundy and Hollowed, 2005), therefore, the shallow concentration of capelin may be indicative of spawning activity. Other possible explanations are discussed below.

At broad spatial scales, the distribution of age-1 pollock (Figures 12, 14) appeared to be associated with potentially productive regions of the Bering Sea shelf. Highest densities of age-1 pollock were usually located in the middle and outer domains north of the Pribilof Islands. Enhanced nutrients or prey aggregation and retention on the middle and outer shelf may lead to consistent prey availability. Kachel et al. (2002) compared the oceanography of the inner and middle domains and found higher concentrations of nutrients at depth in the middle domain and showed pumping of nutrients to the surface occurs in the region of the inner front. Springer et al. 1996 showed that the outer shelf regions are characterized by high primary production. Common prey of age-1 pollock include: copepods, euphausiids, and age-0 pollock (Lang et al., 2000). Coyle et al. (2011) found *Calanus marshallae*, an important zooplankton prey for age-1 pollock, was more abundant in the middle domain than in the inner domain in cold years. Ressler et al. (2012) found pockets of high euphausiid abundance in north of the Pribilofs and along the shelf break, but the highest concentrations of euphausiids were often located in the southern portions of the middle and outer domain; however, they also noted that the spatial distribution of euphausiid abundance may have reflected the impact of predation by pollock, making interpretation of association between these species difficult. The consistent pattern of age-1 pollock distribution northwest of the Pribilof Islands (Fig. 12, 14) could make this region a predictable hotspot for place-based foragers that take age-1 pollock as prey (Piatt et al., 2006; Decker et al., 1995; Sigler et al., 2012).

The BEST/BSIERP program hypothesized that climate and ocean conditions influence the intensity of predator-prey relationships which may impact location of zoogeographic provinces through bottom-up processes, and that reduced cold pool extent would increase overlap of inner domain forage fish and

piscivores. Our results suggest changes in spatial distribution and shifts in overlap of capelin and age-1 pollock in response to changing ocean conditions. Predicted density of age-1 pollock shows their spatial distribution expanded southward in cold years, perhaps in response to a similar shift in the cold pool, though this pattern was more dramatic for demersal (Fig. 12) than for midwater age-1 pollock (Fig. 14). Our findings and those of other investigators suggest that capelin and age-1 pollock have adopted spatial distributions that buffer them from groundfish predators. Ciannelli and Bailey (2005) suggested that the distribution of capelin is a predator avoidance response and suggested that the inner domain represents a refuge from capelin predators such as Pacific cod. In support of this hypothesis, Decker et al. (1995) note that capelin were more prevalent in seabird diets prior to the 1977 regime shift and the subsequent outburst of gadoid / flatfish (some of which consume capelin). These findings would suggest that as Pacific cod, and more recently arrowtooth flounder, abundance expanded in the middle domain (Mueter and Litzow 2008, Spencer 2008), the spatial distribution of capelin contracted to the inner domain. Our analysis showed age-1 pollock tolerated cooler bottom temperatures (<1° C) in the middle domain, a finding consistent with earlier studies by Wyllie Echevveria and Wooster (1998). Wyllie Echevveria and Wooster (1998) proposed tolerance for cooler waters buffered age-1 pollock from groundfish predators such as adult pollock and arrowtooth flounder. More recent studies confirm that adult pollock and arrowtooth flounder appear to expand inshore into the middle domain in warm years as the area of the cold pool contracts (Overland and Stabeno 2004, Spencer 2008, Fig 8. in Ressler et al. 2012). Synthesis of these findings suggests that the overlap between age-1 pollock and groundfish predators may be buffered because age-1 pollock aggregated in cooler waters in the north in warm years and cold years. These data do not provide evidence that warm ocean conditions will result in increased predator prey interactions for age-1 pollock with other groundfish predators, as long as a cold pool forms in the northern Bering Sea.

The BEST/BSIERP program posed a third hypothesis, that reduced cold pool extent would increase the competitive interactions between forage fish. On the contrary, our data suggest that competitive interactions between age-1 pollock and capelin are higher in cold years. In cold years, the spatial distribution of demersal age-1 pollock extended to the south, and the spatial distribution of capelin was concentrated in the near-shore regions of the inner domain, and capelin and age-1 pollock co-occurred more frequently (Fig. 8). However, this assumes that the vertical distribution during foraging was similar (i.e. that the demersal pollock feed nearer the surface where the capelin are most abundant). The mechanisms underlying these shifts in distribution are unknown, but may be related to winds, spring ice, storms and initial thermal conditions that influence the strength of the inner front (Kachel et al. 2002) or currents (Stabeno et al., 2012) that may also influence frontal boundaries. Other studies in the Gulf of

Alaska (GOA) showed that habitats of age-1 pollock and capelin were spatially partitioned by fronts. Hollowed et al. (2007) found that in the GOA, age-1 pollock resided in the tidal mixed shallow water region of high primary production, while capelin typically resided in deeper waters of troughs off the eastside of Kodiak Island. Logerwell et al. (2007 and 2010) found that when age-1 pollock were absent or the front weakened, capelin crossed into shallow water. This finding suggests that age-1 pollock and capelin may exhibit complex interactions and may be distributed with respect to fronts or other physical oceanographic features. It is notable that age-1 pollock typically occupied shallower water than capelin in the GOA, while the reverse was observed in the Bering Sea. Comparative analysis of these differences may provide an opportunity to improve our understanding of species specific responses to predation, or competitive interactions or a combination of these factors. Process studies are needed to assess whether barriers partitioning age-1 pollock and capelin would be weaker in cold years.

Age-1 pollock and age-0 pollock

Our study also suggests complex interactions between age-0 and age-1 pollock in the middle domain. Age-0 pollock were dispersed broadly across the Bering Sea shelf consistent with previous studies (e.g. Wespestad et al., 2000), but densities were generally highest in the south, while age-1 pollock densities were highest in the north, though their distributions overlapped in the middle domain, particularly in warm years (Fig. 10, 12). The southern middle domain was a region of strong stratification in all years (Figure 3, Stabeno et al., 2010), which could have led to vertical separation of age-1 and age-0 pollock (Traynor, 1986, Bailey, 1989). Vertical and spatial partitioning of habitat by age-0 and age-1 pollock can be explained as a response to prey availability, ontogenetic changes in behavior, and avoidance of predators. Laboratory and field observations showed that age-0 pollock were typically distributed above the thermocline during summer, but that this pattern was not true in all cases (Olla et al. 1996). Laboratory experiments showed age-0 pollock responded to bright light, prey concentrations, and predators with larger juveniles moving deeper than smaller juveniles. Swartzman et al. (2002) reported that size influenced the probability that age-0 pollock would move through the thermocline. They found age-0s greater than 55 mm exhibited diel migrations through the thermocline, while smaller age-0s did not. Unpublished observations taken during BASIS surveys also showed large concentrations of age-0 pollock below as well as above the thermocline in some years (J. Horne, Personal communication, University of Washington, Seattle, WA). BASIS surface trawl data used here would not detect these deeper concentrations, and thus may be indicative of the distribution pattern of smaller age-0s and a conservative estimate of the density of age-0 fish.

Francis and Bailey (1983) hypothesized that stratification creates a refuge from predation for age-0 pollock, and Coyle et al. (2011) reported that water column stability over the middle domain was

associated with increased survival of age-0 pollock. However, while the surface waters may serve as a refuge from groundfish predators such as adult pollock and Pacific cod, it may not serve as a refuge from salmon. Age-0 pollock were a major dietary component of western Alaska salmon during years with warm sea temperatures and low abundance of large zooplankton on the eastern Bering Sea shelf (Farley et al., 2009, Farley and Trudel, 2009, Farley and Moss, 2009). Immature salmon captured along the eastern Bering Sea shelf during years with warm sea temperatures were also feeding on walleye pollock (Davis et al. 2009) with immature chum salmon feeding almost exclusively on age-0 pollock (J. Murphy, personal comm. NOAA/AFSC Auke Bay Laboratory, 17109 Point Lena Loop Road, Juneau, AK). The years with warm sea temperatures and low abundances of large zooplankton (Coyle et al. 2011, Stabeno et al., 2012a) coincided with increased relative abundance of western Alaska juvenile salmon (Farley et al. 2009) and immature chum salmon. These observations suggest that the rate of predation on age-0 pollock by salmon may be mediated by the abundance of alternate prey. Willette et al. (2001) found a similar predation mediation mechanism was occurring in Prince William Sound.

The area occupied by age-0 pollock decreased in cold years, perhaps as a result of their decreased abundance, an increased exposure to predation, or because their prey (which includes copepods, euphausiids, and small fishes; Coyle et al., 2011) was more abundant. Olla et al. (1996) reviewed the literature on the onset of group behavior in walleye pollock, finding that juvenile pollock exhibited an innate attraction to each other, forming denser groups when they were exposed to predators and spreading out under conditions of patchy or dispersed food. The energy density of age-0 pollock and the abundance of large copepods and euphausiids was higher in cold years than in warm years (Moss et al. 2009, Hunt et al. 2011, Ressler et al. 2012), implying better feeding conditions. The increased dispersion of age-0s in warm years (though overall abundance was greater) when prey availability was reduced is consistent with the hypothesis that age-0 pollock may have spread out in warm years in search of food. Secondly, if onset of schooling behavior is triggered by the predation risk and summer stratification present in the middle domain creates a refuge from predation, then the onset of schooling or grouping behavior in age-0 pollock may be delayed until fall when the stratification of the middle domain breaks down.

Habitat partitioning by forage fish

This analysis provides evidence for habitat partitioning by forage fish on the Bering Sea shelf. Statistical inference indicates that interannual variability in the spatial extent of the cold pool is an important feature defining the ocean habitats used by forage fishes. Examination of geostrophic flow features in 2008 also suggests a possible association between cross-shelf flow patterns and the spatial distribution of midwater age-1 pollock in the outer domain. These relationships portend that climate change may influence habitat associations of, and interactions between, forages fishes. Recent studies project that by 2050, the Bering

Sea will warm by 2° C (Hollowed et al. 2009). This warming is likely to impact sea ice extent, the area of the cold pool, and the strength of frontal boundaries. Our study suggests that interspecies interaction between age-1 pollock and capelin in the future may be low because the spatial overlap between species was reduced in warm years. The inshore distribution of capelin and greater tolerance by age-1 pollock of colder temperatures than their predators (e.g. adult walleye pollock and arrowtooth flounder) may continue to buffer their exposure to predation by larger fishes, as long as a cold pool continues to form on the northern Bering Sea shelf in summer (Stabeno et al. 2012a,b). Finally, Mueter et al. (2011) project that as temperatures warm it will result in increased stress on age-0 pollock due to less abundant high lipid zooplankton prey (Coyle et al., 2011, Stabeno et al., 2012a), and on-shelf expansion of predators (Spencer et al., 2008). Our study suggests that this stress will be further exacerbated by the broader spatial distribution of age-0 pollock, if consequent spatial overlap with age-1 pollock is not mitigated by vertical habitat partitioning.

ACKNOWLEDGEMENTS

We thank Angie Grieg for technical support that improved this paper. We thank Michael Sigler and the editorial staff at AFSC for useful comments and suggestions. The manuscript was improved by the careful reading of four reviewers. We express our thanks to the officers and crew of the NOAA ship *Miller Freeman* and *Oscar Dyson* and the Fishing vessels *Aldebaran, Epic Explorer, Northern Explorer*, and *Sea Storm*. This project was supported by NPRB BSIERP and was BEST/BSIERP publication #34. This is contribution number 3653 from NOAA's Pacific Marine Environmental Laboratory. The findings and conclusions in this paper are those of the authors and do not necessarily represent the views of the National Marine Fisheries Service.

Chapter 5: Defining eco-regions

Although funded through a separate mechanism (the Comparative Analysis of Marine Ecosystem Organization program, NMFS), recent analyses conducted by researchers at the Resource Ecology and Fishery Management Division of the Alaska Fisheries Science Center also correspond with research objectives articulated through this grant. This research aimed to better define species distributions and association with physical habitat variables and delineate distinct ecological regions with the eastern Bering Sea based on biological community organization and response to physical habitat. This research and it relevance to NPRB objectives are described briefly in the hypotheses regarding oceanographic influences on fish distributions.

Chapter 5.a. Analytical approach to deliniating ecological regions in marine systems

This paper is in revision for details refer to:

Baker, M. R. and A. B. Hollowed. In Revision. Delineating ecological regions in marine systems: synthesis of physical structure and community composition to inform spatial management. Deep Sea Research II.

ABSTRACT

Species distribution and abundance patterns are driven by many factors, including threshold environmental tolerances and resource preferences and species interactions. To visualize how individual species were distributed relative to dominant physical drivers (temperature and depth) in the ecosystem, we developed contour plots of mean weighted biomass for all species consistently sampled via bottom trawl methods and compared trends between function guilds within the eastern Bering Sea. To compare species distributions in geographic terms, we determined weighted abundance (biomass) and the coefficient of variation in species abundance over the available time series (1982-2012) and used inverse distance weighting to interpolate and develop surface plots of core habitat and patterns in variation in habitat use over time (use of marginal habitat). We also applied random forest methods to quantify the extent to which environmental variables predict distribution patterns for individual species and species guilds. Partial dependence plots were developed to illustrate distinct environmental thresholds for species within the system and variable importance was evaluated to assess the relative importance of each environmental predictor variable to species distribution.

INTRODUCTION

Physical structure and physical forcing mechanisms combine with biological responses and interactions at the species level and within communities to organize marine systems in unique ways at multiple spatial scales. We depicted species distributions across habitat gradients. In particular, we examined the role of habitat in moderating species distributions and interactions, assessed the importance of habitat in defining species distributions, and quantified the importance of dominant physical variables for individual species. By identifying species distributions and delineating distinct ecoregions in the eastern Bering Sea, distinct distribution patterns among species within function guilds were identified. These approaches have since been applied in other Alaska systems (e.g. Aleutian Islands, Gulf of Alaska). Patterns elucidate trends in species abundance, identify potential competitive and predatory interactions, and characterize resource partitioning among species within guilds. In addition, this research demonstrates how distinct climatic periods will shift habitat gradients. Understanding how habitat governs species interactions and impact managed species is a key element of Essential Fish Habitat and the Habitat Assessment Improvement plans developed and implemented by NOAA.

METHODS

To assess importance of physical variables on individual species distributions, we applied random forest methods. Random forests employ ensemble learning, generating multiple classifiers and aggregating results (package randomForest, R Development Core Team 2011) to develop synthesized output. Building on classification and regression tree models, random forests account for interactions among predictor variables with no underlying assumptions of normally distributed data. Successive regression trees are constructed using an independent bootstrapped sample of the dataset; each node is split using the best among a subset of predictors randomly chosen at that node. By combining the predictions from multiple trees, random forest methods achieve high classification accuracy. Building on random forest outputs, partial dependence plots were applied to provide a graphical description of the marginal effect of each physical variable on the predicted probability of species presence. Given a regression function (e.g. species presence) dependent on many variables (e.g. habitat and environmental variables), we determined the marginal or threshold effect of each variable for each species. Variable importance plots were developed to show the relative importance of each variable to species presence, calculated as the increase in model prediction error when data for that particular variable is permuted while all other variables remain unchanged (e.g. the misclassification rate for data not included in the bootstrap sample, divided by the standard error).

RESULTS

Contour plots of species distribution by temperature and depth

Stark and distinct contrasts are evident in the distribution of species within different functional guilds as a function of two main physical drivers within the eastern Bering Sea – temperature and depth. The presence of resident cold bottom temperature (i.e. cold pool) is clearly evident in the system and this dominant feature appears to shape and constrain species distributions in many instances. Within each functional group for fish, we noted similar trends in thermo-bathemetric preferences. There are important also differences by age and life stage as demonstrated by walleye pollock (*Gadus chalcogrammus*, Fig. 1). Pelagic planktivores (Fig. 2, panel 1) are found almost exclusively in shallow areas of the shelf and show significant habitat partitioning as a function of temperature. Pelagic piscivores (Fig. 2, panel 2) are found almost exclusively at depth and within relatively narrow temperature tolerances, demonstrating distinct partitioning by temperature. With the exception of Bering flounder (*Hippoglossoides robustus*, which resides exclusively within colder waters), these species avoid the cold pool. Demersal piscivores (Fig. 2, panel 3) are relatively evenly distributed across the shelf, and relatively impervious to temperature and depth constraints, such that their plots closely mirror plots of the system itself (Fig. 1, top plot). Benthivores (Fig. 3, panel 1) range broadly across the shelf, most relatively widely distributed across temperature, but, in some instances, segregated by depth. We found strong evidence for resource partitioning in most invertebrate groups (Fig. 3, panels 2-6). Sessile benthic invertebrates may serve as a useful proxy for habitat. Although bivalve (e.g. mussel, scallop, clam) distributions are clearly correlated with substrate type, contour plots of temperature and depth also distinctly display habitat partitioning among these species. Cnidarians species groups (e.g. anemones, corals, sea pens) also differentiate by temperature and depth profile. Ascidians and sponges are found primarily within a narrow depth band corresponding to the middle domain. Aggregate classes of echinoderms (brittle stars, basket stars, sea stars, urchins, sand dollars) display unique patterns with abundance concentrated across temperature gradients in the middle domain (and inner domain for sea stars) and at depth (except sandollars), but with a prominent gap between, suggesting distinct species groupings at these two depths.

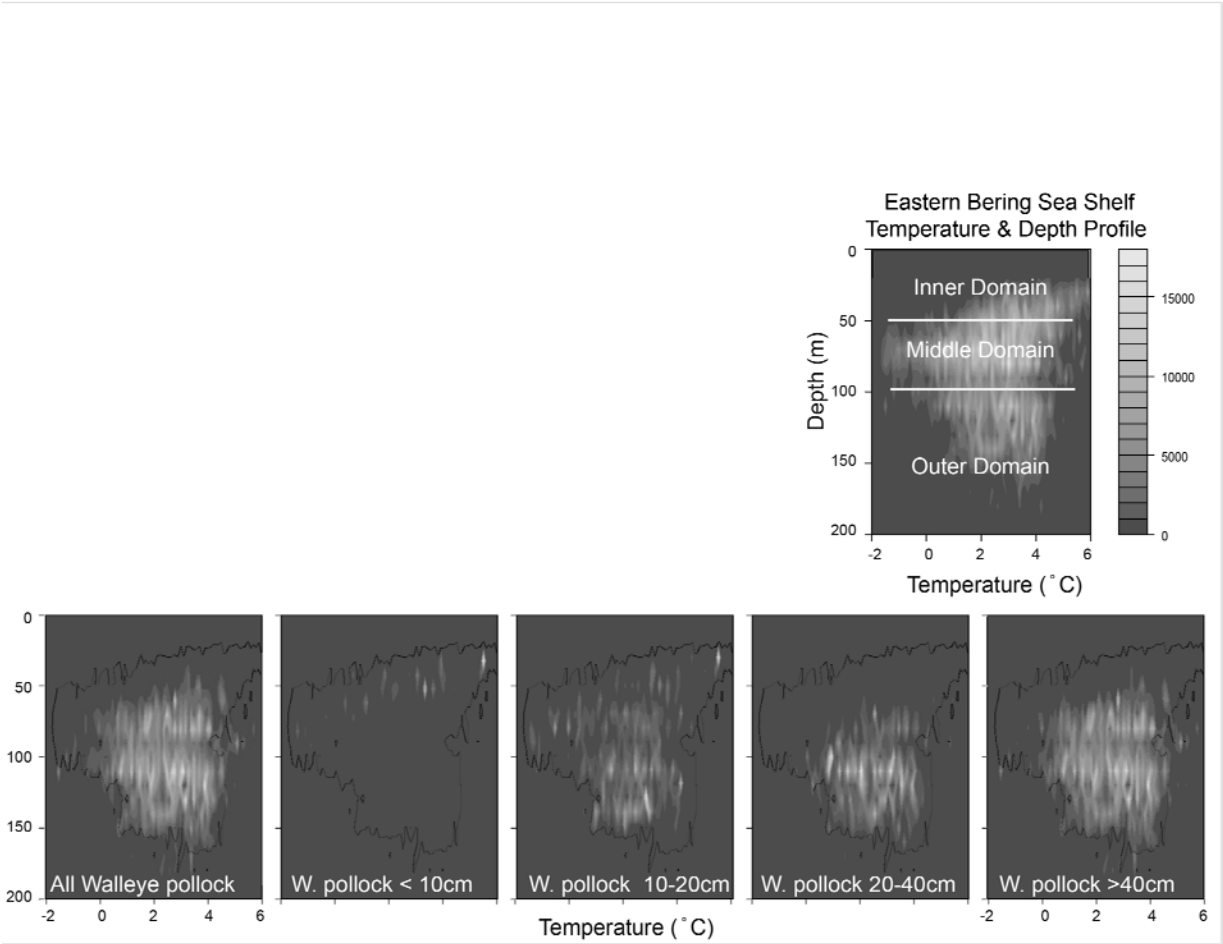

Figure 1. Contour plots of relative species density (biomass) according to temperature and depth (lighter areas indicate higher densities). A contour plot of the entire system is shown as the top figure with distinctions indicating the three main domains of the eastern Bering Sea shelf and a black outline of the system-wide footprint is included on each species graph for reference.

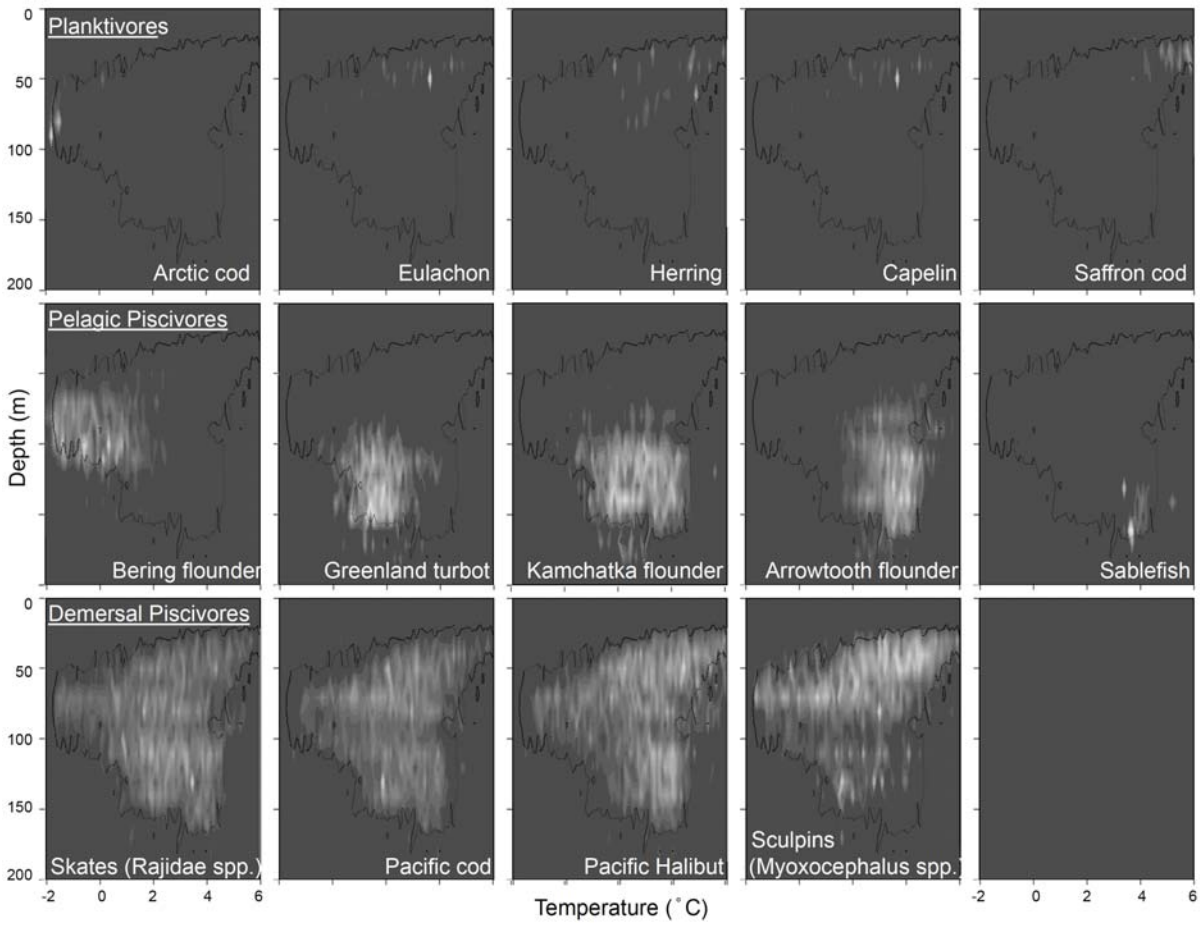

Figure 2 (panels 1-3). Contour plots of relative species density (biomass) according to temperature and depth (lighter areas indicate higher densities). A black outline of the system-wide footprint is included on each species graph for reference.

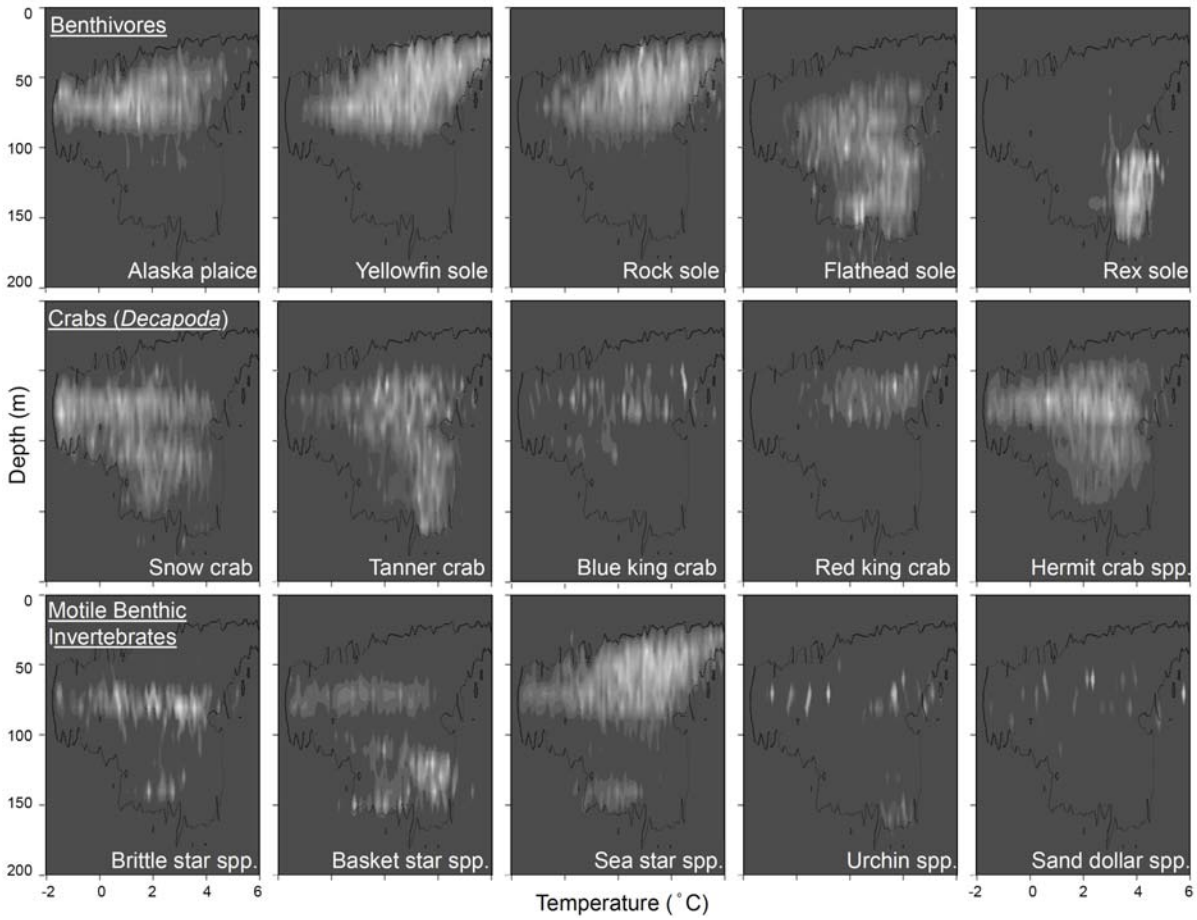

Figure 3 (panels 1-3). Contour plots of relative species density (biomass) according to temperature and depth (lighter areas indicate higher densities). A black outline of the system-wide footprint is included on each species graph for reference.

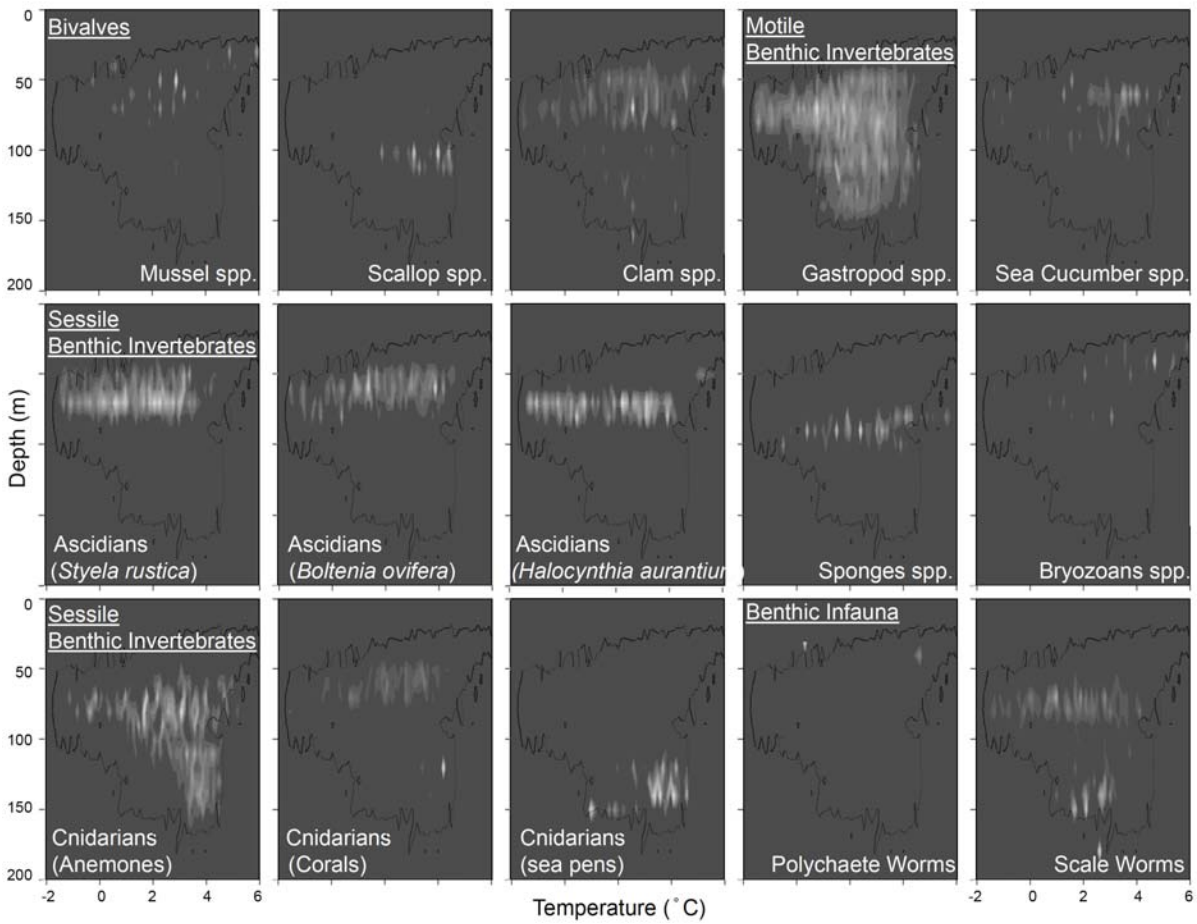

Figure 3 (panels 4-6). Contour plots of relative species density (biomass) according to temperature and depth (lighter areas indicate higher densities). A black outline of the system-wide footprint is included on each species graph for reference.

Maps of Species Distribution (Total Abundance and Coefficient of Variation in Abundance)

Integrating data across the entire time series allowed us to outline areas of core habitat for each species or species group (Fig. 4). The use of time series in these maps allows us to examine variation in abundance as a means to evaluate distribution patterns. Maps of CV of abundance provide a useful complement to maps of total abundance (Fig. 5). As expected, sessile benthic invertebrates are relatively invariant in their abundance in space and time, such that these animals serve as reliable proxies for habitat type. More surprisingly, highly mobile pelagic planktivores also demonstrate relatively consistent habitat use, with fluctuations in abundance in core habitat and minimal range expansion. Variation in biomass abundance was contained within areas of core habitat, such that as abundance and/or growth in these populations rise and fall, densities increase and decrease within core habitat, absent range expansion. This is in stark contrast to patterns displayed by benthivores as well as most demersal and pelagic piscivore species,

where variation in abundance occurs predominantly at the margins of core habitat. Benthivores display shifts in range across the shelf but minimal variation in core habitat. Pelagic piscivores display variation in the northern range of the continental shelf, but minimal variation in core habitat. Demersal piscivores display relatively high variation across most of shelf, but relatively constant in areas of core habitat with fluctuations in abundance associated with marginal habitats and in the area of the cold pool.

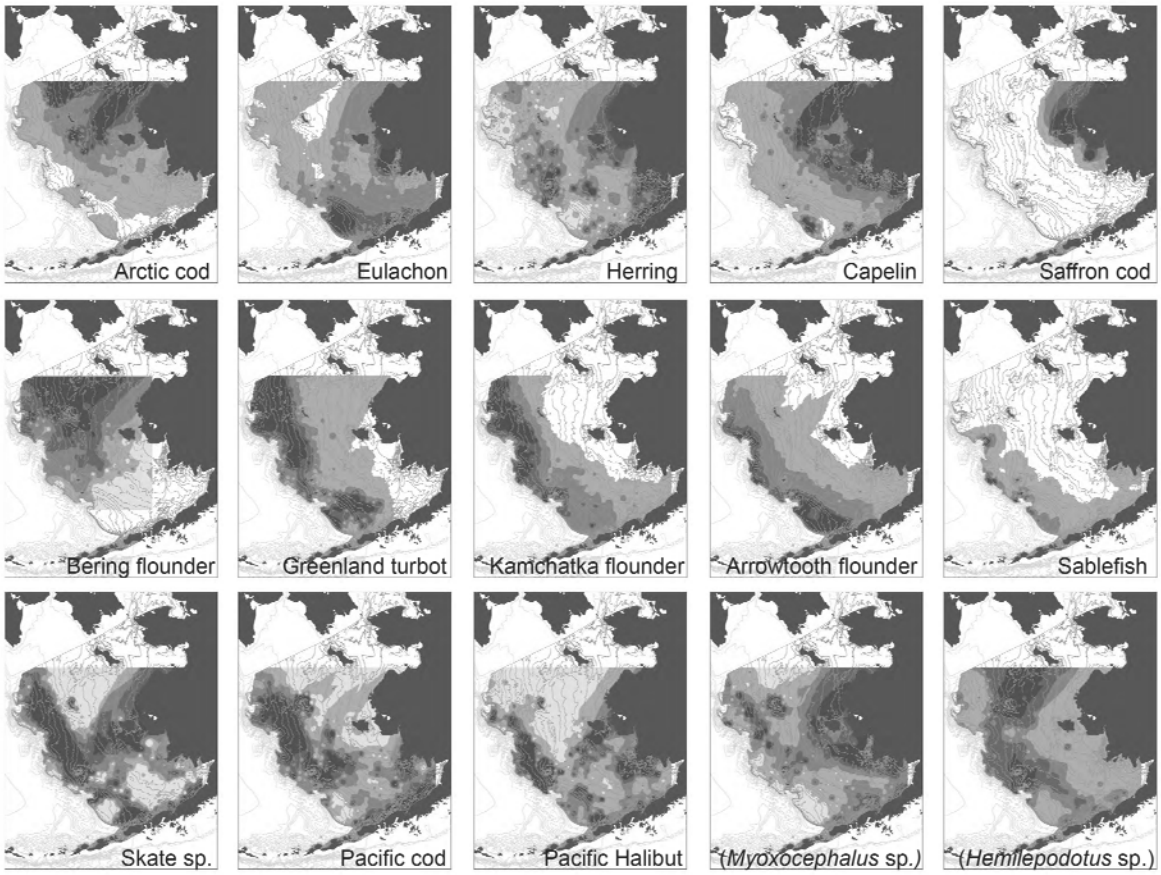

Figure 4. Maps of core habitat (Inverse Distance Weighting) of relative abundance (species biomass) over the time series. Darker areas denote higher concentrations and core habitats.

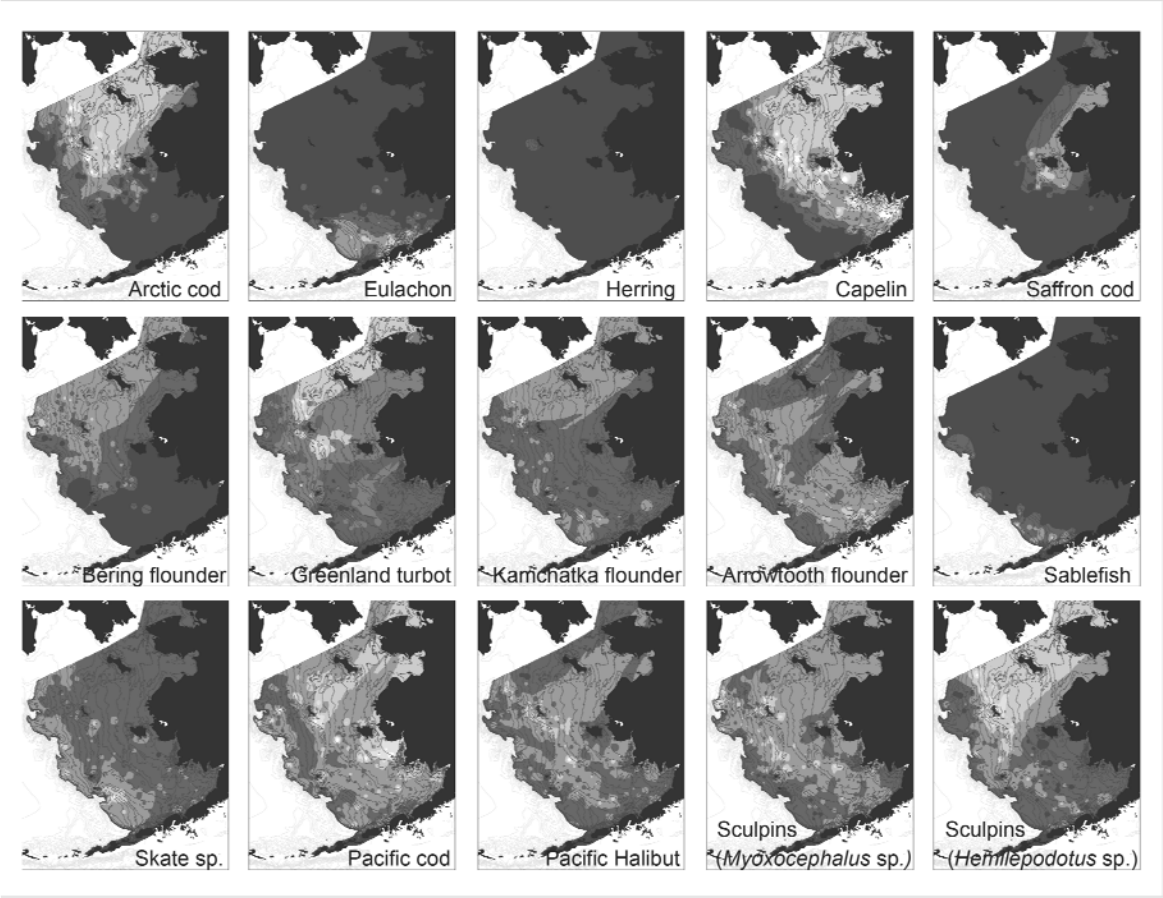

Figure 5. Maps of core habitat (Inverse Distance Weighting) of the coefficient of variation in abundance (species biomass) over the time series. Lighter areas denote areas of consistent use/presence..

Partial dependence plots

We developed partial dependence plots for four ecologically dominant fish species (Gaichas and Francis 2008) in the system (Fig. 6). These plots indicate important breakpoints and nonlinear trends. Partial dependence plots confirmed and quantified trends identified through contour plots and distribution maps. Pacific cod (*Gadus macrocephalus*) range widely and appear relatively indifferent to most physical variables. Pacific halibut (*Hippoglossus stenolepis*) are more sensitive to bottom temperature and depth (100m) thresholds and prefer substrate coarseness of a particular range (25-50). Walleye Pollock are sensitive to bottom (4°C) and surface (6°C) temperature thresholds. Arrowtooth flounder (*Atheresthes stomias*) are strongly constrained by bottom (2°C) and surface (5°C) temperature thresholds as well as thresholds related to stratification and substrate.

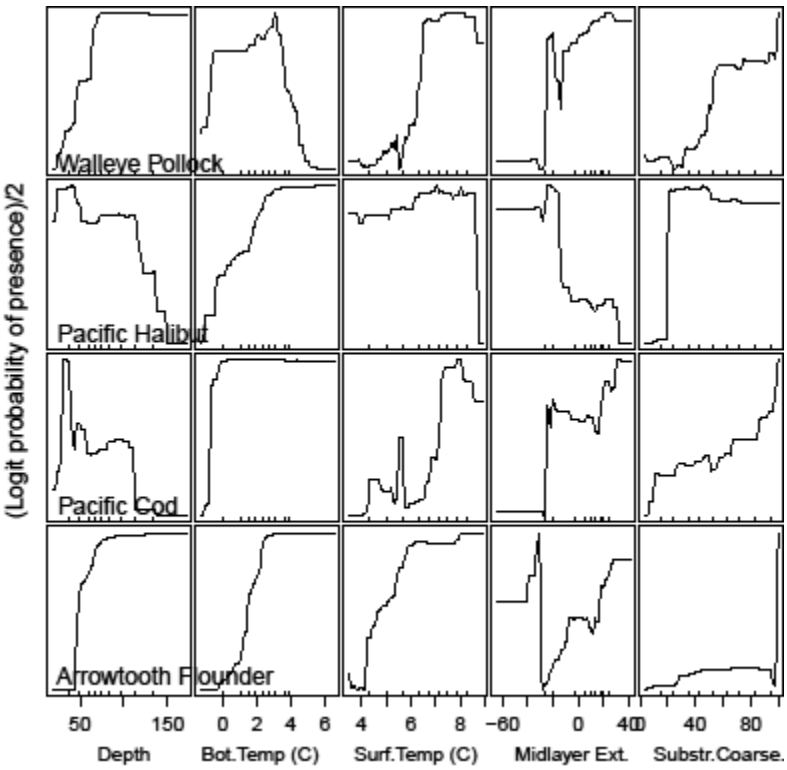

Figure 6. Partial dependence plots (random forest output) detailing threshold shifts in species abundance (logit probability of presence) for individual physical predictor variables, controlling for other variables.

Variable importance measures

Variable importance measures for prominent species in each functional guild suggest differences among guilds. Common dominant predictors for each group of species were: arctic species (species with >50% biomass in areas <2˚C) – latitude; demersal piscivores – bottom temperature, latitude, substrate and stratification; pelagic piscivores – substrate and temperature; pelagic planktivores – top layer depth (stratification) and latitude. For benthivores there were few common dominant predictor variables. These results allow us to better understand the underlying drivers of species distribution. Although pelagic piscivore distributions are largely confined to depth, bottom temperature and substrate had more influence on their distribution, suggesting these predators might extend their range to the inner shelf, absent the resident cold pool, which has important implications for predatory interactions with forage fish and juvenile walleye pollock.

DISCUSSION

We introduce an approach to integrate biological and physical datasets and present a detailed overview of physical drivers influencing individual species distributions within the eastern Bering Sea. This study

revealed evidence for resource partitioning among species or species groups within the broad functional categories of pelagic planktivores, benthivore flatfish, crabs, cnidarians, ascidians, echinoderms, benthic worms, and bivalves. Alternatively species within the category of demersal piscivores show considerable overlap and evidence for competition for similar resources. Pelagic piscivores are of particular interest as they demonstrate a certain degree of partitioning (mostly by temperature) but also common responses to environmental forcing, suggesting that the substantial rise in abundance of this group over the time series is likely driven by environmental conditions and prey availability favorable to this group in aggregate. Shifts in the location, extent and intensity of cold bottom temperatures may dramatically alter predator prey dynamics in this system, especially with regard to the presence of arrowooth flounder.

Heterogeneity in biological and physical processes complicated our efforts to distinguish significant drivers in the spatial distributions of fishes and crabs. Contour plots provide a clear and easily interpreted visual and useful tool for understanding species distributions and overlap, informative to interpreting predatory and competitive interactions and resource partitioning. Due to their relative stationarity, sessile benthic invertebrates may serve as useful proxies for habitat type and structure, particularly in the absence of detailed information on substrate. Variable importance and partial dependence plots highlighted significant areas of variation and identify critical environmental thresholds at the level of individual species. Contrasting patterns in species abundance and variation in abundance (i.e. within or adjacent to core habitat) provides insight into how species or guilds respond to environmental forcing. While most guilds appear to expand and contract their range in marginal habitats as a function of intrapopulation density trends or favorable conditions as per the constant density model (Iles and Sinclair 1982, Hilborn and Walters 1992), pelagic planktivore and arctic species appear restrained within their core range as per the proportional model (Myers and Stokes 1989; Petitgas 1998). For pelagic planktivore species, this is likely a response to predation; core habitats represent not only optimal conditions (e.g. recruitment, growth, forage potential) but also refuge from predation. This is particularly apparent by contrasting the range of the predominant pelagic planktivore species (e.g. juvenile walleye pollock, capelin, saffron cod, arctic cod, Pacific herring) with the predominant pelagic predators (e.g. arrowtooth flounder, Kamchatka flounder, Bering flounder, Greenland turbot, sablefish). These trends should be further explored related to assumptions of localized response of species density to global changes in abundance, especially as per the basin model, which assumes density changes as a result of relationships between habitat suitability and local density (MacCall 1990). Despite the frequent fluctuations in optimal habitat driven by the extent of the cold pool, arctic species also appear limited in their capacity for range or population expansion. This may be related to productivity or mobility constraints.

CONCLUSIONS

Our maps of species distributions illustrate the extent to which species might compete for common resources or segregate and exhibit resource partitioning based on habitat overlap. Our findings suggest that certain populations may be more sensitive to assumptions of spatial homogeneity than others. Our analyses evaluated species distributions in relation to the static and dynamic features of the physical environment, particularly in how static habitat characteristics such as depth and substrate type interact with dynamic features such as temperature to drive shifts in species abundance and distribution.

This research illustrates an approach to identify and delineate distinct ecological regions with large marine systems using statistical and geospatial methods integarteing data on community composition and physical habitat. Outputs of this research can be used in concert with similar analyses to better inform spatial management and understanding of species interactions at regional scales.

Chapter 5.b. Deliniating ecological regions in marine systems: synthesis of physical structure and community composition to inform spatial management.

This paper is in revision for details refer to:

Baker, M. R. and A. B. Hollowed. 2014. Delineating ecological regions in marine systems: synthesis of physical structure and community composition to inform spatial management. Deep Sea Research II.

ABSTRACT

Understanding spatial structure in marine systems and delineating meaningful spatial boundaries are integral to ecosystem approaches to fisheries management. Physical structure and drivers combine with biological responses and interactions to organize marine systems in unique ways at multiple scales. We apply multivariate statistical methods to define spatially coherent ecological units or ecoregions in the eastern Bering Sea, as one approach to define management units in large marine ecosystems. We use random forests to quantify the relative importance of habitat and environmental variables to the distribution of individual species and quantify multi-species or community composition turnover along environmental gradients. Outputs are used to identify discrete ecoregions with distinct physical and biological attributes and to evaluate the relative importance of predictor variables to determining regional boundaries. Depth, bottom temperature and frontal boundaries were dominant factors defining distinct biological communities in this system, with a distinct latitudinal split in the middle shelf at ~60 °N. Our results indicate that distinct climatic periods will shift habitat gradients and that dynamic physical variables such as temperature and stratification are important to understanding temporal stability of ecoregion boundaries. We note distinct patterns between functional guilds in how the system is utilized, but also evidence for subtle resource partitioning among individual species within each aggregate guild. By integrating physical and biological data, we partition ecosystems along ecologically significant gradients, which can serve as the basis for defining spatial management units or aid in understanding structural shifts in species abundance and community dynamics over time.

METHODS

We integrated bottom trawl survey data and environmental indices to identify threshold shifts in community composition across the Bering Sea as a means to define spatially coherent ecological regions. We employed random forest methods to evaluate the extent to which environmental variables predict distribution patterns and to quantify species responses to physical variables (e.g. temperature, depth, substrate, stratification). We evaluated the marginal effect and relative importance of each physical variable (i.e. the effect of the variable, holding other variables constant) on the abundance of individual species to identify thresholds along physical gradients. We then integrated across predominant species within the system to quantify multispecies compositional turnover along environmental gradients (R Package gradient, Forest, Ellis et al., 2012). This allowed us to distinguish where critical thresholds and shifts in community assemblages occur. By using ordination to overlay relative species abundance on a biplot projection representing multiple attributes of the physical system we were able to determine how individual species distributions compare, and cluster sampling stations (via partitioning around medoid methods, pam) according to similar biological communities to define distinct ecological regions.

RESULTS

Importance of predictor variables and important breakpoints along variable gradients

Cumulative plots display thresholds in species abundance and distribution to environmental factors (Fig. 1).These outputs were integrated across all consistently sampled species in the system and binned split importance in random forest tree outputs, and location on each predictor gradient were reported to identify breakpoints in biological communities along environment gradients (Fig. 2). Important breakpoints in aggregate community composition are noted at latitude (57°N, 60°N), longitude (-164°W, -168°W, -174°W), surface temperature (5°C, 7°C, 9°C), bottom temperature (0°C, 2°C, 4°C), depth (50m, 100m), and four grades of substrate coarseness. Based on the eigenvalue or latent root, depth was the strongest explanatory factor in predicting distinct community composition, followed by latitude, bottom temperature, longitude, range of temperature within the water column, bottom layer depth, surface temperature midlayer extent and substrate characteristics (Fig 3).

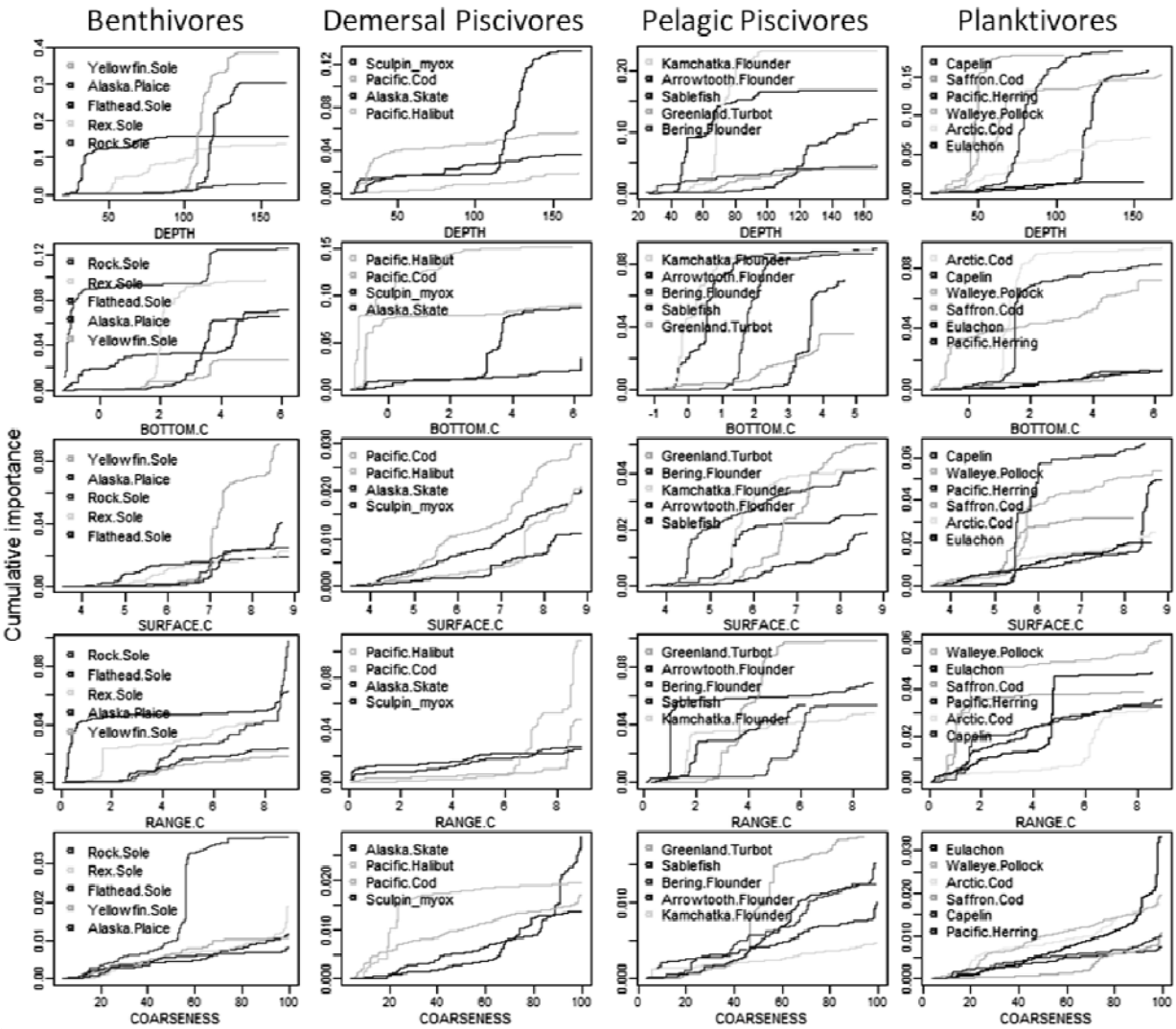

Figure 1. Cumulative importance plots (gradient forest output) display cumulative shift (in R^2 units) of individual species abundance across various environmental predictors. The common scale allows for comparisons across species within function guilds. Plots display prominent species from benthivore, pelagic planktivore, demersal piscivore and pelagic piscivore guilds (clockwise from top left). Species are listed (top down) in order of the height of the line on the far right of each graph.

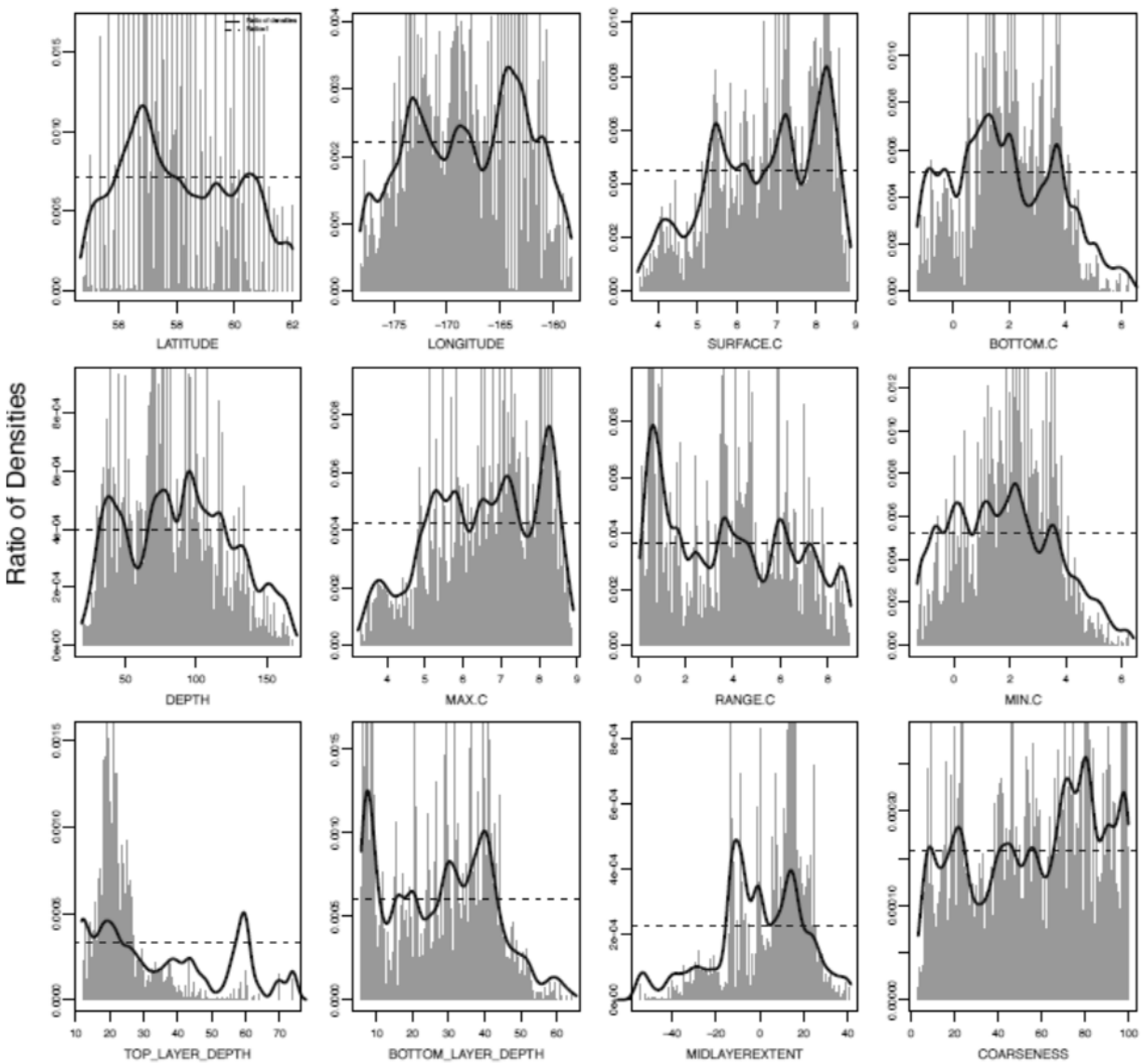

Figure 2. Splits density plots show importance changes in the abundance of multiple species along a given physical gradient, indicating a rate of change in community composition. Plots display binned importance of splits from multiple trees relative to the variable measure on the horizontal axis (gray histogram). Density plots (lines) illustrate kernel density of splits standardized by observation density.

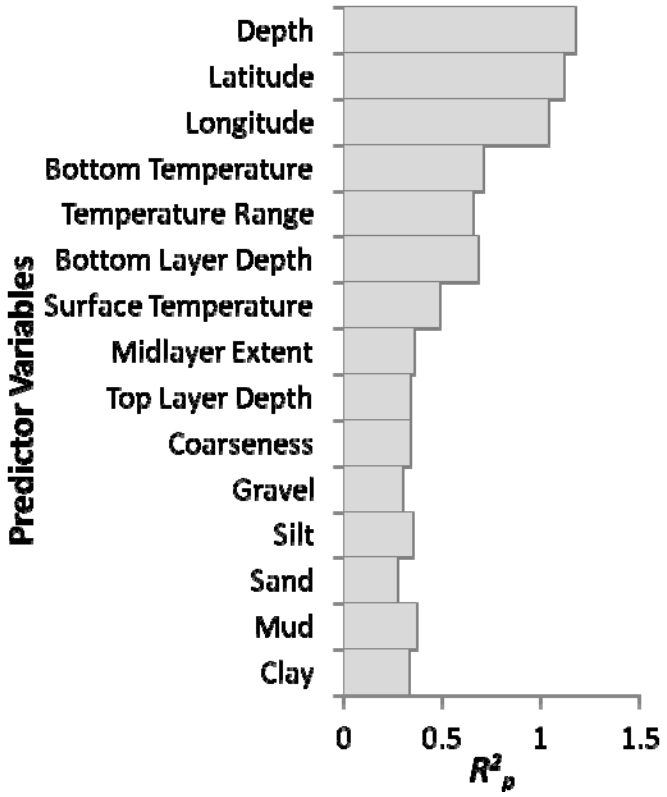

Figure 3. Mean predictor importance weighted by species R^2 by inferred community composition for gradient forest outputs.

Biplot of biological space and delineation of EBS ecoregions

Shifts in biological community composition along environmental gradients in cumulative functions were used to transform environmental data layers into biological composition based on species responses to environmental predictor variables. The transformed multi-dimensional biological space is displayed as a principle components analysis biplot (Fig. 4). Coordinate position represents inferred biological community compositions, as associated with the physical predictor variables. To examine how individual species distribute across the system, we superimposed the weighted mean location of select species at each sampling station (Fig. 5). Using clustering (PAM) to aggregate survey stations based on similar community composition, we defined six distinct ecoregions within the EBS shelf (Fig. 6, top map). We noted distinct trends moving from the inner to outer shelf and a latitudinal break at ~60°N. Across the time series, the inner shelf represents a consistent ecological region and a distinct region is also identified along the outer shelf or slope. Within the middle domain and at the island complexes, complex dynamics are observed, reflecting the dynamic nature of the environmental conditions within this area and complex cross-shelf processes. Attributes of individual ecoregions are summarized (Table 1). Outputs for warm (2001-2005) and cold (2006-2010) periods were similar to each other and to the output integrated over the

entire time series (Fig. 6, lower panels), suggesting relatively stable structuring of the system over time. Still, important differences existed, mainly that the Northern domain extends southward in cold years and restricts northward in warm years. Interestingly, this seems to represent a constraint to subarctic species, rather than an explicit benefit to arctic species, given the response to the extent of the cold pool (Fig. 8).

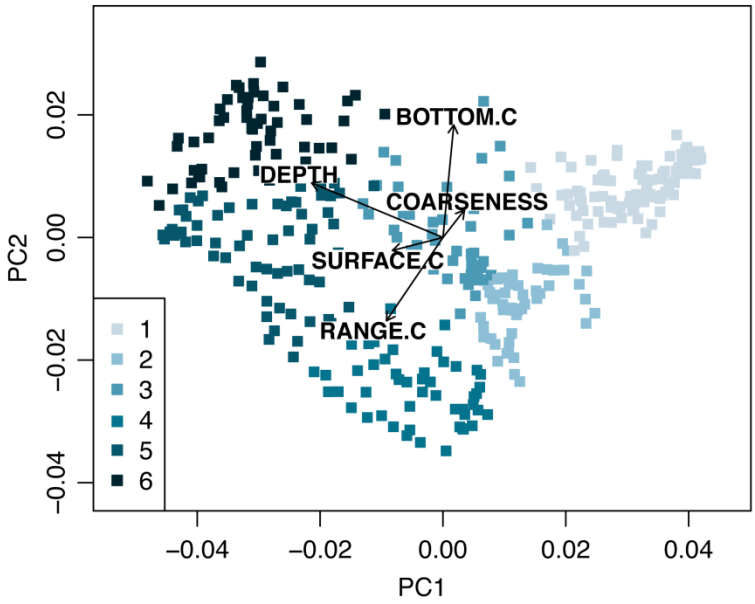

Figure 4. Biplot of inferred community composition based on predictor cumulative functions of physical environmental predictors transformed into a common biological importance scale, where coordinate position represents inferred community composition patterns. Each individual point represents a sample station in the standard EBS bottom trawl survey. Color indicates results of clustering (PAM), such that survey stations are grouped according to distinct physical environments.

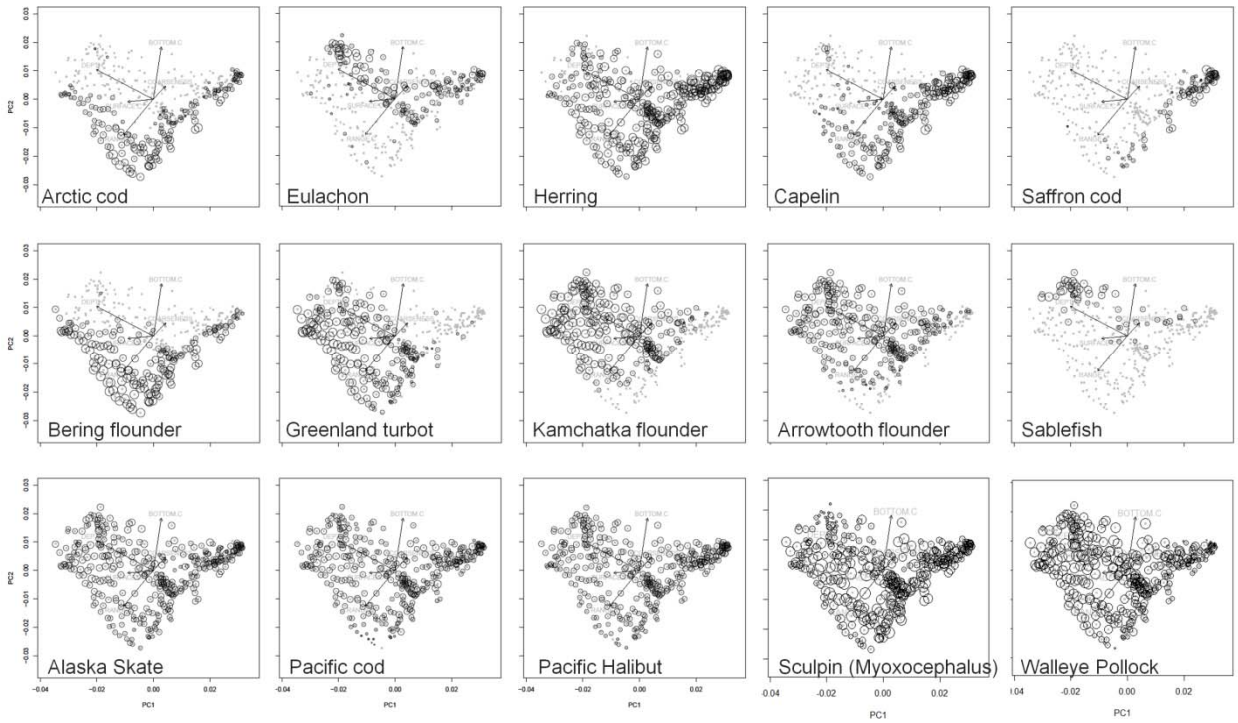
Arctic cod
Eulachon
Herring
Capelin
Saffron cod
Bering flounder
Greenland turbot
Kamchatka flounder
Arrowtooth flounder
Sablefish
Alaska Skate
Pacific cod
Pacific Halibut
Sculpin (Myoxocephalus)
Walleye Pollock
PC1
PC2

5698

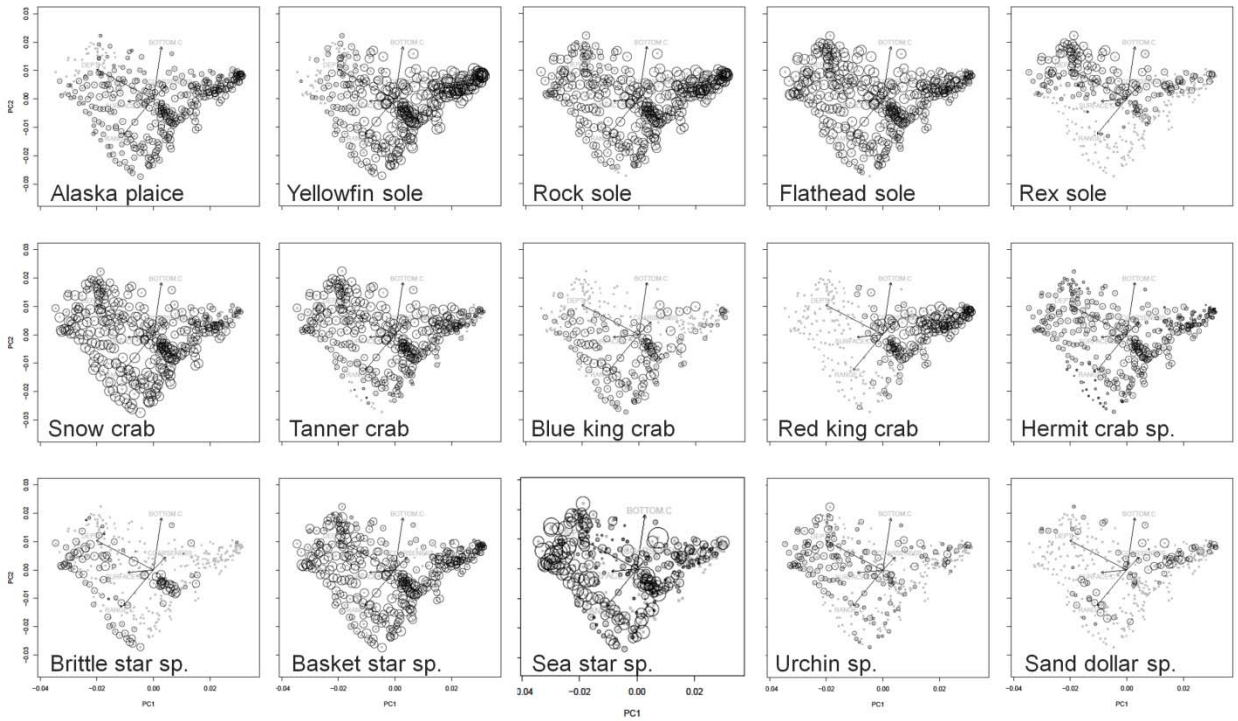
Alaska plaice
Yellowfin sole
Rock sole
Flathead sole
Rex sole
Snow crab
Tanner crab
Blue king crab
Red king crab
Hermit crab sp.
Brittle star sp.
Basket star sp.
Sea star sp.
Urchin sp.
Sand dollar sp.
PC1
PC2

5699

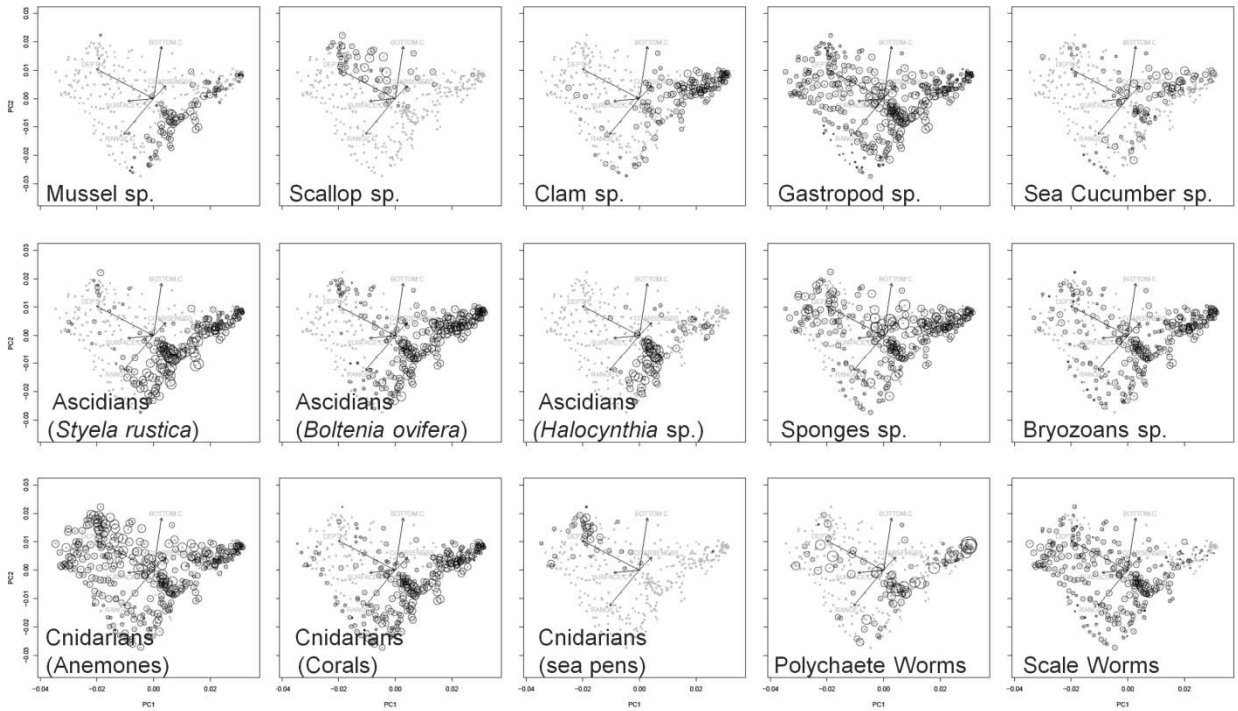

Figure 5. Results demonstrate how individual species respond to multiple environmental variables and how individual species distributions compare to the system as a whole. Species are organized by function guild: panel 1, planktivore forage fishes; panel 2, pelagic piscivores; panel 3, demersal piscivores and walleye pollock; panel 4, benthivore flatfishes ; panel 5, crabs species; panel 6, aggregated echinoderm species; panel 7, aggregated mollusk species; panel 8 and 9, aggregated fixed invertebrates and worms; panel 10, seastars. Note that invertebrates are included in random and gradient forest analyses as individual species, but aggregated here to generalize trends.

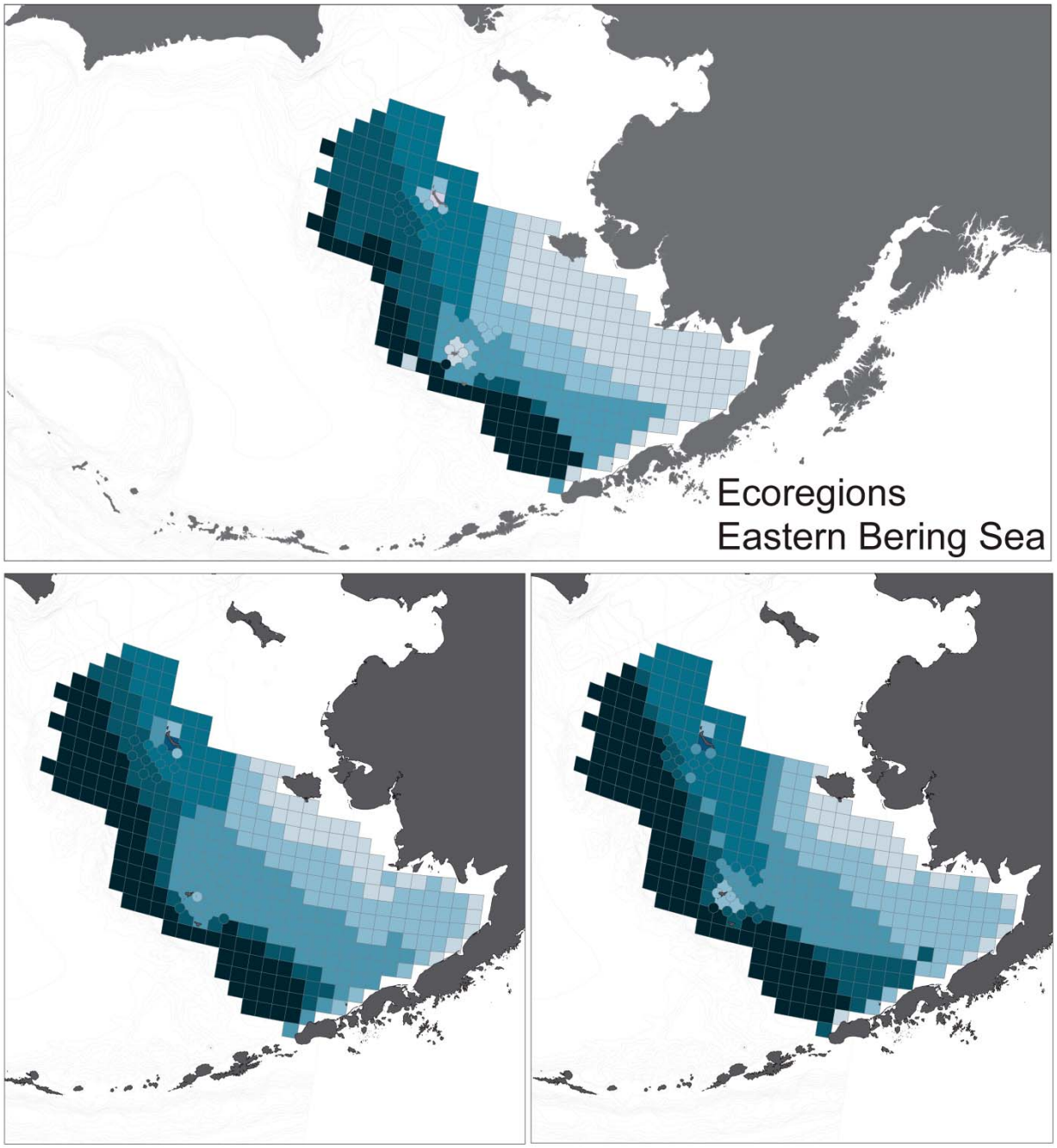

Figure 6. Delineation of ecoregions based on clustering stations through partitioning around medoid methods to represent inferred community assemblages, or distinct ecological regions. Ecoregions are displayed for the entire timeseries as well as for recent cold and warm periods.

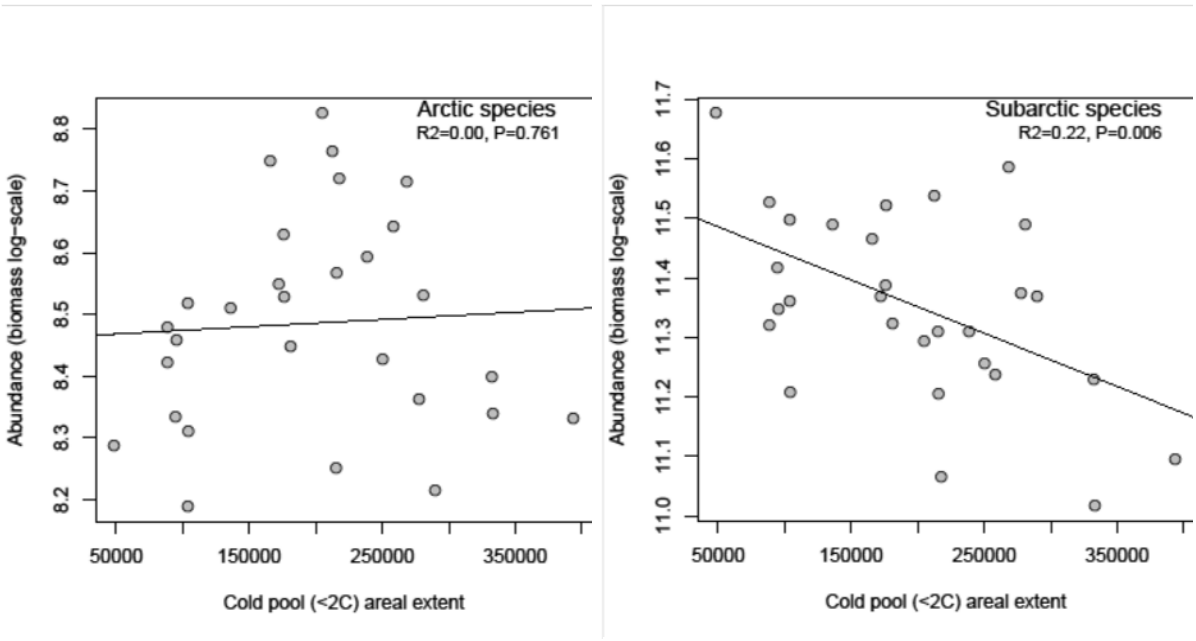

Figure 7. Response of arctic and subarctic species (aggregate annual abundance in biomass) to the areal extent of the eastern Bering sea cold pool.

DISCUSSION

Using data, indices and analyses made available by NPRB funding, we present a detailed overview of selected physical drivers influencing individual species distributions within the EBS and illustrate an approach to integrate biological and physical data to delineate ecoregions using statistical and geospatial methods of biological community composition and physical habitat. Identifying ecologically significant units within LMEs is a necessary and important step in defining units for spatial management and ecosystem approaches management. Our results delineate distinct regional habitats within the EBS LME and aim to characterize the ecological value of habitats, integrate spatially discrete environmental effects and species interactions into stock assessments, and inform multispecies models. Our analyses identified areas with common community and detailed biological and physical characteristics in these areas that may drive difference between regions. These results and this approach may be informative to delineate ecoregions within a nested and hierarchical system of spatial management (Levin et al. 2009).

CONCLUSIONS

Our research approached questions of broad-scale ecological interest in a manner that may inform practical understanding of species dynamics at regional scales. The designation of ecoregions provides an important baseline for future analyses of the effects of climate change and fishing. Our ability to integrate multiple data sources to provide a more comprehensive characterization of the physical habitat of the

eastern Bering Sea directly benefited from and provides justification for the augmentation of surveys, reported elsewhere in this report. Our results aim to distinguish regional patterns within a nested and hierarchical system of spatial management. We also highlight an analytical method that allows us to characterize unique regions and to evaluate ecological dynamics at regional scales and to project the range and scope of an ecoregion within a given timeframe as functions of variables that shift in space over time.

This research establishes a mean index for core species reanges and variation in distribution over time as a baseline to gauge future shifts related to climate or harvest pressures. This research also establishes critical thresholds for species responses to environmental variables that will help determine species overlap and potential competitive and predatory interactions between species in retrospective analyses and projected simulations. This is particularly relevant to parameterize potential species interactions and mortality estimates increasing included in multispecies models and assessments.

ACKNOWLEDGEMENTS

Comparative Analysis of Marine Ecosystem Organization, NOAA Habitat Assessment Improvement Program, ME Clarke, R Hilborn, T Branch, K Holsman, K Aydin, S Gaichas, J Collie, R Bell, S Kotwicki, T Buckley, G Hunt, F. Mueter, I. Ortiz, J. Overland, P. Spencer, and S. Zador

PHYSICAL CHARACTERISITCS					
ECOREGION	LATITUDE	DEPTH	TEMPERATURE	STRATIFICATION	SUBSTRATE
Inner Shelf	Extensive spread across latitude (55-60) and longitude (-158 to -170)	Shallow (Range: 19-69m) (Mean=42±12m SD)	Stable temperatures. Relatively cold surface (5±1˚C) and warm bottom (3±1˚C) temperatures. Narrow range in min/max values (2-7˚C) and low variation within the water column (1˚C).	Extensive top layer depth extending mostly to seafloor	Coarse (Mean=80±21) with high variation (3-100). Substrate entirely sand and gravel.

Middle/Inner (South)	Middle latitudes (57-61)	Relatively shallow Consistent depths (Range: 41-69m) (Mean=61±7m SD)	Relatively cold surface 96±1°C) and bottom (1±0°C) temperatures. Considerable range in min/max values (0-7°C), and some variation within the water column (4°C).	Extensive stratification (top layer depth 19±3, bottom layer depth 22±3 with minimal middle layer 3±5).	Relatively coarse (Mean=56±16). Substrate largely sand with areas of mud and silt.
Southern	Low latitude (55-58)	Mid-range (Range: 67-96m) (Mean=79±8m SD)	Moderate surface (7±1°C) and bottom (2±1°C) temperatures. Moderate range in min/max values (2-8°C), and some variation within the water column (4°C).	Minimal but variable middle layer (top layer depth 23±8, bottom layer depth 29±6 minimal but variable middle layer 6±12).	Consistently coarse (Mean =68±19). Substrate largely sand with extensive areas of mud and silt.
Northern	High latitude (58-62)	Mid-range (Range: 58-94m) (Mean=75±10m SD)	Coldest bottom temperatures Warm surface (7+0°C) and cold bottom (0+1°C) temperatures. Wide range in min/max values (0-9°C), and extensive variation within the water	Even partition of water column (top layer depth 17±2, bottom layer depth 32±5, middle layer 15±4)	Low coarseness (Mean=27±15). Substrate largely mud with areas of silt and clay.

			column (XX).		
Middle/Outer (North)	High latitude (56-62)	Consistently deep (Range: 94-148m) (Mean=114±15m SD)	Moderate range temperatures (surface 8±0°C, bottom 2±1°C). Wide range in min/max values (-1-8°C), and extensive variation within the water column (7°C).	Highly stratified (top layer depth 21±2, bottom layer depth 45±5 with extensive middle layer 24±6).	Low coarseness (Mean=23±15). Substrate mud, silt, clay and sand.
Shelf Break	Extensive spread across latitude (51-61)	Deep Wide range, including deepest and shallowest areas sampled (Range: 12-171m) (Mean=131±43m SD)	Stable temperatures Relatively warm surface (8°C) and bottom (4°C) temperatures. Moderate range in min/max values (1-9°C), and some variation within the water (4°C).	Highly variable water column Top layer depth (28±10m), mid-layer depth 19±24, bottom layer depth 47±19)	Moderately coarse (Mean=48±21) with high variation (3-100). Substrate equal parts mud, silt, and sand.
BIOLOGICAL CHARACTERISITCS					
ECOREGION					
Inner Shelf	Relatively high concentrations of forage fish (saffron cod, capelin, eulachon, herring) and flat fish (yellowfin sole, Alaska plaice, rocksole). Arctic species (eelpout, snailfish) and pelagic piscivores (arrowtooth flounder, Kamchatka flounder, Greenland turbot) are absent. High abundance of fixed sessile invertebrates (e.g. ascidian, bryozoans, sponges, tube worms), sea cumber and red king crab.				
Middle/Inner (South)	Relatively uniform representation of fish species, with lower relative abundance of warm and deepwater species (e.g. rex sole, eulachon, sablefish, Kamchatka and arrowtooth founder, rockfish), demersal piscivore (e.g. Pacific halibut, Pacific cod, skates) and flat fish species (e.g. yellowfin sole, flathead sole, rock sole, Alaska plaice)				

	and higher relative abundance of arctic species (e.g. arctic cod, snailfish, Bering flounder), fixed sessile invertebrates, and polychaetes.
Southern	Relatively low abundance of arctic species (e.g. arctic cod, snailfish, Bering flounder) and relatively high abundance of pelagic piscivores (e.g. Kamchatka and arrowtooth founder), scallop, sand dollar, sea cucumber, and sponge.
Northern	Predominant area for arctic species (e.g. arctic cod, snailfish, eelpout, Bering flounder) and also for populations of Greenland turbot, capelin, coral and blue king crab. Deep water (e.g. sablefish, rockfish), or warm water and southern ranging species (e.g. Kamchatka flounder, arrowtooth flounder, eulachon) species are largely absent.
Middle/Outer (North)	Relatively high abundance of pelagic piscivore (e.g. Greenland turbot, Kamchatka and arrowtooth flounder) and arctic fish species (e.g. e.g. arctic cod, snailfish, Bering flounder, eelpout), echinoderm (e.g. brittle star, basket star, sea star, urchin), crab (e.g. blue king crab, hermit, Tanner, snow), gastropod, and octopus. Also characterized be relatively low abundance of fixed sessile invertebrates (e.g. coral, ascidian, bryozoans) and benthic infauna.
Shelf Break	Exclusive habitat of deepwater species (e.g. sablefish, rockfish) and high abundance for pelagic piscivores (Kamchatka and arrowtooth flounder). Also characterized by the absence of arctic species and low relative abundance of forage fishes and benthic flatfishes.

Chapter 6: Predicting eastern Bering Sea adult walleye pollock (*Gadus chalcogrammus*) winter distribution

This section describes a method to estimate pollock winter spawning distribution based on acoustic data collected from ships of opportunity. The material in this section is the work of Steven Barbeaux (PI and PhD student) and was published as:

Barbeaux, S. J. 2012. Scientific acoustic data from commercial fishing vessels: Eastern Bering Sea walleye pollock (*Theragra chalcogramma*). Ph.D. thesis, School of Aquatic and Fisheries Sciences, University of Washington, Seattle.

A manuscript that will be submitted to a peer reviewed journal has been developed with a tentative title of:

A Generalized Additive Optimum Projection Model for predicting Eastern Bering Sea walleye pollock winter distribution

ABSTRACT

Although the Eastern Bering Sea (EBS) walleye pollock (*Gadus chalcogrammus;* hereafter pollock) has been intensely studied, due to harsh winter conditions, survey effort on adult pollock has been concentrated in the summer. The lack of comprehensive survey data on adult pollock distribution in the EBS during the winter creates a gap in our knowledge of this important species during a critical period in its life history. This study applies a leave one-year-out cross-validation method to develop a generalized additive optimum projection model (OPM) to investigate the use of oceanographic data to project winter pollock density and distribution. Density and distribution of EBS winter pollock was measured through acoustic data collected from commercial fishing vessels during normal fishing operations. Adult pollock in the EBS were found to have specific depth (85-113 m) and temperature (>2°C) preferences. When temperatures declined as winter progressed or in winters where the shallow and northern shelf areas were covered with cold water pollock distribution contracted and in extreme years was restricted to the outer continental shelf edge at the maximum depth preference. When temperatures increased or during winters with warmer water temperatures pollock expanded northward and into shallower waters within their preferred depth range. Assuming winter adult

distribution mirrors spawning location, results of this study suggest that EBS pollock spawning locations may be more variable than currently assumed. This variability likely affects the timing of spawning and the eventual destination of pollock eggs and larvae, directly influencing recruitment strength and overall recruitment variability.

INTRODUCTION

Although the Eastern Bering Sea (EBS) walleye pollock (*Gadus chalcogrammus*; hereafter referred to as pollock) has been intensely studied, due to harsh winter conditions, survey effort on adult pollock has been concentrated in the summer. In the past decade, no trawl surveys and only two acoustic surveys (2001 and 2002) have been conducted in the EBS during the winter. The lack of comprehensive survey data on adult pollock distribution in the EBS during the winter creates a gap in our knowledge of this important species during a critical period in its life history.

Swartzman *et al*. (1995) observed that, in summer, bottom depth and ocean temperature fronts influenced the distribution and dynamics of adult pollock schools. Adult pollock avoided temperatures less than 0° C, preferring mid-water temperatures near 2.5°C and depths between 70 and 130 m. If pollock behave similarly in winter and early spring when water temperatures less than 0° C expand across the EBS shelf, then pollock distribution on the EBS shelf would be condensed to a smaller area. Since EBS shelf waters are well mixed in the winter, sea surface temperature is correlated with mid-water temperatures (Stabeno *et al*. 2007). Therefore the extent and location of pollock distribution in the winter should be predictable at high spatial and temporal resolutions from bathymetry and satellite derived measurements of sea surface temperature and ice coverage.

Even though scientific survey data on pollock distributions are not available for winter, an alternative approach to determining pollock distribution is to collect acoustic data from commercial fishing vessels operating in the EBS during this period. Unlike trawl catch data, opportunistic acoustic data are collected continuously, including times when vessels search for fish and transit between fishing grounds and port. By including data from un-fished areas, opportunistically collected acoustic data provide a more complete picture of pollock distribution and relation to environmental covariates than that available from other fishery dependent data (e.g. catch-per-unit-effort (CPUE)). Opportunistic acoustic data provide a unique spatial and temporal index of pollock density that can potentially be used to identify effects of environmental conditions on pollock distribution during winter months.

Effects of temperature and bottom depth on pollock distributions have been shown to be non-linear (Swartzmann *et al*. 1995), necessitating an additive modeling approach (Stone 1985) to appropriately characterize relationships. Generalized additive models (GAM, Hastie and Tibshirani 1990) have been widely used to study ecological processes, in particular to describe relationships between

oceanographic conditions and fish distributions (e.g. Swartzman *et al*. 1992, Murase *et al*. 2009), due to their flexibility when modeling non-linear relationships and addressing spatial autocorrelation. There are however constraints in the use of GAMS to quantify functional relationships. The high degree of flexibility of the non- or semi-parametric smoothers used in GAMs can reproduce nearly any functional relationship and interaction (Wood 2006). When fit using likelihood or generalized cross-validation (GCV; Wood 2006) methods, this flexibility causes the models to select overly complicated models and erroneously identify noise as trend (Shao 1993, Racine 2000, Arlot and Celisse 2010). GAM overfitting is particularly problematic with opportunistic data like those used in this study. The opportunistic acoustic data are collected non-systematically, are unbalanced between years, and sampling intensity varies across environmental covariates. Therefore, although GAMs describe data well, without implementing additional validation measures GAMs tend to have little predictive power outside the range of the data to which they are fit (Jensen *et al*. 2005).

The first objective of this study was to investigate how well oceanographic data predict winter pollock densities on the EBS shelf. To reduce the tendency for the GAM to overfit data, this study developed and applied a leave one-year-out cross-validation method where data from three out of four years were used to predict the distribution in the fourth. The results of the validation were used to develop an optimum projection model for winter pollock density and distribution on the EBS shelf.

This study also postulates that although EBS pollock move seasonally, their distribution is bounded by inter-annually consistent and seasonally invariant preferences for or against environmental conditions that identify EBS pollock preferred habitat (Vandermeer 1972; Heifetz *et al.*1986; Righton *et al.* 2010). The spatial extent of EBS pollock preferred habitat will vary over time with changes in oceanographic conditions. This concept of a spatially variable preferred habitat is analogous to the N-dimensional realized niche described by Hutchinson (1953, 1957), which has been widely applied in ecology. In limnology the environmental components of the N-dimensional realized niches for freshwater fishes (Magnuson *et al*. 1979, Magnuson *et al*. 1990, Huff *et al*. 2005) have been described using the abundance weighted mean environmental covariate to index niche center and one standard deviation about this mean to index niche width (Birks *et al*. 1990). In an extension of this concept, species-specific realized niche widths have been used to predict population abundance and changes in fish distribution under different climate change scenarios (Magnuson *et al*. 1990). To evaluate whether pollock realized niche was consistent between winter and summer, realized niche estimates were calculated for both the Alaska Fisheries Science Center summer bottom trawl survey data (Lauth 2010) and winter opportunistic acoustic data parametrically following the parametric limnological model and using the validated GAM prediction model.

METHODS

Data collection and processing

From January 2002 through March 2005 acoustic data were collected from four commercial fishing vessels during normal fishing operations in the winter EBS pollock fishery (Barbeaux et al. 2013). All vessels participating in the study were equipped with hull mounted 38 kHz SIMRAD ES-60 echosounders. Processing the data included removing the ES60 triangle wave (Ryan and Kloser 2004), reviewing the data for errors and identifying pollock aggregations, creating bottom lines, and producing spatially and temporally indexed uncalibrated backscatter (s_A m^2nmi^{-2}; Simmonds and MacLennan 2005) at 100 meter intervals along the vessel cruise track. Barbeaux et al. (2013) provides system parameters and description of the methods used in data collection and processing.

Each observation was characterized using the decimal time of day, date in Alaska Standard Time (DAY), bottom depth (BD), sea surface temperature (SST), distance in kilometers to ice edge defined as greater than 75% ice coverage (DI), and location (Z) in universal transverse mercator (UTM) coordinates in kilometers for northern zone 3. SST and DI were obtained from the National Climate Data Center (NCDC 2008). The NCDC data for the Bering Sea with a spatial grid of 0.25° were available at a temporal resolution of one day. Water column temperatures on the EBS shelf in areas less than 150 m bottom depth are not vertically stratified in January through April and SST provide a reliable index of water column temperatures (Figure 5 from Stabeno *et al.* 2007). For this reason the analysis was limited to the shelf area with bottom depths less than 150 meters.

A 100 km^2 grid was created for the EBS shelf using a random start location. The data were then aggregated by vessel, year, 100 km^2 grid cell, and 24-hour temporal bins. A 100 km^2 and 24-hour spatial and temporal aggregation was chosen as the bin size in deference to the spatial and temporal analysis conducted in Barbeaux et al. (2013) where it was found that at smaller resolutions vessel and fishing effects could mask fish distributional effects. The mean uncalibrated acoustic backscatter (s_A m^2nmi^{-2}), BD, SST, DI, and Z were calculated for each spatio-temporal bin. Assuming that backscatter measurements from an individual vessel were consistent within a year, the backscatter data were standardized using a normal-score transformation (Goovaertz 1997) for each year and vessel combination.

Total pollock catch weights were calculated for specific areas and times following Barbeaux and Dorn (2003). Catch data from observed hauls in the North Pacific Groundfish Observer Program database were extrapolated (Barbeaux and Dorn 2003) to total catch estimates obtained from landings

data from the Alaska Department of Fish and Game's (ADF&G) landings database using a ratio of landings to observed catch. Where observer data were available the trawl end position was used for catch location. The extrapolated catch estimates from the area surrounding each 100 km^2 grid cell at 100 km and 500 km radii were summed to obtain estimates of cumulative catch per day for each grid cell (CC100 and CC500, respectively).

Generalized additive model configuration and validation

Geographic regression GAMs with twenty-one different model configurations (Table 1) were examined to test the hypothesis that a significant portion of the variability in winter pollock density on the EBS shelf could be predicted from annual pollock biomass, sea surface temperature, bathymetry, location, local cumulative catch at either a 100 or 500 km radii from the observation, and distance to the ice edge, or a combination of the six variables and their interactions. Temperature, bottom depth, and location were found by Swartzman *et al*. (1992, 1995) to be significant explanatory variables for adult pollock density. The depletion modeling conducted in Chapter 3 demonstrated that fishery removals have a measureable impact on the density of pollock and suggested that analysis at 100 km and 500 km may differ. The ice edge is a prominent feature in the EBS during the winter and spring. Hunt *et al*. (2002) describe an increase in production near the ice edge in the late winter and early spring that could influence pollock density.

Tensor product smoothers (te) and thin plate regression splines (s) were used for the non-additive smoothers (Wood 2006). To address spatial autocorrelation (Swartzman *et al.* 1992), I used thin plate regression splines over location (Z). Thin plate regression splines were also employed for smoothes of single covariates. Tensor product smoothes were used to model interaction terms between covariates with differing units as with SST (^{o}C), BD (m), or DI (km) or among all three (Wood 2006). CC100 and CC500 were fit within the model with a linear slope parameter.

Model selection for descriptive models was conducted using generalized cross-validation (GCV; Wood 2006). The best descriptive model (BDM) was selected as the model with the lowest GCV using all the available data. Due to GCV overfitting data and selecting models that perform poorly in prediction outside the available data, an iterative leave-one-year out cross validation (LYOCV) method was developed to generate an optimum projection model (OPM). I define projection in this study as prediction outside the available dataset or the use of a model to predict using environmental data not used in its development. The best predictive model (BPM) is the model that best predicts the available data from the iterative LYOCV. The candidate BPMs were fit to data from three out of four years using restricted maximum likelihood (REML, Patterson and Thomson 1971, Wood 2006). The data from the fourth year was used as a validation data set and the set of validation measures were

calculated following Power (1993) for each of the four possible year combinations. Validation measures included prediction bias as $\overline{\varepsilon} = \frac{\sum_{i=1}^{m} \varepsilon_{vi}}{m}$, where m is the number of validation data points, and $\varepsilon_{vi} = \hat{x}_{vi} - x_{vi}$, where $\hat{x}_{vi}$ is the predicted value for observation i in validation year v and x_{vi} is the observed value in validation year v for observation i. The standardized bias was calculated as, W $= \frac{\overline{\varepsilon}\sqrt{m}}{s}$, where s is the standard deviation of the observations from the training data set. The standardized predictive sum of square errors (Q_e) was calculated as $Q_e = \frac{\sum_{i=1}^{m} \varepsilon_{vi}^2}{ms^2}$. An Anderson-Darling test (AD Test) was used to insure that the prediction residuals were normally distributed (Stephens 1986). Mean square error, $MSE_v = \frac{\sum_{i=1}^{m} \varepsilon_{vi}^2}{m}$, was calculated to check prediction model fit. For comparing alternative models the Theil's inequality coefficient (Theil 1966) was calculated as $U^2 = \frac{\sum_{i=1}^{m} \varepsilon_{vi}^2}{\sum_{i=1}^{m} x_{vi}^2}$, here the value of U is bounded ($0 \leq U \leq \infty$) such that if $\hat{x}_{vi} = x_{vi}$, then U = 0. If U = 1, then $\hat{x}_{vi} = 0$, a naïve zero-change prediction. If U was greater than 1, then the predictive power of the model is worse than a naïve zero change prediction and should be rejected (Power 1993). Finally I calculated the Janus quotient (Gadd and Wold 1964) to measure the predictive accuracy and consistency of the system structure between validation and training datasets. The Janus quotient was the ratio of the validation MSE over the training MSE calculated as $J^2 = \frac{MSE_v}{MSE_t}$, where $MSE_t = \frac{\sum_{j=1}^{n} (\hat{x}_{tj} - x_{tj})^2}{n}$ for observation i in training years t, and where n is the number of observations in the training data set. J varies between 0 and ∞, values of 1 indicate that relationships among dependent and independent variables were the same between the training and validation datasets. Although there is no significance test for the Janus quotient, an increase in J indicates an increase in overfitting (Power 1993).

The degree of smoothness for each of the splines was determined in an iterative step-wise fashion for each covariate. The 19 model candidates were fit iteratively using the *gam* function in the **mgcv** R library by fixing the basis dimension (k; Wood 2006) for one of the splines at a value between 3 and 20 and allowing the k value of the other covariates in the model to be selected through restricted maximum likelihood with k set at a default maximum of 10*p* (Wood 2006), where *p* is the number of covariates in the smooth or spline. The k with the lowest mean Theil's inequality coefficient ($\overline{U}$) for the four possible training and validation combinations was selected as optimum. The k was then fixed for this covariate at the optimum, and the 19 models were again fit iteratively by fixing k for another covariate between 3 and 20. The optimum k for a second spline was then selected to minimize $\overline{U}$. This process was repeated for the remaining smoothers until the optimum k for each spline was

estimated. The BPM was then selected as the configuration with the lowest overall $\overline{U}$. To test for effects due to the order of covariate fitting on final model selection, the iterative fitting process was repeated for each possible order of covariates. To obtain the OPM, the BPM was fit to all of the data using REML with the basis dimensions set to the optimum for all smoothers. Projections of daily pollock densities for winter 2002 through 2006 were then created from the OPM using oceanographic data for the entire EBS shelf.

Summer bottom trawl data

To evaluate summer versus winter pollock habitat preferences, the realized niche centers and widths for temperature and depth were calculated for winter as the mean uncalibrated opportunistic acoustic backscatter ($\bar{s}_A$ m^2nmi^{-2}) at 100 km^2 by 24-hour cells and catch per unit effort ($kg \cdot km^{-2}$) from National Marine Fisheries Service annual summer bottom trawl surveys for 2002 through 2005 (Walters 2003, Walters 2004, Lauth 2006). The bottom trawl data were collected for most of the EBS shelf south of 62° N longitude between 20 m and 200 m bottom depth. Thirty minute trawl samples were collected near the centers of each cell of a 20 nmi by 20 nmi (1,372 km^2) grid covering the survey area. Near bottom temperatures were measured using a Sea-Bird SBE-39 datalogger (Sea-Bird Electronics Inc., Bellevue, WA) attached to the headrope of the net. Bottom temperatures and depths used in this analysis were averages over the duration the net was on bottom for each 30 minute tow. The realized niche center was calculated as $\hat{u} = \frac{\sum_{i=1}^{n} x_i y_i}{\sum_{i=1}^{n} x_i}$, where y is the environmental variable (temperature or bottom depth), y_i is the value of y in sample i, x_i is the abundance or backscatter value in sample i, and n is the number of observations. The realized niche width was calculated as the weighted standard deviation $\left[\frac{\sum_{i=1}^{n} x_i (y_i - \hat{u})}{\sum_{i=1}^{n} x_i}\right]^{1/2}$ (Huff *et al*. 2005).

To assess consistency between winter and summer GAM derived bottom depth and temperature relationships the BPM was fit to the summer bottom trawl data. The normalized (Goovaertz 1997) bottom trawl CPUE was used as the dependent variable. Bottom temperature was substituted for sea surface temperature and distance to the ice edge was removed from the model. The basis dimensions were set to the optimum values from the winter BPM and the model was fit using REML.

RESULTS

Data description

Acoustic data were collected from four factory trawlers (Vessels A through D) participating in the winter Bering Sea pollock fishery from 2002 through 2005. In 2002 Vessels A and B collected

16,600 km of acoustic data, in 2003 vessels A, B, and C collected 38,700 km of acoustic data, in 2004 Vessel B collected 9,700 km of acoustic data, and in 2005 Vessels A, B, and D collected 24,200 km of acoustic data . Temporal coverage in each year extended from the start of the winter fishery in late January through mid- to late March. Spatial coverage in the southeastern portion of the EBS was inter-annually consistent, but coverage in the northwest was variable with little spatial coverage in 2002 and 2004.

Restricting observations to only those less than 150 m depth and binning the data into 100 km^2 grid cells by day and night and 24-hour period resulted in a dataset of 6,473 observations. At this resolution there were no significant differences between the normal score values of backscatter between day and night (Welch two sample t-test, p-value = 0.53). Sea surface temperatures in areas sampled ranged between -0.11 °C and 5.71 °C with a median of 3.32 °C and a standard deviation of 0.89 °C. The largest range of temperatures was observed in 2003. The highest and lowest sea surface temperatures were both encountered in 2003. The 2005 data collection had the smallest temperature range and did not include any observations lower than 1.95°C. Bottom depth in areas sampled ranged from 50 m to 150 m, with a median depth of 93 m. The distance to the ice edge in areas sampled ranged from 113 km to 645 km, with a median distance of 321 km, and a standard deviation of 116 km. Similar to sea surface temperature, distance to the ice edge had the greatest range of values in 2003 including both the farthest (645 km) and closest (113 km) distances. The smallest range was observed in 2004, between 178 km and 461 km.

For the winter EBS pollock fishery 95% ±1% of the large (≥ 38 m) vessel fleet and 64%± 7% of the small (< 38.1 m) vessel fleet catch by weight in 2002 through 2005 had an observer on board and location was recorded to the nearest tenth of a degree (0.03 km). The small vessel fleet accounted for 45% of the pollock catch in all four years.

For both fleets combined, 82% of all pollock catch by weight was monitored and recorded by an onboard observer. The locations of unobserved hauls were self-reported by fishers on landings reports by Alaska Department of Fish and Game (ADF&G) reporting area. The ADF&G reporting areas are 1 degree longitude by 0.5 degree latitude blocks (~2,500 km^2), except near land where they are smaller. Locations of the unobserved landings were extrapolated to observed catch locations by ADF&G reporting area and therefore some unknown amount of bias in location at the resolution of this analysis was possible.

Descriptive model selection

The best descriptive model (BDM) with the lowest generalized cross-validation score was Model 10 (Table 1) and included all covariates. The BDM had a GCV score of 0.831, an explained deviance of 20.3%, and estimated degrees of freedom (EDF) of 97.92. The BDM was configured using a three-dimensional tensor-product surface fit to bottom depth, sea surface temperature, and distance to ice edge; a two-dimensional thin plate regression spline on location; and a linear fit through annual cumulative catch at a 100 km radius from the observation. The BDM found significant non-linear interactions among bottom depth, distance to ice edge, and sea surface temperature (Fig. 1) using 70.00 estimated degrees of freedom to fit the three-dimensional tensor product spline. The two-dimensional spline on location used 25.92 estimated degrees of freedom to fit an irregular surface with three high points. One high point was located in the southeast EBS, ~50 km north of Unimak Island, another located 50 km south-southwest of the Pribilof Islands, and a third was located 100 km east-northeast of the Pribilof Islands (Fig. 2A).

Table 1. Results for descriptive model comparisons with generalized cross-validation (GCV) score, explained deviance (E.Dev), and estimated degrees of freedom (EDF). Model covariates are location in UTM kilometers (Z), distance to ice edge (DI), bottom depth (BD), sea surface temperature (SST), cumulative daily catch at a 100 km and 500 km radius from each observation (CC100 and CC500). Thin plate regression splines (s) and tensor product smoothers (te) are indicated in each model. The shaded model is the selected descriptive model.

Model	Configuration	GCV	E.Dev. (%)	EDF
1	~CC500 + s(Z)+te(DI,BD,SST)	0.835	19.8	97.4
2	~CC500 +s(Z)+s(DI)+s(BD)+s(SST)	0.853	16.4	48.9
3	~CC500 +s(Z)+s(BD)+s(SST)	0.862	15.2	41.5
4	~CC500 +s(Z)+s(DI)+s(BD)	0.867	14.8	42.6
5	~CC500 +s(Z)+s(DI)+s(SST)	0.860	15.4	41.4
6	~CC500 +s(Z)+s(DI)	0.875	13.6	34.6
7	~CC500 +s(Z)+s(BD)	0.873	13.8	34.9
8	~CC500+s(Z)+s(SST)	0.869	14.2	34.3
9	~CC500+s(Z)	0.881	12.7	27.4
10	~CC100 +s(Z)+te(DI,BD,SST)	0.831	20.3	97.9
11	~CC100 +s(Z)+s(DI)+s(BD)+s(SST)	0.849	16.8	49.2
12	~CC100 +s(Z)+s(BD)+s(SST)	0.858	15.7	42.2
13	~CC100 +s(Z)+s(DI)+s(BD)	0.862	15.2	42.7
14	~CC100 +s(Z)+s(DI)+s(SST)	0.856	15.8	42.2
15	~CC100 +s(Z)+s(DI)	0.871	14.0	35.4
16	~CC100 +s(Z)+s(BD)	0.869	14.3	36.5
17	~CC100+s(Z)+s(SST)	0.865	14.7	35.5
19	~CC100+s(Z)	0.877	13.2	28.4

19	~s(Z)	0.892	11.6	26.4

* the Hessian was not positive definite.

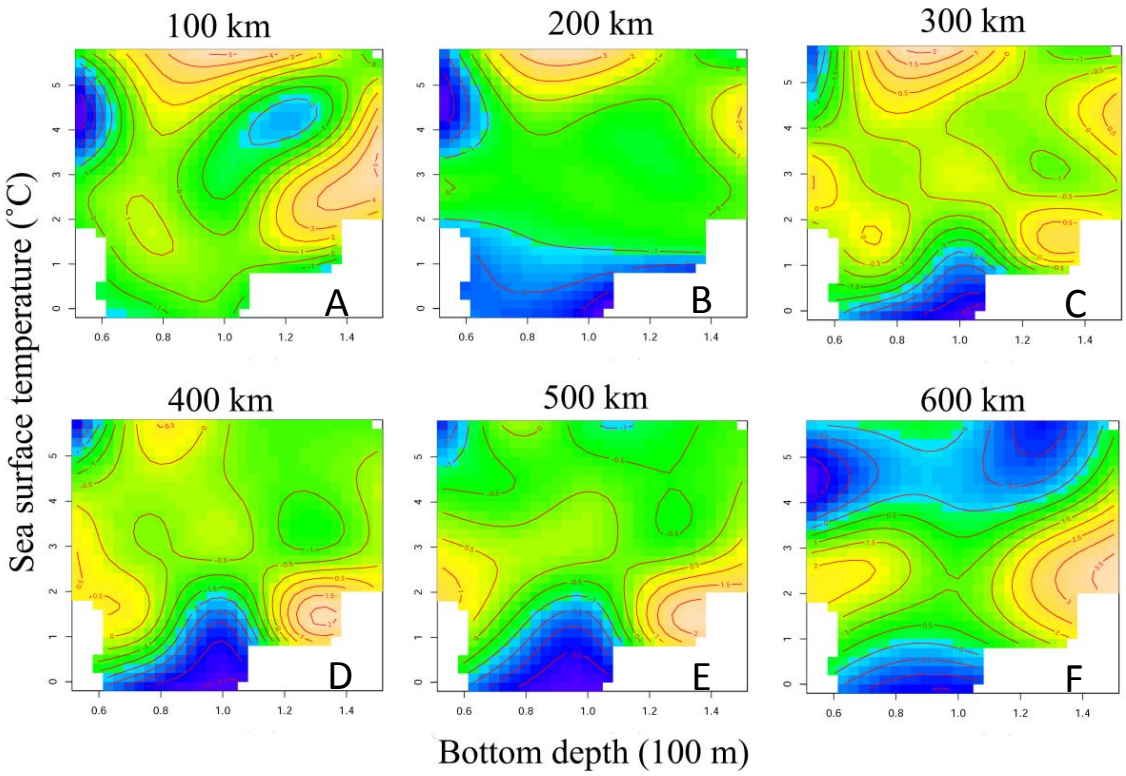

Figure 1. Sea surface temperature and bottom depth effects surfaces at A) 100 km, B) 200 km, C) 300 km, D) 400 km, E) 500 km, and F) 600 km distances to the ice edge for the best descriptive model (BDM) on normalized backscatter (s_A) with 70.00 estimated degrees of freedom. Note in these plots white areas indicate no data, filled areas indicate data at the temperature and depth for at least one distance from the ice edge and does not necessarily mean there were data at the specific distance from the ice edge shown.

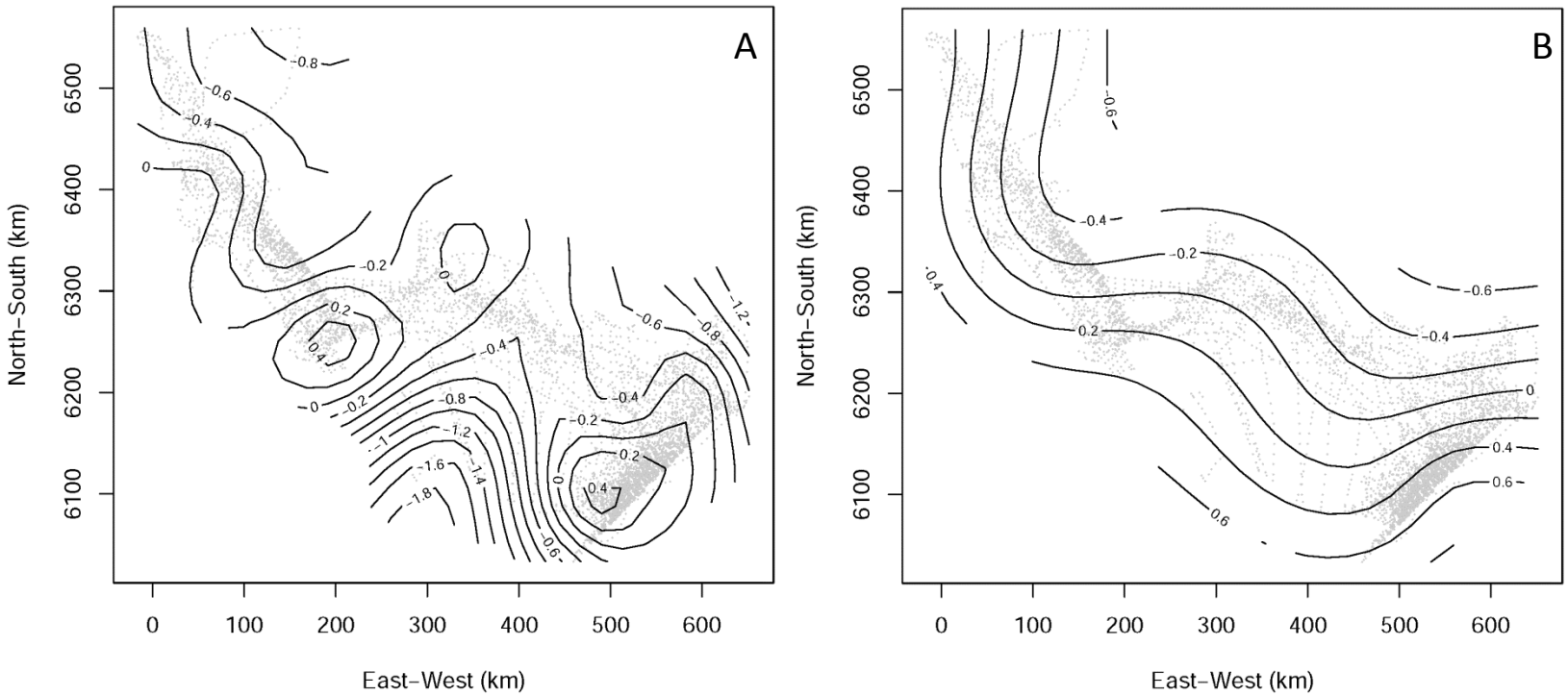

Figure 2 A) Location effect surface for the best descriptive model (BDM) on normalized backscatter (s_A) with 25.92 estimated degrees of freedom and B) location effect for the optimum projection model (OPM) on normalized backscatter showing higher predicted normalized backscatter to the southwest. Locations in both are specified in UTM for northern zone 3 in kilometers. Gray points are observation locations.

The next closest model with a GCV score of 0.835 and explained deviance of 19.8% had the same model structure but with a linear fit to the daily cumulative catch at a 500 km radius (CC500) instead of 100 km. The descriptive model fits found that the location of the observation was the best single descriptive covariate explaining up to 11.6% of the deviance. The remaining covariates explained between 0.9% and 1.8% individually, and in aggregate with interactions explained 8.7% of the deviance. The linear fit to cumulative catch explained 1.6% to 1.1% of the deviance for CC100 and CC500. The cumulative catch parameter was negative in all model configurations reducing the normalized backscatter to between $4.2 \pm 0.5 \times 10^{-6}$ per ton of catch for the 100 km radius and $1.4 \pm 0.4 \times 10^{-6}$ per ton of catch for the 500 km radius.

To explore the effects of annual variability on pollock distribution and our ability to explain relationship variability, an exploratory analysis was conducted fitting the BDM with an annual covariate on both the location spline and covariate smoothes for each year. The annual effects model improved the fit substantially with significant fits for each of the annual specific splines and smoothes with a total EDF of 304.7. The annual effects model increased the explained deviance to 32% while reducing the GVC score to 0.748. Using the GCV model selection criterion, an annual location and SST, BD, and DI with interactions effects would provide the best descriptive model, suggesting a significant annual difference in the relationship among pollock density and environmental covariates. Much of the improvement in the model fit was due to the edge effect where the increased number of parameters allowed additional flexibility in the smoothers to fit observations where there were few data.

Predictive model selection

The iterative LYOCV method using mean Theil's inequality coefficient ($\bar{U}$) for final model selection revealed two model configurations that were nearly identical. Model 2 and Model 11 included all covariates, but with no interactions among covariates (Table 2). The two model configurations differed in that Model 2 used a 500 km radius for exploring the effects of cumulative catch while Model 11 used a 100 km radius. The difference in the Theil's inequality coefficient between the two models was less than 0.0001 with $\bar{U}$ of 0.9639 and 0.9640. The $\bar{Q}_e$ were also very nearly the same at 0.92920 and 0.92917. Although neither were significant (α=0.05), the Model 3 standardized bias ($\bar{W}$ = 0.776) was slightly larger than the Model 11 standardized bias ($\bar{W}$ = -0.580). A basis dimension fixed at 9 for the Model 2 thin-plate regression spline on location achieved the best model predictions as measured by the lowest mean Theil's inequality coefficient, Q_e, MSE, and MAE. The best Model 11 predictions were achieved with the location spline basis dimension fixed at 6. The best model predictions for Model 2 were achieved using a thin-plate regression spline on sea surface temperature

with a basis dimension fixed at 6 and for Model 11 with the basis dimension on SST fixed at 5. For both models the basis dimensions for splines on bottom depth and distance to ice edge at 6 and 3 provided the best predictions. These results were consistent in that they were not dependent on which covariate was initially fixed in the iterative analysis. Although both predictive models were very similar, Model 2 was selected as the best prediction model (BPM) because it had the lowest Theil's inequality coefficient.

Table 2 Results from iterative leave-one-year-out cross-validation. This table shows the configuration and results from each run for the optimum selected model of the 323 possible tested from each run (19 models by 3 through 20 fixed degrees of freedom). The optimum model and fixed degrees of freedom are presented for each run. FREE means the spline or smooth was fit rather than fixed with a default maximum basis dimension of 10*p*, where *p* is the number of covariates in the smooth or spline. Covariates tested were location (Z), sea surface temperature (SST), bottom depth (BD), and distance to ice (DI). The average across the four possible year combinations of Theil's inequality coefficient ($\bar{U}$), standardized predictive sum of square errors ($\bar{Q}_e$), Janus quotient ($\bar{J}^2$), and standardized bias ($\bar{W}$) are presented for model runs with annual cumulative catch for 500 km and 100 km radii from the observations (CC500 and CC100). The shaded model is the best predictive model (BPM). Contains the values from starting the iterative fitting with the thin plate regression spline on sea surface temperature first (SST 1-4), bottom depth first (BD 2-4) and distance to the ice edge first (DI 2-4).

		Degrees of Freedom							
Run	Model	Z	SST	BD	DI	$\bar{U}$	$\bar{Q}$	$\bar{J}^2$	$\bar{W}$
	CC500								
SST 1	Model 7	9	FREE	FREE	FREE	0.974	0.949	1.069	-1.00
SST 2	Model 3	9	5	FREE	FREE	0.967	0.935	1.070	-1.01
SST 3	Model 3	9	5	6	FREE	0.967	0.934	1.064	-0.98
SST 4	Model 2	9	5	6	3	0.964	0.929	1.068	0.78
	CC100								
SST 1	Model 16	6	FREE	FREE	FREE	0.974	0.948	1.045	-1.13
SST 2	Model 12	6	4	FREE	FREE	0.968	0.937	1.053	-1.93
SST 3	Model 12	6	4	6	FREE	0.967	0.935	1.046	-1.90
SST 4	Model 11	6	4	6	3	0.964	0.929	1.049	-0.59
	CC500								
BD 2	Model 7	9	FREE	6	FREE	0.973	0.948	1.070	-1.09
BD 3	Model 4	9	FREE	6	3	0.972	0.945	1.070	0.11

BD 4	Model 2	9	5	6	3	0.964	0.929	1.068	0.78
	CC100								
BD 2	Model 16	6	FREE	6	FREE	0.973	0.947	1.043	-1.14
BD 3	Model 13	6	FREE	6	3	0.973	0.948	1.048	0.37
BD 4	Model 11	6	4	6	3	0.964	0.929	1.049	-0.59
	CC500								
DI 2	Model 4	9	FREE	FREE	3	0.972	0.946	1.071	0.068
DI 3	Model 4	9	FREE	6	3	0.972	0.945	1.070	0.108
DI 4	Model 2	9	5	6	3	0.964	0.929	1.068	0.78
	CC100								
DI 2	Model 13	6	FREE	FREE	3	0.974	0.949	1.050	0.33
DI 3	Model 16	6	FREE	6	0	0.973	0.947	1.043	-1.15
DI 4	Model 11	6	4	6	3	0.964	0.929	1.049	-0.59

Comparison of descriptive and predictive models

For predictions of acoustic backscatter the iterative LYOCV selected a less complex model configuration than GCV. The BPM contained all covariates, but unlike the BDM it did not contain any interactions. Further, the splines used in the BPM used only 23 EDF compared to the 95.92 EDF used in the smoothers and splines fit within the BDM. For comparisons the BDM was fit using the iterative LYOCV, and the mean Theil's inequality coefficient, and the Janus quotient calculated across the four possible combinations. The mean Theil's inequality coefficient for the BPM was 0.96 and for the BDM was 1.14. The BPM is therefore better than the null model for projection, while the BDM being greater than 1.0 was worse and would not be used for projection. The average Janus quotient was 1.07 for the BPM and 1.78 for the BDM. A Janus quotient near one suggests that the BPM was not overfit. The higher Janus quotient for the BDM confirms that the BDM was more overfit and a less optimum configuration for projection than the BPM.

Optimum projection model

The BPM with splines configured using the optimum basis dimensions was fit using REML to the data from all years to obtain OPM. The two-dimensional thin plate regression spline on location for the OPM had 8.57 estimated degrees of freedom with higher estimated backscatter values towards the west and southwest (Fig. 2B). The sea surface temperature spline used 4.61 EDF and had a smooth unimodal shape with a mode backscatter value at 2.8°C, and decreasing backscatter at both lower and higher temperatures (Fig. 3A) with zero incepts at 2.4°C and 3.8°C. The bottom depth spline

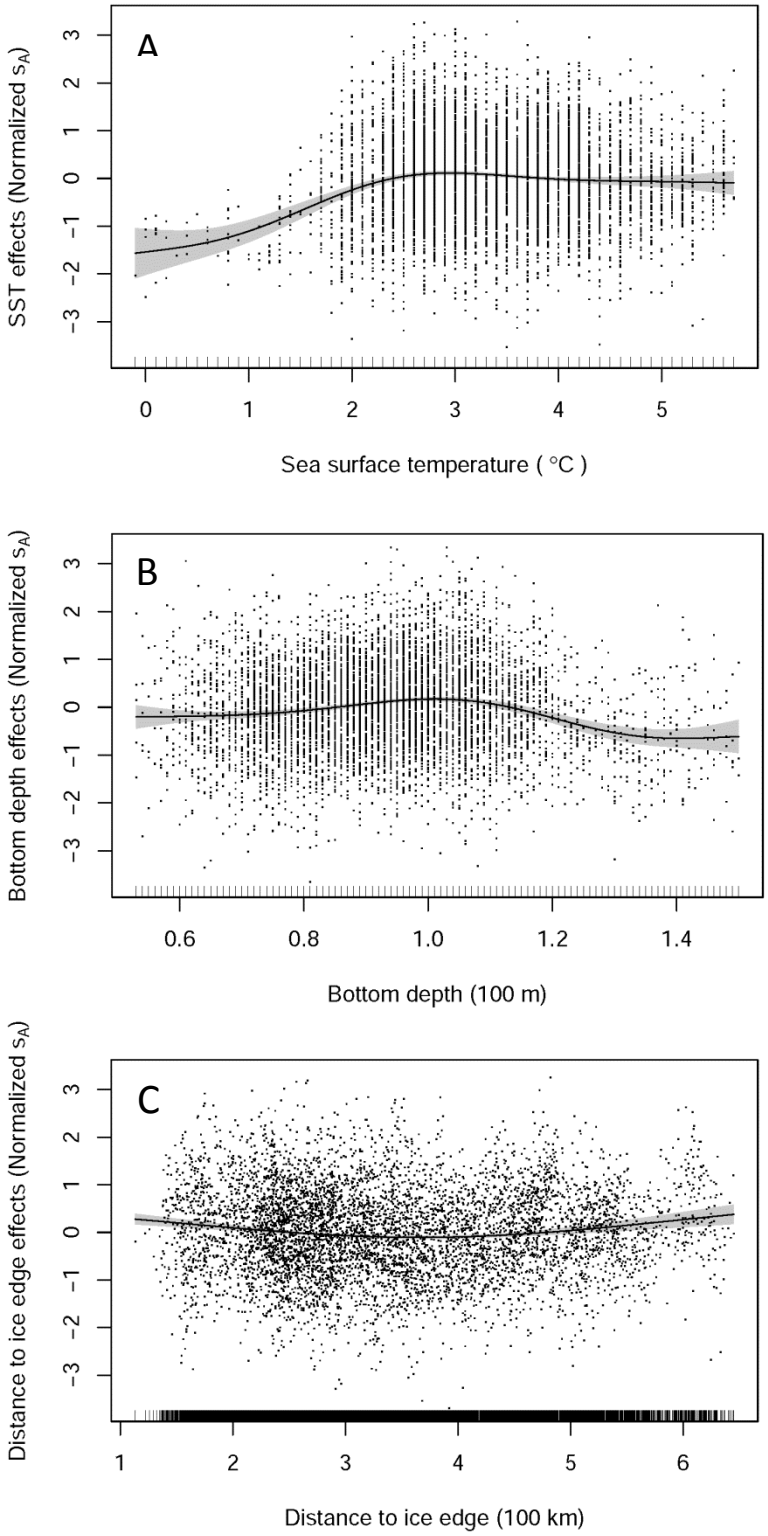

Figure 3. Effects of A) sea surface temperature, B) bottom depth, and C) distance to ice edge on the normalized backscatter (s_A) from the optimum projection model (OPM). Shaded areas are 2 standard errors around estimated effects.

used 5.20 EDF and had a smooth unimodal shape with a mode at 101 m and lower values both at deeper and shallower bottom depths (Fig. 3B) with zero intercepts at 85 m and 113 m. The distance to the ice edge spline used 1.97 EDF and had a smooth U-shaped with the minimum value at 350 km (Fig. 3C). The linear fit to annual cumulative catch at a 500 km radius from the observation was negative with a slope of -1.671×10^{-6}, equating to a decrease of 0.00167 in the normalized backscatter for every 1,000 t of catch. The OPM accounted for spatial autocorrelation at scales greater than 50 km, but residuals still retained some autocorrelation at scales less than 50 km (Fig. 4). Because the location spline in the BDM had a higher degree of flexibility, the BDM was better able to account for small-scale spatial autocorrelation in the observations. The OPM explained 12.9% of the deviance in the available data; 6.2% by location, 2.1% by bottom depth, 1.5% by sea surface temperature, 1.4% by annual cumulative catch within 500 km of the observation, and 0.5% by distance to the ice edge.

Since the strength of the relationship between pollock density and environmental covariates may differ among years, an annual effect was explored for both the spline on sea surface temperature and bottom depth within the OPM. Annual splines on sea surface temperature and bottom depth showed only marginal improvements in fit with increases to explained deviance of 1.1% and 1.0% for SST and BD, and 1.7% for annual splines on both with the added cost of 14.97, 13.80, and 25.35 additional estimated degrees of freedom to the OPM.

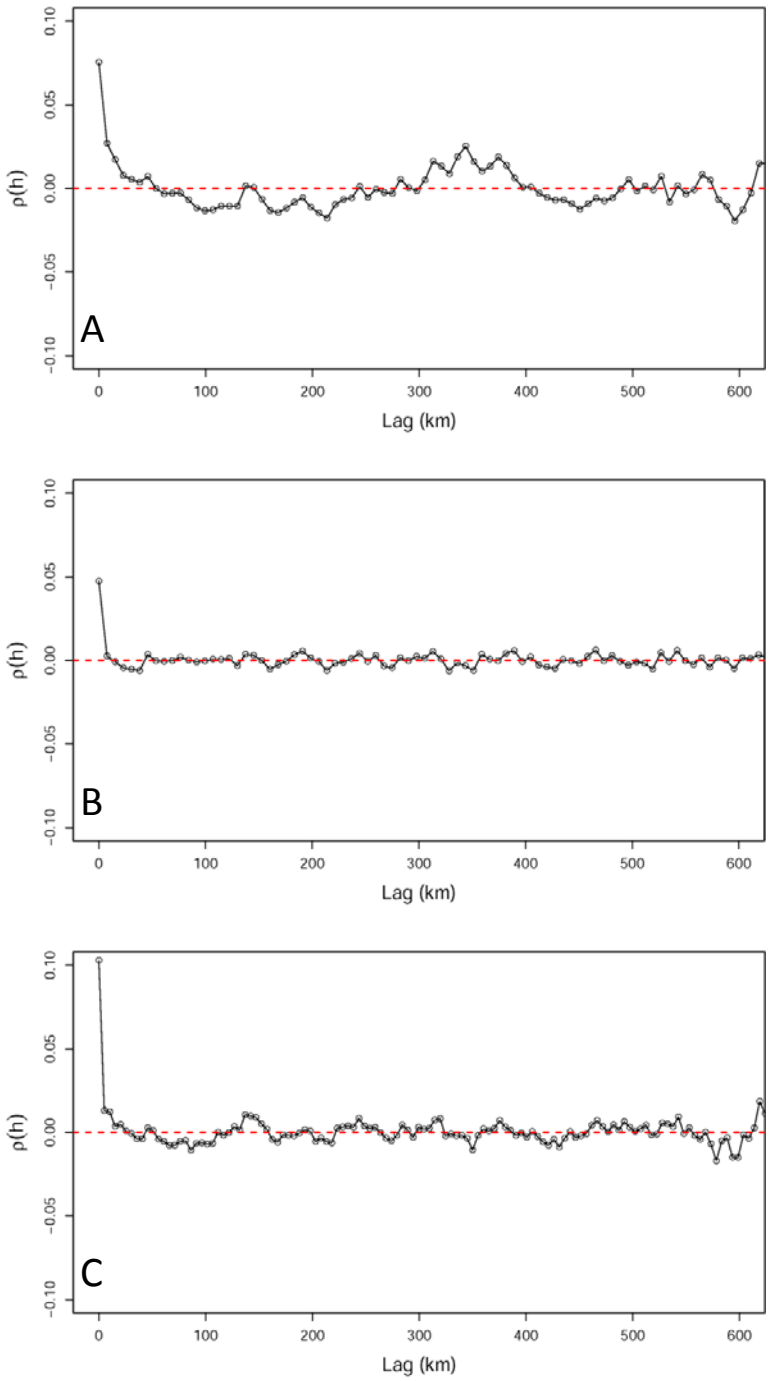

Figure 4. Spatial correlograms for the A) unmodeled normalized backscatter data, B) residuals of the best descriptive model (BDM), and C) residuals of the optimum projection model (OPM) showing spatial autocorrelation in the backscatter data and limited spatial autocorrelation in both the BDM and OPM residuals.

For bottom depth the shape of the annual splines remained unimodal with peaks between 96 and 104 m, the change in the shape of the curve occurred at the tails of the depth distribution where samples were sparse (Fig. 5). For sea surface temperature peak temperatures for 2002 through 2005 were variable with a range between 2.4°C to 3.2°C (Fig. 6). Like the annual bottom depth splines, the main differences in the shapes of the fitted annual splines were primarily in the extreme values where samples were sparse.

Predictions of EBS pollock preferred habitat from the OPM for 2002 through 2006 for January 20, the opening day of the pollock fishery (Fig. 7), show considerable annual variability in available preferred habitat for EBS pollock. The extent of cold water (< 1°C) drives this variability in the projection model. In years when cold water extended across the shelf (i.e. 2002, 2005, and 2006), projected pollock distribution was restricted to the southeast and along the shelf edge. In warmer years (i.e. 2003 and 2004) the projected pollock distribution extended onto the northern shelf, but only in waters within their preferred depth. The prediction standard errors (Fig. 8) were highest at the extreme depths and temperatures where there were few or no samples in the observations. High standard errors within the projection occurred at temperatures colder than 1° C, following the isotherm as shelf waters warmed and cooled. High standard errors of the projection also occurred at depths less than 50 m and greater than 130 m including areas surrounding the Pribilof Islands in the center of the figure and along the Aleutian Peninsula at the southeastern edge of the figure where high abundance is estimated for all years. Standard errors along the 100 m isobath in the southeast remain low, while the northeast projections on the 100 m isobaths are more uncertain due to the south and southwesterly incursion of colder waters from the north and northeast in colder years.

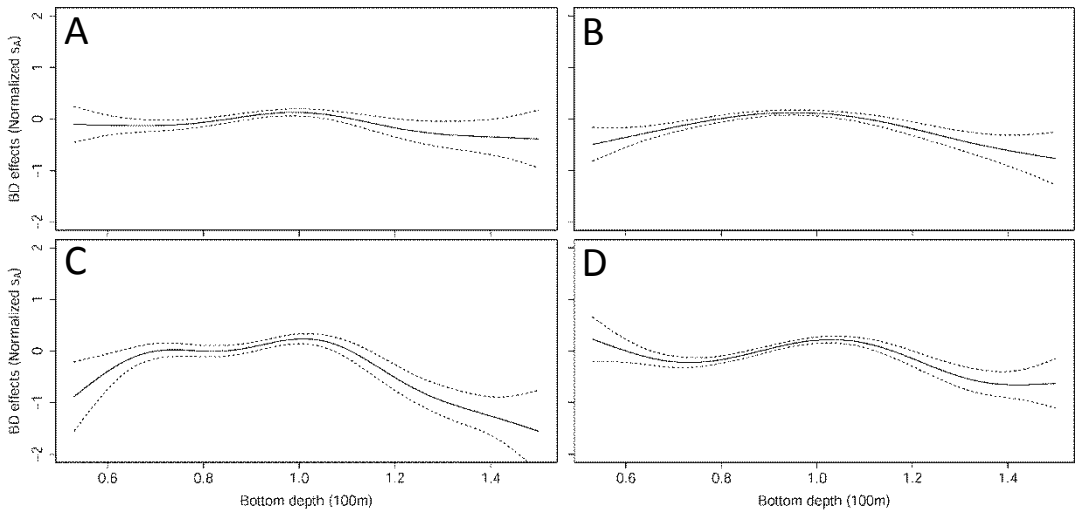

Figure 5 Bottom depth effects on normalized backscatter (s_A) from an exploratory GAM analysis fitting the optimum projection model (OPM) with annual splines on bottom depth for A) 2002, B) 2003, C) 2004, and D) 2005. Note the low variability in peak mode for bottom depth effect and consistent shape between 80 and 120 meters where the majority of data were collected.

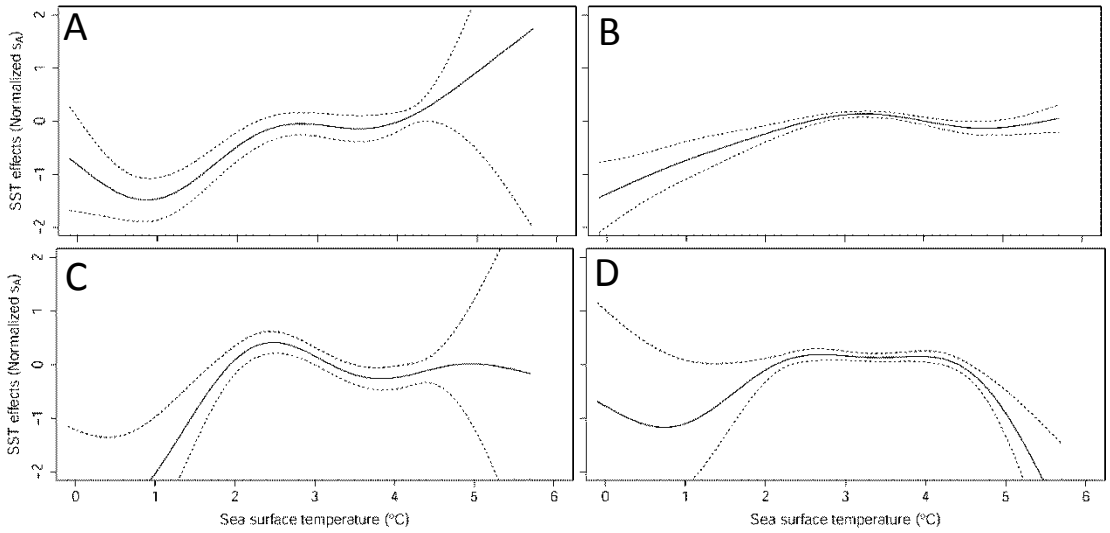

Figure 6. Sea surface temperature effects on normalized backscatter (s_A) from an exploratory GAM analysis fitting the optimum projection model (OPM) with annual splines on sea surface temperature for A) 2002, B) 2003, C) 2004, and D) 2005. Note the peak temperature for pollock abundance varying between 2.4°C and 3.2°C.

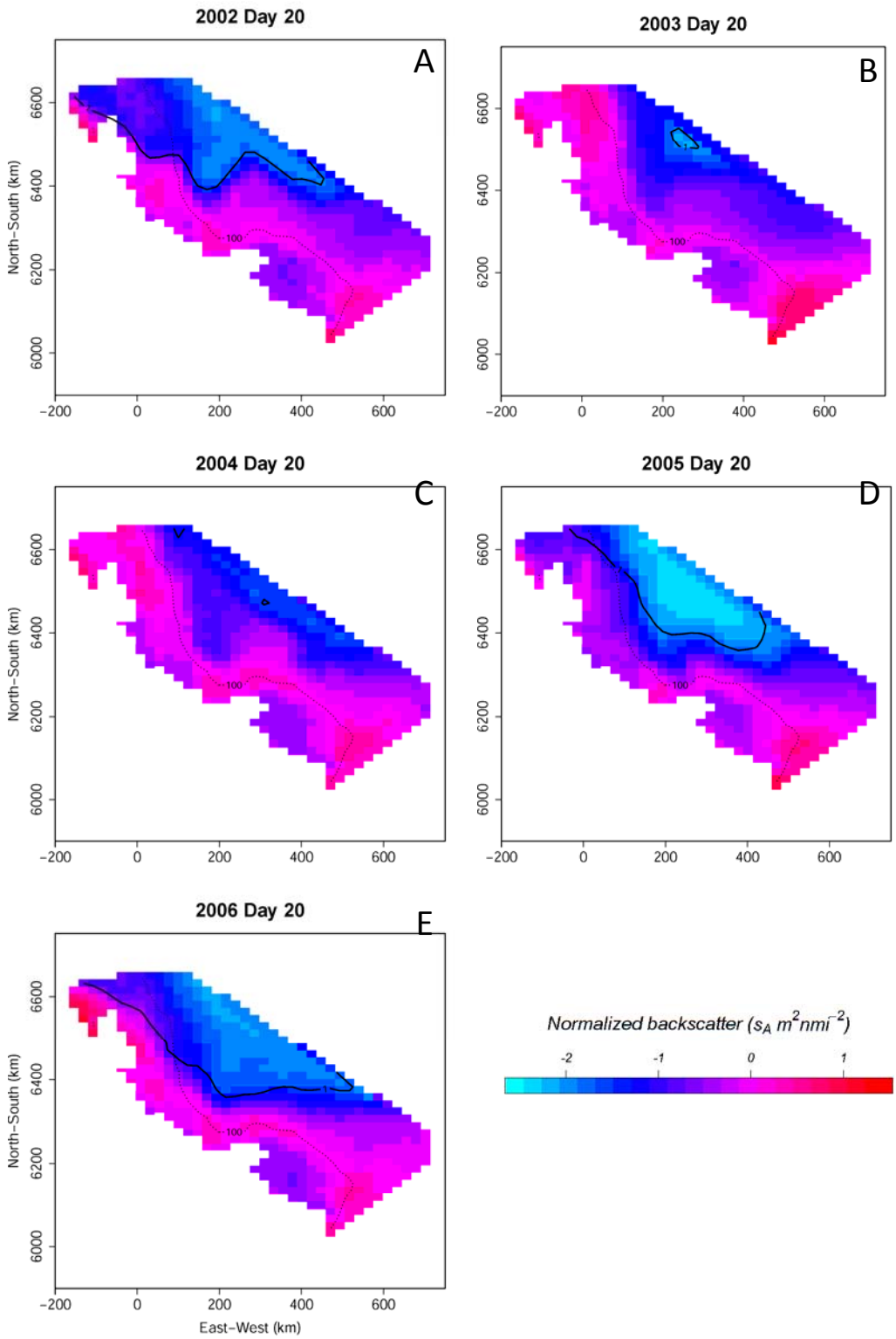

Figure 7 Projections of EBS pollock preferred habitat on January 20 for A) 2002, B) 2003, C) 2004, D) 2005, and E) 2006. The 1 °C isotherm is indicated in the solid black line, the 100 m isobath by a dotted black line.

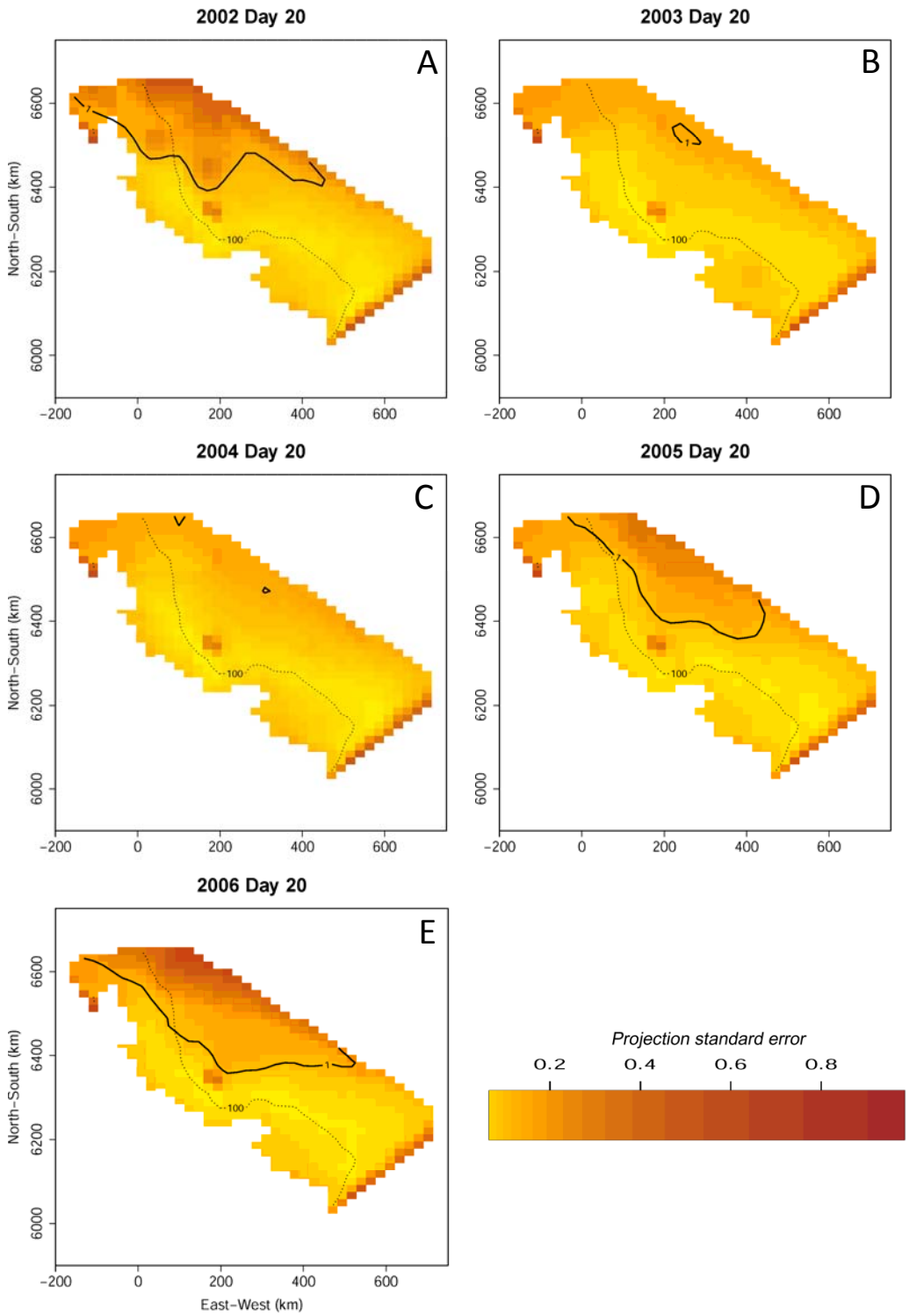

Figure 8 Prediction error from projections of EBS pollock preferred habitat on January 20 for A) 2002, B) 2003, C) 2004, D) 2005, and E) 2006. The 1 °C isotherm is indicated in the solid black line, the 100 m isobath by a dotted black line.

Comparison of winter acoustic and summer bottom trawl data

Comparison of EBS pollock realized niche centers (RNC) and widths (RNW) for depth and water temperature from the summer bottom trawl surveys (Table 3), the winter opportunistic data, and the OPM area above the zero intercept are presented in Figure 9. There was low inter-annual variability for both temperature RNC and bottom depth RNC and winter and summer RNW for 2002 through 2005 nearly completely overlapped one another for both temperature and depth. Figure 9 illustrates the non-symmetry in the shape of the OPM derived realized thermal and bathymetric niches as they do not completely overlap with the RNW in all years for either environmental covariate.

The BPM model fit to the summer bottom trawl survey provided an explained deviance of 39.2% using 15.4 EDF. Both bottom depth and bottom temperature were significant factors in the model (p-values < 0.001) explaining 10% and 5% of the deviance. Location with EDF = 5.0 provided the majority of the explanatory power, accounting for 24.1% of the deviance. The temperature spline curve (EDF = 4.1) was unimodal with a mode at 2.8°C, the same as the winter OPM mode (Fig. 10 and Table 4). However, the summer curve was wider than the winter curve with zero intercepts at 1.4°C and 4.9°C. The bottom depth spline curve (EDF = 5.3) was unimodal with a mode at 93 m. The summer mode was shallower than the winter mode (101 m). The summer bottom depth curve was also wider than the winter curve with zero intercepts at 57 m and 116 m.

Table 3 Realized bottom depth and temperature niche centers (RNC) and widths (RNW) for 2002 through 2005 summer bottom trawl surveys (BTS) and winter opportunistic acoustic data (OAD) showing overlap of summer and winter pollock temperature and depth realized niches.

		Bottom depth (m)		Temperature (°C)	
Year	Data source	RNC	RNW	RNC	RNW
2002	BTS	89	23	2.7	1.0
2002	OAD	89	17	3.0	0.5
2003	BTS	95	32	3.3	1.2
2003	OAD	93	16	3.8	1.1
2004	BTS	90	27	3.3	1.1
2004	OAD	91	13	3.1	0.5
2005	BTS	102	25	3.4	1.1
2005	OAD	96	15	3.5	0.6

Table 4 Modes and upper (UZI) and lower (LZI) zero intercepts for the winter optimum projection model and best predictive model fit to the summer bottom trawl survey data (BPM_{BTS}).

	Temperature (°C)			Bottom depth (m)		
Model	Mode	LZI	UZI	Mode	LZI	UZI
OPM	2.8	2.4	3.8	101	85	113
BPM_{BTS}	2.8	1.4	4.9	93	57	116

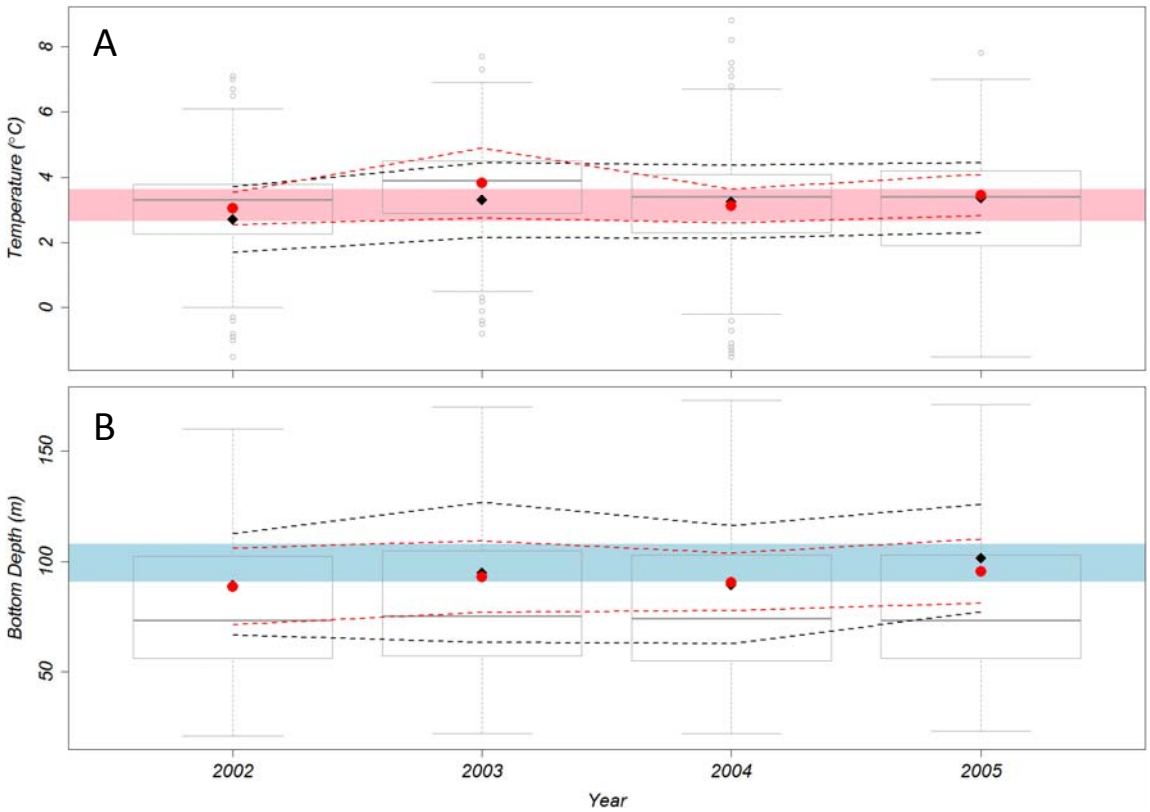

Figure 9 Boxplots of pollock distribution by A) temperature (°C) and B) bottom depth (m) with realized niche centers from the Alaska Fisheries Science Center summer bottom trawl survey (Lauth 2011) catch per unit effort (black diamonds) and from the winter opportunistic acoustic data collection (red circles) with the realized niche width indicated by the dashed lines. The shaded areas are areas of the splines above zero in the optimum projection model for each covariate.

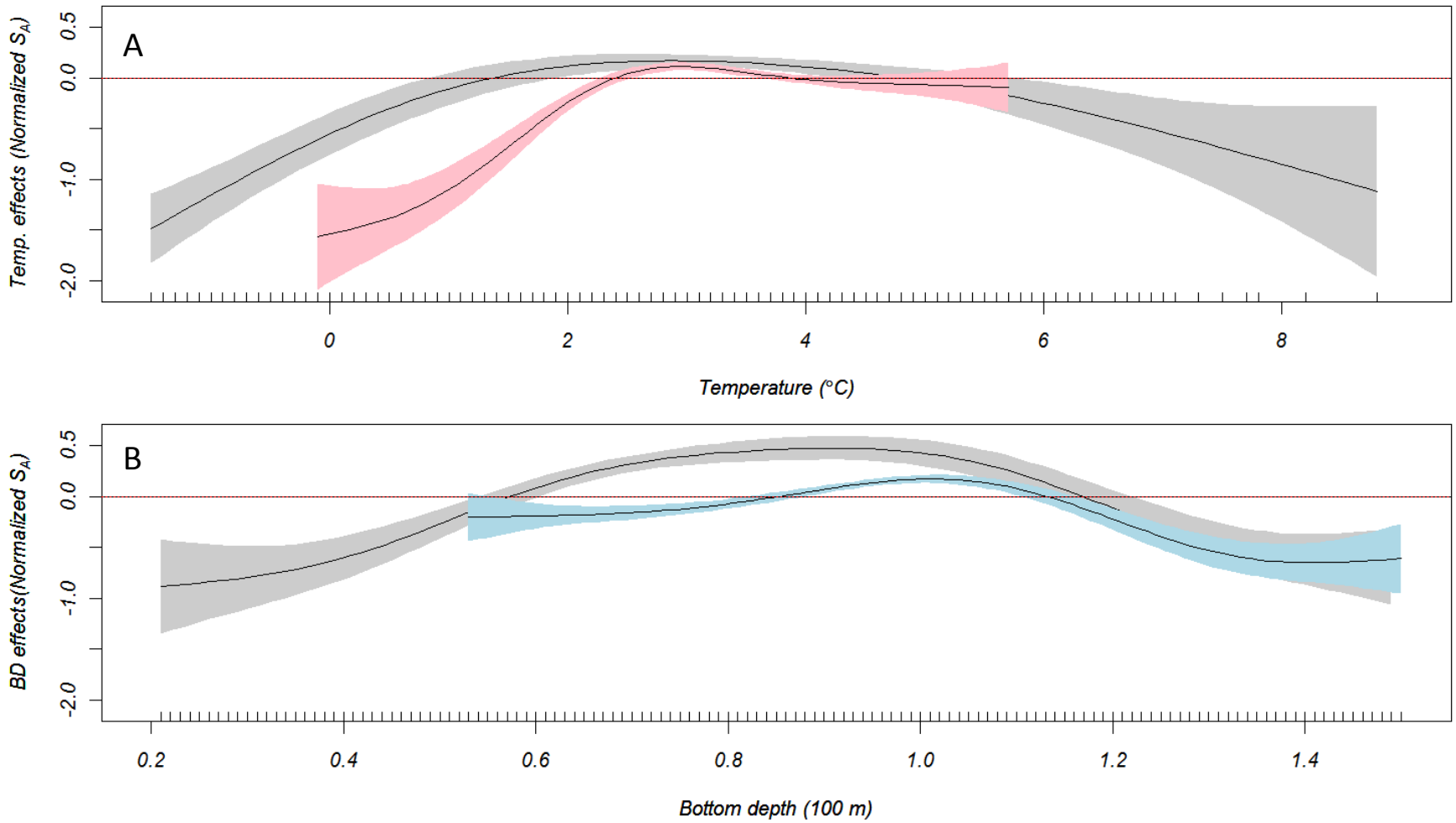

Figure 10 Comparison of effects of A) temperature and B) bottom depth from GAM fits to winter opportunistic acoustic data (overlaid pink and blue curves) and summer bottom trawl survey data (underlying gray curves). The bottom trawl temperatures are bottom temperatures. The opportunistic acoustic data temperatures are sea surface temperatures.

DISCUSSION

Model performance

The purpose of this study was to determine whether available environmental covariates could be used to predict pollock distribution at a daily resolution during winter on the EBS shelf. Cumulative catch, sea surface temperature, bottom depth, and distance to the ice edge were significant predictors of winter pollock density on the EBS shelf. However, in both the descriptive and predictive models, the majority of model deviances remained unexplained. The lack of descriptive power in the BDM can be attributed, in part, to inter-annual variability. An additional ~11% explained deviance was gained in the BDM by adding annual location splines and annual 3-dimensional smoothers on SST, BD, and DI. There were considerable differences in the shapes of the splines and smoothers suggesting that the BDM did not identify consistent inter-annual relationships between pollock density and environmental variables.

The OPM improved marginally when the splines were allowed to vary annually (+1% explained deviance). Shapes of the annual 1-dimensional splines fit to SST and BD deviated only slightly from the OPM fit or from each other, primarily at the bounds of the available data where there were few samples. Therefore it is reasonable to assert that the OPM provided a means of characterizing inter-annually consistent effects of these covariates even though large proportions of the variability remained unexplained.

Pollock exhibited a more patchy distribution than the environmental variables used in this study, with high variability over short spatial and temporal lags (Barbeaux et al. 2013). Therefore a high percentage of explained deviance would not be expected using only these variables. Spatial and temporal projections made from the OPM provide time-dependent snapshots of possible pollock habitat, but there remains a high degree of uncertainty in these projections. Differences in juvenile pollock density, vertical and horizontal distribution in the laboratory have been tied to light levels and temperature gradients (Olla and Davis 1990). Given the high degree of mixing that occurs on the EBS shelf during winter (Stabeno *et al.* 2007), the lack of continuity in pollock distributions at small-scales is not attributable to small-scale variability in oceanographic conditions. Differences in light levels have been shown to affect adult pollock density and vertical distribution in the EBS (Kotwicki *et al.* 2009, Barbeaux et al. 2013) and therefore some daytime variability in pollock density at small scales is likely due to differences in light levels. Finally unaccounted variability and lack of distributional continuity in EBS winter pollock distribution may be related to stochastic movement of aggregations within their preferred habitat and as such may be unpredictable at the daily temporal and 100 km^2 spatial resolution analyzed in this study. If the low predictability is due to stochastic movement within

preferred habitat then decreasing the resolution of the analysis should achieve better predictive power. The higher explained deviance (39.2%) from fitting the BDM to the summer bottom trawl data may be due in part to the lower resolution of the bottom trawl data.

Comparison with summer data

This study postulates that although pollock migrate between summer feeding areas and winter spawning grounds (Bailey *et al.* 1999, Kotwiki *et al*. 2005), their distribution is bounded by seasonally invariant environmental requirements and preferences. If true then spatial distributions of pollock may differ from summer to winter, but the effects of water temperature and bottom depth on pollock distribution should be similar and inter-annually consistent. Realized niche analyses of summer bottom trawl survey data from 2002 through 2005 suggest that realized temperature and depth niche centers for pollock did not change significantly either annually or seasonally with overlapping RNW for all years and seasons. As expected realized niche widths for both temperature and depth were wider in summer, subsuming winter RNWs for three of four years for temperature and all years for bottom depth. Similarly, GAMs of summer bottom trawl data show wider unimodal curves than those from GAMs fit to winter data for both temperature and bottom depth.

Although the winter zero intercepts were completely within the summer zero intercepts, there was a difference between the winter and summer modes that was not captured in the realized niche analysis. A possible explanation for the expansion of summer pollock into a wider proportion of depth and temperature habitat is that although pollock have a temperature preference that is consistent between winter and summer, pollock are more selective of water conditions during winter spawning then during summer feeding when they spread inshore with prey.

Another possible explanation for the apparent differences between summer and winter realized niches is that bottom temperature doesn't adequately characterize temperatures inhabited by pollock in the summer due a strong summer thermocline. The analytic methodology employed in Swartzman *et al*. (1995), the use of GAMs to quantify relationships between pollock abundance and environmental covariates, was similar to this study. Swartzman *et al.* (1995) used pollock abundance above 50 m derived from mid-water acoustic surveys and water column temperatures at 50 m. The purpose of restricting data was to counter possible effects of the thermocline on pollock distribution. The shapes and modes of the splined effects were strikingly similar between Swartzman *et al.* (1995) and the OPM for both bottom depth and water temperature (Fig. 11). Both analyses show unimodel curves for the bottom depth effect with a peak ~100 m and unimodal curves for water temperature with a peak at ~2.5°C for Swartzman *et al.* (1995) at 50 m and 2.8°C for winter sea surface temperature in this

study. When thermocline effects are taken into account, preferred pollock habitat characterized by depth and temperature were similar for summer and winter.

Future applications

The winter distribution of adult pollock may be critical to recruitment variability in EBS pollock. There are two theoretical mechanisms in which available preferred habitat could influence pollock recruitment. The most recent hypotheses on the mechanisms controlling EBS pollock recruitment assume EBS pollock are phylopatric with inter-annually consistent spawning locations (Bachelor *et al*. 2010).

Assuming winter adult distribution mirrors spawning location, results of this study suggest that EBS pollock spawning location may be more variable than currently assumed. This study found that adult pollock in the EBS move to avoid water temperatures below 2°C. The winter extent of cold water across the shelf is variable. In winters where the shelf is covered with cold water, pollock distribution is restricted to the outer continental shelf edge. During winters with warmer (>2°C) water temperatures, pollock may spread over the shelf. Such differences in distribution may impact spawning location and timing and the eventual destination of the floating pelagic pollock eggs and larvae.

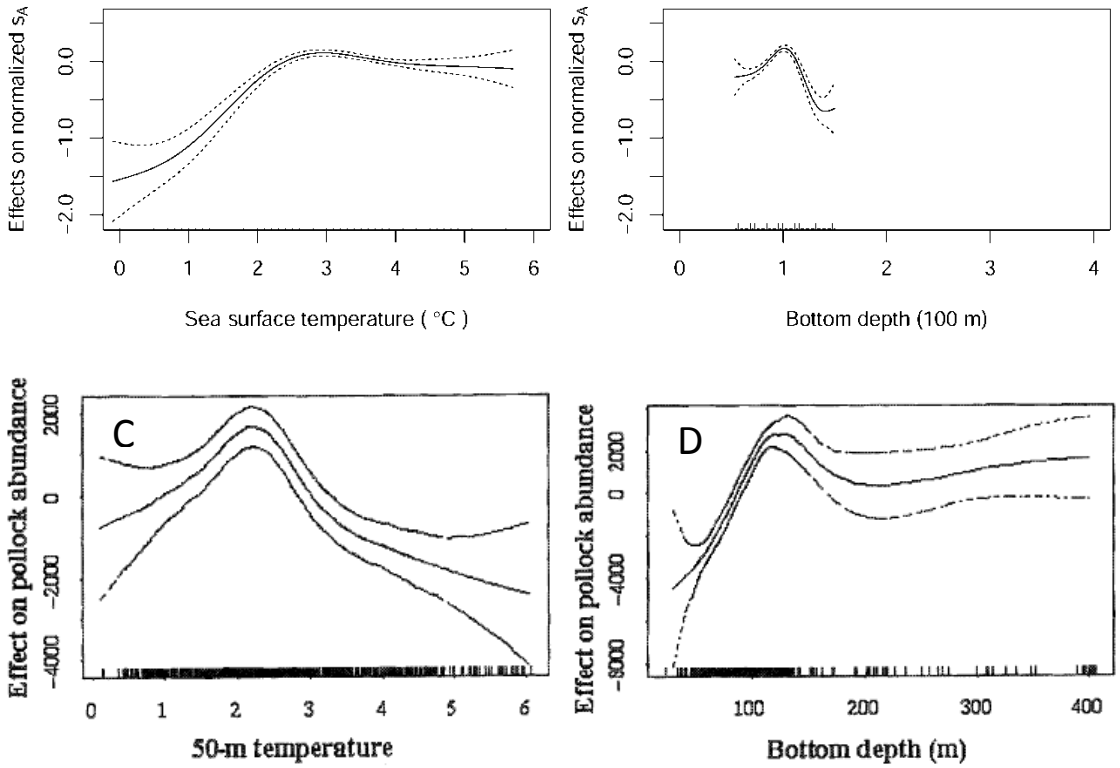

Figure 11. GAM derived effects of A) bottom depth and B) sea surface temperature on the normalized backscatter (s_A) from the optimum projection model (OPM) on winter acoustic data 2002 through 2005, and C) bottom depth and D) sea surface temperature from Figure 4 of Swartzman *et al*. (1995) GAM derived effects of bottom depth (m) and water column temperature (°C) at 50 meters from summer 1988 acoustic survey data.

Wespestad *et al*. (2000) suggested that cannibalism was the main factor determining recruitment variability in EBS pollock. They postulate that warm water in winter and spring results in high transport of larvae and therefore more separation between young of the year and adult pollock than in cold years when across-shelf transport is low. Mueter *et al*. (2011) postulate that, although they are not the sole factors determining recruitment, winter and spring temperatures influence the separation of adults, juveniles, and larvae. Hunt *et al.* (2011) postulate that warm years with early ice retreat produces fewer large zooplankton and predation on age-0 pollock is increased, including cannibalism by juvenile and adult pollock. Smart *et al*. (2012) found further separation of larval stages and juvenile pollock based on water temperatures and differential growth and mortality by larval stage between warm and cold years. These findings suggest that the amount of available preferred winter habitat may be an important predictor of pollock recruitment. Results suggest that an index of available pollock preferred winter habitat could be developed from the OPM and should be evaluated as a covariate for the prediction of pollock recruitment in the future.

Chapter 7: Opportunistic Data Collection as an Index of Local Depletion

This paper is in revision for details refer to:

Barbeaux, S. J., J. K. Horne, and J. N. Ianelli. 2014. A novel approach for estimating location and scale specific fishing exploitation rates of eastern Bering Sea walleye pollock (*Theragra chalcogramma*). Fisheries Research 153: 69-82. Available online 3 February 2014 (http://dx.doi.org/10.1016/j.fishres.2014.01.004)

Chapter 7: Overview

In further studies developed from the opportunistic acoustic data (Barbeaux et al. 2013) collected from commercial fishing vessels, a depletion model was explored that investigates the effects of the commercial fishery on pollock abundance over a range of resolutions (100 km^2 to 50,000 km^2). This project also provides an index of pollock abundance in the eastern Bering Sea (Barbeaux et al. 2014). Although there are annual bottom trawl surveys and biennial acoustic surveys conducted for this species, they measure the summer feeding population distribution and abundance. These snapshots may not accurately portray the population targeted in the winter fishery. Given the continued collection of acoustic data from eastern Bering Sea pollock catcher processor vessels, a Leslie depletion index of winter pollock abundance could be developed using the methodology developed in this project.

Chapter 8: A framework for modeling fish and shellfish responses to future climate change

Chapter 8: Overview

At the very beginning of the project, investigators recognized the need to develop a unified framework for projecting the implications of climate change on marine fish. Investgators worked with BEST/BSIERP climatologists and oceanographers to identify cost effective ways of projecting future stock size using output from global climate models. This project set the stage for the development of the BEST/BSIERP Management Strategy Evaluation models (see Mueter et al. 2011; Ianelli et al. 2011).

The material in this section was published as:

Hollowed, A.B., Bond, N., Wilderbuer, T., Stockhausen, W., A'mar, Z. T., Beamish, R., Overland, J., Schirripa, M. 2009. A framework for modeling fish and shellfish responses to future climate change. ICES Journal of Marine Science 66:1584-1594.

ABSTRACT

A framework is outlined for a unified approach to forecasting the implications of climate change on production of marine fish. The framework involves five steps: 1) identification of mechanisms underlying the reproductive success, growth and distribution of major fish and shellfish populations; 2) assessment of the feasibility of down-scaling implications of climate scenarios derived from Intergovernmental Panel on Climate Change (IPCC) models for regional ecosystems to select and estimate relevant environmental variables; 3) evaluation of climate model scenarios and select IPCC models that appear to provide valid representations of forcing for the region of study; 4) extraction of environmental variables from climate scenarios and incorporation into projection models for fish and shellfish; and 5) evaluation of the mean, variance, and trend in fish and shellfish production under a changing ecosystem. This framework is applied to forecast summer sea surface temperature in the Bering Sea from 2001-2050. The mean summer surface temperature was predicted to increase by 2°C by 2050. The forecasting framework was also used to estimate impacts of climate change on production of northern rock sole (*Lepidopsetta polyxystra*) through projected changes in cross-shelf transport of larvae in the Bering Sea. Results suggest that climate change will lead to a modest increase in the production of strong year classes of northern rock sole.

INTRODUCTION

The recent report of the Intergovernmental Panel on Climate Change (IPCC) concludes that "*There is very high confidence that the global average net effect of human activities since 1750 has been one of warming"* (http://www.ipcc.ch/graphics/gr-ar4-wg1.htm), IPCC, 2007). These changes in climate, in concert with associated environmental disturbances and other drivers, are expected to have lasting impacts on the properties of marine ecosystems and the goods and services extracted from them. With a few exceptions, the IPCC AR4 assessment provides qualitative rather than quantitative predictions of impacts on marine resources (Fischlin *et al*., 2007). The report identifies several sources of uncertainty that contributed to the reliance on qualitative statements including: inadequate representation of the interactive coupling between ecosystems and the climate system; limitations of climate envelope models used to project responses of individual species to climate change; interactions between climate change and changes in human use and management of ecosystems. Since the publication of the report, analysts have endeavored to evaluate the climate-ecosystem couplings (Di Lorenzo *et al.*, 2008) and new techniques for selecting climate scenarios for use in projections (Overland and Wang, 2007; Wang *et al.*, 2010). This paper presents a framework to use these new results to make quantitative forecasts of climate change impacts on fish and shellfish that can be used as part of a coordinated global effort to assess these impacts on commercial fish and their fisheries throughout the world's oceans.

Since the publication of the IPCC AR4 report, scientists around the world have formed interdisciplinary research teams to improve our understanding of the linkages between climate forcing on marine ecosystems and the response of marine fish and shellfish (Brander, 2008; Hollowed *et al.*, 2008; ICES, 2008). These groups are exploring techniques for quantifying the impacts of climate change on the reproductive success, growth and distribution marine fish and shellfish. ICES and PICES sought to facilitate these global research efforts by forming a joint ICES/PICES working group that wouldl promote the development of quantitative forecasts of climate impacts on fish and shellfish in the world's oceans (http://www.ices.dk/workinggroups/ViewWorkingGroup.aspx?ID=331).

Three modeling approaches are typically applied to evaluate the impacts of climate change on fish and shellfish resources:

- Statistical downscaling: Regional scenarios are estimated from IPCC model projections and are used to forecast time series of regional environmental variables (e.g. monthly temperature, advection, prey availability, predator abundance, habitat volume) that are incorporated into stock projection models to estimate future fish or shellfish production.

- Dynamical downscaling on regional scales: IPCC model output is coupled to regional ocean models to project changes in nutrients, phytoplankton, zooplankton and higher trophic level responses and feedbacks.
- Dynamic global models: Fully coupled biophysical models at the global scale that operate at time and space scales relevant to coastal domains.

It is likely that all three modeling approaches will draw on information derived from the correlative, mechanistic and analogue studies (Fischlin *et al*., 2007). Extensions of these modeling approaches could include simulations to evaluate the performance of different management strategies under changing ocean conditions (A'mar *et al.* 2009).

There are tradeoffs between all three modeling approaches. From a physical perspective, statistical downscaling requires that each of the local environmental variables can be linked to the climate or regional forcing that can be projected by the IPCC global climate models (GCMs). In many cases the functional relationships between the local environmental conditions and the climate or regional forcing have not been ascertained or they are uncertain. From a biological perspective, developing forecasts based on environmental variables may not perform well because the responses of fish and shellfish to changes in environmental conditions are represented by simplified interactions that may miss nonlinear responses or feedbacks within the system (Steele, 2009; Hsieh *et al.,* 2005). However, complex biophysical models may suffer from the lack of information on key parameters and a high likelihood of model misspecification. The tradeoffs between modeling approaches and the knowledge that the results will be used to form high stakes management decisions suggest that multiple modeling approaches should be considered and skill assessments should be regularly performed to inform the public on the inherent uncertainties associated with the projections (Stow *et al.*, 2009).

We recognize that reliable biological projections necessitate getting the climate forcing correct. In this regard, present-day models have demonstrated the ability to simulate the past few decades of the mean climate reasonably well (Reichler and Kim 2008), and presumably, this skill also applies to their 21st century forecasts. Due to the chaotic nature of the climate system, it is impossible to forecast the timing and phases of future swings in the climate system. While specific forecasts are therefore not feasible, the models do appear capable of being used to explore the probable changes in the overall properties of the climate forcing.

The global need for baseline quantitative information on potential climate change impacts on fish and shellfish warrants a two-pronged approach. Rapid progress can be made using statistical downscaling

where environmental variables are projected and incorporated into existing stock projection models using existing knowledge of mechanisms linking fish and shellfish response to biophysical forcing. Time series generated for this effort can be used in retrospective analyses to evaluate the performance of models and validation of hypothesized functional relationships. In parallel, the longer-term, and more costly, effort involved in developing sufficient understanding to implement dynamic downscaling by developing coupled biophysical models should be commenced as a means of addressing complex feedbacks in marine ecosystems. This paper describes a framework for making the first type of forecast.

METHODS

The proposed statistical framework involves the following steps:

- Identification of mechanisms that explain environmental influences on the reproductive success, growth and/or distribution of major fish and shellfish populations.
- Identification of the key environmental variables needed to model fish and shellfish responses to environmental variability.
- Assessment of the feasibility of using IPCC model simulation results to predict the environmental variables.
- Comparison of IPCC model hindcasts to observed 20th century conditions on a regional basis to select, and weigh, the IPCC model scenarios to develop an ensemble for use in projections.
- Estimation of environmental variables using the ensemble projection and incorporate time series of environmental variables in stock projection model(s) for fish and shellfish.
- Evaluation of the effects of harvest strategy under changing ecosystem conditions.

Methods for Selecting Environmental Variables

In most regions, fisheries oceanographers have conducted retrospective and process studies designed to improve our understanding of the processes linking ecosystem forcing to reproductive success, growth, and distribution of commercial species (For recent examples see symposium volumes edited by Dann and Fogarty, 2000; Fogarty 2001; Royer and Dagg, 2002; Batchelder *et al.*, 2005). These fisheries oceanography programs provide a basis for selection of environmental variables for use in predicting climate change impacts on commercial fish and fisheries.

Once the environmental variables have been identified, fisheries oceanographers and climate scientists should meet to explore the feasibility of extracting variables from IPCC model projections. This step often requires an exploration of techniques to connect the climate forcing to the environmental factors at the spatial and temporal scales relevant to fish and fisheries. The newly formed ICES/PICES working

group on Forecasting Climate Change Impacts on Fish and Shellfish facilitates this type of communication and scientific exchange.

Methods for Projecting Environmental Variables

There are a variety of ways to formulate future climate scenarios based on the results of IPCC models (e.g., Tebaldi *et al.*, 2005). In general, it is prudent to consider the output from multiple models due to the uncertainties inherent in any individual climate projection. These uncertainties arise because the models are imperfect, of course, and because of the intrinsic variability of the climate system. In other words, from a single simulation it can be very difficult to separate a meaningful signal from the climate "noise" that exists over a vast range of time scales. One approach is to apply a quasi-Bayesian method to construct weighted ensemble mean projections of regional environmental conditions. This method is based on the idea that different models have different strengths and weaknesses, and that the better models for a particular parameter in a particular region should be given greater consideration. Our procedure represents an adaptation of the method developed by Raftery *et al.* (2005) for combining the results from numerical weather prediction (NWP) models for short-term weather forecasts, and is outlined below.

The various IPCC model outputs are evaluated, and rated, based on the fidelity of their hindcasts for the latter half of the 20th century in terms of replicating observed conditions. The errors in these hindcasts are computed for individual parameters and for specific regions. Multiple criteria are considered for each parameter including replication of the means, as well as modeled versus observed variances, and potentially additional measures such as trends and seasonality. The errors are then used to construct "distances" between the model and observations for each model simulation. The distances form the basis for assigning weights for each model using the following expression

$$W_i = \exp(-D_i/D_m),$$

where, W_i is the weight for the individual model run i, D_i is the individual model distance error, and D_m is the mean of the model error distances. The ensemble weighted mean projections are then given by

$$F_{ens}(t) = \sum_{i=1}^{n} W_i \times F_i ,$$

where, F_i (t) are the bias-corrected model projections at time t . The weights, W_i, are also used to compute the variance/uncertainty in the model projections incorporating both inter-model and intra-model forecast variability. As pointed out by Raftery *et al.* (2005) among others, the Bayesian approach has many optimal properties from a statistical perspective.

An Example of the Selection Method

We provide an example of the technique described above using summertime sea surface temperature (SST) over the Bering Sea shelf as the parameter of interest. This parameter represents an important aspect of the oceanography, and is associated not just with the suitability of the habitat for temperature-sensitive species, but is also related to the stratification, and hence the vertical mixing of nutrients into the euphotic zone and ultimately primary production (Hunt *et al*. 2002).

Evaluation of the 20th century model hindcasts was carried out for the region extending from 55° to 65°N latitude, and 165° to 175° W longitude for the average SST over the months of July through September. This evaluation is restricted to the subset of models found to replicate the essential character of the Pacific Decadal Oscillation (PDO, Mantua *et al.*, 1997). The PDO represents the leading mode of variability in SST in the North Pacific, and can be considered an "acid test" of a model's ability to account for the atmospheric variability, oceanic circulation, and air-sea coupling in the North Pacific. The models that pass the PDO test (Overland and Wang, 2007) have been evaluated with respect to their simulations of the mean, interannual variance, and average trend (1948-2007) in seasonally averaged SST over the shelf (Figure 1). The validating data set was obtained from the NCEP Reanalysis (Kistler *et al.*, 2001).

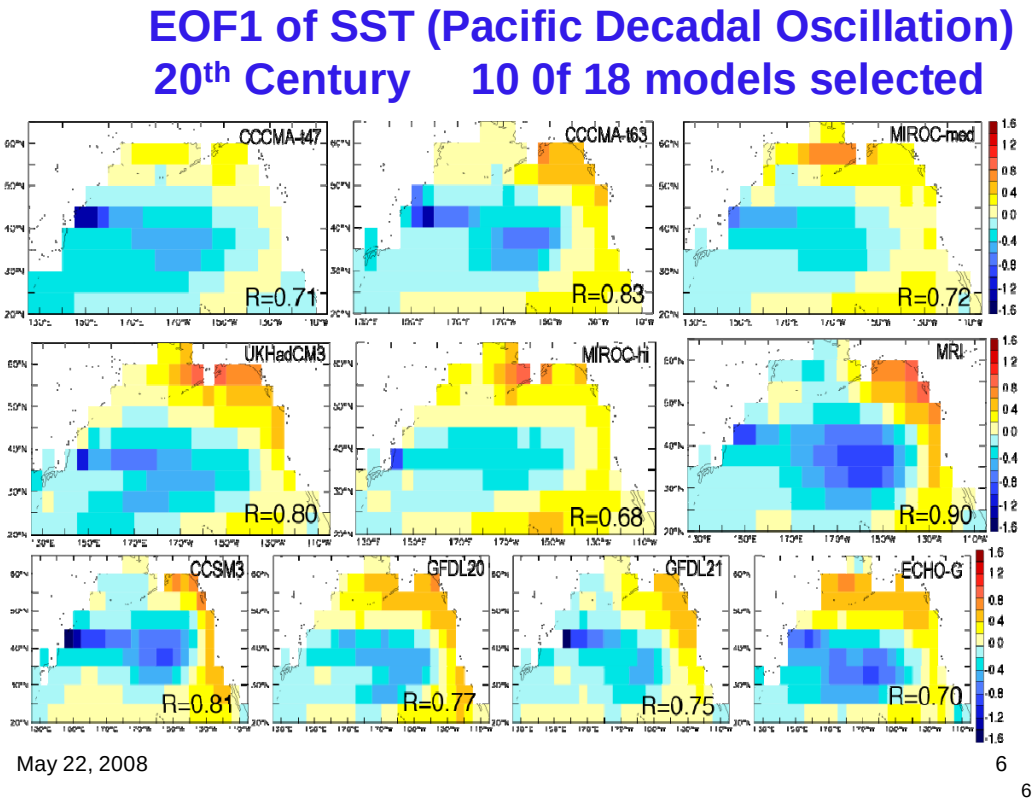

Figure 1. Fit of 10 of 18 IPCC models to the first principal component (EOF1) of SST in the North Pacific.

The weights of the models considered, based on the accuracy of their hindcasts in terms of reproducing the mean, variance and trend in the observed SST of the Bering Sea shelf over the last half of the 20th century, described above, are shown in Figure 2[3]. The highest and second-highest rated models are the high-resolution Canadian model (CCCMAT-63) and the medium-resolution Japanese model (MIROC-med), respectively; the two lowest rankings are for the U. S. Geophysical Fluid Dynamics Laboratory (GFDL) models, GFDL2.0 and GFDL2.1. The latter two models included both sizable errors in their hindcasts of both the mean and trend in SST (they indicated substantial cooling over the latter half of the 20th century). It seems reasonable that their contributions to the ensemble mean, even with bias-correction, receive little weight.

[3] The normalized errors that these weights are based on range from about 0.5 to 10,

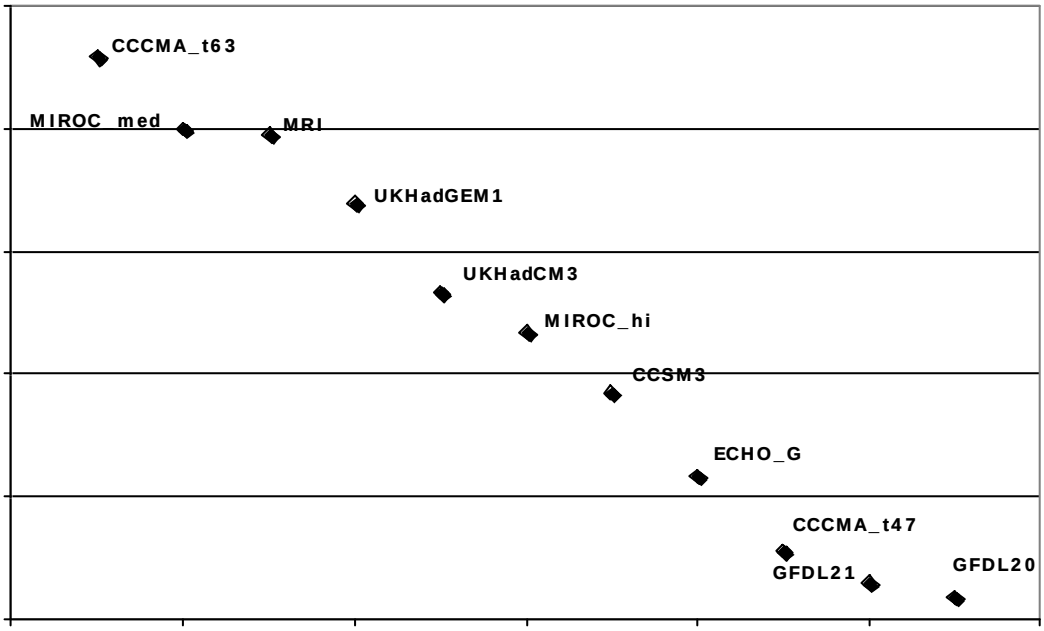

Figure 2. Weights for various models used in forming ensemble mean using a Bayesian model averaging approach. The criteria used for evaluating the models were the accuracy of their hindcasts in terms of reproducing the mean, variance and trend in the observed SST of the Bering Sea shelf over the last half of the 20th century.

A time series of the SST for the first half of the 21st century based on an ensemble weighted mean is shown in Figure 3. This projection is based on the model simulations incorporating the middle-of-the-road A1B emission scenario. The results of the IPCC simulations vary relatively little with the assumed emission scenario for the first half of the 21st century. Much more dramatic differences between the various scenarios are simulated for the second half of the 21st century, which represents another source of uncertainty. The ensemble results for the late summer SST on the Bering Sea shelf feature a near constant warming trend of about 0.4 C per decade. Note that the ensemble mean effectively averages out most of the year-to-year variability that exists in the individual model simulations. The Bayesian method indicates an expected standard deviation of approximately 1°C (as illustrated by the vertical bars in Figure 3) about the ensemble mean in any particular year, with a small increase with time in this uncertainty over the 2000-2050 period of consideration.

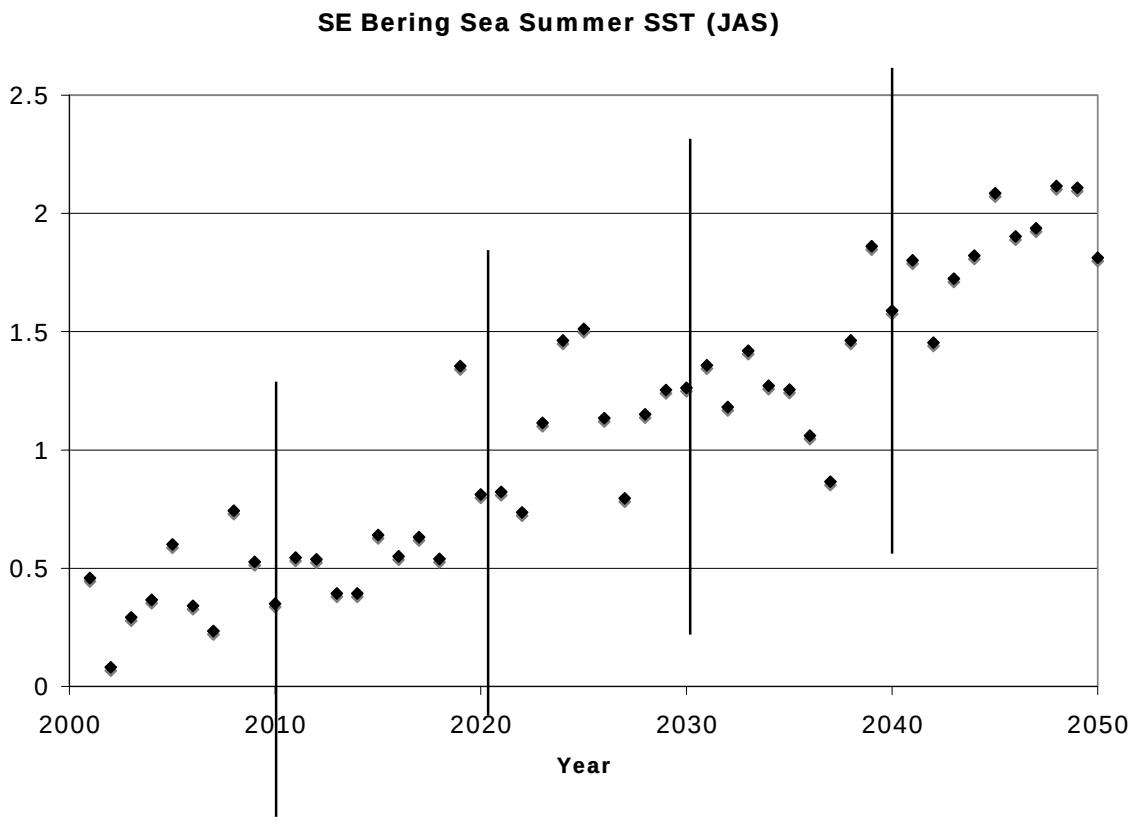

Figure 3. Weighted ensemble mean of IPCC forecasts of SST under A1B emissions scenario. The vertical lines for selected years extend from the mean minus one standard deviation to the mean plus one standard deviation, based on combining the inter-model and intra-model variance in the individual projections.

Methods for Projecting Fish and Shellfish

There are several published methods for incorporating environmental forcing into population dynamics equations (Peterman *et al.*, 2000; Arregui *et al.*, 2006; Maunder and Watters, 2003). Three categories of models hold particular promise for use in projecting climate change impacts on fish and shellfish recruitment. Category 1 models project recruitment (R) by modifying average recruitment ($\bar{R}$) by an environmental variable (I) (equation 1 below) where n is the number of variables and their associated constants (a_i). In this case, the environmental variable (s) would be drawn from the projected ensemble from IPCC models output derived using the weighting method described above.

$$R_{y+1} = \left(\bar{R}_1 e^{\left(\sum_{i=1}^{n} a_i I_{i,y}\right)} e^{(\varepsilon_y - \sigma_R^2/2)} \right); \varepsilon_y \sim N(0, \sigma_R^2).$$

The error term ε_y allows the user to project the expected range of variability in recruitment by simulating 50 year recruitment scenarios with random draws from a distribution of expected recruitment. The potential range of process error associated with the selection of climate change scenarios can be incorporated by projecting recruitment using different climate change scenarios and weighting the mean recruitment projections by the weights provided by the retrospective assessment of the performance of the climate models described above. Density dependent processes are not considered in Category 1 type models.

Category 2 models modify the spawner recruitment relationship to incorporate environmental variables (I) and random variability ε_y (Hilborn and Walters, 1992). For example, a Ricker type spawner recruitment model could be constructed as follows:

$$R_t = \left(\alpha * S_t * e^{-(\beta S + a_1 I_{1,t} + a_2 I_{2,t} + \ldots)} e^{(\varepsilon_y - \sigma_R^2 / 2)} \right).$$

This approach has been used in several retrospective studies designed to assess the performance of models with and without environmental forcing (Peterman *et al.*, 2000; Wilderbuer *et al.*, 2002). The expected range of variability in recruitment due to climate forcing could be simulated by incorporating environmental variables derived from an ensemble of IPCC model outputs derived from the weighting method described above.

Category 3 type models utilize spawner – recruitment functions that incorporate processes at multiple life stages. Some species exhibit dynamic and complex processes due to multiple bottlenecks occurring over several life stages (Rothschild, 2000). Phase transitions in the spawner recruitment relationship may occur due to time lags in the recruitment response of predators and prey (Bailey, 2000). Brooks and Powers (2007) propose a generalized method for modeling the spawner recruitment relationship when key governing factors are exhibited over several life stages. This modeling approach tracks stage-specific processes and accounts for density-dependent impacts on the predation rate. Alternatively, predation effects could be modeled explicitly using a multispecies modeling approach (Jurado-Molina *et al.*, 2005). In Category 3 type models, time series of environmental variables would be derived from ensembles of IPCC model output for different life stages (seasons).

Some ecosystems may exhibit threshold responses (regime shifts) to changing climate conditions (Anderson and Piatt, 1999; Chavez *et al.*, 2003; Beaugrand *et al.*, 2003; Peterson and Schwing, 2003; Scheffer and Carpenter, 2003; Hseih *et al.*, 2005). Threshold responses (regime shifts) to abrupt shifts in climate may reflect changes in the carrying capacity of the ecosystem. Category 1 type models would address shifts in the carrying capacity by partitioning the retrospective time series into regimes and estimating $\overline{R}$ and σ_R^2 for the different regimes. Shifts in the carrying capacity would be addressed in Category 2 and 3 models by incorporating indicators of prey abundance and habitat volume directly into the spawner- recruitment relationship.

The framework presented here could be modified to address the implications of climate change on spatial distributions related to range extensions or contractions (Meuter and Litzow, 2008). Shifts in the range or migration patterns of marine fish or shellfish could be indirectly incorporated by including indicators that represent the volume of suitable habitat (Jacobson *et al.*, 2005; Agostini *et al.*, 2006; Pelletier and Mahévas, 2005).

Stock assessment scientists typically project the stock forward to assess the near term consequences of different harvest strategies (see Punt, 2003; Goodyear, 2004, 2005; Methot, 2005; Schnute *et al.*, 2007, and http://nft.nefsc.noaa.gov/index.html). For Category 2 and 3 type models, analysts have the option of estimating parameters for the spawner-recruitment relationship within a stock assessment or outside of the stock assessment (Haltuch, 2008; Schirripa *et al.*, 2009). Simulation testing and short-term forecasting is recommended to assess the skill of the model relative to observed responses of fish and shellfish. These tests will provide a measure of the uncertainty associated with the model (Schirripa *et al*., 2009). This could be accomplished as part of the periodic stock assessment cycle. This approach will allow analysts to make adjustments to the model to incorporate new information.

MANAGEMENT SCENARIOS

Projections of the distribution, abundance and growth of fish and shellfish populations should include scenarios regarding the expected trends in anthropogenic impacts (Easterling *et al.*, 2007). Time trends in the world markets for fish and shellfish are likely to influence the local demand for sea food (Pinnegar *et al.*, 2006). Collaborations with economists and social scientists will be needed to develop scenarios for the cost of shipping, food preferences and new technological innovations for storage and product development. Collaborations with resource managers will be needed to develop scenarios for future harvest management practices (A'mar *et al.*, 2009). Scenarios for time trends in habitat enhancement (e.g.

artificial reefs) and stock enhancement (marine ranching) will also be needed to adequately forecast the production, distribution and growth of marine fish and shellfish populations throughout the world.

AN APPLICATION FOR NORTHERN ROCK SOLE

Northern rock sole (*Lepidopsetta polyxystra*) is a major flatfish species in the North Pacific Ocean and has a large biomass in the eastern Bering Sea. The species supports a substantial fishery in the Bering Sea and are also harvested in the Gulf of Alaska. Temporal trends in northern rock sole production have been found to be consistent with the hypothesis that decadal scale (or shorter) climate variability influences marine survival during the early life history period (Wilderbuer *et al.*, 2002). After spawning in February-March, northern rock sole larvae are subject to advection from wind, currents, and tidal forcing during April-June. Using an ocean surface current model (OSCURS, Ingraham *et al.*, 1988), Wilderbuer *et al.* (2002) found that wind-driven advection of larvae towards favorable nursery areas in the inner domain coincided with above-average recruitment. The inner domain of the Bering Sea is a productive region due to tidal mixing (Coachman, 1986; McRoy *et al*., 1986). Ocean forcing resulting from onshelf (easterly) winds during the 1980s and again in 2001-2003 coincided with periods of above-average recruitment whereas offshelf (westerly) or midshelf (northerly) winds during the 1990s corresponded with periods of poor or average recruitment (Figure 4). This suggested that patterns of future recruitment for northern rock sole will depend on wind patterns that are influenced by future climate conditions. Thus, to predict future recruitment for northern rock sole, it is also necessary to predict future climate conditions.

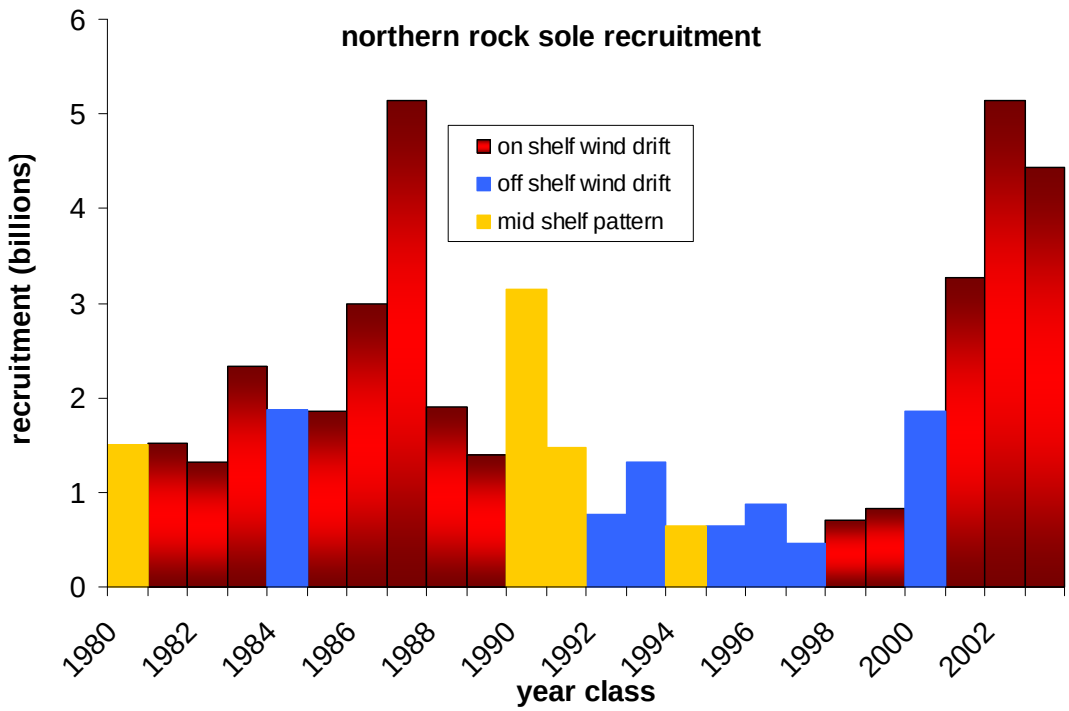

Figure 4. "Observed" recruitment of northern rock sole (estimated from a statistical age-structured model used in the 2007 annual stock assessment). Bar colors reflect classification according to springtime climate condition: onshelf wind drift (red), offshelf wind drift (blue), and midshelf wind drift (yellow).

Following the framework for projecting environmental variables outlined above, spring wind and the associated advection on the Bering Sea shelf was estimated from a weighted ensemble of IPCC model output. Again, the various IPCC models used were rated based on how well their hindcasts for the latter half of the 20th century matched observations. The two specific criteria for this rating were the IPCC model's ability to reproduce the overall mean April-June winds on the southeast Bering Sea shelf, and the interannual variance in the seasonal mean winds. It turns out the models, in general, were able to hindcast the winds more accurately than the SST. The normalized errors in the modeled mean and variance in the winds ranged from about 0.1 to 2. In addition, a different ranking emerged for the climate models for the cross-shelf wind index (Figure 5) than for the late summer SST example presented earlier (Figure 2).

While the MIROC_med and MRI models ranked high for both parameters, and the ECHO-G ranked low for both, other models, such as the CCCMA_t63 and GFDL2.1 were decidedly better for one parameter versus the other. The weights for each model with respect to the cross-shelf winds were then used to form a projection of the winds out to 2050 and converted to ending longitude of surface-drifting larvae. These projections, with the attendant year-to-year variability provided by the Bayesian scheme, indicate a slight

tendency towards increased shoreward transports with substantial variability on top of this weak trend (Figure 6).

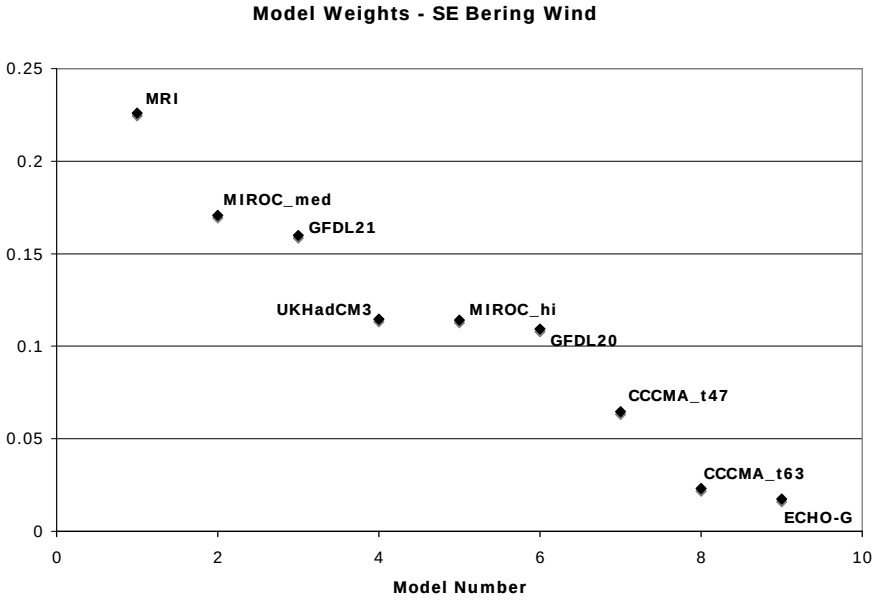

Figure 5. Weights for various models used in forming ensemble mean using a Bayesian model averaging approach. The criteria used for evaluating the models were the accuracy of their hindcasts in terms of reproducing the mean, variance and trend in the observed wind of the Bering Sea shelf over the last half of the 20th century.

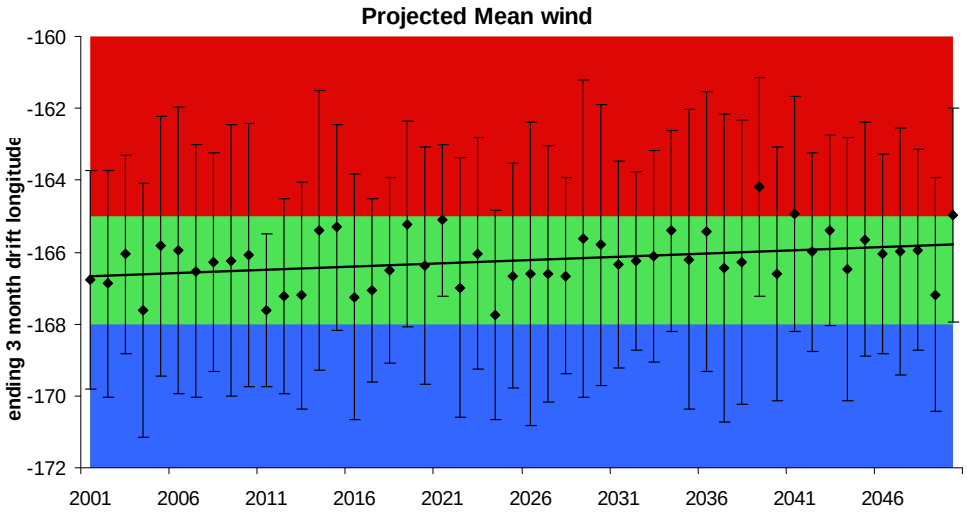

Figure 6. Predicted mean and standard deviation of the longitudinal endpoint of projected larval drift from springtime winds for 2001-2050. Red region represents projected endpoints from onshore drift climate scenario, green region represents mid-shelf drift scenario, and blue region represents off-shelf drift scenario.

Based on these results from the IPCC climate models, the future production of northern rock sole was projected for the period (2001 to 2050) using a method similar to the Category 1 type recruitment function. A hierarchical bootstrap algorithm was applied to estimate for annual variability in future springtime climate (i.e. wind direction and subsequent larval drift) as well as variability in recruitment under a given climate condition. First, three climate conditions (corresponding to the three production regimes identified by Wilderbuer et al., 2002) were characterized according to the range of the ending longitude (*L)* expected for larval drift under each condition: A) onshelf drift (L<165° West), B) midshelf drift (165° West <L≤168° West), and C) offshelf drift (168° West ≤ L). Then, for each projected year, the corresponding predicted mean drift ending longitude and variance from the IPCC model results were used (Figure 6) to draw a sample ending drift longitude from a normally-distributed population. Next, the climate condition corresponding to the sample longitude was identified based on the limits shown in Figure 6. Finally, a value for recruitment was randomly selected (with replacement) from the set of "observed" recruitments (Figure 4) corresponding to the given climate condition. This was repeated 20,000 times to generate bootstrap realizations for each projected year. For each year, the probability of occurrence for each climate condition was computed (Figure 7), as well as the mean and distribution of recruitment (Figure 8).

Not surprisingly, the temporal trend in probability of occurrence of each climate scenario follows a pattern similar to that of the mean ending longitude of larval drift. These results suggest a moderate increase in expected recruitment with time because the trend indicates more frequent occurrence of the onshelf climate condition (A in Figure 7) with time, which corresponds to the highest expected mean recruitment. However, Figure 7 does not incorporate the variation in recruitment which is displayed in Figure 8.

Once the variation of recruitment within a climate condition is incorporated, any trend toward larger recruitments with time is much reduced (Figure 8). The mean of expected recruitment displays a comparatively smaller trend toward larger values with time while the median displays no trend whatsoever. The reduction in trend from mean to median occurs because of the asymmetrical nature of the distribution of recruitment under each of the three climate conditions. As such, the model suggests that, to the best of our current knowledge, rock sole production will not be substantially impacted by future climate change--at least in regard to the effects of that change on patterns of springtime larval advection.

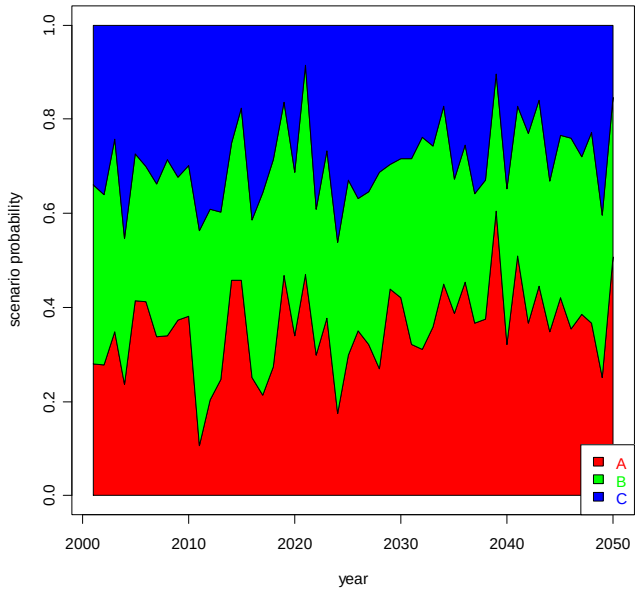

Figure 7. Cumulative probability of future springtime climate conditions (A, B, C) based on 20,000 bootstrapped samples/year (A= onshore winds, B = mid-shelf winds, C = off-shore winds).

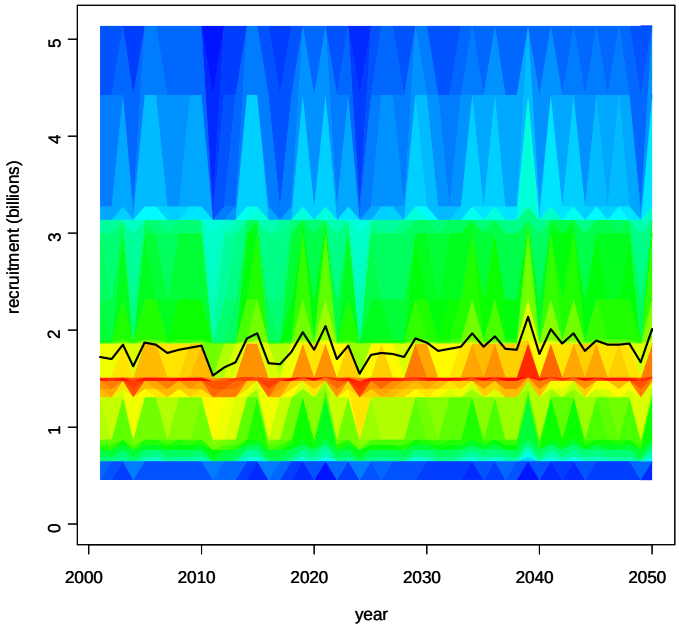

Figure 8. Projected mean (black line) and quantiles(colored shading) for northern rock sole productivity (recruitment) by year. Quantiles are color-coded symmetrically from the median (bright red) to 0 or 100% (dark blue).

DISCUSSION

A framework for forecasting the implications of climate change on production of marine fish was presented that incorporates estimates of key environmental variables derived from IPCC global climate model outputs in stock projection models. The wide range of possible outcomes from the AR4 models presents a challenge. To deal with possible systematic errors in these models and the uncertainty in their simulations in general, a method was developed for weighting individual model forecasts. This method yields estimates of means and variances in environmental variables projected into the future on the time and space scales relevant to fish and shellfish populations. The framework also utilizes known linkages between environmental variability and fish and shellfish production. Statistical projection methods enable scientists to simulate the likely impacts of climate change on fish and shellfish, incorporating the uncertainty associated with climate projections and process error in the projection model. Stock projection models are utilized to project the expected value and its associated uncertainty.

There is considerable debate within the scientific community as to the best practices for downscaling IPCC model output for use in projecting the impacts of climate change on marine ecosystems (ICES, 2008). Comparison of the model weights for summer SST and spring winds illustrates that IPCC GCMs have different strengths and weaknesses in the Bering Sea. The Bayesian weighting technique suggested herein is designed to limit the use of unrealistic and improbable climate trajectories. The use of a pre-simulation skill assessment should also reduce uncertainty that arises from structural incompleteness in the models (ICES, 2008). Importantly, it allows for the estimation of error bounds and for quantifying levels of confidence.

Future work could evaluate results using alternative selection processes and weighting schemes. For example, Smith et al. (2009) present an alternative Bayesian modeling approach to estimate uncertainty in ensembles of climate models. In some cases, the environmental variable needed for projection may not be readily available from IPCC model output. When this occurs, analysts will need to determine the empirical relationships linking climate forcing to regional biologically relevant variables, as well as the associated uncertainty. These relationships could be used to improve the estimates of time series of environmental variables derived from ensembles of IPCC climate model output and will provide a measure of the associated uncertainty in the projections resulting from downscaling.

We acknowledge that some doubts remain about the credibility of the GCMs being used to make climate projections. For example, Koutsoyiannis et al. (2008) compared the 20th century hindcasts from a variety of models with observations and found a mis-match on decadal time scales. We contend that this was not

a valid test of the models, due to the chaotic nature of the climate system. The lack of predictability for specific events (e.g., relatively warm or cool conditions for a particular region and time interval) does not imply that the models cannot be used to anticipate overall changes in the properties of the climate from a stochastic perspective.

As in the case of stock assessment models, the approach described here is a simplification of the complex processes controlling population responses to climate drivers. The predictive skill of climate models is uncertain and this is likely to grow with time making simulations at the end of the time series less reliable (Smith et al., 2007). When coupled with the possibility of behavioral, genetic or other forms of adaptation, our uncertainty is further increased. However, Levin et al. (1997) recommends that mechanistic models should be developed that begin with what is understood (or hypothesized) about the interactions of individual units with a goal towards identifying emergent behavior that can be expressed as statistical ensembles. The framework presented in this paper encourages scientists to build on the long history of fisheries oceanographic research available in many of the world's large marine ecosystems to formulate scenarios for potential impacts of climate change on marine fish and their fisheries.

The framework relies on existing knowledge of linkages between environmental forcing and fish production and these linkages may be unreliable. The effects of short-, medium-, and long-term environmental influences on fish stocks are complex and uncertain for most species, and predictions of stock status are dependent upon accurate forecasts of the appropriate environmental indices and the stability of the relationships between climate and the stock (Fréon et al., 2005). There are many examples where proposed relationships between fish or shellfish recruitment and climate have not held up over time (Myers, 1998; Bull and Livingston, 2001; De Oliveira *et al.* 2005; Francis *et al*., 2006). The imprecision inherent in the projections of climate-recruitment relationships can be attributed to: a) misspecification of or changes over time in the links between climate and recruitment; b) error and uncertainty in estimating the characteristics of the links based on historical data; and c) error and uncertainty in the forecasts of the climate indices. Francis (2006) suggests that cross-validating the environmental variables included as influences on stock dynamics may assist in determining more reliable relationships between recruitment and climate. Relationships may also fail when ecosystem linkages have non-linear underpinnings (Scheffer and Carpenter, 2003). To address this issue time series could be analyzed to assess the dimensionality of the system at different time scales (Sugihara and May, 1990; Sugihara, 1994; Hseih *et al.*, 2005a).

The framework for projecting climate change impacts on fish and shellfish presented here was intentionally designed to parallel the modeling approach used for stock assessment. The expectation is that the parameters and functional forms assumed for stock assessment will be regularly evaluated as part of the public review of stock assessments and the on-going peer review of fisheries oceanographic research. As understanding of the functional relationships between environment and fish production evolves, this information can be rapidly updated in the climate change projections. As part of the periodic reviews, skill assessments could become an integral aspect of the proposed framework to continually update models as new information is acquired (Stow *et al.* 2009).

There are alternative modeling approaches that could be considered for forecasting climate change impacts on commercial species. As mentioned in the Introduction, it is also possible to conduct experiments involving integrated dynamical models. For example, Rose *et al.* (2006) coupled a regional ocean circulation model with a nutrient-phytoplankton-zooplankton component to an individual based model with bioenergetic models to explore the implication of changes in ocean forcing on fish growth. This type of model could be modified to investigate the effects of climate change by treating the IPCC model output as boundary and initial conditions for a regional ocean model. Numerical "experiments" could be performed with the biophysical model under different climate scenarios to develop the environmental variables for use in stock projection models (e.g. Category 2-*type* model) or outputs could be drawn from trophically linked spatial models. Levin *et al.* (1997) suggest that this class of model system should be used when the added amount of detail can be supported by observations that can be measured. The detailed information needed for validation and parameterization of dynamic models is difficult and expensive to collect, as illustrated by the ambitious effort of the Bering Sea under the auspices of the Bering Sea Integrated Research Program (BSIERP)-Bering Sea Ecosystem Study (BEST) program (http://bsierp.nprb.org).

The forecasting framework was applied in the Bering Sea region to demonstrate the method for selecting IPCC model output and developing a weighted ensemble for an environmental variable of interest (July-September SST). This method revealed that the CCCMAT-63 and the MIROC-M models produced the most accurate estimates of mean, variance and trends in Bering Sea SST for the last half of the 20th Century. The weighted ensemble shows mean SSTs are expected to increase by 2° C by 2050. This implies that the typical summer by around 2050 will be as warm as the warmest summers of the present day (Overland and Stabeno, 2004). These changes are likely to impact the spatial distribution of many fish and shellfish populations in the region (Mueter and Litzow, 2007) and may impact the seasonal production cycle (Hunt *et al.*, 2002).

The impact of climate change on Bering Sea northern rock sole production provides an example of the Category 1 type forecast. Specifically, the model incorporates uncertainty at the level of both future climate change and the biological response to that climate. The results suggest that qualitative forecasts of the impact of climate on fish and shellfish that are based on IPCC model scenarios alone (Figure 7) could overestimate the biological response (Figure 8). Incorporating the distribution of recruitments under different climate regimes into the forecast contributed to the perception of the climate impact.

Several assumptions were necessary to complete the example forecast. For simplicity, recruitment was assumed to be independent of stock size. This allowed us to bootstrap over recruitments within a climate scenario, rather than using deviations from a climate-specific stock-recruitment relationship. As such, projections of future stock size were not needed. A more sophisticated model that incorporated climate-mediated changes in density dependence would be an example of a Category 2 model. Such a model might incorporate additional realism by including serial autocorrelation in recruitment through its dependence on stock size, but at the expense of added complexity associated with projecting stock size from one year to the next.

The example model incorporates only the impact of projected changes in cross-shelf transport on recruitment of northern rock sole. Changes in SST are not expected to change the tidal mixing that occurs in the inner domain and creates a nutrient rich nursery area for northern rock sole. Furthermore, retrospective studies show that SST was not significantly related to recruitment (Wilderbuer *et al.*, 2002). We therefore expect that changes in SST will not have a strong impact on recruitment of northern rock sole and that cross-shelf transport will continue to be the most influential environmental variable influencing it.

The northern rock sole example forecasts recruitment based on our current understanding of the linkages between climate and recruitment. There may be other potential processes (e.g., prey availability, growth, predation rates) that could be influenced by increases in SST. In the case of northern rock sole, retrospective studies do not provide evidence that recruitment is significantly influenced by warm surface temperature. If evidence becomes available, then these temperature effects on processes could be addressed using a Category 2 or 3 type model that tracks, for example, the effect of temperature on the dynamics of growth through the population. However, because the functional form and parameter values for this temperature dependence are unknown for northern rock sole, developing a model that incorporates SST would be purely hypothetical. Until the requisite field and laboratory experiments

necessary to elucidate linkages are undertaken, incorporating temperature effects would be an academic endeavor. Expanded field and laboratory studies are needed to evaluate the potential response of fish to projected environmental conditions.

Stochastic simulations allow for a comparison of the mean and median estimates of recruitment over time. In the next 10-20 years, interannual and decadal scale variability is likely to dominate trends in cross shelf transport of northern rock sole larvae. Recruitment of this species is likely to continue to vary. After 2025, mean recruitment is expected to trend upward at a modest rate while the median recruitment remains stable. The reduction in trend from mean to median is due to the asymmetrical nature of the distribution of recruitment under each of the three climate conditions.

The examples shown here address the uncertainty resulting from model selection, environmental process error, measurement error in the assessment, and process error in the spawner recruitment relationship. In our analysis process error in the spawner recruitment relationship was incorporated using a bootstrap method. An alternative approach would be estimate probability distributions for parameters used in the relationship between the environment and recruitment to provide an estimate of the parameter uncertainty as an addition to the process and observation error already inherent within the framework.

If interdisciplinary research teams around the world use this or a similar framework to assess climate change impacts on marine fish and shellfish, then comparative studies can be used to evaluate hypothesized relationships. Myers (1998) advocated this approach, suggesting that hypothesized relationships could be verified and validated with separate tests and analyses using meta-analyses across ecosystems, geographical areas, and/or species to explore other links between climate and recruitment. If regional modeling teams apply the framework and meet to compare results, we anticipate that a more comprehensive assessment of climate change impacts on the availability of fish and shellfish resources throughout the world will be available for consideration by future IPCC review panels.

ACKNOWLEDGEMENTS

We wish to thank Muyin Wang who helped to provide the IPCC model output used our analysis. We also thank Keith Brander and two anonymous reviewers for their helpful comments and suggestions.

Chapter 9: Summary of key findings and outcomes

The goal of our project was to perform research to assess the following BSIERP core hypotheses:

HYPOTHESIS 1.

Climate-induced changes in physical forcing will modify the availability and partitioning of food for all trophic levels through bottom-up processes. Specifically:

> *b. Reduced frequency and intensity of summer storms will reduce surface mixing and increase sea surface temperature, thereby increasing stratification. A substantial decrease in summer winds will result in a mixed layer that is shallower than the euphotic zone, extensive subsurface primary production and depletion of nutrients in the entire water column. There will be no fall phytoplankton bloom. A moderate decrease or no change in the intensity of summer storms will reduce replenishment of nutrients to the euphotic zone, lowering summer primary and secondary production. Both scenarios will reduce juvenile fish production by reducing their condition (energy density) and over-wintering capability.*

The underway oceanographic instruments on NOAAS Oscar Dyson as well as the rugged CTD instruments on the bottom trawl surveys provided new insights into the processes influencing summer stratification in the Bering Sea. The bottom trawl survey CTD measurements provide some of the first observations of the summer mixed layer depth (MLD) on a shelf-wide scale, showing how it varies in space and time (Figure 1.27). These provide essential data points that can be used in a longer time series in conjunction with regional winds to test whether summer winds and the MLD will indeed decrease with global warming. The summer MLD was less than 30 m over much of the region. Salinity was high at the shelf break and low at the coast, but that trend is interrupted by low-salinity water around and south of St. Matthew Island (Figures 1.7, 1.18, 1.25). Horizontal gradients were typically strongest roughly along the 50-m and 100-m isobaths that traditionally separate the inner- and outer-shelf from the middle-shelf. The summer MLD has a more complex behavior than that along the oft-studied 70-m isobath. It reaches deeper to the bottom along the coast southeast of Nunivak Island in water depths both less and greater than 50 m, implying that the frontal boundary of the well-mixed, inner shelf is not always at the 50-m isobath as had been deduced from scattered, cross-shelf transects. We found that the upper-to-lower-layer density difference changed with latitude. The greatest upper-to-lower layer density difference is found across the shelf north of 59°N, but its horizontal extent was much less in 2009. The temperature difference is the main contributor to the vertical density difference over most of the shelf, but salinity plays a larger role at times near Unimak Pass, at the shelf-break, around St. Matthew Island and near the

coast. Near-surface measurements from a moving ship revealed relationships between nitrate, oxygen and phytoplankton carbon that can be understood in terms of the classical Redfield ratio during the spring bloom when nitrate is depleted, and oxygen and chlorophyll increase owing to primary production.

HYPOTHESIS 2.

Climate and ocean conditions influencing water temperature, circulation patterns and domain boundaries impact fish reproduction, survival and distribution, the intensity of predator-prey relationships and the location of zoogeographic provinces through bottom-up processes. Specifically:

a. As heat content increases, the area suitable for spawning and foraging by subarctic species will expand northward and subarctic species will occupy areas formerly occupied by Arctic species.

b. Reduced cold pool extent will increase overlap of inner domain forage fish and outer domain piscivores.

c. Strength of frontal boundaries will weaken due to absence of the summer cold pool, allowing expansion of the inner domain and juvenile and forage fish habitat there. Weaker winds will enhance this effect.

e. Expected decreases in benthic productivity will negatively affect feeding and survival of small flatfish and crab thereby lowering population levels.

As noted above, the augmentation of the NMFS bottom trawl survey with CTDs provided new insights into the location of horizontal gradients (H2c). Maps of oceanographic variables measured during January-March and June-August surveys show the evolution of these ecosystem conditions on the southeastern Bering Sea shelf. Oceanographic conditions were cold throughout the study period, therefore, we were not able to statistically determine whether weaker gradients were observed in years of reduced cold pool extent. However, our work did demonstrate that these measurements can be collected annually, and over time, they should provide valuable insight into this question. As noted above, we observed that the frontal boundary of the well-mixed, inner shelf is not always at the 50-m isobath. This finding underscores the need for continuation of the augmentation of NMFS surveys to provide observations of the location of the frontal boundary. Summer bottom trawl CTD measurements revealed geostrophic currents on the eastern Bering Sea shelf. In two years there was clockwise circulation around St. Matthew Island owing to low-density water there.

Retrospective analysis provided strong evidence of niche partitioning of forage fish and some groundfish across the eastern Bering Sea shelf. Depth alone was not sufficient to explain the observed spatial distributions. Light, bottom temperature, prey availability (euphausiids), and predator abundance were also selected as explanatory variables for vertical and horizontal distributions of fish. Analysis of groundfish data (Chapter 3) revealed that the cold pool impacted the east-west movement of some species with an expansion of some the outer domain species onto the shelf in warm years. This finding suggests that the *strength of frontal boundaries will weaken due to absence of the summer cold pool, allowing intrusion of outer domain species into the middle domain*. Retrospective analysis of forage fish distributions (Chapter 4) revealed that interannual variability in the spatial extent of the cold pool was an important feature defining the ocean habitats used by forage fishes. Our studies showed that greater overlap of age-0 and age-1 pollock occurred in cold years although the estimates were uncertain.

Examination of geostrophic flow features in 2008 also suggests a possible association between cross-shelf flow patterns and the spatial distribution of midwater age-1 pollock in the outer domain. *Retrospective analysis of of age-0 and age-1 pollock and capelin distributions (Chapter 4) did not supported hypothesis H2c.* We found that the spatial overlap of capelin and age-1 pollock was higher in cold years than in warm years. Acoustic data collected in the late summer during the BASIS survey showed that capelin were found in mid-water throughout the middle domain (Parker-Stetter et al., In Press).

In Chapter 5, to facilitate further analysis of shifts in the location of zoogeographic provinces and shifts in the composition of biological communities, we have developed an analytic method to characterize unique ecological regions, evaluate ecological dynamics and biological and biological-physical interactions at regional scales, and develop a baseline against which to evaluate future effects of climatic variability and directional change. The attributes of these regions are summarized in the table (Chapter 5). Spatial maps of species-specific variation in habitat occupancy over time (coefficient of variation in species abundance) suggest that forage fish remain in discrete and relatively constrained core habitat within the inner shelf, regardless of climatic conditions. In contrast, outer domain pelagic piscivores expand into the northern (e.g. Kamchatka flounder, Greenland turbot) and middle (arrowtooth flounder) areas of the eastern Bering Sea shelf in warm periods with increased access to inner domain forage fish and juvenile walleye pollock (Chapter 5). Patterns in range variation for demersal piscivores such as Pacific cod and Pacific halibut are similar, such that these piscivores also expand their range into the middle and northern areas of the Bering Sea shelf, with increased access to inner shelf forage fish and arctic species. In

summary, the combined observations from Chapters 3, 4 and 5 suggest that in warm years *reduced cold pool extent will increase overlap of middle domain forage fish and outer domain piscivores.*

The framework for projecting climate change impacts on the future production of commercial fish and fisheries (Chapter 8) provided some of the first regional projections of future ocean conditions. This study projected that by 2050, the Bering Sea will warm by 2° C and this warming is likely to impact sea ice extent, the area of the cold pool, and the strength of frontal boundaries. This study also showed that climate change is not expected to have a strong influence on cross-shelf advection. These changes are expected to reduce interspecies interaction between age-1 pollock and capelin in the future. The inshore distribution of capelin and the apparent greater tolerance by age-1 pollock of colder temperatures than their predators (e.g. adult walleye pollock and arrowtooth flounder) may continue to buffer their exposure to predation by larger fishes, as long as a cold pool continues to form on the northern Bering Sea shelf in summer (Stabeno et al. 2012b).

Evidence from Chapters 1 and 3 suggest that there will be a limit to the expansion of several commercial groundfish stocks to the north due to the persistence of the cold pool in the northern Bering Sea (Hollowed et al. 2013). We find that the areal extent of the cold pool is an important driver for abundance of subarctic species (Chapter 5). We also provide evidence that ecoregional boundaries shift in response to short-term climatic regimes (2001-2005 versus 2006-2010), such that northern ecoregions and areas occupied by arctic species within the eastern Bering Sea retract northwards in warm phases.*Thus, H2a is not supported for several stocks.*

Collection of underway acoustic data from ships of opportunity in winter (Chapter 6) provided some insights hypothesis 2a with respect to the role of ocean temperature on the area suitable for spawning species. In this study, cumulative catch, sea surface temperature, bottom depth, and distance to the ice edge were significant predictors of winter pollock density on the EBS shelf. However, in both the descriptive and predictive models, the majority of model deviances remained unexplained. The lack of descriptive power in the model suggested that it may be difficult to identify consistent inter-annual relationships between pollock density and environmental variables in winter.

HYPOTHESIS 3

Later spring phytoplankton blooms as a result of early ice retreat will increase zooplankton production, thereby resulting in increased abundances of piscivorous fish (pollock, cod and arrowtooth flounder) and a community controlled by top-down processes [Oscillating Control Hypothesis] with the possible trophic consequences:

a. Competition with abundant, piscivorous fish species for forage species will lead to a decline in murres, kittiwakes and fur seals.

c. In a top-down control community, fishing will reduce the degree of top-down control of forage species (including juvenile pollock) by adult pollock, cod and arrowtooth flounder. Owing to light exploitation rates, top-down control by arrowtooth flounder will increase, as will their level of competition with piscivorous fish, seabirds and marine mammals. As a result of these two processes, arrowtooth flounder will determine ultimate community composition, such that the climax community will be arrowtooth flounder-dominated (similar to the Gulf of Alaska).

In Chapters 2 and 3, we demonstrated that spatially combining acoustic-trawl and bottom-trawl survey results for pollock was the best way to analyze spatial distribution (rather than using the results of one of these surveys alone; Kotwicki et al. 2013). This allowed us to make a full comparison of the distribution of pollock and new information on the distribution of euphausiids. Pollock predation on euphausiids is substantial (Ressler et al. 2012); however, the evidence we have suggests that variations in euphausiid standing stock are driven <u>*by bottom-up and not top-down forcing*</u>: cold temperatures appear favorable to euphausiids, while the effect of predation by their single most important consumer, pollock, appears to be relatively weak (Ressler et al. in review, Chapter 2). In turn, pollock distribution also seems strongly driven by temperature, with less pollock biomass found in the coldest temperatures as previous research has suggested, and only weakly associated with the distribution of euphausiid prey (Ressler et al. unpublished, Chapter 2). Although, bottom-up physical forcing does appear to control the abundance of food available for higher trophic levels, the conceptual linkages were not as originally envisioned by BSIERP. Our study shows that *cold* conditions favor the presence of more euphausiids, which are key zooplankton forage for pollock and many other animals. The mechanisms for this are still unclear. Ocean conditions also do appear to structure trophic relationships: the spatial relationship of euphausiids and pollock appears to be influenced by temperature.

As noted above, Arrowtooth flounder (*Atheresthes stomias*) are strongly constrained by bottom (2°C) and surface (5°C) temperature thresholds (Chapters 3 and 5). The area of the eastern Bering Sea contained within these temperature thresholds reduces in warm climatic phases, which will allow range expansion

of arrowtooth flounder and may increase top-down control by arrowtooth flounder, absent control through fishing.

HYPOTHESIS 4

Climate and ocean conditions influencing circulation patterns and domain boundaries will affect the distribution, frequency and persistence of fronts and other prey-concentrating features and thus the foraging success of marine birds and mammals largely through bottom-up processes. Specifically:

a. Climate-ocean changes will displace predictably located, abundant prey (hot spots).

In Chapter 5, we demonstrate that forage fish are highly reactive to surface temperature (e.g. 5-6°C for capelin, walleye pollock, saffron cod; 8-9°C for herring), bottom temperature (e.g. 1-2°C for arctic cod, capelin) or specific temperature ranges within the water column (e.g. 4-6°C for eulachon). Shifts in temperature ranges and frontal boundaries in conjunction with static habitat variables such as depth and substrate will displace predictably located prey concentrations.

NEW SURVEY METHODS

Ongoing NOAA monitoring surveys in the Bering Sea (Bottom trawl survey, B91, and Acoustic surveys, B58) provided the backbone of summer fieldwork and were fundamental to collecting the data we needed for our project.

We showed that using acoustic backscatter and net samples to survey a key zooplankton forage taxon, euphausiids, was feasible (Smith et al. 2010, 2012, Ressler et al. 2012). This result is especially valuable since euphausiids in the Bering Sea were not monitored on a regular basis previous to our project. If continued, the survey method will produce results that can be used for stock and ecosystem monitoring and for ecological studies. However, the acoustic properties of euphausiids are highly variable and not as well known as those for pollock; more research is needed to better understand euphausiid target strength (the conversion between acoustic backscatter and numbers of euphausiids), and to reconcile the differences between acoustic, net, and model estimates of euphausiid biomass in the Bering Sea.

Our work showed that acoustic surveys detect four main acoustic backscattering classes in the eastern Bering Sea (Woillez et al. 2012). The first two are walleye pollock and euphausiids; our project used data from an existing acoustic-trawl survey of pollock and developed an acoustic method for survey euphausiids. But there are two other main acoustic classes that are not well described, probably

consisting of a mixture of larval fishes and gelatinous zooplankton. The results provided by Woillez et al. (2012) could serve as a baseline for future work to describe the composition of these classes and to further assess their ecological significance.

Chapter 10: BEST-BSIERP Bering Sea Project Connections

Chapter 10.a. Principal Investigators Views on Integrated Research Projects

Our research team supports continuation of integrated research projects. We particularly support the effort to partner with the National Science Foundation in efforts to expand the expertise of the research teams. The communication between PIs in a program with over 90 PIs is a daunting task. The group leaders came up with a workable approach to communication. Despite all efforts to integrate the observationalists with the modelers the modeling lagged so far behind the observations that it was difficult to for there to be a true synthesis of findings until after the project was completed. A news letter might have been an effective way of communicating findings amongst investigators. The

Chapter 10.b. Observations used by other BEST-BSIERP Bering Sea Project investigators

Our research results, in particular the observations of euphausiid and walleye pollock biomass from surveys 2004-2010, were used by other BSIERP projects, manuscripts, and in synthesis of BEST and BSIERP results. For example:

-Euphausiid and pollock data were used in the principal publication from Project B95, B92. Title: Top predator hotspot persistence:

Sigler, M., K. Kuletz, P.H. Ressler, N. Friday, C.D. Wilson, and A. Zerbini, 2012. Apex predators and hot spot persistence in the southeast Bering Sea. Deep-Sea Research II 65-70: 292–303.

- These data were used to model the distribution of marine mammals as detected by visual observers aboard acoustic-trawl surveys (Projects B58 and B66). These results are currently part of a manuscript that is in preparation (A. Zerbini, personal communication).

-These data were used in a revision of the Oscillating Control Hypothesis:

Hunt Jr., G.L., K.O. Coyle, L. Eisner, E.V. Farley, R. Heintz, F. Mueter, J.M. Napp, J.E. Overland, P.H. Ressler, S. Salo, and P.J. Stabeno. 2011. Climate impacts on eastern Bering Sea food webs: A synthesis of new data and an assessment of the Oscillating Control Hypothesis. ICES Journal of Marine Science 68: 1230–1243. doi:10.1093/icesjms/fsr036

-Time series of fish size, spatial distribution, and abundance from the NMFS acoustic trawl survey (euphausiids and pollock), bottom trawl survey and fisheries data were use in comparisons with

ecosystem model results. In addition oceanographic variables were used in verifying the spatial distribution of the cold pool:

Ressler, P.H., Gibson, G., Ortiz, I., Aydin, K., and Herman, A.J. Confronting models with observations (and observations with models): euphausiids in the eastern Bering Sea, poster presented at the BEST-BSIERP PI Meeting, 27-30 March 2012, Anchorage, AK.

-Food habits data collected during acoustic trawl surveys were used by Project B61, and joint publications are still in preparation (T. Buckley, personal communication).

- The framework for developing climate enhanced stock projection models developed by our project team formed the foundation for projection modeling approaches used by Mueter et al. (2011) and Ianelli et al. (2011).

Chapter 10.c. Contributions to BEST-BSIERP Bering Sea Project Synthesis

-BEST synthesis: these data contributed to ongoing NSF-funded synthesis projects. These synthesis efforts coincide with the BSIERP synthesis phase; the following manuscript is an example of one of the early outcomes:

Ressler, P.H., De Robertis, A., and Kotwicki, S., in review. The spatial distribution of euphausiids and pollock in the eastern Bering Sea does not imply top-down control by predation. Marine Ecology Progress Series.

-We leveraged the expertise gained from working on BSIERP projects to collaborate on three BEST scientific papers. Computer programs that we developed to calibrate and analyze underway oceanographic measurements on Dyson were used on five USCG Healy, R/V Knorr and R/V Thomas G. Thompson BEST cruises in 2008-2010. Underway solar radiation and chlorophyll-a observations from Healy and Knorr were employed in a vertically generalized productivity model (VGPM) to estimate net primary production on the Bering Sea shelf (Lomas et al., 2012). Likewise, underway measurements of temperature, salinity, nitrate and chlorophyll-a were used to estimate the air-sea CO2 flux, net community production rate and phytoplankton population abundance as Thompson crossed the Gulf of Alaska in 2010 on its way to a BEST Bering Sea cruise (Palevsky et al., 2013). Computer software developed to analyze CTD data from the bottom trawl survey was used to calculate the bottom temperature on spring 2007 and 2008 Healy cruises. De Robertis and Cokelet (2012) related the bottom temperature to macrozooplankton and pollock distributions and showed that pollock avoid cold bottom temperatures less than 0.5°C.

- Estimates of pollock spawning location are being used by Duffy Anderson et al. as release points for coupled bio-physical larval drift trajectory models.

Chapter 10.d. Management or Policy Implications and Contributions to inform decisions of the North Pacific Fishery Management Council

-New insights into survey results improve the ongoing contribution of bottom trawl and acoustic-trawl survey data to pollock stock assessment and eastern Bering Sea ecosystem assessment, and our index of euphausiid abundance now contributes as well. The work of Kotwicki et al. directly contributes to the annual Bering Sea pollock Stock Assessment and Fishery Evaluation report. Kotwicki's research on environmental factors influencing the vertical distribution of adult pollock is used to inform the estimation of survey catchability. For examples, see

> Zador, S., and Gaichas, S., 2010. Ecosystem considerations for 2011, Appendix C. In: Stock assessment and fishery evaluation report for the groundfish resources of the Bering Sea/Aleutian Islands regions. North Pacific Fishery Management Council, Anchorage, AK. URL: http://access.afsc.noaa.gov/reem/ecoweb/Eco2010.pdf
>
> Ianelli, J.N., Barbeaux, S., Honkalehto, T., Kotwicki, S., Aydin, K., and Williamson, N., 2010. Eastern Bering Sea Walleye Pollock Stock Assessment. In: Stock assessment and fishery evaluation report for the groundfish resources of the Bering Sea/Aleutian Islands regions. North Pacific Fishery Management Council, Anchorage, AK. URL: http://www.afsc.noaa.gov/REFM/docs/2010/EBSpollock.pdf

- Results from B62 demonstrated that forage fish and adult groundfish exhibit niche partitioning and that climate variability influences the spatial boundaries and thus, volume of niches. The Ecoregion study developed a suite of statistical models and analytical protocols that can be used to define species specific habitat windows and eco-regions. Extensions of this approach have clear management applications. First, future distributions of species specific habitat windows or ecoregions can be estimated using projected environmental conditions derived from ROMS/NPZ model output to provide input into fishers choice models. Second, these projected spatial distributions can be utilized to assess the volume of sutiable habitat in the future. These habitat volumes can be incorporated as an input into climate enhanced multi-species or single species stock projection models. Our results contributed to a better understanding of the hypothesis 2: Climate and ocean conditions influencing water temperature, circulation patterns and

domain boundaries impact fish reproduction, survival and distribution, the intensity of predator-prey relationships and the location of zoogeographic provinces through bottom-up processes.

-Results of the winter acoustics project demonstrated in the GAM analysis of pollock distribution in relation to environmental covariates could be developed into an index of pollock preferred habitat. Such an index would be useful in predicting annual pollock survival and recruitment.

-Results of project B62 demonstrated that the previous predictions that groundfish would exhibit marked spatial shifts to the north in response to climate change needed to be re-evaluated. The persistence of the cold pool in the northern Bering Sea is expected to serve as a thermal barrier to rapid expansion of fish into the Arctic Ocean. This information will be used to inform decisions regarding the NPFMC's evaluation of proposals to open selected regions of the northern Bering Sea research area to commercial fishing.

-The framework for developing climate enhanced stock projection models for use in evaluating the effectiveness of different management strategies under changing climatic conditions will likely be used by the NPFMC in future evaluations of Plan amendments and in evaluations of cumulative effects for Programmatic Environmental Impact Statements.

-The research conducted as part of B62 provided the foundation for the development of quantitative projections of the implications of climate change on the distribution and abundance of marine fish species in the southeast Bering Sea. These projections will allow the North Pacific Fishery Management Council to evaluate the relative performance of different harvest strategies under changing climate conditions. These projections will contribute to the smooth and orderly adoption of harvest policy in the future.

-The implication of climate change on the volume of ecoregions can be modeled as a proxy for estimation of density dependent responses in the spawner recruitment curves used in stock assessments.

-Acoustic data collected from ships of opportunity provided important information on localized depletion inside and outside of Steller Sea Lion critical habitat. This information was used in the recent Steller Sea lion EIS.

-The assessment of the vulnerability of marine species to expand or move into the high Arctic has been used by policy makers in discussions of international fishery management and policy.

Chapter 10.e. Integration with BEST-BSIERP Bering Sea modeling projects

Investigators from B62 organized three project coordination meetings with the modelers. These meetings provided an opportunity for the modelers to learn what the observationalists were seeing and learing about the statistical relationship between fish distributions and regional environmental condtions. Likewise, these meetings provided an opportunity for the observationalists to learn and comment on how the their data would be utilized by the modelers.

Anne Hollowed worked with other modelers to develop a modeling framework that was later used by the retrospective team and the management strategy teams to assess the implications of climate change on the productivity and management of walleye pollock in the Bering Sea. She contributed to the following four modeling papers:

Hollowed, A. B., N.A. Bond, T. K. Wilderbuer, W. T. Stockhausen, Z. T. A'mar, R. J. Beamish, J. E. Overland, M. J. Schirripa. 2009. A framework for modeling fish and shellfish responses to future climate change. ICES J. Mar. Sci. 66(7):1584-1594.

Ianelli, J. A. Hollowed, A. Haynie, F. Mueter, N. Bond. 2011a. The challenges of developing fisheries stock assessment approaches, harvest control rules, and management strategies to satisfy and adapt to increasingly complex management objectives in a changing environment. ICES Journal Marine Science 68(6): 1297-1304.

Mueter, F. J., N. A. Bond, J. N. Ianelli, A. B. Hollowed. 2011. Expected declines in recruitment of walleye pollock (Theragra chalcogramma) in the eastern Bering Sea under future climate change. ICES Journal of Marine Science 68(6):1284-1296.

Punt, A. E., T. A'Mar, N. A. Bond, D. S. Butterworth, C. L. de Moor, J. A. A. De Oliveira, M. A. Haltuch, A. B. Hollowed, and C. Szuwalski. 2013. Fisheries Management under Climate and Environmental Uncertainty: Control Rules and Performance Simulation. ICES J. Mar. Sci doi:10.1093/icesjms/fst057.

Chapter 10.f. Contributions to inform research and natural resource management in the Arctic.

Anne Hollowed synthesized the information learned from the BEST-BSIERP Bering Sea project to conduct a vulnerability analysis to evaluate the potential for fish and shellfish movement from the Bering Sea into the Arctic Ocean. She shared this information at international meetings on Arctic research and produced the following paper.

Hollowed, A.B., B. Planque, H. Loeng. 2013. Potential Movement of Fish and Shellfish Stocks from the Sub-Arctic to the Arctic Ocean. Fisheries Oceanography 22(5):355-370.

Chapter 10.g. Oceanographic data shared with other components (Cokelet).

Data sets archived at ERL, Boulder, CO

Cokelet, E.D., 2012a. Underway Seawater Sampling Aboard F/V Aldebaran in Winter & Summer 2008, Forage Distribution and Ocean Conditions (B62). UCAR/NCAR Earth Observing Laboratory, Boulder, CO, BSIERP Data Archive, http://data.eol.ucar.edu/codiac/dss/id=245.B62-001, last accessed 9 January 2012.

Cokelet, E.D., 2012b. Underway Seawater Sampling Aboard F/V Aldebaran in Winter & Summer 2009, Forage Distribution and Ocean Conditions (B62). UCAR/NCAR Earth Observing Laboratory, Boulder, CO, BSIERP Data Archive, http://data.eol.ucar.edu/codiac/dss/id=245.B62-007, last accessed 13 June 2012.

Cokelet, E.D., 2012c. Underway Seawater Sampling Aboard F/V Aldebaran in Winter & Summer 2010, Forage Distribution and Ocean Conditions (B62). UCAR/NCAR Earth Observing Laboratory, Boulder, CO, BSIERP Data Archive, http://data.eol.ucar.edu/codiac/dss/id=245.B62-008, last accessed 13 June 2012.

Cokelet, E.D., 2013a. Underway Seawater Sampling Aboard NOAA ship Oscar Dyson in 2008, Forage Distribution and Ocean Conditions (B62). UCAR/NCAR Earth Observing Laboratory, Boulder, CO, BSIERP Data Archive, http://data.eol.ucar.edu/codiac/dss/id=245.B62-009, last accessed 17 September 2013.

Cokelet, E.D., 2013b. Underway Seawater Sampling Aboard NOAA ship Oscar Dyson in 2009, Forage Distribution and Ocean Conditions (B62). UCAR/NCAR Earth Observing Laboratory, Boulder, CO, BSIERP Data Archive, http://data.eol.ucar.edu/codiac/dss/id=245.B62-010, last accessed 17 September 2013.

Cokelet, E.D., 2013c. Underway Seawater Sampling Aboard NOAA ship Oscar Dyson in 2010, Forage Distribution and Ocean Conditions (B62). UCAR/NCAR Earth Observing Laboratory, Boulder, CO, BSIERP Data Archive, http://data.eol.ucar.edu/codiac/dss/id=245.B62-011, last accessed 17 September 2013.

Cokelet, E.D., 2013d. NOAA Bering Sea Bottom Trawl Survey CTD data in 2008, Forage Distribution and Ocean Conditions (B62). UCAR/NCAR Earth Observing Laboratory, Boulder, CO, BSIERP Data Archive, http://data.eol.ucar.edu/codiac/dss/id=245.B62-012, last accessed, 26 September 2013.

Cokelet, E.D., 2013e. NOAA Bering Sea Bottom Trawl Survey CTD data in 2009, Forage Distribution and Ocean Conditions (B62). UCAR/NCAR Earth Observing Laboratory, Boulder, CO, BSIERP Data Archive, http://data.eol.ucar.edu/codiac/dss/id=245.B62-013,, last accessed 26 September 2013.

Cokelet, E.D., 2013f. NOAA Bering Sea Bottom Trawl Survey CTD data in 2010, Forage Distribution and Ocean Conditions (B62). UCAR/NCAR Earth Observing Laboratory, Boulder, CO, BSIERP Data Archive, http://data.eol.ucar.edu/codiac/dss/id=245.B62-014, last accessed 26 September 2013.

Ressler, P.H., 2008. Depth-integrated euphausiid (Family Euphausiidae) backscatter in June and July 2008 (B62). UCAR/NCAR Earth Observing Laboratory, Boulder, CO, BSIERP Data Archive, http://data.eol.ucar.edu/codiac/dss/id=245.B62-003

Ressler, P.H., 2009. Depth-integrated euphausiid (Family Euphausiidae) backscatter in June, July, and August 2009 (B62). UCAR/NCAR Earth Observing Laboratory, Boulder, CO, BSIERP Data Archive, http://data.eol.ucar.edu/codiac/dss/id=245.B62-005

Ressler, P.H., 2010. Depth-integrated euphausiid (Family Euphausiidae) backscatter in June and July 2010 (B62). UCAR/NCAR Earth Observing Laboratory, Boulder, CO, BSIERP Data Archive, http://data.eol.ucar.edu/codiac/dss/id=245.B62-005

Ressler, P.H., 2008. Depth-integrated midwater pollock biomass in June and July 2008 (B62). UCAR/NCAR Earth Observing Laboratory, Boulder, CO, BSIERP Data Archive, http://data.eol.ucar.edu/codiac/dss/id=245.B62-004

Ressler, P.H., 2009. Depth-integrated midwater pollock biomass in June, July, and August 2009 (B62). UCAR/NCAR Earth Observing Laboratory, Boulder, CO, BSIERP Data Archive, http://data.eol.ucar.edu/codiac/dss/id=245.B62-003

Ressler, P.H., 2010. Depth-integrated midwater pollock biomass in June, July, and August 2010 (B62). UCAR/NCAR Earth Observing Laboratory, Boulder, CO, BSIERP Data Archive, http://data.eol.ucar.edu/codiac/dss/id=245.B62-006

Bottom trawl data was made available to other Bering Sea project researchers upon request, and is publically available on the following AFSC webite http://www.afsc.noaa.gov/RACE/groundfish/survey_data/data.htm

Chapter 11: Project Publications

Baker, M. R. and A. B. Hollowed. 2014. Delineating ecological regions in marine systems: synthesis of physical structure and community composition to inform spatial management. Deep Sea Research II.

Barbeaux, S. J., J. K. Horne, and J. N. Ianelli. 2014. A novel approach for estimating location and scale specific fishing exploitation rates of eastern Bering Sea walleye pollock (*Theragra chalcogramma*). Fisheries Research 153: 69-82. Available online 3 February 2014 (http://dx.doi.org/10.1016/j.fishres.2014.01.004)

Barbeaux, S., J. Horne, and M. Dorn. 2013. Characterizing walleye pollock (Theragra chalcogramma) winter distribution from opportunistic acoustic data. ICES Journal of Marine Science 70:1162-1173

Barbeaux, S. 2012. Scientific Acoustic Data from Commercial Fishing Vessels: Eastern Bering Sea Walleye Pollock (Theragra chalcogramma). University of Washington. PhD dissertation.

Barbeaux, S., J. Horne, and M. Dorn. 2009. Analyzing fish spatial and temporal distribution patterns using uncalibrated acoustic data from multiple vessels. ICES CM 2009/I:04

De Robertis, A., and E. D. Cokelet (2012), Distribution of fish and macrozooplankton in ice-covered and open-water areas of the eastern Bering Sea, *Deep Sea Research Part II: Topical Studies in Oceanography*.

Hollowed, A. B., S. J. Barbeaux, E. Farley, E. D. Cokelet, S. Kotwicki, P. H. Ressler, C. Spital, C. D. Wilson. 2012. Effects of climate variations on pelagic ocean habitats and their role in structuring forage fish distributions in the Bering Sea. *Deepsea Research II,* 65-70: 230-250.

Hollowed, A. B., N.A. Bond, T. K. Wilderbuer, W. T. Stockhausen, Z. T. A'mar, R. J. Beamish, J. E. Overland, M. J. Schirripa. 2009. A framework for modeling fish and shellfish responses to future climate change. ICES J. Mar. Sci. 66(7):1584-1594.

Hollowed, A.B., B. Planque, H. Loeng. 2013. Potential Movement of Fish and Shellfish Stocks from the Sub-Arctic to the Arctic Ocean. Fisheries Oceanography 22(5):355-370.

Ianelli, J. A. Hollowed, A. Haynie, F. Mueter, N. Bond. 2011. The challenges of developing fisheries stock assessment approaches, harvest control rules, and management strategies to satisfy and adapt to increasingly complex management objectives in a changing environment. ICES Journal Marine Science 68(6): 1297-1304.

Kotwicki, S. and Lauth R.R. 2013. Detecting temporal trends and environmentally-driven changes in the spatial distribution of groundfishes and crabs on the eastern Bering Sea shelf. Deep-Sea Research Part II: Topical Studies in Oceanography.

Kotwicki, S., De Robertis, A., Ianelli, J. N., Punt, A. E., and Horne, J. K. 2013. Combining bottom trawl and acoustic data to model acoustic dead zone correction and bottom trawl efficiency parameters for semi-pelagic species. Canadian Journal of Fisheries and Aquatic Sciences. 70: 208-219.

Mueter, F. J., N. A. Bond, J. N. Ianelli, A. B. Hollowed. 2011. Expected declines in recruitment of walleye pollock (Theragra chalcogramma) in the eastern Bering Sea under future climate change. ICES Journal of Marine Science 68(6):1284-1296.

Lomas, M., S. Moran, J. Casey, D. Bell, M. Tiahlo, J. Whitefield, R. Kelly, J. Mathis, and E. Cokelet (2012), Spatial and seasonal variability of primary production on the Eastern Bering Sea shelf, *Deep Sea Research Part II: Topical Studies in Oceanography*.

Mordy, C. W., E. D. Cokelet, C. Ladd, F. A. Menzia, P. Proctor, P. J. Stabeno, and E. Wisegarver (2012), Net community production on the middle shelf of the eastern Bering Sea, *Deep Sea Research Part II: Topical Studies in Oceanography*.

Palevsky, H.I., Ribalet, F., Swalwell, J.E., Cosca, C.E., Cokelet, E.D., Feely, R.A., Virginia Armbrust, E., Quay, P.D., 2013. The influence of net community production and phytoplankton community structure on CO2 uptake in the Gulf of Alaska. Global Biogeochem. Cy.

Punt, A. E., T. A'Mar, N. A. Bond, D. S. Butterworth, C. L. de Moor, J. A. A. De Oliveira, M. A. Haltuch, A. B. Hollowed, and C. Szuwalski. 2013. Fisheries Management under Climate and Environmental Uncertainty: Control Rules and Performance Simulation. ICES J. Mar. Sci doi:10.1093/icesjms/fst057.

Ressler, P.H., De Robertis, A., Warren, J.D., Smith, J.N., and Kotwicki, S., 2012. Developing an acoustic index of euphausiid abundance to understand trophic interactions in the Bering Sea ecosystem. Deep-Sea Research II 65-70: 184-195. http://www.sciencedirect.com/science/article/pii/S096706451200029X

Ressler, P.H., De Robertis, A., and Kotwicki, S., in review. The spatial distribution of euphausiids and pollock in the eastern Bering Sea does not imply top-down control by predation. Marine Ecology Progress Series.

Smith, J.N., P.H. Ressler, and J.D. Warren. 2010. Material properties of Bering Sea euphausiids and other zooplankton. Journal of the Acoustical Society of America 128(5): 2664-2680. http://asadl.org/jasa/resource/1/jasman/v128/i5/p2664_s1?isAuthorized=no

Smith, J.N., Ressler, P.H., and Warren, J.D., 2013. A distorted wave Born approximation target strength model for Bering Sea euphausiids. ICES Journal of Marine Science 70:204-214. http://icesjms.oxfordjournals.org/content/70/1/204.short

Woillez, M., P.H. Ressler, C.D. Wilson, and J.K. Horne, 2012. Multifrequency species classification of acoustic-trawl survey data using semi-supervised learning with class discovery. JASA Express

Letters 131(2), DOI: 10.1121/1.3678685.
http://asadl.org/jasa/resource/1/jasman/v131/i2/pEL184_s1?bypassSSO=1

Publications in preparation

Cokelet, E.D. (2014) 3-D water properties and thermohaline circulation on the Eastern Bering Sea Shelf, submitted to *Deep Sea Research Part II: Topical Studies in Oceanography*.

Chapter 12: Posters and Oral Presentations at Scientific Conferences or Seminars

Chapter 12.a. Oral presentations

Baker

1. Baker, MR, Hollowed, AB, Branch, T. 2013. Oral Presentation. "Patterns influencing species dynamics within and between functional guilds in the northeast Pacific and the role of environmental gradients in shaping interactions". ICES Annual Science Conference, Reykjavik, Iceland, September 2013.
2. Baker, MR, Hollowed, AB, Clarke, ME, Hilborn, R. 2013. Oral Presentation. "Influence of climate and environmental forcing on ecosystem structure in northeast Pacific systems". ICES Annual Science Conference, Reykjavik, Iceland, September 2013.
3. Baker, MR 2013. Oral Presentation. "Synthesis of physical structure and community composition to inform spatial management". Resource Assessment and Conservation Engineering Seminar Series, Alaska Fisheries Science Center, Seattle, WA, February 2013.
4. Baker, MR 2012. Oral Presentation. "Quantitative approaches to spatial management: delineating ecological regions and identifying biophysical drivers of community composition". Friday Harbor Laboratories Lecture Series, San Juan Island, WA, November 2012.
5. Baker, MR, Hollowed, AB. 2012. Oral Presentation. "Habitat and shifting climate: species distributions and interactions in arctic and subarctic systems in the north Pacific". ICES Annual Science Conference, Bergen Norway, September 2012.
6. Baker, MR, Hollowed, AB. 2012. Oral Presentation. "Spatial considerations for analyses of trophic stability in marine ecosystems". Alaska Marine Science Symposium, Anchorage, AK, January 2012.
7. Baker, MR, Hollowed, AB, Clarke, ME, Hilborn, R. 2011. Oral Presentation. "Spatial considerations for analyses of trophic stability in marine ecosystems". American Fisheries Society Annual Meeting, Seattle, WA, September 2011.

Barbeaux

1. Barbeaux, S. C. Spital, A. Greig, and A. Hollowed. Oral Presentation. "Generalized additive mixed-model analysis of Alaska pollock (Theragra chalcogramma) distribution employing fisheries dependent and satellite derived oceanograpich data". BSIERP PI meeting, Girdwood, AK October, 2008

2. Barbeaux, S. 2009. Oral Presentation. "Using opportunistic acoustic data to examine winter distributional dynamics of walleye pollock (Theragra chalcogramma)". BSIERP PI meeting. Seattle, WA August 2009.
3. Barbeaux 2009. Oral Presentation. "Analyzing fish spatial and temporal distribution patterns using un-calibrated acoustic data from multiple vessels". Annual Science Conference, ICES. Berlin, Germany. September 2009.
4. Barbeaux 2009. Oral Presentation. "Analyzing fish spatial and temporal distribution patterns using un-calibrated acoustic data from multiple vessels". UW Quantitative Seminar Series, Seattle, WA. December 2009.
5. Barbeaux 2010. Oral Presentation. "Assessment of Fishery Induced Depletion Using Opportunistically Collected Acoustic Data". Fishery Dependent Information Conference. Galway, Ireland. August 2010.
6. Barbeaux 2012. Oral Presentation. "Assessment of fishery induced depletion using opportunistically collected acoustic data". 17th Annual Western Groundfish Conference, Seattle, WA. February 2012.
7. Barbeaux 2012. Oral Presentation. "Monitoring on a shoestring: The use of commercial fishing vessels as inexpensive sampling platforms for long-term biological and oceanographic monitoring". 2nd ICES/PICES Conference for Early Career Scientists, Ocean of Change. Majorca Island, Spain. April 2012.
8. Barbeaux 2012. Oral Presentation. "A novel approach for estimating location and scale-specific fishing exploitation rates of eastern Bering Sea walleye pollock (*Theragra chalcogramma*)". PICES Science Board Symposium, Annual Meeting, Hiroshima, Japan, October 2012.

Cokelet

1. Stabeno, P.J., E.D. Cokelet and C. Ladd, Definition of summer ocean domains in warm and cold ocean conditions in the Bering Sea, BSIERP "Fish Component Modelers Meeting", 11-13 August 2009, Seattle, WA.
2. Mordy, C.W., E.D. Cokelet and P.J. Stabeno, Summer nutrient distributions, BSIERP "Fish Component Modelers Meeting", 11-13 August 2009, Seattle, WA.
3. Ressler, P.H., E.D. Cokelet, A.B. Hollowed, Walline, S. Kotwicki and C. Wilson, Summer and mid-water spatial distributions relative to prey fields, BSIERP "Fish Component Modelers Meeting", 11-13 August 2009, Seattle, WA.

4. Cokelet, E.D., Winter oceanography, BSIERP "Fish Component Modelers Meeting", 11-13 August 2009, Seattle, WA
5. Cokelet, E.D., Bottom trawl survey oceanography: poleward thermohaline circulation on the eastern Bering Sea shelf, FOCI Seminar, 11 April 2012, Seattle, WA.
6. Cokelet, E.D., Bottom trawl survey oceanography: poleward thermohaline circulation on the eastern Bering Sea shelf, AFSC Groundfish Seminar, 17 May 2012, Seattle, WA.
7. Cokelet, E. D, Geostrophic Circulation and Water Masses of the Eastern Bering Sea Shelf, 23 Jan 2013, Alaska Marine Science Symposium, Anchorage, AK.

Hollowed

1. Hollowed 2007. Oral presentation. "Forecasting climate impacts on future production of commercially exploited fish and shellfish, Phase II". PICES meeting, Victoria, B.C., Canada.
2. Hollowed 2008. Oral Presentation. "Fish population response to future climate drivers". National Stock Assessment Workshop, Port Townsend, WA.6-8 May 2008.
3. Hollowed 2009. Oral Presentation, **Invited**, "Recipes for adaptation: marine management under climate change and ocean acidification/ workshop". Washington DC. May 18-19.
4. Hollowed 2009. Oral Presentation. **Invited. "**Forecasting climate change impacts on Alaskan ecosystems when processes are uncertain", Applying IPCC-class Models of Global Warming to Fisheries Prediction. Princeton, New Jersey. June 16-18, 2009.
5. Hollowed 2009. Oral Presentation, **Invited**. "A framework for modeling fish and shellfish responses to future climate change". The American Fisheries Society Symposium 10: Stock Assessments: Environmental Factors, Nashville, Tenn. August 31-September 3.
6. Hollowed 2009. Oral Presentation. "Overview of Forage Fish Component: Part 2", BEST/BSIERP PI meeting, October 13, 2009, Girdwood, Alaska.
7. Hollowed 2009. Oral Presentation. "Future conditions in the Bering Sea: Applications to walleye pollock and flatfish". POC/FUTURE Topic Session: Outlooks and forecasts of marine ecosystems form an earth system science perspective: challenges and opportunities, October 29, 2009, Jeju Island, Republic of Korea.
8. Hollowed 2010. **Invited**. Oral Presentation. "A review of modeling frameworks for forecasting climate change impacts on fish and fisheries". Ocean Sciences Meeting, Session IT41B. The California Current Ecosystem: Managing Fisheries Resources in the Face of Climate Variability and Change. Portland, OR, February 25, 2010.

9. Hollowed 2010. Oral Presentation. "Scenario based models for predicting stakeholder responses to a changing climate: a case study for the Eastern Bering Sea". ICES, PICES, FAO international symposium on Effects of Climate Change on Fish and Fisheries, Sendai, Japan, April 29, 2010
10. Hollowed 2010. Oral Presentation. "Scenario based models for predicting stakeholder responses to a changing climate: a case study for the Eastern Bering Sea". National Stock and Habitat Assessment Workshop. St. Petersburg, Florida. 17-20 May 2010.
11. Hollowed 2010. Oral Presentation. "Projections of Key Environmental Parameters for the Bering Sea: Empirical Downscaling from Global Climate Models", FATE PI meeting, Woods Hole, MA June 21, 2010.
12. Hollowed 2010. Oral Presentation. "Comparison of the effects of climate variations on pelagic ocean habitats and their potential role in structuring the forage fish distributions in the Bering Sea and Gulf of Alaska". ICES CM 2010/S-20. ICES ASC, Nantes, France September 2010.
13. Hollowed 2010. Oral Presentation. "Effects of climate change on pelagic ocean habitats and their potential role in structuring Bering Sea and Gulf of Alaska ecosystems". PICES Topic Session 8, Portland, Oregon, October 2010.
14. Hollowed 2010. **Invited** Oral Presentation. "Untangling climate and fishing impacts on marine ecosystems". Presentation to the National Academies of Sciences 71st Ocean Studies Board meeting, Seattle, WA, November 10, 2010
15. Hollowed 2011. **Invited** Oral Presentation. "From Climate Change to Fish on Your Plate: Managing Fisheries in a Changing World". In Symposia "Adapting to a clear and present danger: climate change and ocean ecosystems". AAAS Annual Meeting, Washington D.C. February 19, 2011.
16. Hollowed 2011. Oral Presentation. "Fish, forage, and ocean conditions 2", BSIERP PI meeting, Anchorage, AK. March 2011
17. Hollowed 2011 "Forecasting climate change impacts on forage fish distributions in the Bering Sea" (W1-7500) ESSAS Open Science Meeting, Seattle, WA, 22 May, 2011.
18. Hollowed 2011 **Invited**. "Barriers to prediction and opportunities for research". Arctic Coastal States Arctic Fisheries Workshop, June, 2011.
19. Hollowed 2011 **Invited** Oral Presentation. "Global perspectives on climate change effects on fish and fisheries. 141st American Fisheries Society Annual Meeting, Seattle, WA September, 2011
20. Hollowed 2011 **Invited** Oral Presentation. "21st century climate change impacts on marine fisheries". World Meteorological Organization International Workshop on Climate and Ocean Fisheries, Rarotonga, Cook Islands 3-5 October 4, 2011.

21. Hollowed 2012. Oral Presentation. "Fish, forage, and ocean conditions 2", BSIERP PI meeting, Anchorage, AK. March 28, 2012.

22. Hollowed 2012. **Invited Keynote** Oral Presentation. "Climate change effects on fish and fisheries: current outlooks and a roadmap for interdisciplinary research". 2nd ICES/PICES Conference for Early Career Scientists, Ocean of Change. Majorca Island, Spain. April 24-27, 2012.

23. Hollowed 2012. Oral Presentation. "Modeling fish and shellfish responses to climate change. Trade-offs in model complexity". 2nd International Symposium: Effects of Climate Change on the World's Oceans, Yeosu, Korea. May 19, 2012.

24. Hollowed 2012. Oral Presentation. "Potential movement of fish and shellfish stocks from the sub-Arctic to the Arctic Ocean: Part B evaluation of the vulnerability of fish and shellfish stocks to changing environmental conditions". ICES ASC, Bergen Norway, September 2012.

25. Hollowed 2012. Oral Presentation. "Projecting future status and trends of commercial fish and fisheries under shifting management strategies and climate change". PICES Science Board Symposium, Annual Meeting, Hiroshima, Japan, October 2012.

26. Hollowed 2013. **Invited Plenary** Speaker. "Managing fisheries and ecosystems under a variable and changing climate in the North Pacific". International Symposium/Workshop Climate variability and change on marine resources and fisheries in the South Pacific: Toward a South Pacific Integrated Ecosystem Studies Program (SPICES), Concepcion, Chile, January 2013.

27. Hollowed 2013 **Invited** Speaker, Potential movement of fish and shellfish stocks from the sub-Arctic to the Arctic. Lowell Wakefield Symposium, Anchorage, Alaska. March 2013.

28. Hollowed 2013 Oral Presentation, Is a change in our course of action needed? US-CSIRO-NFRDI workshop on "Setting Biological Reference Points in a Changing Climate", Seattle, WA, August 2013.

29. Hollowed 2013 **Invited Speaker**, "Projected changes in the Arctic – An overview". Workshop on Climate Change Effects on Biological Productivity and Fisheries, September 2013, Reykjavik, Iceland

30. Hollowed 2013 **Invited Speaker**, "An overview of the historical climate change and climate variability in the Bering Sea and consequences on biological productivity". Workshop on Climate Change Effects on Biological Productivity and Fisheries, September 2013, Reykjavik, Iceland.

<u>Kotwicki</u>

1. Kotwicki, S. Alex De Robertis, John Horne, Jim Ianelli, and Andre Punt. Incorporation of habitat data in modeling acoustic dead zone correction and survey bottom trawl efficiency parameters for semi-pelagic species. AFS 2011 Seattle.
2. Kotwicki, S., Alex De Robertis, John Horne, Jim Ianelli, and Andre Punt. How many pollock are hiding in acoustic and bottom trawl blind zones. WGC 2012
3. Kotwicki, S., Alex De Robertis, John Horne, Jim Ianelli, and Andre Punt. Combining bottom trawl and acoustic data to quantify expected biases in abundance estimates from bottom trawl and acoustic surveys. ICES ASC September 2012.
4. Kotwicki, S., Jim Ianelli, André E. Punt, and Patrick Ressler. Improving survey derived indices of abundance by combining bottom trawl and acoustic data. ICES ASC September 2012.
5. Kotwicki, S., Alex De Robertis, John Horne, Jim Ianelli, and Andre Punt. The tricky craft of counting pollock. RACE seminar, March 2013.
6. Kotwicki, S., Alex De Robertis, Jim Ianelli, André E. Punt, and John Horne. Incorporating experimentally derived estimates of survey efficiency into stock assessment. ICES WGISDAA group meeting, March 2013.
7. Kotwicki, S., Jim Ianelli, André E. Punt. Combining bottom trawl and acoustic data to estimate density dependent bottom trawl efficiency. ICES ASC, September 2013.

Lauth

1. Duane Stevenson and Robert Lauth. “Latitudinal trends and temporal shifts in the catch composition of bottom trawls conducted on the eastern Bering Sea shelf” ESSAS 2011, Seattle, WA.
2. Robert Lauth. “The 2010 eastern and northern Bering Sea shelf bottom trawl survey; a first-time synoptic view of groundfishes and crabs” Alaska Marine Science Symposium 2010, AFSC Seminar 2011.

Ressler

1. Ressler, P.H., De Robertis, A., Wilson, C.D., Stabeno, P.J. Trends in walleye pollock and euphausiid abundance on the Bering Sea shelf since 2004. Talk given by Ressler at the Alaska Marine Science Symposium in Anchorage, AK, January 19-23, 2009.
2. Ressler, P.H., De Robertis, A. A multifrequency acoustic indicator of euphausiid abundance in the eastern Bering Sea. Talk given by Ressler at the annual meeting of the ICES Working Group on Fisheries Acoustics Science and Technology in Ancona, Italy, May 18-22, 2009.
3. Ressler, P.H., Kotwicki, S. Spatial association between walleye pollock and euphausiids on the eastern Bering Sea shelf, 2004 – 2008. Talk given by Ressler at the Ocean Sciences meeting, Portland, OR, February 21-26, 2010.
4. Ressler, P.H., De Robertis, A., Warren, J.D., Smith, J.N., Kotwicki, S. Using an acoustic index of euphausiid abundance to understand trophic interactions in the Bering Sea ecosystem. Talk given by Ressler at the annual meeting of the ICES Working Group on Fisheries Acoustics Science and Technology in San Diego, CA, April 27-30, 2010.
5. Ressler, P.H., De Robertis, A., Kotwicki, S. Understanding the ocean through integrated ecosystem research: the BEST-BSIERP Bering Sea Project. Talk given by Ressler at the Museum of the Aleutians, Dutch Harbor, AK, June 2010.

Warren

1. Warren, J.D., Smith, J.N., Ressler, P.H. Density and soundspeed measurements of various Bering Sea Zooplankton. Talk given by Warren at the 157th Meeting of the Acoustical Society of America, Portland, Oregon, May 18–22, 2009.
2. Warren, J.D., Smith, J.N., Ressler, P.H. Measurements of physical properties of Bering Sea zooplankton and their use to improve estimates of euphausiid Target Strength. Talk given by Warren at the annual meeting of the ICES Working Group on Fisheries Acoustics Science and Technology in San Diego, CA, April 27-30, 2010.
3. Warren, J.D., Smith, J.N., Ressler, P.H., Demer, D.A. Improved Assessment of Arctic and Antarctic Zooplankton: From Acoustic Scattering Models to a Better Understanding of Polar Ecosystems. Invited talk given by Warren at the 159th meeting of the Acoustical Society of America, Baltimore, MD, April 2010.

Chapter 12.b. Posters

1. Baker, M., A. Hollowed, M. E. Clarke, R. Hilborn. Role of habitat in moderating species distributions and interactions. ICES/PICES Early Career Science Conference, Majorca, Spain. April 2012.
2. Loeng, H., A. Hollowed and B. Planque. From the Sub-Arctic to the Arctic Ocean International Polar Year, Montreal, Canada April 2012.
3. Hollowed, A. B., E, Curchitser, C. Stock, C. I. Zhang. Trade-offs associated with different modeling approaches for assessment of fish and shellfish responses to climate change. Ocean Sciences Meeting, Salt Lake City, February 2012.
4. Spencer, P., N. Bond, A. Hollowed. A simple model for estimating the rate of predation of arrowtooth flounder on walleye pollock on the Bering Sea shelf over the first half of the 21st century. ESSAS 2nd Open Science Meeting, Seattle, WA. May 2011.
5. Kathy J. Kuletz, Elizabeth A. Labunski, Patrick Ressler, Anne Hollowed, and Mike Sigler. "A broadscale perspective for seabird predator-prey dynamics on the Bering Sea shelf". Alaska Marine Science Symposium, Anchorage, Alaska. January 2010.
6. Anne B. Hollowed, Ed Farley, Chris Wilson, Patrick Ressler, Stan Kotwicki, and Ned Cokelet. "Biogeography of forage fishes in the eastern Bering Sea". BSIERP PI meeting October 2008.
7. Anne Hollowed, Marissa Smith, Steven Barbeaux, James Ianelli and Sigrid Salo. "Effect of climate change on walleye pollock in the eastern Bering Sea". Alaska Marine Science Symposium, Anchorage, AK Jan. 2008.
8. Ressler, P.H., Gibson, G., Ortiz, I., Aydin, K., Herman, A.J. Confronting models with observations (and observations with models): euphausiids in the eastern Bering Sea. Poster presented by Ressler at the BEST-BSIERP PI Meeting, Anchorage, AK, 27-30 March, 2012 .
9. Woillez, M., Ressler, P. H., Wilson, C.D., and Horne, J.K. Horne. Multi-frequency species classification of acoustic-trawl survey data using semi-supervised learning and class discovery. Presented by Woillez at ASA/AFS Special Workshop on Acoustic Challenges in Aquatic Ecosystem Assessment, Seattle, WA, 26-27 May, 2011.
10. Ressler, P.H., De Robertis, A., Warren, J.D., Smith, J.N., Kotwicki, S. Using an acoustic index of euphausiid abundance to understand the impact of fish predation and climate conditions on the euphausiid standing stock of the Bering Sea shelf. Presented by Warren at the 5th International Zooplankton Production Symposium, Pucón, Chile, 14-18 March, 2011.
11. M. Woillez, Ressler, P.H., Wilson, C.D., Horne, J.K. Spatio-temporal patterns of near-surface acoustic backscattering in the eastern Bering Sea based on multi-frequency analysis and

geostatistical methods. Poster given by Woillez at the ICES Annual Science Conference, Nantes, France, September 2010.

12. Warren, J.D., Smith, J.N., Ressler, P.H. Are fat krill "loud" ?: Effect of food availability on the acoustic scattering properties of krill and implications for acoustic assessment of zooplankton biomass. Poster given by Warren at the Ocean Sciences meeting, Portland, OR, February 21-26, 2010.
13. Stan Kotwicki and Robert Lauth "Temperature, density effects and temporal trends in spatial distribution of groundfish in the Eastern Bering Sea", 2011 BSIERP PI meeting, Anchorage, AK and 2011 ESSAS, Seattle, WA.
14. Robert Lauth "Long-term monitoring of the marine ecosystem in the Bering and Chukchi Seas" 2011 Alaska Sea Grant, 27th Lowell Wakefield Fisheries Symposium, Anchorage, AK.
15. Baker, MR, Hollowed, AB 2013. Poster. "Role of habitat in moderating species interactions". Alaska Marine Science Symposium. Anchorage, AK, January, 2013.
16. Baker, MR, Hollowed, AB 2012. Poster. "Spatial considerations for analyses of trophic stability in marine ecosystems". ICES/PICES Conference for Early Career Scientists, Palma de Mallorca, Spain, March 2012.
17. Baker, MR, Hollowed, AB 2012. Poster. "Spatial considerations for analyses of trophic stability in marine ecosystems".Western Groundfish Conference, Seattle, WA, February 2012.
18. Cokelet, E. D., C. W. Mordy, P. J. Stabeno, N. Kachel, P. Proctor and D. Righi, A Comparison of Oceanographic Sections Across the Bering Sea Shelf: Spring and Summer 2008, BSIERP PI Meeting, 14-16 October, Girdwood, AK.
19. Hollowed, A. B., E. Farley, C. Wilson, S. Kotwicki and E. D. Cokelet, Biogeography of Forage Fish in the Eastern Bering Sea, BSIERP PI Meeting, 14-16 October, Girdwood, AK.
20. Cokelet, E. D., C. W. Mordy, P. J. Stabeno, N. Kachel, P. Proctor and D. Righi, Evolution of the Bering Sea Shelf's Mixed Layer and Photic Zone: Ice to Summer, poster presentation to the Alaska Marine Science Symposium, 19-22 January 2009, Anchorage, AK.
21. Cokelet, E.D. 2010. 3D Hydrographic measurements on the eastern Bering Sea shelf from the 2008 Bering Sea bottom trawl survey, poster presentation at the BEST-BSIERP PI Meeting, 13-15 October 2009, Girdwood, AK.
22. Cokelet, E.D. 2010. 3D Hydrographic measurements from the Bering Sea bottom trawl survey, poster presentation at the AGU Ocean Sciences Meeting, 22-26 February 2010, Portland, OR.
23. De Robertis, A. & Cokelet, E.D. 2010. Fish and macrozooplankton distribution in ice-covered and open-water areas of the eastern Bering Sea, poster presentation at the AGU Ocean Sciences Meeting, 22-26 February 2010, Portland, OR.

24. Prokopenko, M.G., J. Granger, C. Mordy, P. DiFlore, N. Cassar, N. Cokelet, N. Kachel, D. Kachel, R. Sambrotto, D. Sigman & B. Moran. 2010. Spring primary production on the eastern Bering Sea shelf as estimated from oxygen/argon rations and triple oxygen isotopes, poster presentation at the AGU Ocean Sciences Meeting, 22-26 February 2010, Portland, OR.
25. Sullivan, M.E., C.W. Mordy, P.J. Stabeno, N.B. Kachel, D.G. Kachel, S.A. Salo & E.D. Cokelet, History of an ecosystem spring setup as seen in annual ice cover, poster presentation at the AGU Ocean Sciences Meeting, 22-26 February 2010, Portland, OR.
26. Cokelet, E.D. 2011. Bottom Trawl Survey CTD Measurements, poster presented at the BEST-BSIERP PI Meeting, 22-24 March 2011, Anchorage, AK.
27. Cokelet, E. D, Poleward thermohaline circulation on the southeast Bering Sea shelf, poster presented at AGU/ASLO Ocean Sciences Meeting, 22 Feb 2012, Salt Lake City.
28. Palevsky, H. I.; Ribalet, F.; Cosca, C. E.; Swalwell, J. E.; Cokelet, E. D.; Quay, P. D.; Feely, R. A.; Armbrust, E. V., Explaining a narrow region of high CO2 uptake in the Gulf of Alaska: the role of biological production and phytoplankton community structure, poster presented at AGU/ASLO Ocean Sciences Meeting, 23 Feb 2012, Salt Lake City.
29. Cokelet, E. D., Poleward thermohaline circulation on the eastern Bering Sea shelf: Results from the NOAA/AFSC Bottom Trawl Survey, poster presented at the BEST-BSIERP PI Meeting, 28-30 March 2012, Anchorage, AK.
30. Barbeaux, S. C. Spital, A. Greig, and A. Hollowed. 2009. Poster. “Generalized additive mixed model analysis of Alaska pollock (Theragra chalcogramma) distribution employing fisheries-dependent and satellite-derived oceanographic data”. Trilateral Committee for Wildlife and Ecosystem Conservation and Management Poster Session. May 2009.

Chapter 13: Outreach

Education and outreach activities specific to this project included four categories of activitiies: teachers-at-sea who participated in BSIERP cruises, summer interns who participated in cruises and worked with us on data analysis, graduate students who used project data as part of their thesis or dissertation, and outreach presentations.

TEACHERS AT SEA:

NOAA Teachers-at-Sea participated in the summer acoustic-trawl surveys in each BSIERP field year: Two teachers participated in the summer of 2009 and five participated in the summer of 2010. Web logs and lesson plans developed by these teachers are available at http://teacheratsea.noaa.gov/, and 2010 teachers were featured as a part of a BSIERP web page about the acoustic trawl survey (http://bsierp.nprb.org/fieldwork/2010/pollock-acoustic.html). We interacted with two PolarTREC teachers at sea on the July BEST USCGC *Healy* cruise, answering questions that students asked on the website and providing background information. We also worked with professional photographers covering the BEST/BSIERP research on the April-May and July *Healy* cruises. One, Galean Rosenwaks, maintains a website about her adventures (http://arctic.globaloceanexploration.com/).

INTERNS:

Patrick Ressler supervised Amanda Guenther, a summer intern in 2009, worked on measuring euphausiids in the Bering Sea and estimating their density near the seafloor. Her experience is briefly described at http://www.afsc.noaa.gov/Education/Internships/2009/intern_guenther.htm Amanda also presented results of her internship project on a poster at the Water Management Association of Ohio's Annual Fall Conference held in Columbus, Ohio, in November 2009. The poster and a description of her summer internship experience is available at http://www.afsc.noaa.gov/internships/interns/2009_AGuenther.htm Patrick Ressler also helped Troy Buckley in supervising an AFSC student intern in summer 2011 (Kelsey Kappler) who worked on comparing food habits of pollock with acoustically-estimated euphausiid densities using summer 2010 samples.

THESES AND DISSERTATIONS:

The euphausiid material properties and target strength work conducted as part of this project formed the basis for the master's thesis of Joy Smith at Stony Brook University.

The Groundfish Trends in the eastern Bering Sea shelf bottom trawl survey project formed the basis for the PhD thesis of Stan Kotwicki at the University of Washington. The title of his theis is *"Combining bottom trawl and acoustic data to improve survey derived population and spatial indices of semi-pelagic species."*

The Opportunistic data collection as an index of local depletion project and the Predicting Eastern Bering Sea adult walleye pollock (Theragra chalcogramma) winter distribution project Barbeaux, S. 2012. Scientific Acoustic Data from Commercial Fishing Vessels: Eastern Bering Sea Walleye Pollock (Theragra chalcogramma). University of Washington. PhD dissertation.

OUTREACH PRESENTATIONS:

Mike Sigler and Patrick Ressler presented a 'tag-team' talk on BEST-BSIERP research at the Museum of the Aleutians in Dutch Harbor, AK, in June 2010. They presented an overview of the program as well as some specific information about BSIERP projects involving the acoustic-trawl and bottom trawl pollock surveys, project B62 research. The talk was well attended by members of the local community. Sigler and Ressler repeated the talk the next morning (by invitation) for industry members and skippers at the Unisea fish processing plant. An article about these talks and PDF versions of the presentations were featured on the BEST-BSIERP home page, and then moved to the acoustic survey web page, http://bsierp.nprb.org/fieldwork/2010/pollock-acoustic.html Ressler, P.H., De Robertis, A., Kotwicki, S. Understanding the ocean through integrated ecosystem research: the BEST-BSIERP Bering Sea Project. Talk given by Ressler at the Museum of the Aleutians, Dutch Harbor, AK, June 2010.

Chapter 14: Literature Citied

Aglen, A. 1996. Impact of fish distribution and species composition on the relationship between acoustic and swept-area estimates of fish density. ICES Journal of Marine Science 53:501–505.

Aglen, A., Engås, A., Huse, I., Michalsen, K., and Stensholt, B. K. 1999. How vertical fish distribution may affect survey results. ICES Journal of Marine Science 56:345–360.

Agostini, V.N., Francis, R.C., Hollowed, A.B., Pierce, S., Wilson, C., and Hendrix A.N. 2006. The relationship between hake (*Merluccius productus*) distribution and poleward sub-surface flow in the California Current System. Canadian Journal of Fisheries and Aquatic Sciences 63:1648-1659.

Alton, M.S., Bakkala, R.G., Walters, G.E., and Munro, P.T., 1988. Greenland turbot Reinhardtius hippoglossoides of the eastern Bering Sea and Aleutian Islands region. U.S. Dep. Commer., NOAA Tech. Rep. NMFS-71, 31 p.

Alverson, D. L., and Pereyra, W.T. 1969. Demersal fish explorations in the northeast Pacific Ocean – An evaluation of exploratory fishing methods and analytical approaches to stock size and yield forecasts. Journal of the Fisheries Research Board of Canada 26:1985–2001.

Amakasu, K. and Furusawa, M. 2006. The target strength of Antarctic krill (*Euphausia superba*) measured by the split-beam method in a small tank at 70 kHz. ICES Journal of Marine Science 63:36-45.

A'mar, Z.T., Punt, A.E. and Dorn, M.W. 2009. The evaluation of two management strategies for the Gulf of Alaska walleye pollock fishery under climate change. ICES Journal of Marine Science 66:1614-1633.

Ambrose, W.G., Jr., Clough, L.M, Tilney, P.R., and Beer, L. 2001. Role of echinoderms in benthic remineralization in the Chukchi Sea. Marine Biology 139 937–949.

Anderson, C. I. H., Horne, J. K., and Boyle, J. 2007. Classifying multifrequency fisheries acoustic data using a robust probabilistic classification technique. Journal of the Acoustical Society of America 121:230-237.

Anderson, L.A. 1995. On the hydrogen and oxygen content of marine phytoplankton. Deep Sea Research Part I: Oceanographic Research Papers 42:1675-1680.

Anderson, P.J., and Piatt, J.F. 1999. Community reorganization in the Gulf of Alaska following ocean climate regime shift. Marine Ecology Progress Series, 189: 117-123.

Anderson, V.C. 1950. Sound scattering from a fluid sphere. Journal of the Acoustical Society of America 22(4):426-431.

Arlot, S., and A. Celisse. 2010. A survey of cross-validation procedures for model selection. Statistics Surveys 4: 40-79.

Armstrong, F.A.J., Stearns, C.R., and Strickland, J.D.H. 1967. The measurment of upwelling and subsequent biological processes by means of the Technicon AutoAnalyzer and associated equipment. Deep-Sea Research 14, 381-389.

Arregui, I., Arrizabalaga, H., Kirby, D.S. and Martin-Gonzalez, J.M. 2006. Stock-environment-recruitment models for North Atlantic albacore (*Thunnus alalunga*). Fisheries Oceanography, 15(5): 402-412.

Atkinson, D.B., Rose, G.A., Murphy, E.F., and Bishop, C.A., 1997. Distribution changes and abundance of northern cod (Gadus morhua), 1981-1993. Canadian Journal of Fisheries and Aquatic Sciences 54 (Suppl. 1):132-138.

Aydin, K. and Mueter, F. 2007. The Bering Sea - A dynamic food web perspective. Deep-Sea Research II 54:2501–2525.

Bacheler, N.M., Ciannelli, L., Bailey, K.M., Duffy-Anderson, J.T. 2010. Spatial and temporal patterns of walleye pollock (*Theragra chalcogramma*) spawning in the eastern Bering Sea inferred from egg and larval distributions. Fisheries Oceanography 19: 107-120.

Baier, C. T. and Napp, J. M. 2003. Climate-induced variability in Calanus marshalle populations. Journal of Plankton Research 25(7):771-782.

Bailey, K.M. 1989. Interaction between the vertical distribution of juvenile walleye pollock Theragra chalcogramma in the eastern Bering Sea, and cannibalism. Marine Ecology Progress Series 53:205-213.

Bailey, K.M. 2000. Shifting control of recruitment of walleye pollock (*Theragra chalcogramma*) after a major climate and ecosystem change. Marine Ecology Progressive Series, 198: 215-224.

Bailey, K., Quinn II, T.J., Bentzen, P. and Grant, W.S. 1999. Population Structure and Dynamics of Walleye Pollock, *Theragra chalcogramma*, Advances in Marine Biology 37:179-255.

Balls, R., 1948. Herring fishing with the echometer. Journal du Conseil International pour l'Exploration de la Mer 15:193-206.

Barbeaux, S.J., and Dorn, M.W. 2003. Spatial and temporal analysis of eastern Bering Sea echo integration-trawl survey and catch data of walleye pollock, *Theragra chalcogramma*, for 2001 and 2002. U.S. Dep. Commer., NOAA-TM-AFSC-136, 34 p.

Barbeaux, S.J., Horne, J. and Dorn, M.W. 2013. Characterizing walleye pollock (*Theragra chalcogramma*) winter distribution from opportunistic acoustic data. ICES J. Mar. Sci. Advanced Access first published online May 22, 2013.

Bartolino, V., Ciannelli, L., Bacheler, N.M., and Chan, K.S. 2011. Ontogenetic and sex-specific differences in density-dependent habitat selection of a marine fish population. Ecology 92:189-200.

Batchelder H. P., Lessard, E.J., Strub, P.T. and Weingartner, T. J. (editors). 2005. U.S.GLOBEC biological and physical studies of plankton, fish and higher trophic level production, distribution, and variability in the northeast Pacific Deep-Sea Research Part II, 52(1-2).

Beaugrand, G., Brander, K. M., Lindley, J. A., Souissi, S., and Reid, P. C. 2003. Plankton effect on cod recruitment in the North Sea. Nature, 436: 661-664.

Biernacki, C., Celeux, G., and Govaert, G. 2000. Assessing a Mixture Model for Clustering with the Integrated Completed Likelihood. IEEE Transactions on Pattern Analysis and Machine Intelligence 22:719-725.

Birks, H.J.B., Line, J.M., Juggins, S., Stevenson, A.C. and ter Braak, C.J.F. 1990. Diatoms and pH re-construction. Philisophical Transactions of the Royal Society B 327:263–278.

Bluhm, B.A., Iken, K., Mincks Hardy, S., Sirenko, B.I., Holladay, B.A. 2009. Community structure of epibenthic megafauna in the Chukchi Sea. Aquatic Biology 7:269–293.

Booth, B.C., Lewin, J., and Lorenzen, C.J. 1988. Spring and summer growth rates of subarctic Pacific phytoplankton assemblages determined from carbon uptake and cell volumes estimated using epifluorescence microscopy. Marine Biology 98:287-298.

Boschi, E. E. 2000. Biodiversity of marine decapod brachyurans of the Americas. Journal of Crustacean Biology 20(Special No. 2):337–342.

Brander, K. 2008. A history of climate – related research in ICES. ICES Insight, 45: 32-35.

Brierley, A.S., and Watkins, J.L. 1996. Acoustic targets at South Georgia and the South Orkney Islands during a season of krill scarcity. Marine Ecology Progress Series 138:51-61.

Brierley, A.S., Watkins, J.L., and Murray, A.W.A. 1997. Interannual variability in krill abundance at South Georgia. Marine Ecology Progress Series150:87–98.

Brinton, E., Ohman, M. D., Townsend, A. W., Knight, M. D., and Bridgeman, A.L. 2000. Euphausiids of the World Ocean. World Biodiversity Database CD-ROM Series, Springer Verlag. ISBN 3-540-14673-3.

Brodeur, R.D., Wilson, M.T., Ciannelli, L., Doyle, M. and Napp, J.M. 2002. Interannual and regional variability in distribution and ecology of juvenile pollock and their prey in frontal structures of the Bering Sea. Deep-Sea Research II 49:6051-6067.

Brooks, E. N., and Powers, J. E. 2007. Generalized compensation in stock-recruitment functions: properties and implications for management. ICES Journal of Marine Science, 64: 413-424.

Brooks, J. L., and Dodson, S. I., 1965. Predation, body size, and composition of plankton. Science 150:28-35.

Bull B., and Livingston, M. E. 2001. Links between climate variation and year class strength of New Zealand hoki (*Macruronus novaezelandiae*): an update. New Zealand Journal of Marine and Freshwater Research, 35: 871–880.

Burnham, K. P., and Anderson, D. R. 2010. Model selection and multimodel inference. Springer, New York, 514 pp.

Campbell, R.W., and Dower, J.F. 2003. Role of lipids in the maintenance of neutral bouyancy by zooplankton. Marine Ecology Progress Series 263:93-99.

Carpenter, S. R., and Kitchell, J. F. E. 1993. The trophic cascade in lakes. Cambridge University Press, Cambridge, 385 pp.

Chavez, F. P., Ryan, J., Lluch-Cota, S. E., Ňiquen M. C. 2003. From anchovies to sardines and back: multidecadal change in the Pacific ocean. Science, 299: 217-221.

Cheung, W. W. L., Lam, V. W. Y., Sarmiento, J. L., Kearney, K., Watson, R., and Pauly, D. 2009. Projecting global marine biodiversity impacts under climate change scenarios. Fish and Fisheries 10:235-251.

Christensen, N. L., Bartuska, A. M., Brown, J. H., Carpenter, S., D'Antonio, C., Francis, R., Jerry F. Franklin, J.F., MacMahon, J.A., Noss R.F., Parsons, D.J., Peterson, C.H., Turner, M.G., and Woodmansee, R. G. 1996. The report of the Ecological Society of America committee on the scientific basis for ecosystem management. Ecological Applications 6(3):665-691.

Chu, D., and Wiebe, P.H. 2005. Measurements of sound-speed and density contrasts of zooplankton in Antarctic waters. ICES Journal of Marine Science 62:818-831.

Chu, D., and Ye, Z. 1999. A phase-compensated DWBA representation of the bistatic scattering by weakly scattering objects: Applications to zooplankton. Journal of the Acoustical Society of America 106:1732-1743.

Chu, D., Foote, K.G. and Stanton, T.K. 1993. Further analysis of target strength measurements of Antarctic krill at 38 and 120 kHz: Comparison with deformed cylinder model and inference of orientation distribution. Journal of the Acoustical Society of America 93(5):2985-2988.

Chu, D., Wiebe , P. H., and Copley , N. 2000. Inference of material properties of zooplankton from acoustic and resistivity measurements. ICES Journal of Marine Science 57:1128-1142.

Chuchukalo, V.I., Kuznetsova N.A., and Napazakov, V.V. 1996. Seasonal distribution of euphausids in the Bering and Okhotsk Sea and adjacent waters of Pacific Ocean. Izvestiya TINRO 119:256-281.

Ciannelli, L., and Bailey, K.M. 2005. Landscape dynamics and resulting species interactions: the cod-capelin system in the southeastern Bering Sea. Marine Ecology Progress Series 291:227-236.

Ciannelli, L., Brodeur, R.D., and Napp, J.M. 2004. Foraging impact on zooplankton by age-0 walleye pollock (*Theragra chalcogramma*) around a front in the southeast Bering Sea. Marine Biology 144:515-525.

Ciannelli, L., Chan, K., Bailey, K.M. and Stenseth, N.C. 2004. Nonadditive effects of the environment on the survival of a large marine fish population, Ecology 85:3418–3427.

Ciannelli, L., Fauchald, P., Chan, K., Agostini, V., and Dingsor, G. 2008. Spatial fisheries ecology: Recent progress and future prospects. Journal of Marine Systems 71(3-4):223-236.

Clarke, A. 1992. Is there a latitudinal diversity cline in the sea? Trends in Ecology and Evolution 7:286–287.

Clarke, A., and Johnston, N.M. 1999. Scaling of metabolic rate with body mass and temperature in fish. Journal of Animal Ecology 68:893–905.

Clutter, R. I., and Anraku, M., 1968. Avoidance of samplers. In Zooplankton sampling, p. 57-76. UNESCO Monographs in Oceanographic Methodology 2., Unesco Press, Paris, France, 174 p.

Coachman, L.K. 1986. Circulation, water masses, and fluxes on the southeastern Bering Sea shelf. Continental Shelf Research, 5: 23–108.

Coachman, L.K., Aagaard, K., and Tripp, R.B. 1975. Bering Strait: the regional physical oceanography. Univ of Washington Pr.

Conti, S.G. and Demer, D.A. 2006. Improved parameterization of the SDWBA for estimating krill target strength. ICES Journal of Marine Science 63:928-935.

Cokelet, E.D. 2012a. Underway Seawater Sampling Aboard F/V Aldebaran in Winter & Summer 2008, Forage Distribution and Ocean Conditions (B62). UCAR/NCAR Earth Observing Laboratory, Boulder, CO, BSIERP Data Archive, http://data.eol.ucar.edu/codiac/dss/id=245.B62-001, last accessed 9 January 2012.

Cokelet, E.D. 2012b. Underway Seawater Sampling Aboard F/V Aldebaran in Winter & Summer 2009, Forage Distribution and Ocean Conditions (B62). UCAR/NCAR Earth Observing Laboratory, Boulder, CO, BSIERP Data Archive, http://data.eol.ucar.edu/codiac/dss/id=245.B62-007, last accessed 13 June 2012.

Cokelet, E.D. 2012c. Underway Seawater Sampling Aboard F/V Aldebaran in Winter & Summer 2010, Forage Distribution and Ocean Conditions (B62). UCAR/NCAR Earth Observing Laboratory, Boulder, CO, BSIERP Data Archive, http://data.eol.ucar.edu/codiac/dss/id=245.B62-008, last accessed 13 June 2012.

Cokelet, E.D. 2013d. Underway Seawater Sampling Aboard NOAA ship Oscar Dyson in 2008, Forage Distribution and Ocean Conditions (B62). UCAR/NCAR Earth Observing Laboratory, Boulder, CO, BSIERP Data Archive, http://data.eol.ucar.edu/codiac/dss/id=245.B62-009, last accessed 17 September 2013.

Cokelet, E.D. 2013e. Underway Seawater Sampling Aboard NOAA ship Oscar Dyson in 2009, Forage Distribution and Ocean Conditions (B62). UCAR/NCAR Earth Observing Laboratory, Boulder, CO, BSIERP Data Archive, http://data.eol.ucar.edu/codiac/dss/id=245.B62-010, last accessed 17 September 2013.

Cokelet, E.D. 2013f. Underway Seawater Sampling Aboard NOAA ship Oscar Dyson in 2010, Forage Distribution and Ocean Conditions (B62). UCAR/NCAR Earth Observing Laboratory, Boulder, CO, BSIERP Data Archive, http://data.eol.ucar.edu/codiac/dss/id=245.B62-011, last accessed 17 September 2013.

Cokelet, E.D., 2013g. NOAA Bering Sea Bottom Trawl Survey CTD data in 2008, Forage Distribution and Ocean Conditions (B62). UCAR/NCAR Earth Observing Laboratory, Boulder, CO, BSIERP Data Archive, http://data.eol.ucar.edu/codiac/dss/id=245.B62-012, last accessed September 2013.

Cokelet, E.D., 2013h. NOAA Bering Sea Bottom Trawl Survey CTD data in 2009, Forage Distribution and Ocean Conditions (B62). UCAR/NCAR Earth Observing Laboratory, Boulder, CO, BSIERP Data Archive, http://data.eol.ucar.edu/codiac/dss/id=245.B62-013, last accessed September 2013.

Cokelet, E.D., 2013i. NOAA Bering Sea Bottom Trawl Survey CTD data in 2010, Forage Distribution and Ocean Conditions (B62). UCAR/NCAR Earth Observing Laboratory, Boulder, CO, BSIERP Data Archive, http://data.eol.ucar.edu/codiac/dss/id=245.B62-014, last accessed September 2013.

Cokelet, E.D., 2014. 3-D water properties and thermohaline circulation on the eastern Bering Sea shelf. submitted to Deep Sea Research Part II: Topical Studies in Oceanography.

Coyle, K.O. 2000. Acoustic estimates of zooplankton biomass and distribution: application of canonical correlation to scaling of multifrequency acoustic data. Canadian Journal of Fisheries and Aquatic Sciences 57:2306-2318.

Coyle, K.O., Chavtur, V.G., and Pinchuk, A. I. 1996. Zooplankton of the Bering Sea: A review of Russian-language literature. Ecology of the Bering Sea. Alaska Sea Grant Report No. 96-01:97-134, Fairbanks, AK.

Coyle, K.O., Eisner, L.B., Mueter, F.J., Pinchuk, A.I., Janout, M.A., Cieciel, K.D., Farley, E.V., and Andrews, A.G. 2011. Climate change in the southeastern Bering Sea: impacts on pollock stocks and implications for the oscillation control hypothesis. Fisheries Oceanography 20(2):139-156.

Coyle, K.O., Hunt, Jr., G.L., M.B. Decker, and Weingartner, T.J. 1992. Murre foraging, epibenthic sound scattering, and tidal advection over a shoal near St. George Island, Bering Sea. Marine Ecology Progress Series 83:1-14.

Coyle, K.O., and Pinchuk, A.I. 2002. The abundance and distribution of euphausiids and zero-age pollock on the inner shelf of the southeast Bering Sea near the Inner Front in 1997-1999. Deep-Sea Research II 49:6009-6030.

Coyle, K.O., Pinchuk, A.I., Eisner, L.B., and Napp, J.M. 2008. Zooplankton species composition, abundance, and biomass on the eastern Bering Sea shelf during summer: The potential role of water-column stability and nutrients in structuring the zooplankton community. Deep-Sea Research II 55:1775-1791.

Cui, X., Grebmeier, J.M., Cooper, L.W., Lovvorn, J.R., North, C.A., Seaver, W.L., and Kolts, J.M. 2009. Spatial distributions of groundfish in the northern Bering Sea in relation to environmental variation. Marine Ecology Progress Series 393:147–160.

Currie, D.J., Mittelbach, G.G., Cornell, H.V., Field, R., Guegan, J.-F., Hawkins, B.A., Kaufman, D.M., Kerr, J.T., Oberdorff, T., O'Brien, E., and Turner, J.R.G. 2004. Predictions and tests of climate-based hypotheses of broad-scale variation in taxonomic richness. Ecology Letters 7:1121–1134.

Dagg, M.J., Clarke, M.E., Nishiyama, T. and Smith, S.L. 1984. Production and standing stock of copepod nauplii, food items for larvae of the walleye pollock *Theragra chalcogramma* in the southeastern Bering Sea. Marine Ecology Progress Series 19:7-16.

Dalpadado, P., Ingvaldsen, R. B., Stige, L. C., Bogstad, B., Knutsen, T., Ottersen, G., and Ellertsen, B. 2012. Climate effects on Barents Sea ecosystem dynamics. ICES Journal of Marine Science 69:1303–1316.

Dalpadado, P., and Skjoldal, H.R. 1996. Abundance, maturity and growth of the krill species *Thysanoessa inermis* and *T. longicaudata* in the Barents Sea. Marine Ecology Progress Series144:175-183.

Danielson, S., Eisner, L., Weingartner, T., and Aagaard, K. 2011. Thermal and haline variability over the central Bering Sea shelf: Seasonal and interannual perspectives. Continental Shelf Research 31:539-554.

Dann, N. and Fogarty, M. J. 2000. Recruitment dynamics of exploited marine populations: physical-biological interactions: Part 1. Ed. By M. J. Fogarty. ICES Journal of Marine Science 57 (2): 189-190.

Davis, N.D., Volkov, A.V., Efimkin, A.Y., Kuznetsova, N.A., Armstrong, J.L., and Sakai, O. 2009. Review of BASIS salmon food habits studies. North Pacific Anadromous Fish Commission Bulletin 5:197-208.

De Roberts, A., and Cokelet, E.D. 2012. Fish and macrozooplankton distribution in ice-covered and open-water areas of the eastern Bering Sea. Deep-Sea Research II 65–70:217–229.

De Robertis, A., and Higginbottom, I. 2007. A post-processing technique to estimate the signal-to-noise ratio and remove echosounder background noise. ICES Journal of Marine Science 64:1282-1291.

De Robertis, A., McKelvey, D., and Ressler, P.H. 2010. Development and application of empirical multi-frequency methods for backscatter classification. Canadian Journal of Fisheries Aquatic Sciences 67:1459-1474.

Decker, M.B., and Hunt, Jr., G.L. 1996. Murre foraging at the frontal system surrounding the Pribilof Islands, Alaska. Marine Ecology Progress Series:139:1-10.

Decker, M.B., Hunt, Jr., G.L., and Byrd, Jr., G.V. 1995. The relationships among sea-surface temperature, the abundance of juvenile walleye pollock (*Theragra chalcogramma*), and the reproductive performance and diets of seabirds at the Pribilof Islands, southeastern Bering Sea. P. 425-437. In R. J. Beamish (editor) Climate change and northern fish populations. Special Publication 121 of the Fish. Canadian Journal of Fisheries and Aquatic Sciences.

Demer, D.A., and Conti, S.G. 2003. Validation of the stochastic distorted-wave Born approximation model with broad bandwidth total target strength measurements of Antarctic krill. ICES Journal of Marine Science 60:625-635.

Demer, D.A.and Conti, S.G. 2003a. Reconciling theoretical versus empirical target strengths of krill: effects of phase variability on the distorted-wave Born approximation. ICES Journal of Marine Science, 60:429-434.

Demer, D.A. and Conti, S.G. 2003b. Validation of the stochastic distorted-wave Born approximation model with broad bandwidth total target strength measurements of Antarctic krill. ICES Journal of Marine Science 60:625-635.

Demer, D.A. and Conti, S.G. 2005. New target-strength model indicates more krill in the Southern Ocean. ICES Journal of Marine Science 62:25-32.

Dempster, A.P., Laird, N. M., and Rubin, D. B. 1977. Maximum likelihood from incomplete data via EM algorithm. Journal of the Royal Statistical Society Series B (Methodology) 39:1–38.

Denbo, D.W., 1993. Plot Plus, Scientific Graphics System. NOAA Pacific Marne Environmental Laboratory.

De Oliveira, J.A.A., and Butterworth, D.S. 2005. Limits to the use of environmental indices to reduce risk and/or increase yield in the South African anchovy fishery. African Journal of Marine Science 27: 191–203.

Di Lorenzo, E., Schneider, N., Cobb, K.M., Franks, P.J.S., Chhak, K., Miller, A.J., McWilliams, J.C., Bograd, S.J., Arango, H., Curchister, E., Powell, T.M. and Riviere, P. 2008. North Pacific gyre oscillation links ocean climate and ecosystem change. Geophysical Research Letters 35: L08607.

Dorn, M.W. 1995. The effects of age composition and oceanographic conditions on the annual migration of Pacific whiting, *Merluccius productus*. California Cooperative Oceanic Fisheries Investigations Reports 36:97-105.

Dwyer, D.A., Bailey, K.M., and Livingston, P.A., 1987. Feeding habits and daily ration of walleye pollock (*Theragra chalcogramma*) in the eastern Bering Sea, with special reference to cannibalism. Canadian Journal of Fisheries and Aquatic Sciences 44:1972-1984.

Easterling, W. and Aggarwal, P., Batima, P., Brander, K. M., Erda, L., Howden, S. M., Kirilenko, A., Morton, J., Soussana, J.-F., Schmidhuber, J., and Tubiello, F. N. 2007. Food, fibre and forest products. *In* Climate Change 2007: Impacts, Adaptation and Vulnerability. Contribution of Working Group II to the Fourth Assessment Report of the Intergovernmental Panel on Climate Change, pp. 273-313. Ed. M. L. Parry, O. F. Canziani, J. P. Palutikof, P. J. vander Linden and C. E. Hanson. Cambridge University Press, Cambridge, UK.

Ellis, N., Smith, S. J., and Pitcher, C. R. 2012. Gradient forests: calculating importance gradients on physical predictors. Ecology 931:156-168.

Endo, Y. 1993. Orientation of Antarctic krill in an aquarium. Nippon Suisan Gakkaishi 59(3):465-468.

Ernst, B., Orensanz, J.M., and Armstrong, D.A. 2005. Spatial dynamics of female snow crab (*Chionoecetes opilio*) in the eastern Bering Sea. Canadian Journal of Fisheries and Aquatic Sciences 62:250-268.

Everson, I., and Bone, D.G. 1986. Effectiveness of the RMT8 system for sampling krill (*Euphausia superba*) swarms. Polar Biology 6(1):83-90.

FAO. 2009. The State of World Fisheries and Aquaculture 2008, Part 1. World review of fisheries and aquaculture. FAO Fisheries and Aquaculture Department, Viale delle Terme di Caracalla, 00153 Rome, Italy, 176 p. http://www.fao.org/docrep/ 011/i0250e/ i0250e00 .htm

FAO. 2012. The State of World Fisheries and Aquaculture 2012, Part 1. World Review of Fisheries and Aquaculture. FAO Fisheries and Aquaculture Department, Rome. URL: http://www.fao.org/docrep/016/i2727e/i2727e00.htm.

Farley, E.V., Jr., and Moss, J.M. 2009. Growth rate potential of juvenile chum salmon on the eastern Bering Sea shelf: an assessment of salmon carrying capacity. North Pacific Anadromous Fish Commission Bulletin 5:265 – 277.

Farley, E. V., Jr., Murphy, J., Moss, J., Feldmann, A., and Eisner, L. 2009. Marine ecology of western Alaska juvenile salmon, p. 307-330. In C. C. Krueger and C. E. Zimmerman (Editors), Pacific Salmon: Ecology and Management of Western Alaska's Populations. American Fisheries Society Symposium 70, Bethesda, Maryland.

Farley, Jr., E.V., Trudel, M. 2009. Growth rate potential of juvenile sockeye salmon in warmer and cooler years on the Eastern Bering Sea shelf. Journal of Marine Biology Volume 2009, Article ID 640215.

Feder, H.M., Jewett, S.C., and Blanchard, A. 2005. Southeastern Chukchi Sea (Alaska) epibenthos. Polar Biology 28:402–421.

Feder, H.M., Jewett, S.C., Blanchard, A.L. 2007. Southeastern Chukchi Sea (Alaska) macrobenthos. Polar Biology 30:261–275.

Feder, H.M., Naidu, A.S., Jewett, S.C., Hameedi, J.M., Johnson, W.R., and Whitledge, T.E. 1994. The northeastern Chukchi Sea: benthos-environmental interactions. Marine Ecology Progress Series 111:171–190.

Fernandes, P. G. 2009. Classification trees for species identification of fish-school echotraces. ICES Journal of Marine Science 66:1073–1080.

Fischlin, A., Midgley, G. F., Price, J. T., Leemans, R., Gopal, B., Turley, C., Rounsevell, M.D.A., Dube, O. P., Tarazona, J., and Velichko, A. A. 2007. Ecosystems, their properties, goods and services. Climate Change 2007: Impacts, Adaptation and Vulnerability. *In* Contribution of Working Group II to the Fourth Assessment Report of the intergovernmental Panel on Climate Change, pp. 211-272. M. L. Parry, O.F. Canziani, P. P. Palutikof, P. J. vander Linden, and C. E. Hanson Ed. By Cambridge University Press Cambridge, UK.

Fofonoff, N.P., Hayes, S., and Millard, R.C. 1974. WHOI/Brown CTD microprofiler: methods of calibration and data handling. Woods Hole Oceanographic Institution Tech. Rep. WHOI-74-89, 1-66.

Fogarty, M. J. 2001. Recruitment dynamics of exploited marine populations: physical-biological interactions. Part 2. Ed. By M. J. Fogarty. ICES Journal of Marine Science 58(5): 936.

Foote, K.G. 1990. Speed of sound in *Euphausia superba*. Journal of the Acoustical Society of America 87(4):1405-1408.

Foote, K.G., Everson, I., Watkins, J.L., and Bone, D.G. 1990. Target strengths of Antarctic krill (*Euphausia superba*) at 38 and 120 kHz. Journal of the Acoustical Society of America 87(1):16-24.

Foote, K.G., Knudsen, H.P., Vestnes, G., MacLennan, D.N., and Simmonds, E.J. 1987. Calibration of acoustic instruments for fish density estimation: A practical guide. *In* ICES Cooperative Research Report, Vol. 144. International Council for the Exploration of the Sea, Copenhagen, Denmark.

Foote, K.G., and Stanton, T.K., 2000. Chapter 6: Acoustical Methods. *In* Harris, R.P., Wiebe, P.H., Lenz, J., Skjoldal, H.R., Huntley, M., (Eds.), Zooplankton Methodology Manual. Academic Press, San Diego, CA, pp. 223-253.

Forman, K.A. and Warren, J.D. 2009. Variability in the density and sound-speed of coastal zooplankton and nekton. ICES Journal of Marine Science 67(1):10-18. doi:10.1093Nices msNfsp217.

Forman, K.A. and Warren, J.D. 2010. Variability in the density and sound-speed of coastal zooplankton and nekton. ICES Journal of Marine Science 67(1):10-18. doi:10.1093/icesjms/fsp217.

Francis, R.C., Bailey, K.M. 1983. Factors affecting recruitment of selected gadoids in the northeastern Pacific and east Bering Sea. In Year to Year: Interannual Variability of the Environment and Fisheries of the Gulf of Alaska and the Eastern Bering Sea, W.S. Wooster (ed.), Washington Sea Grant, University of Washington, Seattle, WA, 17–22.

Francis, R.I.C.C. 2006. Measuring the strength of environment-recruitment relationships: the importance of including predictor screening within cross-validations. ICES Journal of Marine Science 63: 594–599.

Francis, R I.C.C., Hadfield, M. G., Bradford-Grieve, J. M., Renwick, J. A., and Sutton. P. J. H. 2006. Links between climate and recruitment of New Zealand hoki (*Macruronus novaezelandiae*) now unclear. New Zealand Journal of Marine and Freshwater Research 40: 547–560.

Fréon, P., Cury, P., Shannon, L., and Roy, C. 2005. Sustainable exploitation of small pelagic fish stocks challenged by environmental and ecosystem changes: A review. Bulletin of Marine Science, 76: 385–462.

Frost, B.W., 1993. A modelling study of processes regulating plankton standing stock and production in the open subarctic Pacific Ocean. Progress in Oceanography 32:17-56.

Gadd, A., and Wold, H. 1964. The janus coefficient: a measure for the accuracy of prediction, In: H.O.A. Wold (Editor), Economic Model Building: Essays on the Causal Chain Approach. North-Holland, Amsterdam, 229-235pp.

Gaichas, S.K. and Francis, R.C. 2008. Network models for ecosystem-based fishery analysis: a review of concepts and application to the Gulf of Alaska marine food web. Canadian Journal of Fisheries and Aquatic Sciences 65(9):1965-1982.

Garrison, L.P., Link, J.S. 2000. Fishing effects on spatial distribution and trophic guild structure of the fish community in the Georges Bank region. ICES Journal of Marine Science 57:723-730.

Genin, A., Haury, L., Greenblatt, P. 1988. Interactions of migrating zooplankton with shallow topography: predation by rockfishes and intensification of patchiness. Deep-Sea Research I 35 (2):151-175.

Gill, A.E. 1982. Atmosphere-ocean dynamics. Academic press.

Gliwicz, Z.M. 1986. A lunar cycle in zooplankton. Ecology 67 (4):883-897.

Godø, O. R. 1994. Factors affecting the reliability of groundfish abundance estimates from bottom trawl surveys. *In* A. Fernö, and S. Olsen (Editors) Marine Fish Behaviour in Capture and Abundance Estimation, pp. 166–199. Fishing News Books, Oxford.

Godø, O. R., and Engås, A. 1989. Swept area variation with depth and its influence on abundance indices of groundfish from trawl surveys. Journal of Northwest Atlantic Fishery Science 9:133–139.

Godø, O.R., and Wespestad, V.G. 1993. Monitoring changes in abundance of gadoids with varying availability to trawl and acoustic surveys. ICES Journal of Marine Science 50:39–51.

Goodyear, C. P. 2004. FSIM – A simulator for forecasting fish population trends and testing assessment methods. Collective Volume of Scientific Papers ICCAT, 56(1): 120-131.

Goodyear, C. P.. 2005. FSIM Version 4.0 User's Guide, August 2005. C. Philip Goodyear, 1214 N. Lakeshore Drive, Niceville, FL 32578. 49 p.

Gorska, N., Ona, E. and Korneliussen, R. 2005. Acoustic backscattering by Atlantic mackerel as being representative of fish that lack a swimbladder. Backscattering by individual fish. ICES Journal of Marine Science 62:984-995.

Goovaerts, P. 1997. Geostatistics for Natural Resources Evaluation. Oxford University Press, New York. 483 pp.

Grebmeier, J.M., Feder, H.M., and McRoy, C.P. 1989. Pelagic-benthic coupling on the shelf of the northern Bering and Chukchi Seas. II. Benthic community structure. Marine Ecology Progress Series 51:253–268.

Grebmeier, J.M., McRoy, C.P., and Feder, H.M. 1988. Pelagic-benthic coupling on the shelf of the northern Bering and Chukchi Seas. I. Food supply source and benthic biomass. Marine Ecology Progress Series 48, 57–67.

Grebmeier, J.M., Overland, J.E., Moore, S.E., Farley, E.V., Carmack, E.C., Cooper, L.W., Frey, K.E., Helle, J.H., McLaughlin, F.A., and McNutt, S.L. 2006. A major ecosystem shift in the northern Bering Sea. Science 311:1461–1464.

Greenblatt, P. 1981. Sources of acoustic backscattering at 87.5 kHz. Journal of the Acoustical Society of America 70(1):134-142.

Greenlaw, C.F. 1977. Backscattering spectra of preserved zooplankton. Journal of the Acoustical Society of America 62:44-52.

Greenlaw, C.F., and Johnson, R.K. 1982. Physical and acoustical properties of zooplankton. Journal of the Acoustical Society of America, 72(6):1706-1710.

Grumbine, R. E. 1994. What is ecosystem management? Conservation Biology, 8(1):27–38.

Haflinger, K. 1981. A survey of benthic infaunal communities of the southeastern Bering Sea shelf. *In* Hood, W., Calder, J.A. (Editors) The eastern Bering Sea shelf: oceanography and resources, Vol. II. University of Washington Press, Seattle, WA, p. 1091-1103.

Hagen, W., Van Fleet, E.S., and Kattner, G. 1996. Seasonal lipid storage as overwintering strategy of Antarctic krill. Marine Ecology Progress Series 134:85-89.

Haltuch, M. A. 2008. Modeling Human and Climate Impacts on the Management of the Pacific North West Groundfish Fishery. PhD. dissertation, University of Washington, Seattle, WA, 187p.

Hamazaki, T., Fair, L., Watson, L., and Brennan, E. 2005. Analyses of Bering Sea bottom-trawl surveys in Norton Sound: absence of regime shift effect on epifauna and demersal fish. ICES Journal of Marine Science 62:597–1602.

Hankin, S.C., Davison, J., O'Brien, K., and Harrison, D.E. 1992. FERRET: A computer visualization and analysis tool for gridded data, NOAA Data Report ERL PMEL-38. NOAA Pacific Marine Environmental Laboratory, Seattle, WA, 1-164.

Hankin, S.C., Harrison, D.E., and Davison, J. 1991. FERRET, an interactive data visualization analysis and management system for gridded data sets, NOAA Technical Memorandum ERL PMEL-38. NOAA Pacific Marine Environmental Laboratory, Seattle, WA.

Hare, S.T. 2010. Assessment of the Pacific halibut stock at the end of 2009. Available at: http://www.iphc.washington.edu/papers/sa09.pdf.

Hargens, A.R. 1972. Freezing resistance in polar fishes. Science 176:184–186.

Harvey, H.R., Pleuthner, R, Lessard, E.J., Bernhardt, M., and Shaw, C.T. 2012. The composition of euphausiids in the Bering Sea: physical and biochemical properties of *Thysanoessa inermis*, *Thysanoessa raschii*, and *Thysanoessa longipes* over seasons and years. Deep-Sea Research II 65-70:173–183.

Hastie, T.J., and Tibshirani, R.J. 1990. Generalized Additive Models. Monographs on Statistics and Applied Probability 43. Chapman and Hall, London.

Hatch, S.A. and G.A. Sanger. 1992. Puffins as samplers of juvenile pollock and other forage fish in the Gulf of Alaska. Marine Ecology Progress Series 80:1–14.

Hedges, J., Baldock, J.A., Gelinas, Y., Lee, C., Peterson, M., Wakeham, S.G., 2002. The biochemical and elemental compositions of marine plankton: A NMR perspective. Marine Chemistry 78, 47-63.

Heifitz, J., Murfy, M. and Koski, V. 1986. Effects of logging on winter habitat of juvenile salmonids in Alaskan streams, North American Journal of Fisheries Management 6:52-58.

Hermann, A.J., Gibson, G.A., Bond, N.A., Curchister, E.N., Hedstrom, K., Cheng, W., Wang, M., Cokelet, E.D., Stabeno, P.J., 2014. Projected future biophysical states of the Bering Sea. submitted to Deep Sea Research Part II: Topical Studies in Oceanography.

Hewitt, R.P., and Demer, D.A. 2000. The use of acoustic sampling to estimate the dispersion and abundance of euphausiids, with an emphasis on Antarctic krill, *Euphausia superba*. Fish. Res. 47(2–3):215–229.

Hewitt, R.P., Watkins, J., Naganobu, M., Sushin, V., Brierley, A.S., Demer, D., Kasatkina, S., Takao, Y., Goss, C., Malyshko, A., Brandon, M., Kawaguchi, S., Siegel, V., Trathan, P., Emery, J., Everson, I., and Miller, D., 2004. Biomass of Antarctic krill in the Scotia Sea in January/February 2000 and its use in revising an estimate of precautionary yield. Deep-Sea Research II 51:1215-1236.

Hilborn, R., and Walters, C.J. 1992. Quantitative fisheries stock assessment: Choice, dynamics and uncertainty. Chapman and Hall. 570 p.

Hilborn, R., and Walters, C. J. 1992. Quantitative fisheries stock assessment: choice, dynamics and uncertainty. Reviews in Fish Biology and Fisheries 2(2):177-178.

Hillebrand, H. 2004. On the generality of the latitudinal diversity gradient. American Naturalist 163:192–211.

Hjellvik, V., Michalsen, K., Aglen, A., and Nakken, O. 2003. An attempt at estimating the effective fishing height of the bottom trawl using acoustic survey recordings. ICES Journal of Marine Science 60:967–979.

Holliday, D.V. and Pieper, R.E. 1995. Bioacoustical oceanography at high frequencies. ICES Journal of Marine Science 52:297-304.

Hollowed, A.B., Beamish, R.J., Okey, T.A., and Schirripa, M.J. 2008. Reports of PICES/NPRB workshops on forecasting climate impacts on future production of commercially exploited fish and shellfish. PICES Scientific Report No. 34. North Pacific Marine Science Organization (PICES), P. O. Box 6000 Sidney, British Columbia, Canada V8L 4B2.

Hollowed, A. B., Bond, N.A., Wilderbuer, T.K., Stockhausen, W.T., A'mar, Z.T., Beamish, R.J., Overland, J.E., and Schirripa M.J. 2009. A Framework for modeling fish and shellfish responses to future climate change. ICES Journal of Marine Science 66(7):1584-1594.

Hollowed, A.B., Planque, B. and Loeng, H. 2013. Potential movement of fish and shellfish stocks from the sub-Arctic to the Arctic Ocean. Fisheries Oceanography 22(5): 355-370.

Hollowed, A. B., Wilson, C.D., Stabeno, P.J., and Salo, S.A., 2007. Effect of ocean conditions on cross-shelf distribution of walleye pollock (*Theragra chalcogramma*) and capelin (*Mallotus villosus*). Fisheries Oceanography 16(2):142-154.

Honkalehto, T., Jones, D., McCarthy, A., McKelvey, D. Guttormsen, M., Williams, K. and Williamson, N. 2009. Results of the Echo Integration-Trawl Survey of Walleye Pollock (*Theragra chalcogramma*) on the U.S. and Russian Bering Sea Shelf in June and July 2008. U.S. Department of Commerce, NOAA Technical Memorandum NMFS-AFSC-194, 56 p. http://www.afsc.noaa.gov/Publications/AFSC-TM/NOAA-TM-AFSC-194.pdf.

Honkalehto, T.A., McCarthy, A., Ressler, P., Stienessen, S., Jones, D. 2010. Results of the acoustic-trawl survey of walleye pollock (*Theragra chalcogramma*) on the U.S. and Russian Bering Sea shelf in June - August 2009 (DY0909). AFSC Processed Rep. 2010-03, 57 p. Alaska Fish. Sci. Cent., NOAA, Natl. Mar. Fish. Serv., 7600 Sand Point Way NE, Seattle WA 98115. Available from http://www.afsc.noaa.gov/Publications/ProcRpt/PR2010-03.pdf.

Honkalehto, T., A. McCarthy, P. Ressler, K. Williams, and D. Jones. 2012. Results of the acoustic-trawl survey of walleye pollock (*Theragra chalcogramma*) on the U.S. and Russian Bering Sea shelf in June - August 2010 (DY1006). AFSC Processed Rep. 2012-01, 59 p. Alaska Fish. Sci. Cent., NOAA, Natl. Mar. Fish. Serv., 7600 Sand Point Way NE, Seattle WA 98115. URL: http://www.afsc.noaa.gov/Publications/ProcRpt/PR2012-01.pdf.

Honkalehto, T., Patton, W., de Blois, S., Williamson, N. 2002. Echo integration-trawl survey results for walleye pollock (*Theragra chalcogramma*) on the Bering Sea shelf and slope during summer

1999. U.S. Dep. Commer., NOAA Tech. Memo. NMFS-AFSC-125, 66 p. Available from http://www.afsc.noaa.gov/Publications/AFSC-TM/NOAA-TM-AFSC-125.pdf.

Honkalehto, T., Williamson, N., Jones, D., McCarthy, A., and McKelvey, D. 2009. "Results of the echo integration-trawl survey of walleye pollock (*Theragra chalcogramma*) on the U.S. and Russian Bering Sea shelf in June and July 2008." U. S. Dep. Commer., NOAA Tech. Memo., NMFS-AFSC-194, 56 p. URL: http://www.afsc.noaa.gov/Publications/AFSC-TMNNOAA-TM-AFSC-194.pdf.

Horne, J. K. Acoustic approaches to remote species identification: a review. 2000. Fisheries Oceanography 9:356–371.

Hsieh, C., Glaser, S.M., Lucas, A.J., and Sugihara, G. 2005. Distinguishing random environmental fluctuatios from ecological catastrophes for the North Pacific Ocean. Nature 435: 336-340.

Huff, D., Hubler, S., Borisenko, A. 2005. Using Field Data to Estimate the Realized Thermal Niche of Aquatic Vertebrates, North American Journal of Fisheries Management 25:346-360.

Hunt Jr., G.L., K.O. Coyle, L. Eisner, E.V. Farley, R. Heintz, F. Mueter, J.M. Napp, J.E. Overland, P.H. Ressler, S. Salo, and P.J. Stabeno. 2011. Climate impacts on eastern Bering Sea food webs: A synthesis of new data and an assessment of the Oscillating Control Hypothesis. ICES Journal of Marine Science 68: 1230-1243.

Hunt, G.L., Stabeno, P.J., Strom, S., Napp, J.M. 2008. Patterns of spatial and temporal variation in the marine ecosystem of the southeastern Being Sea, with special reference to the Pribilof Domain. Deep-Sea Research II 55:1919–1944.

Hunt Jr., G.L., Stabeno, P.J., Walters, G., Sinclair, E., Brodeur, R.D., Napp, J.M., and Bond, N.A. 2002. Climate change and control of energy flow in the southeastern Bering Sea. Progress in Oceanography 55: 5–22.

Hunt, G.L. Jr., Stabeno, P., Walters, G., Sinclair, E., Brodeur, R.D. 2002. Climate change and control of the southeastern Bering Sea pelagic ecosystem. Deep-Sea Research II 49:5821–5853.

Hutchinson, G. E. 1953. The concept of pattern in Ecology. Proceedings of the National Academy of Science Philosophy A 105:1-12.

Hutchinson, G. E. 1957. Concluding remarks. Cold Spring Harbor Symp. on Quant. Biol. 22: 415-427.

Hutchinson, W. F. 2008. The dangers of ignoring stock complexity in fishery management: The case of the North Sea cod, Biological Letters 4:693-695.

Ianelli, J.N., Barbeaux, S., Honkalehto, T., Kotwicki, S., Aydin, K., and Williamson, N. 2008. Assessment of the walleye pollock stock in the eastern Bering Sea. *In* Stock assessment and fishery evaluation report for the groundfish resources of the Bering Sea/Aleutian Islands regions. North Pacific Fishery Management Council, Anchorage, AK.

Ianelli, J.N., Barbeaux, S., Honkalehto, T., Kotwicki, S., Aydin, K., and Williamson, N. 2009. Assessment of the walleye pollock stock in the eastern Bering Sea. *In* Stock assessment and fishery evaluation report for the groundfish resources of the Bering Sea/Aleutian Islands regions. North Pacific Fishery Management Council, Anchorage, AK.

Ianelli, J.N., Barbeaux, S., Honkalehto, T., Kotwicki, S., Aydin, K., and Williamson, N. 2010. Assessment of the Walleye Pollock stock in the Eastern Bering Sea. *In* Stock assessment and fishery evaluation report for the groundfish resources of the Bering Sea/Aleutian Islands regions. North Pacific Fishery Management Council, Anchorage, AK.

Ianelli, J. Hollowed, A., Haynie, A., Mueter, F., Bond, N. 2011a. The challenges of developing fisheries stock assessment approaches, harvest control rules, and management strategies to satisfy and adapt to increasingly complex management objectives in a changing environment. *ICES Journal Marine Science* 68(6): 1297-1304.

Ianelli, J.N., Honkalehto, T., Barbeaux, S., Kotwicki, S. Aydin, K, Williamson, N. 2011. Assessment of the walleye pollock stock in the eastern Bering Sea. *In* Stock assessment and fishery evaluation report for the groundfish resources of the Bering Sea/Aleutian Islands regions. North Pacific Fishery Management Council, Anchorage, AK.

Ianelli, J.N., Honkalehto, T., Barbeaux, S., Kotwicki, S., Aydin, K., Williamson, N. 2012. Assessment of the Walleye Pollock stock in the Eastern Bering Sea. *In* Stock assessment and fishery evaluation report for the groundfish resources of the Bering Sea/Aleutian Islands regions. North Pacific Fishery Management Council, Anchorage, AK.

Ianelli, J.N., Buckley, T., Honkalehto, T., Walters, G., and Williamson, N. 2001. Eastern Bering Sea Walleye Pollock Stock Assessment. *In* Stock assessment and fishery evaluation report for the groundfish resources of the Bering Sea/Aleutian Islands regions. North Pacific Fishery Management Council, Anchorage, AK.

ICES. 2008. Report of the Workshop on Cod and Future Climate Change (WKCFCC), 17–20 June 2008, ICES, Copenhagen. ICES CM 2008/OCC:09. 98 pp.

Iida, T. and Saitoh,S.I. 2007. Temporal and spatial variability of chlorophyll concentrations in the Bering Sea using emperical orthogonal function (EOF) analysis of remote sensing data. Deep-Sea Research II. 54:2657-2671.

Iken, K., Konar, B., Benedetti-Cecchi, L., Cruz-Motta, J. J., Knowlton, A. 2010. Large-scale spatial distribution patterns of echinoderms in nearshore rocky habitats. PLoS ONE 5(11), e13845.

Iles, T. D., and Sinclair, M. 1982. Atlantic herring: stock discreteness and abundance. Science 215(4533):627-633.

Ingraham, W. J., Jr., and Miyahara, R. K. 1988. Ocean Surface Current Simulations in the North Pacific Ocean and Bering Sea (OSCURS – Numerical Model). U.S. Department of Commerce, National Oceanic and Atmospheric Administration Technical Memorandum, NMFS F/NWC – 130, 155pp.

IPCC, 2007: Climate Change 2007: Synthesis Report. Contribution of Working Groups I, II and III to the Fourth Assessment Report of the Intergovernmental Panel on Climate Change [Core Writing Team, Pachauri, R.K and Reisinger, A.(Eds.)]. IPCC, Geneva, Switzerland, 104 pp.

Jacobson, L. D., Bograd, S. J., Parrish, R. H., Mendelssohn, R., and Schwing, F. B. 2005. An ecosystem-based hypothesis for climatic effects on surplus production in California sardine (*Sardinops sagax*) and environmentally dependent surplus production models. Canadian Journal of Fisheries and Aquatic Sciences 62: 1782-1796.

Jensen, O.P, Seppelt, R., Miller, T.J., and Bauer, L.J. 2005. Winter distribution of blue crab *Callinectes sapidus* in Chesapeake Bay: application and cross-validation of a two-stage generalized additive model. Marine Ecology Progress Series 299:239–255.

Jewett, S.C., Clough, L.M., Blanchard, A.L., Ambrose, W.G., Feder, H.M., Hoberg, M.K., and Whiting, A.V. 2009. Nearshore macrobenthos of northern Kotzebue Sound, Alaska, with reference to local sewage disposal. Polar Biology 32:1665–1680.

Jewett, S.C., and Feder, H.M. 1981. Epifaunal invertebrates of the continental shelf of the eastern Bering and Chukchi Seas. *In* Hood, W., Calder, J.A. (Editors) The eastern Bering Sea shelf: oceanography and resources, Vol. II. University of Washington Press, Seattle, WA, pp. 1131-–1153.

Jones, B.A., Lavery, A.C., and Stanton, T.K. 2009. Use of the distorted wave Born approximation to predict scattering by inhomogeneous objects: Applications to squid. Journal of the Acoustical Society of America 125:73-88.

Juardo-Molina, J., Livingston, P.A., and Ianelli. J.N. 2005. Incorporating predation interactions in a statistical catch-at-age model for a predator-prey system in the eastern Bering Sea. Canadian Journal of Fisheries and Aquatic Sciences 62:1865-1873.

Kachel, N.B., Hunt Jr., G.L., Salo, S. A., Schumacher, J.D., Stabeno, P.J., and Whitledge, T.E. 2002. Characteristics and variability of the inner front of the southeastern Bering Sea. Deep-sea Research II 49:5889-5909.

Kang, D., Iida, K., Mukai, T. and Hwang, D. 2004. Acoustic target strength of Japanese common squid, *Todarodes pacificus*, and important parameters influencing its TS: swimming angle and material properties. OCEANS '04. MTTS/IEEE TECHNO-OCEAN '04(1):364-369.

Karp, W. A., and Walters, G. E. 1994. Survey assessment of semipelagic gadoids: the example of walleye pollock, *Theragra chalcogramma*, in the eastern Bering Sea. Marine Fisheries Review:56:8–22.

Kasatkina, S.M., Gross, C., Emery, J.H., Takao, Y., Litvinov, F.F., Malyshko, A., Shnar, V.N., and O.A.Berezhinsky. 2004. A comparison of net and acoustic estimates of krill density in the Scotia Sea during the CCAMLR 2000 Survey. Deep-Sea Research II 51:1289-1300.

Kils, U. 1981. The swimming behavior, swimming performance and energy balance of Antarctic krill, Euphausia superba. BIOMASS Science Series No.3.

Kimura, D.K. 1989. Variability, tuning, and simulation for the Doubleday-Deriso catch-at-age model. Canadian Journal of Fisheries and Aquatic Sciences 46:941-949.

Kimura, D. A., and Somerton, D. A. 2006. Review of statistical aspects of survey sampling for marine fisheries. Reviews in Fisheries Science 14:245–283.

Kinder, T.H., and Schumacher, J.D. 1982. Hydrography over the continental shelf of the southeastern Bering Sea, in: Hood, D.W., Calder, J.A. (Eds.), The Eastern Bering Sea Shelf. University of Washington Press, Seattle, 31-52.

Kistler, R., Kalnay, E., Collins, W., Saha, S., White, G., Woollen, J., Chelliah, M., Ebisuzaki, W., Kanamitsu, M., Kousky, V., van den Dool, H., Jenne, R., Fiorino, M. 2001: The NCEP-NCAR

50-year Reanalysis: Monthly means CD-ROM and documentation. Bulletin of the American Meteorological Society 82, 247–267.

Knight, C.A., Cheng, C.C., and DeVries, A.L. 1991. Adsorption of α-helical antifreeze peptides on specific ice crystal surface planes. Biophysical Journal 59:409–418.

Kobari, T., Tadokoro, K., Shiomoto, A., and Hashimoto, S. 2003. Geographical variations in prosome length and body weight of *Neocalanus* copepods in the North Pacific. Journal of Oceanography 59(3):3-10.

Køgeler, J.W., Falk-Petersen, S., Kristensen, Å., Pettersen, F. and Dalen, J. 1987. Density- and sound speed contrasts in sub-Arctic zooplankton. Polar Biology 7:231-235.

Konar, B, Iken K., Cruz-Motta, J.J., Benedetti-Cecchi, L., and Knowlton, A. 2010. Current patterns of macroalgal diversity and biomass in northern hemisphere rocky shores. PLoS ONE 5(10):e13195.

Korneliussen, R. J., Heggelund, Y., Eliassen, I. K., and Johansen, G.O. 2009. Acoustic species identification of schooling fish. ICES Journal of Marine Science 66:1111–1118.

Kotwicki, S. and Lauth R.R. 2013. Detecting temporal trends and environmentally-driven changes in the spatial distribution of bottom fishes and crabs on the eastern Bering Sea shelf. Deep-Sea Research Part II: Topical Studies in Oceanography, 94: 231-243

Koslow, J.A. 1981. Feeding selectivity of schools of northern anchovy, *Engraulis mordax*, in the Southern California Bight. Fishery Bulletin 79 (1):131-142.

Kotwicki S., Buckley T.W., Honkaletho T., and Walters G. 2005. Variation in the distribution of walleye pollock with temperature and implications for seasonal migration. Fishery Bulletin 103:574-587.

Kotwicki, S., De Robertis, A., von Szalay, P., and Towler, R. 2009. The effect of light intensity on the availability of walleye pollock (*Theragra chalcogramma*) to bottom trawl and acoustic surveys. Can J. Fish. Aquat. Sci. 66:983–994.

Kotwicki, S. and Lauth, R.R. 2013. Detecting temporal trends and environmentally-driven changes in the spatial distribution of groundfishes and crabs on the eastern Bering sea shelf. Deep-Sea Research II, http://dx.doi.org/10.1016/j.dsr2.2013.03.017.

Kotwicki, S., and Weinberg, K.L. 2005. Estimating capture probability of a survey bottom trawl for Bering Sea skates (*Bathyraja* spp.) and other fish. Alaska Fisheries Research Bulletin 11:135–145.

Koutsoyiannis, D., Efstratiadis, A., Mamassis, N. and Christofides, A. 2008. On the credibility of climate predictions. Hydrological Sciences–Journal–des Sciences Hydrologiques 53(4): 671-684.

Kristensen, Å., Dalen, J. 1986. Acosutic estimation of size distribution and abundance of zooplankton. Journal of the Acoustical Society of America 80 (2):601-611.

Ladd, C., and Stabeno, P.J. 2012. Stratification on the Eastern Bering Sea shelf revisited. Deep-Sea Research Part II: Topical Studies in Oceanography 65:72-83.

Ladd, C., Stabeno, P.J., and O'Hern, J.E. 2012. Observations of a Pribilof eddy. Deep Sea Research Part I: Oceanographic Research Papers 66:67-76.

Lang, G.M., Brodeur, R.D., Napp, J.M., and Schabetsberger., R. 2000. Variation in groundfish predation on juvenile walleye pollock relative to hydrographic structure near the Pribilof Islands, Alaska. ICES Journal of Marine Science 57:265-271.

Lang, G.M., Livingston, P.A., and K.A. Dodd. 2005. Groundfish food habits and predation on commercially important prey species in the eastern Bering Sea from 1997 through 2001. U.S. Dep. Commer., NOAA Technical Memorandum NMFS-AFSC-158, 230p.

Lauth, R. R. 2006. Report to the fishing industry on the results of the 2005 Eastern Bering Sea groundfish survey. AFSC Processed Rep. 2006-07. Alaska Fisheries Science Center, National Marine Fisheries Service, NOAA, 7600 Sand Point Way NE, Seattle WA 98115. 64 p.

Lauth, R. R. 2010. Results of the 2009 Eastern Bering Sea continental shelf bottom trawl survey of groundfish and invertebrate resources. U.S. Department of Commerce, NOAA Technical Memorandum NMFS-AFSC-204, 228p.

Lauth, R.R. 2011. Results of the 2010 eastern and northern Bering Sea continental shelf bottom trawl survey of groundfish and invertebrate fauna. U.S. Department of Commerce, NOAA Technical Memorandum NMFS-AFSC-227, 256 p.

Lavery, A.C., Stanton, T.K., McGehee, D.E., and D. Chu. 2002. Three-dimensional modeling of acoustic backscattering from fluid-like zooplankton. Journal of the Acoustical Society of America 111(3):1197-1210.

Lawson, G.L., Wiebe, P.H., Ashjian, C.J., Chu, D. and T.K. Stanton. 2006. Improved parameterization of Antarctic krill target strength models. Journal of the Acoustical Society of America 119(1):232-242.

Lawson, G.L., Wiebe, P.H., Stanton, T.K., and Ashjian, C.J. 2008. Euphausiid distribution along the Western Antarctic Peninsula- Part A: Development of robust multi-frequency acoustic techniques to identify euphausiid aggregations and quantify euphausiid size, abundance, and biomass. Deep-Sea Research II 55 (2):412-431.

Lee, K., Mukai, T., Lee, D. and Iida, K. 2008. Verification of mean volume backscattering strength obtained from acoustic Doppler current profiler by using sound scattering layer. Fisheries Science 74:221-229.

Legendre, P. 1993. Spatial Autocorrelation: Trouble or New Paradigm? Ecology 74(6):1659-1673.

Lenor, S., Beaugrand, G., and Lecuyer, Ė. 2011. Modelled spatial distribution of marine fish and projected modifications in the North Atlantic Ocean. Global Change Biology 17:115-129.

Levin, P. S., Fogarty, M. J., Murawski, S. A., and Fluharty, D. 2009. Integrated Ecosystem Assessments: Developing the Scientific Basis for Ecosystem-Based Management of the Ocean. PLoS Biol. 7:23-28.

Levin, S. Grenfell, A.B., Hastings, A., Perelson, A.S. 1997. Mathematical and computational challenges in population biology and ecosystem science. Science 275: 334-343.

Livingston, P.A. 1991. Walleye pollock, Groundfish food habits and predation on commercially important prey species in the eastern Bering Sea, 1984-1986. U.S. Department of Commerce, NOAA Technical Memorandum NMFS-FNNWC-207.

Livingston, P.A., Aydin, A., Boldt, J.L., Hollowed, A.B. and Napp, J.M. 2011. Alaska marine fisheries management: Advances and linkages to ecosystem research, pp. 113 - 152. *In* A. Belgrano and C. W. Fowler (Eds.), Ecosystem-based Management for Marine Fisheries: an Evolving Perspective. Cambridge University Press.

Logerwell, E. A., Stabeno, P.J., Wilson, C.D., and Hollowed, A.B. 2007. The effect of oceanographic variability and interspecific competition on juvenile pollock (*Theragra chalcogramma*) and capelin (*Mallotus villosus*) distributions on the Gulf of Alaska Shelf. Deep Sea Research Part II 54:2849-2868.

Logerwell, E.A., Duffy-Anderson, J., Wilson, M., McKelvey, D. 2010. The influence of pelagic habitat selection and interspecific competition on productivity of juvenile walleye pollock (*Theragra chalcogramma*) and capelin (*Mallotus villosus*) in the Gulf of Alaska. Fisheries Oceanography 19:262-278.

Lomas, M., Moran, S., Casey, J., Bell, D., Tiahlo, M., Whitefield, J., Kelly, R., Mathis, J., and Cokelet, E. 2012. Spatial and seasonal variability of primary production on the Eastern Bering Sea shelf. Deep Sea Research Part II: Topical Studies in Oceanography 65:126-140.

Loots, C., Vaz, S., Planque, B. and Koubbi, P. 2010. What controls the spatial distribution of North Sea plaice spawning population? Confronting ecological hypotheses through a model selection framework. ICES Journal of Marine Science 67:244–257.

Lorenzen, C.J. 1966. A method for the continuous measurement of *in vivo* chlorophyll concentration. Deep Sea Research 13:223-227.

MacCall, A. 1990. Dynamic geography of marine fish populations. University of Washington Press, Seattle, pp.153.

Macklin, S.A., Hunt, Jr. G.L., Editors, 2004. The Southeast Bering Sea Ecosystem: Implications for Marine Resource Management (Final Report: Southeast Bering Sea Carrying Capacity). NOAA Coastal Ocean Program Decision Analysis Series No. 24, Silver Spring, MD 20910, 192 pp.

MacLennan, D.N., Fernandes, P.G., and Dalen, J. 2002. A consistent approach to definitions and symbols in fisheries acoustics. Journal of Marine Science 59:365–369.

Magnuson, J.J. 1991. Fish and fisheries ecology. Ecological Applicatons 1: 13–26.

Magnuson, J.J., Crowder, L.B. and Medvick, P.A. 1979. Temperature as an Ecological Resource, American Zoologist 19: 331-343.

Magnuson, J.J., Meisner, J.D. and Hill, D.K. 1990. Potential Changes in the Thermal Habitat of Great Lakes Fish after Global Climate Warming, Transactions of the American Fisheries Society119: 254-264.

Mangel, M., Talbot, L. M., Meffe, G. K., Agardy, M. T., Alverson, D. L., Barlow, J., Botkin, D. B., Budowski, G., Clark, T., Cooke, J., Crozier, R. H., Dayton, P. K., Elder, D. L., Fowler, C. W., Funtowicz, S., Giske, J., Hofman, R. J., Holt, S. J., Kellert, S. R., Kimball, L. A., Ludwig, D., Magnusson, K., Malayang, B. S., Mann, C., Norse, E. A., Northridge, S. P., Perrin, W. F.,

Perrings, C., Peterman, R. M., Rabb, G. B., Regier, H. A., Reynolds, J. E., Sherman, K., Sissenwine, M. P., Smith, T. D., Starfield, A., Taylor, R. J. Tillman, M. F., Toft, C., Twiss, J. R., Wilen, J., Young, T. P. 1996. Principles for the conservation of wild living resources. Ecological Applications 6(2):338-362.

Mantua, N.J., Hare, S.R., Zhang, Y., Wallace, J.M., and Francis, R.C. 1997. A Pacific interdecadal climate oscillation with impacts on salmon production. Bulletin of the American Meteorological Society 78, 1069-1079.

Matsukura, R., Yasuma, H., Murase, H., Yonezaki, S., Funamoto, T., Honda, S., and Miyashita, K. 2009. Measurements of density contrast and sound-speed contrast for target strength estimation of *Neocalanus* copepods (*Neocalanus cristatus* and *Neocalanus plumchrus*) in the North Pacific Ocean. Fisheries Science 75:1377 – 1387.

Mauchline, J. 1980. The biology of euphausiids. *In* Blaxter, J.H.S., Russell, F.S., Yonge, M., (Eds.), Advances in Marine Biology, Vol. 18. Academic Press, London, England, pp. 373-554.

Maunder, M.N., and Watters, G.M. 2003. A general framework for integrating environmental time series into stock assessment models: model description, simulation testing, and example. Fishery Bulletin 101: 89–99.

McConnaughey, R.L. 1995. Changes in geographic dispersion of eastern Bering Sea flatfish associated with changes in population size. *In* Baxter, B.R. (Ed.), Proceedings of the International Symposium on North Pacific Flatfish. Fairbanks: Alaska Sea Grant Report No. 95-04, pp. 385–405.

McGehee, D.E., O'Driscoll, R.L., Martin Traykovski, L.V. 1998. Effects of orientation on acoustic scattering from Antarctic krill at 120 kHz. Deep-Sea Research II 45 (3):1273-1294.

McLachlan, G. J. 1992. Discriminant analysis and statistical pattern recognition. Wiley, New York.

McRoy, C.P., Hood, D.W., Coachman, L.K., Walsh, J.J., and Goering, J.J. 1986. Processes and resources of the Bering Sea shelf (PROBES): The development and accomplishments of the project. Continental Shelf Research 5: 5–22.

Medwin, H. and C.S. Clay. 1998. Fundamentals of Acoustical Oceanography. Academic Press, San Diego, California.

Methot, R.D. 1986. Frame trawl for sampling pelagic juvenile fish. California Cooperative Oceanic Fisheries Investigations Reports 27:267-278.

Methot, R. D. 2005. User Manual for the Assessment Program Stock Synthesis 2 (SS2), Model Version 1.18. April 8, 2005. Northwest Fisheries Science Center, Seattle, WA USA.

Michalsen, K., Godø, O. R., and Fernö, A. 1996. Diel variation in the catchability of gadoids and its influence on the reliability of abundance indices. ICES Journal of Marine Science 53(2):389-395.

Miller, D.J. and Browning, J. 2003. A mixture model and EM-based algorithm for class discovery, robust classification, and outlier rejection in mixed labeled/unlabeled data sets. IEEE Transactions on Pattern Analysis and Machine Learning 25:1468–1483.

Miyashita, K. 2003. Diurnal changes in the acoustic-frequency characteristics of Japanese anchovy (*Eugraulis japonicus*) post-larvae "shirasu" inferred from theoretical scattering models. ICES Journal of Marine Science 60:532-537.

Mizobata, K., Saitoh, S., Shiomoto, A., Miyamura, T., Shiga, N., Imai, K., Toratani, M., Kajiwara, Y., and Sasaoka, K. 2002. Bering Sea cyclonic and anticyclonic eddies observed during summer 2000 and 2001. Progress in Oceanography 55:65-75.

Mizobata, K., Saitoh, S., and Wang, J. 2008. Interannual variability of summer biochemical enhancement in relation to mesoscale eddies at the shelf break in the vicinity of the Pribilof Islands, Bering Sea. Deep Sea Research Part II: Topical Studies in Oceanography 55:1717-1728.

Morse, P.M. and K.U. Ingard. 1968. Theoretical Acoustics. Princeton University Press, Princeton, NJ.

Moss, J. H., Farley, Jr., E.V., Feldman, A.M., and Ianelli, J.N. 2009. Spatial distribution, energetic status and food habits of eastern Bering Sea age-0 walleye pollock. Transactions of the American Fisheries Society 138:497-505.

Mountain, D.G., Murawski, S.A. 1992. Variation in the distribution of fish stocks on the northeast continental shelf in relation to their environment, 1980 –1989. ICES Marine Science Symposia 195:424−432.

Mueter, F., Bond, N., Ianelli, J., and Hollowed, A. 2011. Expected declines in recruitment of walleye pollock (*Theragra chalcogramma*) in the eastern Bering Sea under future climate change. ICES Journal of Marine Science, 68(6): 1297-1304.

Mueter, F.J., and Litzow, M.A. 2008. Sea ice retreat alters the biogeography of the Bering Sea continental shelf. Ecological Applications 18(2):309–320.

Mullin, M.M., and Conversi, A. 1988. Biomasses of euphausiids and smaller zooplankton in the California Current - Geographic and interannual comparisons relative to the Pacific whiting, *Merluccius productus*, fishery. Fishery Bulletin 87:633-644.

Mundy, P.R., and Hollowed, A.B. 2005. Fish and Shellfish. Pp. 79-95. In Phillip R. Mundy (Editors) The Gulf of Alaska: Biology and Oceanography. Alaska Sea Grant College Program, University of Alaska, Fairbanks, 213 p.

Munro, P.T. 1998. A decision rule based on the mean square error for correcting fishing power differences in trawl survey data. Fishery Bulletin 96:538-546.

Murase, H., Nagashima, H., Yonezaki, S., Matsukura, R. and Kitakado, T. 2009. Application of a generalized additive model (GAM) to reveal relationships between environmental factors and distributions of pelagic fish and krill: a case study in Sendai Bay, Japan, ICES Journal of Marine Science 66:1417-1424.

Myers, R.A. 1998. When do environment-recruitment correlations work? Reviews in Fish Biology and Fisheries 8: 285–305.

Myers, R. A., and Stokes, K. 1989. Density-dependent habitat utilization of groundfish and the improvement of research surveys. ICES CM, 500, 15.

Napp, J.M., Baier, C.T., Brodeur, R.D., Coyle, K.O., Shiga, N., and Mier, K., 2002. Interannual and decadal variability in zooplankton communities of the southeast Bering Sea shelf. Deep-Sea Research II 49:5991–6008.

National Marine Fisheries Service (NMFS), 2010. Fisheries of the United States, 2009. Fisheries Statistics Division, National Marine Fisheries Service, NOAA, 1315 East-West Highway, Silver Spring, MD 20910-3282 Available from http://www.st.nmfs.noaa.gov/st1/fus/fus09/fus_2009.pdf.

National Marine Fisheries Service (NMFS), 2012. Fisheries of the United States, 2011, 124 p. Fisheries Statistics Division, National Marine Fisheries Service, NOAA,1315 East-West Highway, Silver Spring, MD 20910-3282.

National Research Council (NRC). 2003. Decline of the Steller Sea Lion in Alaskan Waters: Untangling Food Webs and Fishing Nets. The National Academies Press.Washington D.C.

Nichol, D.G., 1998. Annual and between-sex variability of yellowfin sole, Pleuronectes asper, spring-summer distributions in the eastern Bering Sea. Fishery Bulletin 96:547-561.

Nigam, K., McCallum, A., Thrun, S., and Mitchell, T. 2000. Text Classification from Labeled and Unlabeled Documents using EM. Machine Learning 39:103-134.

Nøttestad, L., Giske, J., Holst, J.C., and Huse, G., 1999. A length-based hypothesis for feeding migrations in pelagic fish. Canadian Journal of Fisheries and Aquatic Sciences 56(Suppl):26-34.

Nye, J.A., Link, J.S., Hare, J.A., and Overholtz, W.J., 2009. Changing spatial distribution of fish stocks in relation to climate and population size on the Northeast United States continental shelf. Marine Ecology Progress Series 393:111-129.

Okkonen, S.R. 2001. Altimeter observations of the Bering Slope Current eddy field. Journal of Geophysical Research: Oceans (1978–2012) 106:2465-2476.

Olla, B. L., and Davis. M.W. 1990. Effects of physical factors on the vertical distribution of larval walleye pollock Theragra chalcogramma under controlled laboratory conditions. Marine Ecology Progress Series 63:105-112.

Olla, B. L., Davis, M.W., Ryer, C.H., and Sogard, S.M. 1996. Behavioral determinants of distribution and survival in early stages of walleye pollock, *Theragra chalcogramma*: a synthesis of experimental studies. Fisheries Oceanography 5(Suppl. 1):167-178.

Ona, E., and Mitson, R.B. 1996. Acoustic sampling and signal processing near the seabed: the dead zone revisited. ICES Journal of Marine Science 53:677–690.

Osuga, D.T., and Feeney, R.E. 1978. Antifreeze glycoproteins from Arctic fish. Journal of Biological Chemistry 253:5338–5343.

Overland, J.E., Alheit, J., Bakun, A., Hurrell, J.W., Mackas, D.L., and Miller, A.J. 2010. Climate controls on marine ecosystems and fish populations. Journal of Marine Systems 79:305-315.

Overland, J.E., and Stabeno, P.J. 2004. Is the climate of the Bering Sea warming and affecting the ecosystem? EOS Transactions American Geophysical Union 85:309–312.

Overland, J.E., and Wang, M. 2007. Future climate of the North Pacific Ocean. EOS Transactions American Geophysical Union 88: 178-182.

Overland, J.E., Wang, M., Wood, K.R., Percival, D.B., and Bond, N.A. 2012. Recent Bering Sea warm and cold events in a 95-year context. Deep-Sea Research II 65–70:6–13.

Palevsky, H.I., Ribalet, F., Swalwell, J.E., Cosca, C.E., Cokelet, E.D., Feely, R.A., Virginia Armbrust, E., and Quay, P.D. 2013. The influence of net community production and phytoplankton community structure on CO2 uptake in the Gulf of Alaska. Global Biogeochemical Cycles.

Parker-Stetter, S.L., Horne, J.K., Farley, E.V., Barbee, D.H., Andrews III, A.G., Eisner, L.B., Nomura, J.M. In Press. Summer distributions of forage fish in the eastern Bering Sea. Deep-Sea Research II.

Patel, R., Pedersen, G., and Ona, E. 2009. Inferring the acoustic dead-zone volume by split-beam echo sounder with narrow-beam transducer on a noninertial platform. The Journal of the Acoustical Society of America 125:698-705.

Pelletier, D., and Mahévas, S. 2005. Spatially explicit fisheries simulation models for policy evaluation. Fish and Fisheries 6: 307-349.

Perry, A.L., Low, P. J., Ellis, J.R., and Reynolds, J.D. 2005. Climate change and distribution shifts in marine fishes. Science 308(5730):1912-1915.

Peterman, R.M., Pyper, B.J., and Grout, J.A. 2000. Comparison of parameter estimation methods for detecting climate-induced changes in productivity of Pacific salmon (*Oncorhyncus* spp.). Canadian Journal of Fisheries and Aquatic Sciences 57: 181-191.

Peterson, W.T., and Schwing, F.B. 2003. A new climate regime in northeast Pacific ecosystems. Geophysical Research Letters 30(17): 1896.

Petitgas, P., 1993. Geostatistics for fish stock assessments: a review and an acoustic application. ICES Journal of Marine Science 50:285-298.

Petitgas, P. 1998. Biomass-dependent dynamics of fish spatial distributions characterized by geostatistical aggregation curves. ICES Journal of Marine Science 55(3):443-453.

Pianka, E.R. 1966. Latitudinal gradients in species diversity: a review of concepts. American Naturalist 100:33–46.

Piatt, J.F., Wetzel, J., Bell, K., DeGange, A.R., Balogh, G.R., Drew, G.S., Greernaert, T., Ladd, C., and Byrd, G.V. 2006. Predictable hotspots and foraging habitat of the endangered short-tailed albatross (*Phoebastria albatrus*) in the North Pacific: implications for conservation. Deep-Sea Research II 53:387-398.

Pinchuk, A. I. and K. O. Coyle. 2008. Distribution, egg production and growth of euphausiids in the vicinity of the Pribilof Islands, southeastern Bering Sea, August 2004. Deep-Sea Research 55:1792-1800.

Pinchuk, A. I. and R. R. Hopcroft. 2006. Egg production and early development of *Thysanoessa inermis* and *Euphausia pacifica* (Crustacea: Euphausiacea) in the northern Gulf of Alaska. Journal of Experimental Marine Biology and Ecology 332(1):206-215.

Pinnegar, J.K., T.P. Hutton, and Placenti, V. 2006. What relative seafood prices can tell us about the status of stocks. Fish and Fisheries 7: 219-226.

Planque, B., C. Loots, P. Petitgas, U. Linstrøm, S. Vaz. 2011. Understanding what controls the spatial distribution of fish populations using a multi-model approach. Fisheries Oceanography 20(1):1-17.

Pohle, G., Iken, K., Clarke, K.R., Trott, T., and Konar, B. 2011. Aspects of benthic decapod diversity and distribution from rocky nearshore habitat at geographically widely dispersed sites. PLoS ONE 6(4): e18606.

Power, M. 1993. The predictive validation of ecological and environmental models. Ecological Modeling 68: 33–50.

Press, W.H., Flannery, B.P., Teukolsky, S.A., and Vetterling, W.T. 1986. Numerical recipes: the art of scientific computing. Cambridge University Press, New York.

Punt, A.E. 2003. Evaluating the efficacy of managing West Coast groundfish resources through simulations. Fishery Bulletin 101: 860-873.

Pyper, B.J., and Peterman, R.M. 1998. Comparison of methods to account for autocorrelation in correlation analyses of fish data. Canadian Journal of Fisheries and Aquatic Sciences 55:2127-2140.

Racine, J. 2000. Consistent cross-validatory model-selection for dependent data: hv-block cross-validation. Journal of Econometrics 99: 39-61.

Raftery, A.E., Gneiting, T., Balabdaoui, F., and Polakowski, M. 2005. Using Bayesian model averaging to calibrate forecast ensembles. Monthly Weather Review 133: 1155–1174.

Redfield, A.C. 1934. On the proportions of organic derivations in sea water and their relation to the composition of plankton, in: Daniel, R.J. (Editors), James Johnstone Memorial Volume. University Press of Liverpool, Liverpool, England, 177-192.

Redfield, A.C., Ketchum, B.H., and Richards, F.A. 1963. The influence of organisms on the composition of seawater, in: Hill, M.N. (Editors), The Sea. Interscience, New York, 26-77.

Reichler, T. and Kim, J. 2008. How well do coupled models simulate today's climate? Bulletin of the American Meteorological Society 89, 303-311.

Reid, P.C., Battle, E.J.V., Batten, S.D., Brander, K.M. 2000. Impacts of fisheries on plankton community structure. ICES Journal of Marine Science 57:495-502.

Reiss, C.S., Cossio, A.M., Loeb, V. and D.A. Demer. 2008. Variations in the biomass of Antarctic krill (*Euphausia superba*) around the South Shetland Islands, 1996-2006. ICES Journal of Marine Science 65(4):497-508.

Ressler, P.H., Brodeur, R.D., Peterson, W.T., Pierce, S.D., Vance, P.M., Røstad, A., Barth, J.A. 2005. The spatial distribution of euphausiid aggregations in the Northern California Current during August 2000. Deep-Sea Research II 52:89-108.

Ressler, P.H., De Robertis, A., Warren, J.D., Smith, J.N., and Kotwicki, S. 2012. Developing an acoustic index of euphausiid abundance to understand trophic interactions in the Bering Sea ecosystem. Deep-Sea Research II 65-70:184-195.

Ressler, P.H., Holmes, J.A., Fleischer, G.W., Thomas, R.E., Cooke, K.D. 2007. A timely review of Pacific hake (*Merluccius productus*) autecology. Marine Fisheries Review 69(1-4):1-24.

Rew, R., Davis, G., Emmerson, S.,and Davies, H. 2009. NetCDF user's guide for C, an interface for data access, version 3 April 1997. Unidata, Boulder, CO.

Richards, F. 1965. Anoxic basins and fjords, in: Riley, J.P., Skirrow, G. (Editors), Chemical Oceanography. Academic Press, London, 611-645.

Righton, D, Andersen, K., Neat, F., Thorsteinsson, V., Steingrund, P., Svedäng, H., K. Michalsen, K., Hinrichsen, H., Bendall, V., Neuenfeldt, S., Wright, P., Jonsson, P., Huse, G., van der Kooij, J.,

Mosegaard, H., Hüssy, K. and Metcalfe, J. 2010. Thermal niche of Atlantic cod Gadus morhua: limits, tolerance and optima, Marine Ecology Progress Series 420: 1-13.

Rijnsdorp, A. D., Peck, M. A., Englehard, G. H., Möllmann, C., Pinnegar, J. K. 2009. Resolving the effect of climate change on fish populations. ICES Journal of Marine Science 66:1570-1583.

Rivoirard, J., K. Simmonds, P. Foote, and N. Bez. 2000. Geostatistics for Estimating Fish Abundance. Iowa State Press (Blackwell), 206 p.

Robinson, C.L.K. 2000. The consumption of euphausiids by the pelagic fish community off southwestern Vancouver Island, B.C. Journal of Plankton Research 22 (9):1649-1662.

Rohde, K. 1992. Latitudinal gradients in species diversity: the search for the primary cause. Oikos 65:514–527.

Rose, C.S., and Nunnallee, E.P. 1998. A study in changes in groundfish trawl catching efficiency due to differences in operating width, and measures to reduce width variation. Fisheries Research 36:139–147.

Rose, K.A., Megrey, B.A., Hay, D., Werner, F., and Schweigert, J. 2006. Climate regime effects on Pacific herring growth using coupled nutrient-phytoplankton-zooplankton and bioenergetics models. Transactions of the American Fisheries Society 137: 278-297.

Rosenzweig, M.L., and Sandlin, E.A. 1997. Species diversity and latitudes: listening to area's signal. Oikos 80:172–176.

Rothschild, B. J. 2000. Fish stocks and recruitment: the past thirty years. ICES Journal of Marine Science 57: 191–201.

Roy, K., Jablonski, D., and Valentine, J.W. 2000. Dissecting latitudinal diversity gradients: functional groups and clades of marine bivalves. Proceedings of the Royal Society of London B 267:293–299.

Roy, K., Jablonski, D., Valentine, J.W., and Rosenberg, G. 1998. Marine latitudinal diversity gradients: tests of causal hypotheses. Proceedings of the National Academy of Sciences 95:3699–3702.

Royer, T., and Dagg, M. (Eds.). 2002. Ecology of the Southeastern Bering Sea. Deep Sea Research Part II 49(26): 5809.

Ruddick, B. 1983. A practical indicator of the stability of the water column to double-diffusive activity. Deep-sea research. Part A. Oceanographic Research Papers 30:1105-1107.

Ryan, T.E., and Kloser, R.J. 2004. Improving the precision of ES60 and EK60 echosounder applications. Report of the Working Group on Fisheries Acoustic Science and Technology (WGFAST), 20-23 April 2004, Gydnia, Poland. ICES CM2004/B:06.

Sameoto, D, 1980. Quantitative measurements of euphausiids using a 120-kHz sounder and their *in situ* orientation. Canadian Journal of Fisheries and Aquatic Sciences 50:334-346.

Sameoto, D., Cochrane, N., Herman, A. 1993. Convergence of acoustic, optical, and net-catch estimates of euphausiid abundance: Use of artificial light to reduce net avoidance. Canadian Journal of Fisheries and Aquatic Sciences 50:334-346.

Schabetsberger, R., Brodeur, R.D., Ciannelli, L., Napp, J.M. and Swartzman, G.L. 2000. Diel vertical migration and interaction of zooplankton and juvenile walleye pollock (*Theragra chaIcogramma*) at a frontal region near the Pribilof Islands, Bering Sea. ICES Journal of Marine Science 57(4):1283-1295.

Schirripa, M. J., Goodyear, C. P., and Methot, R. M. 2009. Testing two methods of incorporating climate data into the assessment of U.S. West Coast sablefish. ICES Journal of Marine Science 66:1605-1613.

Scheffer, M., and S. Carpenter. 2003. Catastrophic regime shifts in ecosystems: linking theory to observation. Trends in Ecology and Evolution 18(12): 648-656.

Schnute, J.T., Maunder, M.N., and Ianelli, J.N. 2007. Designing tools to evaluate fishery management strategies: can the scientific community deliver? ICES Journal of Marine Science 64: 1077-1084.

Schumacher, J.D., Kinder, T.H., Pashinski, D.J., Charnell, R.L., 1979. A structural front over the continental shelf of the eastern Bering Sea. J. Phys. Oceanogr. 9, 79-87.

Shao, J. 1993. Model selection by cross-validation. Journal of American Statistical Association 88: 486-494.

Shaw, T.L., Feinberg, L., Peterson, W.T. 2006. Protocols for measuring molting rate and egg production of live euphausiids. Available from http://www.pices.int/projects/Euphasiid/PICES%20Protocols%20COMPLETE.pdf.

Sigler, M., Kuletz, K., Ressler, R., Friday, N., Wilson, C., Zerbini, A. 2012. Marine predators and persistent prey in the southeast Bering Sea. Deep Sea Research II 65-70:292-303.

Sigler, M.F., Renner, M., Danielson, S.L., Eisner, L.B., Lauth, R.R., Kuletz, K.J., Logerwell, E.A., Hunt Jr., G.L. 2011. Fluxes, fins, and feathers: Relationships among the Bering, Chukchi, and Beaufort Seas in a time of climate change. Oceanography 24(3):250–265.

Simard, Y., Lavoie, D. 1999. The rich krill aggregation of the Saguenay - St. Lawrence Marine Park: hydroacoustic and geostatistical biomass estimates, structure, variability, and significance for whales. Canadian Journal of Fisheries and Aquatic Sciences 56:1182-1197.

Simmonds, J., and MacLennan, D. 2005. Fisheries Acoustics: Theory and Practice. 2nd ed. Blackwell Science Ltd., Oxford, UK, 437 p.

Simpson, J.H., 1981. The Shelf-Sea Fronts: Implications of their Existence and Behaviour. Philosophical Transactions of the Royal Society of London. Series A, Mathematical and Physical Sciences 302:531-543.

Sinclair, E. 1994. Prey selection by northern fur seals (*Callorhinus ursinus*) in the eastern Bering Sea," Fishery Bulletin 92(1):144-156. Smart, T.I., Duffy-Anderson, J.T., Horne, J.K., Farley, E.V., Wilson, C.D. and Napp, J.M.. 2012. Influence of environment on walleye pollock eggs, larvae, and juveniles in the Southeastern Bering Sea. Deep Sea Research II 65-70:196-207.

Smart, T.I., Duffy-Anderson, J.T., Horne, J.K., Farley, E.V., Wilson, C.D. and Napp, J.M.. 2012. Influence of environment on walleye pollock eggs, larvae, and juveniles in the Southeastern Bering Sea. Deep Sea Research II 65-70:196-207.

Smith, D.M., Cusack, S., Colman, A.W., Folland, C.K., Harris, G.R., Murphy, J.M. 2007. Improved sea temperature prediction for the coming decade from a global climate model. Science 317: 796-799.

Smith, G.B. 1981. The biology of walleye pollock. *In* D.W. Hood and J.A. Calder (eds.), The eastern Bering Sea shelf: Oceanography and Resources, Vol. 1, Univ. of Wash. Press, Seattle, WA, pp. 527-551.

Smith, J.N. 2010. Physical characteristics of Bering Sea zooplankton and their use to parameterize an acoustic scattering model for euphausiids. M.S. Thesis, School of Marine and Atmospheric Sciences, Stony Brook University, Stony Brook, NY, 96 p.

Smith, J.N., Ressler, P.H., and Warren, J.D. 2010. Material properties of euphausiids and other zooplankton from the Bering Sea. Journal of the Acoustical Society of America, 128(5):2664-2680.

Smith, J.N., Ressler, P.H., and Warren, J.D. 2013. A distorted wave Born approximation target strength model for Bering Sea euphausiids. ICES Journal of Marine Science 70:204-214.

Smith, K.R., and McConnaughey, R.A. 1999. Surficial sediments of the eastern Bering Sea continental shelf: EBSSED database documentation. U.S. Dep. Commer., NOAA. Tech. Memo NMFS-AFSC-104, 41 pp.

Smith, S.L. 1991. Growth, development and distribution of the euphausiids *Thysanoessa raschii* (M. Sars) and *Thysanoessa inermis* (Krøyer) in the southeastern Bering Sea. Polar Research 10 (1):461–478.

Smith, R.L., Tebaldi, C., Nychka, D., and Mearns, L.O. 2009. Bayesian modeling of uncertainty in ensembles of climate models. Journal of the American Statistical Assocation 104(485):97-116.

Sohn, D., Ciannelli, L., and Duffy-Anderson, J.T. 2010. Distribution and drift pathways of Greenland halibut (*Reinhardtius hippoglossoides*) during early life stages in the eastern Bering Sea and Aleutian Islands. Fisheries Oceanography 19(5):339-353.

Somerton, D.A., Munro, P.T., and Weinberg, K.L. 2007. Whole-gear efficiency of a benthic survey trawl for flatfish. Fishery Bulletin 105:278–291.

Somerton, D.A., and Otto, R.S. 1999. New efficiency of a survey trawl for snow crab, Chionoecetes opilio, and Tanner crab, C. bairdi. Fishery Bulletin 97:617–625.

Spencer, P.D. 2008. Density-independent and density-dependent factors affecting temporal changes in spatial distributions of eastern Bering Sea flatfish. Fisheries Oceanography 17(5):396-410.

Springer, A.M. 1992. A review: Walleye pollock in the North Pacific - how much difference do they really make? Fisheries Oceanography 1(1):80-96.

Springer, A. M., McRoy, C. P., and Turco, K. R. 1989. The paradox of pelagic food webs in the northern Bering Sea – II. Zooplankton communities. Continental Shelf Research 9(4):359-386.

Springer, A.M., McRoy, C.P., and Flint, M. 1996. The Bering Sea green belt: shelf-edge processes and ecosystem production. Fisheries Oceanography(5): 205–223.

Springer, A.M., and Roseneau, D.G. 1985. Copepod-based food webs: auklets and oceanography in the Bering Sea. Marine Ecology Progress Series 21:229-237.

Stabeno, P. J., Bond, N. A., and Salo, S.A. 2007. On the recent warming of the southeastern Bering Sea shelf. Deep Sea Research Part II: Topical Studies in Oceanography 54(23–26):2599-2618.

Stabeno, P.J., Farley, E., Kachel, N., Moore, S., Mordy, C.W., Napp, J.M., Overland, J.E., Pinchuk, A.I., Sigler, M.F. 2012a. A comparison of the physics of the northern and southern shelves of the eastern Bering Sea shelf and some implications for the ecosystem. Deep-Sea Research II 65-70, 14-30.

Stabeno, P.J., Kachel, N.B., Moore, S.E., Napp, J.M., Sigler, M., Yamaguchi, A., Zerbini, A.N., 2012. Comparison of warm and cold years on the southeastern Bering Sea shelf and some implications for the ecosystem. Deep-Sea Research II 65-70:31–45.

Stabeno, P.J., Napp, J., Mordy, C., Whitledge, T., 2010. Factors influencing physical structure and lower trophic levels of the eastern Bering Sea shelf in 2005: Sea ice, tides and winds. Progress in Oceanography, 85(3–4), 180–196.

Stabeno, P.J., Schumacher, J.D., Ohtani, K., 1999. The physical oceanography of the Bering Sea. Pp.1-28. In Dynamics of The Bering Sea, T.R. Loughlin, and K. Ohtani (eds.), Alaska Sea Grant, AK-SG-99-03, Fairbanks, AK, 1–28.

Stanton, T.K. 1988a. Sound scattering by cylinders of finite length I:Fluid cylinders. Journal of the Acoustical Society of America, 83:55-63.

Stanton, T.K. 1988b. Sound scattering by cylinders of finite length II. Elastic cylinders. Journal of the Acoustical Society of America, 83:64-67.

Stanton, T.K. 1989. Sound scattering by cylinders of finite length III: Deformed cylinders. Journal of the Acoustical Society of America, 86:691-705.

Stanton, T.K., and Chu, D. 2000. Review and recommendations for the modeling of acoustic scattering by fluid-like elongated zooplankton: euphausiids and copepods. ICES Journal of Marine Science 57:793-807.

Stanton, T.K., Chu, D, and Wiebe, P.H. 1998b. Sound scattering by several zooplankton groups. II. Scattering models. Journal of the Acoustical Society of America 103(1):236-253.

Stanton, T.K., Chu, D., Wiebe, P.H., and Clay, C.S. 1993a. Average echoes from randomly oriented random-length finite cylinders: Zooplankton models. Journal of the Acoustical Society of America, 96(4):3463-3472.

Stanton, T.K., Chu, D., and Wiebe, P.H. 1996. Acoustic scattering characteristics of several zooplankton groups. ICES Journal of Marine Science 53:289-295.

Stanton, T.K., Clay, C.S., and Chu, D. 1993b. Ray representation of sound scattering by weakly scattering deformed fluid cylinders: Simple physics and application to zooplankton. Journal of the Acoustical Society of America 94(6):3454-3462.

Stanton, T.K., Weibe, P.H., Chu, D., Benfield, M.C., Scanlon, L., Martin, L.V. and Eastwood, R.L. 1994. On acoustic estimates of biomass. ICES Journal of Marine Science 51:505-512.

Stanton, T.K., Wiebe, P.H., and Chu, D. 1998a. Differences between sound scattering by weakly scattering spheres and finite-length cylinders with applications to sound scattering by zooplankton. Journal of the Acoustical Society of America 103(1):254-264.

Stauffer, G. 2004. NOAA protocols for groundfish bottom trawl sur-veys of the Nation's fishery resources. U.S. Department Comerce NOAA Technical Memorandum NMFS-F/SPO-65, 205 p.

Steele, J.H. 2009. Assessment of some linear food web methods. Journal of Marine Systems,76(1-2):186-194.

Stephens, M.A. 1986. Tests based on EDF statistics. In: D'Agostino, R.B. and Stephens, M.A., eds.: Goodness-of-Fit Techniques. Marcel Dekker, New York.

Stevenson, D.E., and Hoff, G.R. 2009. Species identification confidence in the eastern Bering Sea shelf survey (1982–2008). AFSC Processed Report 2009-04, 46 pp. Alaska Fish. Sci. Cent., NOAA, National Marine Fisheries Service, Sand Point Way NE, Seattle WA 98115.

Stevick, P.T., Incze, L.S., Kraus, S.D., Rosen, S., Wolff, N., and Baukus, A. 2008. Trophic relationships and oceanography on and around a small offshore bank. Marine Ecology Progress Series 363:15-28.

Stockwell, D.A., Whitledge, T.E., Zeeman, S.I., Coyle, K.O., Napp, J.M., Brodeur, R.D., Pinchuk, A.I., and Hunt, G.L. 2001. Anomalous conditions in the south-eastern Bering Sea, 1997: nutrients, phytoplankton and zooplankton. Fisheries Oceanography 10 (1):99-116.

Stoker, S. 1981. Benthic invertebrate macrofauna of the eastern Bering/Chukchi continental shelf, *In* Hood, W., Calder, J.A. (Editors), The eastern Bering Sea shelf: oceanography and resources, Vol. II. University of Washington Press, Seattle, WA, p. 1069-1090.

Stone, C. 1985. Additive regression and other nonparametric models. Annals of Statistics 13: 689-705.

Stow, C.A., Jolliff, J., McGillicuddy D.J. Jr., Doney, S. C., Allen, J.I., Friedrichs, M.A.M., Rose, K.A., and Wallhead, P. 2009. Skill assessment for coupled biological/physical models of marine systems. Journal of Marine Systems 76(1-2): 4-15.

Strickland, J.D., and Parsons, T.R. 1968. A practical handbook of seawater analysis. Fisheries Research Board of Canada Ottawa.

Sugihara G. 1994. Nonlinear forecasting for the classification of nature time series. Philosophical Transactions of the Royal Society of London Series A 348: 477-495.

Sugihara G. and May R. 1990. Nonlinear forecasting as a way of distinguishing chaos from measurement error in a data series. Nature 344: 734-741.

Sund, O. 1935. Echo sounding in fishery research. Nature 135:953.

Sundby, S., Nakken, O. 2008. Spatial shifts in spawning habitats of Arcto-Norwegian cod related to multidecadal climate oscillations and climate change. ICES Journal of Marine Science 65:953-963.

Swain, D.P. 1999. Changes in the distribution of Atlantic cod (*Gadus morhua*) in the southern Gulf of St. Lawrence-effects of environmental change or change in environmental preferences? Fisheries Oceanography 8:1–17.

Swain, D.P., Benoit, H.P. 2006. Change in habitat associations and geographic distribution of thorny skate (*Amblyraja radiata*) in the southern Gulf of St Lawrence: density-dependent habitat selection or response to environmental change? Fisheries Oceanography 2:166-182.

Swain, D.P., Wade, E.J. 1993. Density-dependent geographic distribution of Atlantic cod (*Gadus morhua*) in the southern Gulf of St. Lawrence. Canadian Journal of Fisheries and Aquatic Sciences 50:715-733.

Swartzman, G., Huang, C., Kaluzny, S., 1992. Spatial analysis of Bering Sea groundfish survey data using generalized additive models. Canadian Journal of Fisheries and Aquatic Sciences 49(7):1366-1378.

Swartzman, G., Napp, J., Brodeur, R., Winter, A., and Ciannelli, L. 2002. Spatial patterns of pollock and zooplankton distribution in the Pribilof Islands, Alaska nursery area and their relationship to pollock recruitment. ICES Journal of Marine Science 59:1167-1186.

Swartzman, G., Silverman, E. and Williamson, N. 1995. Relating trends in walleye pollock (Theragra chalcogramma) abundance in the Bering Sea to environmental factors. Canadian Journal of Fisheries and Aquatic Science 52: 369-380.

Swartzman, G., Stuetzle, W., Kulman, K., and Wen, N. 1994. Modeling the distribution of fish schools in the Bering Sea: morphological school identification. Natural Resource Modeling 8:177-194.

Swartzman, G., Winter, A., Coyle, K., Brodeur, R., Buckley, T., Ciannelli, L., Hunt, Jr., G., Ianelli, J., and Macklin, A. 2005. Relationship of age-0 pollock abundance around the Pribilof Islands, to other shelf regions of the eastern Bering Sea. Fisheries Research 74:273-287.

Taylor, J.R. 1982. An introduction to error analysis: The study of uncertainties in physical measurements. University Science Books, Mill Valley, CA. pp. 52-74.

Tebaldi, C., Smith, R.L , Nychka, D. and Mearns, L.O. 2005. Quantifying uncertainty in projections of regional climate change: A Bayesian approach to the analysis of multi-model ensembles. Journal of Climate 18:1524-1540.

Teledyne RD Instruments. 2009. Citadel CTD-NV Technical Specifications MM-1032, Rev. 10/10.

Theil, H. 1966. Applied Economic Forecasting. Rand McNally. Chicago, Il.

Traynor, J. J., 1986. Midwater abundance of walleye pollock in the eastern Bering Sea, 1979 and 1982. International North Pacific Fisheries Commission Bulletin 45:121-135.

Traynor, J.J., 1996. Target strength measurements of walleye pollock (Theragra chalcogramma) and Pacific hake (*Merluccius productus*). ICES Journal of Marine Science 53, 253 – 258.

Trevorrow, M. V., Mackas, D. L., Benfield, M. C. 2005. Comparison of multifrequency acoustic and in situ measurements of zooplankton abundances in Knight Inlet, British Columbia. Journal of the Acoustical Society of America 117:3574-3588.

Urick, R.J. 1983. Principles of underwater sound, 3rd edition. McGraw-Hill, Inc. Peninsula Publishing, Los Altos, California.

Vandermeer, J. 1972. Niche theory, Annual Review of Ecology and Systematics 3: 107-132.

Vidal, J, and Smith, S.L. 1986. Biomass, growth, and development of populations of herbivorous zooplankton in the southeastern Bering Sea during spring. Deep-Sea Research II 33(4), 523-556.

von Szalay, P.G., and Brown, E. 2001. Trawl comparisons of fishing power differences and their applicability to National Marine Fisheries Service and Alaska Department of Fish and Game trawl survey gear. Alaska Fishery Research Bulletin 8(2):85-95.

von Szalay P.G., Somerton, D.A. and Kotwicki, S. 2007. Correlating trawl and acoustic data in the eastern Bering Sea: a first step toward improving biomass estimates of walleye pollock (*Theragra chalcogramma)* and Pacific cod (*Gadus macrocephalus*) Fisheries Research 86:77–83.

Walsh, J. J. and McRoy, C. P. 1986. Ecosystem analysis in the southeastern Bering Sea. Continental Shelf Research 5:259–288.

Walters C.J. and Martell S. 2004. Fisheries Ecology and Management. Princeton, New Jersey, Princeton University Press.

Walters, C. 2003. Folly and fantasy in the analysis of spatial catch rate data, Canadian Journal of Fisheries and Aquatic Science 60: 1433-1436.

Wang, M, Overland, J. E., and Bond, N. A. 2010. Climate projections for selected Large Marine Ecosystems. Journal of Marine Systems 79(3-4):258-266.

Warren, J.D., and Demer, D.A. 2010. Abundance and distribution of Antarctic krill (Euphausia superba) nearshore of Cape Shirreff, Livingston Island, Antarctica, during six austral summers between 2000 and 2007. Canadian Journal of Fisheries and Aquatic Sciences 67:1159–1170.

Warren, J.D., and Smith, J.N. 2007. Density and sound speed of two gelatinous zooplankton: ctenophore (*Mnemiopsis leidyi*) and lion's mane jellyfish (*Cyanea capillata*). Journal of the Acoustical Society of America 122(2):574-580.

Warren, J.D., Stanton, T.K., McGehee, D.E., and Chu, D. 2002. Effect of animal orientation on acoustic estimates of zooplankton properties. IEEE J. Ocean. Eng. 27(1):130-137.

Warren, J.D., Stanton, T.K., Wiebe, P. H. and Seim, H. E. 2003. Inference of biological and physical parameters in an internal wave using multiple frequency acoustic scattering data. ICES Journal of Marine Science 60, 1033-1046.

Warren, J.D., and Wiebe, P.H. 2008. Accounting for biological and physical sources of acoustic backscatter improves estimates of zooplankton biomass. Canadian Journal of Fisheries and Aquatic Sciences 65:321-1333.

Weinberg, K.L., Otto, R.S., Somerton, D.A. 2004. Capture probability of a survey trawl for red king crab (*Paralithodes camtschaticus*). Fishery Bulletin 102:740–749.

Wespestad, V. G., Fritz, L.W., Ingraham, W.J., and Megrey, B. A. 2000. On relationships between cannibalism, climate variability, physical transport, and recruitment success of Bering Sea walleye pollock (*Theragra chalcogramma*). ICES Journal of Marine Science 57:268–274.

Wiebe, P.H., Ashjian, C.J., Gallager, S.M., Davis, C.S., Lawson, G.L., and Copley, N.J. 2004. Using a high-powered strobe light to increase the catch of Antarctic krill. Marine Biology 144(3):493-502.

Wiebe, P.H., Boyd, S.H., Davis, B.M., and Cox, J.L., 1982. Avoidance of towed nets by the euphausiid *Nematoscelis megalops*. Fishery Bulletin 80:75–91.

Wiebe, P.H., Chu, D., Kaartvedt, S., Hundt, A., Melle, W., Ona, E., and Batta-Lona, P. 2010. The acoustic properties of *Salpa thompsoni*. ICES Journal of Marine Science 67(3):583-593.

Wiebe, P.H., Stanton, T.K., Benfield, M.C., Mountain, D.G., and Greene, C.H. 1997. High-frequency acoustic volume backscattering in the Georges Bank Coastal Region and its interpretation using scattering models. IEEE Journal of Oceanic Engineering 22(3):445-464.

Wilberg, M.J., Thorson, J.T., Linton, B.C., and Berkson, J. 2010. Incorporating time-varying catchability into population dynamic stock assessment models. Reviews in Fisheries Science 18:7–24.

Wilderbuer, T. K., Hollowed, A.B., Ingraham W.J. Jr., Spencer, P.D., Conners, M.E., Bond, N.A., and Walters, G.E. 2002. Flatfish recruitment response to decadal climatic variability and ocean conditions in the eastern Bering Sea. Progress in Oceanography 55:235-247.

Wildebuer, T.K., and Nichol, D.G., 2011a. Assessment of the northern rock sole stock in the Bering Sea/Aleutian Islands. *In* Stock Assessment and Evaluation Report for the Groundfish Resources

of the Bering Sea/Aleutian Islands Regions, pp. 813-888 (Chapter 8). Available from the North Pacific Fishery Management Council, 605 West 4th Avenue, Suite 306, Anchorage, AK 99501.

Wildebuer, T.K., Nichol, D.G., and Ianelli, J., 2011b. Assessment of yellowfin sole stock in the Bering Sea/Aleutian Islands. *In* Stock Assessment and Evaluation Report for the Groundfish Resources of the Bering Sea/Aleutian Islands Regions, pp. 583-668 (Chapter 4). Available from the North Pacific Fishery Management Council, 605 West 4th Avenue, Suite 306, Anchorage, AK 99501.

Wilderbuer, T.K., and Nichol, D.G. 2010. Northern rock sole, *In* Stock assessment and fishery evaluation report for the groundfish resources of the Bering Sea/Aleutian Islands regions, chapter 7, pp. 781–868. Available from the North Pacific Fishery Management Council, 605 West 4th Ave., Suite 306, Anchorage, AK 99501.

Wilderbuer, T.K., Nichol, D.G., and Ianelli, J. (2010). Yellowfin sole, *In* Stock assessment and fishery evaluation report for the groundfish resources of the Bering Sea/Aleutian Islands regions, chapter 4, pp. 565–644. Available from the North Pacific Fishery Management Council, 605 West 4th Ave., Suite 306, Anchorage, AK 99501.

Willette, T.M., Cooney, R.T., Patrick, V., Mason, D.M., Thomas, G.L., and Scheel, D., 2001. Ecological processes influencing mortality of juvenile pink salmon (*Oncorhynchus gorbuscha*) in Prince William Sound, Alaska. Fisheries Oceangraphy 10(supplement 1):14-41.

Wilson, M.T., Jump, C.M., Buchheister, A., 2009. Ecology of small neritic fishes in the western Gulf of Alaska. II. Consumption of krill in relation to krill standing stock and the physical environment. Marine Ecology Progress Series 392:239-251.

Wood, S. N. 2003. Thin plate regression splines. Journal of the Royal Statistical Society B 65:95-114.

Wood, S.N. 2006. Generalized additive models: an introduction with R. Chapman and Hall, Boca Raton, Florida, 392 pp.

Wood, S.N., Augustin, N.H. 2002. GAMs with integrated model selection using penalized regression splines and applications to environmental modelling. Ecological Modelling 157:157-177.

Worm, B., Hilborn, R., Baum, J.K., Branch, T.A., Collie, J.S., Costello, C., Fogarty, M.J., Fulton, E.A., Hutchings, J.A., Jennings, S., Jensen, O.P., Lotze, H.K., Mace, P.M., McClanahan, T.R., Minto, C., Palumbi, S.R., Parma, A.M., Ricard, D., Rosenberg, A.A., Watson, R., and Zeller, D. 2009. Rebuilding global fisheries. Science 325:578-585.

Worm, B., Myers, R.A. 2003. Meta-analysis of cod-shrimp interactions reveals top-down control in oceanic food webs. Ecology 84 (1):162-173.

Wyllie-Echeverria, T, Wooster, W. 1998. Year-to-year variations in Bering Sea ice cover and some consequences for fish distributions. Fisheries Oceanography 7(2):159-170.

Zador, S., and Gaichas, S. 2010. Ecosystem considerations for 2011, Appendix C. *In* Stock assessment and fishery evaluation report for the groundfish resources of the Bering Sea/Aleutian Islands regions. North Pacific Fishery Management Council, Anchorage, AK.

Zhou, M., Nordhausen, W., Huntley, M. 1994. ADCP measurements of the distribution and abundance of euphausiids near the Antarctic Peninsula in winter. Deep-Sea Research I 41(9):1425-1445.

Zhukova, N.G., Nesterova, V.N., Prokopchuk, I.P., and Rudneva, G.B., 2009. Winter distribution of euphausiids (Euphausiacea) in the Barents Sea (2000–2005). Deep-Sea Research II 56:1959–1967.

Zimmermann M., Wilkins, M.E., Weinberg, K.L., Lauth, R.R., and Shaw, F.R. 2003. Influence of improved performance monitoring on the consistency of a bottom trawl survey. ICES Journal of Marine Science 60:818–826.

Zuur, A.F., Ieno, E.N., Walker, N.J., Saveliev, A.A., Smith, and G.M. 2009. GLM and GAM for absence-presence and proportional data. P. 1-15. In Mixed Effects Models and Extensions in Ecology with R. Statistics for Biology and Health. Springer Verlag.